

UC Berkeley

UC Berkeley Electronic Theses and Dissertations

Title

Phosphonated Xanthene Fluorophores for Live-Cell Imaging Applications

Permalink

<https://escholarship.org/uc/item/5t07m295>

Author

Turnbull, Joshua Luke

Publication Date

2022

Peer reviewed|Thesis/dissertation

Phosphonated Xanthene Fluorophores for Live-Cell Imaging
Applications

By

Joshua L. Turnbull

A dissertation submitted in partial satisfaction of the
requirements for the degree of

Doctor of Philosophy

in

Chemistry

in the

Graduate Division

of the

University of California, Berkeley

Committee in charge:

Professor Evan. W. Miller, Chair
Professor Christopher J. Chang
Professor Stephen Brohawn

Spring 2022

Phosphonated Xanthene Fluorophores for Live-Cell Imaging Applications

© 2022

By Joshua L. Turnbull

Abstract

Phosphonated Xanthene Fluorophores for Live-Cell Imaging Applications

By

Joshua L. Turnbull

Doctor of Philosophy, Chemistry

University of California, Berkeley

Professor Evan. W. Miller, Chair

Since the original synthesis of fluorescein in 1871, the use of xanthene fluorophores has remained ubiquitous in biology, medicine, and chemical biology. The wide utility of fluorescein and related xanthene dyes is due, in part, to their high brightness and wide range of colors available with simple modifications to the terminal and bridgehead atoms of the xanthene fluorophore core. By comparison, substitution of the pendant carboxylate has remained relatively underexplored. The identity of the substitution at this 3- position can have profound effects on the properties of xanthene fluorophores. We envisioned installation of a biologically relevant phosphonate functionality may provide access to fluorophores with unique properties, such as enhanced water solubility and opportunities for functionalization. Herein we will discuss the first syntheses of novel phosphonated xanthene fluorophores, their associated spectroscopic properties, and the utility of these dyes for both intracellular imaging and membrane potential sensing in living cells.

Table of Contents

Acknowledgements.....	ii
Introduction.....	1
Chapter 1: 3-phosphonofluoresceins: synthesis, spectroscopy, and applications.....	12
Supporting Information for Chapter 1.....	26
Chapter 2: 3-phosphonorhodamines for live cell imaging applications.....	59
Supporting Information for Chapter 2.....	78
Chapter 3: Phosphonated Xanthene Fluorophores for Voltage Sensing Applications.....	145
Supporting Information for Chapter 3.....	159

Acknowledgements

There are so many people I'd like to acknowledge for getting me to this point, the first being my mum. I will forever be grateful for the sacrifices that you made so that I could go and chase my dreams. You have always given your full support to whatever crazy thing I decided to do next, including moving more than 5000 miles across the world to get a PhD in chemistry. Not only has your emotional support got me through the last 25 years, but so has your financial support, and I don't take for granted the privileges that you have given me. Thank you from the bottom of my heart, I hope that I made you proud. To the rest of my family, particularly my grandparents, thank you for everything you have done.

To my PhD advisor, Evan, thank you for every bit of mentorship and guidance over the last five years. Your optimism is infectious and even in my most deflated moments I would leave our meetings reenergized and ready to persevere. I've had the pleasure of learning so many new skills throughout my time in the lab, both scientifically and professionally, and I'm thankful for your continuous encouragement. I'm not sure anyone else could have prepared me as well as you have for my next steps.

The Miller lab has been such an incredible place to work, being surrounded by highly intelligent, humble, and supportive people. It's been special coming to work every day and working alongside not just colleagues, but genuine friends. Friday lunches, karaoke nights at Jaguar and Covid-era lawn hangs are all grad school highlights for me and I'm leaving with so many fond memories. I'd especially like to acknowledge Brittany for not only her important contributions to this work but also continued friendship and emotional support; it was truly special celebrating you at your wedding. I'd also like to acknowledge Ryan for all his hard work and synthetic contributions to this dissertation, I'm adamant I learnt as much from him as I hope he did from me. It's been wonderful watching him grow into an exceptional scientist and I'm excited to follow his journey at Stanford. Every single member of the Miller lab, past and present, has helped foster such a supportive and collaborative environment and I've had a blast.

As someone who thrives off social interactions, the pandemic has been particularly challenging for me. However, I realize how fortunate I am to be surrounded by such wonderful friends, who kept my social calendar busy even when everything was over Zoom. I met Danny and Lauren, days after moving here 5 years ago, and I am incredibly grateful for their friendship and constant support through all the ups and downs of grad school. I can't wait for many more nights of absurd quantities of wine and Danny's delicious cooking. All my friends back in London, I miss them dearly and it was challenging moving so far away, but I'm thankful for all the memories and the times they have flown out to visit. Kameron has been a great friend who constantly reminds me to advocate for myself and has been incredibly helpful through my job search. There's never a dull moment with Ian, thanks for the laughs.

To all my mentors over the years, thank you for helping steer my journey. I can only hope to pay it forward and help provide similar guidance to others. My professors at King's, thank you for developing a course that ignited my passion for chemical biology and advocating for my future. Siyka, thank you for the late nights in Wandsworth talking about life and PhDs, you were a role model that made me see this path as a viable one. Keary, thank you for taking the chance and allowing me to spend a summer in your lab at Scripps as an undergraduate; that summer exposed me to what a PhD in chemistry would really look like, set me on this path and I clearly fell in love with California.

After visiting, I never had any doubts that Berkeley was the right place for me to get my PhD, and I only grew more confident in that decision. I'm particularly grateful for the opportunity

to participate in the chemical biology program and all the experiences I had through my lab rotations. Graduate school certainly had its challenges, and imposter syndrome is something I continuously grapple with. I'd like this dissertation to serve as a constant reminder of this achievement. I'm not sure what my future will look like, but it'll certainly be founded on this success. As Britney Spears once highlighted: success is a state of mind, not about conquering something.

Importantly, thank you to the reader. I hope you find this work as exciting as I have.

Introduction

Since the original synthesis of fluorescein (**Figure 1a**) in 1871,¹ this versatile molecule remains one of the most widely utilized fluorophores in biology, medicine, and chemical biology. Fluorescein labeled antibodies were the first immunofluorescent stains,² and reagents such as fluorescein isothiocyanate, or FITC, remain ubiquitous for the preparation of fluorescent biological conjugates.³ One of the few fluorophores FDA approved for use in humans, sodium fluorescein, has found clinical uses in ophthalmology^{4,5} and more recently, neurosurgery.⁶ A staple in the chemical biology community, countless fluorescein-derived probes and sensors have been reported over the years.⁷⁻⁹ Design of such probes often take advantage of the ability to modulate fluorescence by substitution at the phenolic oxygen, control of spirocyclization, or changes in the rate of photoinduced electron transfer (PeT).¹⁰⁻¹² For example, appending BAPTA, a calcium chelator, to fluoresceins is a common strategy that makes use of PeT to modulate fluorescence and has enabled probing of intracellular calcium dynamics in neurons and brain tissue with high sensitivity and spatiotemporal resolution.¹³⁻¹⁵

The wide utility of fluorescein and related xanthene dyes is due, in part, to their high brightness and wide range of colors available with simple modifications to the terminal and bridgehead atoms of the xanthene fluorophore core. Replacement of the terminal oxygen atoms with amines results in another class of xanthene fluorophores: rhodamines (**Figure 1a**). Rhodamines were first reported less than 20 years after fluoresceins,¹⁶ and have also become widely recognized as fundamental scaffolds for the fluorophore community. In comparison to fluoresceins, rhodamines are relatively insensitive to pH, often exhibit improved photostability and have highly tunable spectral properties all of which have resulted in the widespread adoption of rhodamine derivatives in fluorescent labelling.¹⁷ The alkylation pattern on the terminal amines enables precise tuning of the absorption and emission wavelengths and C-N bond restriction with fused cyclohexane or 4-membered azetidine rings improves brightness and photostability (**Figure 1b**).^{18,19} Replacement of the 10' oxygen atom with carbon,^{20,21} silicon,²²⁻²⁶ phosphorus,²⁷⁻²⁹ or sulfur³⁰ red-shifts excitation and emission wavelengths (**Figure 1b**), avoiding issues related to phototoxicity and autofluorescence and improving tissue penetration. These highly attractive properties and have found widespread use in a variety of biological applications such as fluorogenic labelling,^{26,31,32} far-red voltage sensing,^{33,34} in vivo imaging,³⁵ and super resolution microscopy.³⁶

It was once thought that the 3-carboxylate present on the pendant ring was an indispensable part of the structure of xanthene fluorophores. However, it is now understood that an important role of the 3-substituent is to maintain orthogonality between the xanthene chromophore and the pendant benzene ring.¹⁰ In other words, there is nothing intrinsic about a 3-carboxylate and so long as there is some substituent to restrict free rotation of the pendant ring, a high fluorescence quantum yield can be maintained. Installation of novel chemical functionalities at this position (**Figure 1c**) can have large influences on the chemical properties and behavior of xanthene fluorophores, while the orthogonality of the ring systems leaves the fundamental photophysical properties relatively unperturbed.

Herein we review the implications 3-substitution can have on the properties of xanthene fluorophores and the subsequent biological applications for which they may be used. We comment on traditional and contemporary 3-functionalities that have advanced applications in super resolution microscopy, fluorogenic detection of analytes, and voltage sensing and also highlight the profound opportunities chemical exploration at this position may have in the context of biological imaging.

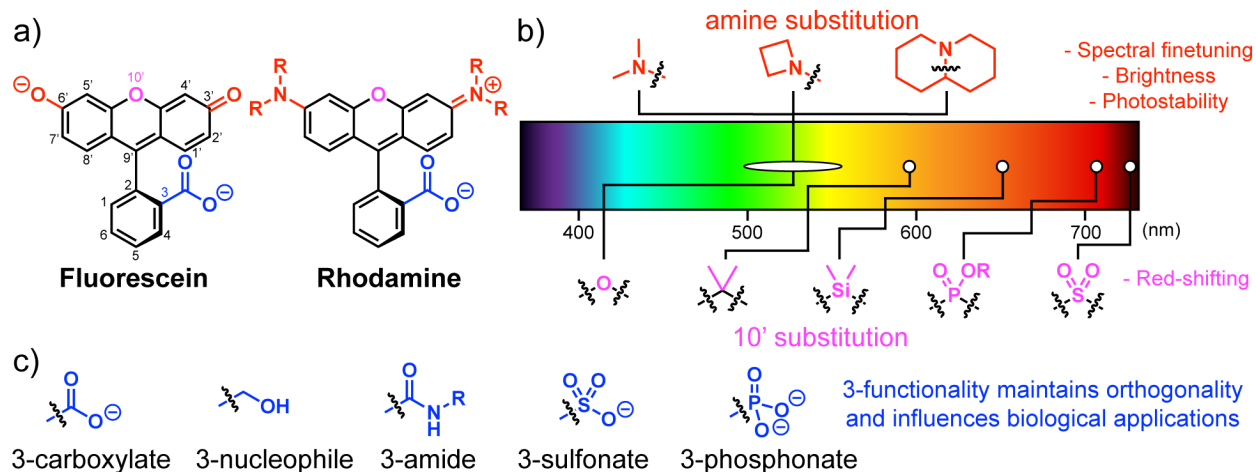


Figure 1. Chemical modification of xanthene fluorophores. (a) general structures of 3-carboxyfluorescein and 3-carboxyrhodamine. (b) amine and 10' substitution influence photophysical properties of xanthene fluorophores. (c) examples of 3-substitutions that maintain orthogonality between the pendant ring and xanthene core and have large implications on subsequent applications.

Carboxy 3-substitution

A key feature of xanthene fluorophores brought about by the presence of the 3-carboxylate is the propensity to spirocyclize into a closed, colorless lactone (**Figure 2a**). This dynamic equilibrium can be sensitive to several environmental factors such as pH,³⁷ polarity,³⁸ and temperature³⁹ and its fluorogenic nature has been fundamental to development of fluorescent tools with unprecedented contrast.

Fluoresceins predominantly adopt the open fluorescent form under physiological conditions, but chemical trapping of the closed lactone is a powerful method for developing fluorogenic sensors.¹² Acetylation of phenolic oxygens is perhaps the most common strategy, and fluorescein diacetate (**Figure 2b**) is a versatile cell viability reagent that readily diffuses across biological membranes where cellular esterases uncage the fluorophore rendering them fluorescent (**Figure 2c**).^{40,41} Expansion of this strategy, including and beyond esterases has led to a plethora of reagents facilitating the measure of specific enzymatic activity in complex systems or site selective uncaging at subcellular precision.^{12,41-45} Although less common, rhodamines can also be locked in the closed form and dipeptidyl rhodamines have served as important substrates for measuring protease activity.^{46,47} Beyond enzymes, reactivity based fluorogenic uncaging allows us to use fluorescence as a readout in response to analytes such as metal ions, reactive oxygen species and endogenous nucleophiles (**Figure 2c**).⁴⁸ Additionally uncaging can be initiated in a photoactivatable manner for a number of applications including super-resolution microscopy.⁴⁹⁻⁵¹

The dynamic equilibrium between the fluorescent zwitterion (Z) and lipophilic lactone (L) forms of rhodamines (**Figure 2d**) has profound implications on their biological imaging applications. Those with high K_{L-Z} values, and thus a preference for the fluorescent zwitterion are environmentally insensitive making them useful for bioconjugation, but their lack of cell permeability often limits their intracellular use.⁵² The K_{L-Z} of 3-carboxy siliconrhodamines, SiRs, are sufficiently low that the closed lactone predominates in aqueous environments, facilitating passage through lipophilic membranes.²⁶ However, upon binding to biological targets, changes in sterics and local environment often shift the equilibrium to the open fluorescent zwitterion (**Figure 2e**).^{26,53} This fluorogenic turn on is highly attractive since background fluorescence is minimal, therefore leading to exceptional contrast in labelling experiments without the need to remove

excess fluorophore. Combining SiRs with covalent targeting ligands such as HaloTag or SNAPTag has led to widespread use in the labelling of many intracellular structures and live-cell super resolution microscopy.^{32,36} Additionally, this environmental sensitivity has led to the development of chemi-genetic probes of voltage and calcium dynamics in which changes in local protein structure modulate fluorescence output through this equilibrium.⁵⁴

More recent advances have sought to fine tune the K_{L-Z} equilibrium of 3-carboxy rhodamines and expand the color palette of fluorogenic labelling probes.^{19,53,55} The K_{L-Z} equilibrium inversely correlates to the absorbance wavelength, in that short wave rhodamines usually predominate as the open zwitterion. Incorporation of electron withdrawing groups on terminal azetidines, or fluorination of the xantheno core have been highlighted as general approaches to decrease K_{L-Z} , improving tissue permeability and fluorogenicity of shorter wave rhodamines (**Figure 2d, f**).^{53,55} Additionally, installation of a neighboring amide has been shown to also stabilize the closed lactone through a neighboring group effect (**Figure 2g**).⁵⁶ On the other hand, near infrared 3-carboxyrhodamines (10' P, S substituted) often exhibit prohibitively low K_{L-Z} values with insufficient tendency to open, rendering them essentially unusable for fluorescence imaging.⁵⁷ Recent approaches to increase K_{L-Z} of such fluorophores have involved fluorination of the pendant ring, presumably lowering the pK_a of the 3-carboxylate and results in K_{L-Z} values within the threshold for super resolution imaging applications (**Figure 2d, f**).^{57,58} Notably, synergy of these approaches facilitates precise finetuning of the K_{L-Z} of rhodamines for specific applications.⁵⁷

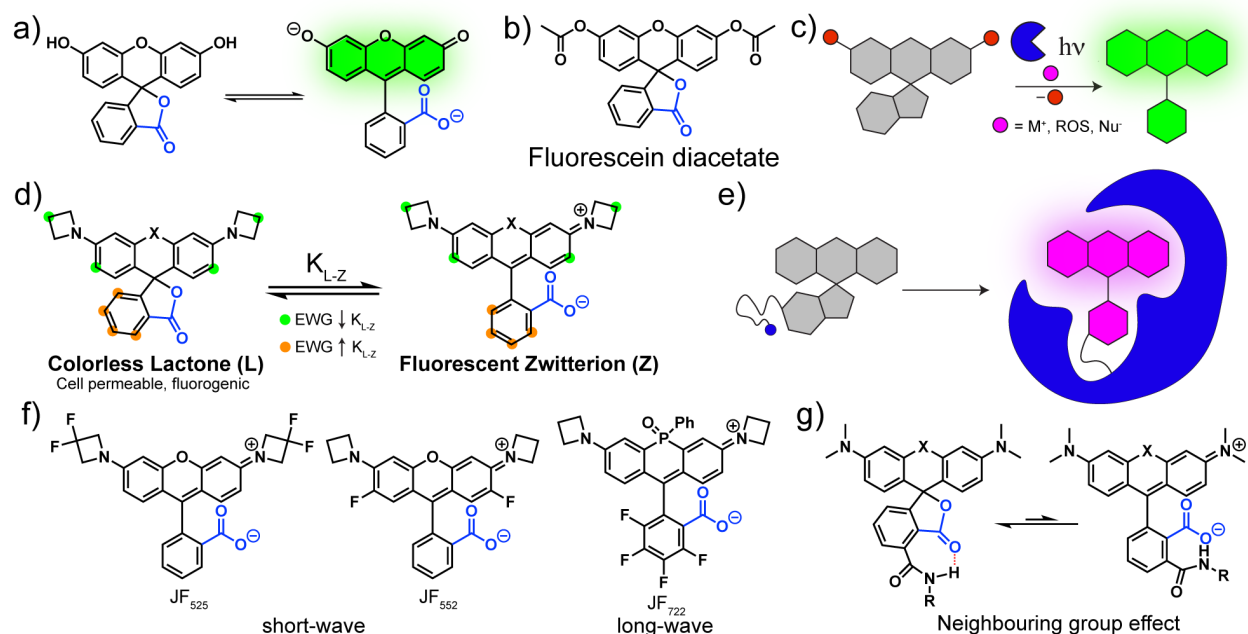


Figure 2. Applications of 3-carboxy substituted xantheno fluorophores. (a) Spirocyclization equilibrium of fluorescein. (b) Chemical structure of fluorescein diacetate. (c) Enzymatic, reactivity based and photoactivated fluorogenic uncaging of xantheno fluorophores. (d) General method for fine-tuning K_{L-Z} of rhodamines by xantheno or pendant ring substitution. (e) Fluorogenic turn on of rhodamines upon protein labelling. (f) Structures of rhodamines with fine-tuned K_{L-Z} constants through fluorination. (g) Finetuning of K_{L-Z} through a neighboring group effect.

Nucleophile 3-substitution

Substitution of the 3-carboxylate for nucleophiles such as hydroxymethyl, aminomethyl or mercaptomethyl can further shift the equilibrium to the closed colorless spirocyclic form (**Figure 3a**).⁵⁹ Interestingly, these fluorophores tend to spontaneously switch to the open fluorescent form

in a transient manner. The thermal equilibrium of this spirocyclization and the lifetime spent in the open form are parameters that influence the blinking behavior and are finetuned by the nucleophilicity of the 3-substituent and electrophilicity of the xanthene fluorophore.⁵⁹ 3-hydroxymethyl siliconrhodamines, HMSiRs (**Figure 3b**) have gained particular attention as spontaneously blinking fluorophores for single molecule localization microscopy (SMLM) applications.^{32,36,53,59,60} Under physiological conditions, HMSiRs exist predominantly (>99%) in the closed spiroether and the stochastic switching to the fluorescent form facilitates the construction of super resolution images (**Figure 3c**), mitigating the need for any fluorophore activation with UV light or strongly reducing dSTORM buffers.⁶¹ Recent advances in calculating the blinking kinetics of HMRs has led to the expansion of the color pallet for multicolor imaging.^{62,63} Additionally improvements in labelling strategies such as through fluorogenic bioconjugation have further enhanced the applications of these fluorophores.⁶⁴

3-hydroxymethyl rhodamines and rhodols have been incorporated into fluorogenic sensors, by chemical trapping of the spiroether with substrates for enzymes such as glycosidases and peptidases.^{65–67} This has led to a variety of probes for visualizing enzymatic upregulation in a variety of cancers such as breast, pancreatic and lung and has demonstrated promise in the optical discrimination of benign vs. malignant tumors.^{68–70} Tuning of the spirocyclization equilibrium, through modification of xanthene amine substitution for example, is important in optimization of the fluorescent turn-on upon enzymatic uncaging.⁶⁶

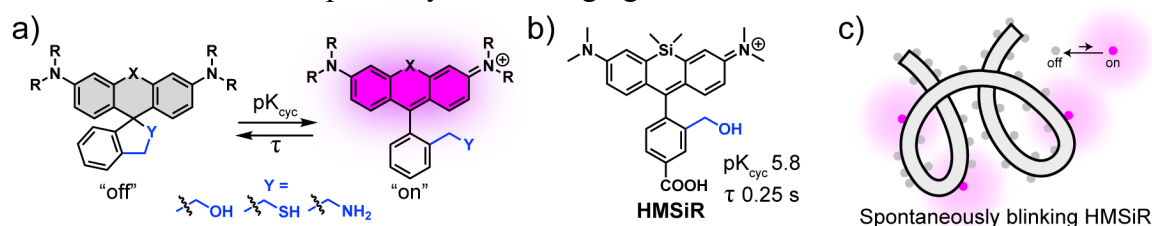


Figure 3. 3-nucleophile substitution for super resolution microscopy. (a) Equilibrium of spontaneously blinking fluorophores influenced by the pK_{cyc} and lifetime, τ spent in the on form. (b) Chemical structure of HMSiR and properties suitable for single-molecule localization microscopy. (c) Schematic of single-molecule localization microscopy with spontaneously blinking fluorophores.

Amide 3-substitution

Parallel to the discovery and optimization of 3-hydroxymethyl substitution for spontaneously blinking fluorophores, amidation of 3-carboxylate substitution shifted the equilibrium of rhodamines to the closed lactam (**Figure 4a**).^{71,72} While carboxy-rhodamines are pH independent, 3-amidorhodamines spirocyclize in a pH dependent manner and exhibit spontaneous blinking behavior at physiological pH.⁷³ The tertiary nature of the amide nitrogen readily facilitates functionalization. For example, installation of a photoswitchable unit led to photoactivatable rhodamines through spiro lactam opening (**Figure 4b**).^{74–76}

Additionally, 3-amides can be functionalized in a modular manner to finetune the spirocyclization equilibrium (**Figure 4b**). Functionalization with electron withdrawing moieties such as sulfonamides enabled precise finetuning of the spiro lactam equilibrium for applications in fluorogenic labelling and super resolution imaging.^{77,78} In contrast to the finetuning discussed previously, the modular nature of amide substitution facilitated more precise finetuning and over a larger range as the amide electronics can be finely controlled. This finetuning is accomplished without chemical modification of the xanthene, meaning photophysical properties remain relatively unperturbed. Additionally, this approach is easily adaptable to other xanthene fluorophores thereby providing improved generalizability. Finally, amidorhodamines were readily

synthesized from carboxyrhodamines, and the modularity of the approach complements synthetic feasibility.^{77,78}

Fluorogenic spirolactam ring opening has been the basis of an abundance of fluorescent probes for specific detection of analytes and ions. Owing to the modularity of amide functionalization, often a chelator is appended and upon ion binding a shift in equilibrium to the open form results in a fluorescence turn on. Alternatively, reactivity-based probes undergo a chemical reaction or amide hydrolysis in the presence of a specific ion or analyte, resulting in a species with a higher propensity to adopt the open, fluorescent form. Several reviews have reported comprehensive summaries of fluorescent sensors that use this approach.^{48,71,72,79}

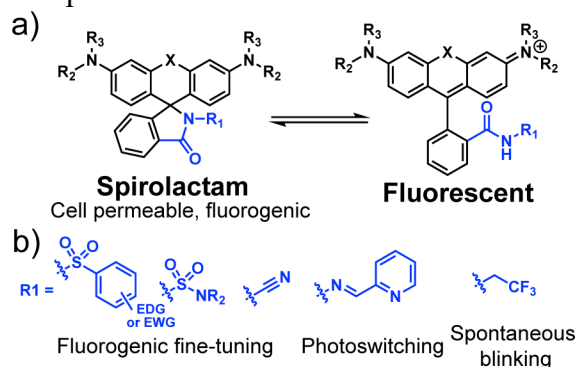


Figure 4. Modular tuning of spirolactamization with 3-amide functionality. (a) Equilibrium between open fluorescent and colorless spirolactam of 3-amide substituted rhodamines. (b) Modular amide substitution influences spirolactam equilibrium for various applications.

Sulfonate 3-substitution

Thus far, the applications of 3-substitution we have highlighted largely focused on controlling the spirolactonization equilibrium of xanthene fluorophores. While in many instances this is a highly attractive property, there are also applications where fluorophore spirolactonization is undesirable. Substitution for a sulfonate at the 3-position typically prevents spirolactonization of xanthene fluorophores, on account of the exceedingly low pK_a .⁸⁰ 3-sulfonate substitution also imparts improved water solubility, an important property for use in biological applications.⁸¹ These properties have made 3-sulfonates an important feature of voltage sensing fluorophores that localize to extracellular membranes in which the 3-sulfonate is responsible for preventing cell permeability and ensuring proper orientation within the membrane.^{33,82–86}

Phosphonate 3-substitution

We recently disclosed the first report of 3-phosphonate substitution in the context of novel 3-phosphonofluoresceins.⁸⁷ Interestingly, we found 3-phosphonate substitution was accompanied by a significant improvement in water solubility, and 3-phosphonofluoresceins behaved like their 3-sulfonate counterparts, displaying no propensity to spirolactonize. Importantly, phosphonates are readily functionalizable. Esterification of the phosphonate facilitates cell permeability where we observe superior accumulation and retention of the fluorophore in living cells. 3-phosphonate substitution is also well suited for incorporation into voltage sensing scaffolds. More recently we have expanded this substitution to other xanthene fluorophores such as rhodamines and silicon-rhodamines. The synthesis, characterization and subsequent live-cell imaging applications of 3-phosphonate substituted xanthene fluorophores will be discussed comprehensively in this dissertation.

Conclusions and outlook

We have highlighted examples of how substitution beyond a 3-carboxylate over recent years has led to the evolution of novel xanthene fluorophores for new applications. This has largely focused on tuning the spirocyclization equilibrium for super resolution imaging, fluorogenic labelling or reaction-based analyte detection. Tuning this equilibrium by 3-substitution has advantages over approaches that rely on chemical modification of the xanthene scaffold. For example, tuning of the xanthene electronics with withdrawing groups is accompanied by spectral shifts, often lower quantum yields and can leave the xanthene prone to nucleophilic attack.^{57,88} Recent reports of tuning spirocyclization with 3-amide substitution are highly attractive due to the modularity of the approach facilitating easy incorporation of a wide number of amines.⁷⁷

On the other hand, there are instances where spirocyclization is undesirable and it is important for the fluorophore to remain in the open fluorescent form. This is useful in examples where fluorescence is being modulated through other pathways such as PeT or where membrane permeability needs to be kept at a minimum, such as in extracellular applications or for improving retention once in cells.

Ultimately, 3-functionality provides the unique advantage of having major influences on the characteristic properties of xanthene fluorophores, such as spirocyclization and water solubility, while leaving photophysical properties such as absorption and emission wavelengths relatively unperturbed. As interest in the chemical exploration of this substituent has grown over recent years, several new biological imaging applications of xanthene fluorophores have emerged including in voltage sensing and single molecule localization microscopy. Perhaps one of the greatest challenges accompanied with new 3-functionalities is synthetic tractability. Often methods that focus on synthetic generalizability do so in the context of xanthene substitution, thus methods that easily facilitate expansion of our repertoire of 3-substituents would be highly sought after. We envision incorporation of novel modalities at the 3-position will be accompanied by the evolution of fluorophores with novel properties and further contribute to our fluorescent molecular toolkit thereby advancing our understanding of complex biological systems.

This dissertation outlines methods to install phosphonic acids and esters at the 3-position of xanthene dyes. Chapter 1 details the synthesis and spectroscopic characterization of a series of novel 3-phosphonofluoresceins. We subsequently demonstrate how phosphonate functionalization facilitates intracellular delivery for prolonged live-cell imaging. Chapter 2 describes the expansion of 3-phosphonate substitution to rhodamines and SiRs via a high-yielding, acid-free synthesis. We highlight the improvement in water solubility accompanied by 3-phosphonate substitution and how intracellular localization is tunable through phosphonate esterification. Finally, Chapter 3 explores the application of xanthene fluorophores with 3-phosphonate substitution in membrane potential sensing.

References

- (1) Baeyer, A. Ueber Eine Neue Klasse von Farbstoffen. *Ber. Dtsch. Chem. Ges.* **1871**, *4* (2), 555–558.
- (2) Coons, A. H.; Creech, H. J.; Norman, J. R.; Berliner, E. The Demonstration of Pneumococcal Antigen in Tissues by the Use of Fluorescent Antibody *J. Immunol.* **1942**, *45* (3), 159.
- (3) Brelje, T. C.; Wessendorf, M. W.; Sorenson, R. L. Multicolor Laser Scanning Confocal Immunofluorescence Microscopy: Practical Application and Limitations. *Methods Cell Biol.* **2002**, *20* (70), 165–244.
- (4) Wilson, S. A.; Last, A. Management of Corneal Abrasions - American Family Physician. *Am. Acad.*

- Fam. Physicians* **2004**, 70 (1), 123–131.
- (5) Marmor, M. F.; Ravin, J. G. Fluorescein Angiography: Insight and Serendipity a Half Century Ago. *Arch. Ophthalmol.* **2011**, 129 (7), 943–948.
 - (6) Cavallo, C.; De Laurentis, C.; Vetrano, I. G.; Falco, J.; Broggi, M.; Schiariti, M.; Ferroli, P.; Acerbi, F. The Utilization of Fluorescein in Brain Tumor Surgery: A Systematic Review. *Journal of Neurosurgical Sciences.* **2018**, 62, (6), 690–703.
 - (7) Johnson, I. D. *Molecular Probes Handbook: A Guide to Fluorescent Probes and Labeling Technologies*; Life Technologies Corporation, 2010.
 - (8) Lavis, L. D.; Raines, R. T. Bright Building Blocks for Chemical Biology. *ACS Chem. Biol.* **2014**, 9 (4), 855–866.
 - (9) D. Lavis, L.; T. Raines, R. Bright Ideas for Chemical Biology. *ACS Chem. Biol.* **2008**, 3 (3), 142–155.
 - (10) Urano, Y.; Kamiya, M.; Kanda, K.; Ueno, T.; Hirose, K.; Nagano, T. Evolution of Fluorescein as a Platform for Finely Tunable Fluorescence Probes. *J. Am. Chem. Soc.* **2005**, 127 (13), 4888–4894.
 - (11) Miura, T.; Urano, Y.; Tanaka, K.; Nagano, T.; Ohkubo, K.; Fukuzumi, S. Rational Design Principle for Modulating Fluorescence Properties of Fluorescein-Based Probes by Photoinduced Electron Transfer. *J. Am. Chem. Soc.* **2003**, 125 (28), 8666–8671. h
 - (12) Grimm, J. B.; Heckman, L. M.; Lavis, L. D. The Chemistry of Small-Molecule Fluorogenic Probes. In *Progress in Molecular Biology and Translational Science*; Elsevier B.V., 2013; Vol. 113, pp 1–34.
 - (13) Minta, A.; Kao, J. P. Y.; Tsien, R. Y. Fluorescent Indicators for Cytosolic Calcium Based on Rhodamine and Fluorescein Chromophores *J. Biol. Chem.* **1989**, 264 (14), 8171–8.
 - (14) Gee, K. R.; Brown, K. A.; Chen, W. N. U.; Bishop-Stewart, J.; Gray, D.; Johnson, I. Chemical and Physiological Characterization of Fluo-4 Ca²⁺-Indicator Dyes. *Cell Calcium* **2000**, 27 (2), 97–106.
 - (15) Roopa; Kumar, N.; Kumar, M.; Bhalla, V. Design and Applications of Small Molecular Probes for Calcium Detection. *Chem. - An Asian J.* **2019**, 14 (24), 4493–4505.
 - (16) Ceresole M. Ger. Pat. 44002, Nov 13, 1887.
 - (17) Beija, M.; Afonso, C. A. M.; Martinho, J. M. G. Synthesis and Applications of Rhodamine Derivatives as Fluorescent Probes. *Chem. Soc. Rev.* **2009**, 38 (8), 2410–2433.
 - (18) Karstens, T.; Kobs, K. Rhodamine B and Rhodamine 101 as Reference Substances for Fluorescence Quantum Yield Measurements. *J. Phys. Chem.* **2002**, 84 (14), 1871–1872.
 - (19) Grimm, J. B.; English, B. P.; Chen, J.; Slaughter, J. P.; Zhang, Z.; Revyakin, A.; Patel, R.; Macklin, J. J.; Normanno, D.; Singer, R. H.; et al. A General Method to Improve Fluorophores for Live-Cell and Single-Molecule Microscopy. *Nat. Methods* **2015**, 12 (3), 244–250. h
 - (20) Grimm, J. B.; Sung, A. J.; Legant, W. R.; Hulamm, P.; Matlosz, S. M.; Betzig, E.; Lavis, L. D. Carbofluoresceins and Carborhodamines as Scaffolds for High-Contrast Fluorogenic Probes. *ACS Chem. Biol.* **2013**, 8 (6), 1303–1310.
 - (21) Grimm, J. B.; Gruber, T. D.; Ortiz, G.; Brown, T. A.; Lavis, L. D. Virginia Orange: A Versatile, Red-Shifted Fluorescein Scaffold for Single- And Dual-Input Fluorogenic Probes. *Bioconjug. Chem.* **2016**, 27 (2), 474–480.
 - (22) Fu, M.; Xiao, Y.; Qian, X.; Zhao, D.; Xu, Y. A Design Concept of Long-Wavelength Fluorescent Analogs of Rhodamine Dyes: Replacement of Oxygen with Silicon Atom. *Chem. Commun.* **2008**, No. 15, 1780–1782.
 - (23) Egawa, T.; Koide, Y.; Hanaoka, K.; Komatsu, T.; CooTeraiper, T.; Nagano, T. Development of a Fluorescein Analogue, TokyoMagenta, as a Novel Scaffold for Fluorescence Probes in Red Region. *Chem. Commun.* **2011**, 47 (14), 4162–4164.
 - (24) Hirabayashi, K.; Hanaoka, K.; Takayanagi, T.; Toki, Y.; Egawa, T.; Kamiya, M.; Komatsu, T.; Ueno, T.; Terai, T.; Yoshida, K.; et al. Analysis of Chemical Equilibrium of Silicon-Substituted Fluorescein and Its Application to Develop a Scaffold for Red Fluorescent Probes. *Anal. Chem.* **2015**, 87 (17), 9061–9069.
 - (25) Grimm, J. B.; Brown, T. A.; Tkachuk, A. N.; Lavis, L. D. General Synthetic Method for Si-

- Fluoresceins and Si-Rhodamines. *ACS Cent. Sci.* **2017**, *3* (9), 975–985.
- (26) Lukinavičius, G.; Umezawa, K.; Olivier, N.; Honigmann, A.; Yang, G.; Plass, T.; Mueller, V.; Reymond, L.; Corrêa Jr, I. R.; Luo, Z.-G.; et al. A Near-Infrared Fluorophore for Live-Cell Super-Resolution Microscopy of Cellular Proteins. *Nat. Chem.* **2013**, *5* (2), 132–139.
- (27) Fukazawa, A.; Usuba, J.; Adler, R. A.; Yamaguchi, S. Synthesis of Seminaphtho-Phospho-Fluorescein Dyes Based on the Consecutive Arylation of Aryldichlorophosphines. *Chem. Commun.* **2017**, *53* (61), 8565–8568.
- (28) Zhou, X.; Lai, R.; Jon Beck, ab R.; Li ab, H.; Stains, C. I. Nebraska Red: A Phosphinate-Based near-Infrared Fluorophore Scaffold for Chemical Biology Applications †. *Chem. Commun* **2016**, *52*, 12290.
- (29) Chai, X.; Cui, X.; Wang, B.; Yang, F.; Cai, Y.; Wu, Q.; Wang, T. Near-Infrared Phosphorus-Substituted Rhodamine with Emission Wavelength above 700 Nm for Bioimaging. *Chem. - A Eur. J.* **2015**, *21* (47), 16754–16758.
- (30) Liu, J.; Sun, Y. Q.; Zhang, H.; Shi, H.; Shi, Y.; Guo, W. Sulfone-Rhodamines: A New Class of near-Infrared Fluorescent Dyes for Bioimaging. *ACS Appl. Mater. Interfaces* **2016**, *8* (35), 22953–22962.
- (31) Shieh, P.; Dien, V. T.; Beahm, B. J.; Castellano, J. M.; Wyss-Coray, T.; Bertozzi, C. R. CalFluors: A Universal Motif for Fluorogenic Azide Probes across the Visible Spectrum. *J. Am. Chem. Soc.* **2015**, *137* (22), 7145–7151.
- (32) Xue, L.; Karpenko, I. A.; Hiblot, J.; Johnsson, K. Imaging and Manipulating Proteins in Live Cells through Covalent Labeling. *Nat. Chem. Biol.* **2015**, *11* (12), 917–923.
- (33) Huang, Y.-L.; Walker, A. S.; Miller, E. W. A Photostable Silicon Rhodamine Platform for Optical Voltage Sensing. *J. Am. Chem. Soc* **2015**, *137*, 10.
- (34) Liu, P.; Miller, E. W. Electrophysiology, Unplugged: Imaging Membrane Potential with Fluorescent Indicators. *Acc. Chem. Res.* **2020**, *53* (1), 11–19.
- (35) Koide, Y.; Urano, Y.; Hanaoka, K.; Piao, W.; Kusakabe, M.; Saito, N.; Terai, T.; Okabe, T.; Nagano, T. Development of NIR Fluorescent Dyes Based on Si-Rhodamine for in Vivo Imaging. *J. Am. Chem. Soc.* **2012**, *134* (11), 5029–5031.
- (36) Wang, L.; Frei, M. S.; Salim, A.; Johnsson, K. Small-Molecule Fluorescent Probes for Live-Cell Super-Resolution Microscopy. *J. Am. Chem. Soc.* **2019**, *141* (7), 2770–2781.
- (37) Martin, M. M.; Lindqvist, L. The PH Dependence of Fluorescein Fluorescence. *J. Lumin.* **1975**, *10* (6), 381–390.
- (38) Zhao, Z. G.; Shen, T.; Xu, H. J. The Absorption and Structure of Fluorescein and Its Ethyl Derivatives in Various Solutions. *Spectrochim. Acta Part A Mol. Spectrosc.* **1989**, *45* (11), 1113–1116.
- (39) Hinckley, D. A.; Seybold, P. G. A Spectroscopic/Thermodynamic Study of the Rhodamine B Lactone \rightleftharpoons Zwitterion Equilibrium. *Spectrochim. Acta Part A Mol. Spectrosc.* **1988**, *44* (10), 1053–1059.
- (40) Hume, E. M.; Krebs; Dowling, H. A.; Wald, G.; Williams, R. J.; Pelton, R. B.; Siegel, F. L. Membrane Properties of Living Mammalian Cells as Studied by Enzymatic Hydrolysis of Fluorogenic Esters. *Proc. Natl. Acad. Sci. U. S. A.* **1966**, *55* (1), 134–141.
- (41) Iwaki, H.; Kamiya, M.; Kawatani, M.; Kojima, R.; Yamasoba, T.; Urano, Y. Fluorescence Probes for Imaging Basic Carboxypeptidase Activity in Living Cells with High Intracellular Retention. *Anal. Chem.* **2021**, *93* (7), 3470–3476.
- (42) Tian, L.; Yang, Y.; Wysocki, L. M.; Arnold, A. C.; Hu, A.; Ravichandran, B.; Sternson, S. M.; Looger, L. L.; Lavis, L. D. Selective Esterase-Ester Pair for Targeting Small Molecules with Cellular Specificity. *Proc. Natl. Acad. Sci. U. S. A.* **2012**, *109* (13), 4756–4761.
- (43) Lavis, L. D.; Chao, T. Y.; Raines, R. T. Synthesis and Utility of Fluorogenic Acetoxymethyl Ethers. *Chem. Sci.* **2011**, *2* (3), 521–530.
- (44) Rotman, B.; Zderic, J. A.; Edelman, M. FLUOROGENIC SUBSTRATES FOR β -D-GALACTOSIDASES AND PHOSPHATASES DERIVED FROM FLUORESCEIN (3, 6-DIHYDROXYFLUORAN) AND ITS MONOMETHYL ETHER. *Proc. Natl. Acad. Sci. U. S. A.*

- 1963**, *50* (1), 1.
- (45) Ritter, C.; Nett, N.; Acevedo-Rocha, C. G.; Lonsdale, R.; Kräling, K.; Dempwolff, F.; Hoebenreich, S.; Graumann, P. L.; Reetz, M. T.; Meggers, E. Bioorthogonal Enzymatic Activation of Caged Compounds. *Angew. Chemie - Int. Ed.* **2015**, *54* (45), 13440–13443.
- (46) Leytus, S. P.; Melhado, L. L.; Mangel, W. F. Rhodamine-Based Compounds as Fluorogenic Substrates for Serine Proteinases. *Biochem. J.* **1983**, *209* (2), 299–307.
- (47) D. Lavis, L.; Chao, T.-Y.; T. Raines, R. Fluorogenic Label for Biomolecular Imaging. *ACS Chem. Biol.* **2006**, *1* (4), 252–260.
- (48) Chan, J.; Dodani, S. C.; Chang, C. J. Reaction-Based Small-Molecule Fluorescent Probes for Chemoselective Bioimaging. *Nat. Chem.* **2012**, *4* (12), 973–984.
- (49) Gee, K. R.; Weinberg, E. S.; Kozlowski, D. J. Caged Q-Rhodamine Dextran: A New Photoactivated Fluorescent Tracer. *Bioorganic Med. Chem. Lett.* **2001**, *11* (16), 2181–2183.
- (50) Wysocki, L. M.; Grimm, J. B.; Tkachuk, A. N.; Brown, T. A.; Betzig, E.; Lavis, L. D. Facile and General Synthesis of Photoactivatable Xanthene Dyes. *Angew. Chemie - Int. Ed.* **2011**, *50* (47), 11206–11209.
- (51) A. Krafft, G.; Randall. Sutton, W.; T. Cummings, R. Photoactivable Fluorophores. 3. Synthesis and Photoactivation of Fluorogenic Difunctionalized Fluoresceins. *J. Am. Chem. Soc.* **2002**, *110* (1), 301–303.
- (52) Panchuk-Voloshina, N.; Haugland, R. P.; Bishop-Stewart, J.; Bhalgat, M. K.; Millard, P. J.; Mao, F.; Leung, W. Y.; Haugland, R. P. Alexa Dyes, a Series of New Fluorescent Dyes That Yield Exceptionally Bright, Photostable Conjugates. *J. Histochem. Cytochem.* **1999**, *47* (9), 1179–1188.
- (53) Zheng, Q.; Ayala, A. X.; Chung, I.; Weigel, A. V.; Ranjan, A.; Falco, N.; Grimm, J. B.; Tkachuk, A. N.; Wu, C.; Lippincott-Schwartz, J.; et al. Rational Design of Fluorogenic and Spontaneously Blinking Labels for Super-Resolution Imaging. *ACS Cent. Sci.* **2019**, *5* (9), 1602–1613.
- (54) Deo, C.; Abdelfattah, A. S.; Bhargava, H. K.; Berro, A. J.; Falco, N.; Farrants, H.; Moeyaert, B.; Chupanova, M.; Lavis, L. D.; Schreiter, E. R. The HaloTag as a General Scaffold for Far-Red Tunable Chemigenetic Indicators. *Nat. Chem. Biol.* **2021**, *17* (6), 718–723.
- (55) Grimm, J. B.; Muthusamy, A. K.; Liang, Y.; Brown, T. A.; Lemon, W. C.; Patel, R.; Lu, R.; Macklin, J. J.; Keller, P. J.; Ji, N.; et al. A General Method to Fine-Tune Fluorophores for Live-Cell and in Vivo Imaging. *Nat. Methods* **2017**, *14* (10), 987–994.
- (56) Bucevičius, J.; Kostiuk, G.; Gerasimaitė, R.; Gilat, T.; Lukinavičius, G. Enhancing the Biocompatibility of Rhodamine Fluorescent Probes by a Neighbouring Group Effect. *Chem. Sci.* **2020**, *11* (28), 7313–7323.
- (57) Grimm, J. B.; Tkachuk, A. N.; Xie, L.; Choi, H.; Mohar, B.; Falco, N.; Schaefer, K.; Patel, R.; Zheng, Q.; Liu, Z.; et al. A General Method to Optimize and Functionalize Red-Shifted Rhodamine Dyes. *Nat. Methods* **2020**, *17* (8), 815–821.
- (58) Grimm, J. B.; Brown, T. A.; Tkachuk, A. N.; Lavis, L. D. General Synthetic Method for Si-Fluoresceins and Si-Rhodamines. **2018**, *18*, 19.
- (59) Uno, S. N.; Kamiya, M.; Yoshihara, T.; Sugawara, K.; Okabe, K.; Tarhan, M. C.; Fujita, H.; Funatsu, T.; Okada, Y.; Tobita, S.; et al. A Spontaneously Blinking Fluorophore Based on Intramolecular Spirocyclization for Live-Cell Super-Resolution Imaging. *Nat. Chem.* **2014**, *6* (8), 681–689.
- (60) Takakura, H.; Zhang, Y.; Erdmann, R. S.; Thompson, A. D.; Lin, Y.; McNellis, B.; Rivera-Molina, F.; Uno, S. N.; Kamiya, M.; Urano, Y.; et al. Long Time-Lapse Nanoscopy with Spontaneously Blinking Membrane Probes. *Nat. Biotechnol.* **2017**, *35* (8), 773–780.
- (61) Jradi, F. M.; Lavis, L. D. Chemistry of Photosensitive Fluorophores for Single-Molecule Localization Microscopy. *ACS Chem. Biol.* **2019**, *14* (6), 1077–1090.
- (62) Tachibana, R.; Kamiya, M.; Morozumi, A.; Miyazaki, Y.; Fujioka, H.; Nanjo, A.; Kojima, R.; Komatsu, T.; Ueno, T.; Hanaoka, K.; et al. Design of Spontaneously Blinking Fluorophores for Live-Cell Super-Resolution Imaging Based on Quantum-Chemical Calculations. *Chem. Commun.* **2020**, *56* (86), 13173–13176.

- (63) Uno, S. N.; Kamiya, M.; Morozumi, A.; Urano, Y. A Green-Light-Emitting, Spontaneously Blinking Fluorophore Based on Intramolecular Spirocyclization for Dual-Colour Super-Resolution Imaging. *Chem. Commun.* **2017**, *54* (1), 102–105.
- (64) Werther, P.; Yserentant, K.; Braun, F.; Kaltwasser, N.; Popp, C.; Baalman, M.; Herten, D. P.; Wombacher, R. Live-Cell Localization Microscopy with a Fluorogenic and Self-Blinking Tetrazine Probe. *Angew. Chemie Int. Ed.* **2020**, *59* (2), 804–810.
- (65) Ueo, H.; Shinden, Y.; Tobo, T.; Gamachi, A.; Udo, M.; Komatsu, H.; Nambara, S.; Saito, T.; Ueda, M.; Hirata, H.; et al. Rapid Intraoperative Visualization of Breast Lesions with γ -Glutamyl Hydroxymethyl Rhodamine Green. *Sci. Reports 2015 51* **2015**, *5* (1), 1–6.
- (66) Asanuma, D.; Sakabe, M.; Kamiya, M.; Yamamoto, K.; Hiratake, J.; Ogawa, M.; Kosaka, N.; Choyke, P. L.; Nagano, T.; Kobayashi, H.; et al. Sensitive β -Galactosidase-Targeting Fluorescence Probe for Visualizing Small Peritoneal Metastatic Tumours in Vivo. *Nat. Commun. 2015 61* **2015**, *6* (1), 1–7.
- (67) Kamiya, M.; Asanuma, D.; Kuranaga, E.; Takeishi, A.; Sakabe, M.; Miura, M.; Nagano, T.; Urano, Y. β -Galactosidase Fluorescence Probe with Improved Cellular Accumulation Based on a Spirocyclized Rhodol Scaffold. *J. Am. Chem. Soc.* **2011**, *133*, 12960–12963.
- (68) Fujita, K.; Kamiya, M.; Urano, Y. Rapid and Sensitive Detection of Cancer Cells with Activatable Fluorescent Probes for Enzyme Activity. *Methods Mol. Biol.* **2021**, *2274*, 193–206.
- (69) Hino, H.; Kamiya, M.; Kitano, K.; Mizuno, K.; Tanaka, S.; Nishiyama, N.; Kataoka, K.; Urano, Y.; Nakajima, J. Rapid Cancer Fluorescence Imaging Using A γ -Glutamyltranspeptidase-Specific Probe For Primary Lung Cancer. *Transl. Oncol.* **2016**, *9* (3), 203–210.
- (70) Takahashi, R.; Ishizawa, T.; Sato, M.; Inagaki, Y.; Takanka, M.; Kuriki, Y.; Kamiya, M.; Ushiku, T.; Urano, Y.; Hasegawa, K. Fluorescence Imaging Using Enzyme-Activatable Probes for Real-Time Identification of Pancreatic Cancer. *Front. Oncol.* **2021**, *11*, 3300.
- (71) Beija, M.; Afonso, C. A. M.; Martinho, J. M. G. Synthesis and Applications of Rhodamine Derivatives as Fluorescent Probes. *Chem. Soc. Rev.* **2009**, *38* (8), 2410–2433.
- (72) Kim, H. N.; Lee, M. H.; Kim, H. J.; Kim, J. S.; Yoon, J. A New Trend in Rhodamine-Based Chemosensors: Application of Spirolactam Ring-Opening to Sensing Ions. *Chem. Soc. Rev.* **2008**, *37* (8), 1465–1472.
- (73) MacDonald, P. J.; Gayda, S.; Haack, R. A.; Ruan, Q.; Himmelsbach, R. J.; Tetin, S. Y. Rhodamine-Derived Fluorescent Dye with Inherent Blinking Behavior for Super-Resolution Imaging. *Anal. Chem.* **2018**, *90* (15), 9165–9173.
- (74) Belov, V. N.; Bossi, M. L. Photoswitching Emission with Rhodamine Spiroamides for Super-Resolution Fluorescence Nanoscopies. *Isr. J. Chem.* **2013**, *53* (5), 267–279.
- (75) Halabi, E. A.; Pinotsi, D.; Rivera-Fuentes, P. Photoregulated Fluxional Fluorophores for Live-Cell Super-Resolution Microscopy with No Apparent Photobleaching. *Nat. Commun. 2019 101* **2019**, *10* (1), 1–10.
- (76) Fölling, J.; Belov, V.; Kunetsky, R.; Medda, R.; Schönle, A.; Egner, A.; Eggeling, C.; Bossi, M.; Hell, S. W. Photochromic Rhodamines Provide Nanoscopy with Optical Sectioning. *Angew. Chemie Int. Ed.* **2007**, *46* (33), 6266–6270.
- (77) Lardon, N.; Wang, L.; Tschanz, A.; Hoess, P.; Tran, M.; D’Este, E.; Ries, J.; Johnsson, K. Systematic Tuning of Rhodamine Spirocyclization for Super-Resolution Microscopy. *J. Am. Chem. Soc.* **2021**, *143* (36), 14592–14600.
- (78) Wang, L.; Tran, M.; D’Este, E.; Roberti, J.; Koch, B.; Xue, L.; Johnsson, K. A General Strategy to Develop Cell Permeable and Fluorogenic Probes for Multicolour Nanoscopy. *Nat. Chem. 2019 122* **2019**, *12* (2), 165–172.
- (79) Yang, Y.; Zhao, Q.; Feng, W.; Li, F. Luminescent Chemodosimeters for Bioimaging. *Chemical Reviews*. January 9, 2013, pp 192–270.
- (80) Gibbs, R. C.; Shapiro, C. V. THE ABSORPTION SPECTRA OF SULFONEFLUORESCEIN AND SOME OF ITS DERIVATIVES. *J. Am. Chem. Soc.* **1928**, *50* (6), 1755–1762.
- (81) Jiao, G. S.; Han, J. W.; Burgess, K. Syntheses of Regioisomerically Pure 5- or 6-Halogenated

- Fluoresceins. *J. Org. Chem.* **2003**, *68* (21), 8264–8267.
- (82) Miller, E. W.; Lin, J. Y.; Frady, E. P.; Steinbach, P. A.; Kristan, W. B.; Tsien, R. Y. Optically Monitoring Voltage in Neurons by Photo-Induced Electron Transfer through Molecular Wires. *Proc. Natl. Acad. Sci. U. S. A.* **2012**, *109* (6), 2114–2119.
- (83) Kulkarni, R. U.; Yin, H.; Pourmandi, N.; James, F.; Adil, M. M.; Schaffer, D. V.; Wang, Y.; Miller, E. W. A Rationally Designed, General Strategy for Membrane Orientation of Photoinduced Electron Transfer-Based Voltage-Sensitive Dyes. **2016**.
- (84) Ortiz, G.; Liu, P.; Naing, S. H. H.; Muller, V. R.; Miller, E. W. Synthesis of Sulfonated Carbofluoresceins for Voltage Imaging. *J. Am. Chem. Soc.* **2019**, *141* (16), 6631–6638.
- (85) Franke, J. M.; Raliski, B. K.; Boggess, S. C.; Natesan, D. V.; Koretsky, E. T.; Zhang, P.; Kulkarni, R. U.; Deal, P. E.; Miller, E. W. BODIPY Fluorophores for Membrane Potential Imaging. *J. Am. Chem. Soc.* **2019**, *141* (32), 12824–12831.
- (86) Kulkarni, R. U.; Vandenberghe, M.; Thunemann, M.; James, F.; Andreassen, O. A.; Djurovic, S.; Devor, A.; Miller, E. W. In Vivo Two-Photon Voltage Imaging with Sulfonated Rhodamine Dyes. *ACS Cent. Sci.* **2018**, *4* (10), 1371–1378.
- (87) Turnbull, J. L.; Benlian, B. R.; Golden, R. P.; Miller, E. W. Phosphonofluoresceins: Synthesis, Spectroscopy, and Applications. *J. Am. Chem. Soc.* **2021**, *143* (16), 6194–6201.
- (88) Umezawa, K.; Yoshida, M.; Kamiya, M.; Yamasoba, T.; Urano, Y. Rational Design of Reversible Fluorescent Probes for Live-Cell Imaging and Quantification of Fast Glutathione Dynamics. *Nat. Chem.* **2016**, *9* (3), 279–286.

Chapter 1

3-phosphonofluoresceins: synthesis, spectroscopy, and applications

Portions of this work were published as:

[Turnbull, J. L.; Benlian, B. R.; Golden, R. P.; Miller, E. W. Phosphonofluoresceins: Synthesis, Spectroscopy, and Applications. J. Am. Chem. Soc. 2021, 143 \(16\), 6194-6201.](#)

Abstract

Xanthene fluorophores, like fluorescein, have been versatile molecules across diverse fields of chemistry and life sciences. Despite the ubiquity of 3-carboxy and 3-sulfonofluorescein for the last 150 years, to date, no reports of 3-phosphonofluorescein exist. Here, we report the synthesis, spectroscopic characterization, and applications of 3-phosphonofluoresceins. The absorption and emission of 3-phosphonofluoresceins remain relatively unaltered from the parent 3-carboxyfluorescein. 3-phosphonofluoresceins show enhanced water solubility compared to 3-carboxyfluorescein and persist in an open, visible light-absorbing state even at low pH and in low dielectric media while 3-carboxyfluoresceins tend to lactonize. In contrast, the spirocyclization tendency of 3-phosphonofluoresceins can be modulated by esterification of the phosphonic acid. The bis-acetoxymethyl ester of 3-phosphonofluorescein readily enters living cells, showing excellent accumulation (>6x) and retention (>11x), resulting in a nearly 70-fold improvement in cellular brightness compared to 3-carboxyfluorescein. In sum, we develop the first synthesis of 3-phosphonofluoresceins, characterize the spectroscopic properties of this new class of xanthene dyes, and utilize these insights to show the utility of 3-phosphonofluoresceins in prolonged intracellular imaging.

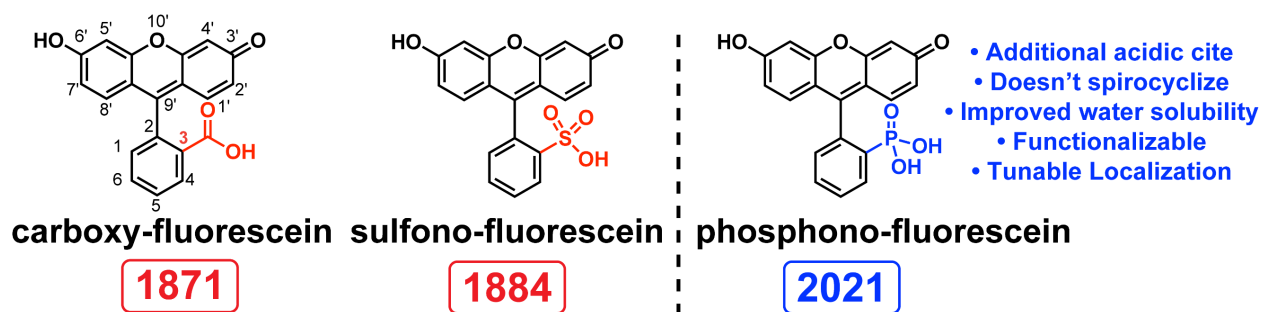
Introduction

Until the realization that the 3-carboxy group of fluoresceins plays no intrinsic role in the fluorescence properties of fluoresceins,¹ almost all reported fluorescein derivatives contained this functional group. While this clearly didn't hinder the broad adoption of fluorescein across the life sciences, one could imagine how any confinement of a chemical structure could be limiting on the potential chemical exploration and hence scope of possible applications. Indeed, the 3-carboxy group is not indispensable for strong fluorescence and is needed to maintain orthogonality between the xanthene chromophore and pendant benzene moiety.¹ In other words, the 3-carboxylate can be replaced with another functional group. This provides a unique opportunity to develop next generation fluoresceins with novel physical properties or that contain unique chemical functionalities to further expand the scope of applications of these dyes. Ideally such substitutions would be achieved without compromising the highly desirable photophysical properties that are responsible for the widespread use of fluoresceins. Minimizing perturbations in brightness or excitation/emission wavelengths will make new fluoresceins easily adaptable for use in current microscopy set ups with little need for adjustment of laser lines or filter sets and would also allow for direct comparison to well characterized carboxy fluoresceins.

While fluoresceins with acidic substituents at the 3-position have been ubiquitous in the literature for some time (3-sulfonofluorescein was reported a mere 13 years after 3-carboxyfluorescein),² we were somewhat surprised to find no report describing 3-phosphonofluorescein, which possesses the biologically relevant acidic phosphonate group (**Scheme 1**). Phosphonates are ubiquitous organophosphorus functionalities, and the chemically inert C–P bond makes them an interesting structural analog of phosphates. Phosphates play a myriad of roles in living organisms and in fact, by mimicking phosphates, phosphonates have found numerous uses in biology and medicine.^{3,4} For example, phosphonates have found widespread use in the development of nucleoside antiretrovirals such as tenofovir.^{5,6} We were curious to explore this unreported class of fluoresceins, namely by investigating the unique properties that a 3-phosphonate would bring in comparison to 3-carboxyfluoresceins and the opportunity this may present with respect to new imaging applications.

There are several properties that are unique to phosphonates that we were interested in exploring. Firstly, the two acidic sites on phosphonates – one pK_a above sulfonic acid but below carboxylic acid, and a second pK_a near physiological pH – might provide opportunities for functionalization.⁷ Organophosphorus chemistry is expansive, and a wide array of functionalities can be derived from phosphonates, such as phosphonate esters, phosphonamides, phosphinates, and phosphine oxides.⁴ Not only did we envision that all of these functionalities could be incorporated into a fluorescein scaffold, but the presence of a 3-phosphonate could serve as a useful chemical handle for fluorescein derivatization. Derivatization of carboxy fluoresceins at the 3-position has led to several fluorogenic sensors of inorganic ions such as copper, zinc, and gold.^{8,9} The persistent ionization at physiological pH has led to the incorporation of phosphonates into molecules to improve water solubility and we rationalized this property would likely improve the water solubility of fluoresceins, an important property for use in biological contexts.^{3,10} Lastly, 3-carboxyfluoresceins spirocyclize at low pH or in low dielectric mediums to a nonfluorescent lactone,^{11,12} and this is often the basis for design of fluorogenic probes, whereas 3-sulfonofluoresceins remain in an open fluorescent state. Since 3-functionality plays a key role in this propensity to spirocyclize and thus influence subsequent applications, we were curious to explore to what degree 3-phosphonofluoresceins would exhibit this behavior.

In this chapter, we discuss the first synthesis of 3-phosphonofluoresceins, characterize the spectral properties of this new class of fluorophore, and describe how we can exploit the properties of 3-phosphonofluoresceins for prolonged imaging of living cells.



Scheme 1. Unique properties of phosphono-fluorescein.

Results and Discussion

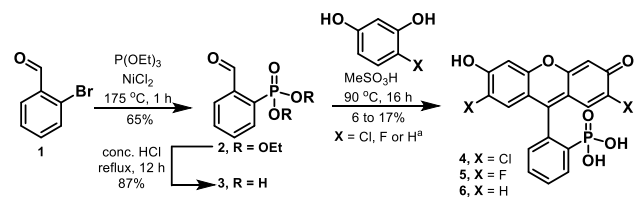
Synthesis of 3-phosphonofluoresceins

Substituting the carboxylate functionality of fluoresceins poses an inherent synthetic challenge. Attempts to displace fluoride from 2-fluorobenzaldehyde with triethylphosphite, in a fashion analogous to the synthesis of 3-sulfonofluorescein precursors,^{13,14} did not produce the desired aryl phosphonate, despite adjusting various conditions such as temperature and pressure. Carbon-phosphorous bonds are often formed through Michaelis-Arbuzov chemistry, in which an alkyl halide undergoes nucleophilic attack from a trialkyl phosphite, displacing the halide and generating a phosphonium intermediate.^{15,16} Subsequent attack from the displaced halide generates pentavalent alkyl phosphonates in a reaction that is used extensively, including in the preparation of Horner-Emmons reagents.^{15,17} Tavs reported the access of analogous aryl phosphonium intermediates through use of transition metal catalysts such as Ni^0 or Pd^0 .^{16,18,19} We found Ni -mediated catalysis enables access of the desired arylphosphonic ester **2** from 2-bromobenzaldehyde **1** in 65% yield (Scheme 2). Importantly, a slight excess of triethyl phosphite is required due to undesired oxidation of the phosphite to the corresponding phosphate at elevated

temperature. A weak nitrogen flow is also prudent to remove the generated ethylbromide to minimize its reaction with triethyl phosphite, which generates diethyl ethyl phosphonate. Both phosphonate side products are high boiling and, since polarity is largely dictated by the phosphonate, are chromatographically difficult to separate from **2**, hence minimizing their production is prudent. This approach enables facile access to up to 10 g quantities of **2** in one step from simple, low-cost starting reagents.

Hydrolysis to phosphonic acid **3** can be performed in concentrated HCl under refluxing conditions to give the free acid in 87% yield. While the diethyl ester precursor (**2**) can be carried directly into the condensation with resorcinols to make 3-phosphonofluoresceins (with hydrolysis of diethylphosphonate occurring *in situ*), we observe improved yields and simpler purification when using free phosphonic acid (**3**). Condensation of **3** with the corresponding resorcinol in neat methanesulfonic acid gives dihalogenated phosphonofluoresceins **4** and **5**. Non-halogenated phosphonofluorescein (**6**) may also be prepared via this route, but cleaner conversion was observed with 85% phosphoric acid at the expense of a longer reaction time.

The purification of crude phosphonofluoresceins is difficult, owing to the high polarity of the water-soluble dyes. Despite crude analytical HPLC traces appearing relatively clean, comparison of a HPLC purified standard by UV/Vis spectroscopy determined that only a fraction (~30%) of the crude isolate mass can be attributed to the fluorophore (**Figure S1**). We hypothesize the impurities are largely attributed to the harsh reaction conditions promoting polymerization of resorcinols, inefficient oxidation to the xanthene and the presence of organic salts, contributing to the mass but likely not able to absorb visible light.²⁰ Despite requiring an *in situ* oxidation to generate the xanthene, performing reactions under nitrogen as opposed to open to air surprisingly results in an almost two-fold increase in purity of the crude isolate (**Figure S1**). We had initially hypothesized that this oxygen free approach would allow us to access the unoxidized fluorophore and potentially aid in purification; however, it has been reported that methanesulfonic acid may act as an oxidant at elevated temperatures.²⁰ Chromatographic purification techniques such as silica flash chromatography require highly polar solvent systems (4:2:1 Ethyl acetate: isopropanol: water with 3% acetic acid as an additive) and is both laborious and only improves impurity to a moderate extent even after multiple iterations (**Figure S1**). Alternative chromatographic techniques such as preparative HPLC and reverse phase silica flash chromatography are more fruitful, yet low throughput owing to the limited solubility of the fluorophores. Ultimately, careful trituration of the crude reaction isolates with mixtures of ice-cold methanol/isopropanol or methanol/acetonitrile enables isolation of pure dyes (**Figure S1**). This approach negates the need for costly and low throughput reverse phase chromatographic techniques, but comes at the cost of reduced isolated yields, ranging from 6 to 17%. It is notable that this synthetic route provides similar yields to those observed with the analogous sulfonated derivatives (**Supporting Info**) and low yields/non-trivial purifications are commonly encountered with such reactions.



^a for X = H the following conditions were used: H₃PO₄ (85%), 130 °C, 2.5 days

Scheme 2. Synthesis of 3-phosphonofluoresceins.

Spectroscopic characterization of 3-phosphonofluoresceins

To examine the influence of phosphonate substitution on fluorescein, we evaluated the spectroscopic properties of 3-phosphonofluoresceins (**4** - **6**) compared to traditional 3-carboxy- and 3-sulfono- fluoresceins. In 0.1 M NaOH_(aq) 2',7'-dichloro-3-phosphonofluorescein (pF.Cl, **4**) absorbs at 498 nm and emits at 517 nm (**Table 1, Figure S2a**), demonstrating a very slight hypsochromic shift relative to 2',7'-dichloro-3-carboxyfluorescein (502 nm/523 nm, **Table 1, Figure S2d**).²¹ The sulfo derivative, 2',7'-dichloro-3-sulfonofluorescein (sF.Cl), however has a slight bathochromic shift and absorbs at 509 nm and emits at 526 nm (**Table 1, Figure S2e**). These small shifts are likely due to slight inductive differences from the *meso* ring. Since the *meso* ring and the xanthene are orthogonal to one another, there should be minimal ground state interactions between the two. As a result, the Stokes shift, extinction coefficients, and quantum yields show only minor variability across the series (**Table 1**). The photostability of **4** is similar to the 3-carboxy and 3-sulfono analogs (**Figure S2g-i**). While photophysical properties among the series remain relatively unperturbed, one large change is the improved water solubility; pF.Cl (**4**) is almost twice as soluble as 2',7'-dichloro-3-carboxyfluorescein, and slightly less soluble than sF.Cl (**Table 1**).

Fluorescein can exist in cationic, neutral, anionic or dianionic forms, making absorption and fluorescence of fluoresceins strongly pH dependent.^{22,23} Halogenated (2',7'- dichloro or difluoro) fluoresceins have lower phenolic pK_a values than the corresponding unhalogenated fluorescein, making dichloro- and difluoro- fluoresceins less sensitive to biologically relevant pH fluctuations.^{21,24} In order to assess the effect of *meso* substitution on the pH sensitivity, we titrated 3-carboxy, 3-sulfono and 3-phosphono- dichlorofluoresceins from pH 2.3 to 9.8 (**Figure 1a, d, and g**). Transition to the dianion can be monitored by measuring the increase in absorption at λ_{\max} with respect to increasing pH (**Figure 1b, e, and h**). The phenolic pK_a of all three dichlorofluoresceins is 4.5, suggesting substitution at the 3 position has little effect on formation of the dianion (**Figure 1c, f, and i**).

The phenolic pK_a values for non-halogenated, 3-phosphonofluorescein (**6**, pK_a = 6.4) and fluorinated 3-phosphonofluorescein (**5**, pK_a = 4.8) also closely match the pK_a value of the analogous 3-carboxy analog (**Figures S3 and S4**).²⁴ Unique to 3-phosphonofluoresceins, after deprotonation to the dianion, a 5 nm hypsochromic shift is observed as pH continues to increase (**Figure 1g, Figure S3a and c**). This likely results from formation of a trianion (**Figure 1i**) due to the extra acidic site on the phosphonate and quantification of this shift with **4** (pF.Cl) reveals a pK_a of 7.8 – in the typical range of acidities for aryl phosphonic acids.⁷

In the neutral form, carboxy fluoresceins spirocyclize to a colorless, non-fluorescent lactone (**Figure 1c**) whereas 3-sulfono-fluoresceins do not (**Figure 1f**). Both sulfono- and phosphono-dichlorofluoresceins have a clear isosbestic point between pH 2.3 and 6.8 (**Figure 1d and g**), resulting from the interconversion of the anionic quinoid and dianion. The same isosbestic point is not observed with 3-carboxy dichlorofluorescein as absorption continuously decreases with pH due to spirocyclization to the neutral lactone at low pH (**Figure 1a**). The observation that carboxy-fluoresceins spirocyclize whereas sulfono- and phosphono-fluoresceins do not can be rationalized by the difference in pK_a values. The 3-substituents on the latter two are strongly acidic, with pK_a values lower than protonation of the xanthene to the cationic form (**Figure S4c**), and thus the neutral form favors an open zwitterion. The carboxylate, however, has a higher pK_a, so a significant portion of the neutral form exists as a closed lactone.²²

Fluorescein can also spirocyclize in low dielectric media and thus doesn't absorb light in the visible region (**Figure S5a,b**, red trace). In low dielectric media, both 3-phosphono- (**Figure S5d-**

f) and 3-sulfo-fluoresceins (**Figure S5c**) possess absorbance profiles akin to the protonated xanthene in the open form. Moving from high to low dielectric, we observe an apparent increase in the pK_a of the phenolic oxygen but no tendency to spirocyclize into the colorless lactone.

Table 1. Properties of fluoresceins.

Dye	3-substituent	X ^a	λ_{max} / nm ^b	λ_{em} / nm ^b	ϵ / M ⁻¹ cm ^{-1b,c}	Φ_f ^b	Solubility ^d
fluorescein	-CO ₂ H	-H	491	514	88,000	0.92	---
2',7'-dichloro-3-carboxy-fluorescein	-CO ₂ H	-Cl	502	523	86,000	0.94	1
2',7'-dichloro-3-sulfonofluorescein (sF.Cl)	-SO ₃ H	-Cl	509	526	87,000	0.89	3.1
2',7'-dichloro-3-phosphonofluorescein (pF.Cl, 4)	-PO ₃ H ₂	-Cl	498	517	88,000	0.90	1.8
2',7'-difluoro-3-phosphonofluorescein (pF.F, 5)	-PO ₃ H ₂	-F	488	508	84,000	0.94	---
3-phosphonofluorescein (pF.H, 6)	-PO ₃ H ₂	-H	487	508	75,000	0.99	---

^a see Scheme 2. ^b in 0.1M NaOH_(aq), relative to fluorescein. ^c At max absorption. ^d measured in PBS relative to 2',7'-dichlorofluorescein.

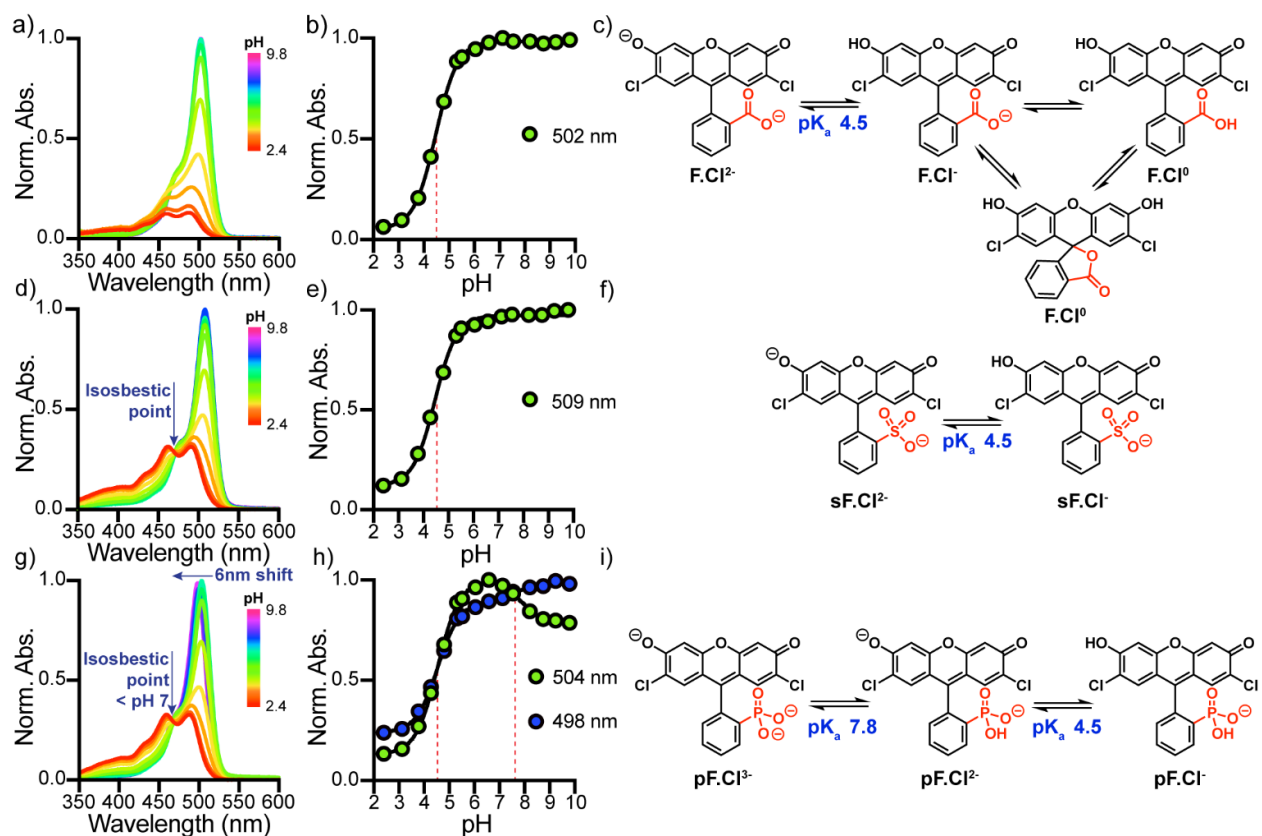
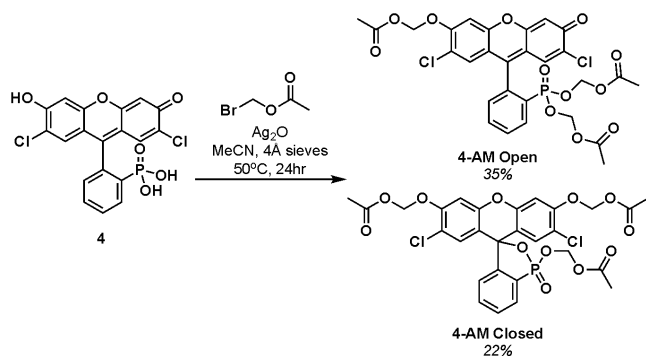


Figure 1. Spectroscopic characterization of the pH dependence of dichlorofluoresceins. Normalized absorbance spectra and corresponding plots of normalized absorbance vs. pH at λ_{max} for carboxy- (a, b), sulfono- (d, e) and phosphono- (g, h) dichlorofluoresceins. Spectra were recorded in 10 mM buffered solutions (see supporting information) containing 150 mM NaCl from pH 2.4 (red) to 9.8 (magenta), and intermediate values of 3.1, 3.8, 4.3, 4.8, 5.3, 5.5, 6.1, 6.6, 7.1, 7.5, 8.2, 8.7 and 9.2 at a dye concentration of 2 μ M. Titration curves fit to sigmoidal dose response curves (solid black) enabled pK_a determination (dashed red). Error bars represent \pm SEM for $n = 3$ independent determinations and if not visible are smaller than the marker. Summary of pH equilibria with determined pK_a values for carboxy- (c), sulfono- (f) and phosphono- (i) dichlorofluorescein.

Intracellular delivery and live-cell imaging

Acetoxy methyl (AM) ethers are commonly employed to deliver anionic fluorophores and small molecules into cells.²⁵ The high pK_a (~13) of the formaldehyde hydrate leaving group provides chemical and hydrolytic stability, therefore AM ether hydrolysis relies on endogenous cellular esterases.²⁶ In the context of fluorescein, this uncaging process is fluorogenic; hydrolysis of the first AM ether releases the dye from its closed, colorless lactone form and hydrolysis of the second AM ether provides the negatively charged phenolate responsible for strong fluorescence. This fluorogenicity has resulted in the widespread use of fluorescein AMs as cell viability reagents and has enabled the intracellular delivery of numerous fluorescein-derived probes.^{26,27} Despite their widespread use, carboxy fluoresceins are rapidly effluxed out of cells, hindering the long-term imaging of live cells.^{28–30} We considered whether the improved water solubility and lower pK_a of 3-phosphonofluoresceins would improve intracellular retention, since this charged group must be masked in some way in order to cross the lipid bilayer. While 3-sulfonyl-fluoresceins also possess high water solubility and low pK_a values, sulfonic esters are potent electrophiles, making them inherently unstable and difficult to chemically mask for intracellular delivery.³¹ On the other hand, phosphonates are commonly masked with biologically labile protecting groups, such as AM esters, to deliver phosphonate or phosphate containing biomolecules into cells.^{32–34} This approach is commonly incorporated into the design of nucleotide (or nucleoside phosphate) prodrugs.^{35,36}



Scheme 3. Synthesis of phosphonofluorescein acetoxy methyl esters and ethers.

Treatment of 3-carboxy-fluoresceins with bromomethyl acetate in the presence of Ag(I) in MeCN, results predominantly in the closed, non-fluorescent, lactonized form with two phenolic AM ethers, although a small amount of the open AM ether/ester can be isolated (**Supporting Info**).²⁶ Owing to the tendency to not spirocyclize, the opposite selectivity is observed with **pF.Cl** (**4**), where the open form (**4-AM open**) is the major product, and the cyclized form (**4-AM closed**) is the minor product (**Scheme 3**). In buffered saline (Hank's balanced salt solution, HBSS), **4-AM open** has absorption centered at 467 nm, and emission profiles characteristic of a singly alkylated xanthene ether (**Figure S6a,b**). No hydrolysis is observed after several hours of incubation in HBSS at 37 °C (**Figure S7**). Incubation in strong base, or in the presence of porcine liver esterase (PLE), however, results in a ~30x fold increase in fluorescence (**Figure S7 and S6a,b**), demonstrating effective release of the free dye, behaving in the same way as the analogous carboxy-fluorescein AM (**Figure S6i,j**). While the closed, 3-carboxy fluorescein AMs absorb no visible light in HBSS (**Figures S6e-h**), **4-AM closed**, with an absorption maximum at 443 nm, displays a spectrum (**Figure S6c,d**) similar to that of the cationic species observed at low pH (**Figure S6b**), suggesting the **4-AM closed** is in an open, zwitterionic form. Subsequent incubation

of **4-AM closed** at 37 °C in HBSS for 2 hours results in a loss of any visible absorption (**Figure S6d**) along with a decrease in m/z corresponding to loss of a single AM group (**Figure S8**). This suggests that in this form, the phosphonate ester of **4-AM closed** is prone to facile hydrolysis (**Figure S9**). The ³¹P NMR chemical shift of **4-AM closed** is significantly downfield (30.3 ppm, **Spectrum S23**) relative to **4-AM open** (14.3 ppm, **Spectrum S20**), likely a result of increased electrophilicity and thus confers decreased hydrolytic stability of **4-AM closed**.

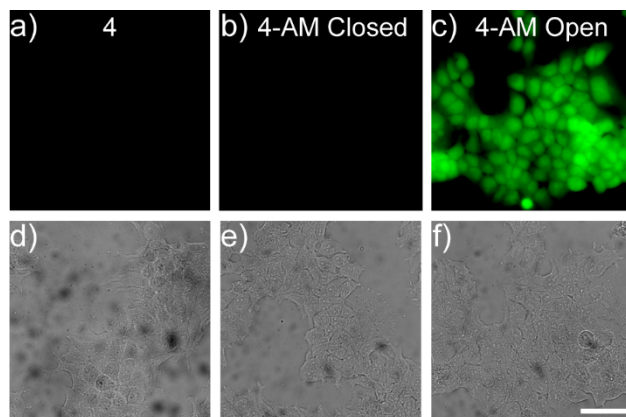


Figure 2. Cell permeability of phosphonofluoresceins. Widefield fluorescence (a-c) and DIC (d-f) images of HEK cells stained with 500 nM **4** (a,d), **4-AM closed** (b,e) and **4-AM open** (c,f) for 20 min at 37 °C. Cells were washed once with HBSS prior to imaging. Scale bar is 50 μ M.

Unsurprisingly, **4**, which contains an unmasked phosphonic acid, is cell impermeable and no uptake into HEK293T (HEK) cells is observed by widefield fluorescence microscopy after 20 minutes of incubation (**Figure 2a,d**). The same is true for **4-AM closed**, suggesting the phosphonate ester is rapidly hydrolyzed in the loading solution and the resulting negative charge precludes the ability to diffuse across the cell membrane (**Figure 2b,e**, **Figure S10**). The strong cellular fluorescence from cells treated with **4-AM open** indicates a high degree of cell permeability followed by fluorogenic uncaging (**Figure 2c,f**). Compared to 3-carboxyfluorescein AM derivatives, **4-AM open** has between 3.5 to 6-fold increase in cellular fluorescence intensity compared to FCI and F-AMs (both open and closed) at 500 nM in HEK cells (**Figure 3a,d**), enabling the phosphono derivative to be used at much lower concentrations. In fact, we saw reasonable fluorescence intensity at 100 nM concentrations, whereas carboxy fluoresceins are often loaded in the μ M range.²⁶

We postulated the increased cellular fluorescence intensity of 3-phosphonofluoresceins may result from improved cellular retention compared to 3-carboxyfluoresceins. Serial washing of cells loaded with FCI-AM (2',7'-dichloro-3-carboxyfluorescein) results in a dramatic loss of fluorescence and after 3 washes cellular fluorescence levels are 8% of original intensities (**Figure 3b,c**). Conversely, with **4-AM open**, cellular fluorescence intensity levels remain at 89% of the original values, even after 3 washes (**Figure 3b,c**), thereby demonstrating an almost 70 fold increase in fluorescence intensity compared to cells stained with FCI-AM. The enhanced cellular retention of 3-phosphonofluoresceins expands the scope of use for prolonged imaging in living cells.

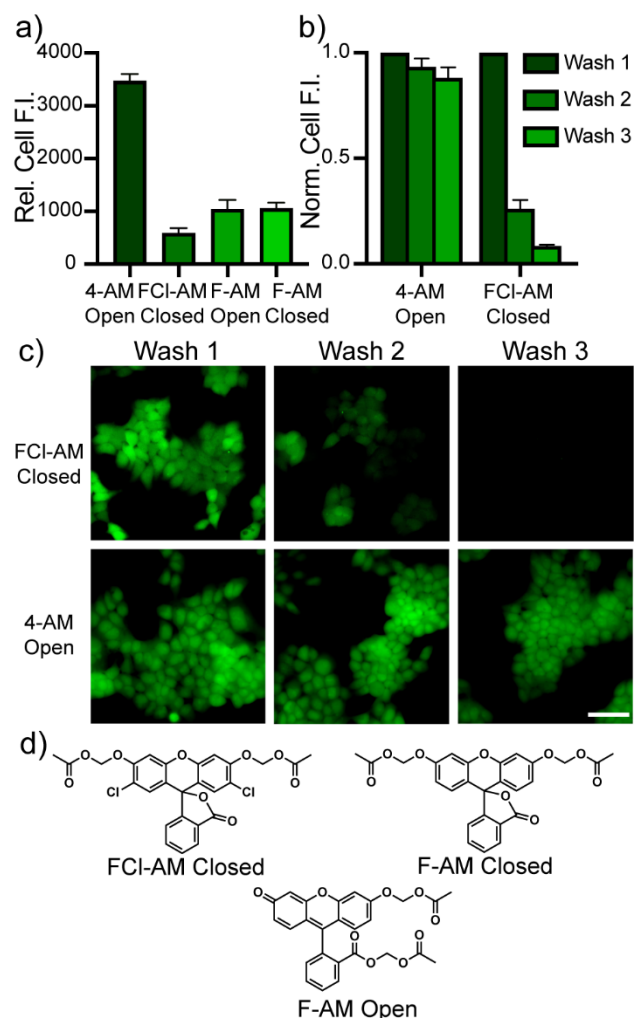


Figure 3. Cellular retention of fluoresceins. (a) Comparison of the relative brightness of fluorescein AMs in HEK cells. (b) normalized intensity and (c) fluorescence images of 4-AM Open and FCI-AM Closed loaded onto HEK cells at 500 nM in HBSS for 20 min. Cells were sequentially washed with fresh HBSS and changes in fluorescence intensity were measured by means of fluorescence microscopy. All dyes were loaded at 500 nM in HBSS for 20 min at 37 °C. Error bars in (a) and (b) are ±SEM for n=4 coverslips. Scale bar is 50 μm. (d) Chemical structures of carboxyfluorescein AMs.

We then incubated HEK cells labelled with FCI-AM closed, 4-AM open and calcein AM (a multiply carboxylated fluorescein derivative, with a net 6 negative charge and excellent cellular retention)^{30,37} in DMEM for up to 60 minutes prior to imaging. Carboxy fluorescein is rapidly effluxed and no fluorescence is seen after the 0 min time point (**Figure 4b**), whereas phosphonofluorescein appears to efflux at a much slower rate, and almost half the intracellular fluorescence is retained after an hour (**Figure 4a**). Anionic transporters such as multidrug resistant-associated proteins (MRP) have been implicated in the efflux of fluorescein from cells and MRP inhibitors such as MK-571 improve retention and accumulation of dyes.³⁸⁻⁴⁰ Incubation of stained HEK cells in DMEM containing MK-571 (50 μM) reduces the rate of dichlorofluorescein efflux after 15 minutes (**Figure 4b ii, iii**), however almost all cellular fluorescence is still lost after 60 minutes (**Figure 4b iii, iv**). On the contrary phosphonofluorescein efflux is almost completely inhibited by MK-571: no change in cellular fluorescence intensity is observed after 60 minutes incubation in the presence of MK-571 (**Figure 4a**). While fluorescein is known to be effluxed by

a variety of transporters, complete inhibition of phosphonofluorescein efflux demonstrates the propensity of the phosphonate to avoid some of these pathways and implicates MRPs as the key contributor to efflux. One could imagine circumstances where moderate efflux of a fluorophore could prove beneficial, such as improving contrast when labelling intracellular structures. On the other hand, phosphonofluorescein efflux can be readily inhibited with the addition of MK-571 for situations where efflux would be undesirable, such as quantitative long-term live cell or in vivo imaging applications (**Figure 5**). Importantly, 3-phosphonofluorescein **4** shows very low cellular toxicity, comparable to calcein-AM,⁴¹ a reagent widely used as a viability marker, when assayed using an MTT reduction assay (**Figure S11**).⁴²

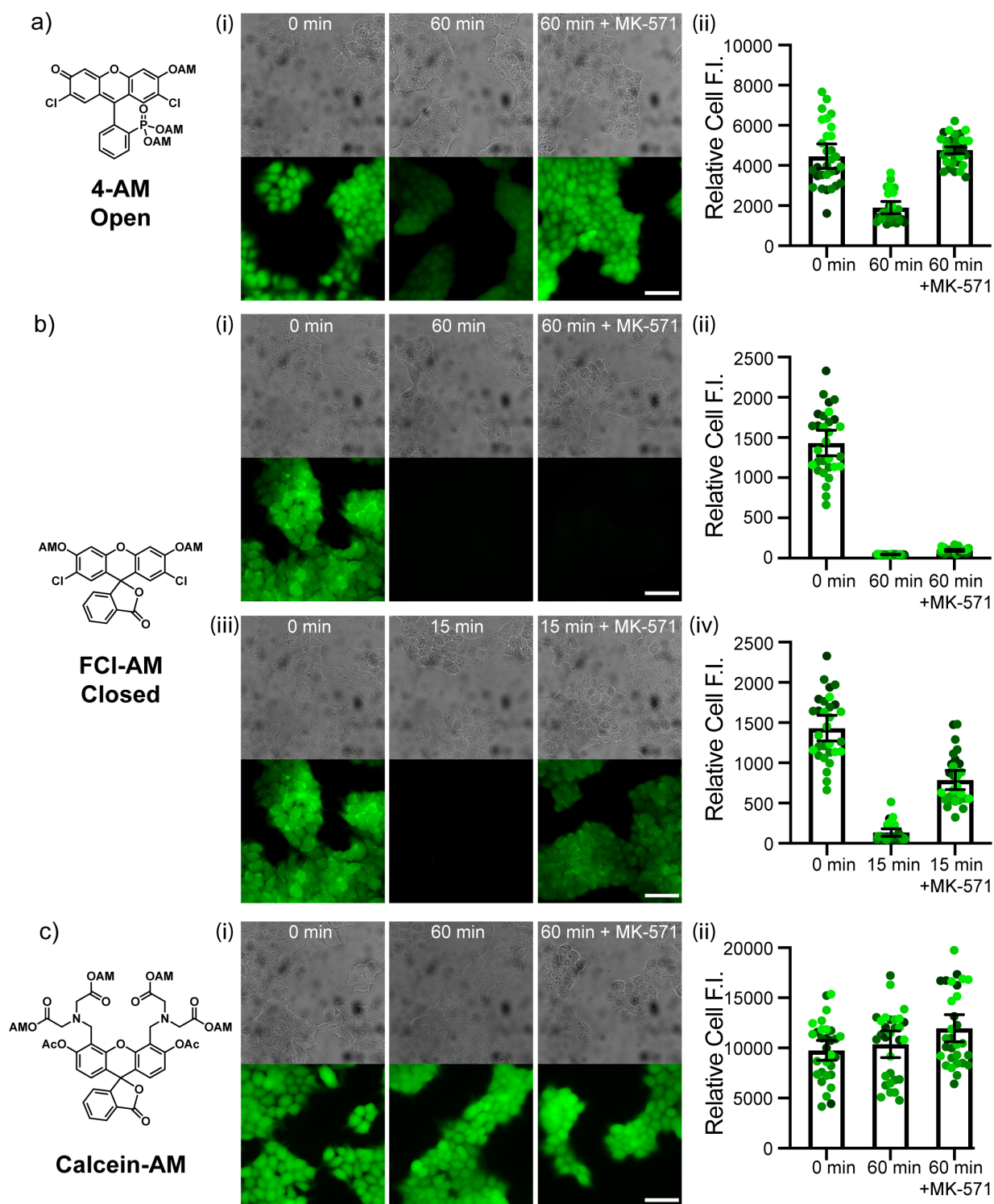


Figure 4. Efflux of fluoresceins. DIC and fluorescence images (i, iii) and associated quantification (ii, iv) of HEK cells loaded with 500 nM **4-AM open** (a), **FCI-AM closed** (b) and **calcein-AM** (c). Cells were incubated with dye for 20 mins and imaged in HBSS (0 min) or dye loading solutions were replaced with DMEM either with or without 50 μ M MK-571 and incubated for a further 60 (i and ii) or 15 (iii and iv) mins prior to imaging. Scale bar is 50 μ m. Images are normalized to the relevant 0 min image. For quantification error bars represent \pm SEM for $n = 30$ images across 6 coverslips (coverslips represented by different shades of green).

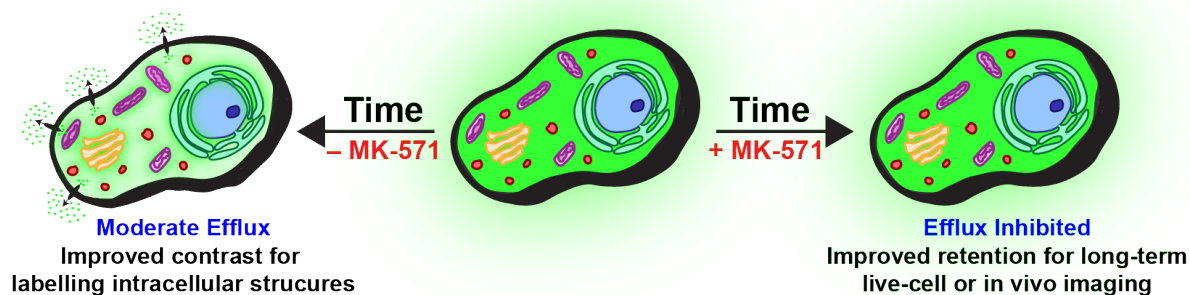


Figure 5. Examples of circumstances when moderate efflux of phosphonofluoresceins could be beneficial or when inhibition with MK-571 would be preferable.

Conclusions and outlook

In summary, we report the first synthesis of 3-phosphonofluoresceins, characterize the spectroscopic properties of this new class of fluorophore, and demonstrate the applicability of 3-phosphonofluorescein to live-cell imaging experiments. The new synthetic route to 3-phosphonofluorescein provides access to unhalogenated and 2',7'-dihalogen-3-phosphonofluoresceins. While the attractive photophysical properties of fluoresceins, such as absorption/emission wavelengths and brightness remain relatively unperturbed 2',7'-dichloro-3-phosphonofluorescein is almost twice as water soluble than its 3-carboxy analog. In addition, 3-phosphonofluoresceins, unlike 3-carboxyfluoresceins, do not spirocyclize, rendering them cell-impermeant. Esterification of the phosphonic acid with biologically labile acetoxy methyl esters allows delivery of 3-phosphonofluoresceins to living cells, where they show an almost 70-fold increase in cellular brightness over carboxy fluorescein resulting from improved accumulation and retention. We imagine that 3-phosphonofluoresceins will be of utility for long-term or *in vivo* imaging applications that rely on a high degree of cellular retention. Ultimately incorporation of a phosphonate at the 3-position provides a new class of fluoresceins with unique characteristics without any compromise in optical properties and we envision this will yield additional opportunities in the context of other xanthene fluorophores such as rhodamines.

References

- (1) Urano, Y.; Kamiya, M.; Kanda, K.; Ueno, T.; Hirose, K.; Nagano, T. Evolution of Fluorescein as a Platform for Finely Tunable Fluorescence Probes. *J. Am. Chem. Soc.* **2005**, *127* (13), 4888-4894.
- (2) Remsen, I. On a New Class of Compounds Analogous to the Phthaleins. *Am. Chem. J.* **1884**, *6*, 180–181.
- (3) Sevrain, C. M.; Berchel, M.; Couthon, H.; Jaffrès, P.-A. Phosphonic Acid: Preparation and Applications. *Beilstein J. Org. Chem.* **2017**, *13*, 2186–2213.
- (4) Iaroshenko, V. Organophosphorus Chemistry: From Molecules to Applications. *Organophosphorus Chem.* Wiley. **2019**.
- (5) De Clercq, E. Acyclic Nucleoside Phosphonates: Past, Present and Future. Bridging Chemistry to HIV, HBV, HCV, HPV, Adeno-, Herpes-, and Poxvirus Infections: The Phosphonate Bridge. *Biochem. Pharmacol.* **2007**, *73* (7), 911–922.
- (6) De Clercq, E. Clinical Potential of the Acyclic Nucleoside Phosphonates Cidofovir, Adefovir, and Tenofovir in Treatment of DNA Virus and Retrovirus Infections. *Clin. Microbiol. Rev.* **2003**, *16* (4), 569–596.
- (7) Franz, R. G. Comparisons of PKa and Log P Values of Some Carboxylic and Phosphonic Acids: synthesis and measurement. *AAPS PharmSci.* **2001**, *3* (2), 10.

- (8) Helal, A.; Kim, H. S.; Yamani, Z. H.; Nasiruzzaman Shaikh, M. Fluorescein-N-Methylimidazole Conjugate as Cu²⁺ Sensor in Mixed Aqueous Media Through Electron Transfer. *J. Fluoresc.* **2016**, *26* (1), 1–9.
- (9) Yan, F.; Fan, K.; Bai, Z.; Zhang, R.; Zu, F.; Xu, J.; Li, X. Fluorescein Applications as Fluorescent Probes for the Detection of Analytes. *TrAC - Trends Anal. Chem.* **2017**, *97*, 15–35.
- (10) Wiemer, A. J.; Wiemer, D. F. Prodrugs of Phosphonates and Phosphates: Crossing the Membrane Barrier. *Top. Curr. Chem.* **2015**, *360*, 115–160.
- (11) Martin, M. M.; Lindqvist, L. The PH Dependence of Fluorescein Fluorescence. *J. Lumin.* **1975**, *10* (6), 381–390.
- (12) Leonhardt, H.; Gordon, L.; Livingston, R. Acid-Base Equilibria of Fluorescein and 2', 7'-Dichlorofluorescein in Their Ground and Fluorescent States. *J. Phys. Chem.* **1971**, *75* (2), 245-249.
- (13) Kulkarni, R. U.; Yin, H.; Pourmandi, N.; James, F.; Adil, M. M.; Schaffer, D. V.; Wang, Y.; Miller, E. W. A Rationally Designed, General Strategy for Membrane Orientation of Photoinduced Electron Transfer-Based Voltage-Sensitive Dyes. *ACS Chem. Biol.* **2017**, *12* (2), 407-413.
- (14) Kovi, R.; Nampalli, S.; Tharial, P. X. Process for Preparation Isosulfan Blue, US20080281127A1, 2008.
- (15) Michaelis, A.; Kaehne, R. Ueber Das Verhalten Der Jodalkyle Gegen Die Sogen. Phosphorigsäureester Oder O-Phosphine. *Ber. Dtsch. Chem. Ges.* **1898**, *31* (1), 1048–1055.
- (16) Debrouwer, W.; Wauters, I.; Stevens, C. V. Methods for the Introduction of the Phosphonate Moiety into Complex Organic Molecules. *Organophosphorus Chem.* **2019**, 249–294.
- (17) Wadsworth, W. S. Synthetic Applications of Phosphoryl-Stabilized Anions. *Org. React.* **1977**, 73–253.
- (18) Tavs, P. Reaktion von Arylhalogeniden Mit Trialkylphosphiten Und Benzolphosphonigsäure-Dialkylestern Zu Aromatischen Phosphonsäureestern Und Phosphinsäureestern Unter Nickelsalzkatalyse. *Chem. Ber.* **1970**, *103* (8), 2428–2436.
- (19) Balthazor, T. M.; Grabiak, R. C. Nickel-Catalyzed Arbuzov Reaction: Mechanistic Observations. *J. Org. Chem.* **1980**, *45* (26), 5425–5426.
- (20) Bacci, J. P.; Kearney, A. M.; Van Vranken, D. L. Efficient Two-Step Synthesis of 9-Aryl-6-Hydroxy-3H-Xanthen-3-One Fluorophores. *Bioorg. Med. Chem. Lett.* **1989**, *264* (2), 9051–9053.
- (21) Leonhardt, H.; Gordon, L.; Livingston, R. Acid-Base Equilibria of Fluorescein and 2', 7'-Dichlorofluorescein in Their Ground and Fluorescent States. *J. Phys. Chem.* **1971**, *75* (2), 245-249..
- (22) Martin, M. M.; Lindqvist, L. The PH Dependence of Fluorescein Fluorescence. *J. Lumin.* **1975**, *10* (6), 381–390.
- (23) Sjöback, R.; Nygren, J.; Kubista, M. Absorption and Fluorescence Properties of Fluorescein. *Spectrochim. Acta Part A.* **1995**, *51* (6), L7–L21.
- (24) Sun, W.-C.; Gee, K. R.; Klaubert, D. H.; Haugland, R. P. Synthesis of Fluorinated Fluoresceins. *J. Org. Chem.* **1997**, *62* (19), 6469-6475.
- (25) Tsien, R. Y. A Non-Disruptive Technique for Loading Calcium Buffers and Indicators into Cells. *Nature.* **1981**, *290* (5806), 527-528.
- (26) Lavis, L. D.; Chao, T. Y.; Raines, R. T. Synthesis and Utility of Fluorogenic Acetoxymethyl Ethers. *Chem. Sci.* **2011**, *2* (3), 521–530.
- (27) Johnson, I. D. *Molecular Probes Handbook: A Guide to Fluorescent Probes and Labeling Technologies*; Life Technologies Corporation, 2010, p 835-836.
- (28) Prosperi, E.; Croce, A. C.; Bottiroli, G.; Supino, R. Flow Cytometric Analysis of Membrane Permeability Properties Influencing Intracellular Accumulation and Efflux of Fluorescein. *Cytometry* **1986**, *7* (1), 70–75.
- (29) Rotman, B.; Papermaster, B. W. Membrane Properties of Living Mammalian Cells as Studied by Enzymatic Hydrolysis of Fluorogenic Esters. *Proc. Natl. Acad. Sci. U.S.A.* **1966**, *55* (1) 134-141.
- (30) Izumi, S.; Urano, Y.; Hanaoka, K.; Terai, T.; Nagano, T. A Simple and Effective Strategy to Increase the Sensitivity of Fluorescence Probes in Living Cells. *J. Am. Chem. Soc.* **2009**, *131* (29), 10189–10200.

- (31) Rusha, L.; Miller, S. C. Design and Application of Esterase-Labile Sulfonate Protecting Groups. *Chem. Commun.* **2011**, 47 (7), 2038–2040.
- (32) Schultz, C.; Vajanaphanich, M.; Harootunian, A. T.; Sammak, P. J.; Barrett, K. E.; Tsien, R. Y. Acetoxymethyl Esters of Phosphates, Enhancement of the Permeability and Potency of CAMP. *J. Biol. Chem.* **1993**, 268 (9), 6316–22.
- (33) Li, W.; Schultz, C.; Llopis, J.; Tsien, R. Y. Membrane-Permeant Esters of Inositol Polyphosphates, Chemical Syntheses and Biological Applications. *Tetrahedron* **1997**, 53 (35), 12017–12040.
- (34) Wiemer, A. J.; Wiemer, D. F. Prodrugs of Phosphonates and Phosphates: Crossing the Membrane Barrier. *Topics in Current Chemistry* **2015**, 360, 115–160.
- (35) Pradere, U.; Garnier-Amblard, E. C.; Coats, S. J.; Amblard, F.; Schinazi, R. F. Synthesis of Nucleoside Phosphate and Phosphonate Prodrugs. *Chem. Rev.* **2014**, 114 (18), 9154–9218.
- (36) Schultz, C. Prodrugs of Biologically Active Phosphate Esters. *Bioorganic Med. Chem.* **2003**, 11 (6), 885–898.
- (37) Diehl, H.; Ellingboe, J. L. Indicator for Titration of Calcium in Presence of Magnesium Using Disodium Dihydrogen Ethylenediamine Tetraacetate. *Anal. Chem.* **1956**, 28 (5), 882–884.
- (38) Sun, H.; Johnson, D. R.; Finch, R. A.; Sartorelli, A. C.; Miller, D. W.; Elmquist, W. F. Transport of Fluorescein in MDCKII-MRP1 Transfected Cells and Mrpl-Knockout Mice. *Biochem. Biophys. Res. Commun.* **2001**, 284 (4), 863–869.
- (39) Shugarts, S.; Benet, L. Z. The Role of Transporters in the Pharmacokinetics of Orally Administered Drugs. *Pharm. Res.* **2009**, 26 (9), 2039–2054.
- (40) Gekeler, V.; Ise, W.; Sanders, K. H.; Ulrich, W. R.; Beck, J. The Leukotriene LTD4 Receptor Antagonist MK571 Specifically Modulates MRP Associated Multidrug Resistance. *Biochem. Biophys. Res. Commun.* **1995**, 208 (1), 345–352.
- (41) Papadopoulos, N. G.; Dedoussis, G. V. Z.; Spanakos, G.; Gritzapis, A. D.; Baxevanis, C. N.; Papamichail, M. An Improved Fluorescence Assay for the Determination of Lymphocyte-Mediated Cytotoxicity Using Flow Cytometry. *J. Immunol. Methods* **1994**, 177 (1–2), 101–111..
- (42) Kumar, P.; Nagarajan, A.; Uchil, P. D. Analysis of Cell Viability by the MTT Assay. *Cold Spring Harbor Protocols* **2018**, 2018 (6).

Chapter 1 Supplementary Information

General procedures

Chemical reagents and anhydrous solvents were purchased from commercial suppliers and used without further purification, besides resorcinol and 4-chlororesorcinol which were recrystallized from toluene prior to use. 2',7'-dichlorofluorescein was synthesized based on literature procedures.¹ Thin layer chromatography (TLC) (silica gel, F254, 250 μm) and preparative thin layer chromatography (PTLC) (Silicycle, F254, 1000 μm) were performed on precoated TLC glass plates and were visualized by fluorescence quenching under UV light. Flash column chromatography was performed on Silicycle Silica Flash F60 (230–400 Mesh) for normal phase or 60 RP-18 (200–400 mesh) for reverse phase, using a forced flow of air at 0.5–1.0 bar. NMR spectra were recorded on Bruker AV-300 MHz, Bruker AVB-400 MHz, Bruker AVQ-400 MHz, Bruker NEO-500 MHz and Bruker AV-600 NMR spectrometers. NMR spectra measured on Bruker AVII-900 MHz, 225 MHz, equipped with a TCI cryoprobe accessory, were performed by Dr. Jeffrey Pelton (QB3). Chemical shifts (δ) are expressed in parts per million (ppm) and are referenced to CDCl_3 (7.26 ppm), DMSO (2.50 ppm), MeOD (3.31 ppm) or D_2O (4.79 ppm). Coupling constants are reported as Hertz (Hz). Splitting patterns are indicated as follows: s, singlet; d, doublet; t, triplet; q, quartet; dd, doublet of doublet; td, triplet of doublets; dt, doublet of triplets; tt, triplet of triplets; ddd, doublet of doublet of doublets; tdd, triplet of doublet of doublets; q, quartet; m, multiplet. High resolution mass spectra (ESI EI) were measured by the QB3/Chemistry mass spectrometry service at University of California, Berkeley. High performance liquid chromatography (HPLC) and low resolution ESI Mass Spectrometry were performed on an Agilent Infinity 1200 analytical instrument coupled to an Advion CMS-L ESI mass spectrometer. The column used was Phenomenex Luna 5 μm C18(2) (4.6 mm I.D. \times 150 mm) with a flow rate of 1.0 mL/min. The mobile phase was MQ-H₂O with 0.05% trifluoroacetic acid (eluent A) and HPLC grade MeCN with 0.05% trifluoroacetic acid (eluent B). Signals were monitored at 210, 254, 350, 460 and 520 nm over 10 min, with a gradient of 10 to 100% eluent B for 8 min, then held at 100% B for 2 min.

Spectroscopic studies

UV-Vis absorbance and fluorescence spectra were recorded using a 2501 Spectrophotometer (Shimadzu) and a Quantamaster Master 4 L-format scanning spectrofluorometer (Photon Technologies International). The fluorometer is equipped with an LPS-220B 75-W xenon lamp and power supply, A-1010B lamp housing with integrated igniter, switchable 814 photon-counting/analog photomultiplier detection unit, and MD5020 motor driver. Samples were measured in 1-cm path length quartz cuvettes (Starna Cells).

The maximum absorption wavelength (λ_{max}), maximum emission wavelength (λ_{em}) and extinction coefficients (ϵ) were taken in 0.1M $\text{NaOH}_{(\text{aq})}$ using 1000x dilutions from stock solutions of dyes in DMSO (2 mM). Photostabilities of dichlorofluoresceins were investigated by continuous illumination of 250 nM solutions (in 0.1 M NaOH) at λ_{max} and monitoring fluorescence intensity every second for 10 minutes. pH titrations were conducted in buffers containing 150 mM NaCl and 10 mM buffer. The following buffer systems were used: phosphate (pH 2.4 – 3.1 and 5.5 – 7.5), acetate (pH 3.8 – 5.3), tris (pH 8.2 – 9.2) and carbonate (pH 9.8). pK_a's were determined by recording absorbance values at wavelengths of interest ($n = 3$) and fitting to sigmoidal dose response curves using GraphPad Prism software. Dielectric titrations were conducted in mixtures

of dioxane and water (0 – 100% in 10% increments) containing 0.01% triethylamine. For spectroscopic comparison of fluorophore purity, stock solutions of fluorophore (from various purification methods) were prepared in DMSO at a theoretical concentration of 2 mM using the molecular weight of the fluorophore. Spectra of each stock solution (1000x dilution in 0.1 M NaOH) were normalized to a HPLC purified standard to determine relative purity by mass.

In vitro AM ester hydrolysis reactions and characterization.

For chemical hydrolysis, 2 μ l AM dyes (1 mM in DMSO) were diluted to 2 mL in 0.1 M NaOH or HBSS (pH 7.4) and characterized by absorbance and fluorescence spectroscopy. For the enzymatic reactions, commercially purified pig liver esterase (PLE, MW = 168 kDa) as a suspension in 3.2 M $(\text{NH}_4)_2\text{SO}_4$ was used as a stock solution of 28.1 mg/mL. 2 μ l AM dyes (1 mM in DMSO) were incubated with or without 1 μ l PLE (final concentration 0.7025 mg/mL) in HBSS (pH 7.4, final volume 40 μ l) for 2 hrs at 37°C. Solutions were either diluted to 2 mL in HBSS and characterized by absorbance and fluorescence spectroscopy or diluted with 200 μ l MeCN, filtered through a 0.22 μ m PTFE filter and characterized by HPLC.

Relative solubility of fluoresceins

Suspensions of 5 mg each of 2',7'-dichloro carboxy-, sulfono- and phosphono- fluoresceins in 1 mL DPBS (pH 7.4) were stirred vigorously for three days. Each suspension was then filtered through a 0.22 μ m PTFE filter into scintillation vials. 2 μ l of the filtrate was diluted to 2 mL in 0.1 M NaOH and the concentration of fluorescein present was determined by UV-Vis spectroscopy.

Cell culture

Human embryonic kidney 293T (HEK) cells were maintained in Dulbecco's modified eagle medium (DMEM) supplemented with 4.5 g/L D-glucose, 10% fetal bovine serum (FBS; Thermo Scientific) and 1% GlutaMax (Invitrogen) at 37 °C in a humidified incubator with 5% CO₂. Cells were passaged and plated in DMEM (as above) onto 12 mm glass coverslips pre-coated with Poly-D-Lysine (PDL; 1 mg/mL; Sigma-Aldrich) at a density of 50,000 cells per coverslip. Imaging was performed 36–48 hours after plating.

For loading experiments, HEK cells were incubated with a 500 nM solution of dye (1 mL) in HBSS at 37 °C for 20 min, prior to transfer to 3 mL fresh HBSS (no dye) for imaging. For dye wash out experiments, this imaging solution was replaced with 3 mL fresh HBSS after each subsequent round of imaging (3 washes). For dye efflux experiments, dyes were loaded as above and coverslips were either imaged immediately in fresh HBSS (0 min time point) or loading solutions were replaced with DMEM (1 mL) with or without the presence of MK-571 (50 μ M) and then incubated for a further 15 or 60 min at 37 °C before imaging in HBSS (3 mL).

For the MTT cytotoxicity assay, HEK cells were passaged and plated in DMEM (as above) into a 96-well glass bottom plate pre-coated with PDL at a density of 10,000 cells per well. The assay was performed 12 hours after plating. Cells were incubated with 500 nM solutions of dye (100 μ l) or a DMSO (0.1%) vehicle control at 37 °C for 20 min. Loading solutions were replaced with fresh DMEM (100 μ l) containing MTT (1.1 mM) and cells were incubated for 4 hours – a negative control containing no HEK cells was included. MTT formazan crystals were solubilized by

addition of 10% SDS-HCl (100 μ l) and a further 2 hour incubation. Absorbance at 570 nm was recorded for each well using a plate reader.

Epifluorescence microscopy

Imaging was performed on an AxioExaminer Z-1 (Zeiss) equipped with a Spectra-X Light engine LED light (Lumencor), controlled with Slidebook (v6, Intelligent Imaging Innovations). Images were acquired with a W-Plan-Apo 63x/1.0 objective (63x; Zeiss) and images were focused onto an OrcaFlash4.0 sCMOS camera (sCMOS; Hamamatsu). The excitation light was delivered from an LED at 475/34 nm and emission was collected with a quadruple emission filter (430/32, 508/14, 586/30, 708/98 nm) after passing through a quadruple dichroic mirror (432/38, 509/22, 586/40, 654 nm LP).

Image analysis

Image analyses were performed in ImageJ (FIJI, NIH). For image intensity measurements, regions of interested were created by thresholding images to create binary masks (cells and background). Background subtracted mean fluorescence intensities were calculated and averaged across five images (each containing at least 15 cells) per coverslip and 4 coverslips were examined for each condition.

Supporting figures

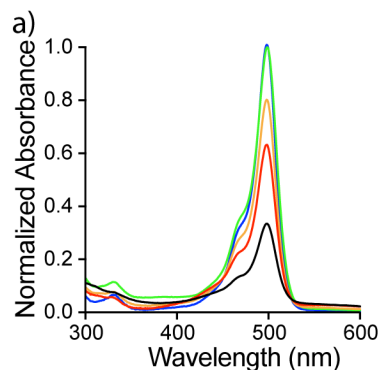


Figure S1. Comparison of the purity of **4** across synthetic and purification techniques.

Normalized absorption spectra of the crude isolate of **4** when the reaction was performed open to air (**black**), under a nitrogen atmosphere (**red**), after three purifications by flash silica chromatography (**orange**) and by precipitation with cold MeOH/*i*PrOH (**blue**). Spectra are normalized to a standard solution of **4** that was purified by HPLC (**green**). All spectra were taken in 0.1M NaOH_(aq) at a theoretical final dye concentration of 2 μ M.

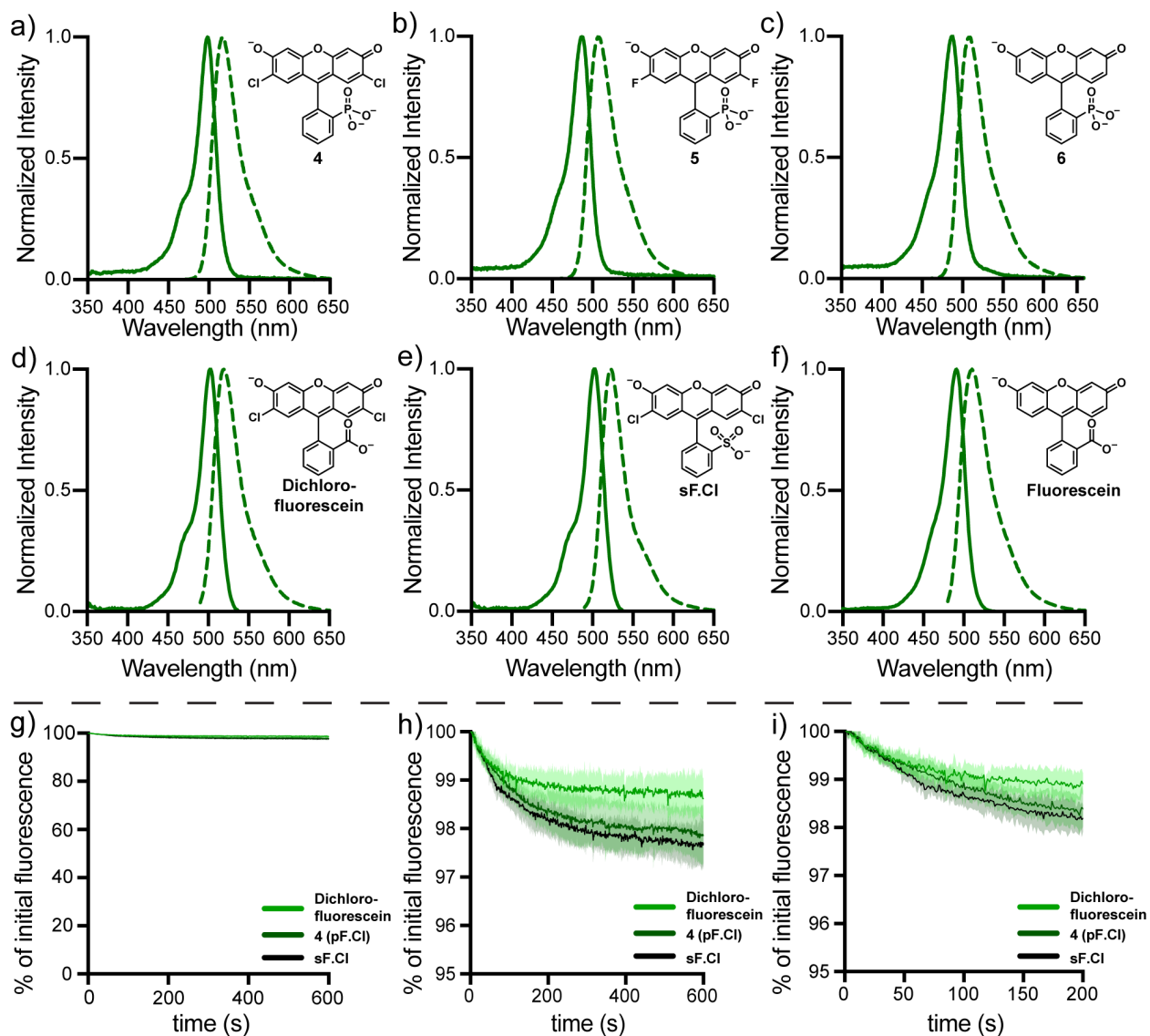


Figure S2. *In vitro* spectroscopy of fluoresceins.

Normalized absorption (solid) and fluorescence (dashed) spectra of **4** (a), **5** (b), **6** (c), 2',7'-dichlorofluorescein (d), 2',7'-dichloro-3-sulfonfluorescein (e) and fluorescein (f). Spectra were recorded in 0.1 M NaOH. For fluorescence spectra, excitation was at 500 nm (a, d, and e) or 490 nm (b, c and f). Photostability of 2',7'-dichlorofluorescein, 2',7'-dichloro-3-sulfonfluorescein and **4** (g – i). Fluorescence was measured under continuous illumination at λ_{max} for 10 minutes. Spectra g – i represent the same data with different axes ranges. Shaded regions represent the standard deviation for $n = 3$ measurements.

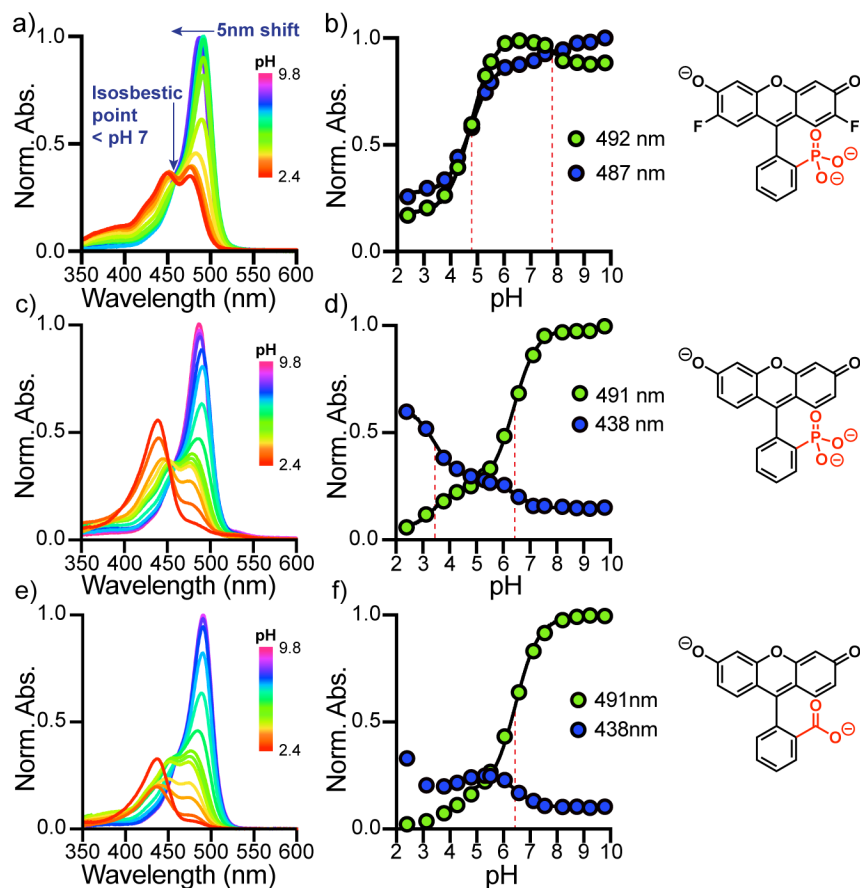


Figure S3. pH characterization of fluoresceins.

Normalized absorbance spectra and corresponding plots of normalized absorbance vs. pH at λ_{\max} for pF.F (**5**) (a, b), pF.H (**6**) (c, d) and fluorescein (e, f). Spectra were recorded in 10 mM buffered solutions containing 150 mM NaCl from pH 2.4 (red) to 9.8 (magenta), and intermediate values of 3.1, 3.8, 4.3, 4.8, 5.3, 5.5, 6.1, 6.6, 7.1, 7.5, 8.2, 8.7 and 9.2 at a dye concentration of 2 μM . Titration curves fit to sigmoidal dose response curves (solid black) enabled pK_a determination (dashed red). Error bars represent $\pm\text{SEM}$ for $n = 3$ independent determinations and if not visible are smaller than the marker

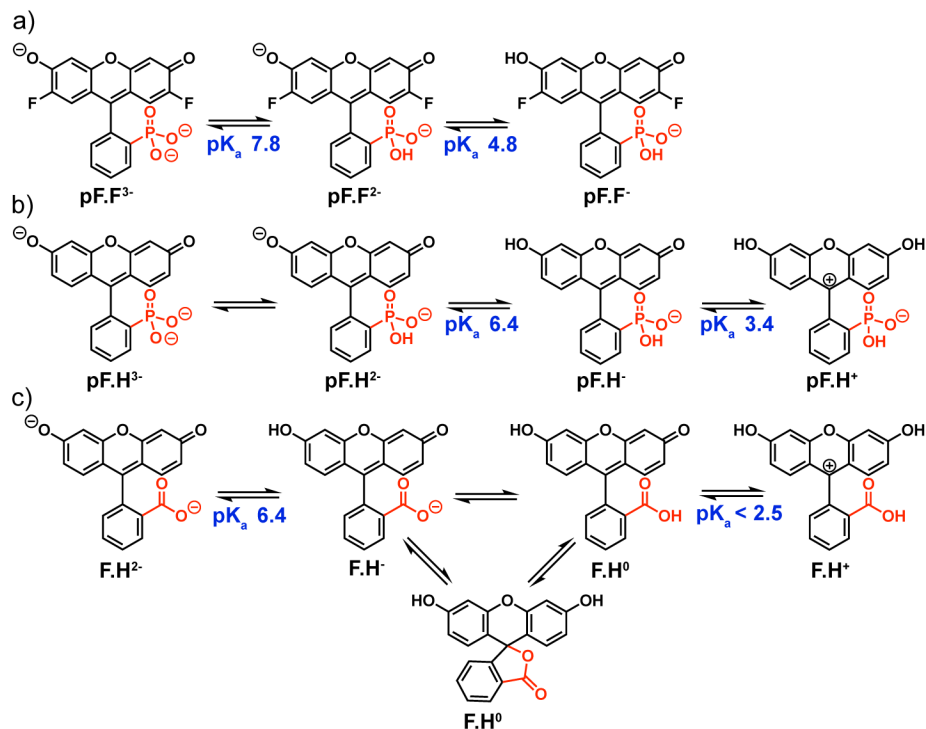


Figure S4. pH equilibria of fluorescein dyes.

Summary of pH equilibria with determined pK_a values (see **Figure S2**) for **5** (a), **6** (b) and fluorescein (c).

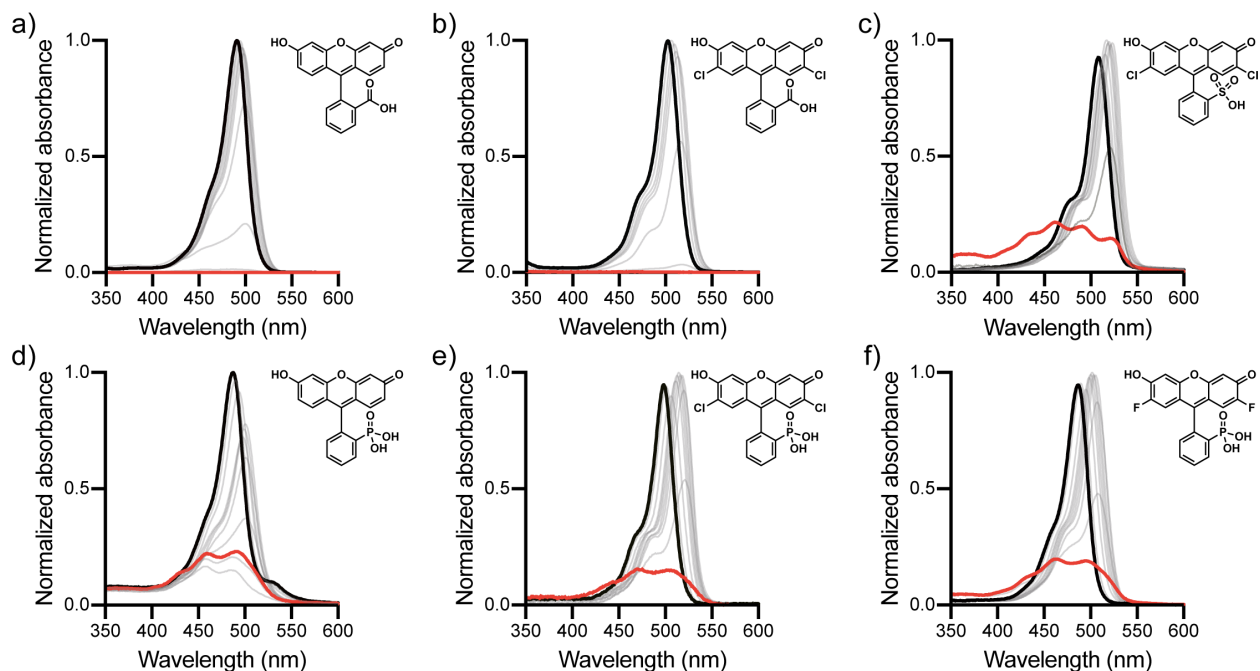


Figure S5. Dielectric titrations of fluorescein dyes.

Plots of normalized absorbance intensity vs. wavelength for a) fluorescein, b) dichlorofluorescein, c) dichlorosulfolfluorescein, d) **6** (PF.H), e) **4** (PF.Cl) and f) **5** (PF.F). 1 mM dye solutions in DMSO were diluted 1000 fold into water/dioxane mixtures from 100% water (black) to 100% dioxane (red) in 10 % increments (grey). All solutions contained 0.01% triethylamine.

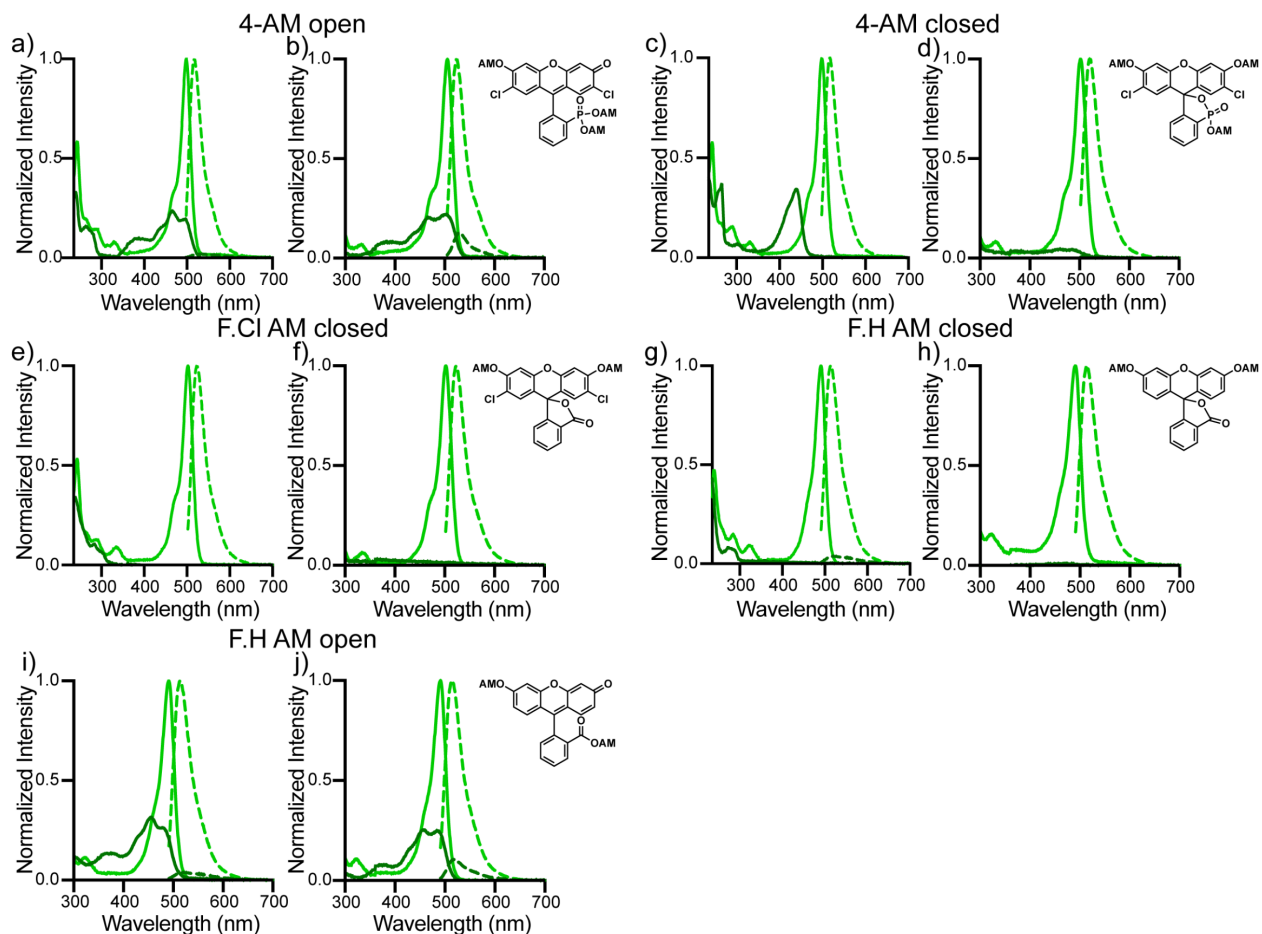


Figure S6. Spectroscopic characterization of fluorescein AMs.

Absorption (solid) and emission (dashed) spectra of 4-AM open (a,b), 4-AM closed (c,d), F.Cl AM closed (e,f), F.H AM (g,h) closed and F.H AM open (i,j). For each dye, the left graph (a, c, e, g, i) represents normalized intensity vs. wavelength for 1 μ M solutions of dye in HBSS (**dark green**) or 0.1 M NaOH (**light green**). The right graph (b, d, f, h, j) represents normalized intensity vs. wavelength for 1 μ M solutions of dye after incubation in HBSS for 2 hrs at 37°C without (**dark green**) or with (**light green**) the presence of PLE.

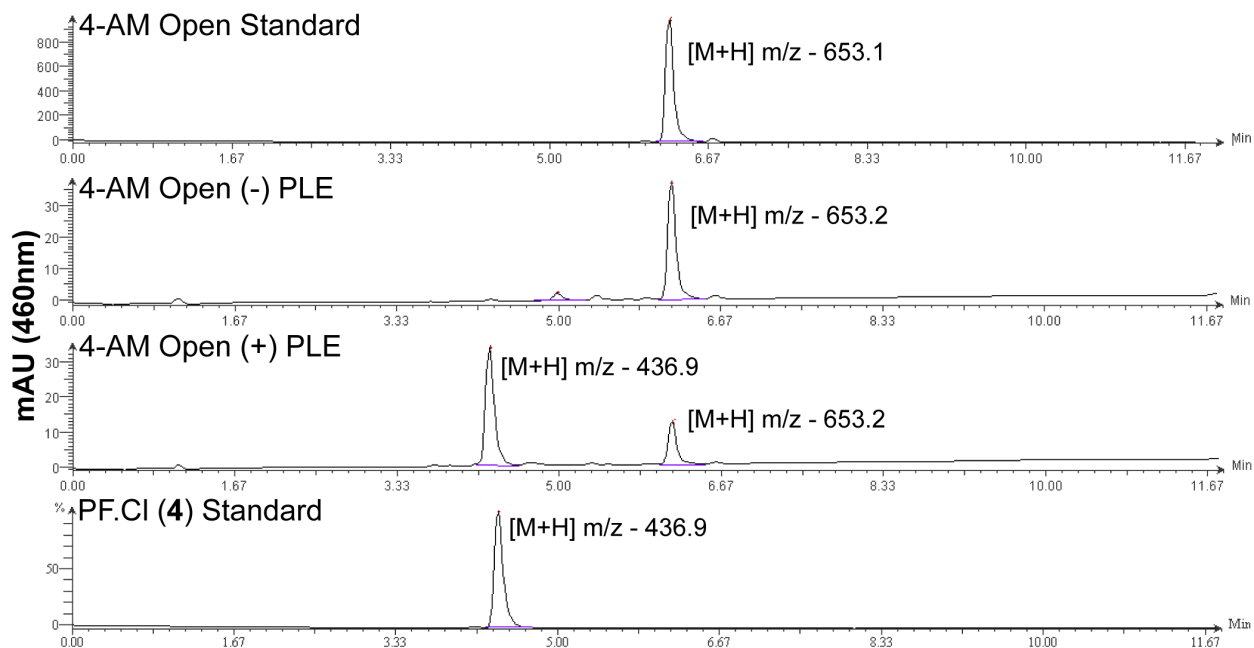


Figure S7. HPLC analysis of PLE reaction with 4-AM open.

4-AM open was incubated with or without PLE in HBSS for 2 hrs at 37 °C. HPLC traces were then compared to those of 4-AM open (not incubated in HBSS) and 4.

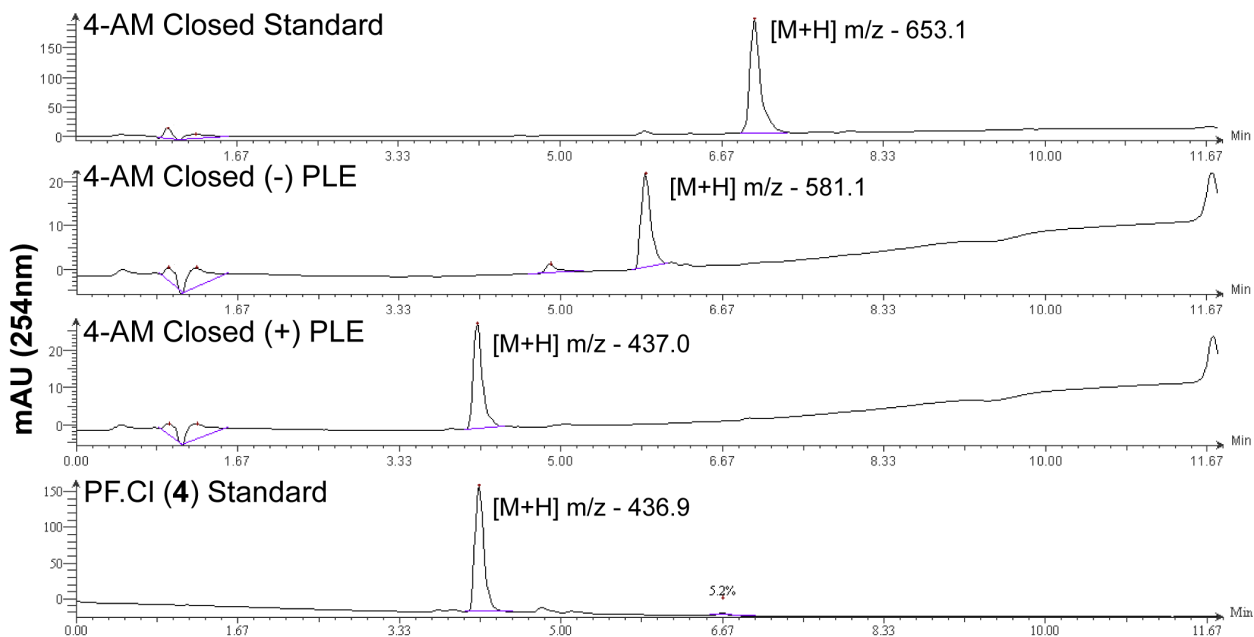


Figure S8. HPLC analysis of PLE reaction with 4-AM closed.

4-AM closed was incubated with or without PLE in HBSS for 2 hrs at 37 °C. HPLC traces were then compared to those of 4-AM closed (not incubated in HBSS) and 4. Note: incubation of 4-AM closed without PLE results in a compound with a mass corresponding to the loss of a single AM ester.

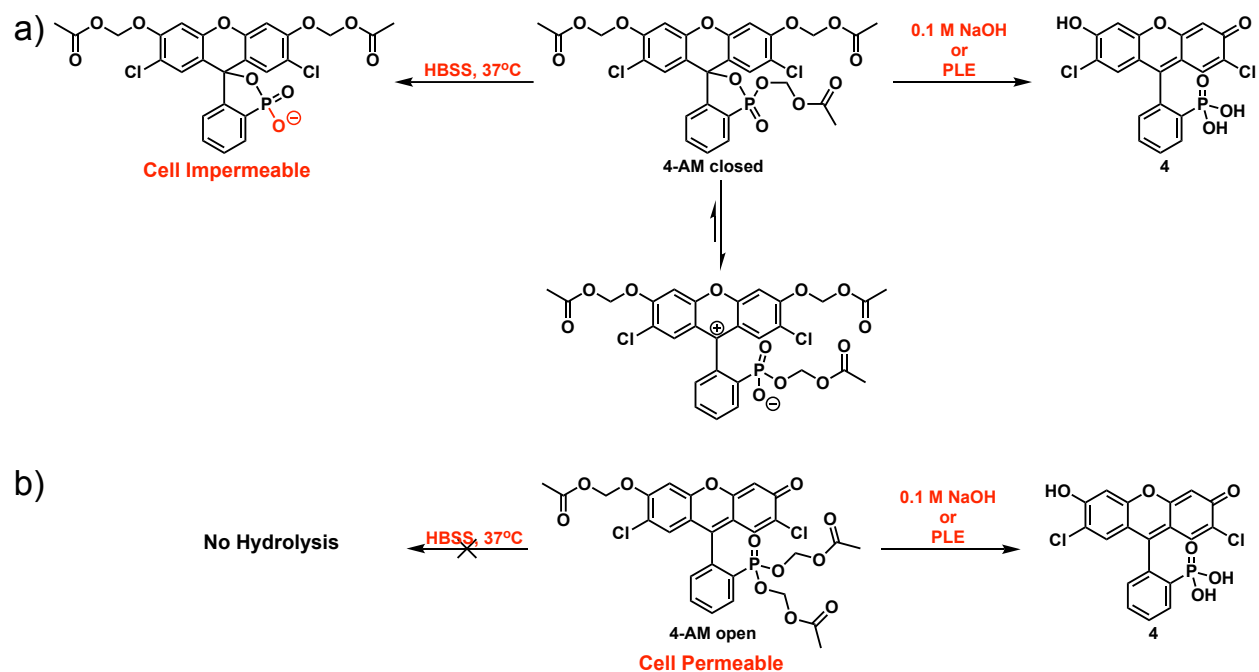


Figure S9. Summary of 4-AM closed and 4-AM open hydrolysis.

Mild hydrolysis of 4-AM closed (a) (HBSS, 37 °C) leads to loss of the phosphonoester and allows the adoption of the spirocyclized form, 4-AM open (b) is not prone to hydrolysis under such mild conditions. Global saponification of AM esters on the phosphonate and phenolic oxygens of 4-AM closed or 4-AM open (a,b) in strong base (0.1 M NaOH) or the presence of PLE results in the open form of 2',7'-dichloro-3-phosphonofluorescein.

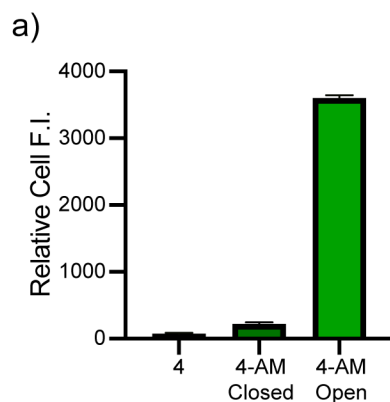


Figure S10. Relative cell brightness of phosphono-fluoresceins.

Comparison of relative cell fluorescence intensity for 4, 4-AM closed and 4-AM open. Dyes were loaded onto HEK cells at 500 nM (in HBSS) for 20 min at 37 °C before being imaged in fresh HBSS. Error bars are \pm SEM for $n = 3$ coverslips.

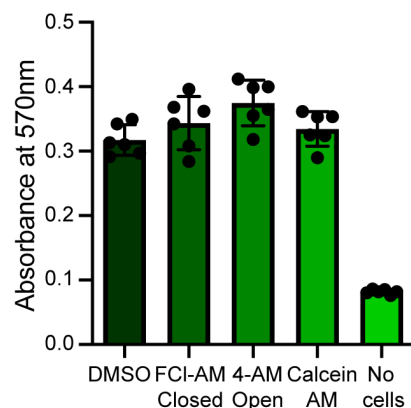
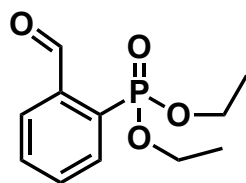


Figure S11. Cytotoxicity of fluoresceins.

MTT assay to determine cytotoxicity of fluoresceins to HEK cells. Cells were incubated with a DMSO vehicle (0.1%) or 500 nM **FCI-AM closed**, **4-AM open** or **calcein-AM** in HBSS for 20 min. Loading solutions were replaced with DMEM containing 1.1 mM MTT and incubated for 4 hours, prior to solubilizing with 10% SDS-HCl and measuring absorbance at 570 nm. Error bars represent \pm SEM for $n = 6$ replicates where each data point is an average of 3 absorbance measurements.

Synthetic procedures



Synthesis of **2**:

diethyl (2-formylphenyl)phosphonate

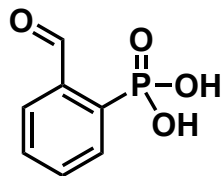
An oven dried Schlenk flask, equipped with a reflux condenser, was charged with NiCl_2 (35 mg, 0.27 mmol, 0.05 eq) and evacuated and backfilled with nitrogen (3x). 2-bromobenzaldehyde (**1**) (0.63 mL, 5.41 mmol, 1 eq) was added and the system was purged with nitrogen for 10 mins. Upon heating to 175°C , triethyl phosphite (1.2 mL, 7 mmol, 1.3 eq) was added and the solution stirred for 1hr under a weak nitrogen flow. Upon cooling to room temperature, the crude orange oil was purified by flash column chromatography (50% EtOAc/Hexanes) to afford **2** (786 mg, 3.25 mmol, 60%) as a colorless oil.

^1H NMR (400 MHz, Chloroform-*d*) δ 10.65 (s, 1H), 8.07 (m, 2H), 7.68 (m, 2H), 4.25 – 4.08 (m, 4H), 1.33 (t, $J = 7.1$ Hz, 6H).

^{31}P NMR (162 MHz, Chloroform-*d*) δ 16.34.

^{13}C NMR (101 MHz, Chloroform-*d*) δ 191.96 (d, $J = 3.8$ Hz), 138.07 (d, $J = 9.8$ Hz), 134.13 (d, $J = 8.9$ Hz), 133.09 (d, $J = 14.1$ Hz), 132.75 (d, $J = 2.9$ Hz), 130.59 (d, $J = 182.4$ Hz), 128.07 (d, $J = 12.6$ Hz), 62.77 (d, $J = 5.7$ Hz), 16.36 (d, $J = 6.3$ Hz).

HR-ESI-MS m/z for $C_{11}H_{15}O_4NaP^+$ $[M+Na]^+$ calcd: 265.0600 found: 265.0602.



Synthesis of **3**:

(2-formylphenyl) phosphonic acid

2 (300 mg, 1.24 mmol) was refluxed in conc. HCl (1.1 mL) for 12 hours. The solution was concentrated to dryness by azeotroping with MeCN. The resulting residue was dissolved in a small volume of MeOH, diluted with DCM, poured into hexanes and filtered to afford **3** (200 mg, 1.08 mmol, 87%) as a beige solid.

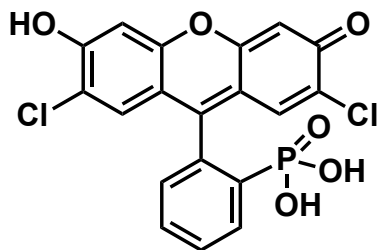
1H NMR (500 MHz, DMSO- d_6) δ 10.73 (s, 1H), 7.96 – 7.87 (m, 2H), 7.75 (tdd, J = 7.4, 2.9, 1.5 Hz, 1H), 7.69 (t, J = 7.6 Hz, 1H).

^{31}P NMR (202 MHz, DMSO- d_6) δ 9.29 (d, J = 12.9 Hz).

^{13}C NMR (126 MHz, DMSO- d_6) δ 192.96 (d, J = 3.8 Hz), 137.59 (d, J = 1.1 Hz), 136.86 (d, J = 164.8 Hz), 133.85 (d, J = 12.9 Hz), 132.93 (d, J = 8.1 Hz), 131.95 (d, J = 2.6 Hz), 127.26 (d, J = 11.7 Hz).

HR-ESI-MS m/z for $C_7H_6O_4P^-$ $[M-H]^-$ calcd: 185.0009 found: 185.0011.

*alternative work up: After cooling to room temperature, the solution was diluted with water (30 mL), washed with DCM (30 mL) and subsequently extracted into 1:3 i PrOH:DCM (30 mL) (3x), dried over Na_2SO_4 and concentrated under vacuum. The residue was suspended in a small amount of DCM, diluted with hexanes and a tan solid was filtered by vacuum filtration.



Synthesis of **4**:

2',7'-dichlorophosphonofluorescein

3 (250 mg, 1.34 mmol) and 4-chlororesorcinol (387 mg, 2.68 mmol) were charged into a round bottom that was subsequently evacuated and backfilled with nitrogen (3x). Methanesulfonic acid

(3 mL) was added and the solution stirred at 90°C for 16 hours. Upon cooling to room temperature, 15 mL water was added and the suspension stirred vigorously in an ice bath for 20 minutes before filtering. The crude brown/red solid was suspended in 4 mL MeOH, placed in an ice bath and diluted slowly with 20 mL ⁱPrOH. A brick red solid was then isolated by vacuum filtration and washed with hexanes to obtain **4** (101 mg, 0.23 mmol, 17%).

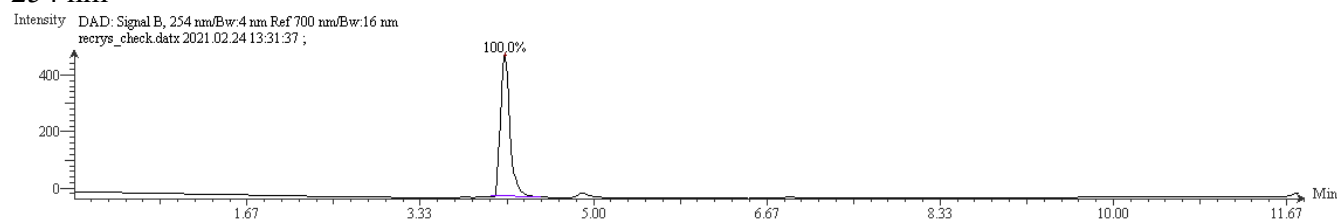
¹H NMR (500 MHz, Deuterium Oxide + < 1% NaOD) δ 7.90 (dd, *J* = 11.7, 7.8 Hz, 1H), 7.49 (t, *J* = 7.2 Hz, 1H), 7.35 (t, *J* = 7.6 Hz, 1H), 7.17 (s, 2H), 6.69 (dd, *J* = 7.5, 3.6 Hz, 1H), 6.53 (s, 2H).

³¹P NMR (202 MHz, Deuterium Oxide + < 1% NaOD) δ 7.34.

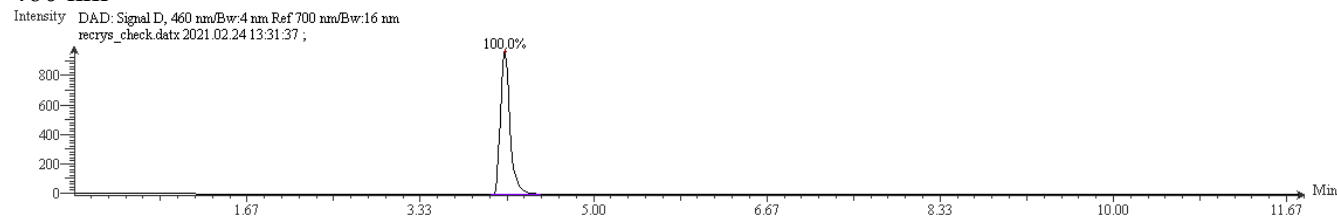
¹³C NMR (126 MHz, Deuterium Oxide + < 1% NaOD) δ 174.23, 160.96 (d, *J* = 3.3 Hz), 157.37, 140.87 (d, *J* = 161.9 Hz), 133.50 (d, *J* = 7.6 Hz), 132.64 (d, *J* = 7.6 Hz), 130.15, 128.97 (d, *J* = 10.9 Hz), 128.58 (d, *J* = 11.2 Hz), 128.05, 127.13, 113.44, 103.73.

HR-ESI-MS *m/z* for C₁₉H₁₀O₆Cl₂P⁻ [M-H]⁻ calcd: 434.9598 found: 434.9603.

254 nm

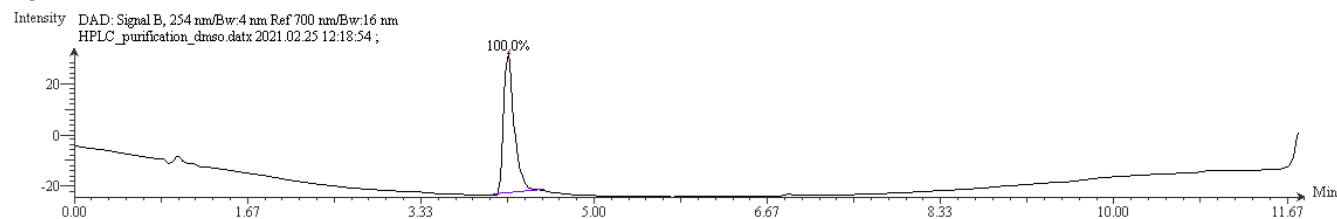


460 nm

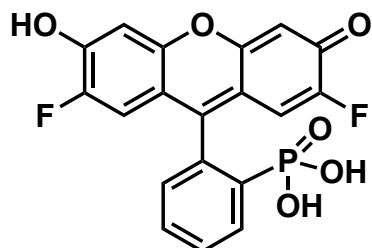
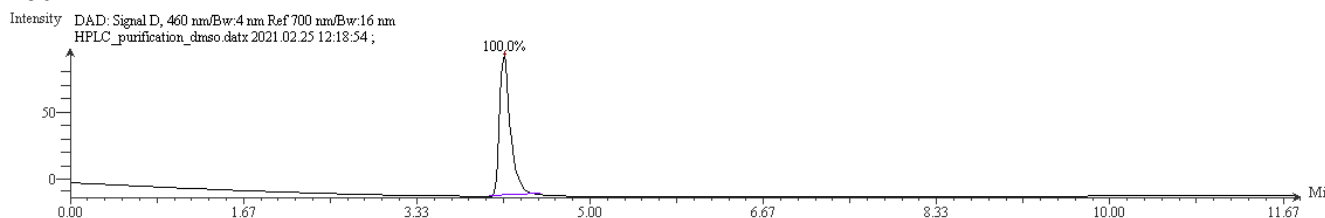


Small amounts of **4** were also obtained by purifying the crude reaction isolate via HPLC as demonstrated below:

254 nm



460 nm



Synthesis of **5**:

2',7'-difluorophosphonofluorescein

3 (300 mg, 1.61 mmol) and 4-fluororesorcinol (413 mg, 3.23 mmol) were charged into a round bottom that was subsequently evacuated and backfilled with nitrogen (3x). Methanesulfonic acid (3 mL) was added and the solution stirred at 90 °C for 16 hours. Upon cooling to room temperature, 20 mL water was added and the suspension stirred vigorously in an ice bath for 20 minutes before filtering. The crude brown/red solid was triturated with 20 mL cold ⁱPrOH and filtered to obtain **5** as a bright orange solid (38 mg, 0.09 mmol, 6%).

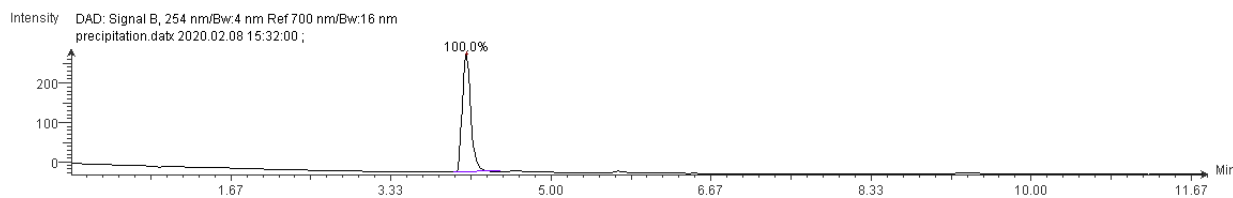
¹H NMR (500 MHz, Deuterium Oxide + <1% NaOD) δ 8.06 (dd, *J* = 11.7, 7.8 Hz, 1H), 7.64 (t, *J* = 8.3 Hz, 1H), 7.51 (t, *J* = 7.5 Hz, 1H), 6.95 (m, 3H), 6.76 (d, *J* = 7.5 Hz, 2H).

³¹P NMR (202 MHz, Deuterium Oxide + < 1% NaOD) δ 7.29 (d, *J* = 11.1 Hz). ¹⁹F NMR (470 MHz, Deuterium Oxide + <1 % NaOD) δ -134.06 (dd, *J* = 11.5, 7.8 Hz).

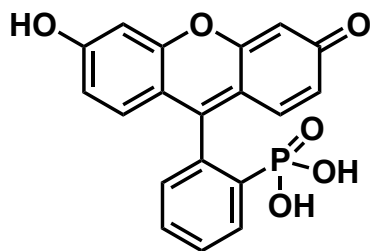
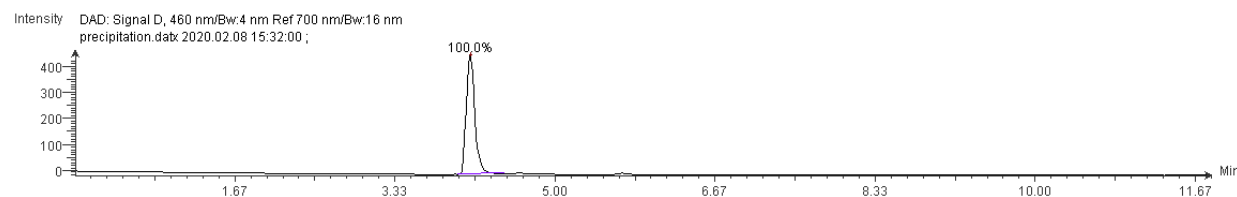
¹³C NMR (126 MHz, Deuterium Oxide + < 1% NaOD) δ 169.54 (d, *J* = 17.8 Hz), 155.97, 155.19, 153.23, 140.74 (d, *J* = 162.0 Hz), 133.94 (d, *J* = 7.7 Hz), 132.66 (d, *J* = 7.5 Hz), 128.83 (d, *J* = 10.9 Hz), 128.58 (d, *J* = 11.0 Hz), 128.03, 113.12 (d, *J* = 22.3 Hz), 112.67 (d, *J* = 9.0 Hz), 104.71 (d, *J* = 4.9 Hz).

HR-ESI-MS *m/z* for C₁₉H₁₀O₆F₂P⁻ [M-H]⁻ calcd: 403.0189 found: 403.0189.

254 nm



460 nm



Synthesis of **6**:

3-phosphonofluorescein

Phosphoric acid (85% in H₂O, 4 mL) was added to a mixture of **3** (150 mg, 0.81 mmol) and resorcinol (195 mg, 1.77 mmol, 2.2 eq) in a 10 mL round bottom and the suspension was stirred at 120°C for 2.5 days. The red solution was cooled to room temperature, poured into 15 mL ice water and stirred in an ice bath for 30 min. A brown solid was collected by filtration, triturated with methanol (50 mL) and filtered again. The filtrate was concentrated to dryness, suspended in a minimal amount of methanol (~ 7 mL) and diluted with excess cold MeCN. Vacuum filtration then yielded **6** as a pale brown solid (29 mg, 0.08 mmol, 10%).

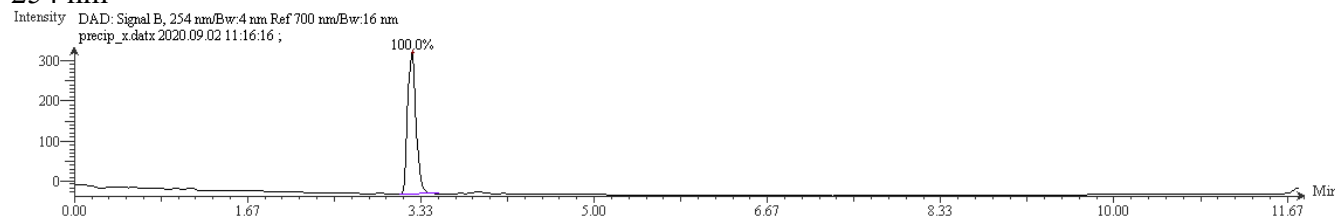
¹H NMR (500 MHz, Deuterium Oxide + <1% NaOD) δ 7.91 (dd, *J* = 11.9, 7.6 Hz, 1H), 7.49 (t, *J* = 7.8 Hz, 1H), 7.37 (t, *J* = 7.5 Hz, 1H), 7.05 (d, *J* = 9.7 Hz, 2H), 6.89 (dd, *J* = 7.1, 3.7 Hz, 1H), 6.53 – 6.48 (m, 4H).

³¹P NMR (162 MHz, Deuterium Oxide + <1% NaOD) δ 7.58.

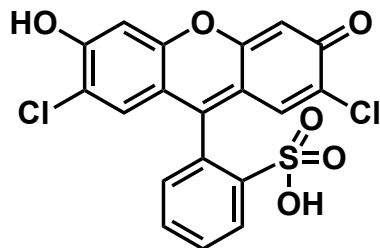
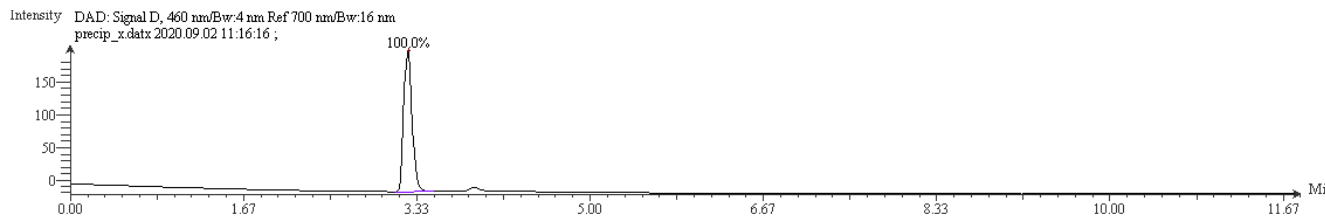
¹³C NMR (126 MHz, Deuterium Oxide + <1% NaOD) δ 180.21, 162.32 (d, *J* = 3.0 Hz), 158.92, 140.75 (d, *J* = 162.7 Hz), 134.29 (d, *J* = 7.7 Hz), 132.94, 132.58 (d, *J* = 7.7 Hz), 128.95 (d, *J* = 11.1 Hz), 128.26 (d, *J* = 11.5 Hz), 127.87 (d, *J* = 2.1 Hz), 122.30, 113.71, 103.21.

HR-ESI-MS *m/z* for C₁₉H₁₂O₆P⁻ [M-H]⁻ calcd: 367.0377 found: 367.0380.

254 nm



460 nm



Synthesis of 2',7'-dichloro-3-sulfonofluorescein.

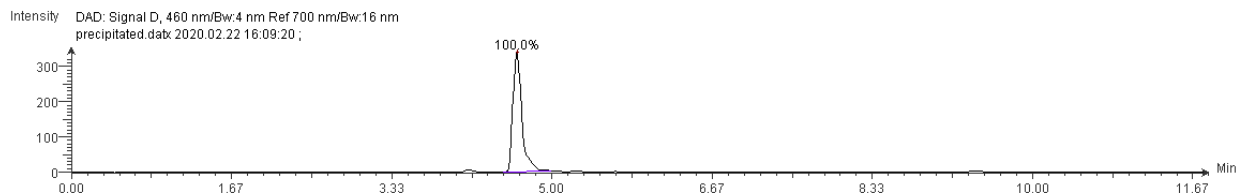
2-formylbenzenesulfonic acid (300 mg, 1.61mmol) and 4-chlororesorcinol (465 mg, 3.23 mmol) were charged into a round bottom that was subsequently evacuated and backfilled with nitrogen (3x). Methanesulfonic acid (3 mL) was added and the solution stirred at 90 °C for 16 hours. Upon cooling to room temperature, 8 mL water was added and the suspension stirred vigorously in an ice bath for 20 minutes before filtering. The crude brown/red solid was suspended in 2 mL MeOH, placed in an ice bath and diluted slowly with 25 mL ¹PrOH. A brick red solid was then isolated by vacuum filtration and washed with hexanes to obtain 2',7'-dichlorosulfonofluorescein (85 mg, 0.19 mmol, 12%).

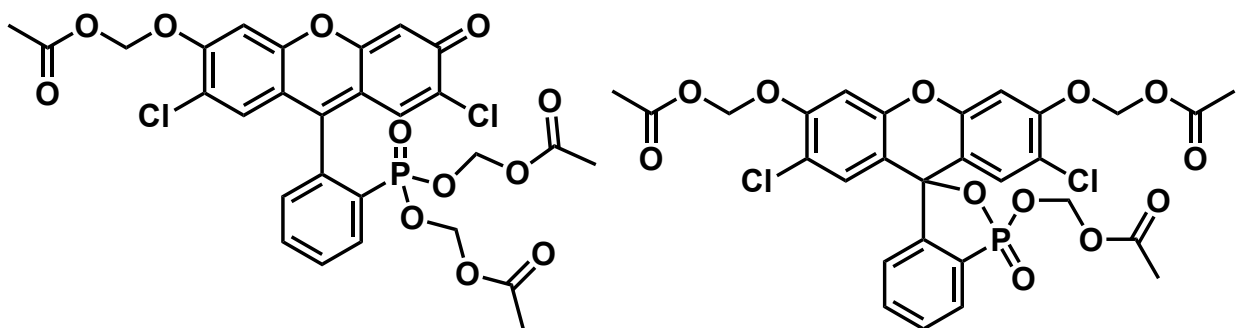
¹H NMR (500 MHz, Deuterium Oxide + <1% NaOD) δ 8.10 (dd, *J* = 8.0, 1.0 Hz, 1H), 7.75 (td, *J* = 7.7, 1.3 Hz, 1H), 7.69 (dd, *J* = 7.7, 1.3 Hz, 1H), 7.15 (m, 3H), 6.64 (s, 2H).

¹³C NMR (126 MHz, Deuterium Oxide + <1% NaOD) δ 174.71, 157.31, 155.38, 141.57, 131.25, 130.40, 130.27, 129.79, 129.30, 127.71, 127.58, 112.77, 103.86.

HR-ESI-MS *m/z* for C₁₉H₁₀O₆Cl₂S⁻ [M-H]⁻ calcd: 434.9502 found: 434.9500.

460 nm





Synthesis of **4-AM open** and **4-AM closed**:

4 (100 mg, 0.23 mmol), Ag₂O (212 mg, 0.92 mmol, 4 eq) and 4Å molecular sieves (250 mg) were charged into a round bottom that was subsequently evacuated and backfilled with nitrogen (3x). MeCN (8 mL) was added and the suspension was stirred at room temperature for 1 hour. Bromomethyl acetate (0.13 mL, 1.38 mmol, 6 eq) was then added slowly and the mixture was warmed to 50°C and stirred for 24 hours. Upon cooling to room temperature, the suspension was diluted with DCM, filtered over celite and concentrated to a yellow oil. Purification by flash column chromatography (75-100% EtOAc/Hexanes) afforded:

4-AM open as an orange powder (53 mg, 0.08 mmol, 35%).

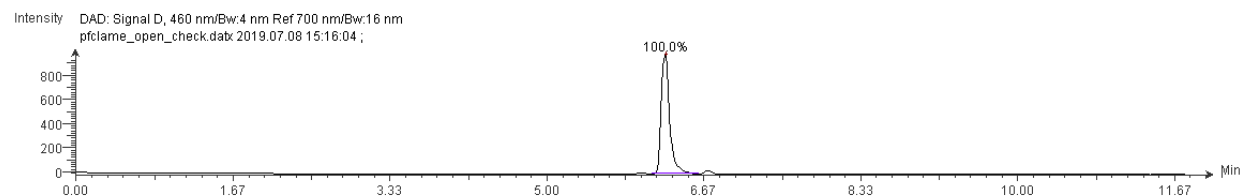
¹H NMR (500 MHz, Chloroform-*d*) δ 8.14 (ddd, *J* = 14.9, 7.7, 1.0 Hz, 1H), 7.84 (tt, *J* = 7.6, 1.4 Hz, 1H), 7.76 (tdd, *J* = 7.6, 3.7, 1.1 Hz, 1H), 7.34 (t, *J* = 6.3 Hz, 1H), 7.27 (s, 1H), 7.01 (s, 1H), 6.94 (s, 1H), 6.61 (s, 1H), 5.92 (s, 2H), 5.50 (q, *J* = 9.5, 5.2 Hz, 1H), 5.47 (q, *J* = 9.5, 5.2 Hz, 1H), 5.41 (dd, *J* = 11.9, 5.2 Hz, 1H), 5.32 (dd, *J* = 14.1, 5.2 Hz, 1H), 2.20 (s, 3H), 2.00 (s, 3H), 1.97 (s, 3H).

³¹P NMR (162 MHz, Chloroform-*d*) δ 14.33.

¹³C NMR (226 MHz, Chloroform-*d*) δ 178.06, 169.48, 169.16, 169.07, 157.77, 156.53, 152.02, 146.66, 135.77, 135.43 (d, *J* = 10.0 Hz), 134.21 (d, *J* = 8.9 Hz), 133.77, 130.51 (d, *J* = 14.0 Hz), 130.18 (d, *J* = 14.5 Hz), 129.24, 128.11, 127.77 (d, *J* = 194.6 Hz), 120.73, 119.94, 117.08, 106.21, 103.29, 85.07, 81.70 (d, *J* = 5.2 Hz), 81.28 (d, *J* = 5.6 Hz), 21.06, 20.74, 20.71.

HR-ESI-MS *m/z* for C₂₈H₂₄O₁₂Cl₂P₁⁺ [M+H]⁺ calcd: 653.0377 found: 653.0379.

460 nm



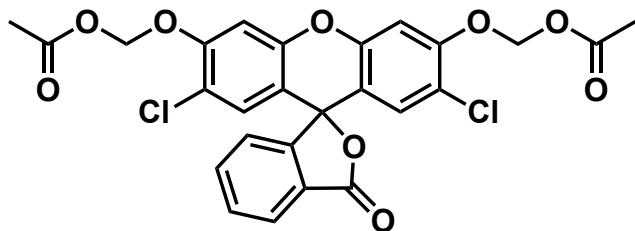
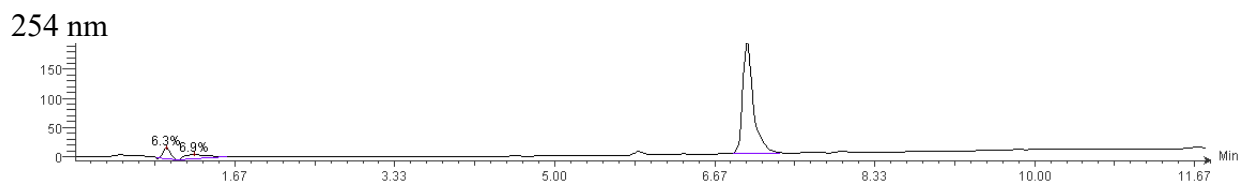
and **4-AM closed** as an off white solid. (33 mg, 0.05 mmol, 22%).

^1H NMR (400 MHz, Chloroform-*d*) δ 7.97 – 7.90 (m, 1H), 7.64 – 7.57 (m, 2H), 7.07 (s, 2H), 7.05 (s, 2H), 7.00 – 6.89 (m, 1H), 5.85 (s, 6H), 2.18 (s, 6H), 2.07 (s, 3H).

^{31}P NMR (162 MHz, Chloroform-*d*) δ 30.27.

^{13}C NMR (226 MHz, Chloroform-*d*) δ 169.73, 169.70, 169.47, 154.09, 150.82 (d, $J = 19.9$ Hz), 149.84, 134.76, 130.32, 130.26, 127.70 (d, $J = 11.4$ Hz), 125.44 (d, $J = 14.5$ Hz), 123.45 (d, $J = 175.6$ Hz), 120.06, 116.11, 104.01, 85.64, 82.59 (d, $J = 5.6$ Hz), 29.92, 21.12.

HR-ESI-MS m/z for $\text{C}_{28}\text{H}_{24}\text{O}_{12}\text{Cl}_2\text{P}_1^+$ $[\text{M}+\text{H}]^+$ calcd: 653.0377 found: 653.0379.



Synthesis of **FCI-AM closed**:

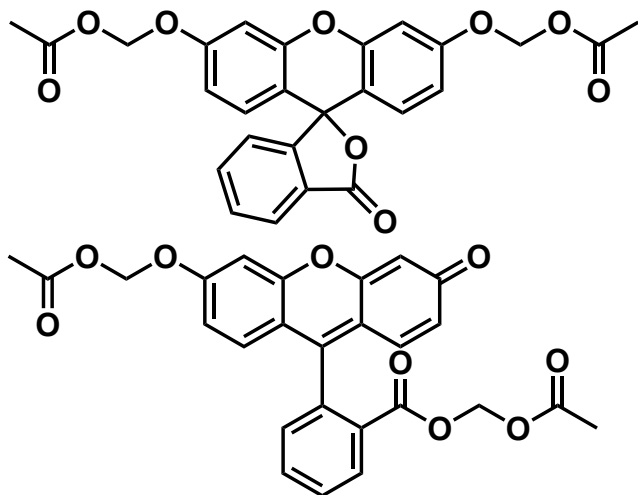
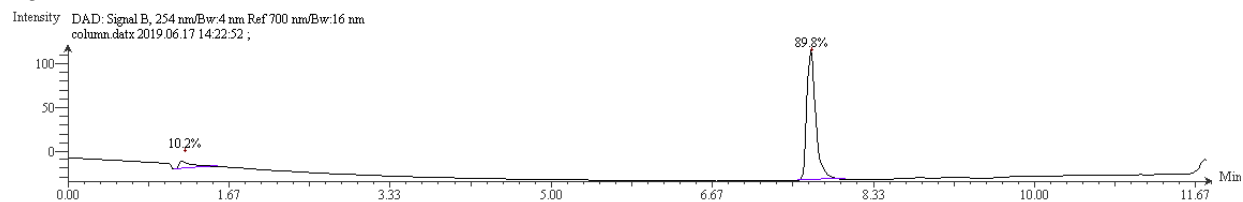
2',7'-dichlorofluorescein (200 mg, 0.5 mmol), Ag_2O (289 mg, 1.25 mmol, 2.5 eq) and 4Å molecular sieves (400 mg) were charged into an oven dried round bottom, which was subsequently evacuated and backfilled with nitrogen (3x). MeCN (7.2 mL) was added and the suspension stirred at room temperature for 1 hour. Bromomethyl acetate (0.2 mL, 2 mmol, 4eq) was added slowly and the mixture was stirred at 50°C overnight. Upon cooling to room temperature the mixture was diluted with DCM (25 mL), filtered over celite and concentrated before purifying by flash column chromatography (1: 4: 5 EtOAc: DCM: Hexanes). **FCI-AM closed** was isolated as a white solid (60.3 mg, 0.11 mmol, 23%).

^1H NMR (400 MHz, Chloroform-*d*) δ 8.07 (dt, $J = 7.1, 0.9$ Hz, 1H), 7.78 – 7.64 (m, 2H), 7.19 – 7.12 (m, 1H), 7.08 (s, 2H), 6.78 (s, 2H), 5.86 (s, 4H), 2.18 (s, 6H).

^{13}C NMR (126 MHz, Chloroform-*d*) δ 169.47, 168.63, 154.06, 151.88, 150.32, 135.63, 130.54, 129.28, 126.23, 125.66, 123.77, 119.69, 113.86, 104.09, 85.42, 81.08, 20.91.

HR-ESI-MS m/z for $\text{C}_{26}\text{H}_{19}\text{O}_9\text{Cl}_2^+$ $[\text{M}+\text{H}]^+$ calcd: 545.0401 found: 545.0402.

254 nm



Synthesis of F-AM open and F-AM closed:

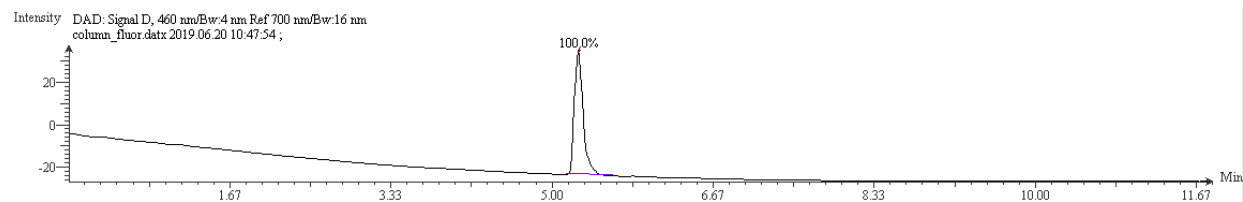
Fluorescein (200 mg, 0.6 mmol), Ag₂O (347 mg, 1.5 mmol, 2.5 eq) and 4Å molecular sieves (400 mg) were charged into an oven dried round bottom, which was subsequently evacuated and backfilled with nitrogen (3x). MeCN (7.2 mL) was added and the suspension stirred at room temperature for 1 hour. Bromomethyl acetate (0.24 mL, 2.4 mmol, 4eq) was added slowly and the mixture was stirred at 50°C overnight. Upon cooling to room temperature the mixture was diluted with DCM (25 mL), filtered over celite and concentrated before purifying by flash column chromatography (1: 4: 5 EtOAc: DCM: Hexanes) to afford:

F-AM open as an orange solid (14.1 mg, 0.03 mmol, 5%).

¹H NMR (300 MHz, Chloroform-*d*) δ 8.31 (dd, *J* = 7.8, 1.3 Hz, 1H), 7.80 (td, *J* = 7.6, 1.4 Hz, 1H), 7.72 (td, *J* = 7.6, 1.4 Hz, 1H), 7.33 (dd, *J* = 7.5, 1.2 Hz, 1H), 7.21 (d, *J* = 2.3 Hz, 1H), 6.97 (d, *J* = 8.9 Hz, 1H), 6.93 – 6.85 (m, 2H), 6.84 – 6.58 (m, 2H), 5.86 (s, 2H), 5.68 (d, *J* = 5.7 Hz, 1H), 5.61 (d, *J* = 5.7 Hz, 1H), 2.17 (s, 3H), 1.94 (s, 3H).

HR-ESI-MS *m/z* for C₂₆H₂₁O₉⁺ [M+H]⁺ calcd: 477.1180 found: 477.1178.

460 nm

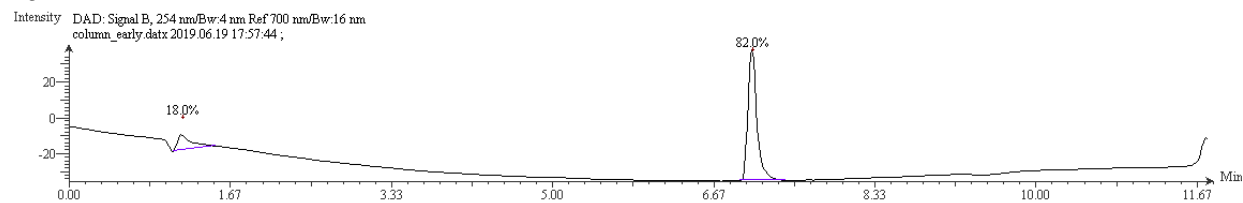


And **F-AM closed** as a white solid (180 mg, 0.38 mmol, 64%).

$^1\text{H NMR}$ (300 MHz, Chloroform- d) δ 8.10 – 7.98 (m, 1H), 7.66 (pd, $J = 7.3, 1.2$ Hz, 2H), 7.16 (dd, $J = 7.3, 1.0$ Hz, 1H), 6.96 (t, $J = 1.4$ Hz, 2H), 6.74 (s, 4H), 5.78 (s, 4H), 2.14 (s, 6H).

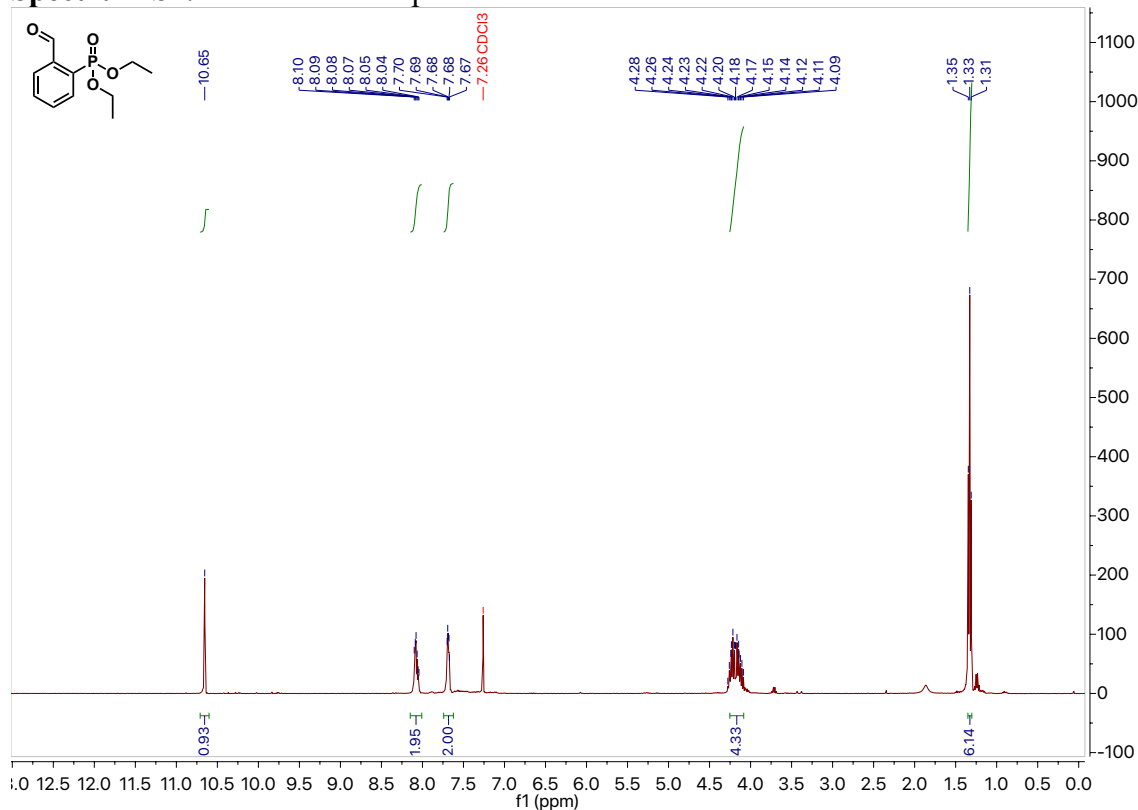
HR-ESI-MS m/z for $\text{C}_{26}\text{H}_{21}\text{O}_9^+$ $[\text{M}+\text{H}]^+$ calcd: 477.1180 found: 477.1178.

254 nm

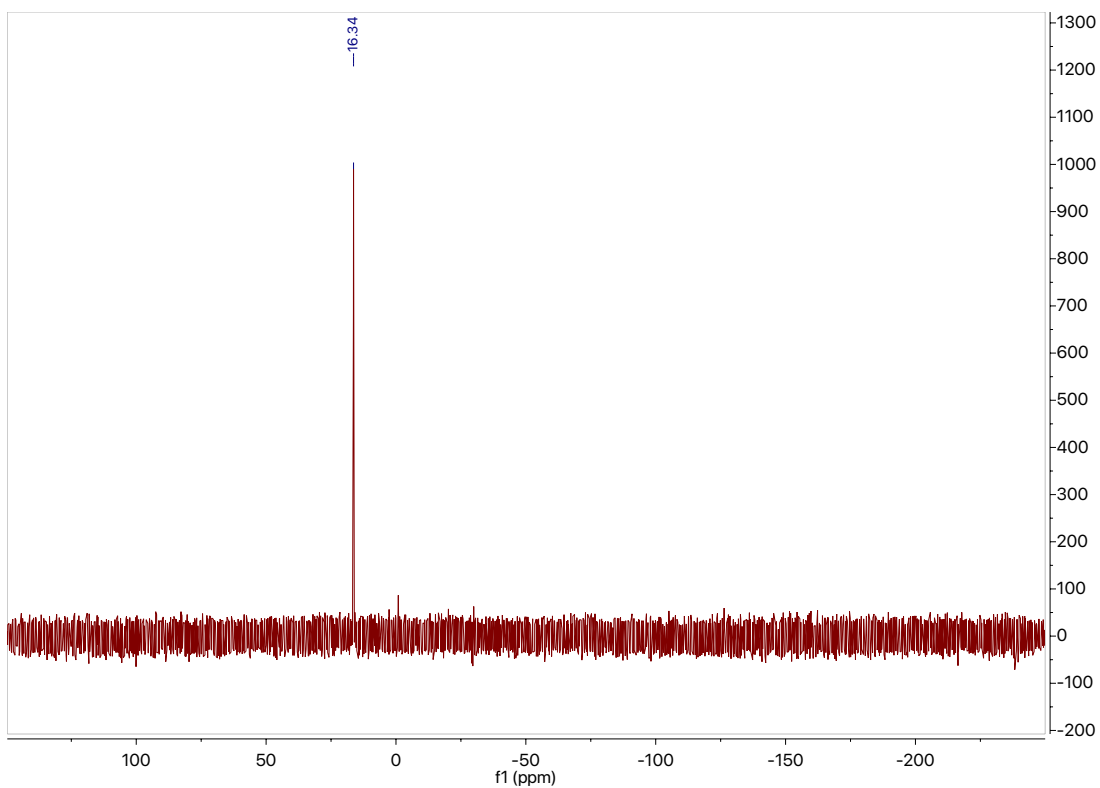


Spectra of compounds.

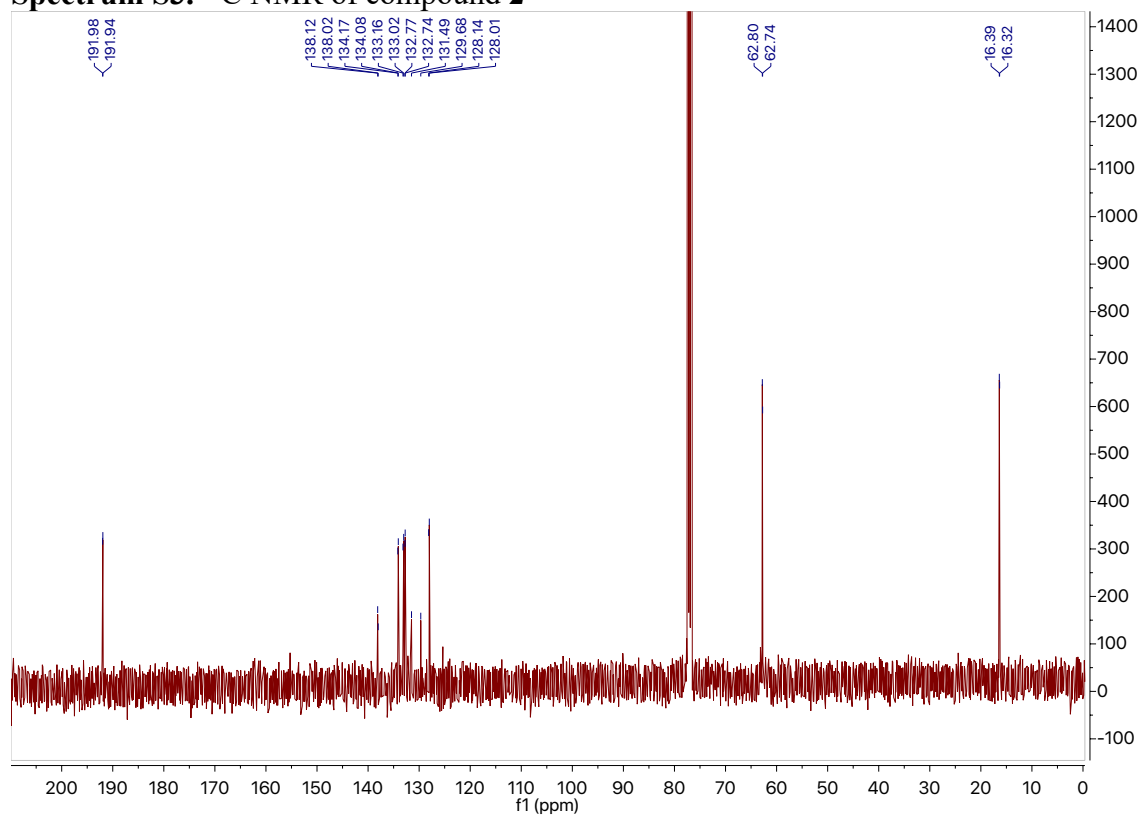
Spectrum S1. $^1\text{H NMR}$ of compound **2**.



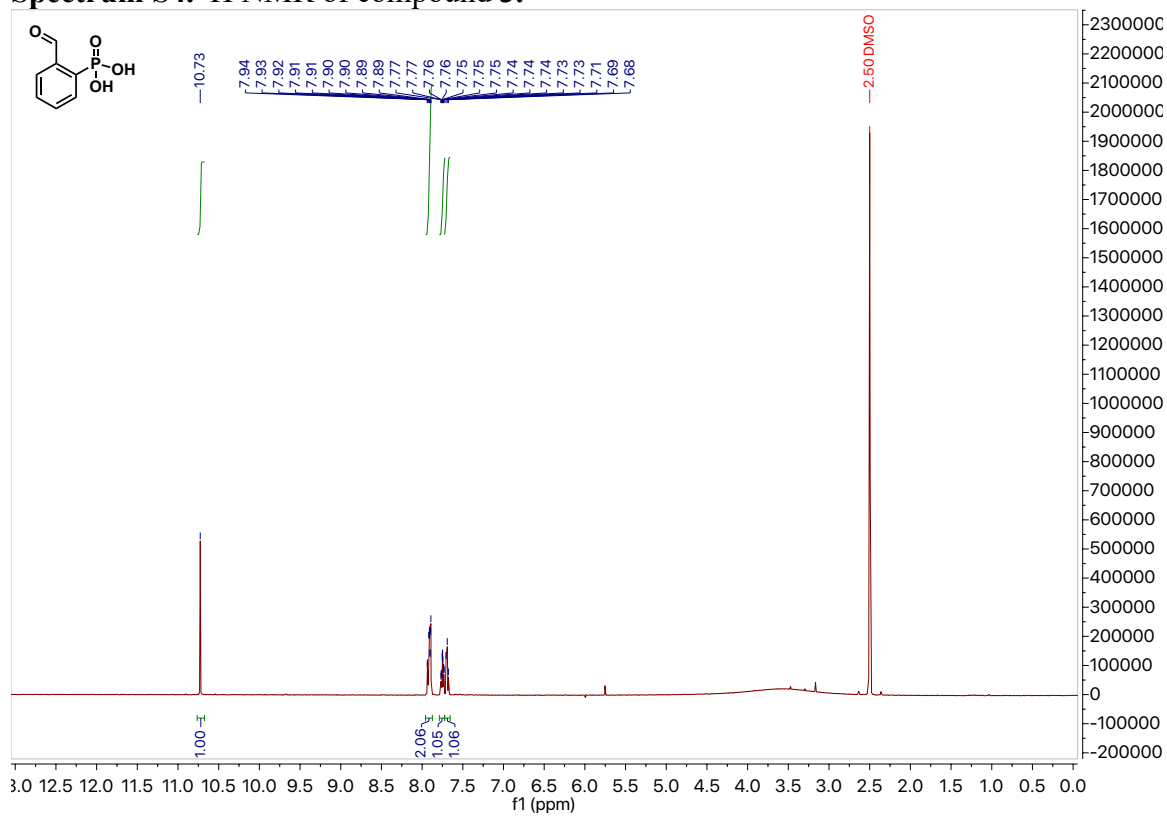
Spectrum S2. ^{31}P NMR of compound **2**.



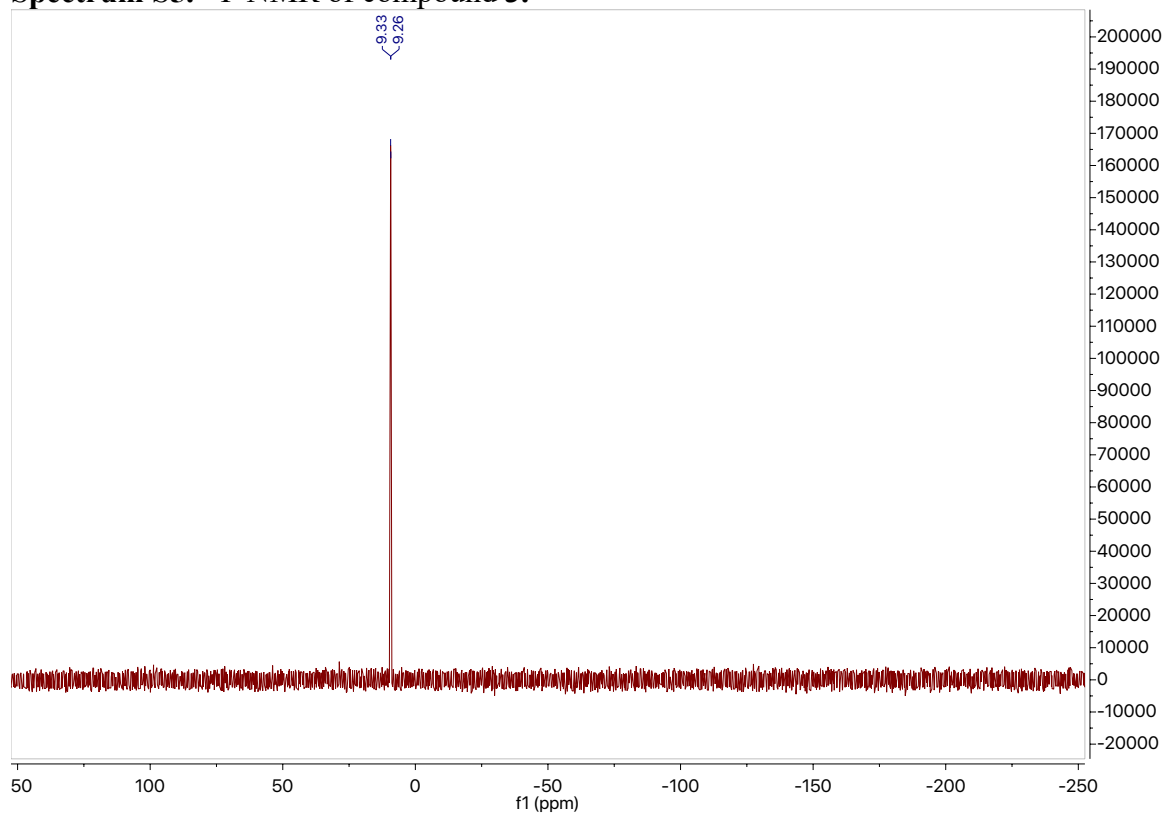
Spectrum S3. ^{13}C NMR of compound **2**



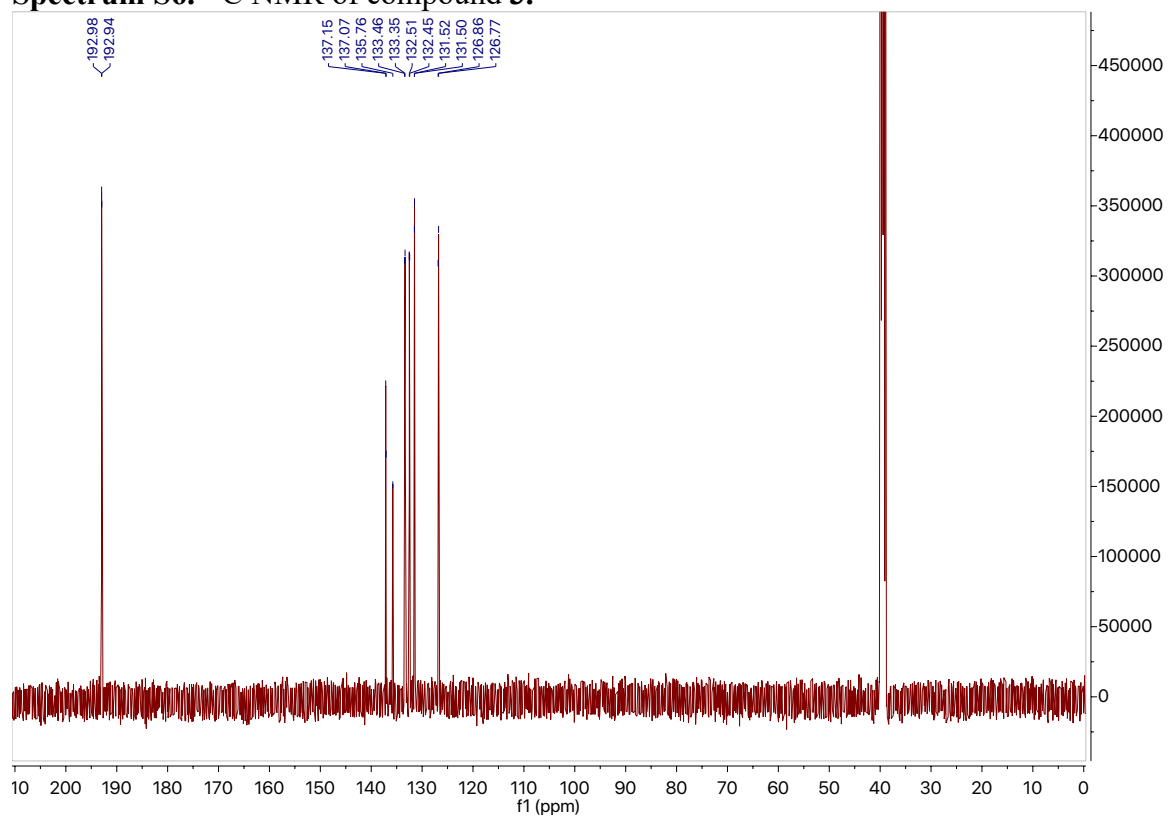
Spectrum S4. ^1H NMR of compound 3.



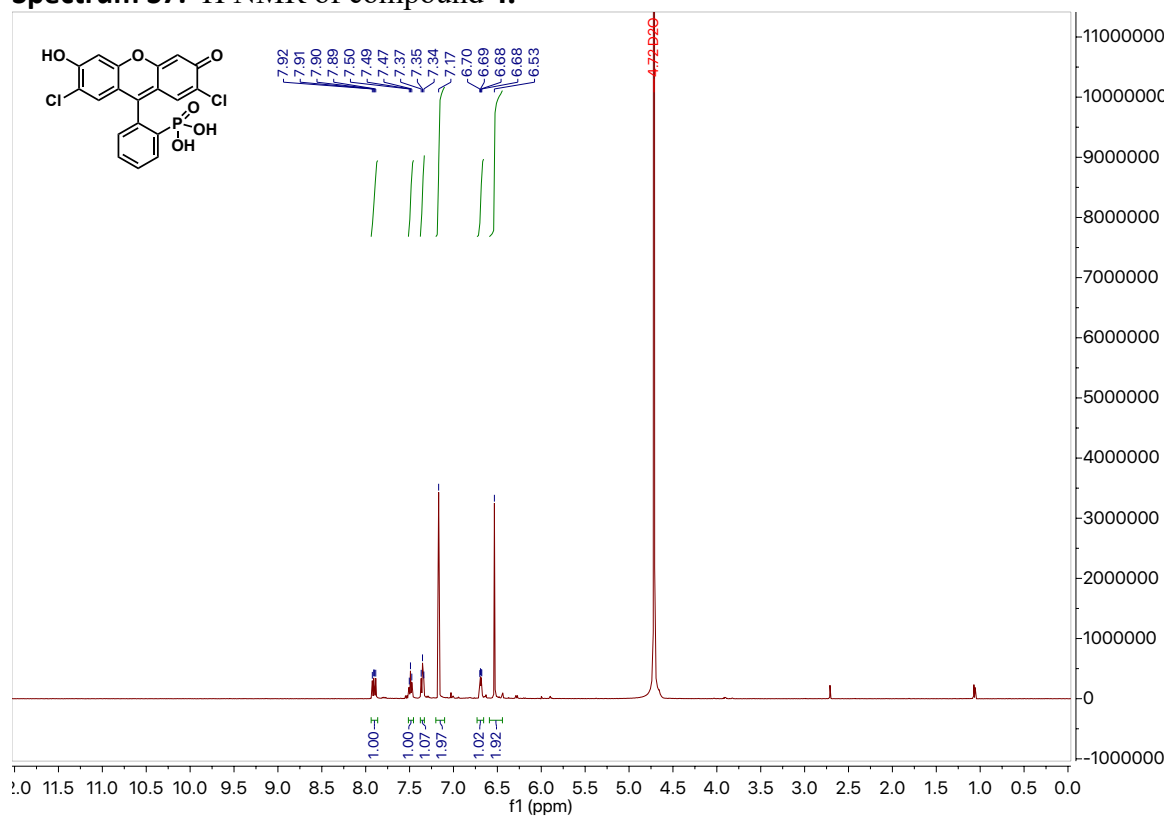
Spectrum S5. ^{31}P NMR of compound 3.



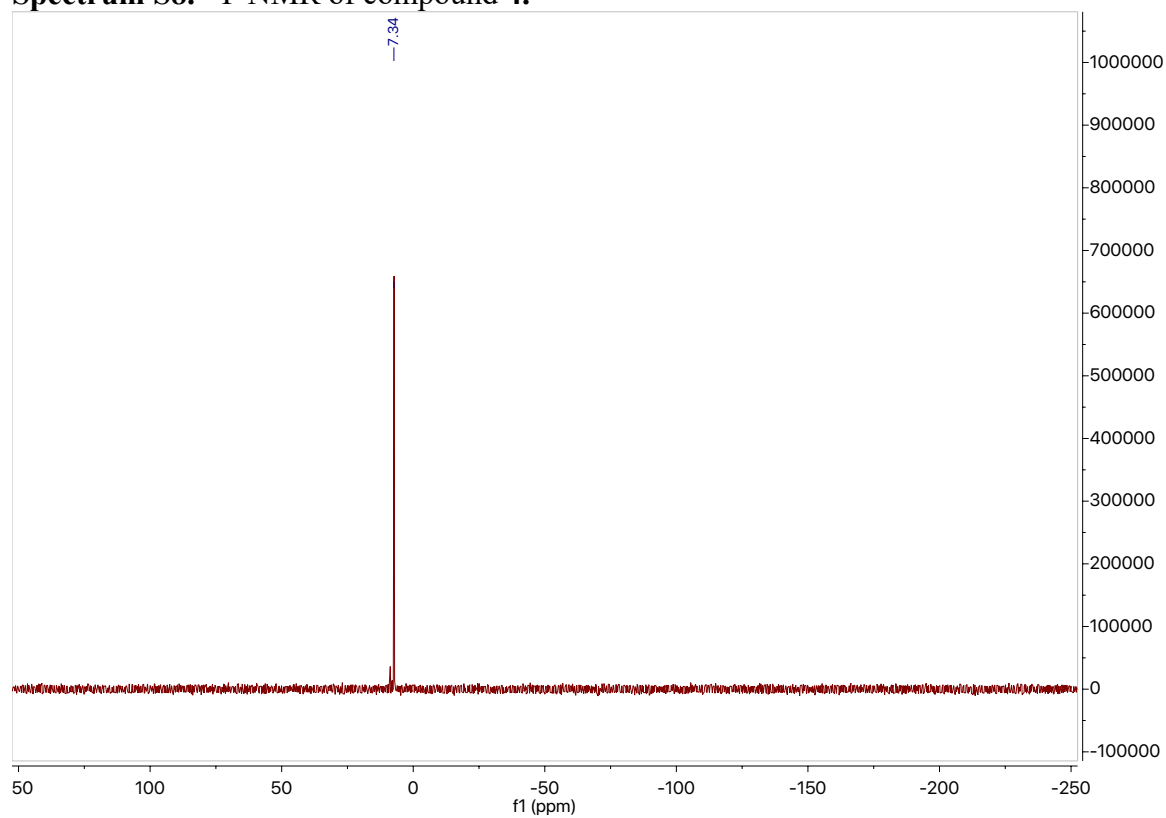
Spectrum S6. ^{13}C NMR of compound 3.



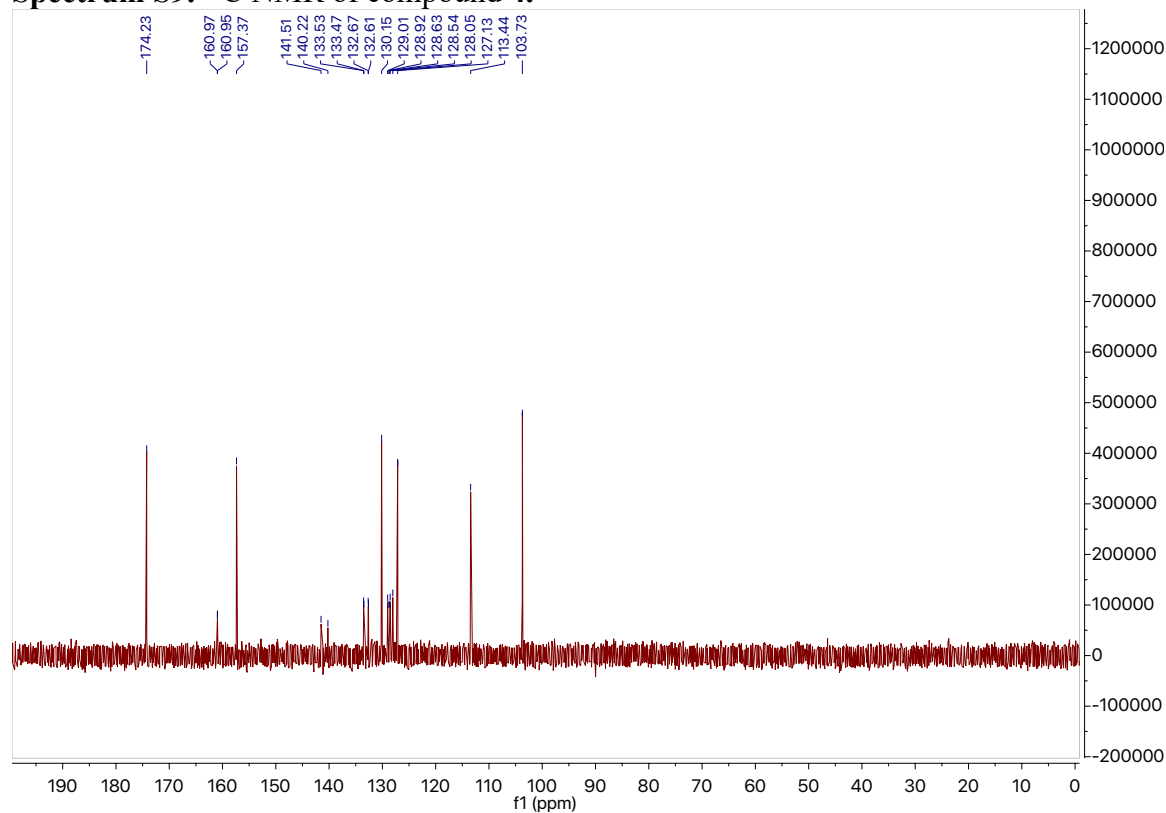
Spectrum S7. ^1H NMR of compound 4.



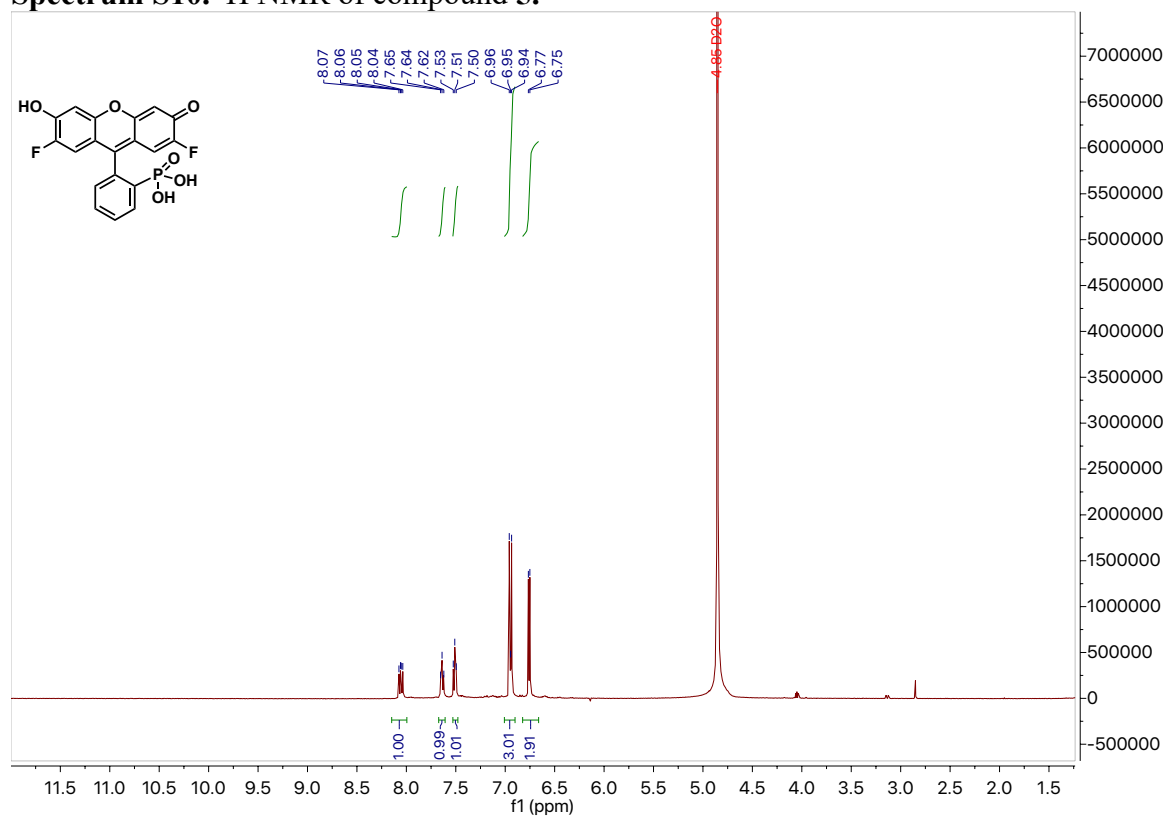
Spectrum S8. ^{31}P NMR of compound 4.



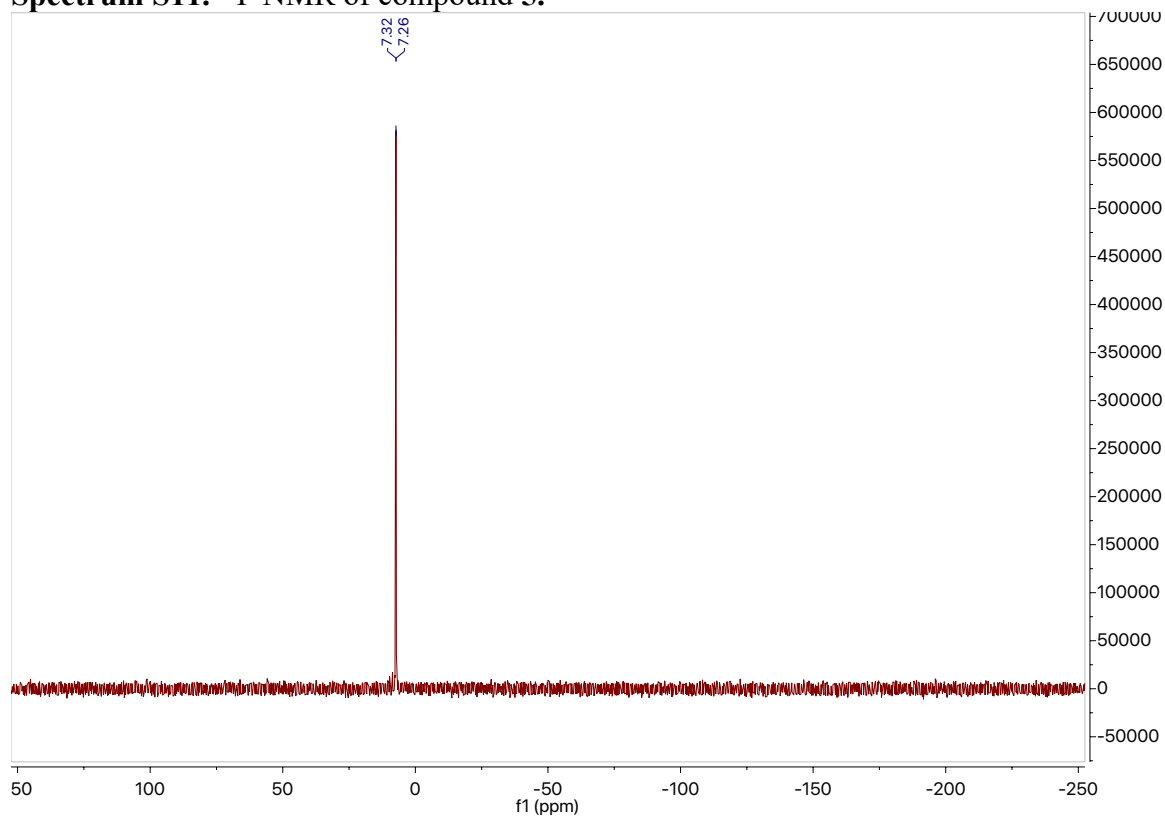
Spectrum S9. ^{13}C NMR of compound 4.



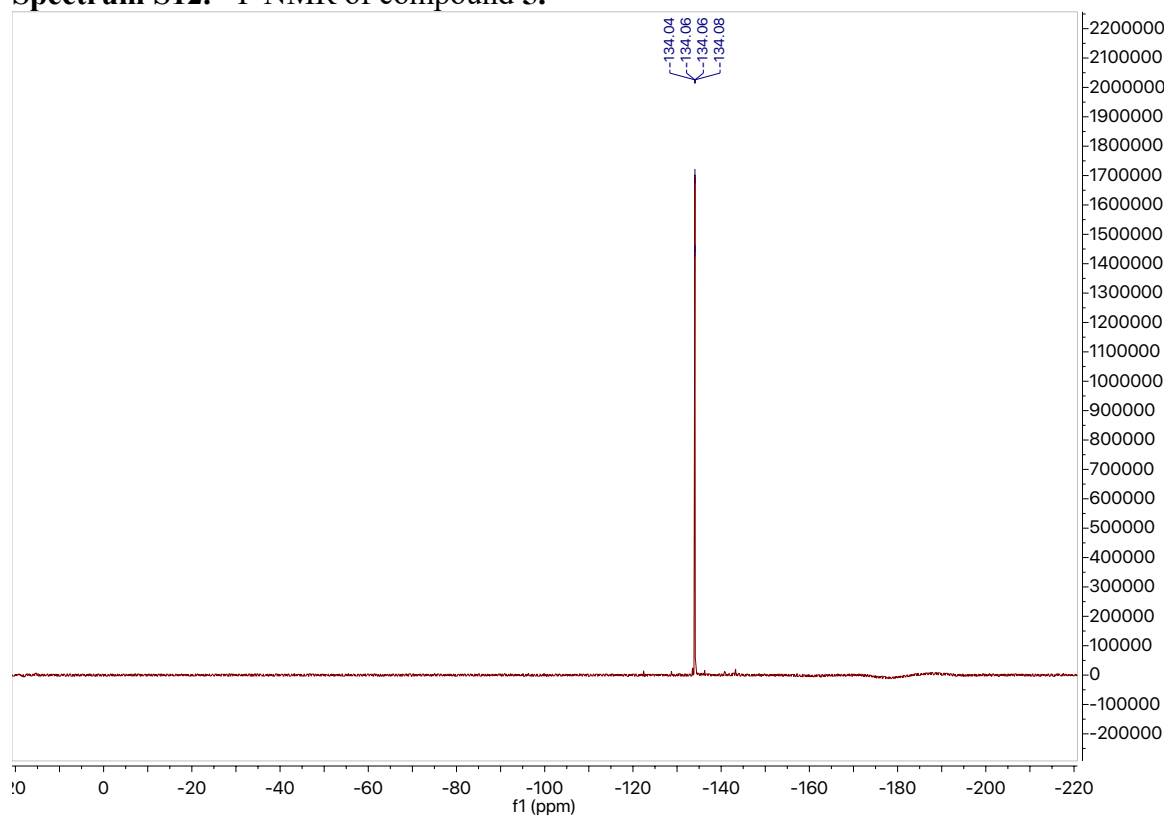
Spectrum S10. ^1H NMR of compound **5**.



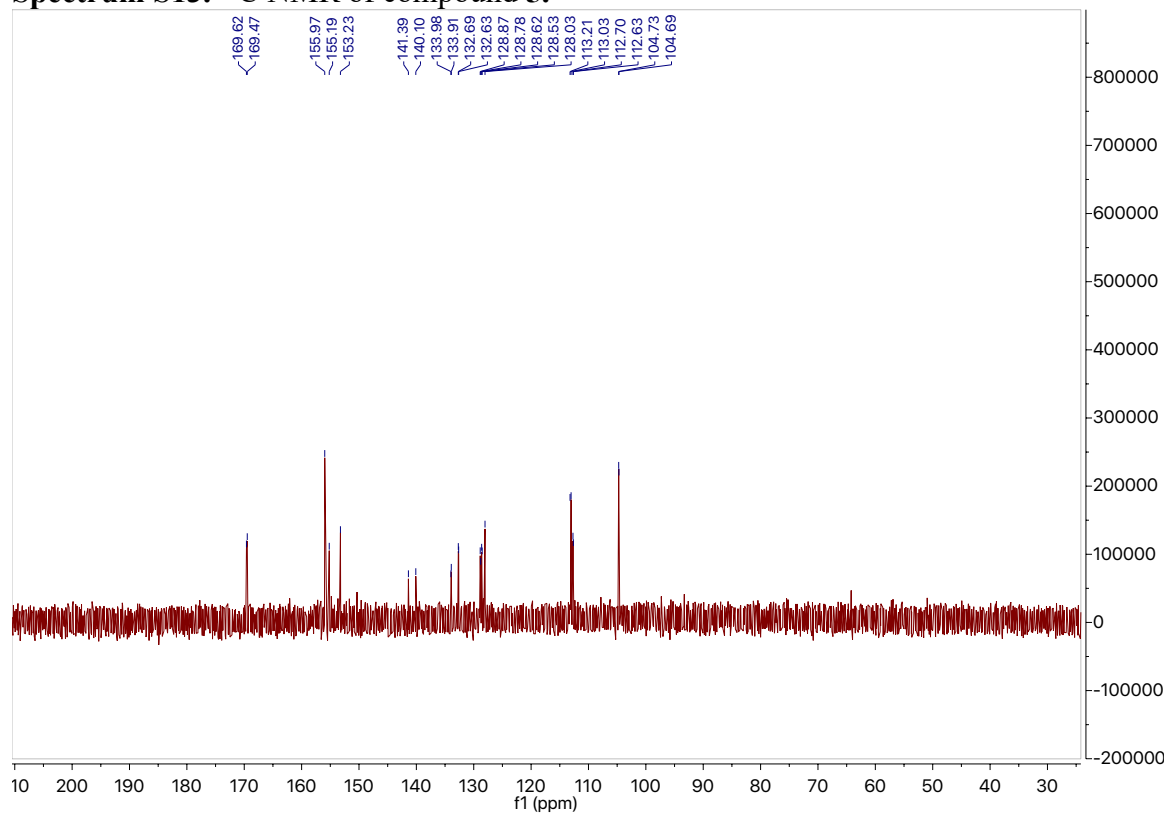
Spectrum S11. ^{31}P NMR of compound **5**.



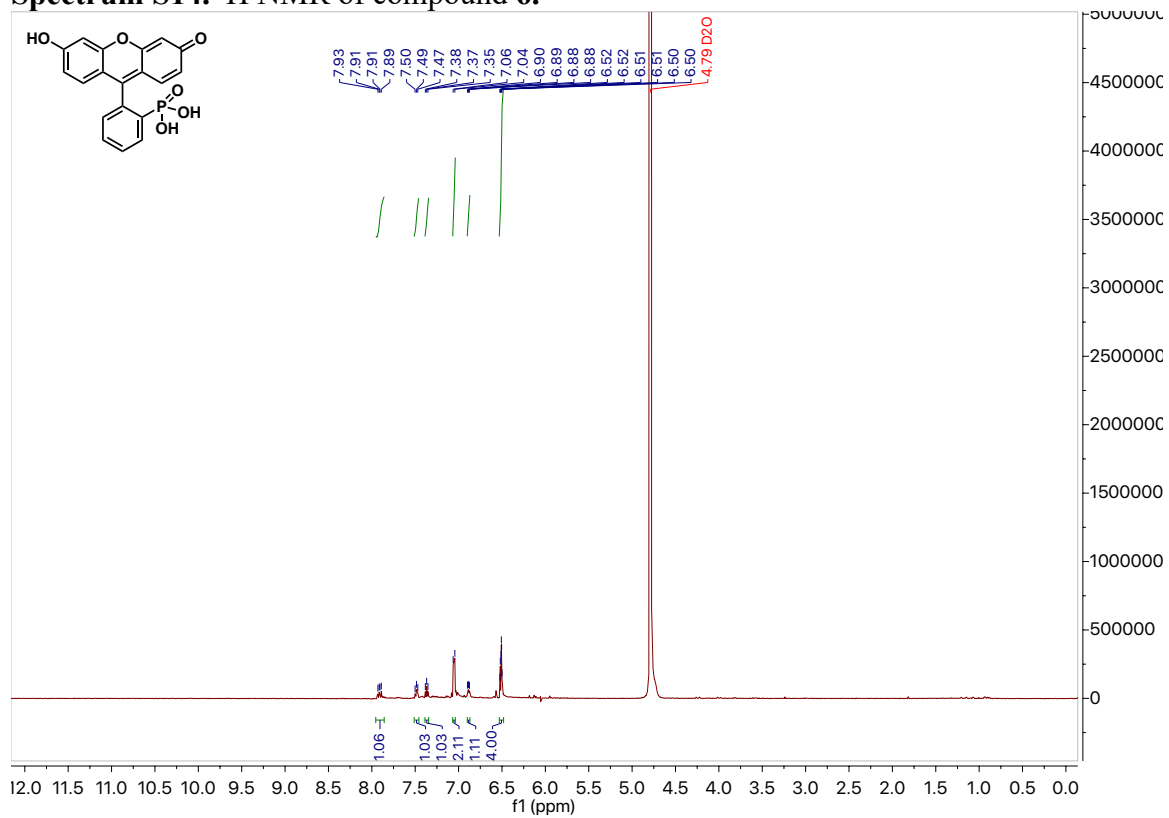
Spectrum S12. ^{19}F NMR of compound 5.



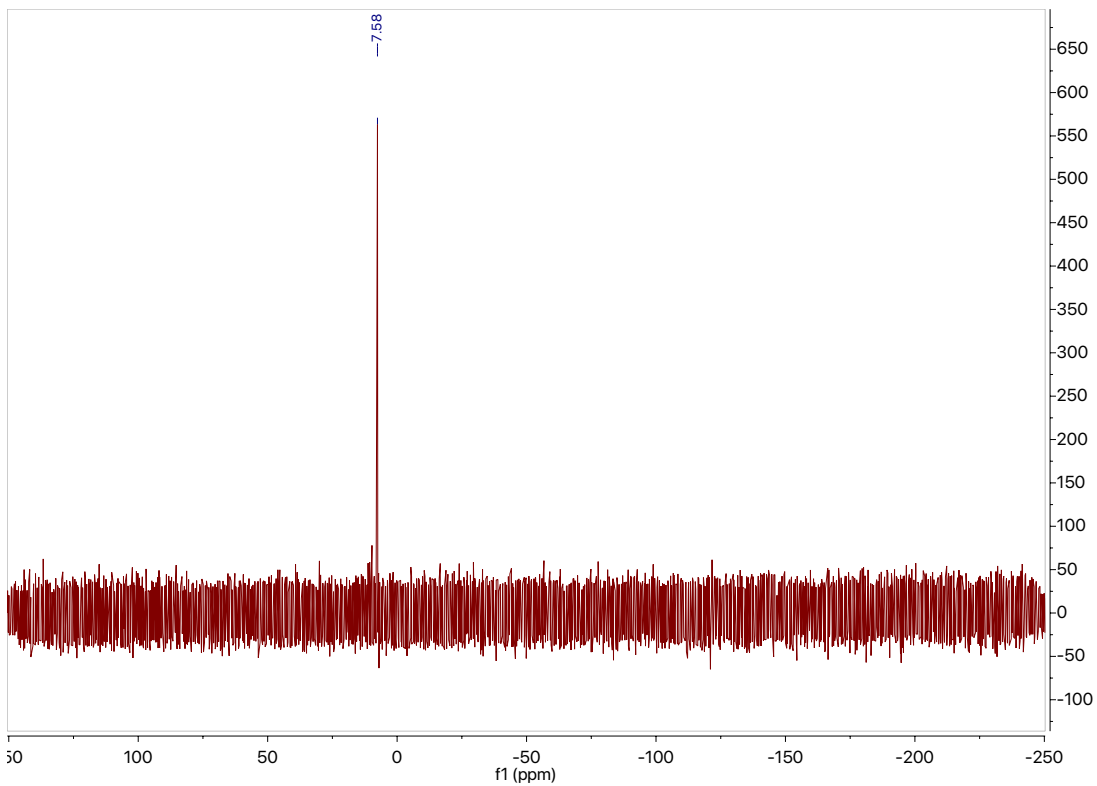
Spectrum S13. ^{13}C NMR of compound 5.



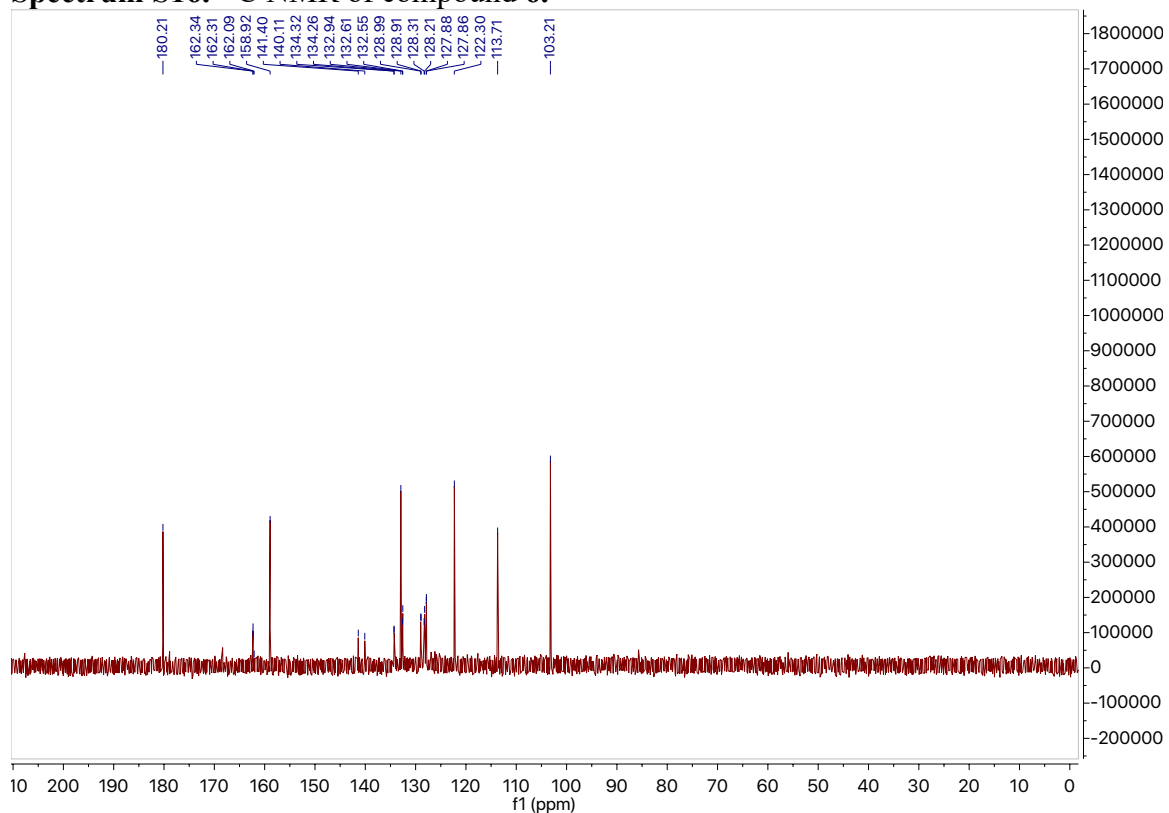
Spectrum S14. ^1H NMR of compound **6**.



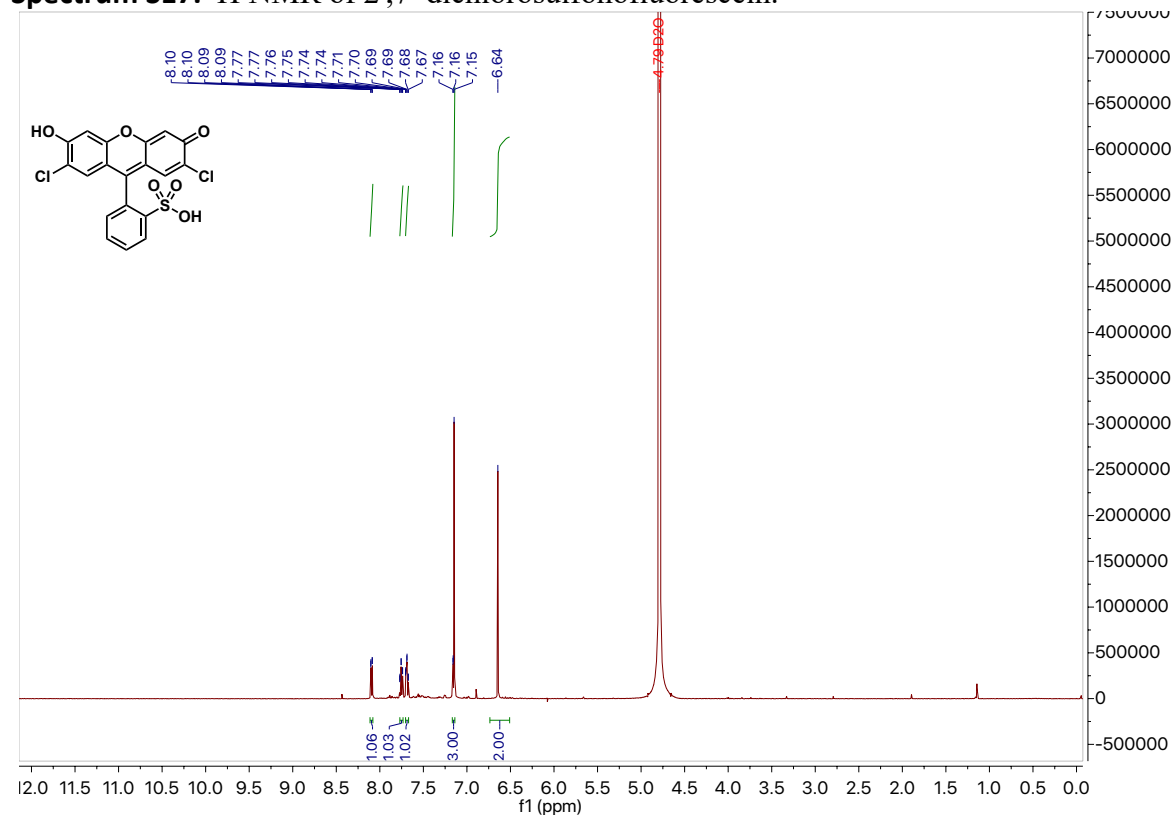
Spectrum S15. ^{31}P NMR of compound **6**.



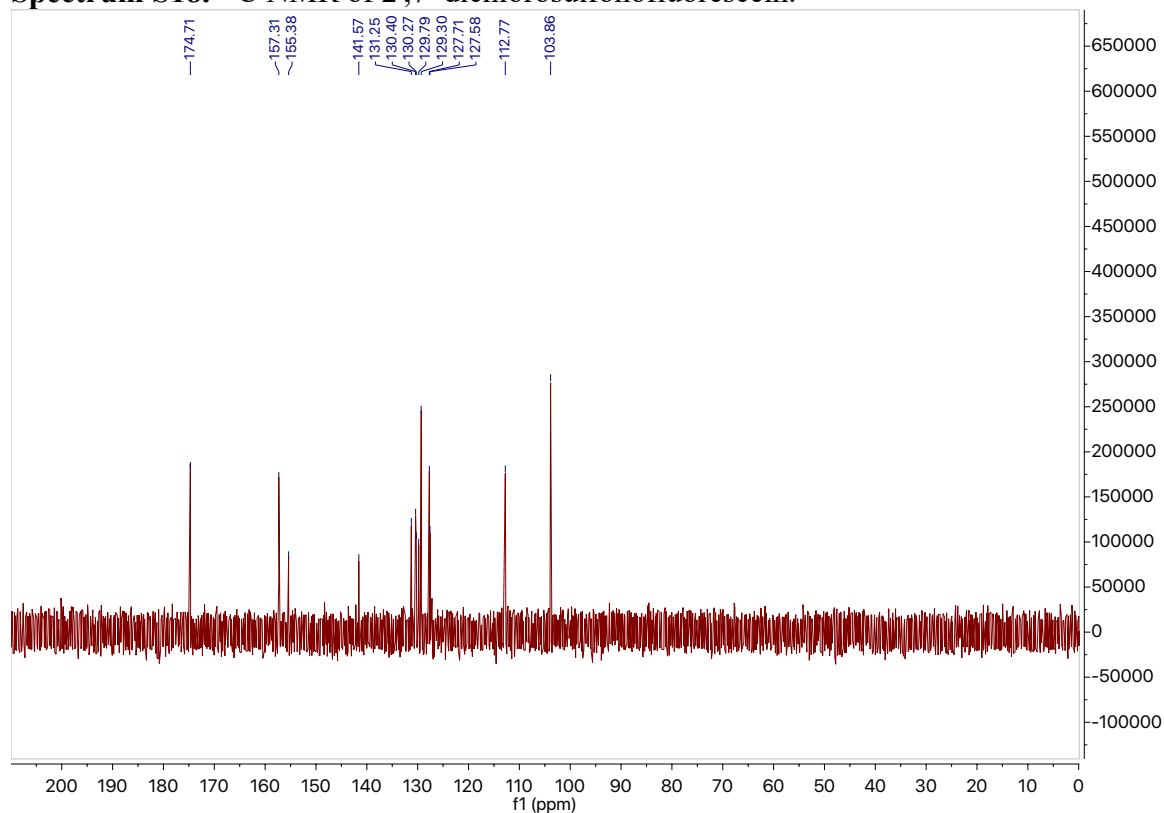
Spectrum S16. ^{13}C NMR of compound 6.



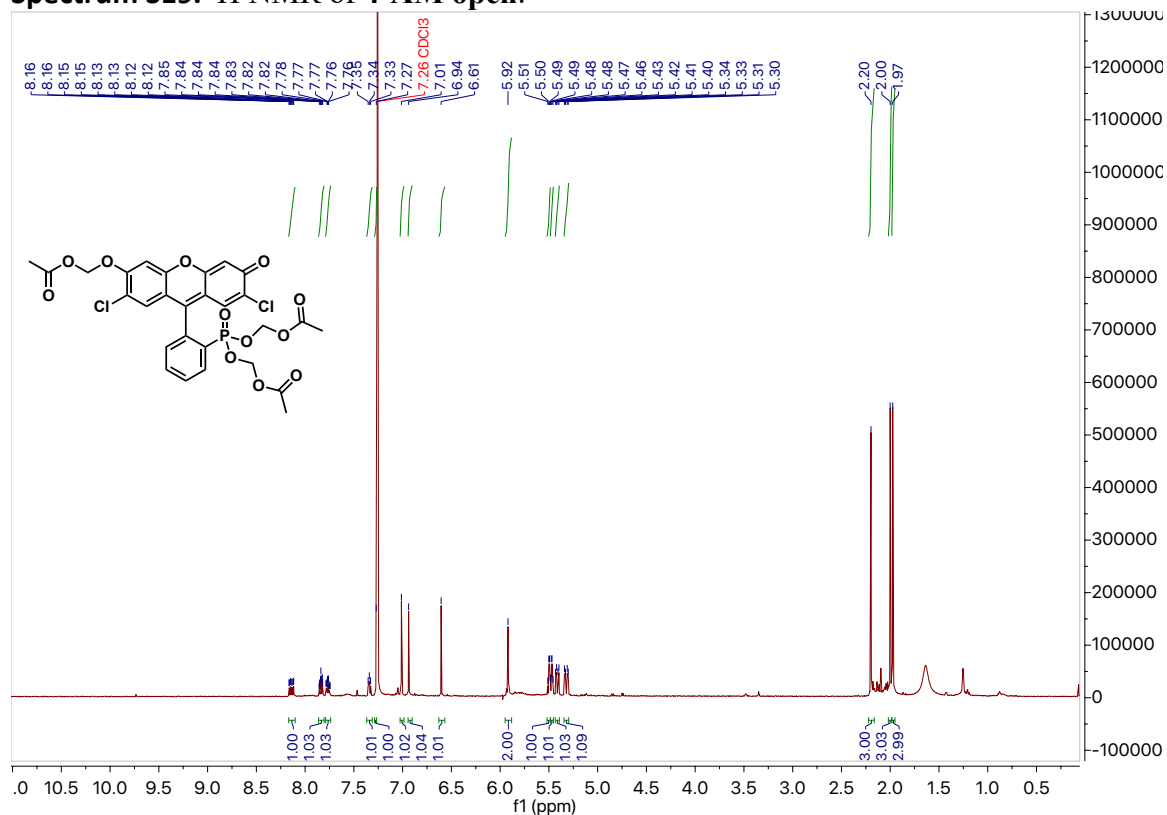
Spectrum S17. ^1H NMR of 2',7'-dichlorosulfonfluorescein.



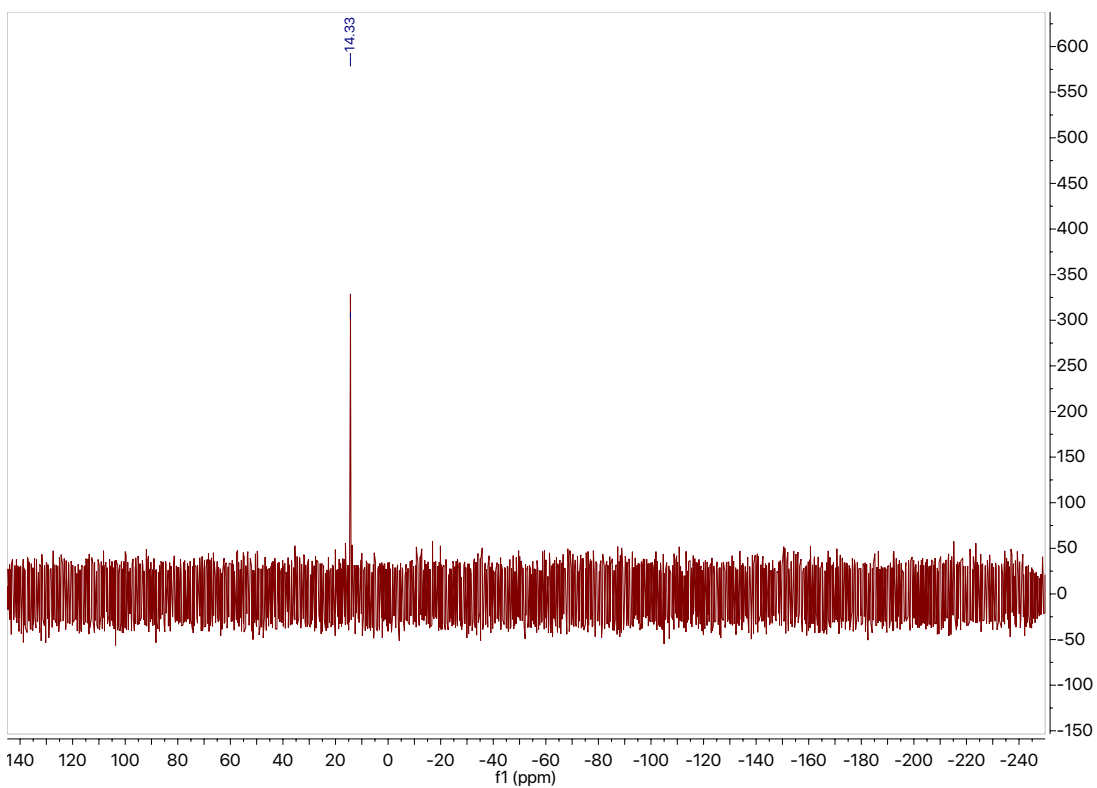
Spectrum S18. ^{13}C NMR of 2',7'-dichlorosulfonofluorescein.



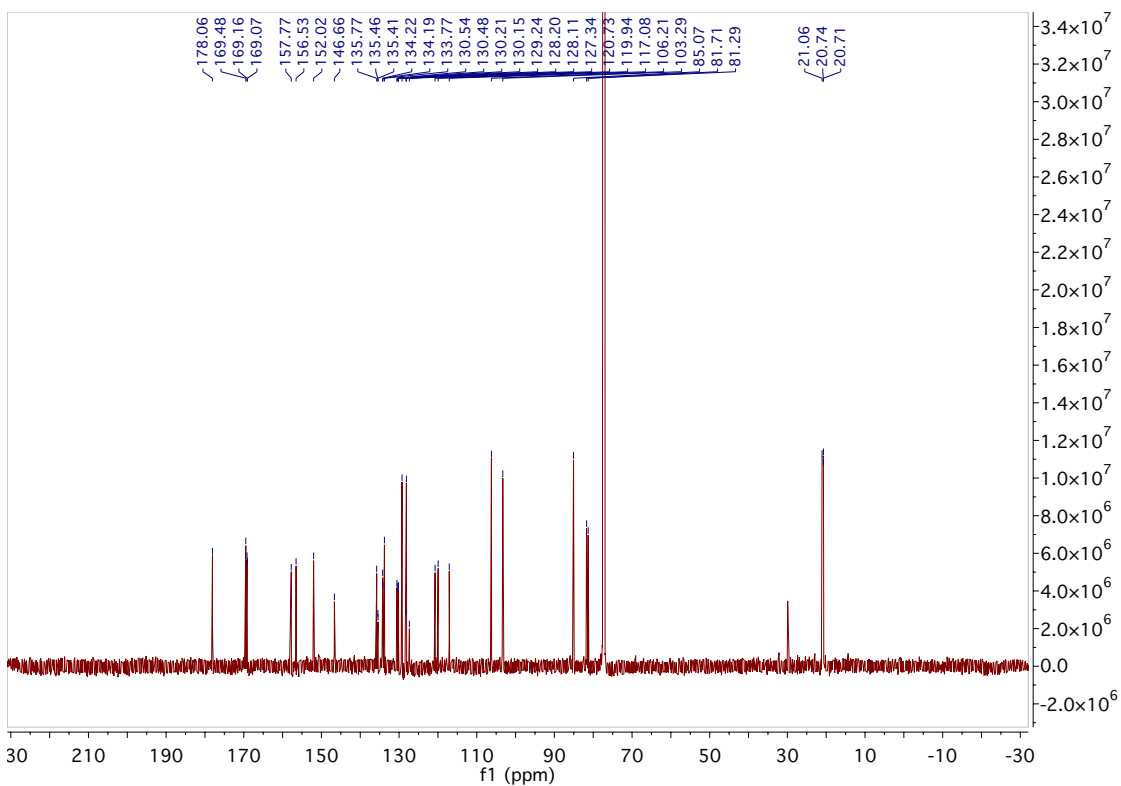
Spectrum S19. ^1H NMR of 4-AM open.



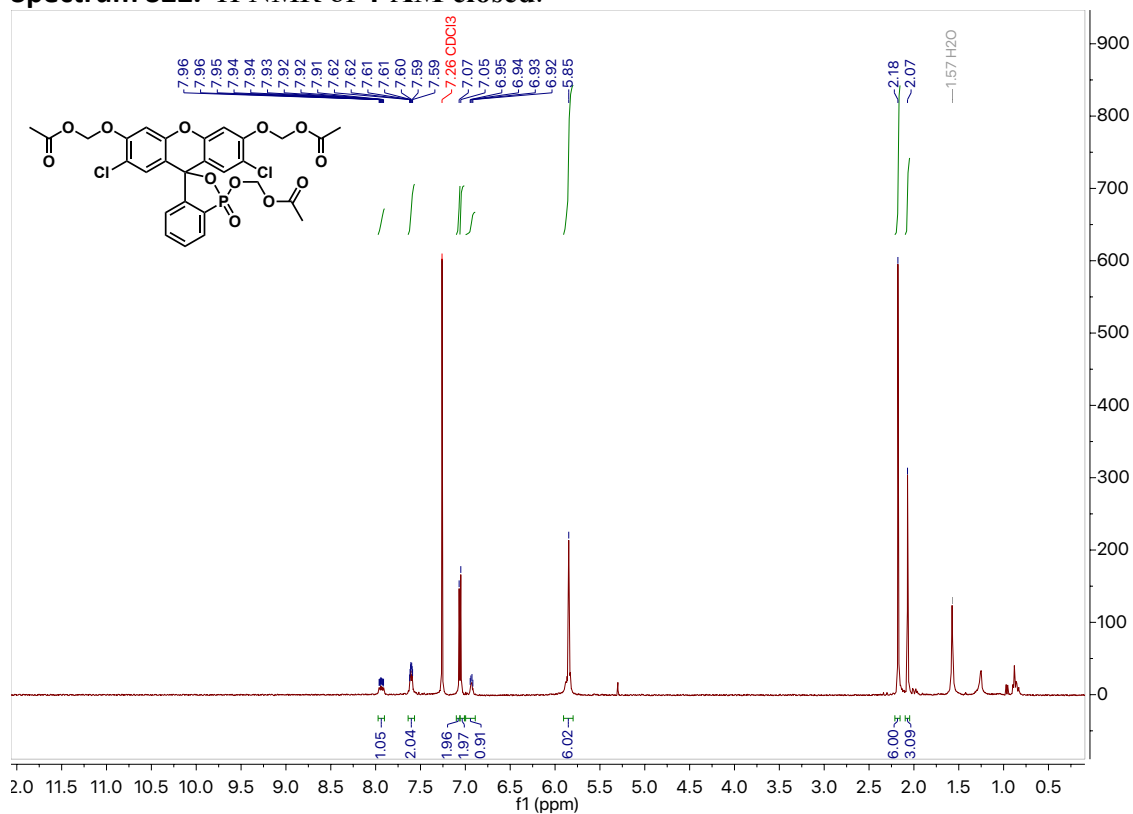
Spectrum S20. ^{31}P NMR of 4-AM open.



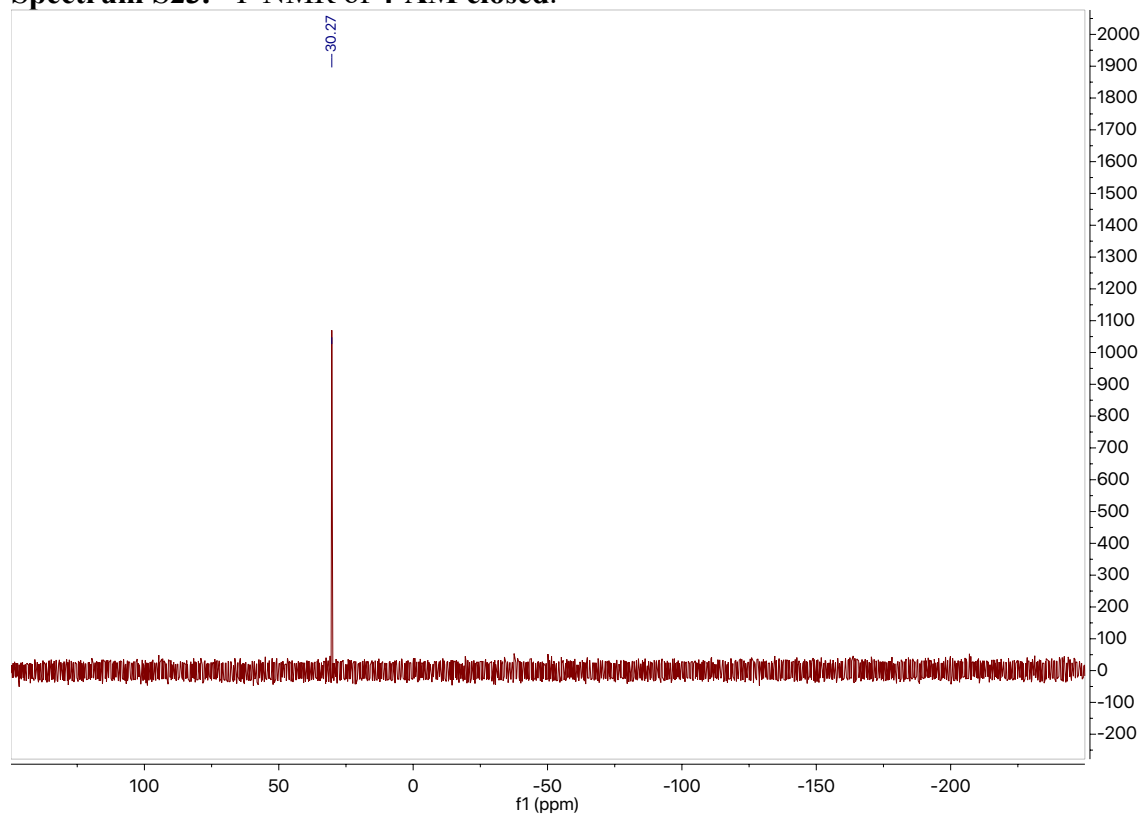
Spectrum S21. ^{13}C NMR of 4-AM open.



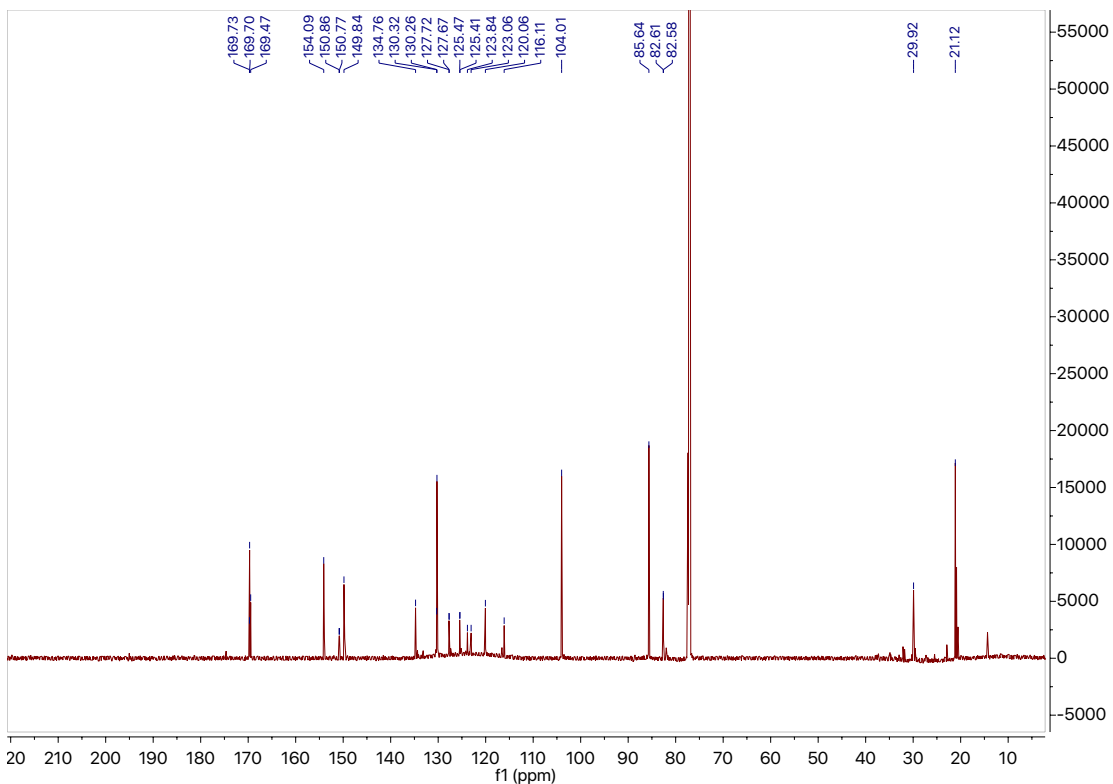
Spectrum S22. ¹H NMR of 4-AM closed.



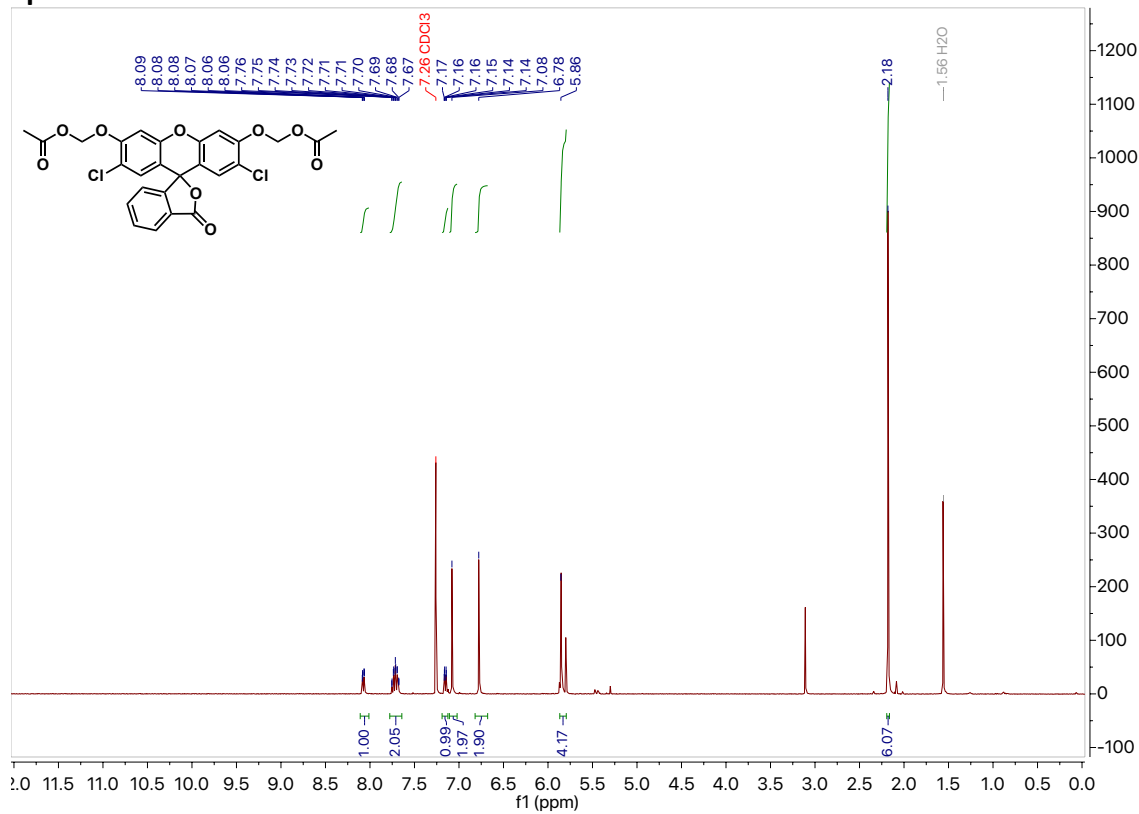
Spectrum S23. ³¹P NMR of 4-AM closed.



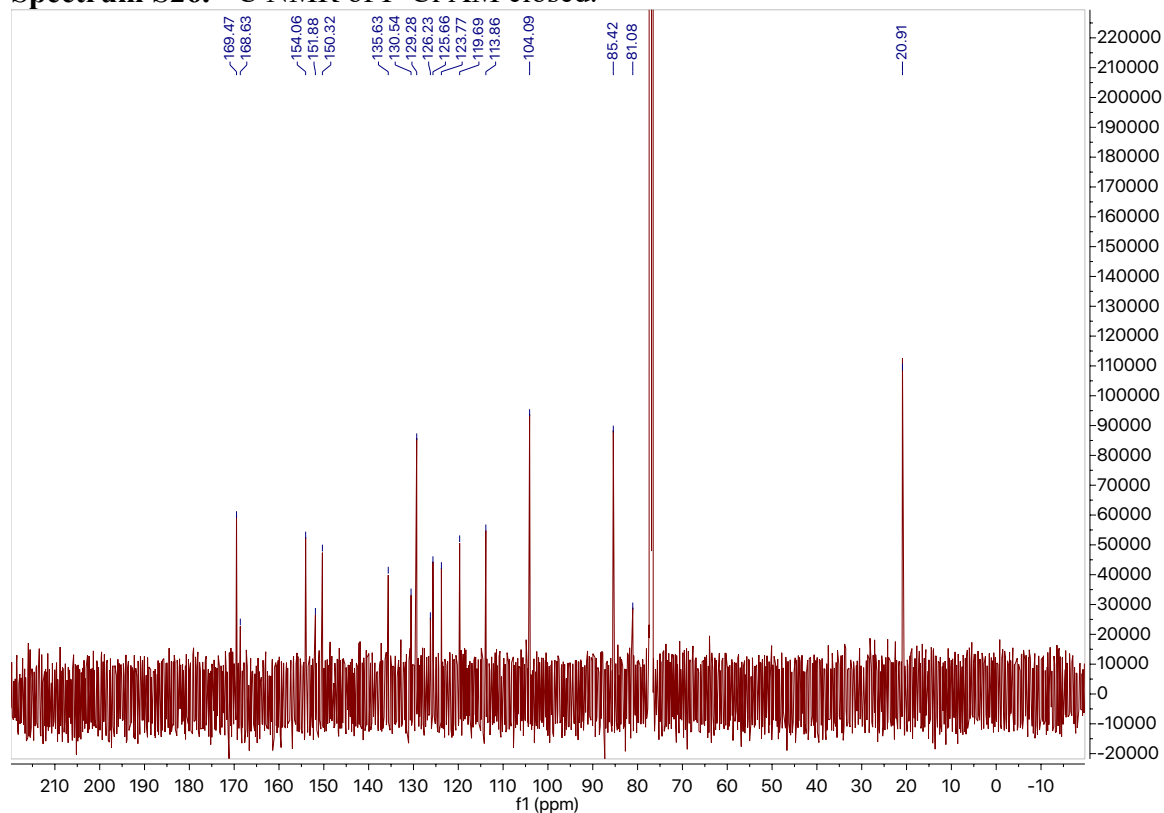
Spectrum S24. ^{13}C NMR of 4-AM closed.



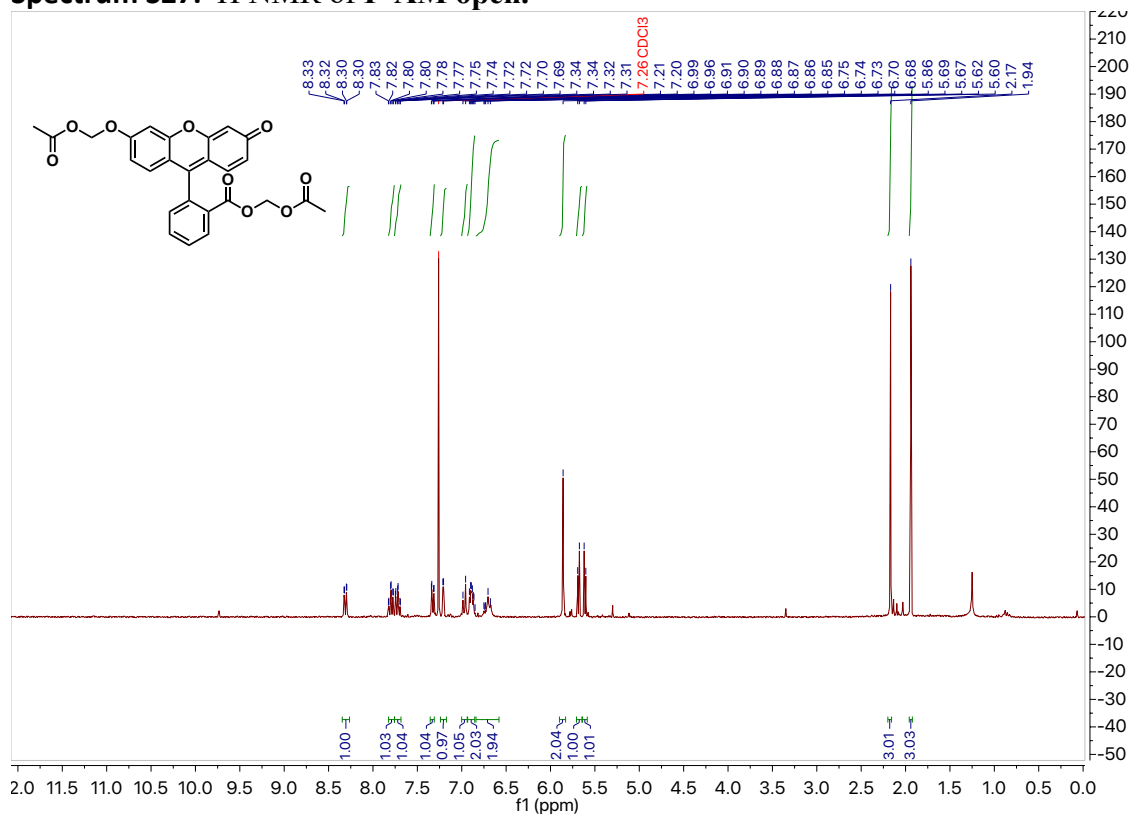
Spectrum S25. ^1H NMR of F-Cl AM closed.



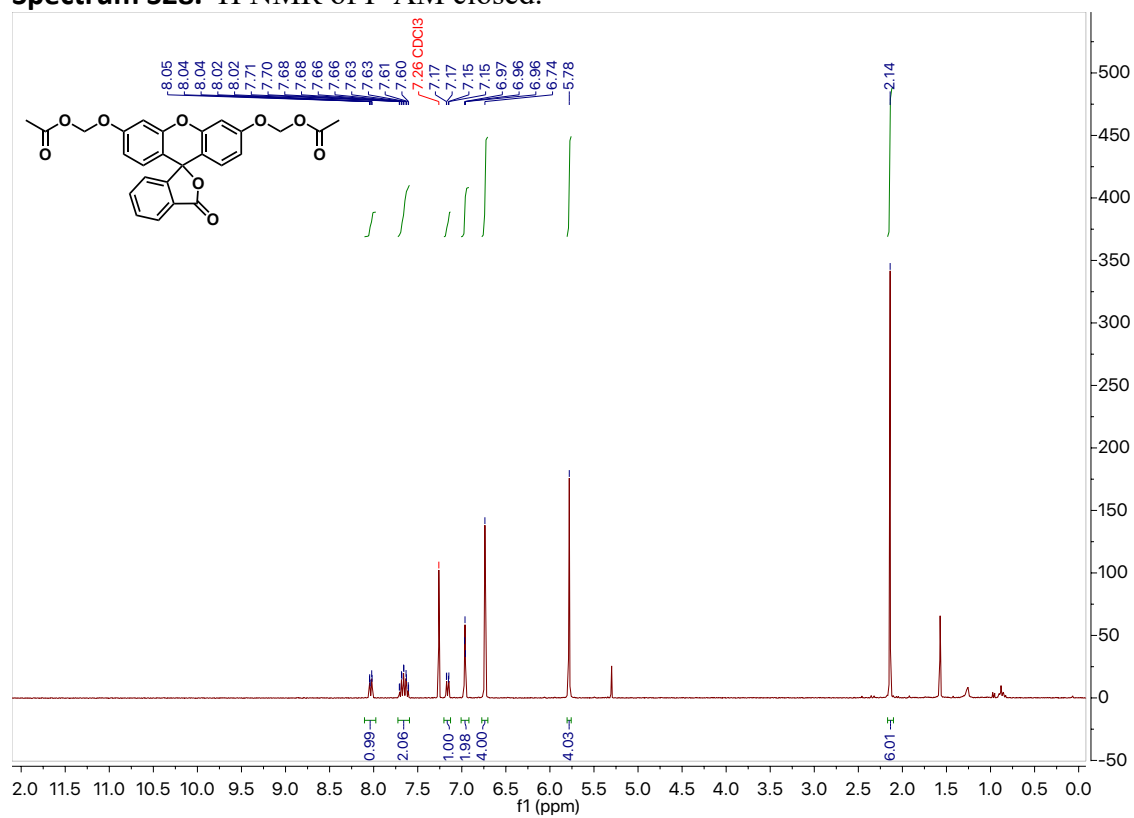
Spectrum S26. ^{13}C NMR of F-Cl AM closed.



Spectrum S27. ^1H NMR of F-AM open.



Spectrum S28. ¹H NMR of F-AM closed.



Chapter 2

Phosphonated Rhodamines for Live Cell Imaging Applications

Part of this work was performed in collaboration with Ryan Golden who assisted with chemical synthesis.

Introduction

Small molecule fluorophores are essential tools that have revolutionized our ability to probe, visualize and understand complex biological systems.^{1,2} The advancement of biological imaging modalities is therefore reliant on our ability to develop novel fluorophores with distinguishing properties. Amine isologues of fluoresceins, rhodamines are highly attractive xanthene fluorophores that have found widespread use across the biological sciences. In comparison to fluoresceins, rhodamines are relatively insensitive to pH, often exhibit improved photostability and have highly tunable spectral properties.³ The alkylation pattern on the terminal amines enables precise tuning of the absorption and emission wavelengths (490 to 600 nm) and C-N bond restriction with fused cyclohexane or 4-membered azetidine rings has been shown to improve brightness.^{4,5} Additionally, the positively charged nature of the xanthene core facilitates cell permeability making rhodamines attractive scaffolds for intracellular or live-cell imaging applications.⁶

Replacement of the 10' oxygen atom with heteroatoms such as carbon,^{7,8} silicon,⁹⁻¹² phosphorus,^{13,14} or sulfur¹⁵ further modifies the spectral properties of rhodamines, typically resulting in greater red shifting of the absorption and emission maxima. Rhodamines with emission maxima in the red to near infrared region of the electromagnetic spectrum are attractive for mitigating phototoxicity and autofluorescence while improving tissue penetration for *in vivo* imaging. Furthermore, expansion of the available color palette through spectral finetuning provides important opportunities for multicolor imaging.

In most cases rhodamines bear a carboxylate at the 3-position on the pendant ring, and despite having profound influence on the associated physical properties, substitution of this functionality is relatively under explored. We recently disclosed a new class of fluoresceins with 3-phosphonate substitutions exhibiting an almost 2-fold improvement in water solubility compared to 3-carboxy analogs.¹⁶ Additionally, we highlighted how the ability to functionalize phosphonates with phosphonate esters provided a method to deliver these anionic fluorophores into living cells where we observed excellent improvements in cellular brightness and retention. Owing to the orthogonality of the xanthene core and the pendant ring, physical changes brought by 3-phosphonate substitution were facilitated without any compromise of the desirable photophysical properties such as brightness and emission. We envisioned that expansion of 3-phosphonate substitution to rhodamines would yield additional opportunities in the applications of xanthene fluorophores, namely increasing water solubility and providing handles for tunable localization.

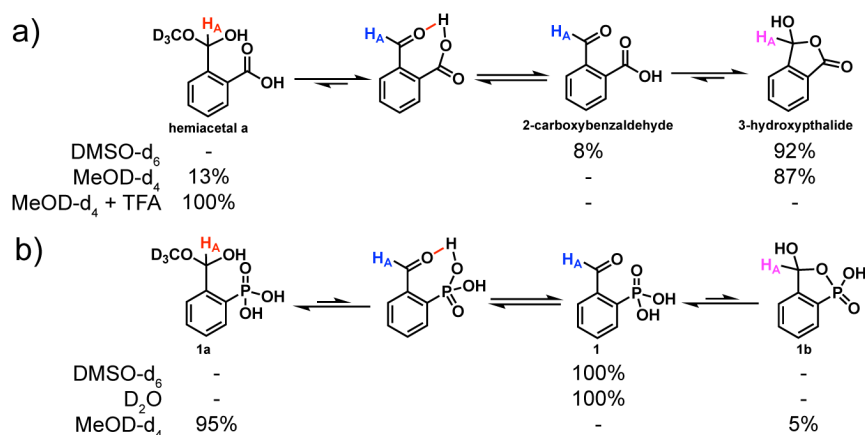
Despite almost 140 years since the first rhodamine was synthesized, synthetic approaches often lack generalizability with respect to varying 3-substitution.¹⁷ In fact, rhodamines are largely constructed by variations of the initially reported Friedel-Crafts condensation. Phthalic anhydrides are heated with aminophenols in the presence of Brønsted or Lewis acids; however, functionalized phthalides often lead to mixture of regioisomers that are difficult to separate.¹⁸ Instead, benzaldehydes are also condensed with aminophenols followed by *in situ* oxidation with exposure to air or use of an organic oxidant such as chloranil.¹⁹ The harsh nature of these condensations often results in low yields, functional group incompatibility and troublesome purifications.^{1,20,21} While acid is prudent to increasing the electrophilicity of benzaldehydes, aniline protonation decreases the nucleophilicity of aminophenols.

A contemporary method to rhodamines has been reported making use of Pd-catalyzed C-N cross coupling of fluorescein ditriflates with various amines.²² While this approach facilitates the synthesis of rhodamines with more exotic amine substitution, not confined by commercial availability of aminophenols, this method is contingent on the ability to easily access reasonable

quantities of the analogous fluorescein. Organometallic approaches to rhodamine synthesis rely on the addition of aryl lithiates into N-alkylated diaminoxanthenes or dilithiated bisphenyl ethers into electrophiles such as aryl esters or phthalic anhydrides.^{23–25} While these methods have alleviated some of the challenges associated with rhodamine condensations, they lack generalizability in the context of 3-substitution and their application to the synthesis of 3-phosphonorhodamines is not straight forward.

Herein we report a mild, acid-free condensation to 3-phosphonorhodamines in exceptional yields. Bought about by intramolecular activation from the *ortho* phosphonic acid, we show that 3-phosphonorhodamines can be synthesized on large scale: often without the need for chromatography, alleviating many of the common challenges associated with purification of charged fluorophores. Additionally, we characterize the properties of 3-phosphonorhodamines, and observe 3-substitution improves water solubility and influences the cellular localization of rhodamine fluorophores. We subsequently expand this chemistry to synthesize red-shifted 3-phosphono silicon rhodamines and find that 3-phosphonate substitution also modulates the spirocyclization equilibrium.

Results and Discussion



Scheme 1. Unique behavior of 2-carboxy and 2-phosphonobenzaldehydes.

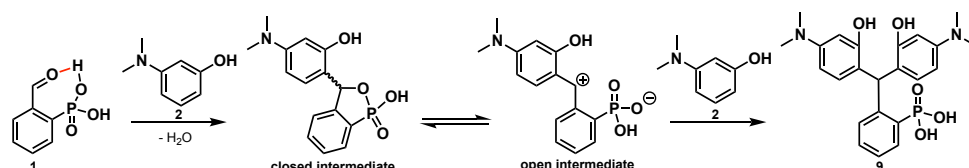
The structure of 2-carboxybenzaldehyde (**Scheme 1a**) remained in doubt for some time, largely since this compound exists in both open and closed, in which the *ortho*-carboxylate lactonizes into the aldehyde, forms.²⁶ NMR analysis in dimethyl sulfoxide (DMSO-d₆) revealed 2-carboxybenzaldehyde exists predominantly (92%) as the lactonized 3-hydroxyphthalide (**Scheme 1a**). It has also been noted that the acidic nature of the 2-carboxylate is responsible for providing intramolecular activation of the aldehyde, increasing electrophilicity.²⁷ We corroborated previous reports of this via ¹H NMR. In a nucleophilic solvent, such as methanol (MeOD-d₄), we observe slight formation (13%) of hemiacetal **a** (**Scheme 1a**), in which methanol has performed nucleophilic attack on the aldehyde. Addition of an exogenous acid, such as trifluoroacetic acid (TFA), pushes the equilibrium completely to the hemiacetal. The phenomenon of this intramolecular activation has previously been utilized in an acid-free synthesis of 3-carboxyrhodamines.²⁸

We asked whether 2-phosphonobenzaldehyde, **1**, would also exhibit this behavior. Unlike 2-carboxybenzaldehyde **1** exists solely in the open aldehyde form in DMSO-d₆ and D₂O. We

observe no sign of lactonization (**Scheme 1b**), suggesting the *ortho*-phosphonate is less nucleophilic than the carboxylate. Interestingly, in MeOD- d_4 we see predominant (95%) formation of the hemiacetal addition product **1a** and a trace amount of the lactonized form **1b** (**Scheme 1b**). We rationalized this conclusion through analysis of ^1H - ^{31}P and ^{13}C - ^{31}P coupling constants (**Table S1**). The acetal proton of **1a** is a singlet, compared to the doublet ($J_{\text{H-P}} = 13\text{Hz}$) observed for **1b** consistent with through-bond coupling (**Spectrum S10**), and the acetal ^{13}C of **1a** had a J-coupling constant comparable to that observed with aldehyde **1** ($J_{\text{C-P}}$ 3.6 Hz and 3.8 Hz respectively), further affirming the relative proximity of the ^{31}P (**Spectrum S12**).

Intrigued by the predominance of the hemiacetal, we rationalized that the *ortho*-phosphonate of **1** must provide excellent intramolecular aldehyde activation and to a greater degree than the analogous *ortho*-carboxylate. We therefore envisioned a synthetic strategy towards 3-phosphonorhodamines that would negate the need for harsh acidic conditions and possibly alleviate the commonly encountered challenges with xantheno fluorophore chemistry such as low yields and troublesome purifications.

Acid-free Friedel Crafts condensations of 3-phosphonorhodamines



Scheme 2. Proposed stepwise formation of triarylmethane intermediate **9**.

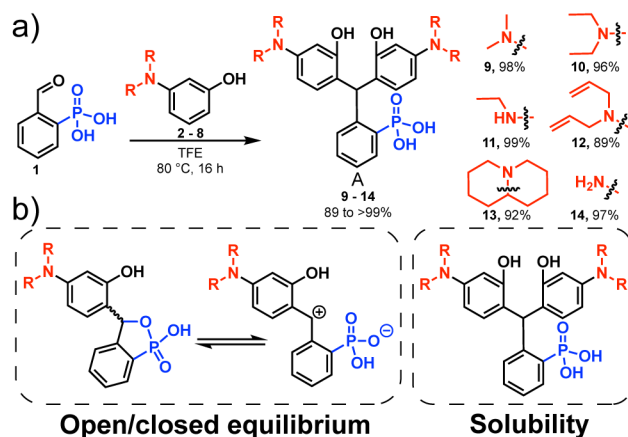
Since the role of strong acid in the Friedel-Crafts condensations of xantheno fluorophores, such as rhodamines, is to activate the aldehyde to promote nucleophilic attack, we hypothesized that the strong intramolecular activation observed with 2-phosphonobenzaldehyde may be sufficient to preclude the need for exogenous acid. We find this is the case. In fact, heating of **1** with 3-(dimethylamino)phenol, **2**, in 2,2,2-trifluoroethanol (TFE) results in clean precipitation of triarylmethane **9** in an excellent 98% yield. Considering the stepwise formation of **9**, we hypothesize the intramolecular activation of **1** is more than sufficient to promote the Friedel-Crafts with **2** to form the corresponding single addition intermediate (**Scheme 2**). This intermediate likely exists as an equilibrium between the lactonized, closed form and open zwitterionic form, and stabilization of the latter would promote reactivity with a second equivalent of aminophenol to yield **9**. In the analogous reaction with 2-carboxybenzaldehyde it was reported that the high ionizing power, low nucleophilicity, and hydrogen bond donating ability of fluorinated alcohols such as TFE were vital for promoting reactivity of the benzylhydrylium intermediate.²⁸⁻³¹ While we observe the highest yields in the reaction between **1** and **2** in TFE, we also saw formation of **9** in methanol in moderate yield (up to 58%, **Scheme 3**, **Table 1**). We attribute this increased reactivity to the greater extent of intramolecular activation of aldehyde **1** and the low pK_a of the phosphonate contributing to stabilization of the open zwitterionic intermediate. We also hypothesize that the electron donating ability of the aniline also plays an important contribution to stability of the open zwitterion intermediate (**Scheme 2**) since reaction between **1** and resorcinol stalls at the single addition, after the initial Friedel-Crafts reaction.

To examine the generalizability of this chemistry we exposed aldehyde **1** to a series of anilines, **2** to **8**, under the same conditions (TFE, 80 °C, 16 hours) and observe precipitation of

triarylmethanes **9** to **15** in excellent yields, ranging from 89 to 99% (**Table 1**). Upon performing this chemistry under more mild conditions (methanol at room temperature) we see a direct correlation between the electron donating ability of the aniline and reactivity, as evident in the increasing yields from 22% to 27% to 65% for **9**, **10** and **13** respectively. This further supports our hypothesis that the second Friedel-Crafts is the rate limiting step and thus stabilization of the zwitterionic intermediate has a large influence on reaction rate.

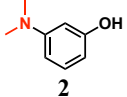
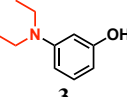
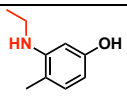
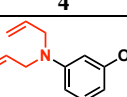
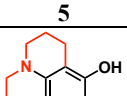
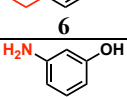
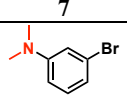
Additionally, we attribute the exceptional yields of **9** to **15** to their insolubility in alcoholic solvents. Friedel-Crafts condensations are reversible, as evidenced by the degradation of the triarylmethane intermediates in the presence of acid.³² Precipitation from the reaction medium therefore drives reaction progression and contributes to the near quantitative yields. The increased hydrophobicity of triarylmethane **13** at elevated temperatures led to slight oxidation to the corresponding rhodamine, diminishing yield of the triarylmethane and complicating purification. We find in these cases performing the reaction under an inert atmosphere is important to prevent oxidation and maximize the yield of the triarylmethane.

Substitution of rhodamine anilines for 4-membered azetidines rings is an effective method for improving the brightness and photostability of rhodamine fluorophores.^{5,33} We wondered whether our acid-free condensation would provide a mild route to 3-phosphono JaneliaFluor derivatives. Despite the apparent generalizability, reaction of **1** with azetidines-containing aniline **S2-1** results in precipitation of an insoluble solid, which we were unable to characterize by ¹H NMR, on account of exceedingly poor solubility (**Scheme S1**). The ring strain of 4-membered rings render azetidines prone to cationic ring opening polymerization, particularly in alcoholic solvents.³⁴ We hypothesize the acidic nature of phosphonobenzaldehyde **1** is sufficient to facilitate formation of the azetidinium salt and initiate the polymerization process. Unfortunately, we even observe polymerization at room temperature.



Scheme 3. (a) an acid free synthesis of phosphonated triarylmethane rhodamine precursors and (b) factors that influence reactivity.

Table 1. Synthesis of triarylmethanes and optimization of reaction conditions.

Aniline	Compound A	Conditions	Yield ^a
 2	9	TFE, 80 °C, 16 h ^b MeOH, 60 °C, 16 h MeOH, rt, 16 h	98% 58% 22%
 3	10	TFE, 80 °C, 16 h MeOH, rt 16 h	96% 27%
 4	11	TFE, 80 °C, 16 h	99%
 5	12	TFE 80 °C, 16 h ^b	89%
 6	13	TFE, 80 °C, 16 h ^b MeOH, rt, 16 h	92% 65%
 7	14	TFE, 80 °C, 16 h	97%
 8	15	TFE, 80 °C, 16 h ^b MeOH, 60 °C, 16 h	93% 54%

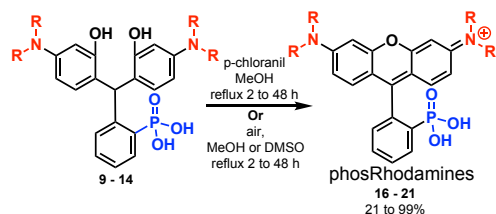
^a isolated yields. ^b for best results, reactions were performed under a nitrogen atmosphere.

After isolating triarylmethane intermediates **9** to **14** isolated in high yields and purity, without the need for any chromatography or crystallization, we next examined conditions for the oxidation to the corresponding 3-phosphonorhodamines **16** to **21** (Scheme 4). In most cases, reflux in methanol with p-chloranil as an oxidant leads to cyclization and oxidation to the corresponding rhodamine. As oxidation to the rhodamines occurs, solubility in methanol increases and so reaction progression can be easily monitored by the dissolution of visible particulates; reaction times vary from 2 to 48 hours and depended on the volume of methanol used. Upon completion, filtration removes any unoxidized fluorophore and trituration with organic solvent to remove excess chloranil yields rhodamines **16** to **19** in excellent yields (Table 2) without need for further purification.

Notably substrates **13** and **14** are sensitive to chloranil oxidation leading to decomposition, possibly a result of the nucleophilic anilines of **14** and electron rich nature of **13**. Instead, reflux in methanol or DMSO with exposure to air is sufficient to promote oxidation to rhodamines **20** and **21** respectively, however these methods are less efficient and require purification by reverse phase silica chromatography. The oxidation to phosRho110, **21**, is particularly low yielding, owing to the limited solubility of the fluorophore and tricky purification. Conversely, tetraallyl rhodamine **19** can be synthesized in an overall 83% yield (2 steps) so we postulated whether we could access **21** through de-allylation of **19** (Scheme S2).

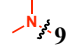
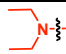
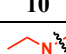
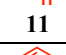
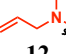
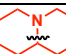
The acidic nature of N,N-dimethylbarbituric acid (NDMBA) makes it uniquely suited for deprotonation by basic amines. NDMBA has therefore found wide use as an allyl scavenger in the Pd-catalyzed de-allylation of allylic amines.³⁵ Treatment of **19** with NDMBA and Pd(PPh₃)₄,

however, affords no reaction (**Table S2, entry A**) and we hypothesize the dissipated positive charge of rhodamines renders the anilines insufficiently basic. Addition of triethylamine however, results in conversion to the desired deallylation product phosRho110, **21** that can be isolated in 52% yield (**Table S2, entry B**). Rhodamine anilines are sufficient leaving groups that do not require activation and, in this regard, behave more like allylic alcohols. We therefore explored common allyl ether Pd-catalyzed deallylation conditions using K_2CO_3 and methanol,³⁶ and while we do observe deallylation, the reaction is sluggish and requires heating for 72 hours to attain reasonable conversion to **21** (**Table S2, entry C**). The crude isolate contained a mixture of de-allyl intermediates. Since the reaction is a heterogenous mixture, we hypothesize the inefficient conversion can be attributed to precipitation of various de-allyl intermediate salts. Future optimization should focus on screening other nucleophile / solvent systems. Allylic ethers can also under go deallylation by first isomerizing to the corresponding enyl ether followed by acid hydrolysis.^{37,38} Heating of **19** with $tBuOK$ in DMSO resulted in a rapid color change and upon addition of aqueous hydrochloric acid (1 M) we observe rapid and quantitative conversion to **21** by analytical HPLC. We were surprised that isomerization of **19** to the corresponding enyl-imminium was able to undergo hydrolysis and this process warrants further mechanistic investigation. This route provides **21** in 71% yield after reverse phase silica chromatography (**Table S2, entry D**).



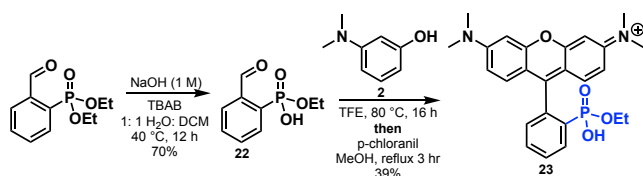
Scheme 4. Oxidation of triarylmethane precursors to phosrhodamines.

Table 2. Oxidation conditions for phosrhodamines.

Triarylmethane	Rhodamine	Yield B ^a	Conditions
 9	16 , phosTMR	99%	<i>p</i> -chloranil, MeOH, reflux, 2-48 h
 10	17 phosRhoB	80%	<i>p</i> -chloranil, MeOH, reflux, 2-48 h
 11	18 , phosRho6G	82%	<i>p</i> -chloranil, MeOH, reflux, 2-48 h
 12	19 phosTAR	93%	<i>p</i> -chloranil, MeOH, reflux, 2-48 h
 13	20 phosJulR	48% ^b	MeOH, reflux, 48 h
 14	21 phosRho110	21% ^{b,c}	DMSO, 100 °C, 12 h

^a isolated yields. ^b after reverse phase silica chromatography. ^c **21** is also accessible by deallylation of **19** in up to 71% yield.

The intramolecular activation provided by the ortho phosphonate (**1**) is fundamental to our ability to access triarylmethane intermediates **9** to **15** in such high yields, and we aimed to explore the scope of this activation further. In particular phosphonic acids have two pK_{as} ($pK_{a1} \sim 1$ to 2 and $pK_{a2} \sim 7$ to 8)³⁹ and we were curious whether an ortho phosphonate monoester would still be capable of providing intramolecular activation for access to functionalized 3-phosphonorhodamines. Hydrolysis of diethyl (2-formylphenyl) phosphonate with aqueous NaOH provides phosphonate monoester **22** in 70% yield (**Scheme 5**). Condensation with **2** followed by chloranil oxidation affords rhodamine **23** in 39% yield with the ethyl ester intact (**Scheme 5**). Importantly the strongly acidic conditions typically required for these condensations would result in phosphonate ester hydrolysis and thus the direct condensation to **23** is a testament to the mild nature of this chemistry and the tolerance of substrates containing acid sensitive functionalities.



Scheme 5. Direct condensation to a functionalized phosTMR.

We have disclosed a relatively generalizable, acid-free synthesis of 3-phosphonorhodamines in exceptional yields. The scalability and the ease of purification of these fluorophores, given the high polarity, presents an exciting opportunity for the development of new fluorescent probes and chemical exploration of the rhodamine scaffold. We highlight that the intramolecular activation provided by the phosphonate is fundamental to the high performance of this chemistry. While we note 2-carboxybenzaldehyde also provides intramolecular activation, reaction with **2** under the same conditions produced carboxyTMR in only 31% yield, after chromatography (**Supporting Info**), more than a 3-fold decrease in the yield of phosTMR, **16**. We propose the lower pK_a of arylphosphonates to be the primary reason for this difference. On the other hand, 2-sulfonobenzaldehyde did not produce sulfoTMR under these conditions, suggesting the pK_a of the arylsulfonic acid is too low and therefore has no proton to activate the aldehyde. As such, sulfoTMR was synthesized by heating with **2** in neat methanesulfonic acid in just 12% yield (**Supporting Info**).

Spectroscopic characterization

To examine the influence of 3-phosphonate substitution on the photophysical properties of rhodamines, we examined the spectroscopic properties of phosTMR, **16** and the ethyl ester analog phosTMR.OEt, **23** in comparison to sulfoTMR and carboxyTMR (**Table 3, Figure 1a-d**). In line with our observations of 3-phosphonofluoresceins,¹⁶ phosTMR displays a slight hypsochromic shift absorbing at 546 nm and emitting at 564 nm, relative to carboxyTMR (549/ 569 nm) in phosphate buffered saline (PBS, pH 7.4). On the other hand, phosTMR.OEt has a slight bathochromic shift in absorbance and identical emission (551/ 569 nm) to carboxyTMR. SulfoTMR absorbs at 556 nm and emits at 574 nm. With a maximal 10 nm difference among the series, 3-substituents have little effect on the spectral profiles of tetramethylrhodamines. The slight differences can be accounted for by inductive differences of the pendant ring that arise from these substitutions. Extinction coefficients and quantum yields also display little variance in response to

3-substitution owing to the maintained orthogonality of the xanthene chromophore and pendant rings.

In the context of fluoresceins, 3-substitution brings about modest changes in water solubility; substitution of the 3-carboxylate with a phosphonate results in a ~2-fold increase in solubility and a 3-fold increase when substituted with a sulfonate.¹⁶ Rhodamines are notoriously more hydrophobic than fluoresceins and their limited water solubility or tendency to aggregate in solution can impede subsequent biological applications.⁴⁰ In fact, development of rhodamines with improved solubility is highly desirable for applications where removal of residual fluorophore is important to improve contrast in applications such as protein labelling or in next generation sequencing.^{41–43} Remarkably we observe a 12.3 fold increase in solubility of phosTMR in PBS relative to carboxyTMR and a 50 fold decrease in solubility of sulfoTMR (**Table 3, Figure S1**). Whereas fluorescein solubility correlates well with the 3-functionality pK_a, relative solubility of rhodamines appear more nuanced exhibiting order of magnitude differences. Without the negative phenolate of fluoresceins, 3-substituents of rhodamines appear to have a greater impact on relative solubility. The zwitterionic nature of rhodamines possibly accounts for large differences in solution enthalpies arising from ionic interactions between the 3-substituent and rhodamine core. Ultimately, we report a phosTMR has a solubility of 5.3 mg/L in PBS compared to approximately 0.4 mg/mL for 67arboxyTMR.

Rhodamine fluorophores are relatively unstable and undergo degradation over time, both in solution and as solids, impeding their use in long imaging experiments or long-term storage. To test the stability, phosTMR and carboxyTMRs were stored as solid powders under identical conditions for 1 year (at room temperature, 15-22 °C, in the dark). Traditional carboxyTMR decomposed into a complex mixture of compounds, resulting, in part from aniline demethylation products (**Figure S2**). On the other hand, phosTMR remarkably showed no signs of any degradation (**Figure S3**). We envision this improved stability will be useful in long term storage of 3-phosphonorhodamines preventing the need for frequent resynthesis or costly storage conditions such as -80 °C freezers.

We next sought to probe the spectral sensitivity of tetramethylrhodamines in response to pH. The absorbance intensity of carboxyTMR, phosTMR, phosTMR.Oet and sulfoTMR are all insensitive to pH changes between pH 2 and 10. We observe 3.5 nm and 8 nm hypsochromic shifts for carboxyTMR and phosTMR respectively in response to decreasing pH (**Figure 1e, f**). We attribute this shift to protonation of the 3-substituent resulting in slight inductive differences of the pendant ring. Fitting of these changes to non-linear sigmoidal curves determined a 3-carboxylate pK_a of 3.4 and 3-phosphonate pK_{a2} of 7.3. We expect the pK_as of phosTMR.Oet and sulfoTMR to be outside of this pH range (<2) and therefore we observe no shift in absorbance wavelength with these fluorophores.

Additionally, we performed spectral characterization of all the novel 3-phosphono rhodamines that were synthesized, **16 – 23 (Table 3)**. As expected, alkylation pattern of the anilines results in spectral finetuning of the absorption and emission wavelengths ranging from 495/ 515 nm (**21**) to 573/ 591 nm (**20**). The absorption intensity of all 3-phosphonorhodamines are insensitive to pH (between 2 and 10) and had phosphonate pK_{a2} values ranging between 7.2 and 7.6 (**Figure S4a-r**).

Table 3. Properties of rhodamines.

Rhodamine	$\lambda_{\max}/\text{nm}^a$	$\lambda_{\text{em}}/\text{nm}^a$	$\epsilon / \text{M}^{-1}\text{cm}^{-1}{}^{a,b}$	Φ^a	Relative solubility ^c
carboxyTMR	549	569	78,000	0.45	1.0
sulfoTMR	556	574	73,000	0.46	0.02
phosTMR, 16	546	564	70,000	0.52	12.3
phosRhoB, 17	553	570	75,000	0.38	-
phosRho6G, 18	520	539	76,000	0.95	-
phosTAR, 19	540	559	53,000	0.68	-
phosJulR, 20	573	591	91,000	0.99	-
phosRho110, 21	495	515	76,000	0.98	-
phosTMR.OEt, 23	551	569	78,000	0.51	-

^a measured in PBS. ^b at maximum absorption. ^c measured in PBS relative to carboxy TMR (see SI).

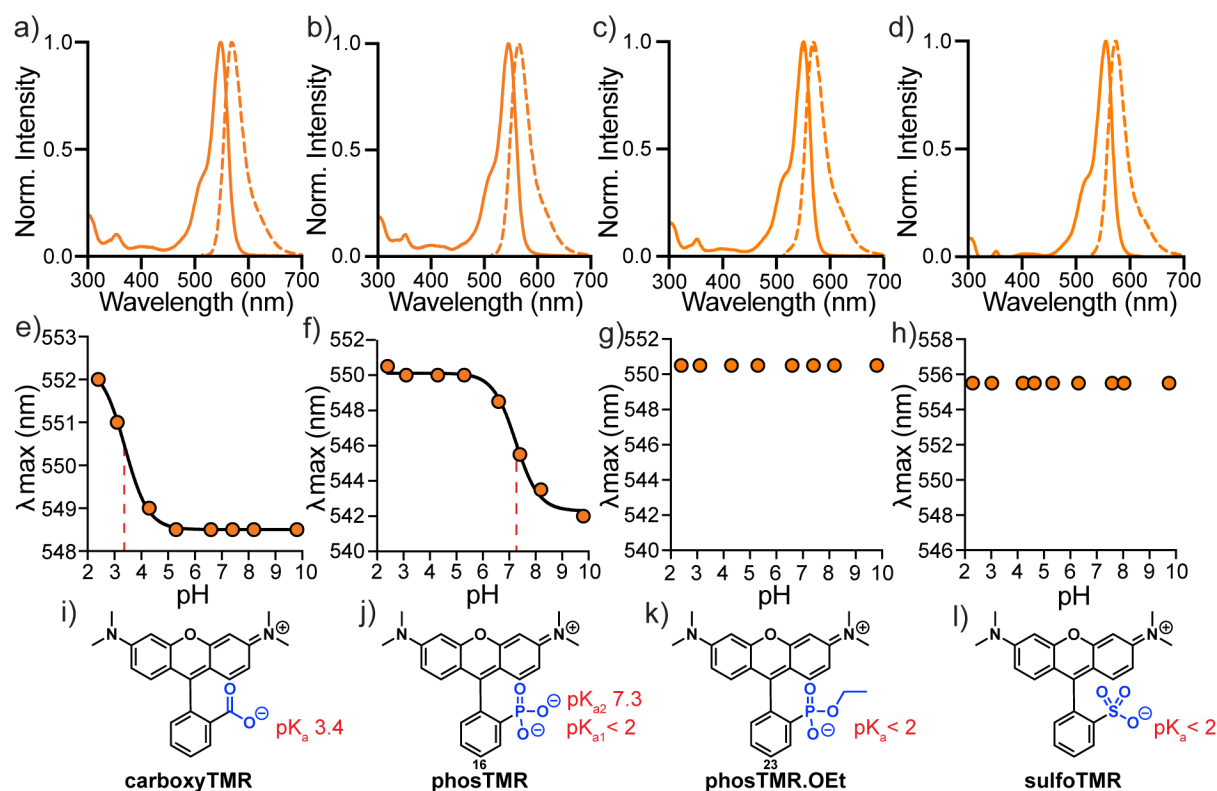
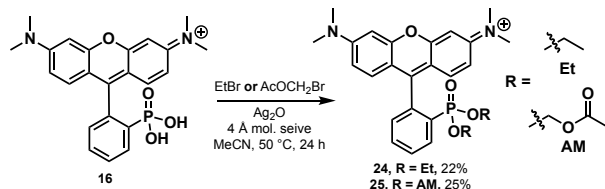


Figure 1. Spectroscopic characterization of tetramethylrhodamines. Normalized absorbance and fluorescence spectra (a-d) in PBS, plots of λ_{\max} vs pH (e-h) and corresponding chemical structures (i-l) for carboxyTMR (a, e, i), phosTMR (b, f, j), phosTMR.OEt (c, g, k) and sulfoTMR (d, h, l). pH titrations were performed in 10 mM buffered solutions (see SI) containing 150 mM NaCl ranging from pH 2.3 to 9.8 at a final dye concentration of 2 μM . Where applicable titration curves were fit to sigmoidal dose response curves (solid black) to enable pKa determination (dashed red). Determined pKa values are reported next to chemical structures (i-l).

Cellular localization



Scheme 6. Synthesis of functionalized 3-phosphonoTMRs.

Biologically labile acetoxy methyl (AM) esters are commonly used to mask anionic functionalities, such as phosphonates, to facilitate cell permeability.^{44,45} We previously harnessed this strategy to deliver 3-phosphonofluoresceins into cells, where hydrolysis by intracellular esterases releases the phosphonic acid, trapping the fluorophore in the cytosol.¹⁶ We wondered whether a similar strategy could be exploited to deliver phosTMRs into cells. Unlike fluoresceins, rhodamines don't possess nucleophilic phenols on the xantheno core and so we also envisioned capping phosTMRs with non-biologically labile functionalities, such as ethyl esters.

Treatment of phosTMR **16** with either ethyl bromide or bromomethyl acetate in the presence of Ag(I) in MeCN yields esterified phosTMRs **24** and **25** in 22% and 25% yield respectively (**Scheme 6**). Acetoxymethyl esters are prone to hydrolysis by cellular esterases, and upon *in vitro* incubation with Porcine Liver Esterase (PLE), both carboxyTMR AM and phosTMR AM, **25** show complete hydrolysis to the corresponding carboxyTMR and phosTMR (**Figures S5 and S6**). Surprisingly, upon incubation in HBSS for 2 hours in the absence of any esterase, carboxyTMR AM shows slight hydrolysis, and phosTMR AM shows about ~50% hydrolysis to the phosphonate monoAM ester (**Figures S5 and S6**). This highlights a degree of hydrolytic instability of the acetoxymethyl esters that may impede future imaging applications, such as cell permeability. On the other hand, phosTMR.2OET, **24** is stable in HBSS showing no sign of hydrolysis after 2 hours, and is also stable when incubated with PLE, suggesting phosphonate esters are less prone to hydrolysis by esterases that specifically target carboxylate esters (**Figure S7**).

Unsurprisingly, **16** is cell impermeable on account of the free phosphonic acid (**Figure 2a**). Zwitterionic **23**, bearing a phosphonate monoester is also cell impermeable (**Figure 2b**), highlighting the ability for a single negatively charged functionality to preclude passage through cellular membranes. Cell-permeable rhodamines such rhodamine 123 localize to mitochondria due to their net positive charge.⁶ Diethyl ester phosTMR **24** also exhibits mitochondrial localization (**Figure 2c**) as confirmed by colocalization with Mitotracker Green™ (**Figure S8**). On the other hand, phosTMR AM **25** displays more cytosolic localization (**Figure 2d**) and we propose this difference stems from intracellular AM hydrolysis yielding phosTMR with a net negative charge (pK_{a2} 7.3). In contrast, carboxyTMR AM appears to retain significant mitochondrial localization (**Figure S9**) and we hypothesize the greater charge density of phosTMR vs. carboxyTMR (net negative vs. net neutral at pH 7.4) accounts for the difference in localization. phosTMR AM also displays excellent cellular retention (**Figure S10a-c, g**) where serial washing of stained cells showed no decrease in fluorescence intensity. On the other hand, after 3 washes we observed a 40% decrease in mitochondrial fluorescence intensity of cells stained with carboxyTMR AM (**Figure S10d-f, g**), suggesting the additional negative charge provided by a 3-phosphonate enhances the inability of rhodamines to pass through cellular membranes. We highlight that not only is the cell permeability profile of phosTMRs tunable by phosphonate functionality, but so is intracellular localization. We envision that tunable localization of rhodamines may have

implications on the subsequent applications of 3-phosphonorhodmaines such as potentially improving labelling efficiency of cytosolic structures.

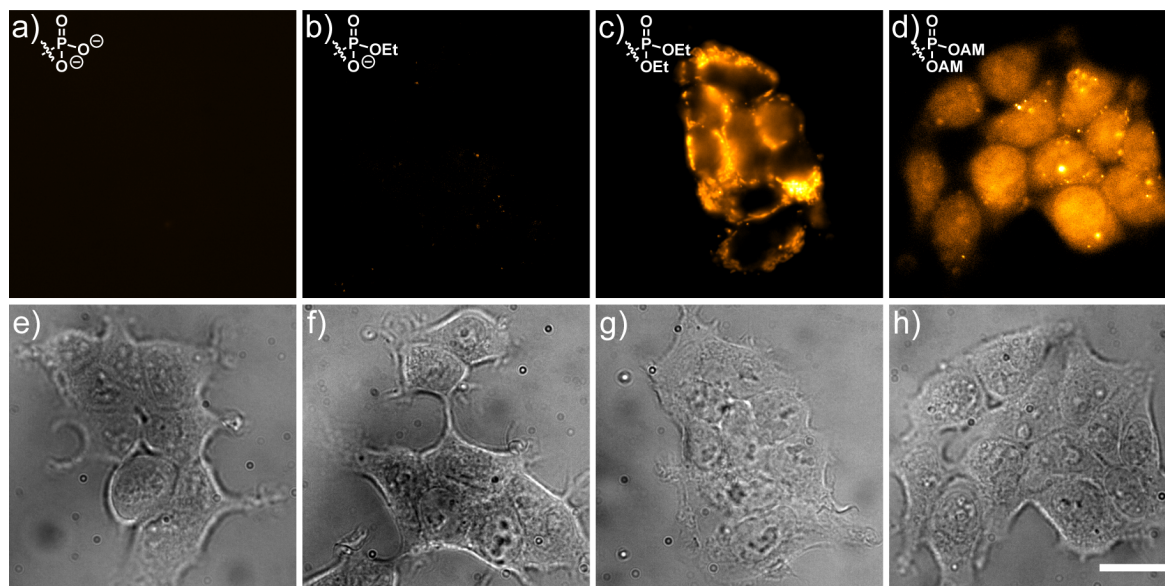
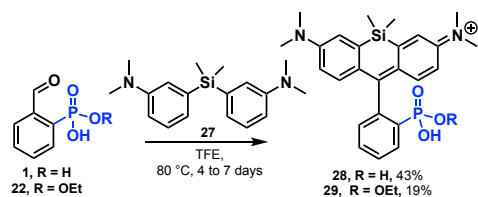


Figure 2. Tunable localization of 3-phosphonoTMRs. Widefield fluorescence (a-d) and DDIC (e-h) images of HEK293T cells stained with 500 nM in HBSS **16** (a, e), **23** (d, f), **24** (c, g) and (d, h) for 20 min at 37 °C. Coverslips were placed into fresh HBSS prior to imaging. Scale bar is 20 μ M.

Synthesis of phosSiRs.



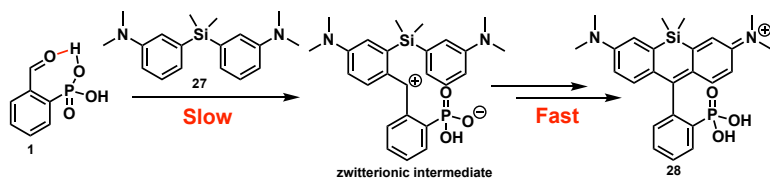
Scheme 7. Synthesis of phosSiRs.

Given the interesting properties of 3-phosphonofluoresceins and rhodamines, we next sought to expand this functionality to red-shifted members of the xanthene fluorophore family. In particular, 10' substitution with dimethylsilane is accompanied by a \sim 100 nm red-shift relative to oxygen substituted counterparts, yielding a new class of fluorophore, silicon-rhodamines (SiRs).⁹ SiRs have highly attractive properties and have found widespread use in a variety of biological applications such as fluorogenic labelling,^{46–48} far-red voltage sensing,⁴⁹ in vivo imaging,^{33,50} and super resolution microscopy.⁵¹

Synthetic approaches to silicon rhodamines have primarily involved organometallic additions or Pd-cross coupling with the ditriflate analogs of silicon fluoresceins and suffer from harsh conditions, lack generalizability or are low yielding.^{5,11} 3-carboxy silicon rhodamines have also been synthesized through Friedel Crafts condensations between 2-carboxybenzaldehydes and diaryl silyl ethers but employ high temperatures and require catalysts, such as CuBr_2 due to low reactivity.⁵² Furthermore these condensations are limited by their low yields and lack of scalability. We wondered whether the intramolecular activation provided by 2-phosphonobenzaldehydes that

provided such successful syntheses of 3-phosphonorhodamines could be expanded to 3-phosphonoSiRs.

Bisphenyldimethyl silane, **27**, can be synthesized in 91% yield via lithiation of 3-bromo-N,N-dimethylaniline, followed by addition of dimethyldichlorosilane (**Supporting Info**). The rate limiting step in our synthesis of 3-phosphonorhodamines (10' oxygen) is the second intermolecular Friedel-Crafts addition of an aniline into the open zwitterionic intermediate (**Scheme 2**). In the case of **27**, the second aniline is preinstalled, and we therefore hypothesized that the intramolecular nature of the second addition into the corresponding zwitterionic intermediate would, in comparison, provide a kinetic advantage (**Scheme 8**). To our surprise, condensation between 2-phosphonobenzaldehyde **1** and **27** is exceedingly slow and requires refluxing in TFE for 7 days to isolate phosTMSiR, **28** in 43% yield (**Scheme 7**). We highlight the comparable yields and scales that have been reported for 3-carboxy SiR condensations.⁵² Additionally, we highlight this synthesis of 3-phosphono SiRs does not require any catalyst or heating under high pressures as is required for 3-carboxy SiRs.⁵² When monitoring the reaction progression by HPLC and NMR we observe only the presence of starting reagents **1** and **27** and the corresponding SiR **28**, with no trace of the expected condensation intermediates. In this case, the initial Friedel-Crafts condensation step must be rate limiting, with the second addition and subsequent oxidation to **28** occurring fast in comparison. Despite the intramolecular activation provided by the ortho-phosphonate, we hypothesize the sterics of the dimer **27** impedes addition into the aldehyde and accounts for the slow reaction kinetics. To improve the rate, we increased temperature and pressure, performing the condensation at 130 °C in a sealed flask and are able to isolate **28** in 29% yield after just 24 hours (**Table S3**). Despite the apparent improvement in kinetics, under these conditions we also observe small amounts of aniline demethylation and formation of the trifluoroethyl phosphonate ester adduct of **28**, which makes purification more intricate. Overlooking the long reaction time required by our initial conditions, the purification of **28** is relatively facile; after trituration with organic solvent **1** and **28** are easily separated by reverse phase silica chromatography. Under the same conditions we can also isolate the phosphonate ethyl monoester analog phosTMSiR.OEt, **29** in 19% yield after 4 days (**Scheme 7**).

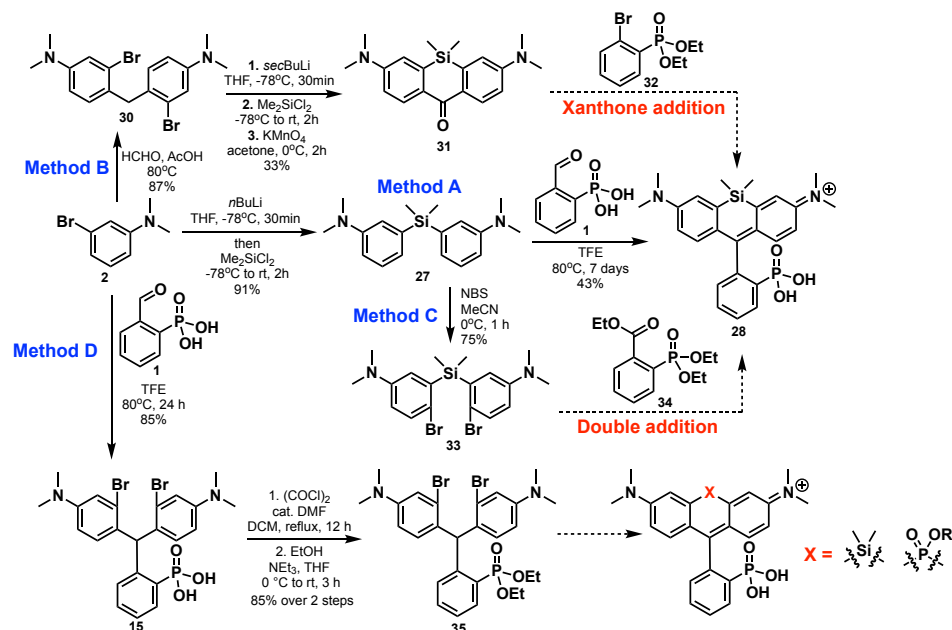


Scheme 8. Proposed stepwise formation of **28** and relative kinetics.

This acid free condensation (**Scheme 9, method A**) provides a mild, moderately yielding route to 3-phosSiRs and we also highlight the compatibility of this method with halogen-containing benzaldehydes to provide a handle for further derivatization (**Chapter 3**). On the other hand, the evidently long reaction times and incompatibility with azetidino-containing bisarylsilanes encouraged us to consider complimentary synthetic strategies. Perhaps the most established route to SiRs involves installation of the pendant ring by addition of a metalated aryl species into a silicon-xanthone.^{5,47,48,53,54} Xanthone **31** (**Scheme 9, method B**) can be synthesized from 3-bromo-N,N-dimethylaniline in 29% yield (4 steps). Aryl phosphonate **32** can be synthesized by Pd-catalyzed Arbuzov of 2-bromo-iodobenzene in 71% yield (**Scheme S3a**) and we envisioned transmetalation could provide a viable nucleophile for addition into xanthone **31**. It has been noted that the electron rich nature of these xanthone electrophiles, and electron poor

nature of the aryl nucleophile creates an electronic mismatch that can result in low yields and often calls for the use of forceful transmetalation reagents such as *tert*-BuLi.¹¹ Inspired by Lavis' and Spars' synthon reversal, we envisioned another route (**Scheme 9 method C**) in which dibrominated bisphenyldimethylsilane **33** could instead undergo transmetalation and addition into an electrophile such as ester **34** to install the phosphonate containing pendant ring.^{11,55} Several reports of SiRs have been synthesized in this manner, allowing for the use of more mild transmetalation reagents, such as Grignard reagents, but often require some degree of optimization or screening.^{11,55} Notably, **34** can be synthesized by Pd-catalyzed Arbuzov of 2-iodobenzoic acid, in which the carboxylic acid also undergoes Arbuzov with excess triethylphosphite resulting in *in situ* formation of the ethyl ester in tandem with phosphonate installation (**Scheme S3b**).

Our overarching goal is to expand 3-phosphonate functionality to the entire family of rhodamine fluorophores, coupling the unique properties of phosphonates with the full spectrum of colors available through 10' substitution. While early-stage 10' heteroatom incorporation can be a strain on subsequent synthetic steps, we envisioned late-stage incorporation of 10' heteroatoms from a common intermediate (**Scheme 9, method D**) could be a highly desirable synthetic improvement. Condensation of aldehyde **1** with 3-bromo-N,N-dimethylaniline provides dibromo-triarylmethane **15** (**Table 1, Scheme 9**) in 85% yield in up to 1g quantities. We imagined making use of the dihalogen handles for lithiation and installation of 10' functionalities as inspired by the synthesis of silicon anthracenes.⁹ Lithiation of **15** with *sec*-BuLi (4 eq) was unsuccessful, likely due to the insolubility of the corresponding tetra-anion in organic solvent, and we therefore decided to protect the phosphonate. Alkylation attempts with ethylbromide resulted in competing alkylation of the anilines, forming the undesired ammonium salts. As an orthogonal protection strategy, reflux of **15** with oxalylchloride in DCM affords the phosphonyldichloride that, due to instability on exposure to air, must be immediately converted to the phosphonate diethyl ester **35** in 85% yield (2 steps). Owing to the instability of triarylmethane intermediates, **35** can be difficult to handle as it is prone to undergo retro Friedel-Crafts to the corresponding 2-phosphonobenzaldehyde on exposure to silica gel. Future efforts should focus on optimizing the purification of this intermediate and screening conditions of subsequent heteroatom incorporation.



Scheme 9. Synthetic methods towards 3-phosphono SiRs.

Spectroscopic characterization of phosSiRs

In acidic EtOH (0.1% TFA) phosTMSiR, **28** absorbs at 652 nm and emits at 670 nm (**Table 4, Figure S11**), demonstrating a 100 nm redshift in both absorption and emission relative to its oxygen substituted counterpart, phosTMR (λ_{\max} 552 nm, λ_{em} 570 nm). We also observe an almost two-fold increase in extinction coefficient, consistent to what is associated with dimethylsilane substitution.⁹ Quantum yields also exhibit almost no variance in response to 3-substitution and are comparable to 10' oxygen substituted counterparts (**Table 4**).

Substitution of the 10' position with silicon shifts the equilibrium of xanthene dyes from the open zwitterion (Z) towards the non-fluorescent closed lactone (L) relative to oxygen substituted rhodamines.¹ This equilibrium (K_{L-Z}) is an important property where the lactonization propensity of SiRs has found useful applications in fluorogenic labelling, super resolution microscopy and improving cell permeability.^{48,56} On the other hand, there are instances where lactonization is prohibitive, such as in facilitating membrane localization of voltage sensing fluorophores.⁴⁹ It is therefore important to fully characterize this equilibrium to guide any future applications of phosSiRs.

SiRs predominantly favor the open zwitterion form (Z) in acidic ethanol. Absorbance in this medium can be used as a proxy for the maximum extinction coefficient, ϵ_{\max} .^{11,33} 3-carboxyTMSiR has a reported ϵ_{\max} of 140,000 M⁻¹cm⁻¹ but demonstrates an almost five-fold decrease in absorbance in aqueous buffer (ϵ_{PBS} 28,000 M⁻¹cm⁻¹), preferentially adopting the L form at physiological pH.¹¹ In contrast, 3-sulfonate substitution, Berkeley Red, exhibits a much lower propensity for lactonization as demonstrated by the almost identical extinction coefficients in ethanol and buffer (**Table 4**, ϵ_{\max} 160,000 M⁻¹cm⁻¹ and ϵ_{PBS} 158,000 M⁻¹cm⁻¹, **Figure S12c**). We hypothesize the significantly lower pK_a of aryl sulfonates is responsible for this shift in equilibrium. phosTMSiR, **28**, on the other hand demonstrates an ϵ_{\max} of 135,000 M⁻¹cm⁻¹ but a 2.4-fold decrease in PBS (ϵ_{PBS} 56,000 M⁻¹cm⁻¹) suggesting a 60% preference for the closed lactone at physiological pH (**Table 1, Figure S12a**). This is interesting as 3-phosphonofluoresceins and 3-phosphonorhodamines did not demonstrate propensity to lactonize. We can also empirically measure the L-Z equilibrium constant ($\text{Log}K_{L-Z}$) by comparing the maximum absorption with the absorption in a 50% dioxane/water mixture (**Supporting Info**). Berkeley Red has a $\text{Log}K_{L-Z}$ value of 2.0 whereas **28** has a significantly lower $\text{Log}K_{L-Z}$ value 0.1 (**Table 4**).

Since the pK_a of the 3-substituent appears to have a large influence on L-Z equilibrium, we were curious to probe the difference between SiRs with a free phosphonic acid, having two pK_as, and a phosphonate monoester with just a single pK_a. pTMSiR.OEt, **29** behaves more like Berkeley Red by having almost identical absorbance in EtOH and PBS (ϵ_{\max} 135,000 M⁻¹cm⁻¹ and ϵ_{PBS} 130,000 M⁻¹cm⁻¹) and a $\text{Log}K_{L-Z}$ of 1.5 demonstrating very little propensity to lactonize (**Table 1, Figure S12b**).

The spirocyclization of SiRs is known to be pH dependent so we titrated **28, 29** and Berkeley Red and monitored changes in absorbance and absorbance maxima between pH 2 and 10 (**Figure S13**). Indeed, we see a pH dependence in the absorption of **28**, with a pK_{cyc} of 7.1, indicating a ~60% preference for the lactonized form at physiological pH (**Figure S13a, c**). On the other hand, **29** and Berkeley Red absorbance is relatively insensitive to pH changes within this range (**Figure S13d, g**). As with oxygen substituted rhodamines, we can probe the pK_a of the 3-substituent by monitoring changes in absorption maxima with respect to pH, resulting from inductive differences from protonation/deprotonation. **28** demonstrates an ~8 nm hypsochromic shift in response to decreasing pH, indicating a phosphonate pK_{a2} of 8.0 (**Figure S13b, c**). The pK_{a1}s of phosphonates and sulfonate of all three fluorophores are lower than 2 given no further changes in absorption in

this pH range (**Figure S13b**). We therefore hypothesize the pK_{a2} of **28** is indicative to the propensity to spirocyclize.

We also probed the influence of solvent polarity on L-Z equilibrium by monitoring changes in absorption and absorbance maxima in dioxane-water mixtures (0 to 100% dioxane + 0.01% triethylamine).⁵⁷ **28** demonstrates an initial increase in absorption with respect to decreasing water content peaking at about 70% zwitterion preference (30% dioxane) before fully lactonizing as dioxane content further increased (**Figure S14a, b**). **29** absorbance is relatively insensitive to dielectric constant, persisting in the zwitterionic form in almost all solutions except 100% dioxane where we observe complete lactonization (**Figure S14d, e**). Berkeley Red also persists as the zwitterion with a slight decrease in absorption in high dioxane content mixtures (>80% dioxane) (**Figure S14g, h**). In all cases we observe an interesting parabolic relationship between absorption and dioxane content (**Figure S14c, f, i**), indicating the effect of dielectric constant on the inductive effect of 3-functionalities.

Table 4. Properties of silicon 10' substituted rhodamines.

Rhodamine	10' substitution	3- substitution	λ_{max} / nm EtOH (PBS) ^a	λ_{em} / nm EtOH (PBS) ^a	ϵ / M ⁻¹ cm ⁻¹ EtOH (PBS) ^a	Φ ^b	Log K _{L-Z} ^c
phosTMR, 16	O	-PO ₃ H ₂	552 (546) nm	570 (564) nm	72,000 (70,000)	0.52	-
phosTMSiR, 28	SiMe ₂	-PO ₃ H ₂	652 (644) nm	670 (660) nm	135,000 (56,000)	0.51	0.1
phosTMSiR.OEt, 29	SiMe ₂	-PO ₃ HEt	655 (648) nm	671 (662) nm	135,000 (130,000)	0.52	1.5
Berkeley Red	SiMe ₂	-SO ₃ H	649 (652) nm	668 (668) nm	160,000 (158,000)	0.53	2.0

^a measured in EtOH +0.1% TFA (and PBS, pH 7.2). ^b measured in 100% ethanol ^c See supporting info.

Conclusions

In summary, we report a novel, mild, and acid-free synthesis of 6 new rhodamine fluorophores bearing 3-phosphonates. This chemistry is reliant on intramolecular aldehyde activation provided by the phosphonic acid functionality. Fluorophore construction is often the bottleneck in fluorescent probe development on account of complex chemistry and low yields and we envision the high yields and scalability of the reported 3-phosphonorhodamine syntheses will facilitate the development of fluorescent tools of increasing complexity. Characterization of 3-phosponoTMRs indicates that 3-substitution has minor influences on photophysical properties but provides an order of magnitude (12.3-fold) improvement in water solubility, a highly sought-after property of rhodamine fluorophores. The functionalizability of phosphonates has profound implications on the cellular permeability and sub-cellular localization of phosTMRs. We subsequently expanded 3-phosphonate substitution to 10' dimethylsilane substituted rhodamines with an accompanied 100 nm red-shifting in absorption and emission. Again, we demonstrate the profound implications phosphonate functionality has on the properties of rhodamines by controlling the lactonization equilibrium; phosTMSiR only exhibits 41% of its maximal absorbance at physiological pH whereas phosTMSiR.OEt exhibits >95%. We hope to expand 3-phosphonate substitution to the entire family of xanthene fluorophores, including rhodols and other 10' substitutions. We envision this expansion will further contribute to our ability to develop new chemical biology tools and provide avenues for new applications.

References

- (1) Lavis, L. D.; Raines, R. T. Bright Building Blocks for Chemical Biology. *ACS Chem. Biol.* **2014**, *9* (4), 855–866.
- (2) D. Lavis, L.; T. Raines, R. Bright Ideas for Chemical Biology. *ACS Chem. Biol.* **2008**, *3* (3), 142–155.
- (3) Beija, M.; Afonso, C. A. M.; Martinho, J. M. G. Synthesis and Applications of Rhodamine Derivatives as Fluorescent Probes. *Chem. Soc. Rev.* **2009**, *38* (8), 2410–2433.
- (4) Karstens, T.; Kobs, K. Rhodamine B and Rhodamine 101 as Reference Substances for Fluorescence Quantum Yield Measurements. *J. Phys. Chem.* **2002**, *84* (14), 1871–1872.
- (5) Grimm, J. B.; English, B. P.; Chen, J.; Slaughter, J. P.; Zhang, Z.; Revyakin, A.; Patel, R.; Macklin, J. J.; Normanno, D.; Singer, R. H.; et al. A General Method to Improve Fluorophores for Live-Cell and Single-Molecule Microscopy. *Nat. Methods* **2015**, *12* (3), 244–250.
- (6) Johnson, L. V.; Walsh, M. L.; Chen, L. B. Localization of Mitochondria in Living Cells with Rhodamine 123. *Proc. Natl. Acad. Sci. U. S. A.* **1980**, *77* (2 II), 990–994.
- (7) Grimm, J. B.; Sung, A. J.; Legant, W. R.; Hulamm, P.; Matlosz, S. M.; Betzig, E.; Lavis, L. D. Carborfluoresceins and Carborhodamines as Scaffolds for High-Contrast Fluorogenic Probes. *ACS Chem. Biol.* **2013**, *8* (6), 1303–1310.
- (8) Grimm, J. B.; Gruber, T. D.; Ortiz, G.; Brown, T. A.; Lavis, L. D. Virginia Orange: A Versatile, Red-Shifted Fluorescein Scaffold for Single- And Dual-Input Fluorogenic Probes. *Bioconjug. Chem.* **2016**, *27* (2), 474–480.
- (9) Fu, M.; Xiao, Y.; Qian, X.; Zhao, D.; Xu, Y. A Design Concept of Long-Wavelength Fluorescent Analogs of Rhodamine Dyes: Replacement of Oxygen with Silicon Atom. *Chem. Commun.* **2008**, No. 15, 1780–1782.
- (10) Hirabayashi, K.; Hanaoka, K.; Takayanagi, T.; Toki, Y.; Egawa, T.; Kamiya, M.; Komatsu, T.; Ueno, T.; Terai, T.; Yoshida, K.; et al. Analysis of Chemical Equilibrium of Silicon-Substituted Fluorescein and Its Application to Develop a Scaffold for Red Fluorescent Probes. *Anal. Chem.* **2015**, *87* (17), 9061–9069.
- (11) Grimm, J. B.; Brown, T. A.; Tkachuk, A. N.; Lavis, L. D. General Synthetic Method for Si-Fluoresceins and Si-Rhodamines. *ACS Cent. Sci.* **2017**, *3* (9), 975–985.
- (12) Egawa, T.; Koide, Y.; Hanaoka, K.; Komatsu, T.; CooTeraiper, T.; Nagano, T. Development of a Fluorescein Analogue, TokyoMagenta, as a Novel Scaffold for Fluorescence Probes in Red Region. *Chem. Commun.* **2011**, *47* (14), 4162–4164.
- (13) Chai, X.; Cui, X.; Wang, B.; Yang, F.; Cai, Y.; Wu, Q.; Wang, T. Near-Infrared Phosphorus-Substituted Rhodamine with Emission Wavelength above 700 Nm for Bioimaging. *Chem. - A Eur. J.* **2015**, *21* (47), 16754–16758.
- (14) Zhou, X.; Lai, R.; Jon Beck, ab R.; Li ab, H.; Stains, C. I. Nebraska Red: A Phosphinate-Based near-Infrared Fluorophore Scaffold for Chemical Biology Applications. *Chem. Commun* **2016**, *52*, 12290.
- (15) Liu, J.; Sun, Y. Q.; Zhang, H.; Shi, H.; Shi, Y.; Guo, W. Sulfone-Rhodamines: A New Class of near-Infrared Fluorescent Dyes for Bioimaging. *ACS Appl. Mater. Interfaces* **2016**, *8* (35), 22953–22962.
- (16) Turnbull, J. L.; Benlian, B. R.; Golden, R. P.; Miller, E. W. Phosphonofluoresceins: Synthesis, Spectroscopy, and Applications. *J. Am. Chem. Soc.* **2021**, *143* (16), 6194–6201.
- (17) Ceresole M. Ger. Pat. 44002, Nov 13, 1887.
- (18) Fu, M.; Zhang, X.; Wang, J.; Chen, H.; Gao, Y. Progress of Synthesis and Separation of Regioisomerically Pure 5(6)-Substituted Rhodamine. *Curr. Org. Chem.* **2016**, *20* (15), 1584–1590.
- (19) Ceresole, M. Verfahren Zur Darstellung von Farbstoffen Aus Der Gruppe Des Meta-Amidophenolphtaleins, 1887.
- (20) Mudd, G.; Pi, I. P.; Fethers, N.; Dodd, P. G.; Barbeau, O. R.; Auer, M. A General Synthetic Route to Isomerically Pure Functionalized Rhodamine Dyes. *Methods Appl. Fluoresc.* **2015**, *3* (4), 045002.
- (21) Deal, P. E.; Kulkarni, R. U.; Al-Abdullatif, S. H.; Miller, E. W. Isomerically Pure

- Tetramethylrhodamine Voltage Reporters. *J. Am. Chem. Soc.* **2016**, *138* (29), 9085–9088.
- (22) B. Grimm, J.; D. Lavis, L. Synthesis of Rhodamines from Fluoresceins Using Pd-Catalyzed C–N Cross-Coupling. *Org. Lett.* **2011**, *13* (24), 6354–6357.
- (23) Wu, L.; Burgess, K. Synthesis and Spectroscopic Properties of Rosamines with Cyclic Amine Substituents. *J. Org. Chem.* **2008**, *73* (22), 8711–8718.
- (24) Lukinavičius, G.; Umezawa, K.; Olivier, N.; Honigmann, A.; Yang, G.; Plass, T.; Mueller, V.; Reymond, L.; Corrêa Jr, I. R.; Luo, Z.-G.; et al. A Near-Infrared Fluorophore for Live-Cell Super-Resolution Microscopy of Cellular Proteins. *Nat. Chem.* **2013**, *5* (2), 132–139.
- (25) Grimm, J. B.; Brown, T. A.; Tkachuk, A. N.; Lavis, L. D. General Synthetic Method for Si-Fluoresceins and Si-Rhodamines. **2018**, *18*, 19.
- (26) Kagan, J. The Structure of Phthalaldehydic Acid. *J. Org. Chem.* **1967**, *32* (12), 4060–4062.
- (27) Rees, C. W.; Sabet, C. R. 107. Mechanism of the Reaction of Phthalaldehydic Acid with Indoles. Intramolecular Catalysis in Aldehyde Reactions. *J. Chem. Soc.* **1965**, *5499* (0), 680–687.
- (28) Dwight, S. J.; Levin, S. Scalable Regioselective Synthesis of Rhodamine Dyes. *Org. Lett.* **2016**, *18*, 5316–5319
- (29) Berkessel, A.; Adrio, J. A.; Hüttenhain, D.; Neudörfl, J. M. Unveiling the “Booster Effect” of Fluorinated Alcohol Solvents: Aggregation-Induced Conformational Changes and Cooperatively Enhanced H-Bonding. *J. Am. Chem. Soc.* **2006**, *128* (26), 8421–8426.
- (30) Bégué, J. P.; Bonnet-Delpon, D.; Crousse, B. Fluorinated Alcohols: A New Medium for Selective and Clean Reaction. *Synlett* **2004**, *2004* (1), 18–29.
- (31) Minegishi, S.; Kobayashi, S.; Mayr, H. Solvent Nucleophilicity. *J. Am. Chem. Soc.* **2004**, *126* (16), 5174–5181.
- (32) Iwata, T.; Kawano, R.; Fukami, T.; Shindo, M. Retro-Friedel-Crafts-Type Acidic Ring-Opening of Triptycenes: A New Synthetic Approach to Acenes. *Chem. - A Eur. J.* **2022**, *28* (12).
- (33) Grimm, J. B.; Muthusamy, A. K.; Liang, Y.; Brown, T. A.; Lemon, W. C.; Patel, R.; Lu, R.; Macklin, J. J.; Keller, P. J.; Ji, N.; et al. A General Method to Fine-Tune Fluorophores for Live-Cell and in Vivo Imaging. *Nat. Methods* **2017**, *14* (10), 987–994.
- (34) Goethals, E. J.; Schacht, E. H.; Bogaert, Y. E.; Ali, S. I.; Tezuka, Y. The Polymerization of Azetidines and Azetidine Derivatives. *Polym. J.* **1980**, *12* (9), 571–581.
- (35) Garro-Helion, F.; Merzouk, A.; Guibé, F. Mild and Selective Palladium(0)-Catalyzed Deallylation of Allylic Amines. Allylamine and Diallylamine as Very Convenient Ammonia Equivalents for the Synthesis of Primary Amines. *J. Org. Chem.* **1993**, *58* (22), 6109–6113.
- (36) Vutukuri, D. R.; Bharathi, P.; Yu, Z.; Rajasekaran, K.; Tran, M. H.; Thayumanavan, S. A Mild Deprotection Strategy for Allyl-Protecting Groups and Its Implications in Sequence Specific Dendrimer Synthesis. *J. Org. Chem.* **2003**, *68* (3), 1146–1149.
- (37) Cunningham, J.; Gigg, R.; Warren, C. D. The Allyl Ether as a Protection Group in Carbohydrate Chemistry. *Tetrahedron Lett.* **1964**, *5* (19), 1191–1196.
- (38) Gent, P. A.; Gigg, R.; Conant, R. The Allyl Ether as a Protecting Group in Carbohydrate Chemistry. Part IV. The 2-Methylallyl Ether Group. *J. Chem. Soc. Perkin Trans. 1* **1973**, 1858–1863.
- (39) Franz, R. G. Comparisons of PKa and Log P Values of Some Carboxylic and Phosphonic Acids: Synthesis and Measurement. *AAPS PharmSci* **2001**, *3* (2), 1–13.
- (40) Johnson, I. D. *Molecular Probes Handbook: A Guide to Fluorescent Probes and Labeling Technologies*; Life Technologies Corporation, 2010.
- (41) Bandichhor, R.; Petrescu, A. D.; Vespa, A.; Kier, A. B.; Schroeder, F.; Burgess, K. Synthesis of a New Water-Soluble Rhodamine Derivative and Application to Protein Labeling and Intracellular Imaging. *Bioconjug. Chem.* **2006**, *17* (5), 1219–1225.
- (42) Grimm, J. B.; Lavis, L. D. Caveat Fluorophore: An Insiders’ Guide to Small-Molecule Fluorescent Labels. *Nat. Methods* **2022**, *19* (2), 149–158.
- (43) Panchuk-Voloshina, N.; Haugland, R. P.; Bishop-Stewart, J.; Bhalgat, M. K.; Millard, P. J.; Mao, F.; Leung, W. Y.; Haugland, R. P. Alexa Dyes, a Series of New Fluorescent Dyes That Yield Exceptionally Bright, Photostable Conjugates. *J. Histochem. Cytochem.* **1999**, *47* (9), 1179–1188.

- (44) Lavis, L. D.; Chao, T. Y.; Raines, R. T. Synthesis and Utility of Fluorogenic Acetoxymethyl Ethers. *Chem. Sci.* **2011**, *2* (3), 521–530.
- (45) Schultz, C.; Vajanaphanich, M.; Harootunian, A. T.; Sammak, P. J.; Barrett, K. E.; Tsien, R. Y. Acetoxymethyl Esters of Phosphates, Enhancement of the Permeability and Potency of CAMP. *J. Bio. Chem.* **1993**, *268* (9), 6316.
- (46) Shieh, P.; Dien, V. T.; Beahm, B. J.; Castellano, J. M.; Wyss-Coray, T.; Bertozzi, C. R. CalFluors: A Universal Motif for Fluorogenic Azide Probes across the Visible Spectrum. *J. Am. Chem. Soc.* **2015**, *137* (22), 7145–7151..
- (47) Koide, Y.; Urano, Y.; Hanaoka, K.; Terai, T.; Nagano, T. Evolution of Group 14 Rhodamines as Platforms for Near-Infrared Fluorescence Probes Utilizing Photoinduced Electron Transfer. *ACS Chem. Biol.* **2011**, *6* (6), 600–608..
- (48) Lukinavičius, G.; Umezawa, K.; Olivier, N.; Honigmann, A.; Yang, G.; Plass, T.; Mueller, V.; Reymond, L.; Corrêa, I. R.; Luo, Z. G.; et al. A Near-Infrared Fluorophore for Live-Cell Super-Resolution Microscopy of Cellular Proteins. *Nat. Chem.* **2013**, *5* (2), 132–139.
- (49) Huang, Y.-L.; Walker, A. S.; Miller, E. W. A Photostable Silicon Rhodamine Platform for Optical Voltage Sensing. *J. Am. Chem. Soc.* **2015**, *137*, 10.
- (50) Koide, Y.; Urano, Y.; Hanaoka, K.; Piao, W.; Kusakabe, M.; Saito, N.; Terai, T.; Okabe, T.; Nagano, T. Development of NIR Fluorescent Dyes Based on Si-Rhodamine for in Vivo Imaging. *J. Am. Chem. Soc.* **2012**, *134* (11), 5029–5031.
- (51) Uno, S. N.; Kamiya, M.; Yoshihara, T.; Sugawara, K.; Okabe, K.; Tarhan, M. C.; Fujita, H.; Funatsu, T.; Okada, Y.; Tobita, S.; et al. A Spontaneously Blinking Fluorophore Based on Intramolecular Spirocyclization for Live-Cell Super-Resolution Imaging. *Nat. Chem.* **2014**, *6* (8), 681–689.
- (52) Wang, B.; Chai, X.; Zhu, W.; Wang, T.; Wu, Q. A General Approach to Spirolactonized Si-Rhodamines. *Chem. Commun.* **2014**, *50* (92), 14374–14377.
- (53) Egawa, T.; Hanaoka, K.; Koide, Y.; Ujita, S.; Takahashi, N.; Ikegaya, Y.; Matsuki, N.; Terai, T.; Ueno, T.; Komatsu, T.; et al. Development of a Far-Red to near-Infrared Fluorescence Probe for Calcium Ion and Its Application to Multicolor Neuronal Imaging. *J. Am. Chem. Soc.* **2011**, *133* (36), 14157–14159.
- (54) Myochin, T.; Hanaoka, K.; Iwaki, S.; Ueno, T.; Komatsu, T.; Terai, T.; Nagano, T.; Urano, Y. Development of a Series of Near-Infrared Dark Quenchers Based on Si-Rhodamines and Their Application to Fluorescent Probes. *J. Am. Chem. Soc.* **2015**, *137* (14), 4759–4765.
- (55) Fischer, C.; Sparr, C. Direct Transformation of Esters into Heterocyclic Fluorophores. *Angew. Chemie - Int. Ed.* **2018**, *57* (9), 2436–2440.
- (56) Uno, S.-N.; Kamiya, M.; Yoshihara, T.; Sugawara, K.; Okabe, K.; Tarhan, M. C.; Fujita, H.; Funatsu, T.; Okada, Y.; Tobita, S.; et al. A Spontaneously Blinking Fluorophore Based on Intramolecular Spirocyclization for Live-Cell Super-Resolution Imaging. *Nat. Chem.* **2014**, *6*, 681-689.
- (57) Åkerlöf, G.; Short, O. A. The Dielectric Constant of Dioxane-Water Mixtures between 0 and 80°. *J. Am. Chem. Soc.* **1936**, *58* (7), 1241–1243.

Chapter 2 Supplementary Information

General procedures

Chemical reagents and anhydrous solvents were purchased from commercial suppliers and used without further purification. For best results 3-aminophenols were purified by flash silica chromatography (100% DCM or 100% EtOAc) immediately prior to use. Thin layer chromatography (TLC) (silica gel, F254, 250 μm) and preparative thin layer chromatography (PTLC) (Silicycle, F254, 1000 μm) were performed on precoated TLC glass plates and were visualized by fluorescence quenching under UV light. Flash column chromatography was performed on Silicycle Silica Flash F60 (230–400 Mesh) for normal phase or 60 RP-18 (200-400 mesh) for reverse phase, using a forced flow of air at 0.5–1.0 bar. NMR spectra were recorded on Bruker AV-300 MHz, Bruker AVB-400 MHz, Bruker AVQ-400 MhZ, Bruker NEO-500 MHz and Bruker AV-600 NMR spectrometers. Chemical shifts (δ) are expressed in parts per million (ppm) and are referenced to CDCl_3 (7.26 ppm), DMSO (2.50 ppm), MeOD (3.31 ppm) or D_2O (4.79 ppm). Coupling constants are reported as Hertz (Hz). Splitting patterns are indicated as follows: s, singlet; d, doublet; t, triplet; q, quartet; dd, doublet of doublet; td, triplet of doublets; dt, doublet of triplets; tt, triplet of triplets; ddd, doublet of doublet of doublets; tdd, triplet of doublet of doublets; q, quartet; m, multiplet. High resolution mass spectra (ESI EI) were measured by the QB3/Chemistry mass spectrometry service at University of California, Berkeley. Analytical high performance liquid chromatography (HPLC) and low resolution ESI Mass Spectrometry were performed on an Agilent Infinity 1200 analytical instrument coupled to an Advion CMS-L ESI mass spectrometer. The column used was Phenomenex Luna 5 μm C18(2) (4.6 mm I.D. \times 150 mm) with a flow rate of 1.0 mL/min. The mobile phase was MQ-H₂O with 0.05% trifluoroacetic acid (eluent A) and HPLC grade MeCN with 0.05% trifluoroacetic acid (eluent B). Signals were monitored at 210, 254, 350, 460 and 520, 560 and 660 nm over 10 min, with a gradient of 10 to 100% eluent B for 8 min, then held at 100% B for 2 min.

Spectroscopic characterization

UV-Vis absorbance and fluorescence spectra were recorded using a 2501 Spectrophotometer (Shimadzu) and a Quantamaster Master 4 L-format scanning spectrofluorometer (Photon Technologies International). The fluorometer is equipped with an LPS-220B 75-W xenon lamp and power supply, A-1010B lamp housing with integrated igniter, switchable 814 photon-counting/analog photomultiplier detection unit, and MD5020 motor driver. Samples were measured in 1-cm path length quartz cuvettes (Starna Cells).

Absorption and emission spectra were taken at a final concentration of 2 μM (rhodamines) or 5 μM (SiRs) in PBS, EtOH (+ 0.1% trifluoroacetic acid) or 50% Water/ dioxane (+ 0.01% triethylamine) using 1000x dilutions from stock solutions of dyes in DMSO. pH titrations were conducted in buffers containing 150 mM NaCl and 10 mM buffer. The following buffer systems were used: phosphate (pH 2.3 – 3.1 and 5.5 – 7.5), acetate (pH 3.8 – 5.3), tris (pH 8.2 – 9.2) and carbonate (pH 9.8). pK_a's were determined by recording absorbance values or maximum absorbance wavelength and fitting to sigmoidal dose response curves using GraphPad Prism software. Dielectric titrations were conducted in mixtures of dioxane and water (0 – 100% in 10% increments) containing 0.01% triethylamine. Quantum yields are relative measurements compared to fluorophores of known quantum yields.

Water solubility

Rhodamines were flushed through a reverse phase silica column (100% MeOH) prior to the experiment to remove any salts. Saturated rhodamine solutions were prepared by adding solid rhodamines portion wise to 2 mL solutions of PBS, with stirring and sonication, until there was an excess of clearly visible solid particulates. The suspensions were filtered through 0.2 μm PTFE filters to remove all solid particulates and the resulting solutions were diluted between 10 to 1000-fold in PBS to ensure a final maximum absorbance reading between 0.1 and 0.8 AU. Absorbance readings at λ_{max} were compared to standard stock solutions of known concentrations and concentrations of each unknown rhodamine solution were calculated. Factoring in the dilution factors, relative solubilities of each rhodamine in PBS were calculated and normalized to 3-carboxytetramethylrhodamine. Each experiment was performed in triplicate.

In vitro AM ester hydrolysis reactions and characterization.

For the enzymatic reactions, commercially purified pig liver esterase (PLE, MW = 168 kDa) as a suspension in 3.2 M $(\text{NH}_4)_2\text{SO}_4$ was used as a stock solution of 28.1 mg/mL. 2 μl AM dyes (2 mM in DMSO) were incubated with or without 1 μl PLE (final concentration 0.7025 mg/mL) in HBSS (pH 7.4, final volume 40 μl) for 2 hrs at 37°C. Solutions were diluted with 200 μl MeCN, filtered through a 0.22 μm PTFE filter and characterized by HPLC comparing to standards.

LogK_{L-Z}

The lactonization equilibrium constant K_{L-Z} was calculated by use of the following equation:

$$K_{L-Z} = \frac{(\varepsilon_{dw} / \varepsilon_{max})}{1 - (\varepsilon_{dw} / \varepsilon_{max})}$$

in which ε_{dw} is the extinction coefficient of the fluorophore in a 1:1 (vol/vol) mixture of spectral grade dioxane and milliQ water with 0.01% (v/v) triethylamine. ε_{max} is the maximum extinction coefficient which was measured in ethanol containing 0.1% (v/v) trifluoroacetic acid. All measurements were performed at 5 μM by diluting 1000-fold from stock solutions in DMSO.

Cell culture

Human embryonic kidney 293T (HEK) cells were maintained in Dulbecco's modified eagle medium (DMEM) supplemented with 4.5 g/L D-glucose, 10% fetal bovine serum (FBS; Thermo Scientific) and 1% GlutaMax (Invitrogen) at 37 °C in a humidified incubator with 5% CO₂. Cells were passaged and plated in DMEM (as above) onto 12 mm glass coverslips pre-coated with Poly-D-Lysine (PDL; 1 mg/mL; Sigma-Aldrich) at a density of 50,000 cells per coverslip. Imaging was performed 16–48 hours after plating.

For loading experiments, HEK cells were incubated with a 500 nM solution of dye (1 mL) in HBSS at 37 °C for 20 min, prior to transfer to 3 mL fresh HBSS (no dye) for imaging. For dye wash out experiments, this imaging solution was replaced with 3 mL fresh HBSS after each subsequent round of imaging (3 washes).

Epifluorescence microscopy

Imaging was performed on an AxioExaminer Z-1 (Zeiss) equipped with a Spectra-X Light engine LED light (Lumencor), controlled with Slidebook (v6, Intelligent Imaging Innovations). Images were acquired with a W-Plan-Apo 63x/1.0 objective (63x; Zeiss) and images were focused onto

an OrcaFlash4.0 sCMOS camera (sCMOS; Hamamatsu). The excitation light was delivered from an LED at 542/33 nm and emission was collected with a quadruple emission filter (430/32, 508/14, 586/30, 708/98 nm) after passing through a quadruple dichroic mirror (432/38, 509/22, 586/40, 654 nm LP).

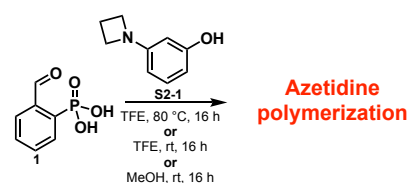
Image analysis

Image analyses were performed in ImageJ (FIJI, NIH). For image intensity measurements, regions of interested were created by thresholding images to create binary masks (cells and background). Background subtracted mean fluorescence intensities were calculated and averaged across five images (each containing at least 15 cells) per coverslip and at least 3 coverslips were examined for each condition.

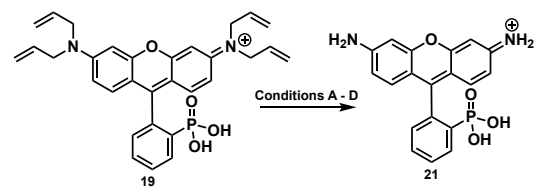
Supplementary figures

Table S1. Summary of 2-carboxy and 2-phosphonobenzaldehyde NMR analyses.

Aldehyde	Solvent	¹ H _A chemical shift (ppm)	¹³ C _A chemical shift (ppm)	³¹ P chemical shift (ppm)	Ratio
2-carboxybenzaldehyde	DMSO- <i>d</i> ₆	6.64 (d, J = 8.1 Hz)	98.32	-	0.92
		10.45 (s)	-	-	0.08
	MeOD- <i>d</i> ₄	6.62 (s)	99.88	-	0.87
		6.42 (s)	105.07	-	0.13
MeOD- <i>d</i> ₄ + TFA	6.42 (s)	105.09	-	1.00	
2-phosphonobenzaldehyde 1	DMSO- <i>d</i> ₆	10.72 (s)	193.39 (d, J = 3.8 Hz)	9.29	1.00
	D ₂ O	10.58 (s)	195.71 (d, J = 4.1 Hz)	10.65	1.00
	MeOD- <i>d</i> ₄	6.02 (s)	102.36 (d, J = 3.6 Hz)	14.44	0.95
		6.29 (d, J = 12.9 Hz)	-	29.47	0.05



Scheme S1. Attempted Friedel-Crafts condensation of azetidine-containing aniline **S2-1**.



Scheme S2. De-allylation of tetraallylrhodamine **19** to phosRho110, **21**.

Table S2. Conditions for deallylation of **19** to **21**.

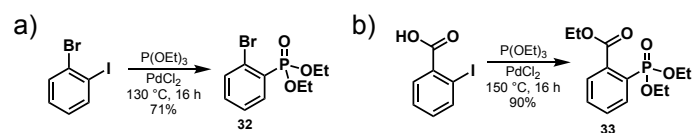
Entry	Conditions	Yield 21
A	NDMBA (6 eq) Pd(PPh ₃) ₄ (4%) DMF 80 °C, 16 h	n.r. ^a
B	NDMBA (6 eq) Pd(PPh ₃) ₄ (4%) 3: 1 DMF: NEt ₃ 80 °C, 16 h	52% ^b
C	K ₂ CO ₃ Pd(PPh ₃) ₄ (4%) MeOH 60 °C, 72 h	~90% ^{a,c}
D	^t BuOK DMF, 100 °C, 10 min then 1 M HCl, 100 °C, 5 min	71% ^b

^a determined by LCMS. ^b isolated. ^c also observed deallylation intermediates.

Table S3. Conditions for Friedel Crafts condensation to **28**.

Entry	Solvent	Temperature	Time	Isolated Yield of 28 ^a	Notes
1	TFE	80 °C	7 days	43%	
2	H ₂ O	150 °C	16 h ^b	22%	Aniline demethylation observed
3	TFE	130 °C	16 h ^b	29% 28 10% TFE adduct	Aniline demethylation observed

^a after reverse phase chromatography. ^b in a sealed bomb flask.

**Scheme S3.** Pd-catalyzed Arbuzov of aryl iodides.

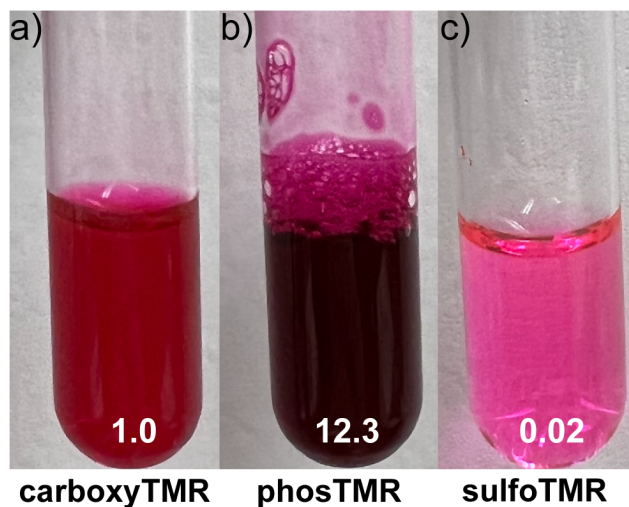


Figure S1. Relative solubility of tetramethylrhodamines. Images of saturated solutions of carboxy- (a), phos- (b) and sulfo- (c) tetramethylrhodamines in PBS after filtration through a 0.2 μm PTFE filter. Relative concentrations (normalized to carboxyTMR) as determined by absorbance spectroscopy are indicated in white.

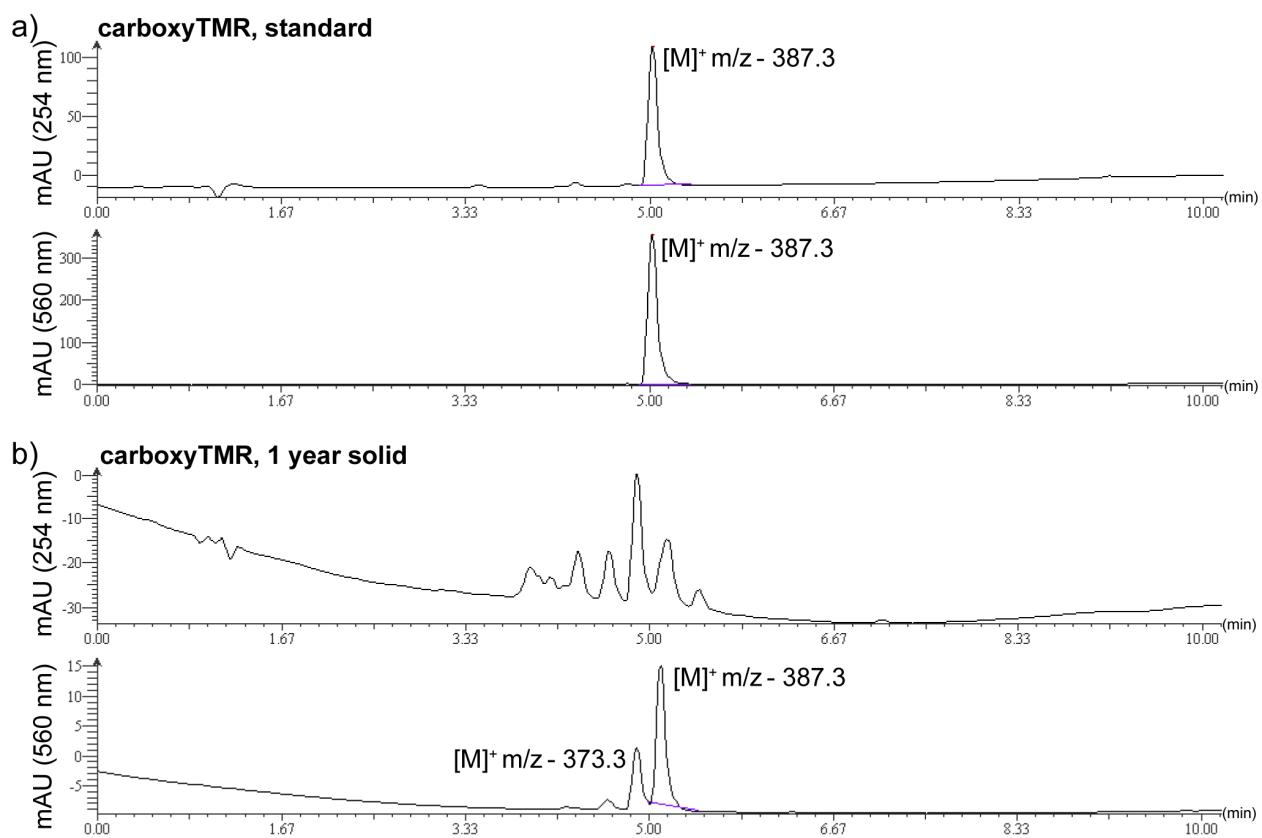


Figure S2. Stability of carboxy TMR. Analytical HPLC traces of a freshly synthesized carboxyTMR standard (a) and sample of carboxyTMR that had been sorted as a solid powder for one year at room temperature in the dark (b). Traces at 254 nm and 560 nm are depicted and where applicable corresponding m/z values are annotated. Note: decomposition of carboxyTMR in 560 nm channel showed demethylation ($\Delta m/z$ -14).

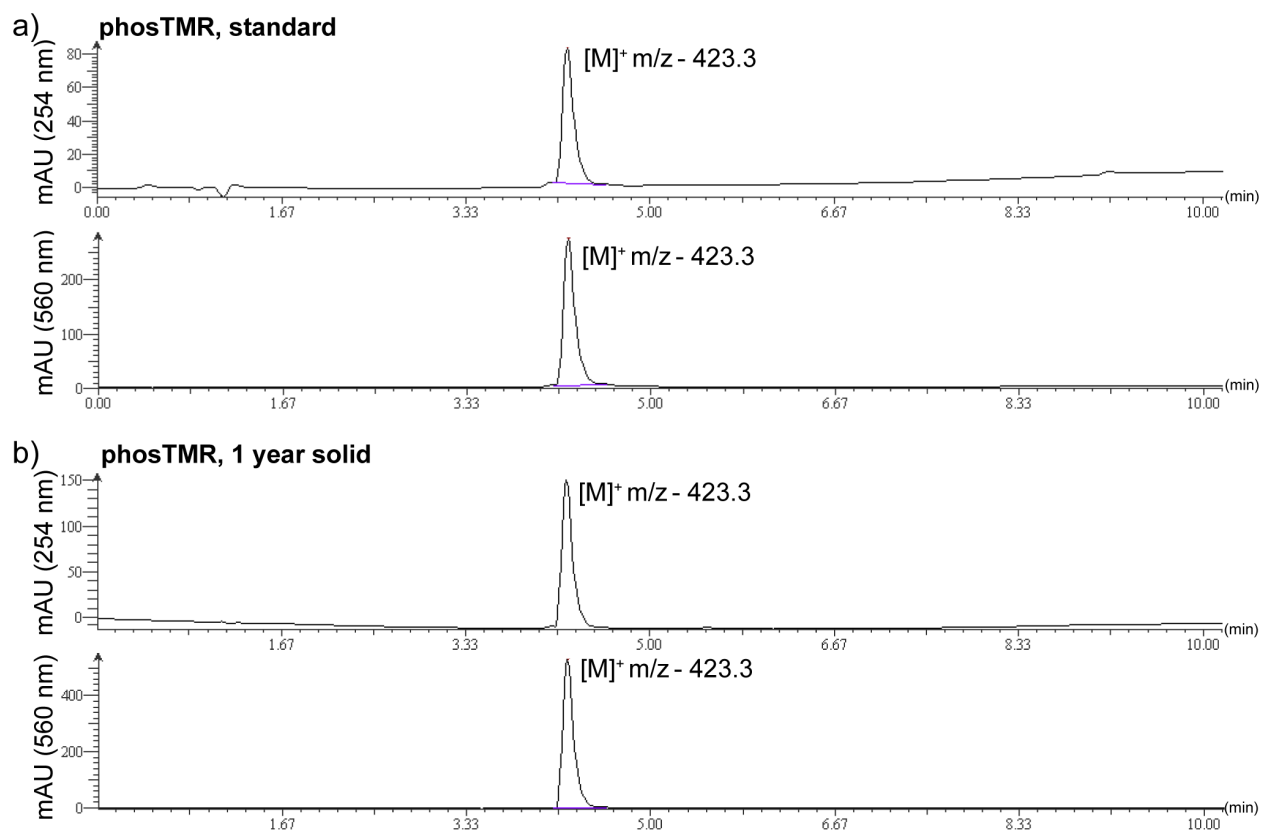


Figure S3. Stability of phosTMR. Analytical HPLC traces of a freshly synthesized phosTMR standard (a) and sample of phosTMR that had been sorted as a solid powder for one year at room temperature in the dark (b). Traces at 254 nm and 560 nm are depicted and corresponding m/z values are annotated. Note: no decomposition was observed.

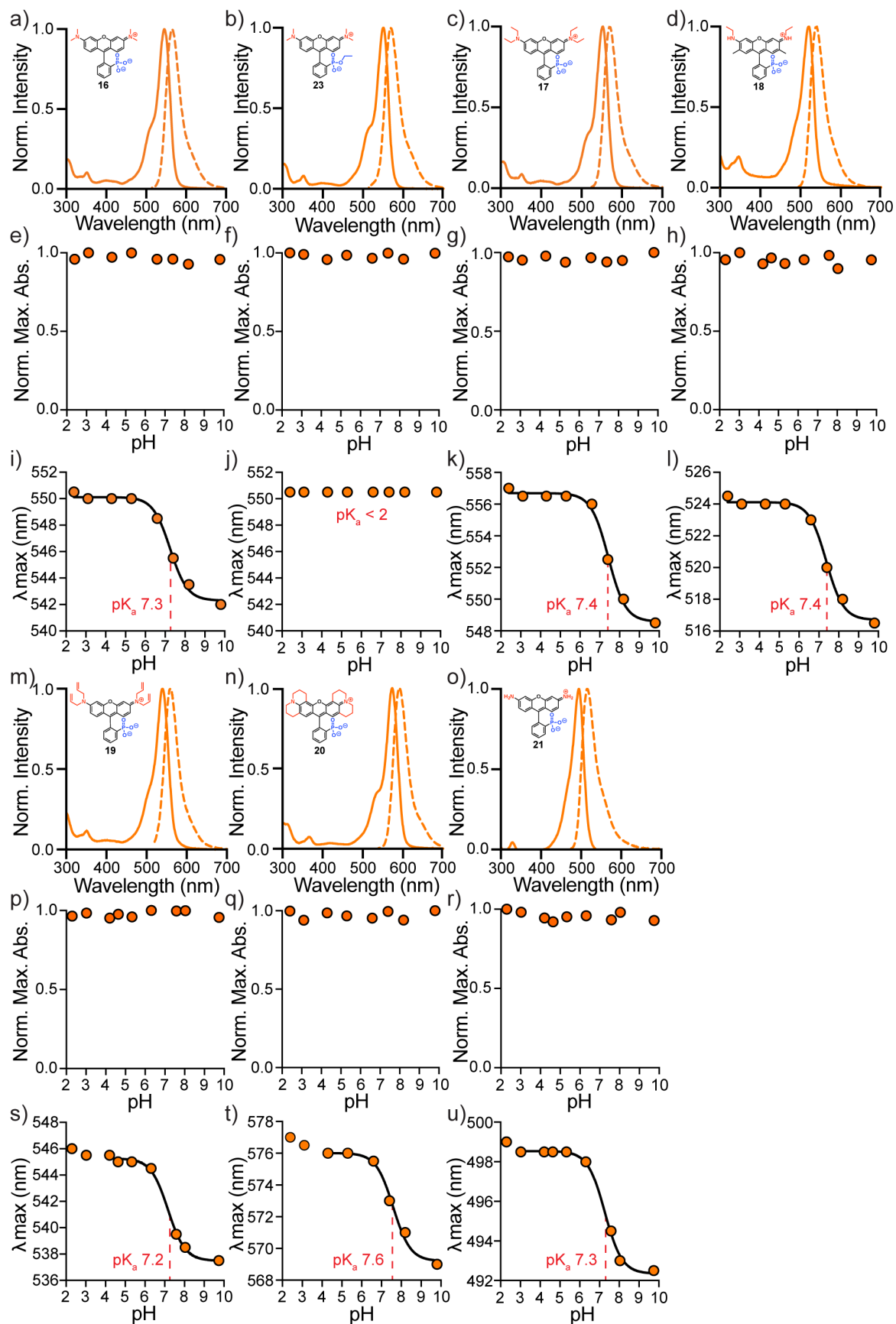


Figure S4. Spectroscopic characterization of 3-phosphonorhodamines. Normalized absorbance and fluorescence spectra (a-d, m-o) in PBS with labeled chemical structures, plots of maximum absorbance vs pH (e-h, p-r), and plots of λ_{max} vs pH (i-l, s-u) for **16** (a, e, i), **23** (b, f, j), **17** (c, g, k), **18** (d, h, l), **19** (m, p, s), **20** (n, q, t), **21** (o, r, u). pH titrations were performed in 10 mM buffered solutions containing 150 mM NaCl ranging from pH 2.3 to 9.8 at a final dye concentration of 2 μM . Titration curves were fit to sigmoidal dose response curves (solid black) to enable pK_a determination (dashed red) and phosphonate pK_{a2} values are indicated in red.

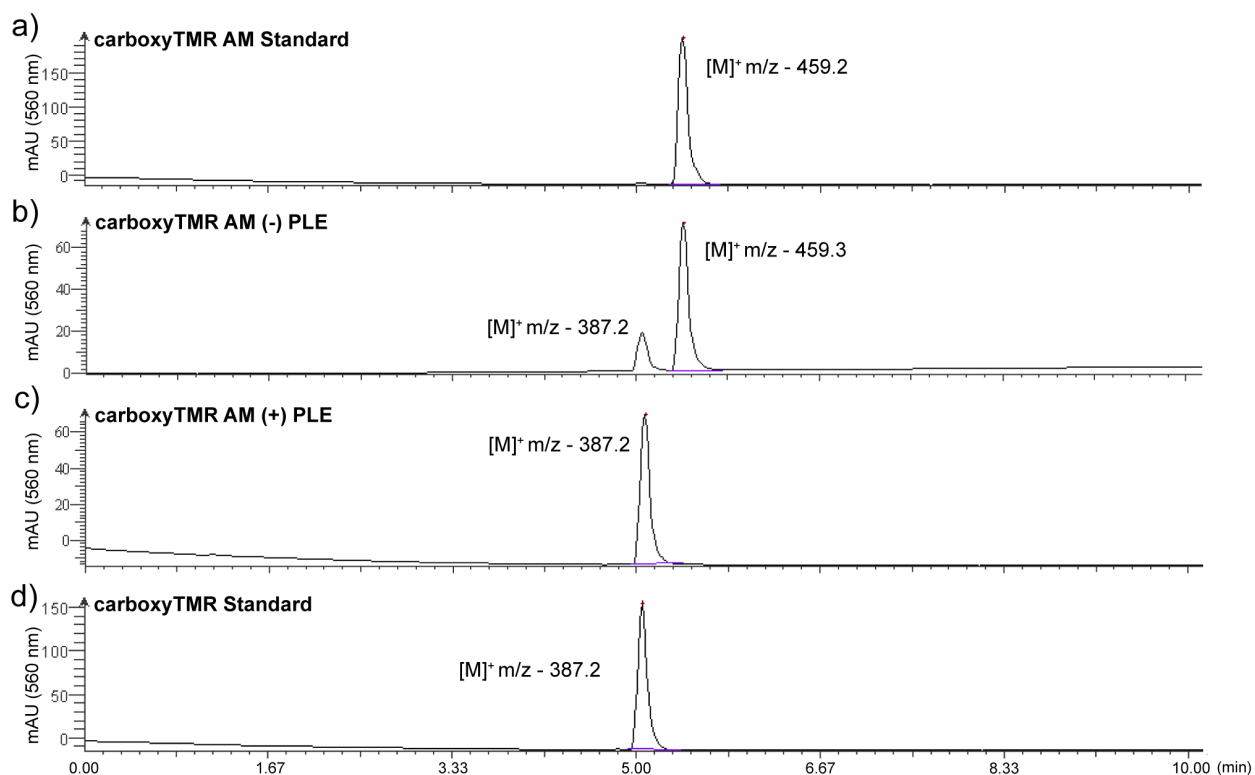


Figure S5. In vitro characterization of carboxyTMR AM hydrolysis.

CarboxyTMR AM was incubated with or without PLE in HBSS for 2 hrs at 37 $^{\circ}\text{C}$. HPLC traces were then compared to those of carboxyTMR AM (not incubated in HBSS) and carboxyTMR standards. Masses are indicated next to the peaks.

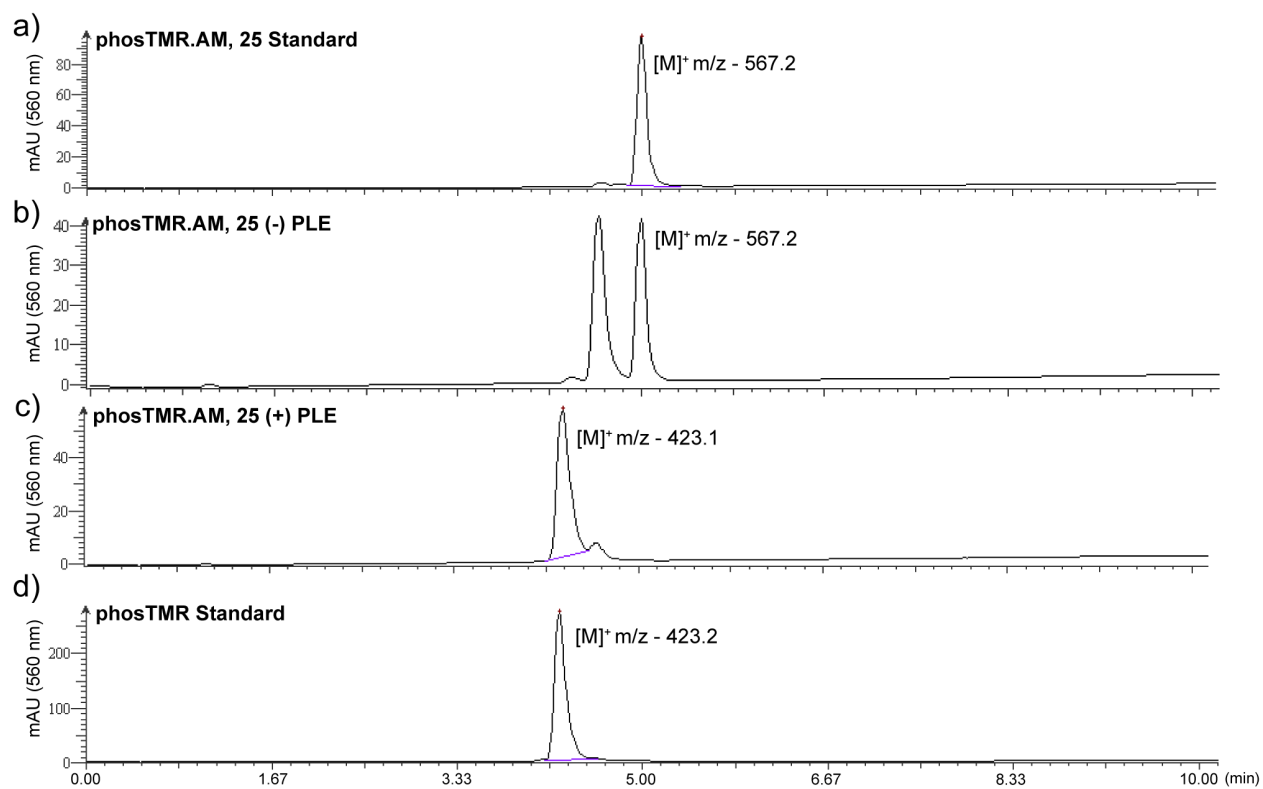


Figure S6. In vitro characterization of phosTMR AM, 25 hydrolysis.

PhosTMR AM, 25 was incubated with or without PLE in HBSS for 2 hrs at 37 °C. HPLC traces were then compared to those of **phosTMR AM, 25** (not incubated in HBSS) and **phosTMR, 19** standards. Masses are indicated next to the peaks unless no mass was observed (b).

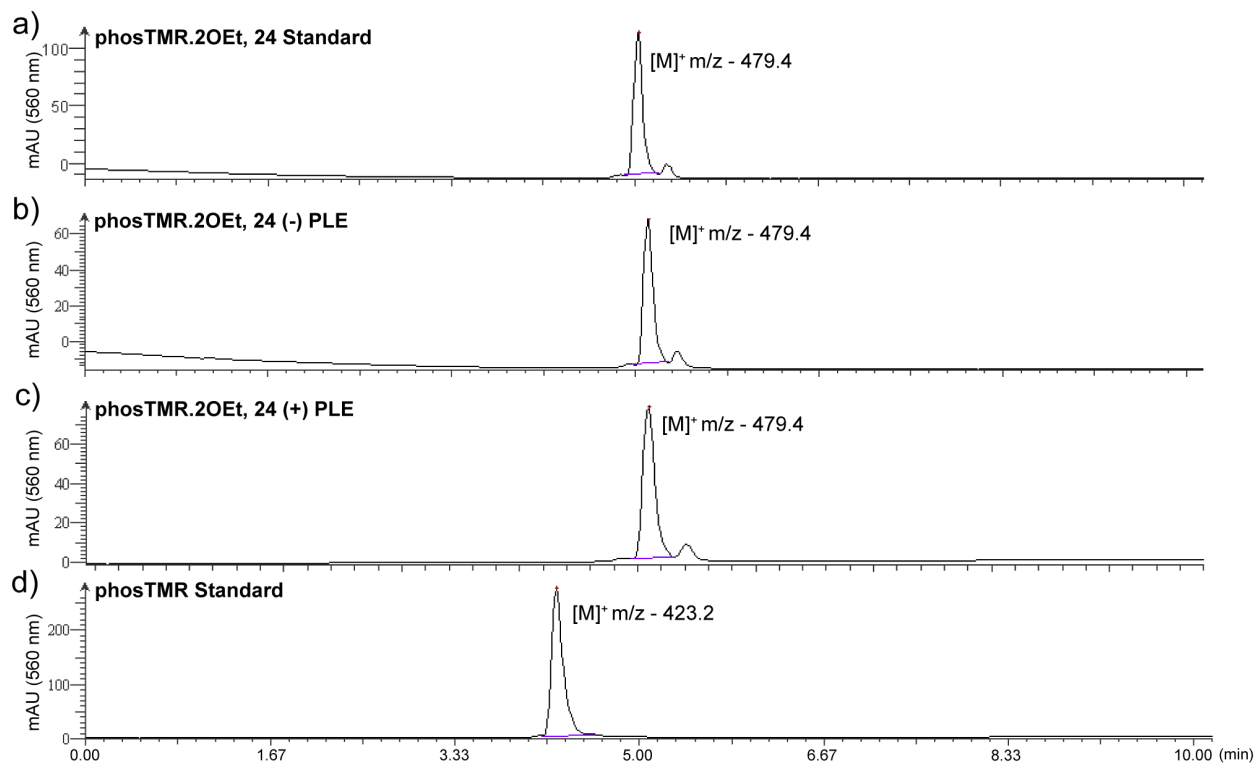


Figure S7. In vitro characterization of phosTMR.2OEt, 24 hydrolysis.

PhosTMR.2OEt, 24 was incubated with or without PLE in HBSS for 2 hrs at 37 °C. HPLC traces were then compared to those of phosTMR.2OEt, 24 (not incubated in HBSS) and phosTMR, 19 standards. Masses are indicated next to the peaks.

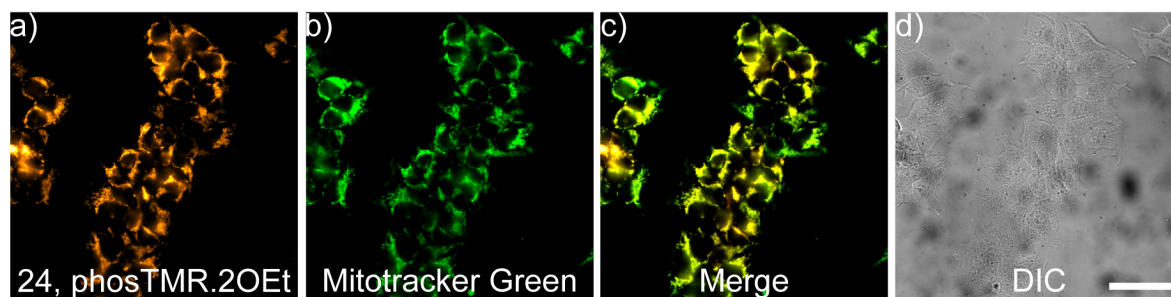


Figure S8. Mitochondrial localization of phosTMR AM, 24. Widefield fluorescence images in the orange (a) and green (b) channels, a merge of images a and b (c) and corresponding DIC image (d) of HEK293T cells stained with 500 nM 24 and 100 nM Mitotracker Green™ in HBSS for 20 minutes at 37 °C. The coverslip was transferred into fresh HBSS prior to imaging. Scale bar is 50 μm.

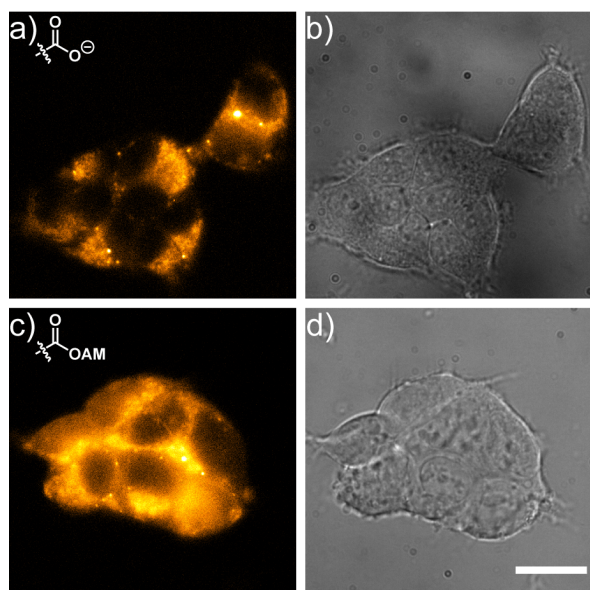


Figure S9. Intracellular localization of 3-carboxytetramethylrhodamines. Widefield fluorescence (a, c) and DIC (b, d) images of HEK293T cells stained with 500 nM carboxyTMR (a, b) and carboxyTMR acetoxymethyl ester (c, d) for 20 minutes at 37 °C. Coverslips were transferred into fresh HBSS prior to imaging. Fluorescence images are normalized to image c. Scale bar is 20 μ M.

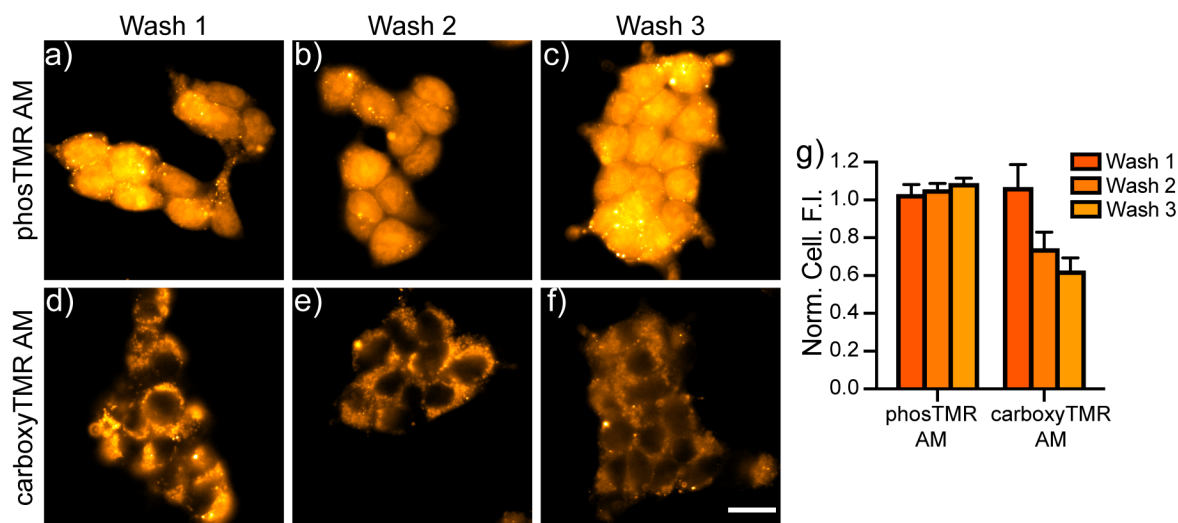


Figure S10. Cellular retention of TMR acetoxymethyl esters. Widefield fluorescence images of HEK293T cells stained with 500 nM phosTMR (a-c) and carboxyTMR (d-f) for 20 minutes at 30 °C. Coverslips were placed into fresh HBSS (1 wash) prior to imaging and coverslips were washed by replacement with fresh HBSS (washes 2 and 3). Scale bar is 20 μ M. Quantification of associated changes in fluorescence intensity (g) through serial washing. Images and quantification for each dye are normalized to the wash 1 condition. Error bars represent + SEM for n = 15 images across 3 coverslips.

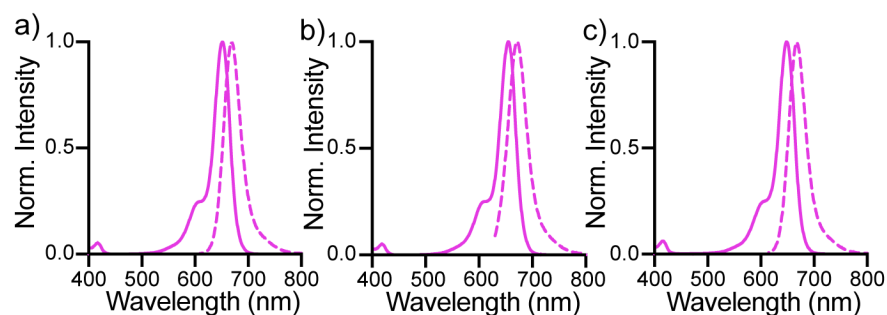


Figure S11. Absorbance and fluorescence spectra of SiRs. Normalized absorbance (solid) and fluorescence (dashed) spectra of phosTMSiR **28** (a), phosTMSiR.OEt **29** (b) and Berkeley Red (c) in EtOH +0.1% (v/v) trifluoroacetic acid. Spectra were recorded at a dye concentration of 1 μ M. Excitation was at 605 nm.

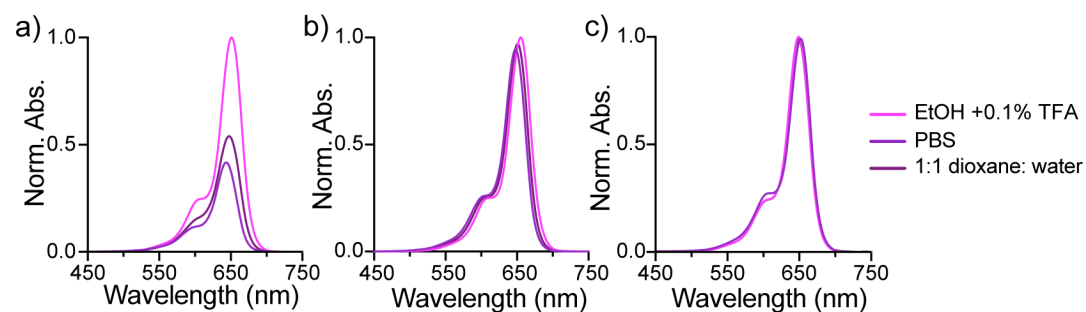


Figure S12. Solvent dependent lactonization of SiRs Normalized absorbance spectra of phosTMSiR **28** (a), phosTMSiR.OEt **29** (b) and Berkeley Red (c) in EtOH+0.1% (v/v) trifluoroacetic acid (—), PBS (—) or a 50% dioxane/ water mixture + 0.1% (v/v) triethylamine (—). In each case spectra are normalized to the EtOH spectrum.

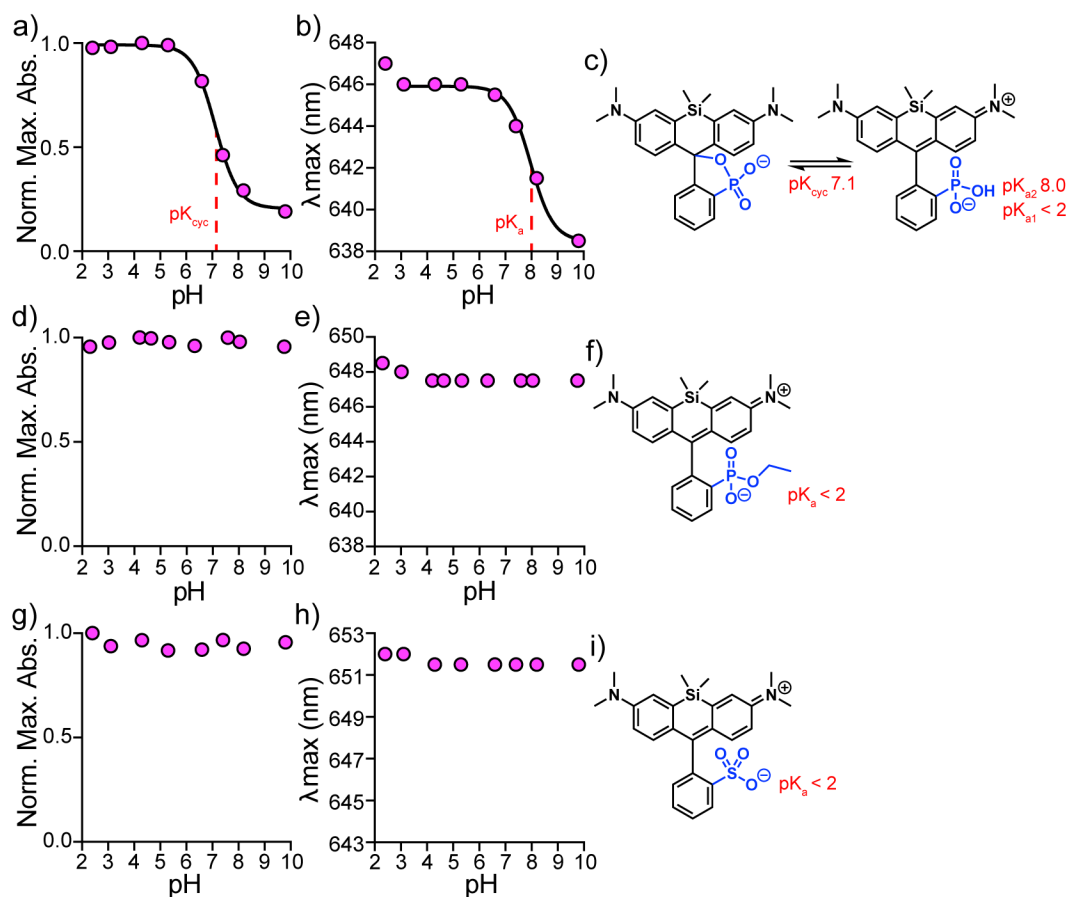


Figure S13. pH dependence of SiR absorbance. Plots of normalized maximum absorbance vs. pH (a, d, g), λ_{\max} vs. pH (b, e, h), and associated chemical structures or Z-L equilibrium (c, f, i) for phosTMSiR **28** (a-c), phosTMSiR.OEt **29** (d-f) and Berkeley Red (g-h). pH titrations were performed in 10 mM buffered solutions containing 150 mM NaCl ranging from pH 2.3 to 9.8 at a final dye concentration of 5 μ M. Where appropriate pH titration curves were fit to sigmoidal dose response curves (solid black) to enable pK_{cyc} or pK_a determination (dashed red) and reported next to the chemical structures.

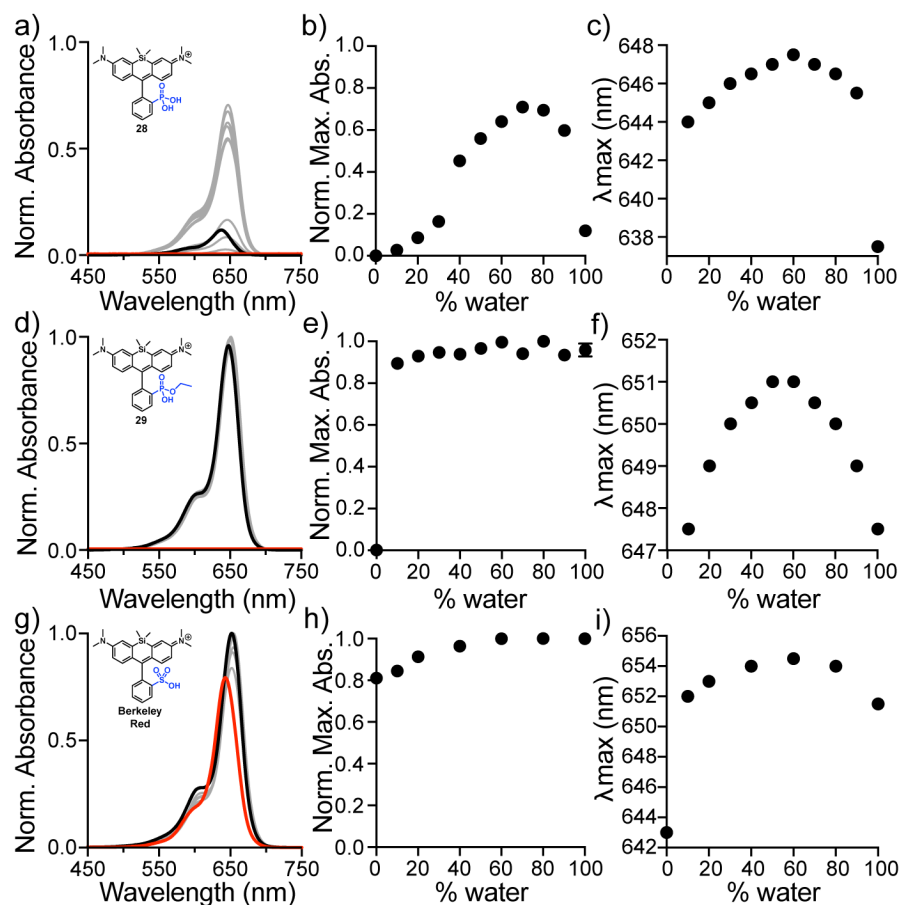


Figure S14. Dioxane-water titrations of SiRs. Normalized absorbance spectra (a, d, g), plots of normalized maximum absorbance vs % water content (b, e, h) and plots of λ_{max} vs % water content (c, f, i) for phosTMSiR **28** (a-c), phosTMSiR.OEt **29** (d-f) and Berkeley Red (g-h). Spectra are normalized to the absorbance spectra of each fluorophore in EtOH + 0.1% (v/v) TFA. Fluorophores were titrated at a final concentration of 5 μM from 100% water (black) to 100% dioxane (red) in 10% increments. All solutions contained 0.01% triethylamine.

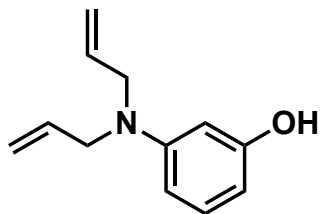
Synthetic procedures

General procedure A for synthesis of triarylmethane intermediates (A):

1 (1 mmol, 1 eq) and 3-aminophenols (2.25 mmol, 2 eq) were charged into a reaction flask that was subsequently evacuated and backfilled with N_2 (x3). 2,2,2-trifluoroethanol was added, and the reaction stirred at 80 $^\circ\text{C}$ overnight. Upon cooling to temperature, trituration with either EtOAc or cold MeOH yielded triarylmethane intermediates.

General procedure B for the synthesis of 3-phosphonorhodamines (B):

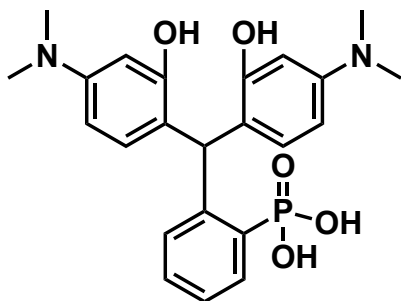
Triarylmethane intermediates (0.5 mmol, 1 eq) and p-chloranil (1 mmol, 2 eq) were refluxed in MeOH for 2 to 24 hours, or until all particulates had dissolved. Upon cooling to room temperature, any remaining solids were removed by vacuum filtration and the filtrate concentrated *in vacuo*. Trituration with EtOAc yielded 3-phosphonorhodamines.



Synthesis of compound 5.

3-aminophenol, **7** (3.0 g, 27.5 mmol, 1 eq) and K_2CO_3 (7.6 g, 5 mmol, 2 eq) were suspended in ethanol (30 mL). While stirring, allyl bromide (5.9 mL, 69 mmol, 2.5 eq) was added and the solution was refluxed for 90 minutes. Upon cooling to room temperature, the suspension was diluted with water and extracted into EtOAc (x3), dried over Na_2SO_4 and concentrated *in vacuo*. The crude oil was purified by flash silica chromatography to attain **5** as a golden oil (4.05 g, 21.4 mmol, 78%).

1H NMR (500 MHz, Chloroform-*d*) δ 7.04 (t, $J = 8.1$ Hz, 1H), 6.30 (d, $J = 7.0$ Hz, 1H), 6.23 – 6.09 (m, 2H), 5.84 (ddt, $J = 17.1, 10.0, 4.9$ Hz, 2H), 5.21 – 5.12 (m, 4H), 3.89 (dt, $J = 4.4, 1.4$ Hz, 4H).



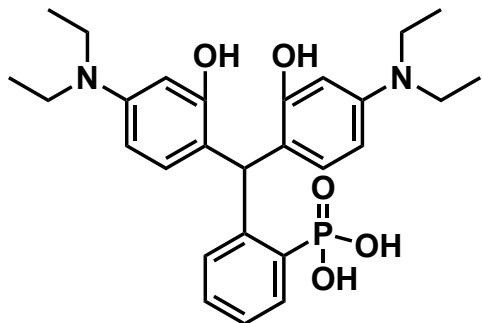
Synthesis of **9**

1 (300 mg, 1.61 mmol, 1 eq) and 3-(dimethylamino)phenol, **2** (496 mg, 3.62 mmol, 2.25 eq) were charged into a round bottom flask that was subsequently evacuated and backfilled with N_2 (x3). Upon addition of TFE (12.5 mL), the solution was stirred at 80 °C for 16 hours. The resulting suspension was concentrated *in vacuo* and triturated with cold methanol, yielding **9** as a white solid (698 mg, 1.58 mmol, 98%).

1H NMR (500 MHz, DMSO-*d*₆) δ 7.67 (dd, $J = 13.7, 7.5$ Hz, 1H), 7.43 (t, $J = 7.6$ Hz, 1H), 7.25 (td, $J = 7.5, 2.7$ Hz, 1H), 7.20 (dd, $J = 7.4, 5.5$ Hz, 1H), 6.61 – 6.53 (m, 3H), 6.08 (m, 4H), 2.78 (s, 12H).

^{31}P NMR (202 MHz, DMSO-*d*₆) δ 14.97

HR-ESI-MS m/z for $C_{23}H_{36}O_5N_2P^-$ [M-H]⁻ calcd: 451.2362 found: 451.2364



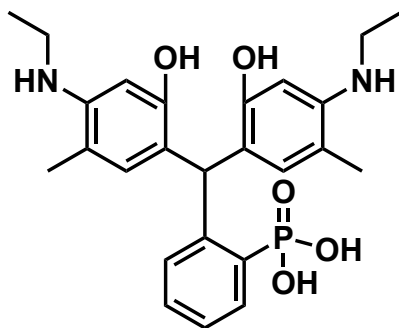
Synthesis of **10**

1 (50 mg, 0.28 mmol, 1 eq) and 3-(diethylamino)phenol, **3** (100 mg, 0.60 mmol, 2.25 eq) were stirred in TFE (7 mL) at 80 °C. The resulting suspension was cooled in an ice bath, filtered and washed with cold methanol, yielding **10** as a white/pale pink solid (128 mg, 0.26 mmol, 96%).

^1H NMR (500 MHz, $\text{DMSO-}d_6$) δ 7.71 – 7.60 (m, 1H), 7.41 (t, $J = 7.5$ Hz, 1H), 7.27 – 7.18 (m, 2H), 6.63 (d, $J = 8.0$ Hz, 2H), 6.54 (s, 1H), 6.06 (s, 4H), 3.23 (q, $J = 6.9$ Hz, 8H), 1.03 (t, $J = 7.0$ Hz, 12H).

^{31}P NMR (202 MHz, $\text{DMSO-}d_6$) δ 14.53.

HR-ESI-MS m/z for $\text{C}_{27}\text{H}_{34}\text{O}_5\text{N}_2\text{P}_1^-$ $[\text{M-H}]^-$ calcd: 497.2211 found: 497.2213



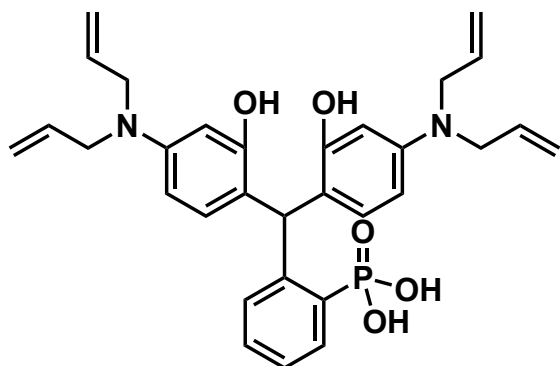
Synthesis of **11**.

1 (75 mg, 0.40 mmol, 1 eq) and 3-(ethylamino)-p-cresol, **4** (137 mg, 0.91 mmol, 2.25 eq) were stirred in TFE (7.5 mL) at 80 °C for 16 hours. The resulting suspension was cooled to room temperature, diluted with methanol (10 mL) and filtered, yielding an off-white solid (136 mg). The filtrate was concentrated *in vacuo*, and trituration with EtOAc yielded a further 55mg of solid. Combined, **11** was isolated as a white/pale purple powder (188 mg, 0.40 mmol, 99%).

^1H NMR (500 MHz, $\text{DMSO-}d_6$) δ 7.66 (ddd, $J = 13.8, 7.9, 1.3$ Hz, 1H), 7.43 (t, $J = 7.6$ Hz, 1H), 7.26 – 7.17 (m, 2H), 6.51 (s, 1H), 6.40 (s, 2H), 5.97 (s, 2H), 3.03 – 2.97 (m, 4H), 1.87 (s, 6H), 1.16 (t, $J = 7.1$ Hz, 6H).

^{31}P NMR (202 MHz, $\text{DMSO-}d_6$) δ 14.84.

HR-ESI-MS m/z for $\text{C}_{25}\text{H}_{30}\text{O}_5\text{N}_2\text{P}^+$ $[\text{M}]^+$ calcd: 469.1898 found: 469.1890



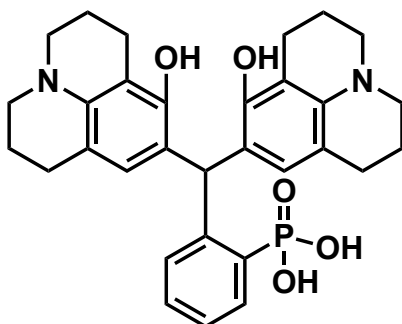
Synthesis of **12**.

1 (200 mg, 1.08 mmol, 1 eq) and **5** (448 mg, 2.37 mmol, 2.2 eq) were added to a round bottom flask that was subsequently evacuated and backfilled with N_2 (x3). Upon addition of TFE (6 mL) the solution was stirred at $80\text{ }^\circ\text{C}$ for 16 hours. Upon cooling to room temperature, the suspension was concentrated *in vacuo* and triturated with EtOAc to yield **12** as a pale pink powder (525 mg, 0.96 mmol, 89%)

^1H NMR (500 MHz, $\text{DMSO-}d_6$) δ 7.66 (dd, $J = 13.7, 7.6$ Hz, 1H), 7.43 (t, $J = 7.6$ Hz, 1H), 7.23 (ddt, $J = 12.9, 8.0, 4.1$ Hz, 2H), 6.54 (d, $J = 8.5$ Hz, 2H), 6.51 (s, 1H), 6.08 – 5.99 (m, 4H), 5.81 (ddt, $J = 15.4, 10.2, 5.1$ Hz, 4H), 5.15 – 5.08 (m, 8H), 3.80 (d, $J = 5.0$ Hz, 8H).

^{31}P NMR (202 MHz, $\text{DMSO-}d_6$) δ 15.03.

HR-ESI-MS m/z for $\text{C}_{31}\text{H}_{36}\text{O}_5\text{N}_2\text{P}^+$ $[\text{M}]^+$ calcd: 547.2356 found: 547.2354



Synthesis of compound **13**.

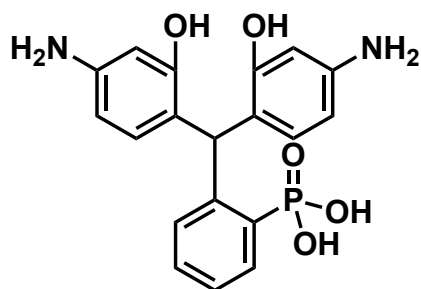
1 (150 mg, 0.81 mmol, 1 eq) and 8-hydroxyjulolidine, **6** (344 mg, 1.82 mmol, 2.25 eq) were charged into a round bottom flask that was subsequently evacuated and backfilled with N_2 (x3). Upon addition of TFE (5 mL), the solution was stirred at $80\text{ }^\circ\text{C}$ for 16 hours. The resulting

suspension was concentrated *in vacuo*, triturated with cold methanol, and filtered, yielding **13** as a white solid (405 mg, 0.74 mmol, 92%).

^1H NMR (400 MHz, DMSO- d_6) δ 7.65 (dd, $J = 13.7, 7.8$ Hz, 1H), 7.45 (t, $J = 7.5$ Hz, 1H), 7.33 – 7.18 (m, 2H), 6.56 (s, 1H), 6.22 (s, 2H), 3.05 – 2.85 (m, 8H), 2.49 – 2.38 (m, 8H), 1.92 – 1.70 (m, 8H).

^{31}P NMR (162 MHz, DMSO- d_6) δ 14.86.

HR-ESI-MS m/z for $\text{C}_{31}\text{H}_{34}\text{O}_5\text{N}_2\text{P}_1^-$ $[\text{M}-\text{H}]^-$ calcd: 545.2211 found: 545.2205



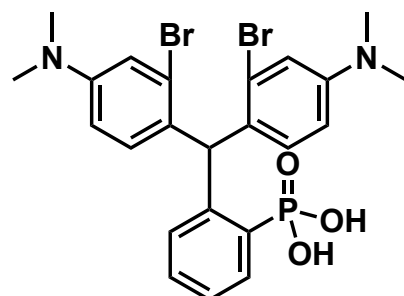
Synthesis of **14**

1 (150 mg, 0.81 mmol, 1 eq) and 3-aminophenol, **7** (220 mg, 2.01 mmol, 2.5 eq) were stirred in TFE (5 mL) at 80 °C for 16 hours. Upon cooling to room temperature, the suspension was filtered and washed with cold methanol to yield **14** as a beige solid (303 mg, 0.79 mmol, 97%).

^1H NMR (500 MHz, DMSO- d_6) δ 7.65 (dd, $J = 13.0, 7.7$ Hz, 1H), 7.38 (q, $J = 7.4$ Hz, 1H), 7.19 (dt, $J = 18.3, 6.2$ Hz, 2H), 6.51 (d, $J = 7.5$ Hz, 2H), 6.14 – 5.88 (m, 5H).

^{31}P NMR (202 MHz, DMSO- d_6) δ 12.91.

HR-ESI-MS m/z for $\text{C}_{19}\text{H}_{18}\text{O}_5\text{N}_2\text{P}_1^-$ $[\text{M}-\text{H}]^-$ calcd: 385.0959 found: 385.0954



Synthesis of **15**.

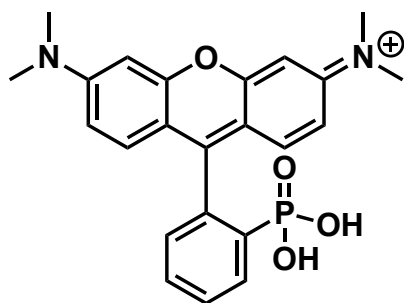
1 (350 mg, 1.74 mmol, 1 eq) and 3-bromo-N,N-dimethylaniline, **8** (972 mg, 5.22 mmol, 3 eq) were charged into a round bottom flask that was subsequently evacuated and backfilled with N_2 (x3).

TFE (3.75 mL) was added, and the solution was stirred at 80 °C for 48 hours. Concentration *in vacuo* and trituration of the resulting residue with EtOAc afforded **15** as a pale pink powder (915 mg, 1.61 mmol, 93%).

^1H NMR (500 MHz, DMSO- d_6) δ 7.86 (ddd, $J = 14.5, 8.0, 1.8$ Hz, 1H), 7.38 (t, $J = 7.9$ Hz, 1H), 7.30 (dt, $J = 7.3, 3.7$ Hz, 1H), 6.83 (d, $J = 2.5$ Hz, 2H), 6.80 – 6.75 (m, 1H), 6.72 (s, 1H), 6.58 (d, $J = 8.6$ Hz, 2H), 6.36 (d, $J = 7.5$ Hz, 2H), 2.85 (s, 12H).

^{31}P NMR (202 MHz, DMSO- d_6) δ 12.52.

HR-ESI-MS m/z for $\text{C}_{23}\text{H}_{24}\text{O}_3\text{N}_2\text{P}_1^-$ $[\text{M}-\text{H}]^-$ calcd: 564.9897 found: 564.9896



Synthesis of **16**.

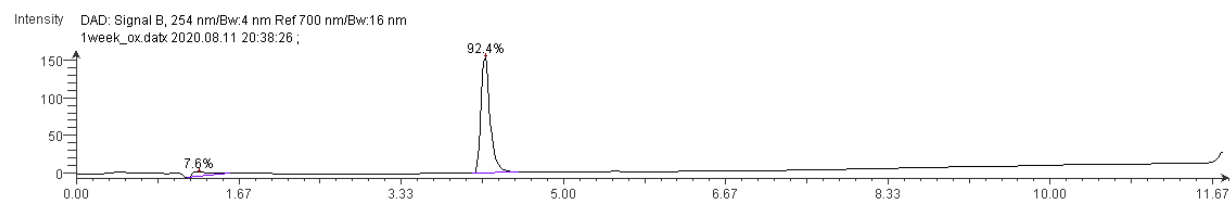
9 (350 mg, 0.8 mmol, 1 eq) and p-chloranil (394 mg, 1.6 mmol, 2 eq) were refluxed in MeOH (50 mL) for 48 hours (or until all solids had dissolved). Upon cooling to room temperature, the solution was filtered, and the filtrate was concentrated *in vacuo*. Trituration with EtOAc yielded **16** as a dark purple solid (335 mg, 0.8 mmol, >99%).

^1H NMR (400 MHz, DMSO- d_6) δ 8.04 (ddd, $J = 13.3, 6.0, 3.5$ Hz, 1H), 7.80 – 7.69 (m, 2H), 7.36 (dd, $J = 5.3, 4.7$ Hz, 1H), 7.08 (dd, $J = 9.4, 1.7$ Hz, 2H), 6.98 (d, $J = 9.5$ Hz, 2H), 6.93 (d, $J = 1.7$ Hz, 2H), 3.27 (s, 12H).

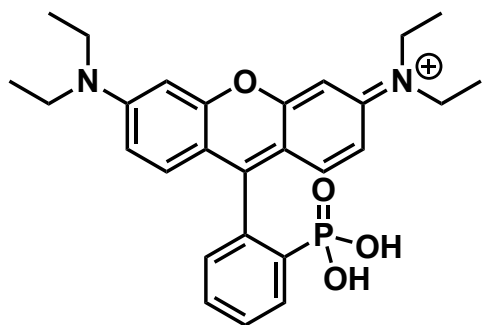
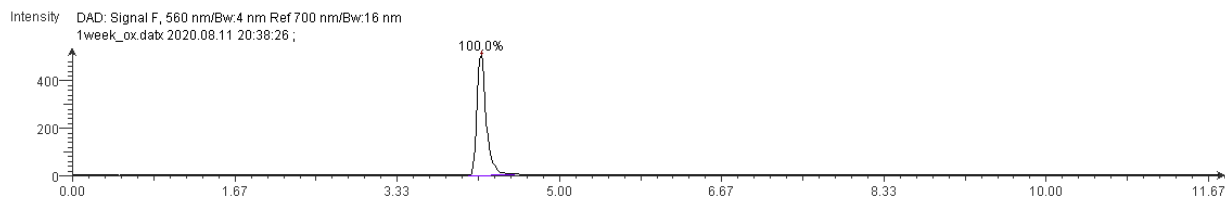
^{31}P NMR (162 MHz, DMSO- d_6) δ 9.70.

HR-ESI-MS m/z for $\text{C}_{23}\text{H}_{24}\text{O}_4\text{N}_2\text{P}^+$ $[\text{M}]^+$ calcd: 423.1468 found: 423.1470

254 nm



560 nm



Synthesis of **17**.

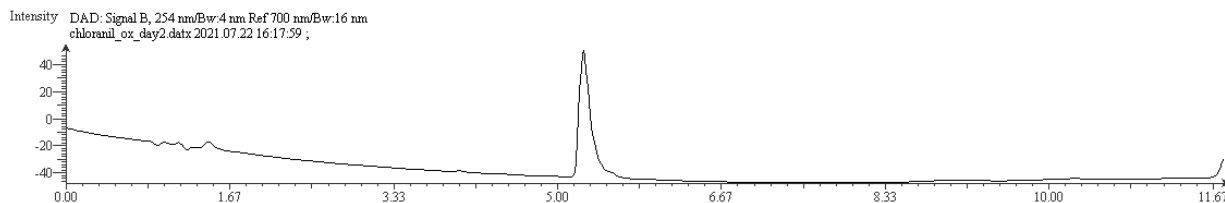
10 (54 mg, 0.11 mmol, 1 eq) and p-chloranil (58 mg, 0.24 mmol, 2 eq) were refluxed in MeOH (15 mL) for 16 hours. Upon cooling to room temperature, the solution was filtered, and the filtrate was concentrated *in vacuo*. Trituration with EtOAc yielded **17** as a dark purple powder (42 mg, 0.09 mmol, 80%).

^1H NMR (500 MHz, Methanol- d_4) δ 8.29 – 7.98 (m, 1H), 7.71 (s, 2H), 7.36 – 7.26 (m, 1H), 7.16 (d, J = 9.5 Hz, 2H), 7.00 (dd, J = 9.5, 2.3 Hz, 2H), 6.93 (d, J = 2.3 Hz, 2H), 3.67 (q, J = 7.2 Hz, 8H), 1.30 (t, J = 7.1 Hz, 12H).

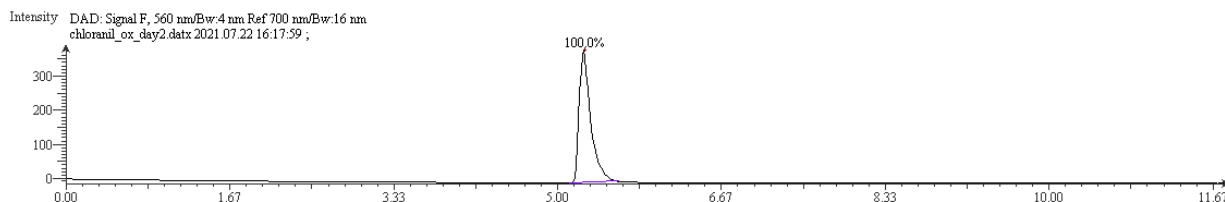
^{31}P NMR (202 MHz, Methanol- d_4) δ 10.34.

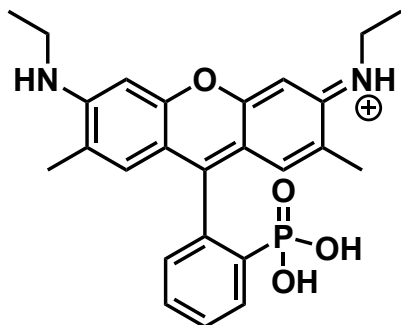
HR-ESI-MS m/z for $\text{C}_{27}\text{H}_{32}\text{O}_4\text{N}_2\text{P}_1^+ [\text{M}]^+$ calcd: 479.2094 found: 479.2100

254 nm



560 nm





Synthesis of **18**.

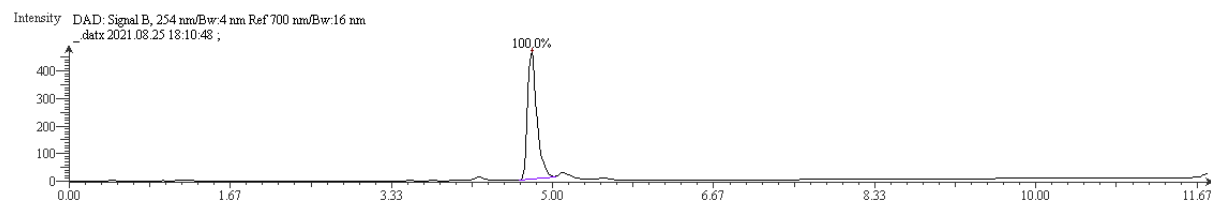
11 (126 mg, 0.27 mmol, 1 eq) and p-chloranil (86 mg, 0.35 mmol, 1.3 eq) were refluxed in MeOH (10 mL) for 20 hours. Upon cooling to room temperature, the solution was filtered, and the filtrate was concentrated *in vacuo*. Trituration with EtOAc yielded **18** as a dark red powder (100 mg, 0.22 mmol, 82%).

^1H NMR (500 MHz, Methanol- d_4) δ 8.19 (dd, $J = 13.8, 7.3$ Hz, 1H), 7.74 – 7.66 (m, 2H), 7.28 – 7.22 (m, 1H), 6.94 (s, 2H), 6.87 (s, 2H), 3.52 (q, $J = 7.2$ Hz, 4H), 2.12 (s, 6H), 1.36 (t, $J = 7.2$ Hz, 6H).

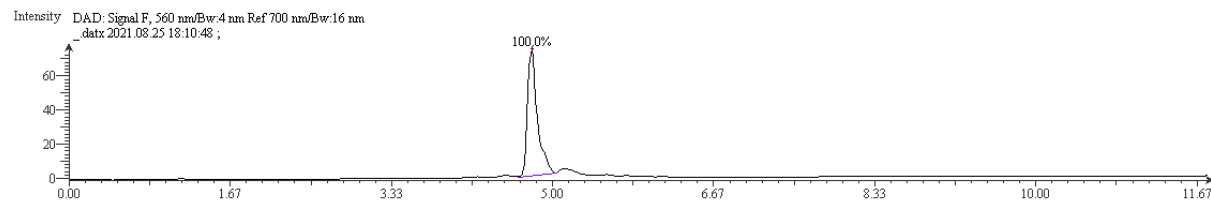
^{31}P NMR (202 MHz, Methanol- d_4) δ 9.68.

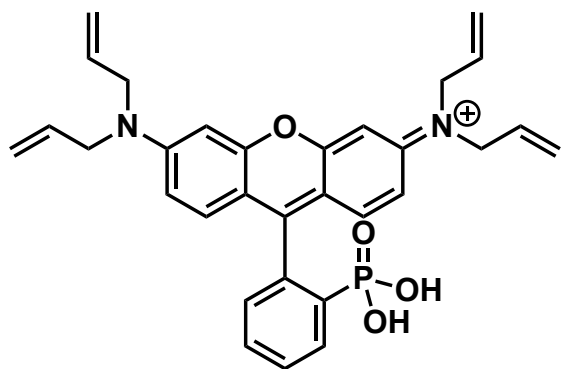
HR-ESI-MS m/z for $\text{C}_{25}\text{H}_{28}\text{O}_4\text{N}_2\text{P}^+$ $[\text{M}]^+$ calcd: 451.1781 found: 451.1774

254 nm



560 nm





Synthesis of **19**.

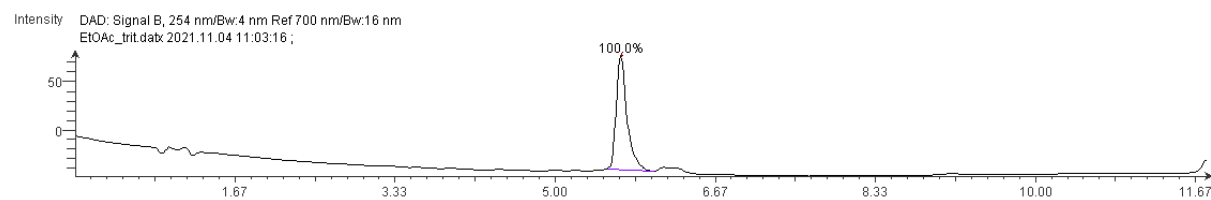
12 (440 mg, 0.81 mmol, 1 eq) and p-chloranil (297 mg, 1.21 mmol, 1.5 eq) were refluxed in MeOH (25 mL) for 12 hours. Upon cooling to room temperature, the solution was filtered, and the filtrate concentrated *in vacuo*. Trituration with EtOAc yielded **19** as a purple powder (397 mg, 0.75 mmol, 93%).

^1H NMR (500 MHz, Methanol- d_4) δ 8.21 – 8.13 (m, 1H), 7.68 (pt, $J = 7.6, 1.8$ Hz, 2H), 7.28 – 7.24 (m, 1H), 7.21 (d, $J = 9.4$ Hz, 2H), 7.01 (dd, $J = 9.5, 2.5$ Hz, 2H), 6.97 (d, $J = 2.4$ Hz, 2H), 5.95 (ddt, $J = 17.2, 10.1, 4.9$ Hz, 4H), 5.32 – 5.16 (m, 8H), 4.26 (dd, $J = 4.8, 2.0$ Hz, 8H).

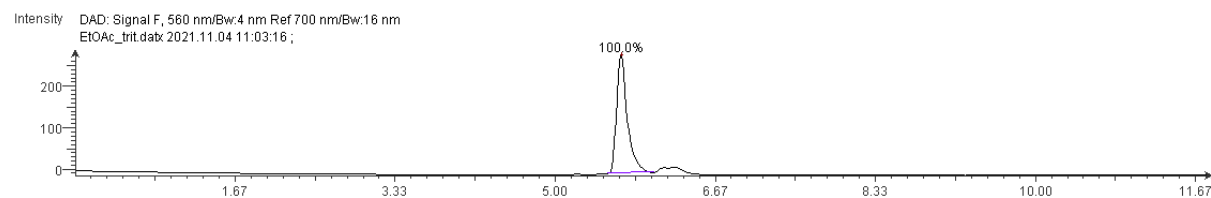
^{31}P NMR (202 MHz, Methanol- d_4) δ 9.29.

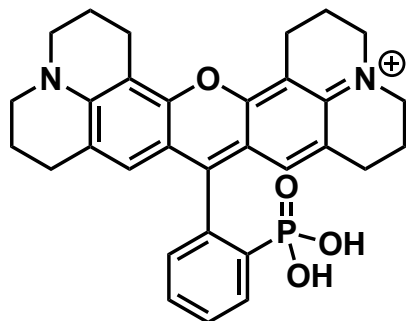
HR-ESI-MS m/z for $\text{C}_{31}\text{H}_{32}\text{O}_4\text{N}_2\text{P}^+$ $[\text{M}]^+$ calcd: 527.2094 found: 527.2094

254 nm



560 nm





Synthesis of **20**.

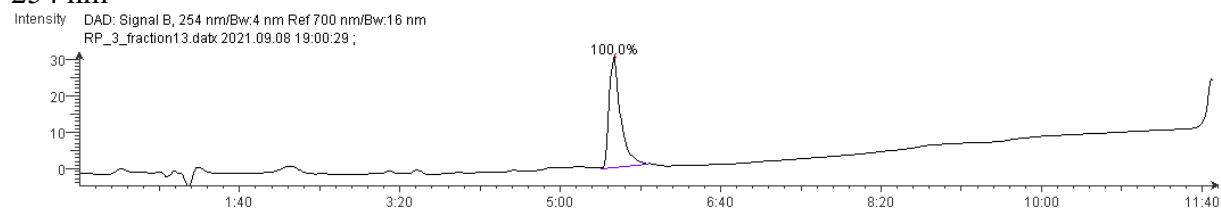
13 (50 mg, 0.09 mmol, 1 eq) was suspended in MeOH (20 mL) and refluxed for 48 hours whilst bubbling compressed air through the suspension. The solution was then cooled in an ice bath, filtered to remove unoxidized starting material, and the filtrate was concentrated *in vacuo*. Trituration with EtOAc yielded a crude solid that was purified by reverse phase silica chromatography (100% MeOH). **20** was isolated as a purple-pink solid (23 mg, 0.04 mmol, 48%).

^1H NMR (500 MHz, Methanol- d_4) δ 8.18 (dd, $J = 12.1, 7.7$ Hz, 1H), 7.59 (t, $J = 7.6$ Hz, 1H), 7.55 (t, $J = 7.4$ Hz, 1H), 7.10 (dd, $J = 7.1, 3.9$ Hz, 1H), 6.74 (s, 2H), 3.52 (t, $J = 5.6$ Hz, 4H), 3.47 (t, $J = 5.7$ Hz, 4H), 3.11 – 3.03 (m, 4H), 2.80 – 2.68 (m, 2H), 2.66 – 2.60 (m, 2H), 2.09 (p, $J = 6.3$ Hz, 4H), 1.97 – 1.90 (m, 4H).

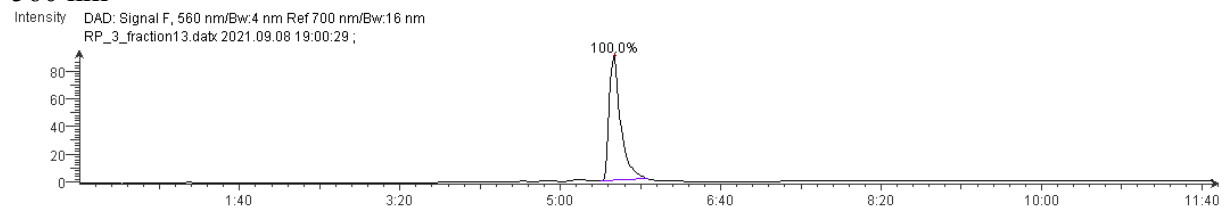
^{31}P NMR (202 MHz, Methanol- d_4) δ 7.76.

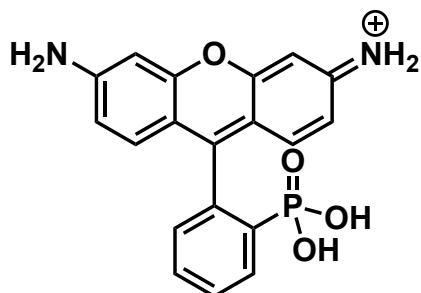
HR-ESI-MS m/z for $\text{C}_{31}\text{H}_{32}\text{O}_4\text{N}_2\text{P}_1^+$ $[\text{M}]^+$ calcd: 527.2094 found: 527.2104

254 nm



560 nm





Synthesis of **21**.

By air oxidation:

14 (100 mg, 0.26 mmol, 1 eq) was dissolved in DMSO (1 mL) and stirred at 100 °C for 12 hours. Upon cooling to room temperature, the crude solution was purified by reverse phase silica chromatography (60% MeOH/ H₂O) affording **21** as a red solid (21 mg, 0.05 mmol, 21%).

By deallylation of **19**:

Method A (**Table S2, entry B**):

19 (50 mg, 0.095 mmol, 1 eq), 1,3-dimethylbarbituric acid (90 mg, 0.576 mmol, 6 eq) and Pd(PPh₃)₄ (4.5 mg, 0.004 mmol, 0.04 eq) were charged into a flame dried Schlenk flask, that was subsequently evacuated and backfilled with N₂ (x3). Upon addition of DMF (0.75 mL) and triethylamine (0.25 mL), the solution was stirred at 80 °C overnight. Upon cooling to room temperature, the solution was diluted with EtOAc and filtered through a pad of celite. The celite was flushed several times with EtOAc to remove excess NDMBA, before elution of the fluorophore by washing with MeOH. Purification by reverse phase silica chromatography (60% MeOH/ H₂O) afforded **21** as an orange/red solid (18 mg, 0.049 mmol, 52 %).

Method B (**Table S2, entry D**):

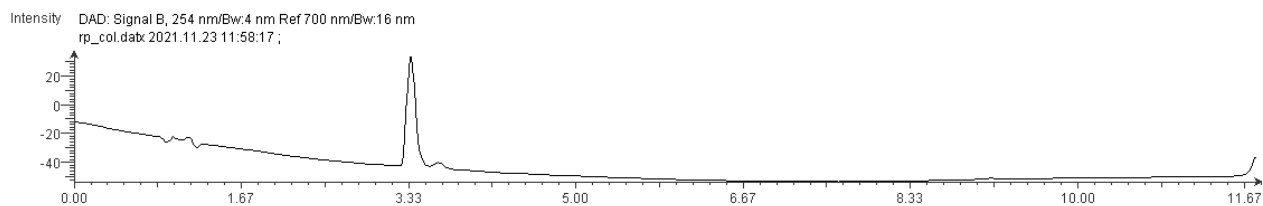
19 (65 mg, 0.12 mmol, 1 eq) and potassium tert-butoxide (95 mg, 0.85 mmol, 7 eq) were dissolved in DMSO (2.5 mL) and stirred at 100 °C for 5 minutes. Upon a color change to a deep brown solution water (7.5 mL) was added. This was followed by acidification with 1 M HCl (1 mL) and continued stirring at 100 °C for 15 minutes. The solution was cooled to room temperature and concentrated to a small volume of liquid < 3 mL. Purification by reverse phase silica chromatography (60% MeOH/ H₂O) afforded **21** as an orange/ red solid (31 mg, 0.085 mmol, 71%).

¹H NMR (500 MHz, Methanol-*d*₄ + 1 drop NaOD) δ 7.86 (dd, *J* = 10.0, 7.7 Hz, 1H), 7.40 (dtt, *J* = 7.5, 3.6, 1.9 Hz, 1H), 7.34 (t, *J* = 7.5 Hz, 1H), 7.10 (d, *J* = 8.7 Hz, 2H), 6.81 (dd, *J* = 7.7, 2.6 Hz, 1H), 6.53 (d, *J* = 2.2 Hz, 2H), 6.49 (dd, *J* = 8.7, 2.2 Hz, 2H).

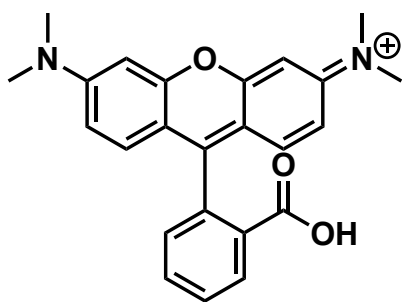
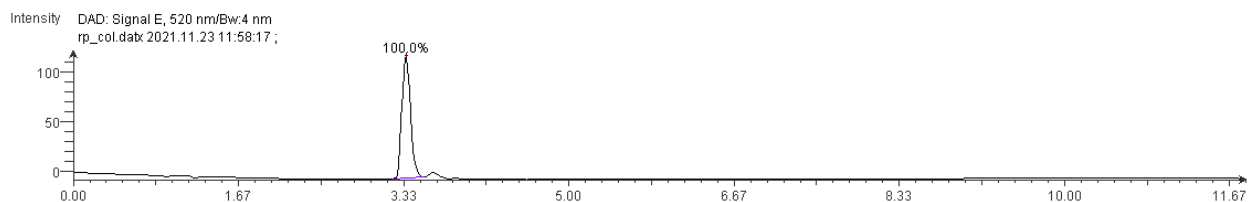
³¹P NMR (202 MHz, Methanol-*d*₄ + 1 drop NaOD) δ 21.52.

HR-ESI-MS *m/z* for C₁₉H₁₆O₄N₂P⁺ [M]⁺ calcd: 367.0842 found: 367.0844

254 nm



520 nm

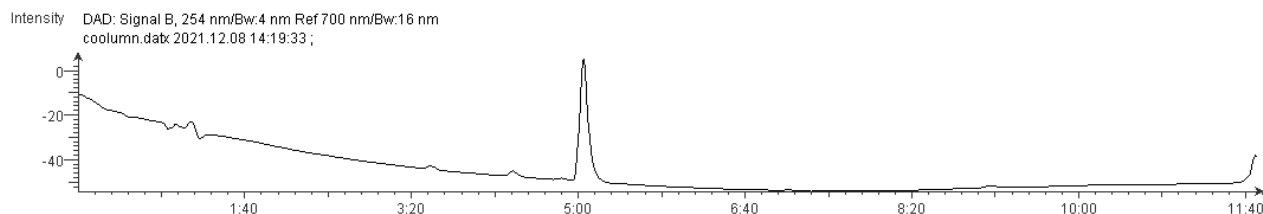


Synthesis of 3-carboxyTMR.

2-carboxybenzaldehyde (159 mg, 1.2 mmol, 1 eq) and 3-dimethylaminophenol, **2** (363 mg, 2.9 mmol, 2.5 eq) were charged into a round bottom flask that was subsequently evacuated and backfilled with N₂ (x3). TFE (10 mL) was added, and the solution was stirred at 80 °C for 3 days. Upon cooling to room temperature, and concentration *in vacuo* the residue was triturated with EtOAc to afford a pale purple solid (237 mg). The solid was combined with chloranil (286 mg, 1.2 mmol, 1 eq) and refluxed in MeOH (15 mL) for 12 hours. The solution was cooled, concentrated *in vacuo*, and purified by flash silica chromatography to afford **3-carboxytetramethylrhodamine** as a pink solid (147 mg, 0.36 mmol, 31%).

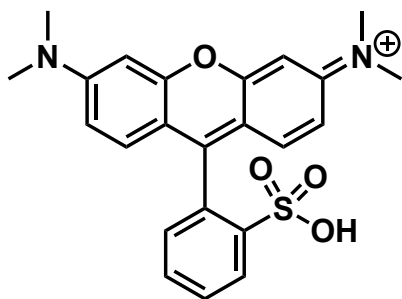
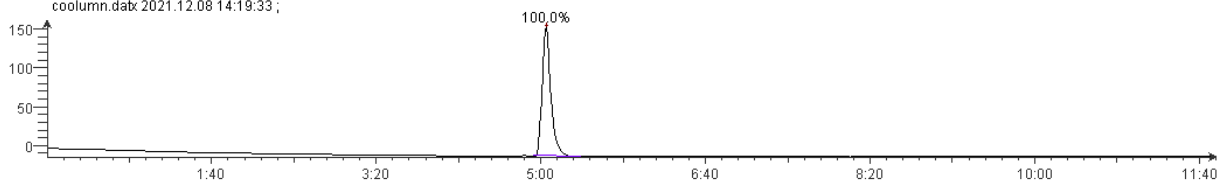
¹H NMR (400 MHz, Methanol-*d*₄) δ 8.23 – 8.12 (m, 1H), 7.73 – 7.67 (m, 2H), 7.33 – 7.27 (m, 1H), 7.24 (d, *J* = 9.5 Hz, 2H), 7.02 (dd, *J* = 9.4, 2.3 Hz, 2H), 6.93 (d, *J* = 2.0 Hz, 2H), 3.28 (s, 12H).

254 nm



560 nm

Intensity DAD: Signal F, 560 nm/Bw:4 nm Ref 700 nm/Bw:16 nm
coolumn.dabx 2021.12.08 14:19:33 ;



Synthesis of 3-sulfoTMR.

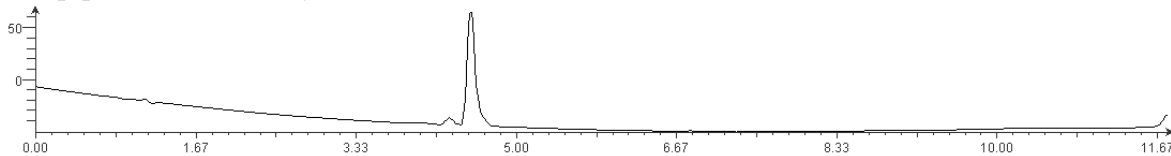
2-sulfonobenzaldehyde (139 mg, 0.75 mmol, 1 eq) and 3-dimethylaminophenol, **2** (257 mg, 1.88 mmol, 2.5 eq) were dissolved in methanesulfonic acid (2 mL) and stirred at 130 °C for 72 hours. Upon cooling to room temperature, the solution was diluted with water (20 mL) and made basic with addition of 10 M KOH. Extraction into 3:1 DCM: ⁱPrOH (x4), drying over Na₂SO₄ and concentration *in vacuo* afforded a deep purple solid which was subsequently purified by reverse phase silica chromatography (60% MeOH/ H₂O). **3** was isolated as a dark purple solid (36 mg, 0.085 mmol, 12%).

¹H NMR (500 MHz, DMSO-*d*₆) δ 8.03 – 7.95 (m, 1H), 7.67 – 7.60 (m, 1H), 7.56 (t, *J* = 7.5 Hz, 1H), 7.18 (d, *J* = 8.1 Hz, 1H), 7.07 – 6.99 (m, 4H), 6.90 (d, *J* = 1.4 Hz, 2H), 3.24 (s, 12H).

HR-ESI-MS *m/z* for C₂₃H₂₃O₄N₂S⁺ [M]⁺ calcd: 423.1373 found: 423.1376

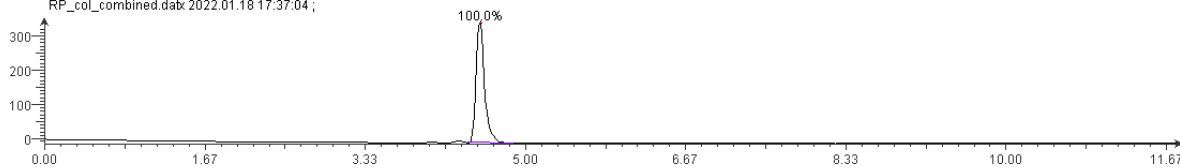
254 nm

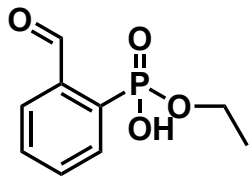
Intensity DAD: Signal B, 254 nm/Bw:4 nm Ref 700 nm/Bw:16 nm
RP_col_combined.dabx 2022.01.18 17:37:04 ;



560 nm

Intensity DAD: Signal F, 560 nm/Bw:4 nm Ref 700 nm/Bw:16 nm
RP_col_combined.dabx 2022.01.18 17:37:04 ;



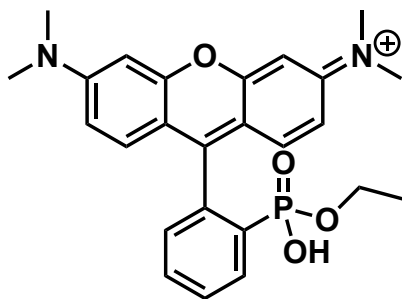


Synthesis of **22**.

diethyl (2-formylphenyl)phosphonate (685 mg, 2.8 mmol, 1 eq) was dissolved in DCM (3 mL) and added to a solution of 1 M NaOH (3 mL) with tetrabutylammonium bromide (273 mg, 0.9 mmol, 0.3 eq). The biphasic mixture was stirred vigorously at 40 °C overnight. Upon cooling to room temperature the mixture was diluted with water and the aqueous layer was washed with EtOAc (x3). The aqueous layer was then acidified with 1 M HCl and extracted into EtOAc (x3). Drying of the pooled organics with Na₂SO₄ and concentration *in vacuo* afforded **22** as a golden viscous oil (415 mg, 1.9 mmol, 70%).

¹H NMR (500 MHz, Chloroform-*d*) δ 10.59 (s, 1H), 8.21 – 7.99 (m, 2H), 7.77 – 7.62 (m, 2H), 4.20 – 4.12 (m, 2H), 1.32 (t, *J* = 7.1 Hz, 3H).

³¹P NMR (202 MHz, Chloroform-*d*) δ 18.45.



Synthesis of **23**.

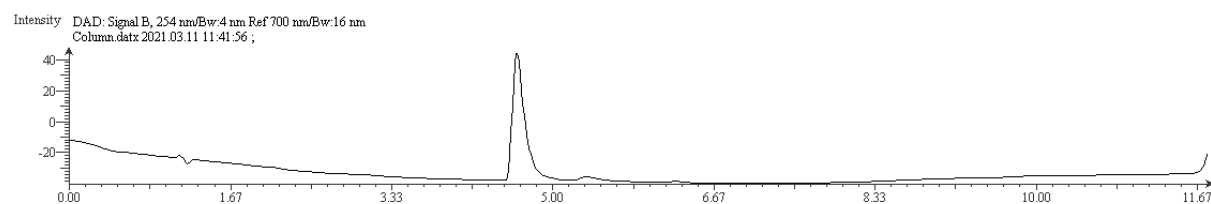
22 (75 mg, 0.35 mmol, 1 eq) and 3-dimethylaminophenol, **2** (112 mg, 0.88 mmol, 2.5 eq) were stirred in TFE (7 mL) at 80 °C overnight. Upon cooling to room temperature, the solution was concentrated *in vacuo* and the residue was triturated with EtOAc to afford a pale purple solid. The solid was combined with chloranil (90 mg, 0.37 mmol, 1.05 eq) and refluxed in MeOH (5 mL) for 3 hours. Purification by flash silica chromatography afforded **23** as a purple solid (62 mg, 0.14 mmol, 39%).

¹H NMR (500 MHz, Chloroform-*d*) δ 8.25 (dd, *J* = 12.0, 7.7 Hz, 1H), 7.58 (t, *J* = 7.8 Hz, 1H), 7.48 (t, *J* = 7.8 Hz, 1H), 7.39 (d, *J* = 9.4 Hz, 2H), 7.05 (dd, *J* = 8.1, 3.5 Hz, 1H), 6.83 (dd, *J* = 9.4, 2.0 Hz, 2H), 6.70 (d, *J* = 1.6 Hz, 2H), 3.73 (q, *J* = 7.0 Hz, 2H), 3.23 (s, 12H), 1.02 (t, *J* = 7.0 Hz, 3H).

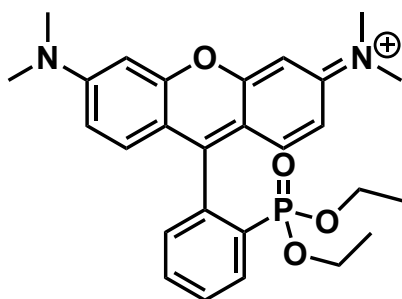
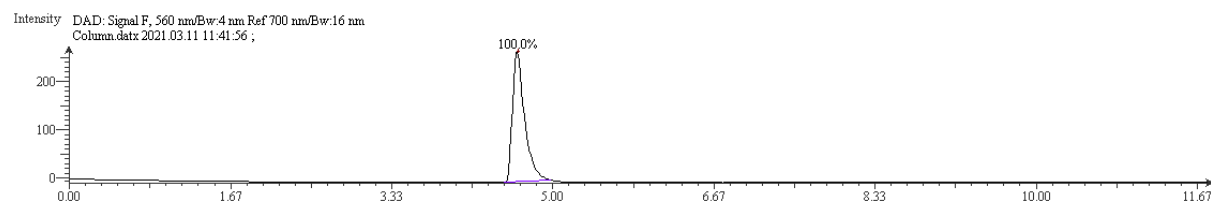
³¹P NMR (202 MHz, Chloroform-*d*) δ 6.17.

HR-ESI-MS *m/z* for C₂₅H₂₈O₄N₂P⁺ [M]⁺ calcd: 451.1781 found: 451.1782

254 nm



560 nm



Synthesis of **24**.

16 (200 mg, 0.47 mmol, 1 eq), Ag₂O (237 mg, 1.18 mmol, 2.5eq) and 4 Å molecular sieves (200 mg) were charged into a flame dried round bottom flask that was subsequently evacuated and backfilled with N₂ (x3). Upon addition of MeCN (12 mL), the suspension was stirred at room temperature for 30 minutes. Bromoethane (0.11 mL, 1.41 mmol, 3.5 eq) was added, and the reaction stirred at 50 °C overnight. A second addition of bromoethane (0.2 mL, 2.1 mmol, 4.5 eq) was added and the reaction stirred for a further 6 hours. Upon cooling to room temperature, the suspension was filtered through a pad of celite and washed with methanol, and the filtrate was concentrated *in vacuo*. Purification by flash silica chromatography (5 to 10% MeOH/DCM) yielded **24** as a purple solid (127 mg, 0.27 mmol, 22%).

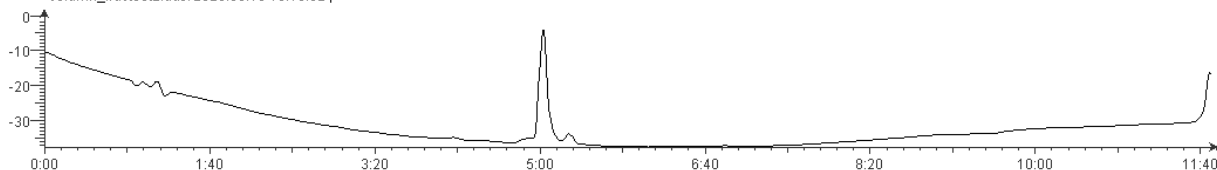
¹H NMR (400 MHz, Chloroform-*d*) δ 8.11 (dd, *J* = 14.0, 7.8 Hz, 1H), 7.79 (t, *J* = 7.2 Hz, 1H), 7.72 (td, *J* = 7.6, 3.4 Hz, 1H), 7.45 – 7.33 (m, 1H), 7.07 (d, *J* = 9.4 Hz, 2H), 6.99 – 6.75 (m, 4H), 3.91 – 3.72 (m, 4H), 3.34 (s, 12H), 1.01 (t, *J* = 7.1 Hz, 6H).

³¹P NMR (162 MHz, Chloroform-*d*) δ 15.16.

HR-ESI-MS *m/z* for C₂₇H₃₂O₄N₂P⁺ [M]⁺ calcd: 479.2094 found: 479.2093

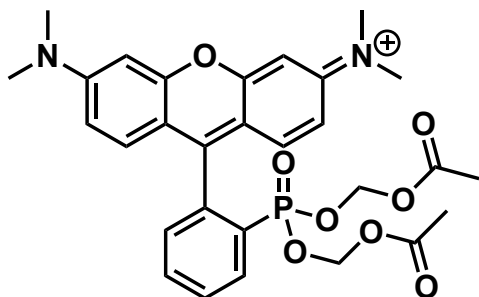
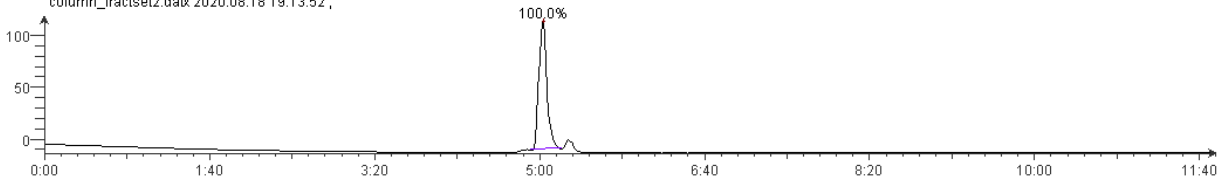
254 nm

Intensity DAD: Signal B, 254 nm/Bw:4 nm Ref 700 nm/Bw:16 nm
column_fractset2.dax 2020.08.18 19:13:52;



560 nm

Intensity DAD: Signal F, 560 nm/Bw:4 nm Ref 700 nm/Bw:16 nm
column_fractset2.dax 2020.08.18 19:13:52;



Synthesis of **25**

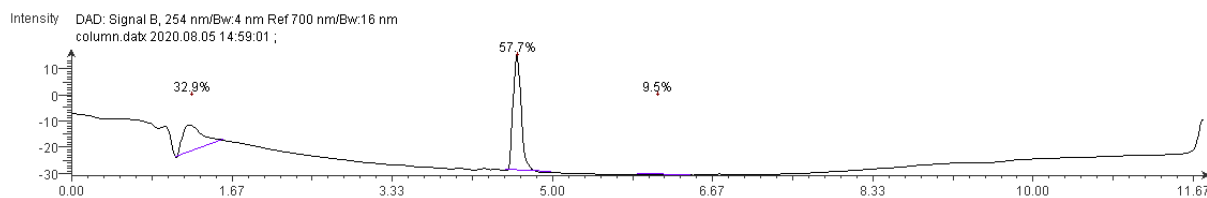
16 (46 mg, 0.11 mmol, 1 eq), Ag₂O (63 mg, 0.27 mmol, 2.5 eq) and 4 Å molecular sieves (50 mg) were charged into a flame dried round bottom flask, that was subsequently evacuated and backfilled with N₂ (x3). Upon addition of MeCN (4 mL), the suspension was stirred at room temperature for 1 hour and then bromomethyl acetate (0.04 mL, 0.039 mmol, 3.5 eq) was added. The suspension was stirred at 50 °C overnight, before cooling to room temperature, and filtering through a pad of celite and washed with DCM. The filtrate was concentrated *in vacuo* and purified by flash silica chromatography (8% MeOH/ DCM) to afford **25** as a purple solid (15 mg, 0.03 mmol, 25%).

¹H NMR (400 MHz, Chloroform-*d*) δ 8.10 (dd, *J* = 14.6, 7.7 Hz, 1H), 7.86 (t, *J* = 7.8 Hz, 1H), 7.82 – 7.68 (m, 1H), 7.41 (t, *J* = 6.3 Hz, 1H), 7.05 (d, *J* = 9.4 Hz, 2H), 6.96 (d, *J* = 8.8 Hz, 2H), 6.91 (s, 2H), 5.51 – 5.12 (m, 4H), 3.37 (s, 12H), 1.99 (s, 6H).

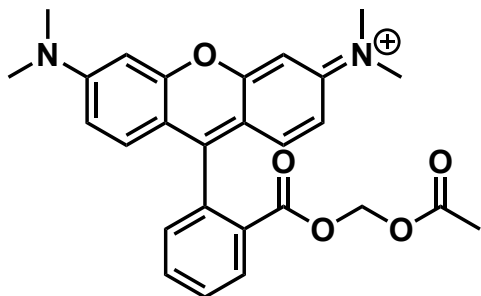
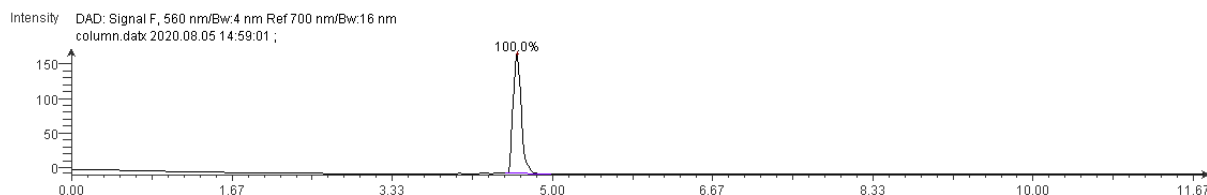
³¹P NMR (162 MHz, Chloroform-*d*) δ 14.34.

HR-ESI-MS *m/z* for C₂₉H₃₂O₈N₂P⁺ [M]⁺ calcd: 567.1891 found: 467.1886

254 nm



560 nm



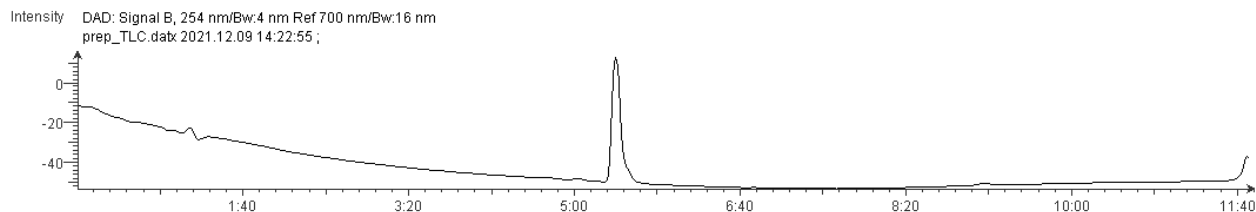
Synthesis of 26

(50 mg, 0.13 mmol, 1 eq), Ag₂O (45 mg, 0.19 mmol, 1.5 eq) and 4 Å molecular sieves (50 mg) were charged into a flame dried reaction vial that was subsequently evacuated and backfilled with N₂ (x3). DMF (1.5 mL) was added, and the reaction warmed to 60 °C. Bromomethyl acetate (0.03 mL, 0.32 mmol, 2.5 eq) was added and the suspension stirred for 16 hours. Upon cooling to room temperature, the mixture was diluted with DCM and filtered through a plug of celite. Concentration *in vacuo*, followed by flash silica chromatography (7.5% MeOH/DCM) afforded **26** as a dark purple solid (19 mg, 0.04 mmol, 32%).

¹H NMR (500 MHz, DMSO-*d*₆) δ 8.26 (dd, *J* = 7.9, 1.3 Hz, 1H), 7.95 (td, *J* = 7.5, 1.4 Hz, 1H), 7.87 (td, *J* = 7.7, 1.4 Hz, 1H), 7.54 (dd, *J* = 7.5, 1.3 Hz, 1H), 7.10 (dd, *J* = 9.5, 2.4 Hz, 2H), 7.01 (d, *J* = 9.5 Hz, 2H), 6.99 (d, *J* = 2.5 Hz, 2H), 5.55 (s, 2H), 3.28 (s, 12H), 1.83 (s, 3H).

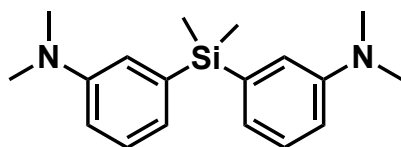
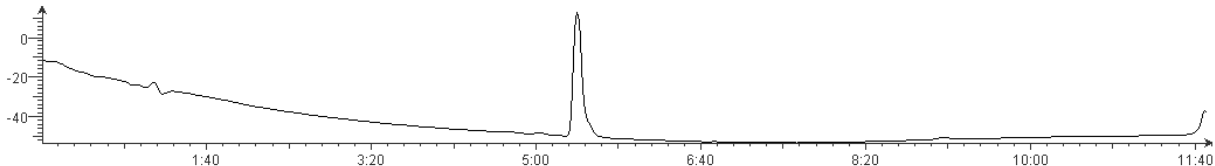
HR-ESI-MS *m/z* for C₂₇H₂₇O₅N₂⁺ [M]⁺ calcd: 459.1914 found: 459.1912

254 nm



560 nm

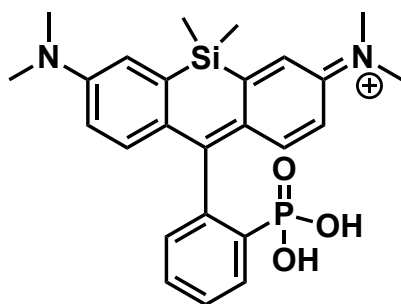
Intensity DAD: Signal B, 254 nm/Bw:4 nm Ref 700 nm/Bw:16 nm
prep_TLC.dax 2021.12.09 14:22:55;



Synthesis of **27**

3-bromo-N,N-dimethylaniline (1.19 g, 5.9 mmol, 2.4 eq) was charged into a flamed dried Schlenk flask that was subsequently evacuated and backfilled with N₂ (x3). THF (11.8 mL) was added and the solution cooled to -78 °C. nBuLi (2.96 mL, 2M in hexanes, 5.9 mmol, 2.4 eq) was added slowly and the solution stirred at -78 °C for 30 minutes. Dichlorodimethyl silane (0.3 mL, 2.5 mmol 1 eq) was added slowly and the solution was slowly warmed to room temperature over 2 hours. The reaction was quenched with sat. ammonium chloride, followed by extraction into EtOAc (x3). The combined organics were washed with brine (x2), dried over Na₂SO₄ and concentrated *in vacuo*. Purification by flash silica chromatography (5% EtOAc/ Hexanes) yielded **27** as a colorless oil (665 mg, 2.23 mmol, 91%).

¹H NMR (400 MHz, Chloroform-*d*) δ 7.23 (t, *J* = 8.1 Hz, 2H), 6.94 (d, *J* = 2.5 Hz, 2H), 6.91 (d, *J* = 7.1 Hz, 2H), 6.77 (dd, *J* = 8.2, 2.3 Hz, 2H), 2.92 (s, 12H), 0.53 (s, 6H).



Synthesis of **28**

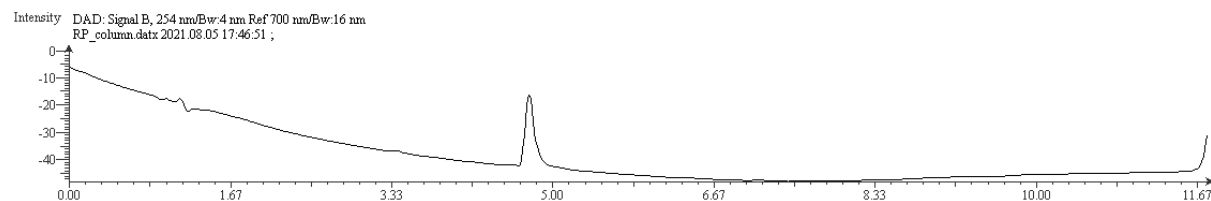
1 (50 mg, 0.27 mmol, 1 eq) and **27** (96 mg, 0.32 mmol, 1.2 eq) were dissolved in TFE (5 mL) and stirred at 80 °C for 7 days. The crude reaction was purified by reverse phase silica chromatography (75% MeOH/ H₂O) to yield **28** as a deep blue solid (54 mg, 0.11 mmol, 43%).

^1H NMR (500 MHz, Methanol- d_4) δ 8.10 (dd, $J = 12.2, 7.4$ Hz, 1H), 7.56 – 7.52 (m, 1H), 7.49 (t, $J = 7.5$ Hz, 1H), 7.24 (d, $J = 2.8$ Hz, 2H), 7.17 (d, $J = 9.6$ Hz, 2H), 7.05 (dd, $J = 7.0, 4.1$ Hz, 1H), 6.68 (dd, $J = 9.6, 2.8$ Hz, 2H), 3.27 (s, 12H), 0.59 (s, 3H), 0.57 (s, 3H).

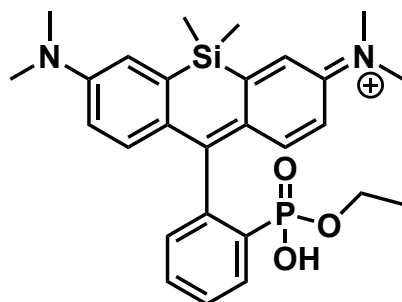
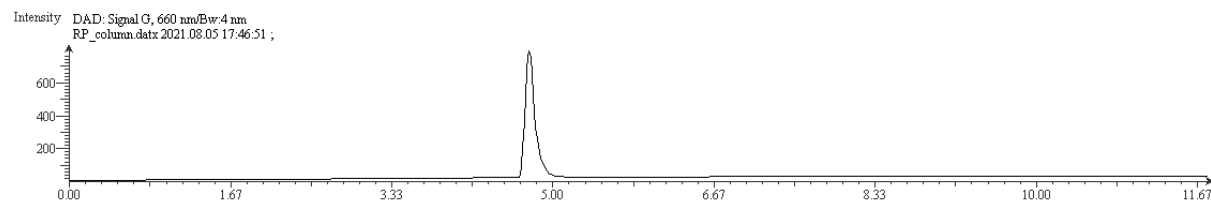
^{31}P NMR (202 MHz, Methanol- d_4) δ 9.80.

HR-ESI-MS m/z for $\text{C}_{25}\text{H}_{30}\text{O}_3\text{N}_2\text{P}_1\text{Si}_1^+$ $[\text{M}]^+$ calcd: 465.1758 found: 465.1766

254 nm



660 nm



Synthesis of **29**.

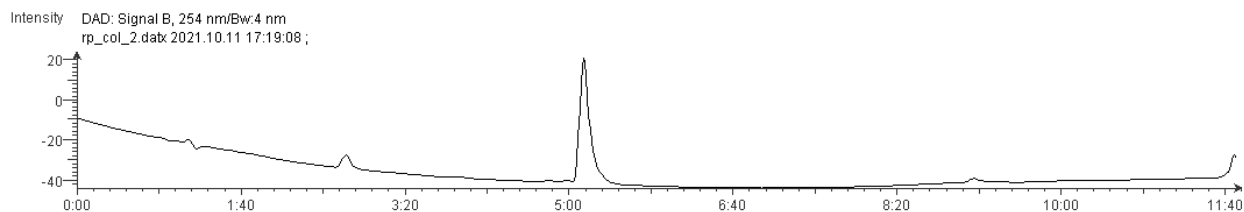
22 (250 mg, 1.17 mmol, 1 eq) and **27** (401 mg, 1.34 mmol, 1.15 eq) were dissolved in TFE (4 mL) and stirred at 80 °C for 4 days. Upon cooling to room temperature, the crude mixture was purified by reverse phase silica chromatography (60 to 100% MeOH/ H_2O) affording **29** as a deep blue solid (110 mg, 0.22 mmol, 19%).

^1H NMR (500 MHz, Methanol- d_4) δ 8.11 (ddd, $J = 12.8, 7.2, 1.8$ Hz, 1H), 7.56 (pt, $J = 7.5, 1.7$ Hz, 2H), 7.27 (d, $J = 2.9$ Hz, 2H), 7.18 – 7.05 (m, 3H), 6.70 (dd, $J = 9.6, 2.9$ Hz, 2H), 3.53 (p, $J = 7.0$ Hz, 2H), 3.31 (s, 12H), 0.86 (t, $J = 7.1$ Hz, 3H), 0.60 (s, 3H), 0.58 (s, 3H).

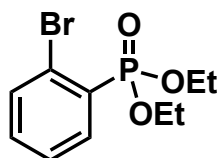
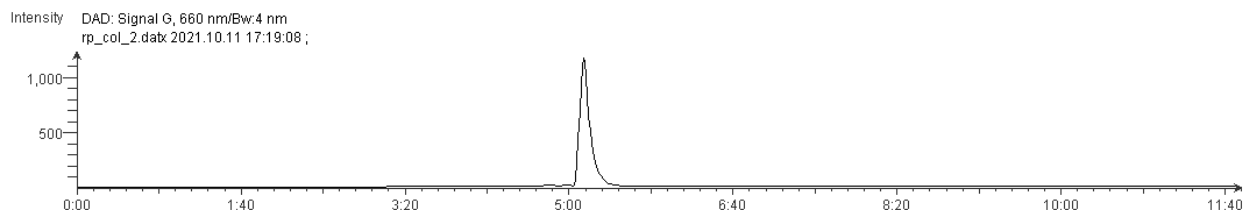
^{31}P NMR (202 MHz, Methanol- d_4) δ 10.18.

HR-ESI-MS m/z for $\text{C}_{27}\text{H}_{34}\text{O}_3\text{N}_2\text{PSi}^+$ $[\text{M}]^+$ calcd: 493.2071 found: 493.2069

254 nm



560 nm

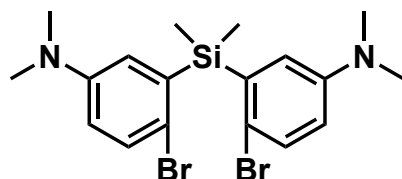


Synthesis of compound 32.

2-bromo-iodobenzene (500 mg, 1.77 mmol, 1 eq) and PdCl₂ were charged into a flame dried reaction vial that was subsequently evacuated and backfilled with N₂ (x3). Triethyl phosphite (0.32 mL, 1.86 mmol, 1.05 eq) was added and the reaction stirred at 130 °C for 16 hours. Upon cooling to room temperature the crude oil was purified by flash silica chromatography (368 mg, 1.26 mmol, 71%).

¹H NMR (500 MHz, Chloroform-*d*) δ 8.08 – 7.96 (m, 1H), 7.67 (ddd, *J* = 7.8, 5.0, 1.6 Hz, 1H), 7.47 – 7.30 (m, 2H), 4.31 – 4.05 (m, 4H), 1.36 (t, *J* = 7.1 Hz, 6H).

³¹P NMR (202 MHz, Chloroform-*d*) δ 14.77.

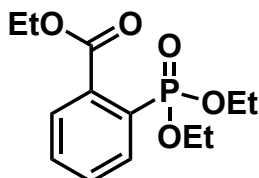


Synthesis of compound 33.

27 (350 mg, 1.17 mmol, 1 eq) was dissolved in MeCN (5 mL) and cooled in an ice bath. N-bromosuccinimide (438 mg, 2.46 mmol, 2.1 eq) was added and the solution stirred at 0 °C for 1.5 hours. Upon quenching with saturated NaHCO₃ and extraction with DCM (x3), the organics were

dried over Na₂SO₄ and concentrated *in vacuo*. Purification by flash silica chromatography (10% DCM/Hexanes) afforded **S6** as a pale yellow solid (398 mg, 0.88 mmol, 75%).

¹H NMR (500 MHz, Chloroform-*d*) δ 7.34 (d, *J* = 8.7 Hz, 2H), 6.83 (d, *J* = 3.2 Hz, 2H), 6.59 (dd, *J* = 8.7, 3.2 Hz, 2H), 2.87 (s, 12H), 0.75 (s, 6H).

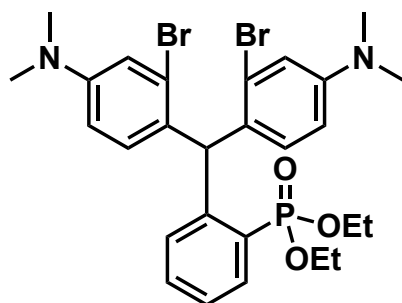


Synthesis of compound **34**.

2-iodobenzoic acid (1.0 g, 4.03 mmol, 1 eq) and PdCl₂ (73.0 mg, 0.40 mmol, 0.1 eq) were charged into a flame dried Schlenk flask that was subsequently evacuated and backfilled with N₂ (x3). Triethyl phosphite (2.77 mL, 16.13 mmol, 4 eq) was added and the solution stirred at 150 °C overnight. Upon cooling to room temperature the crude oil was purified by flash silica chromatography (60% EtOAc/ Hexanes) to isolate **S7** as a golden oil (1.02 g, 3.56 mmol, 89 %).

¹H NMR (400 MHz, Chloroform-*d*) δ 8.03 – 7.92 (m, 1H), 7.75 – 7.66 (m, 1H), 7.63 – 7.49 (m, 2H), 4.39 (q, *J* = 7.2 Hz, 2H), 4.18 – 4.08 (m, 4H), 1.39 (t, *J* = 7.1 Hz, 3H), 1.33 (d, *J* = 7.1 Hz, 6H).

³¹P NMR (162 MHz, Chloroform-*d*) δ 16.27.



Synthesis of compound **35**.

15 (300 mg, 0.53 mmol, 1 eq) was charged into a flame dried round bottom flask equipped with a reflux condenser, that was subsequently evacuated and backfilled with N₂ (x3). DCM (3 mL) and DMF (10 μL) were added and the solution stirred at 30 °C. Slow addition of oxalyl chloride (0.23 mL, 2.64 mmol, 5 eq) produced effervescence and the solution was refluxed for 12 hours. Upon concentration *in vacuo*, the crude residue was quickly evacuated and backfilled with N₂ (x3).* The residue was cooled in an ice bath and dissolved in a mixture of THF (4 mL) and EtOH (2 mL). Addition of triethylamine (0.75 mL) resulted in a suspension that was slowly warmed to room temperature and stirred for 3 hours. The suspension was diluted with 1:1 EtOAc: hexanes and solids were removed by vacuum filtration. Concentration of the filtrate *in vacuo* yielded a brown oil that was redissolved in EtOAc and extracted into 0.1 M HCl (x3). The combined aqueous extracts were made basic by addition of 2 M NaOH, followed by back extraction into EtOAc (x3).

The organic layers were combined, dried with Na₂SO₄ and concentrated to afford **S8** as a slightly pink oil (282 mg, 0.45 mmol, 85%).

*this intermediate is unstable when exposed to air.

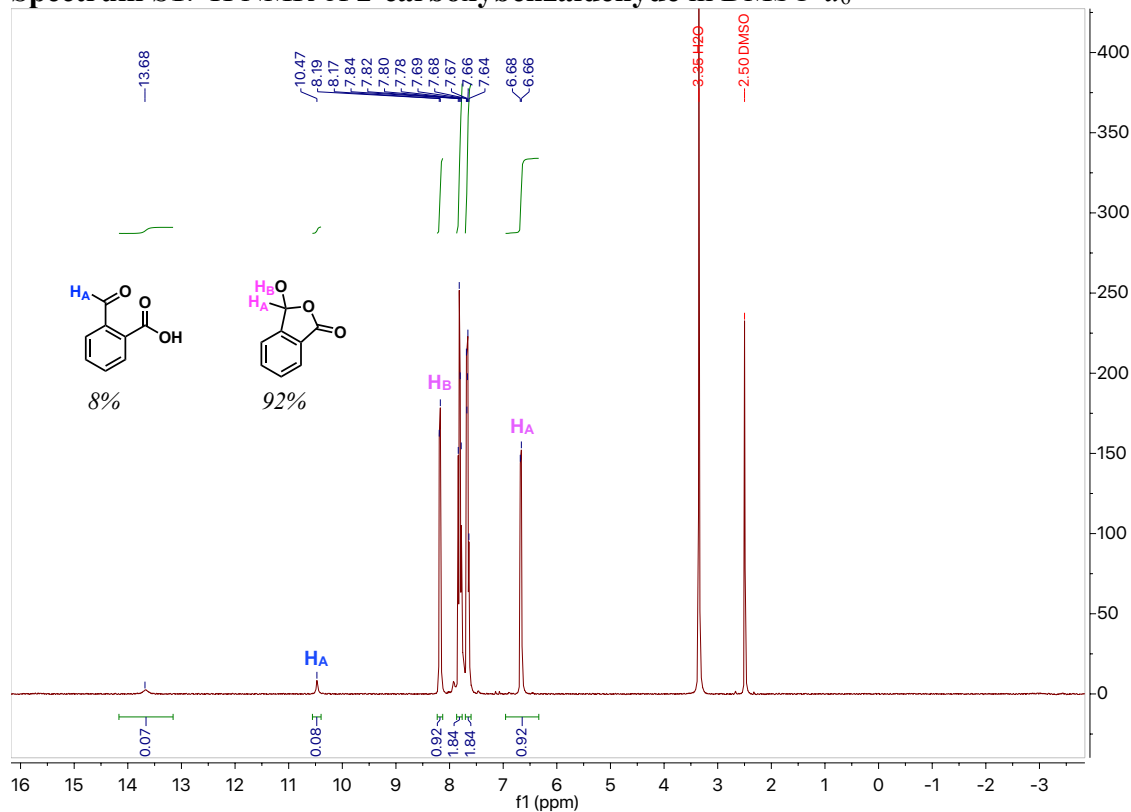
¹H NMR (500 MHz, Chloroform-*d*) δ 8.09 (ddd, *J* = 14.8, 7.6, 1.6 Hz, 1H), 7.40 (tt, *J* = 7.6, 1.5 Hz, 1H), 7.32 (td, *J* = 7.7, 3.2 Hz, 1H), 6.97 (s, 2H), 6.91 (t, *J* = 6.9 Hz, 1H), 6.59 (s, 1H), 6.58 – 6.33 (m, 4H), 4.31 – 3.71 (m, 4H), 2.91 (s, 12H), 1.34 – 1.22 (m, 6H).

³¹P NMR (202 MHz, Chloroform-*d*) δ 18.55.

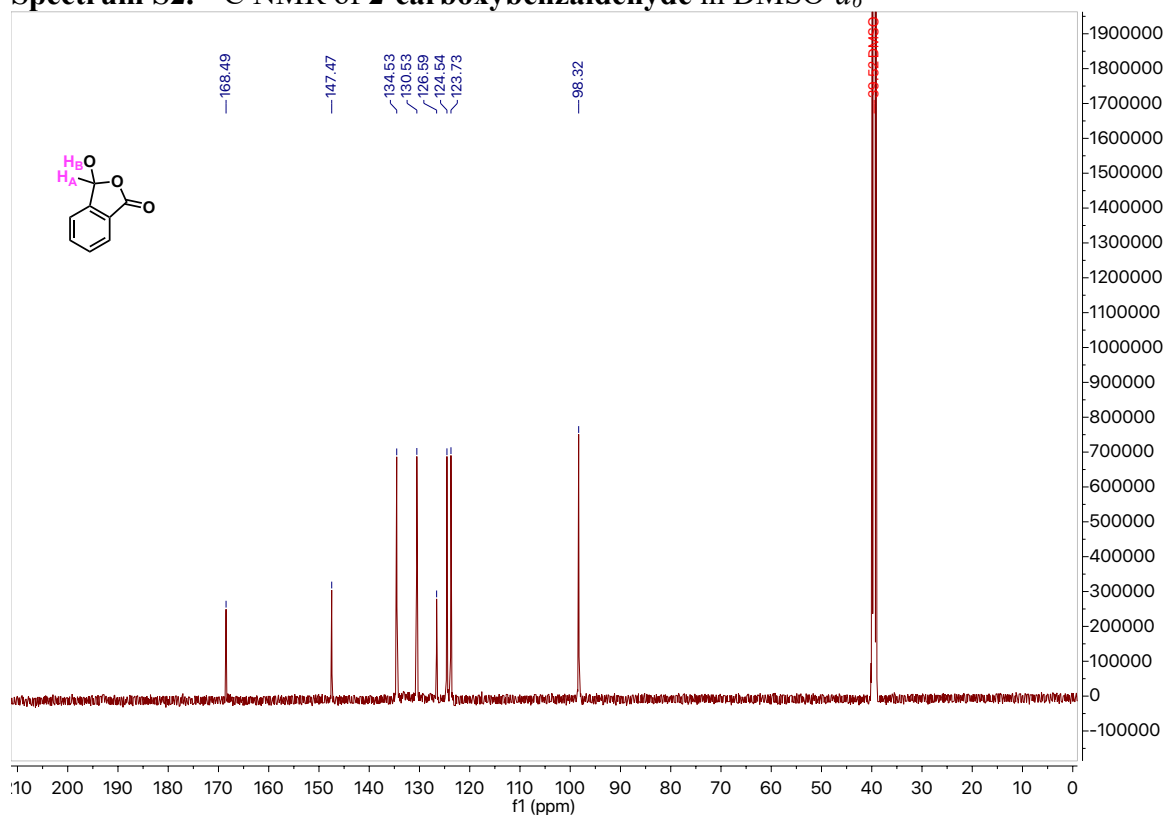
HR-ESI-MS *m/z* for C₂₇H₃₃O₃N₂Br₂P₁⁺ [M+H]⁺ calcd: 623.0668 found: 623.0665

Spectra of compounds

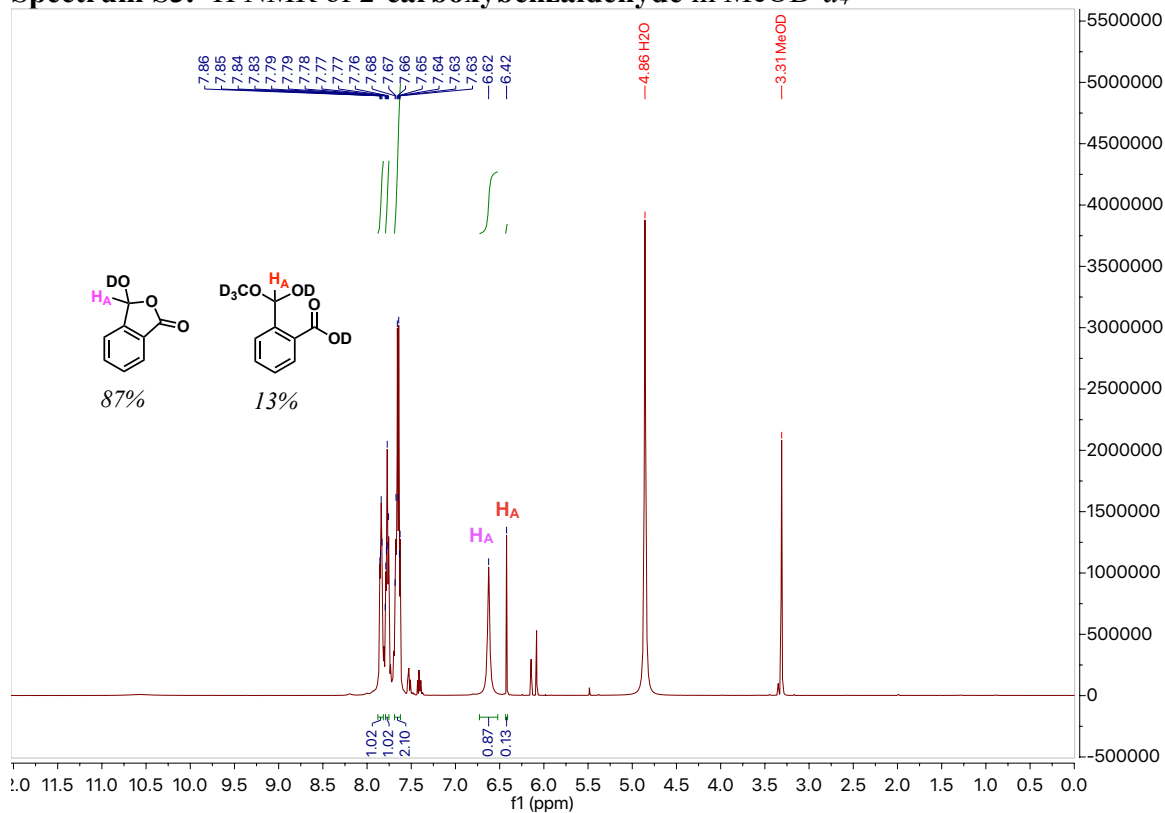
Spectrum S1. ¹H NMR of 2-carboxybenzaldehyde in DMSO-*d*₆



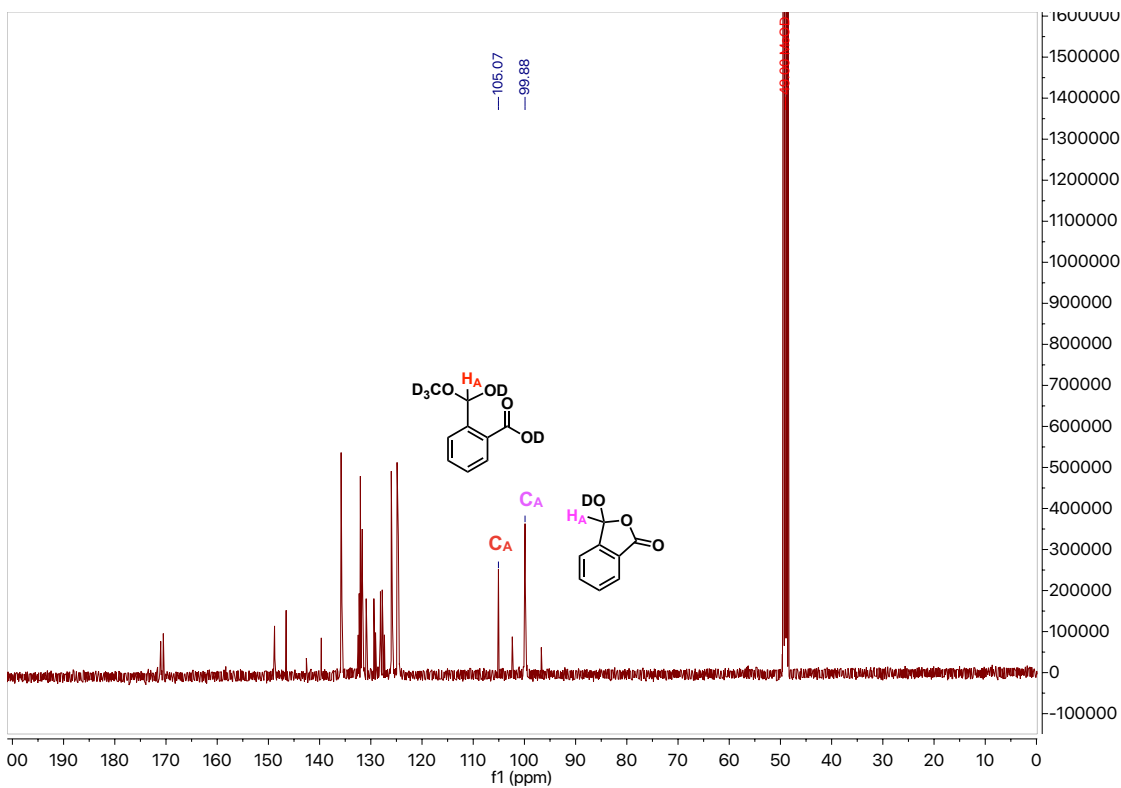
Spectrum S2. ^{13}C NMR of 2-carboxybenzaldehyde in $\text{DMSO-}d_6$



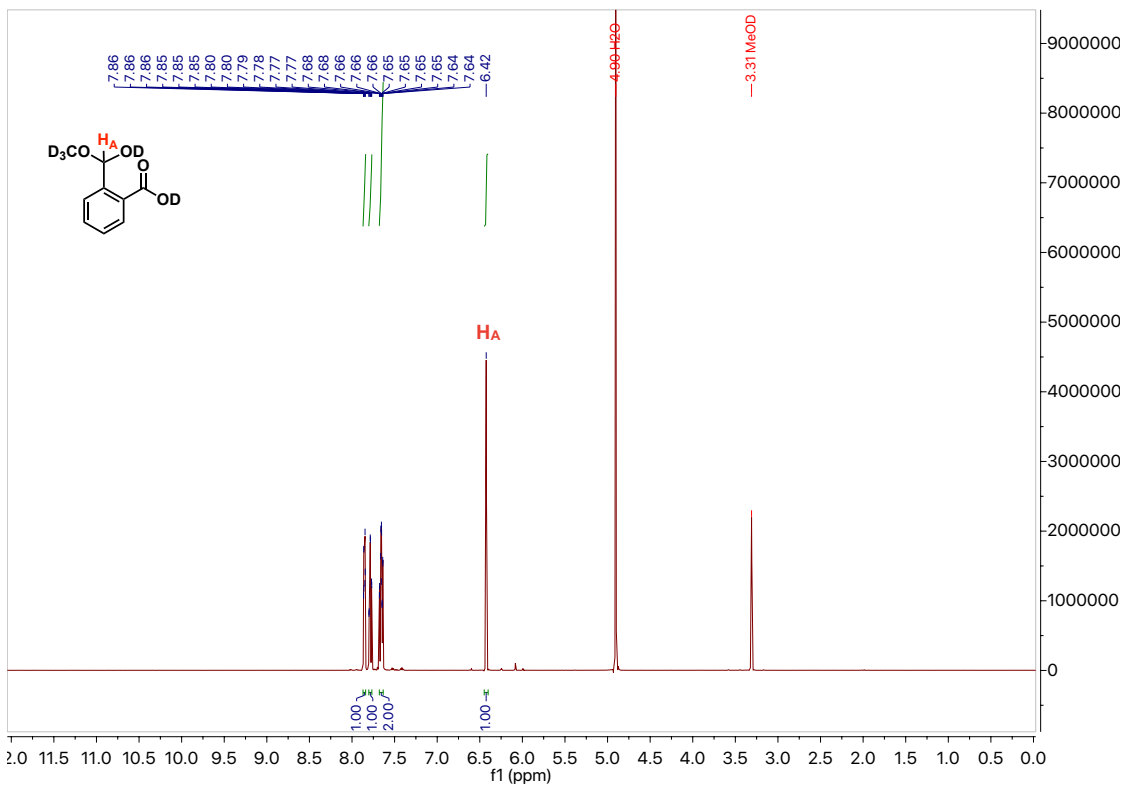
Spectrum S3. ^1H NMR of 2-carboxybenzaldehyde in $\text{MeOD-}d_4$



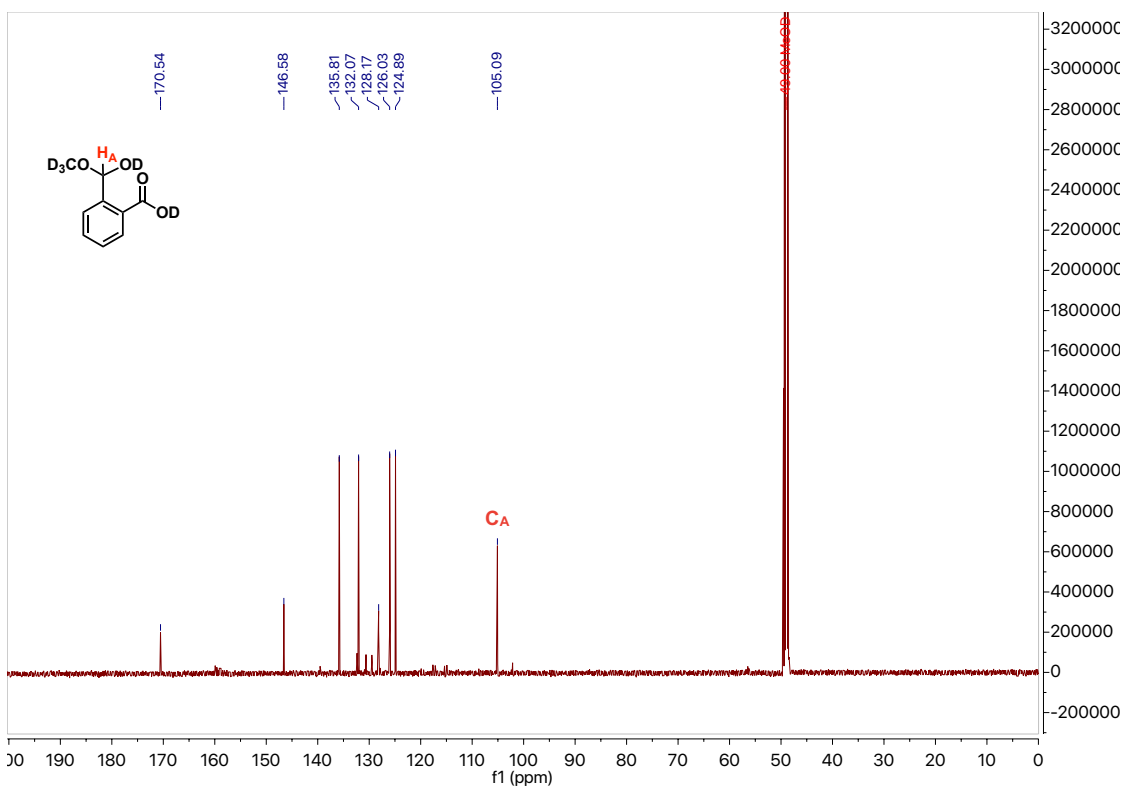
Spectrum S4. ^{13}C NMR of 2-carboxybenzaldehyde in $\text{MeOD-}d_4$



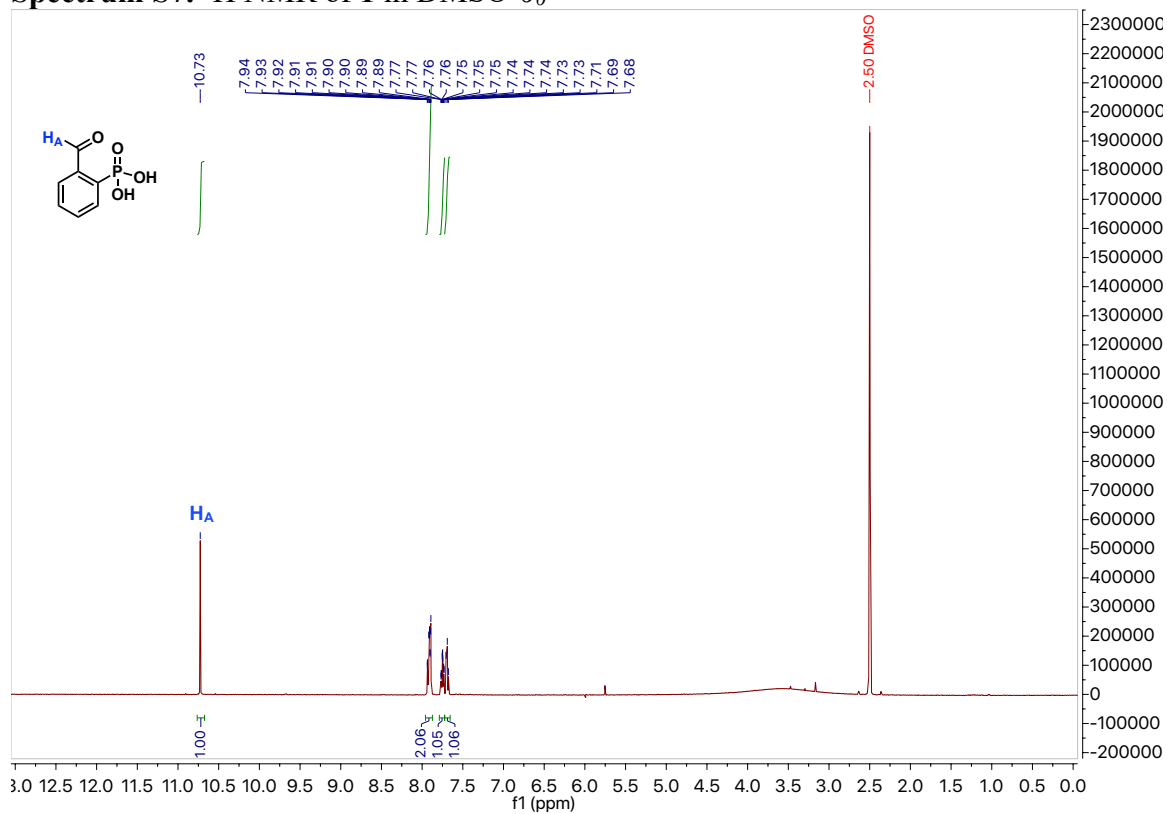
Spectrum S5. ^1H NMR of 2-carboxybenzaldehyde in $\text{MeOD-}d_4$ + TFA



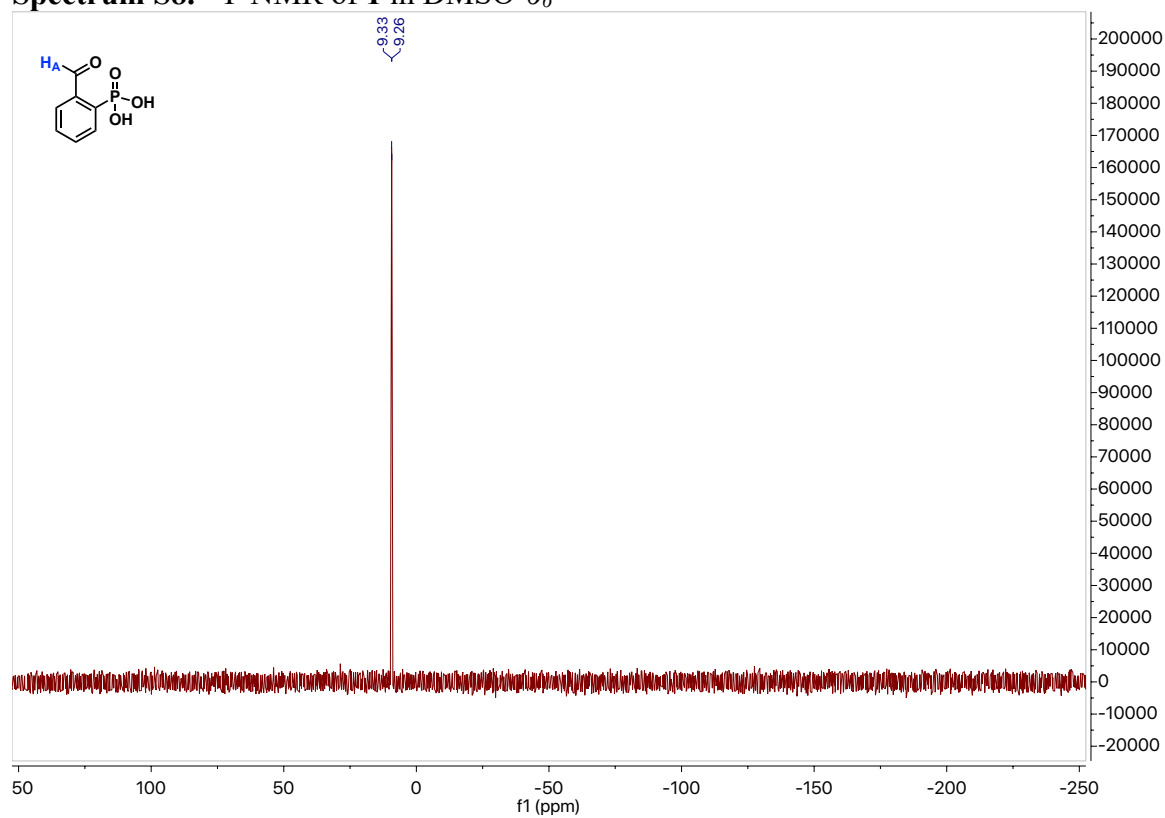
Spectrum S6. ^{13}C NMR of 2-carboxybenzaldehyde in $\text{MeOD-}d_4 + \text{TFA}$



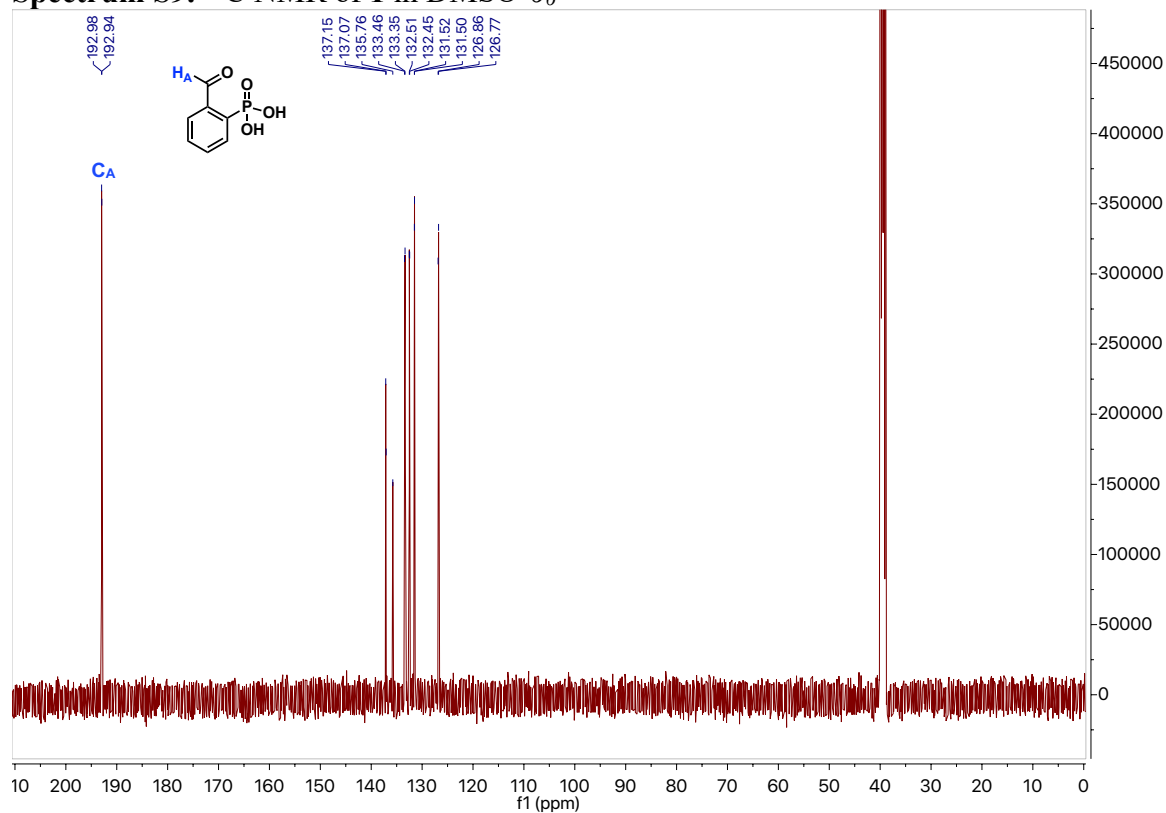
Spectrum S7. ^1H NMR of 1 in $\text{DMSO-}d_6$



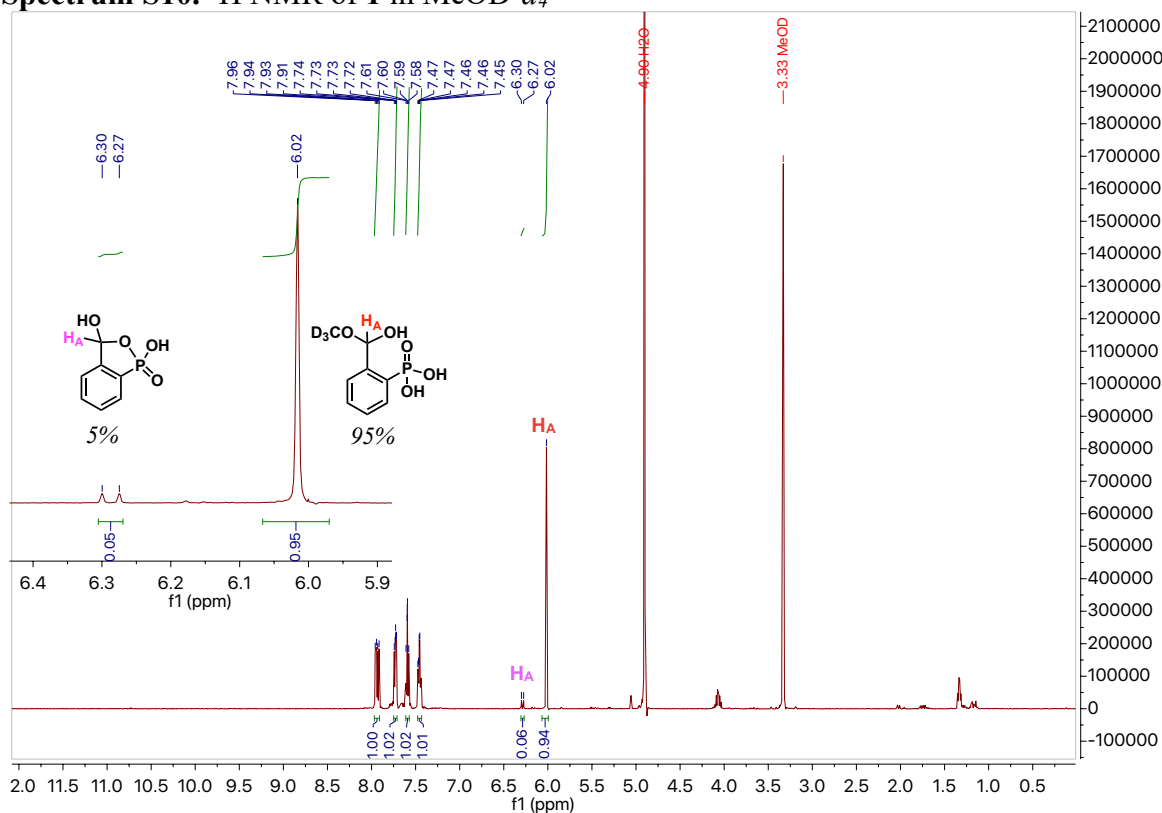
Spectrum S8. ^{31}P NMR of **1** in $\text{DMSO-}d_6$



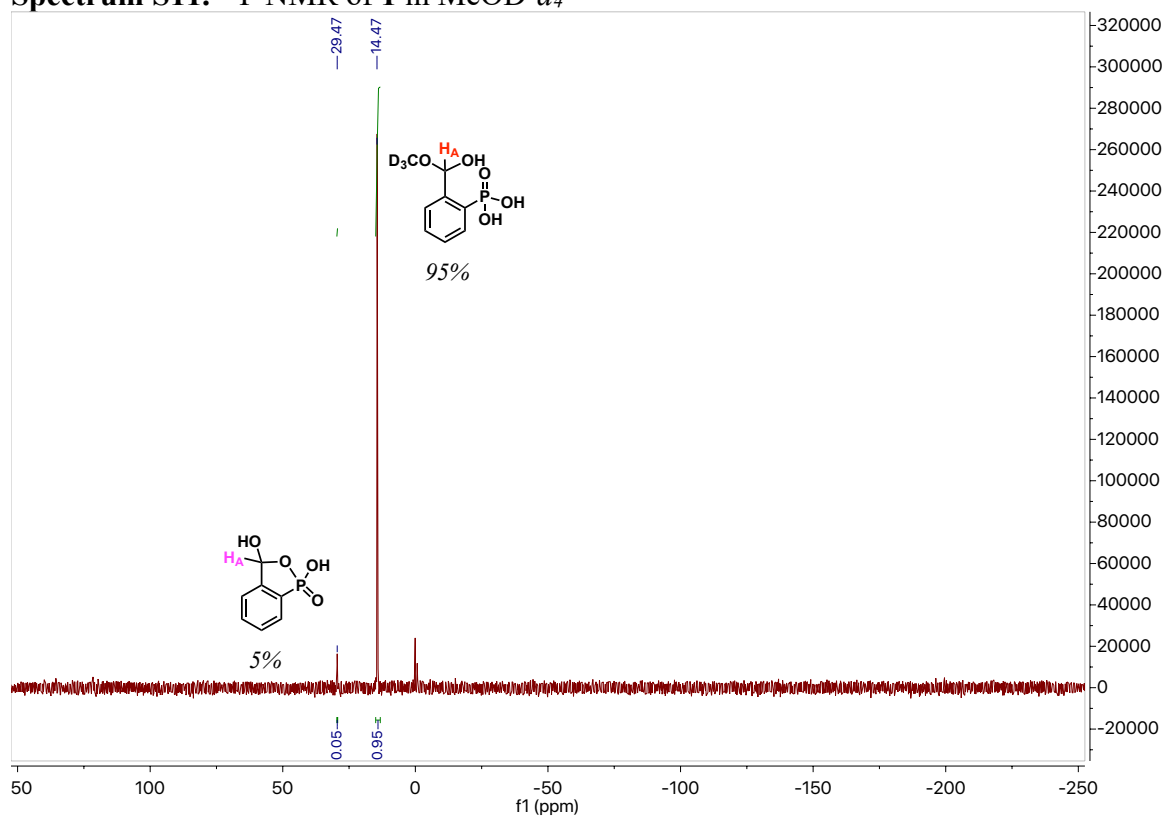
Spectrum S9. ^{13}C NMR of **1** in $\text{DMSO-}d_6$



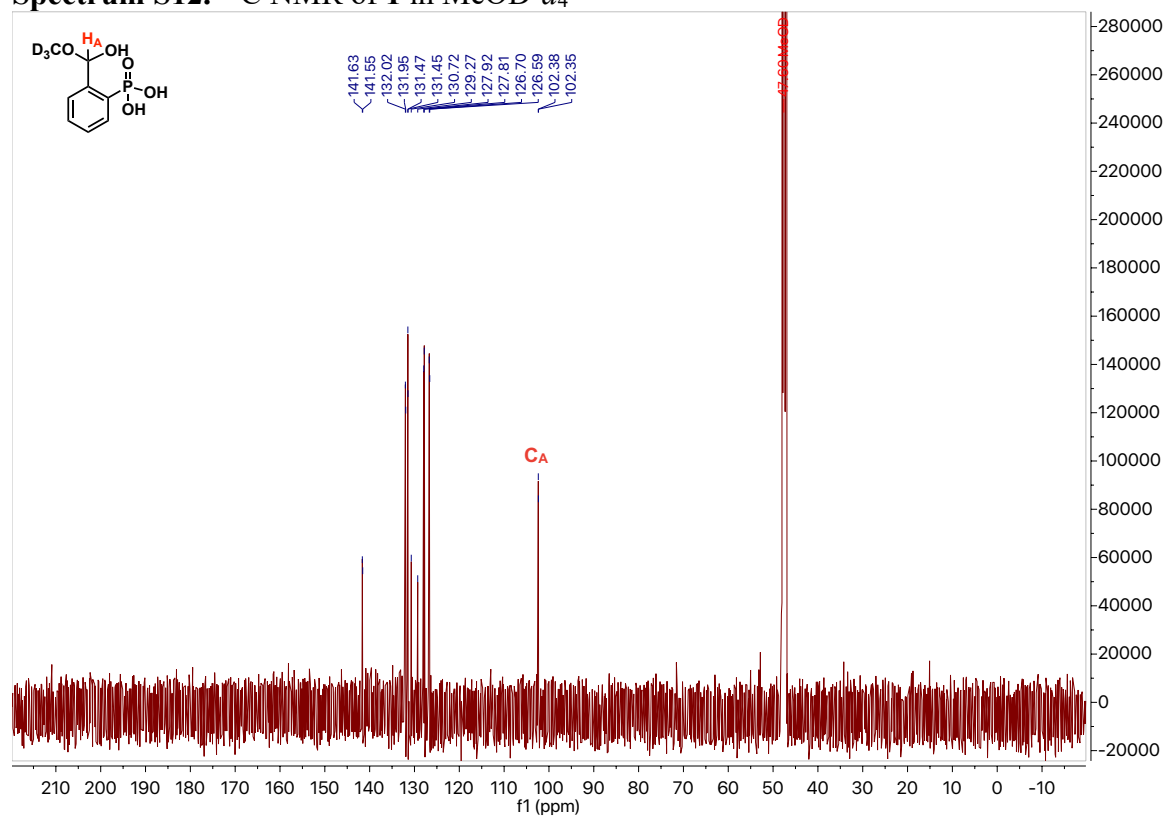
Spectrum S10. ^1H NMR of **1** in $\text{MeOD-}d_4$



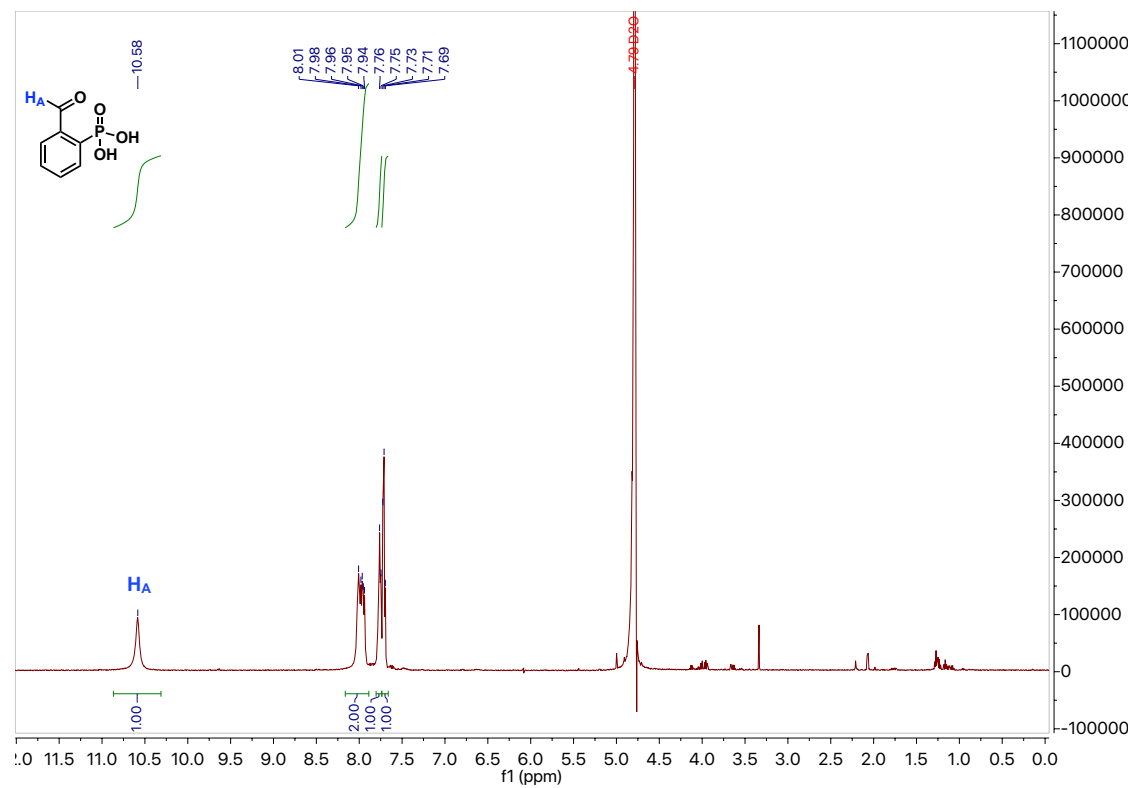
Spectrum S11. ^{31}P NMR of **1** in $\text{MeOD-}d_4$



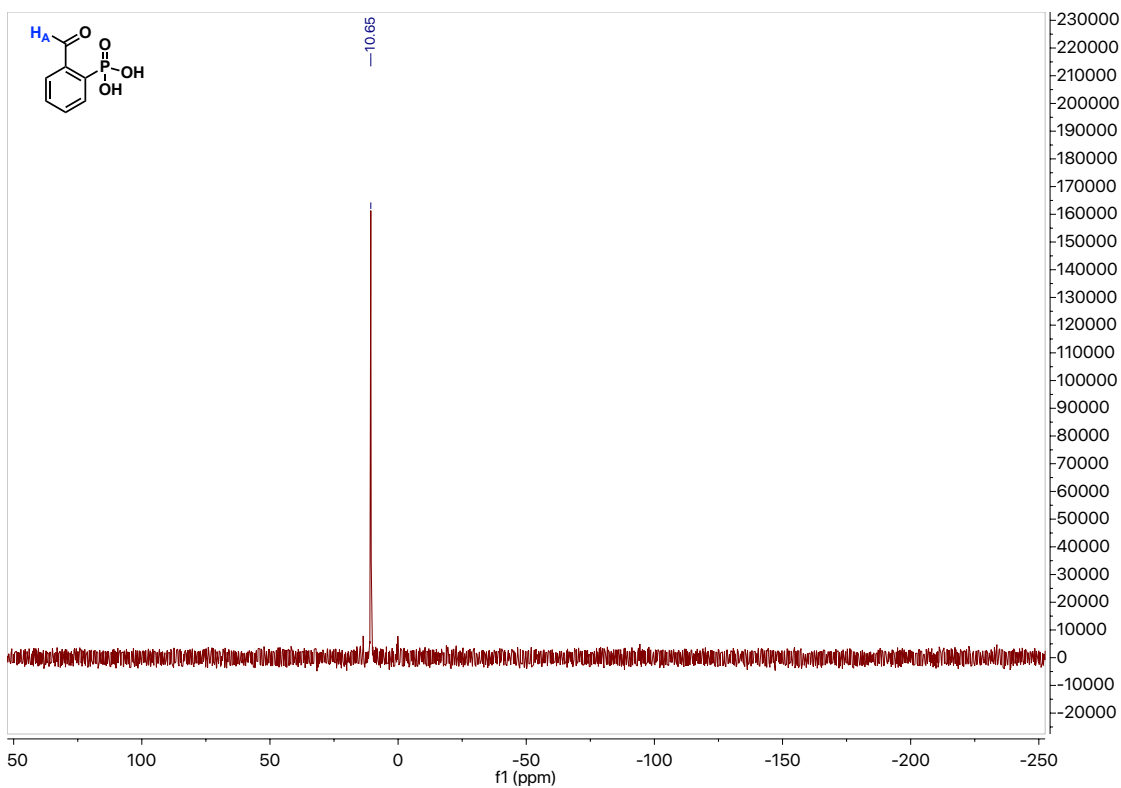
Spectrum S12. ^{13}C NMR of **1** in $\text{MeOD-}d_4$



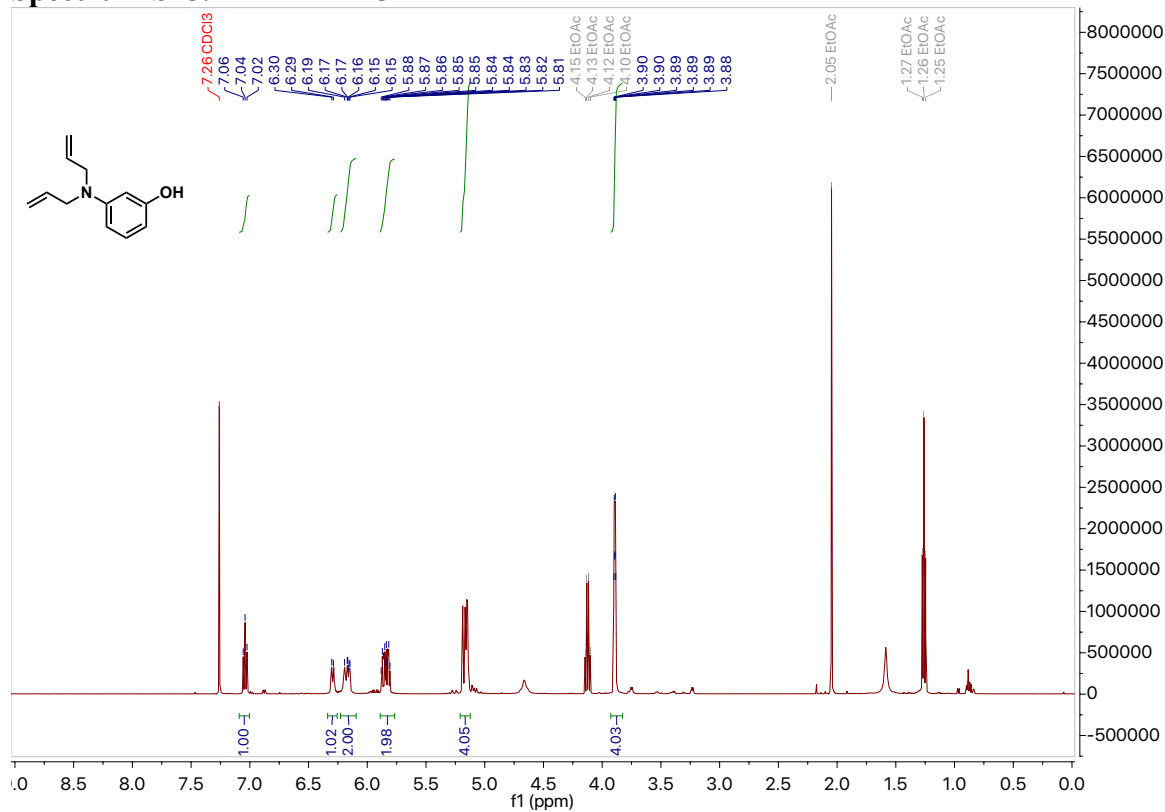
Spectrum S13. ^1H NMR of **1** in D_2O



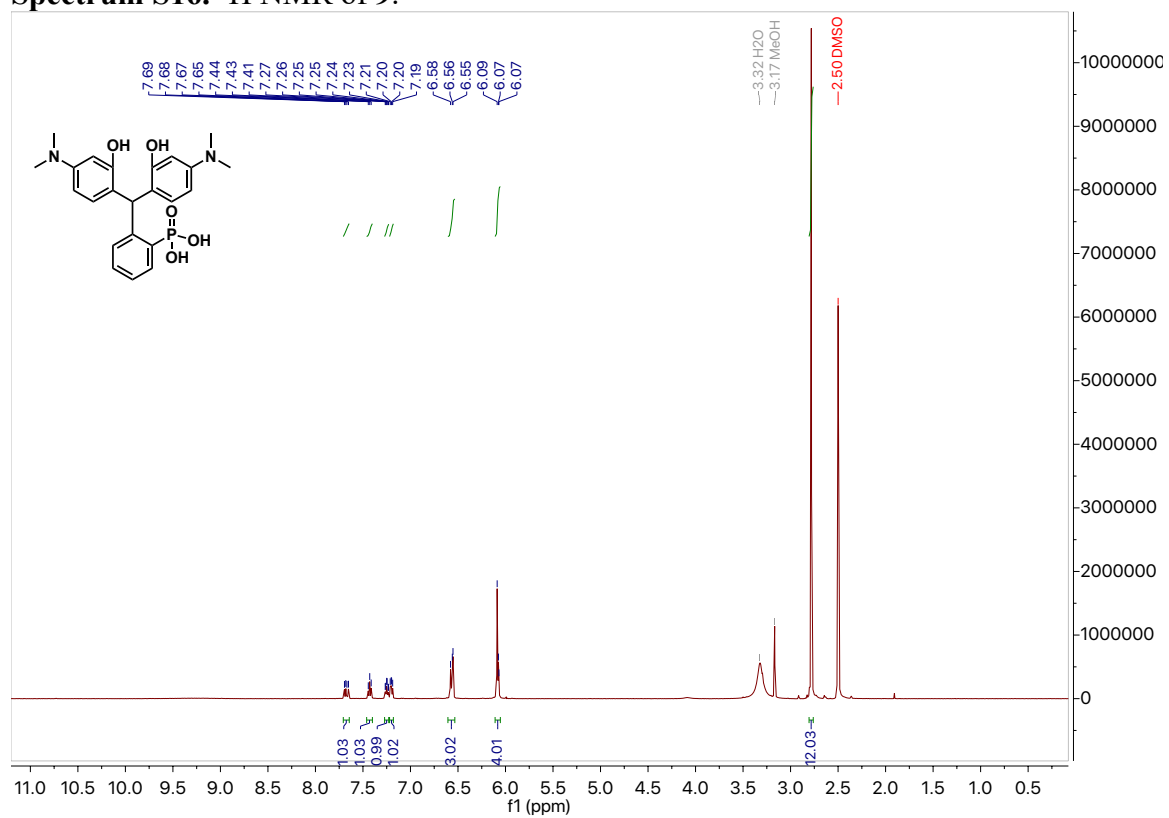
Spectrum S14. ^{31}P NMR of **1** in D_2O



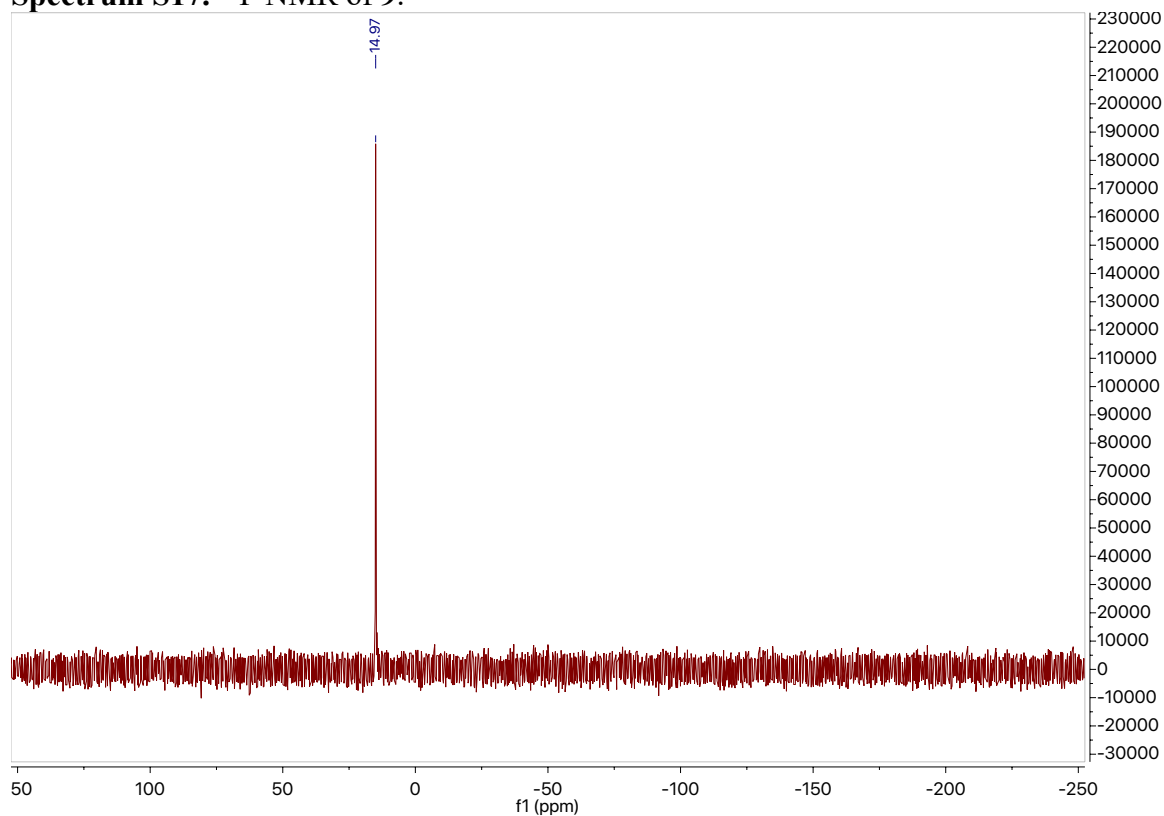
Spectrum S15. ^1H NMR of **5**.



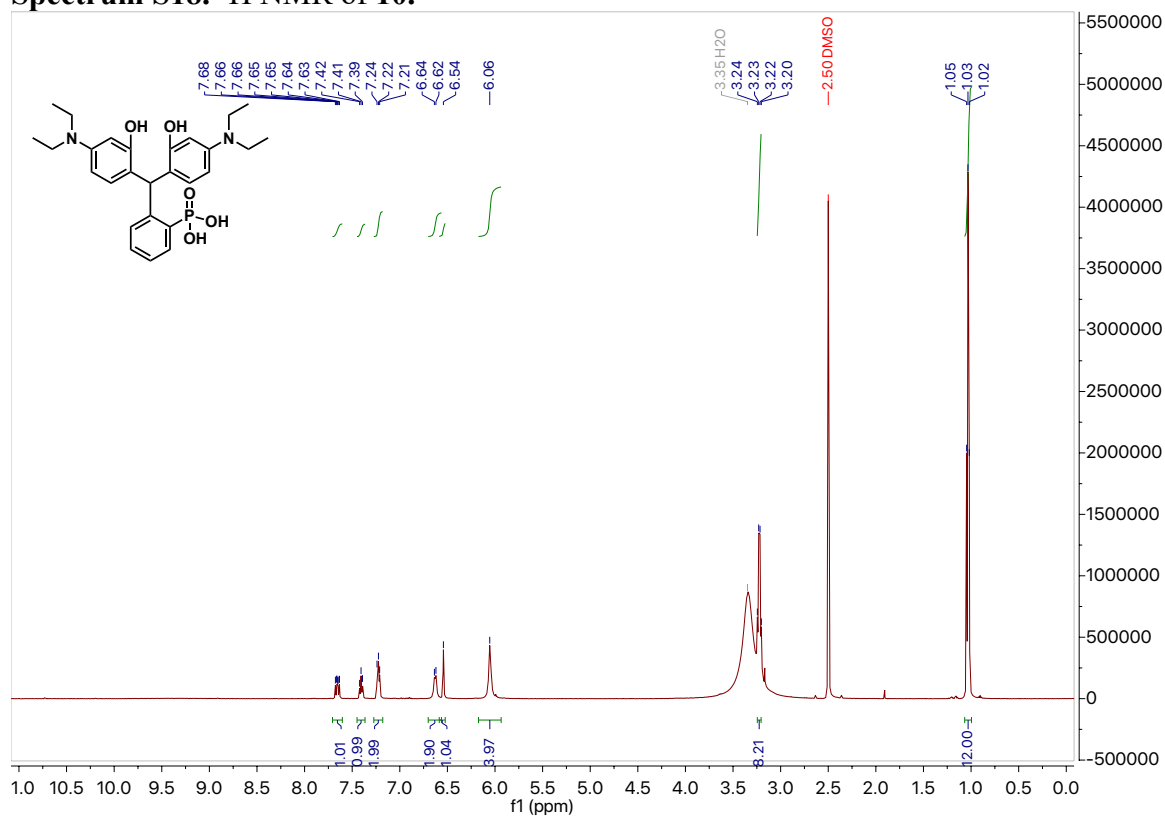
Spectrum S16. ¹H NMR of 9.



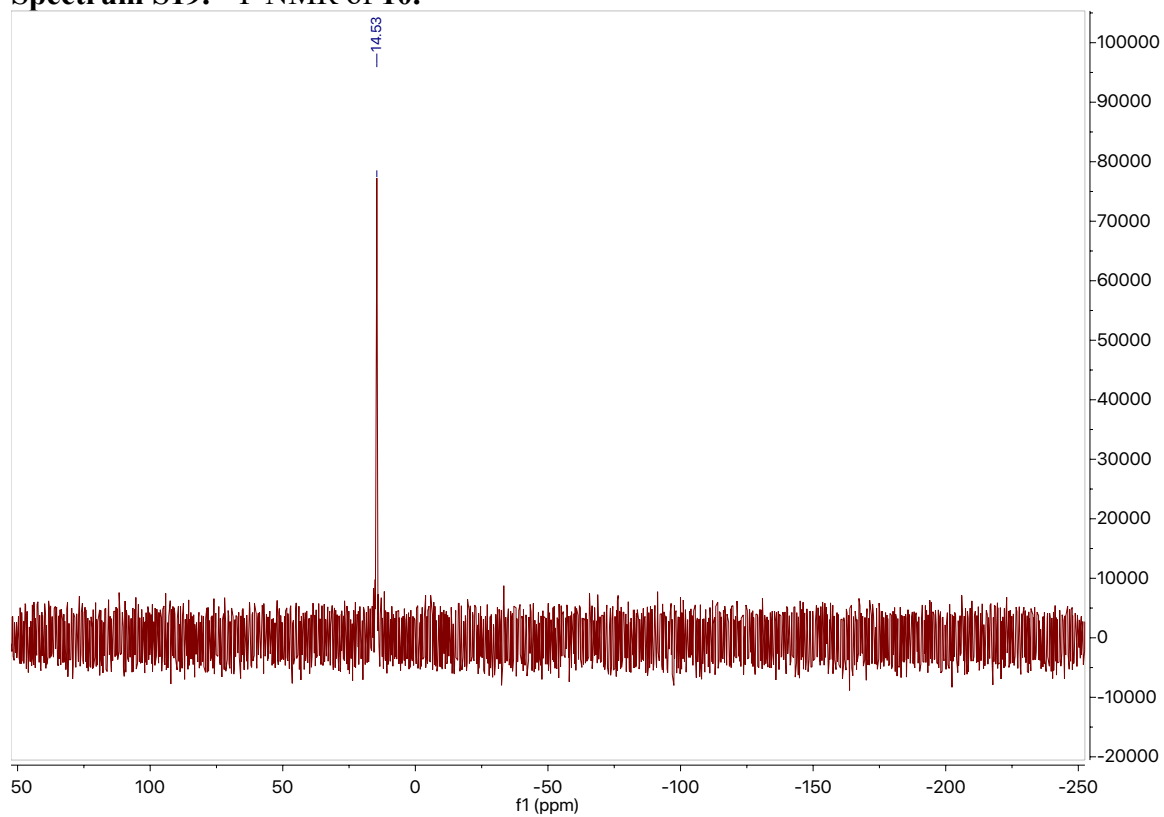
Spectrum S17. ³¹P NMR of 9.



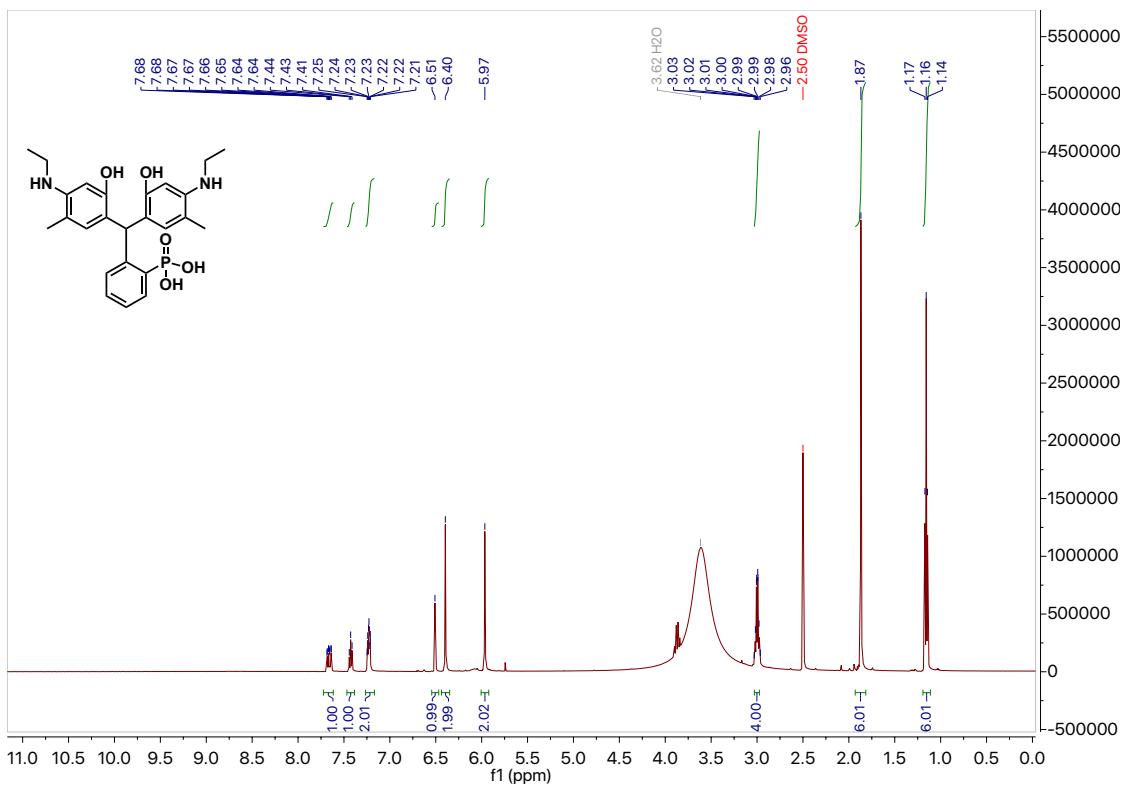
Spectrum S18. ^1H NMR of 10.



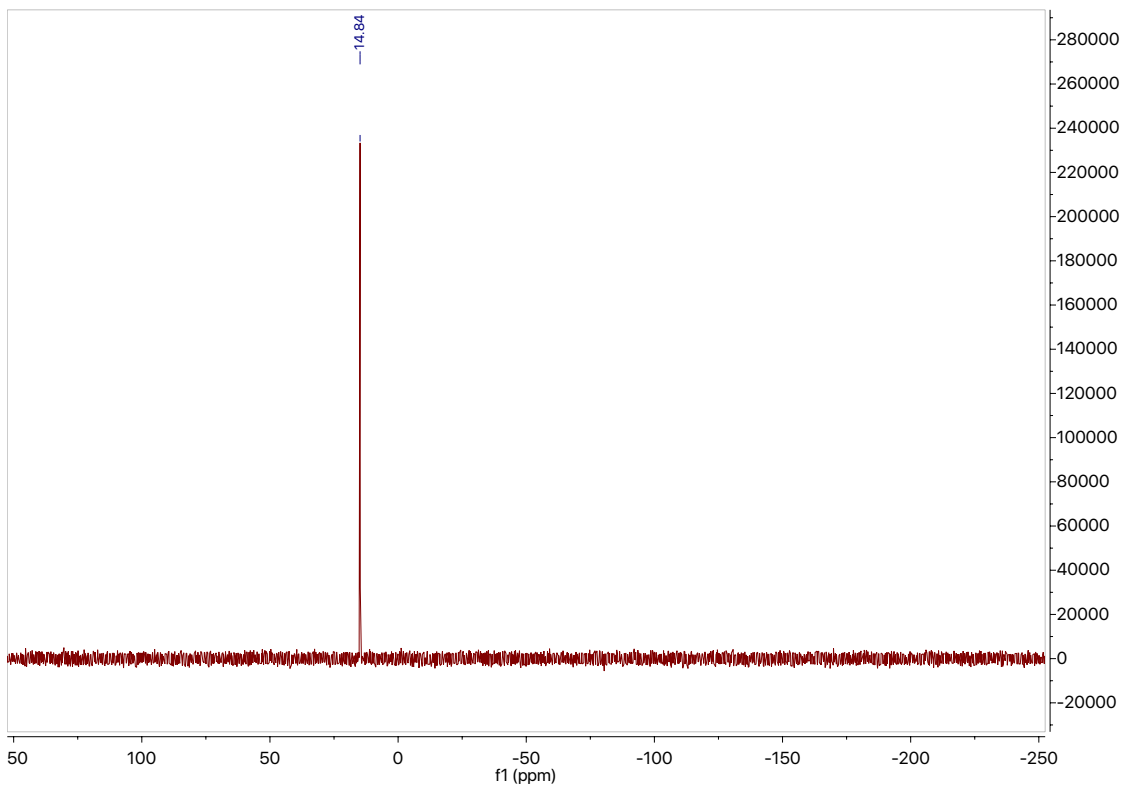
Spectrum S19. ^{31}P NMR of 10.



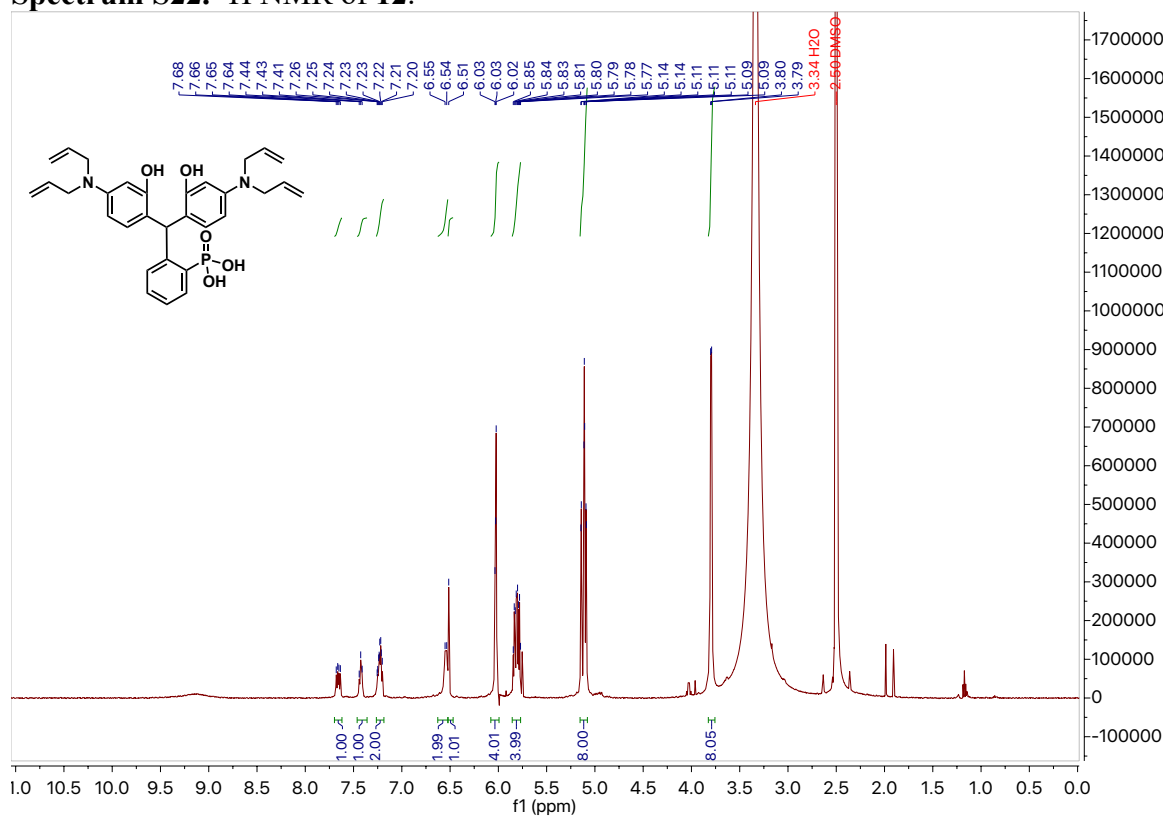
Spectrum S20. ^1H NMR of 11.



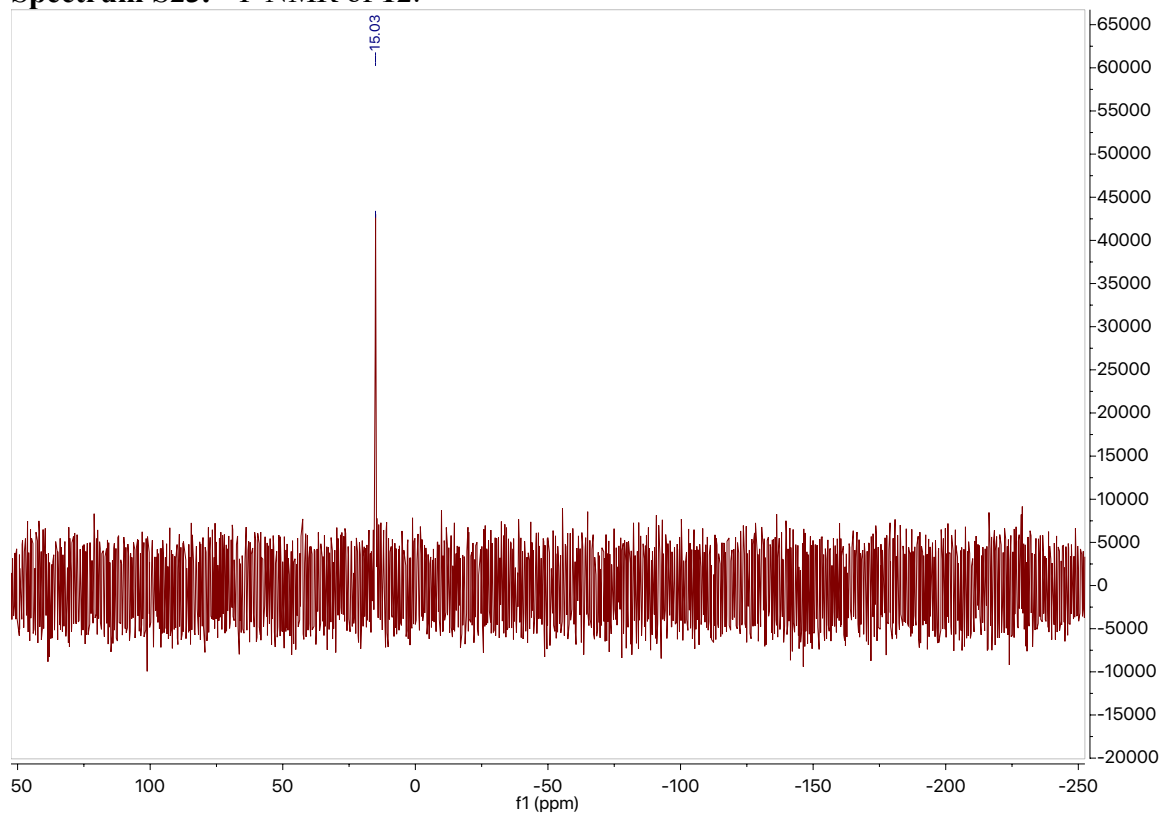
Spectrum S21. ^{31}P NMR of 11.



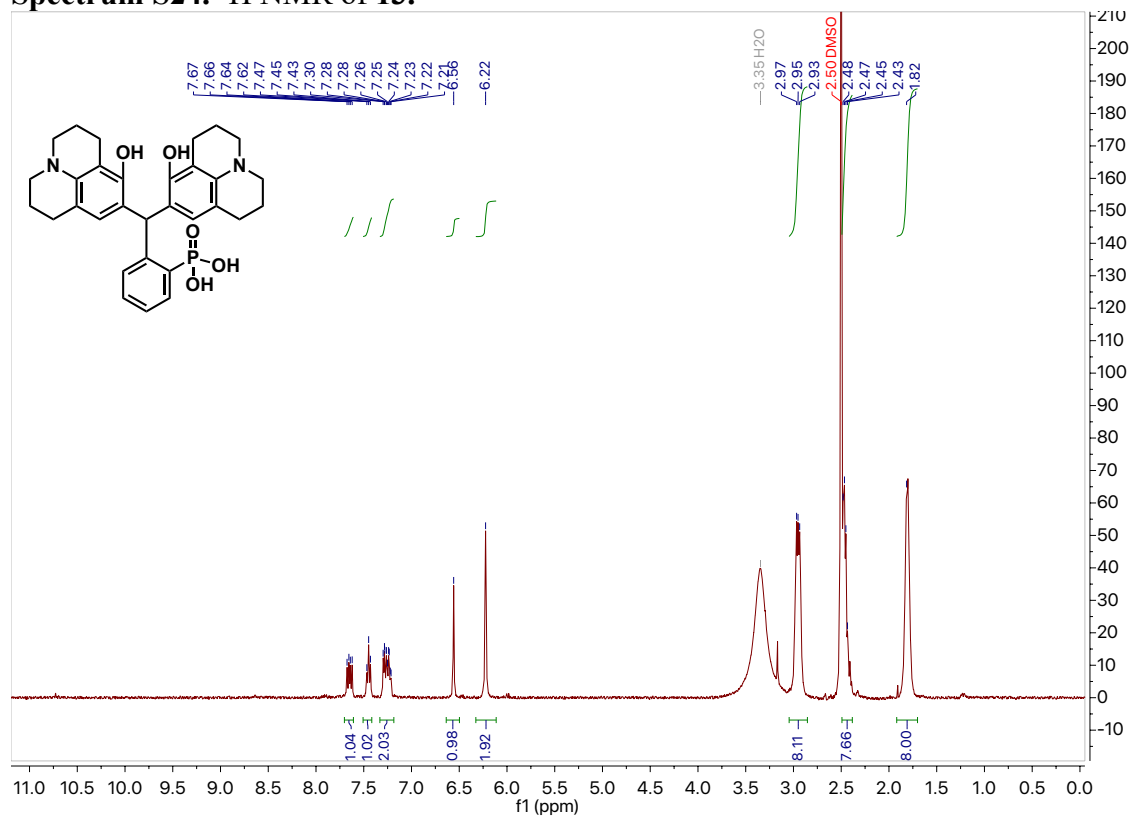
Spectrum S22. ¹H NMR of 12.



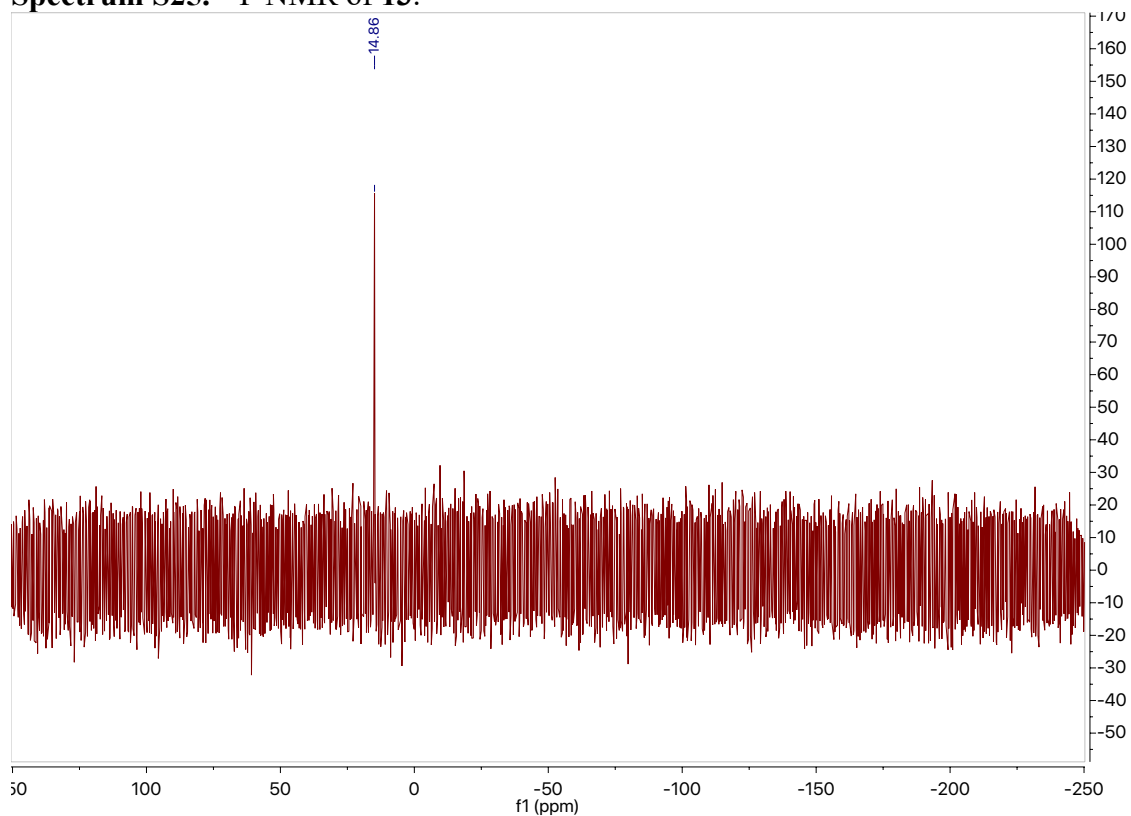
Spectrum S23. ³¹P NMR of 12.



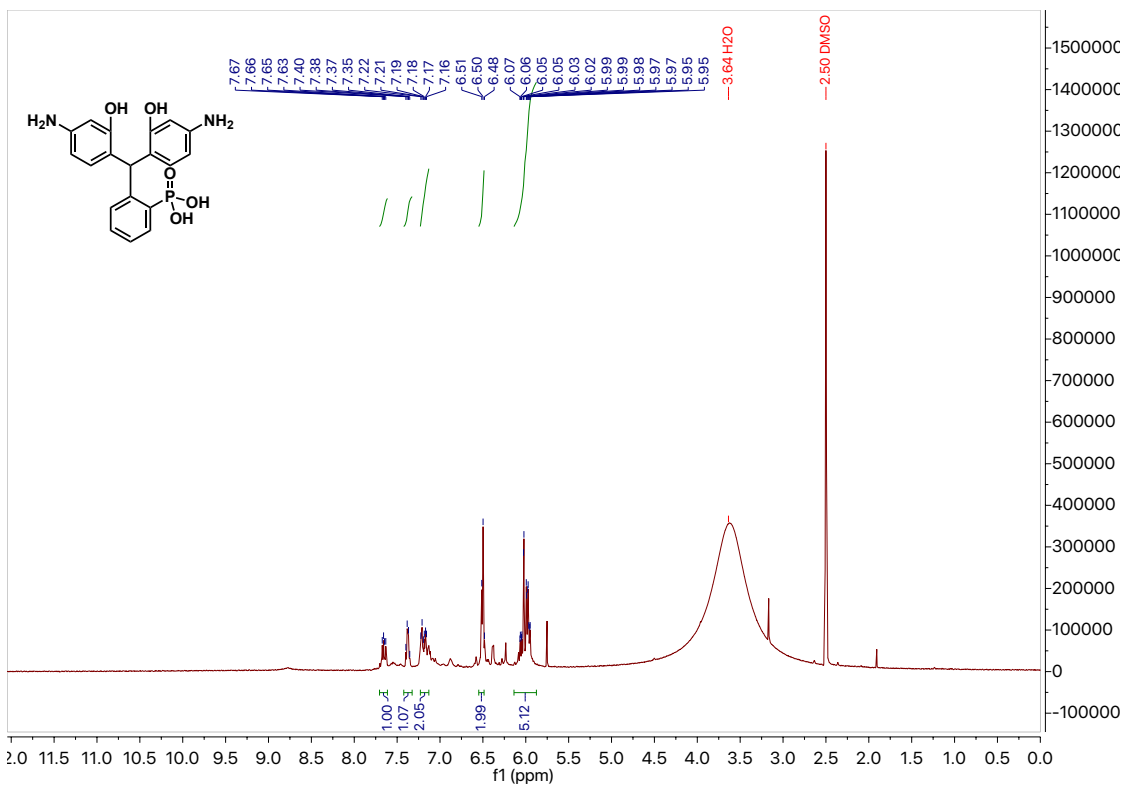
Spectrum S24. ^1H NMR of 13.



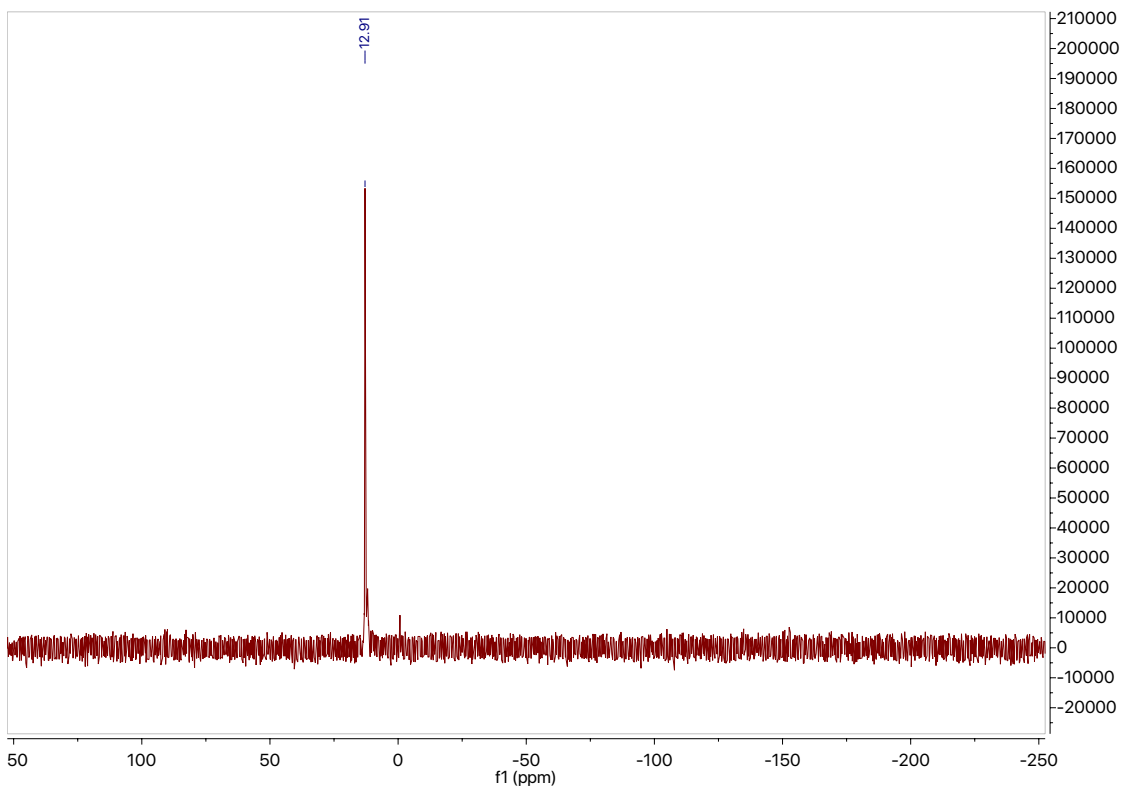
Spectrum S25. ^{31}P NMR of 13.



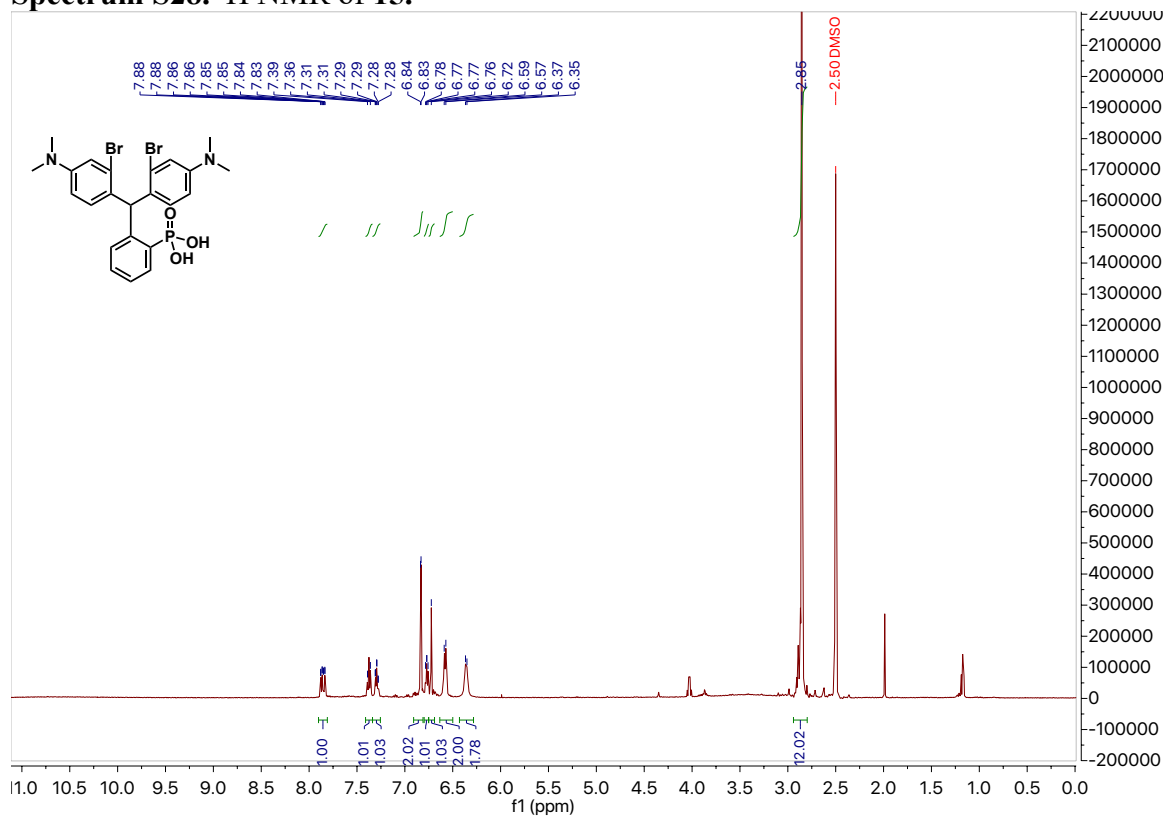
Spectrum S26. ^1H NMR of 14.



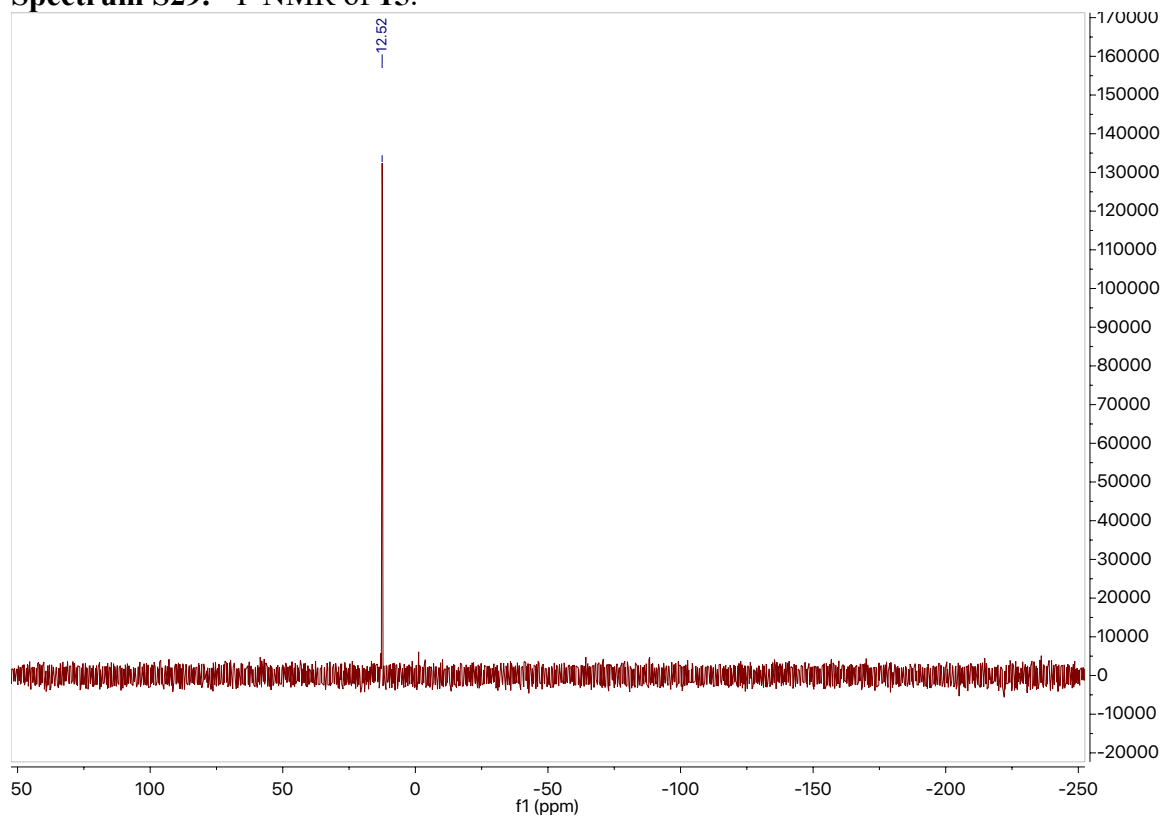
Spectrum S27. ^{31}P NMR of 14.



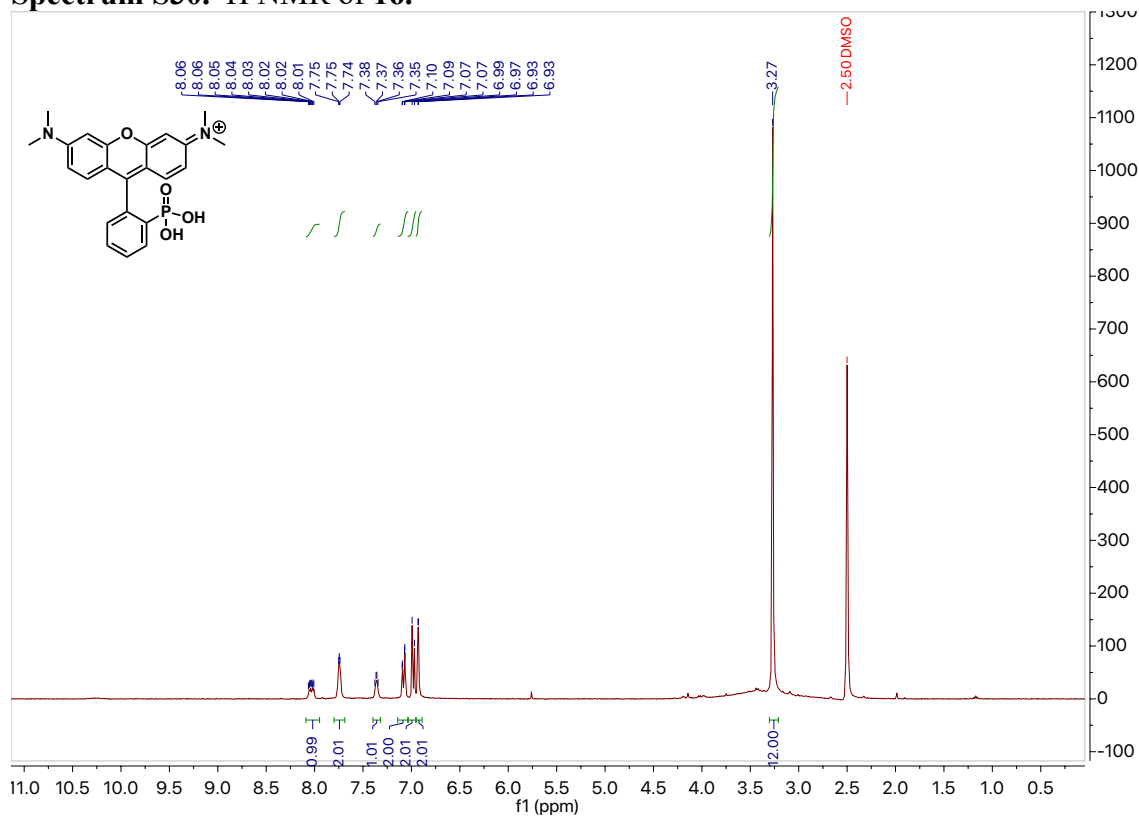
Spectrum S28. ^1H NMR of 15.



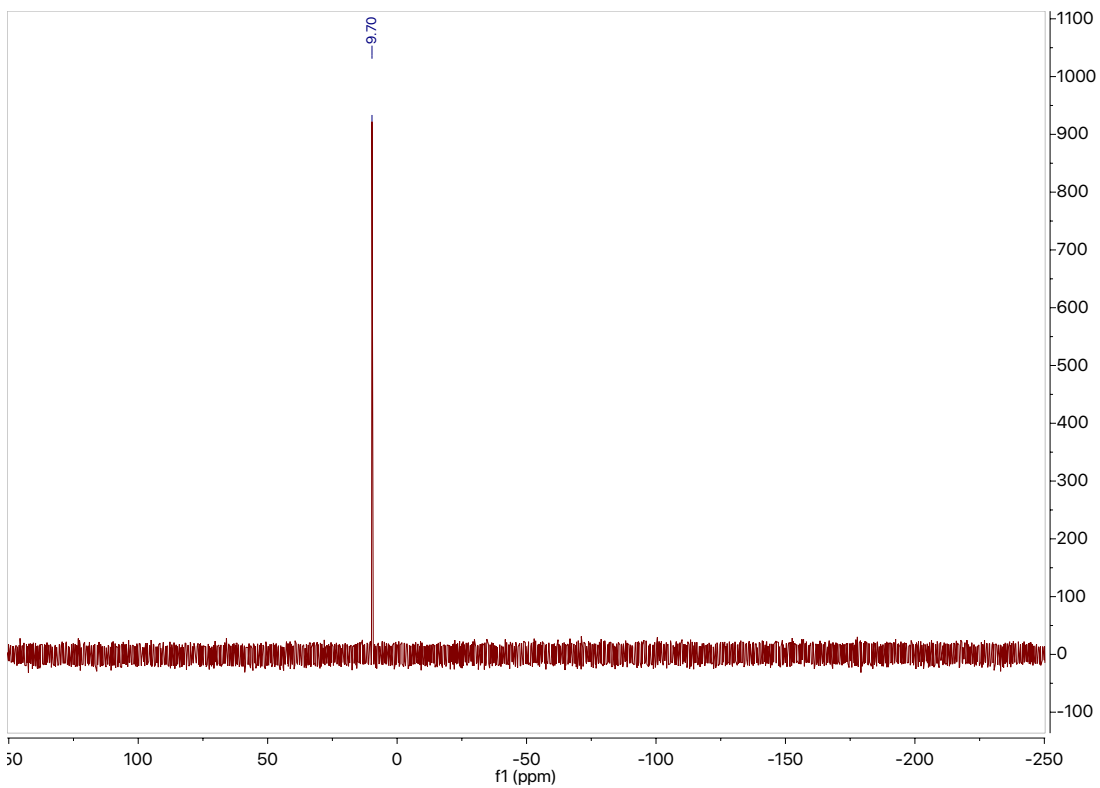
Spectrum S29. ^{31}P NMR of 15.



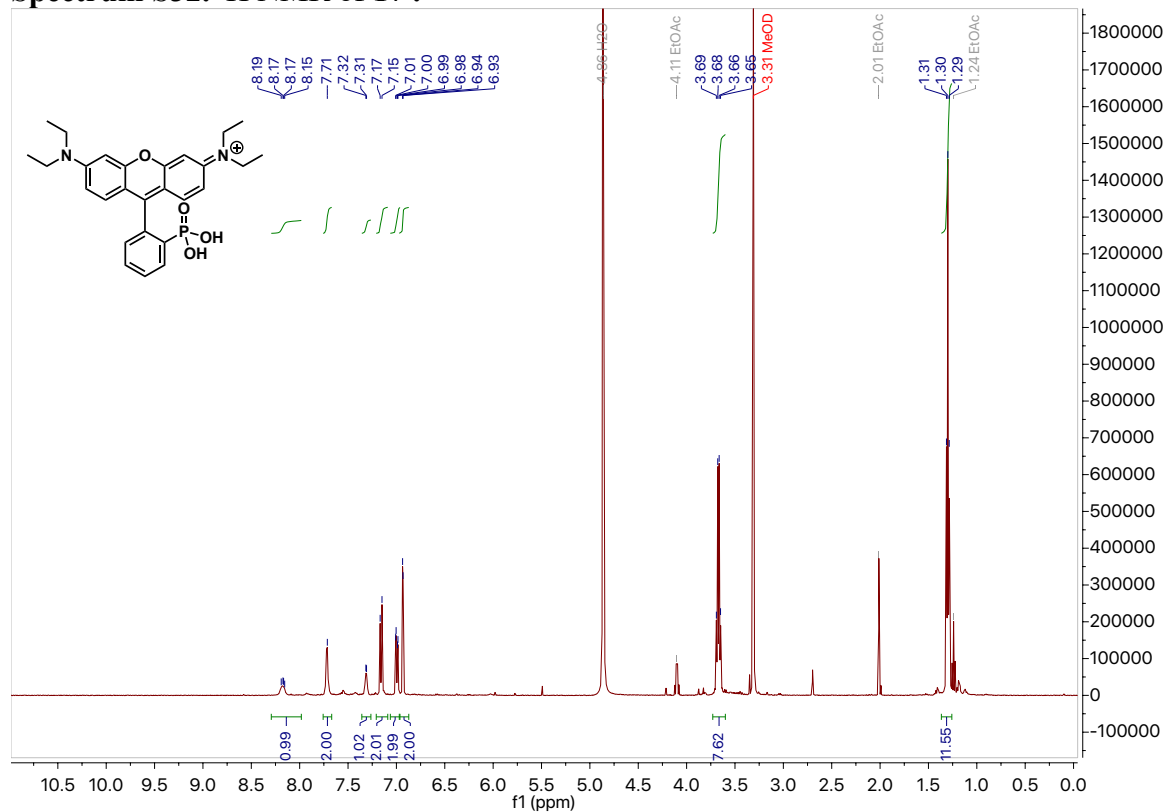
Spectrum S30. ¹H NMR of 16.



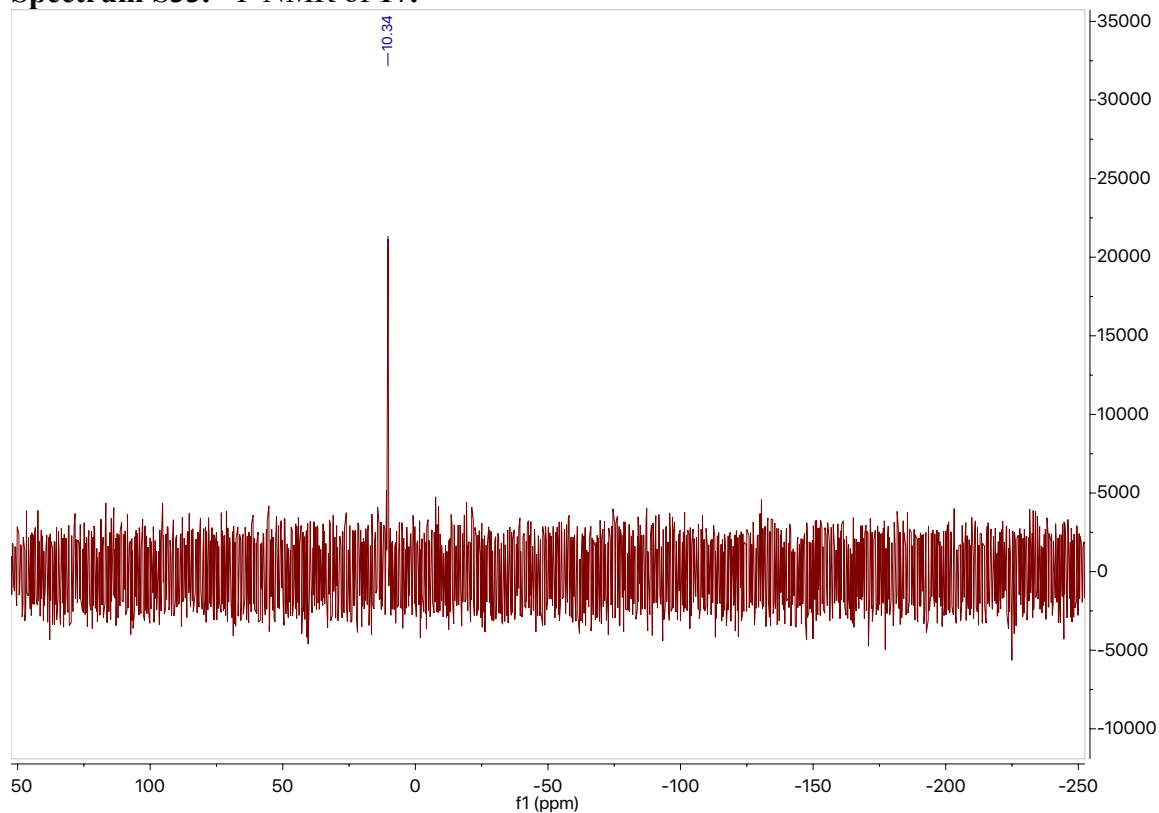
Spectrum S31. ³¹P NMR of 16.



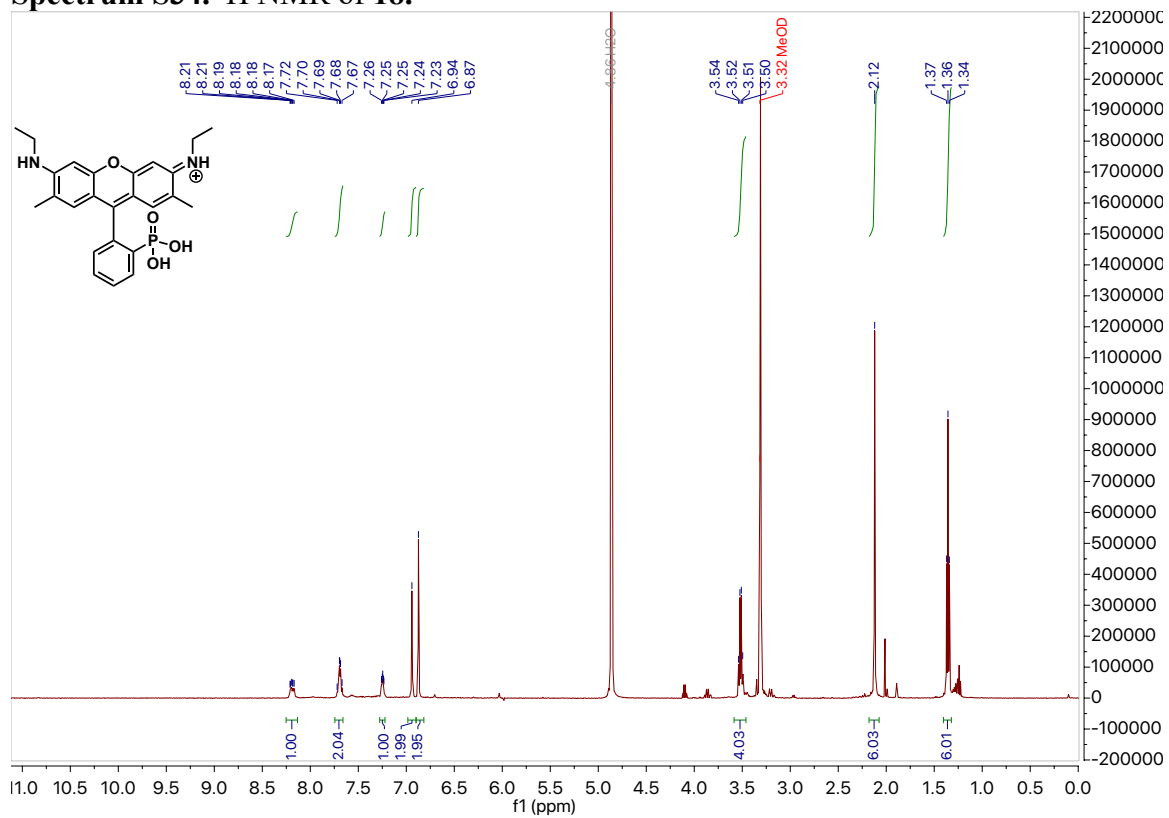
Spectrum S32. ^1H NMR of 17.



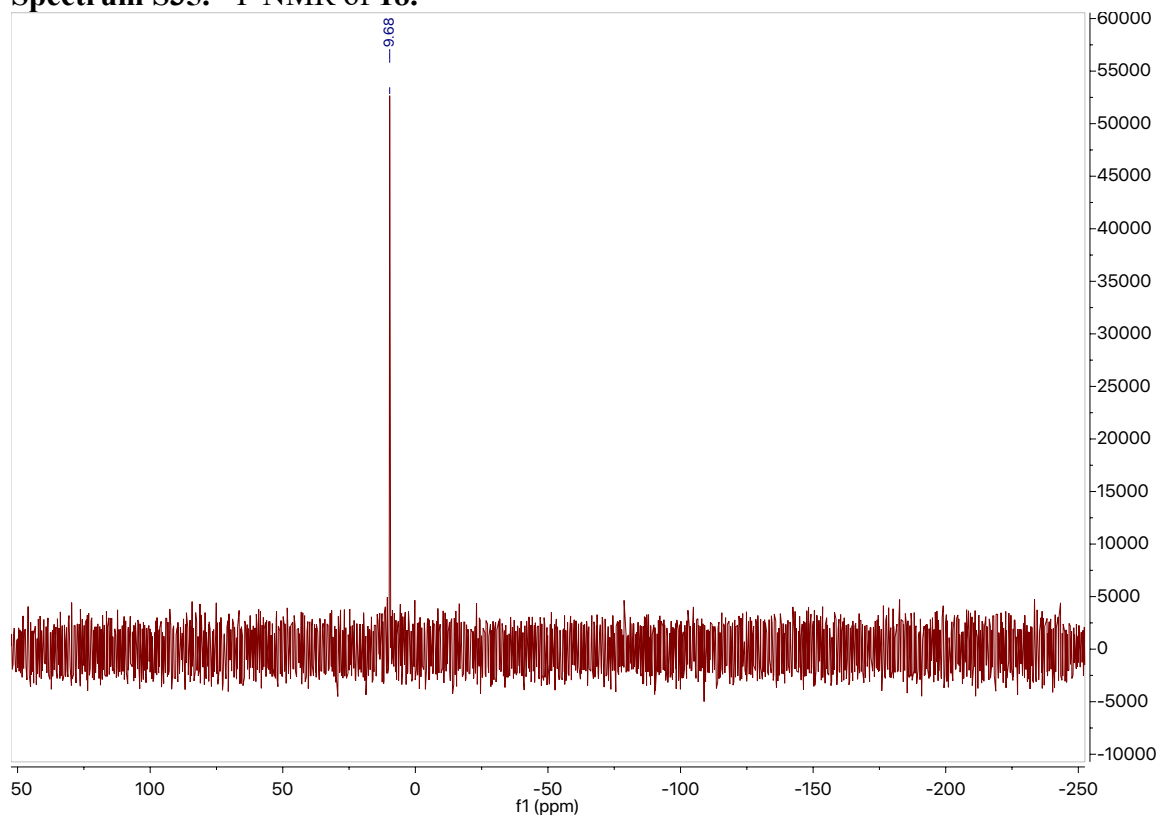
Spectrum S33. ^{31}P NMR of 17.



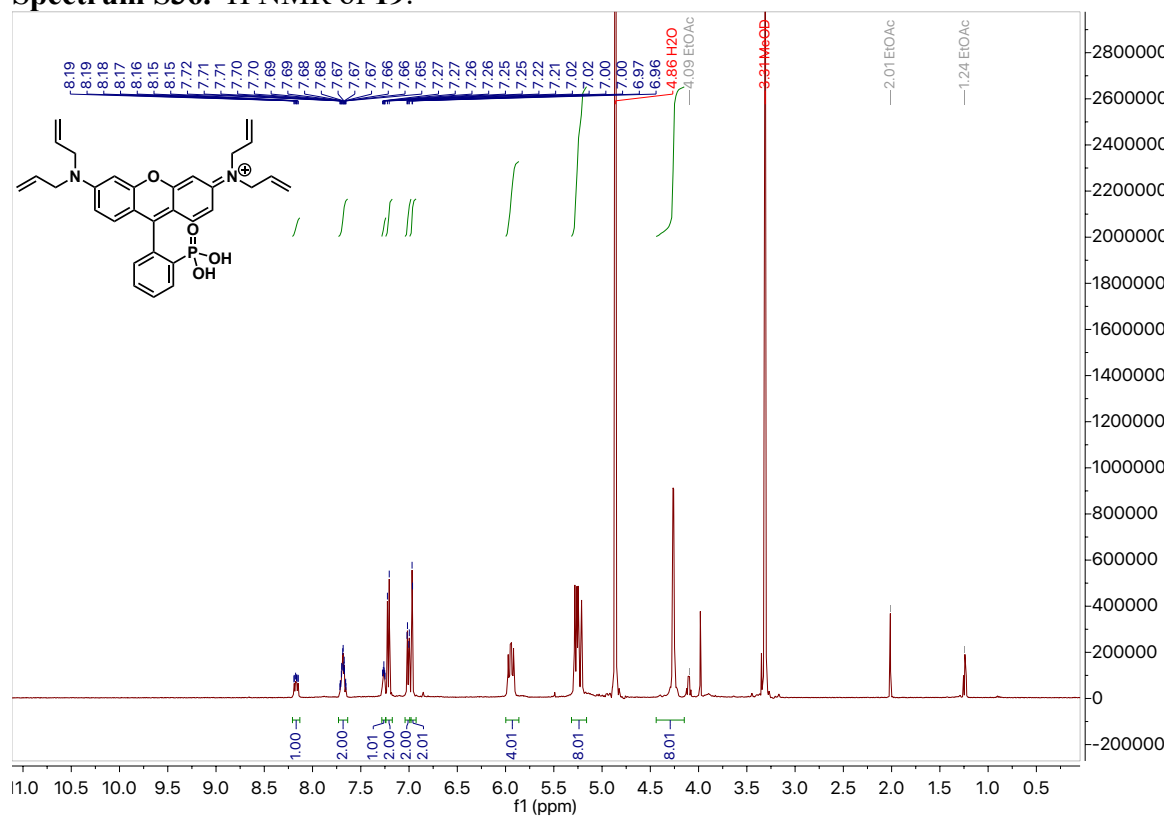
Spectrum S34. ^1H NMR of 18.



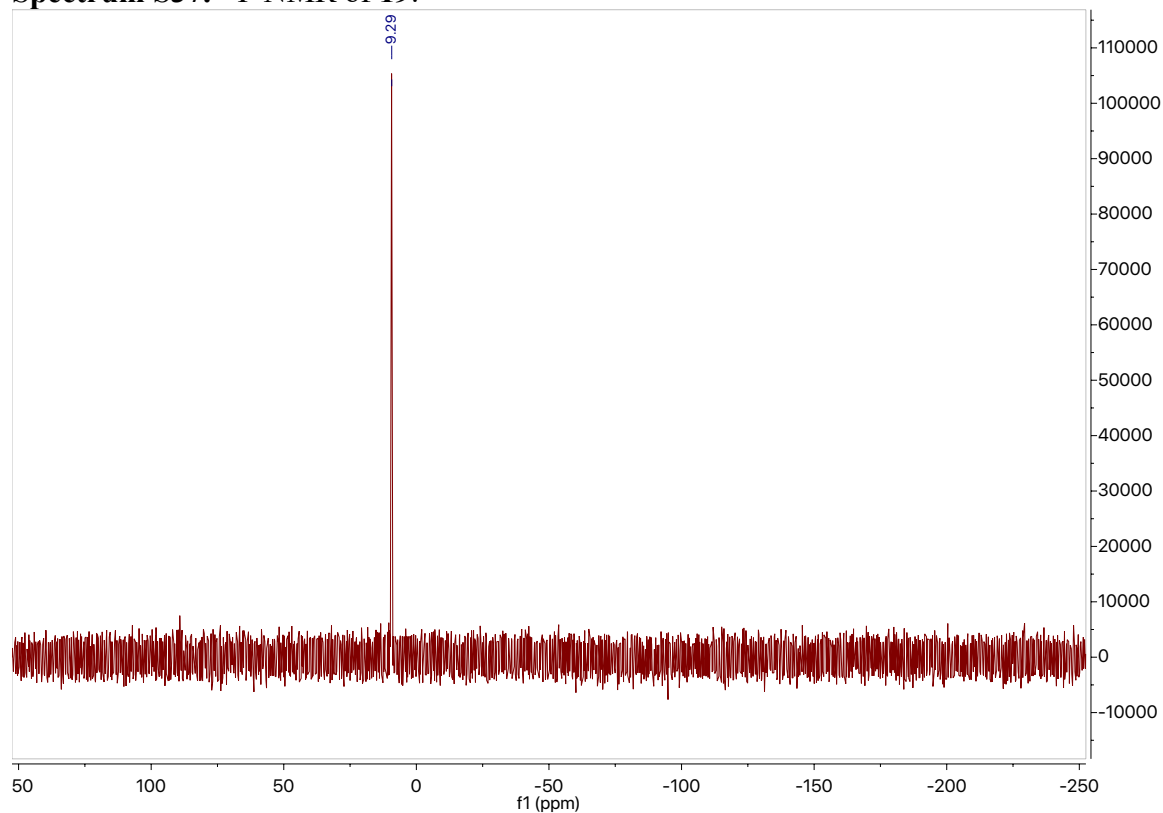
Spectrum S35. ^{31}P NMR of 18.



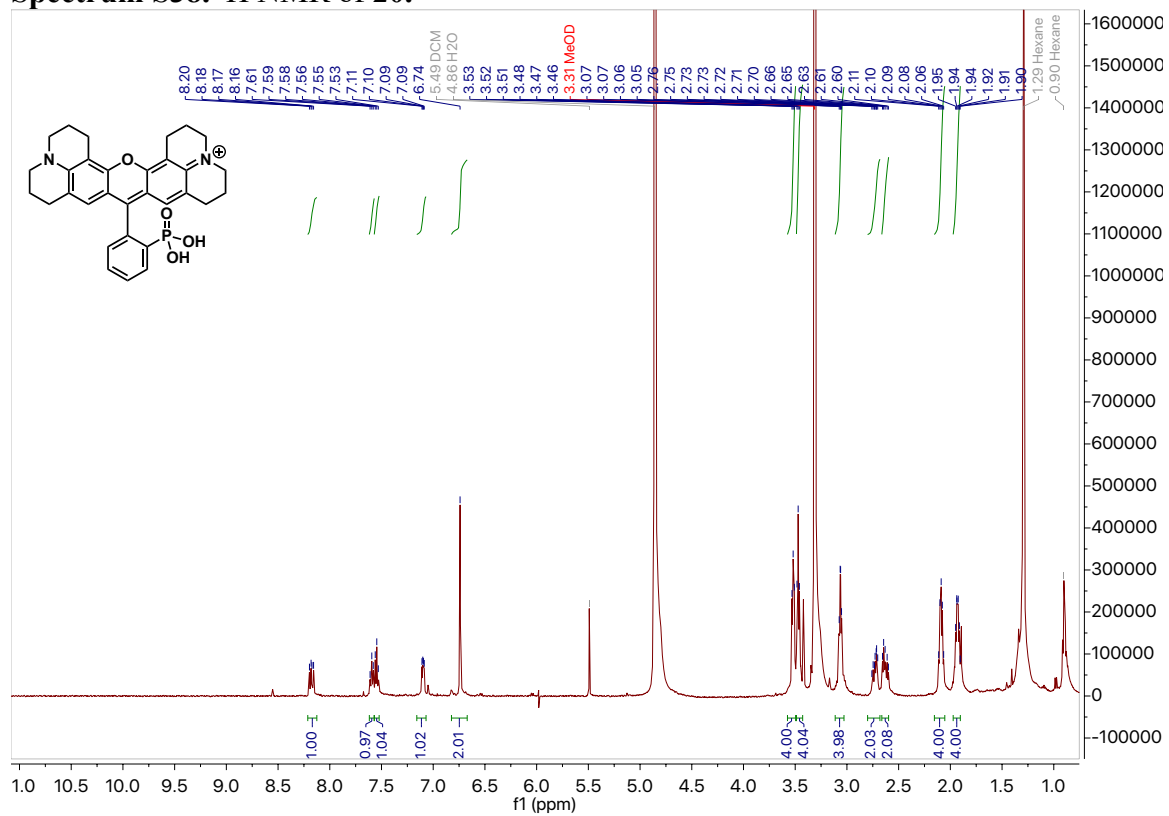
Spectrum S36. ¹H NMR of 19.



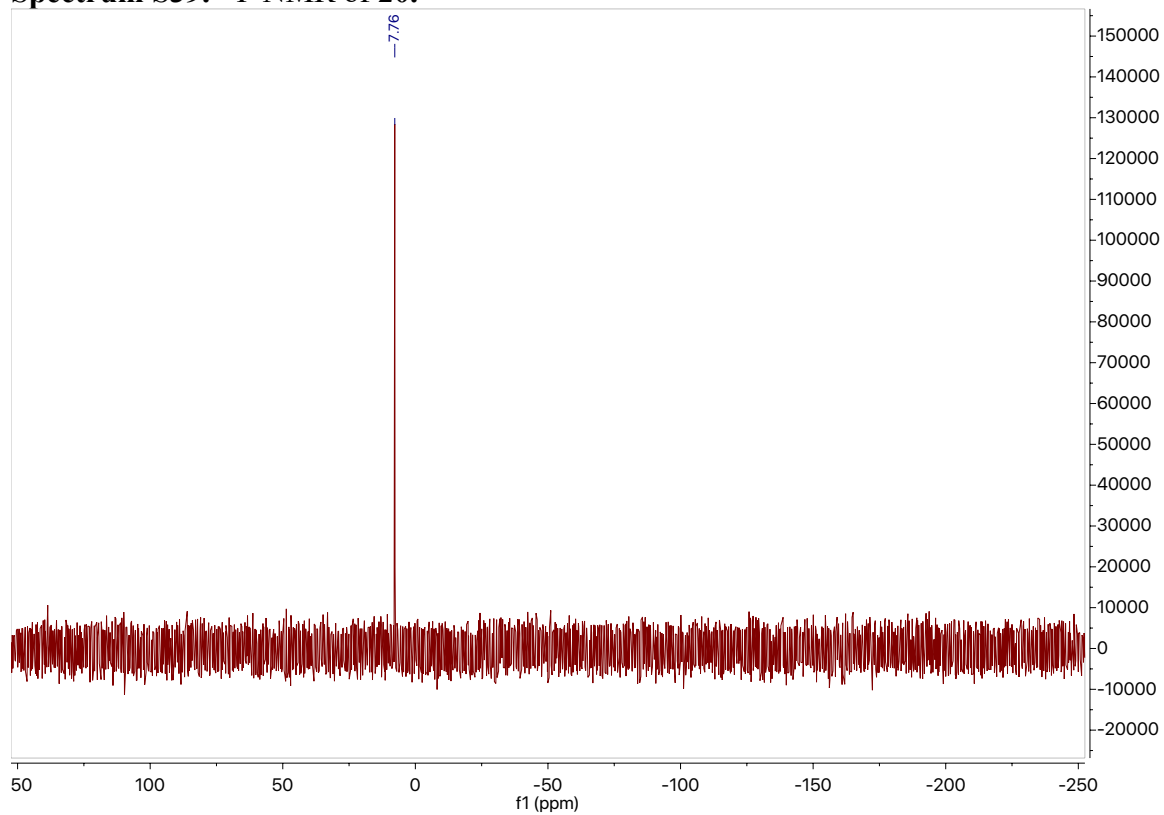
Spectrum S37. ³¹P NMR of 19.



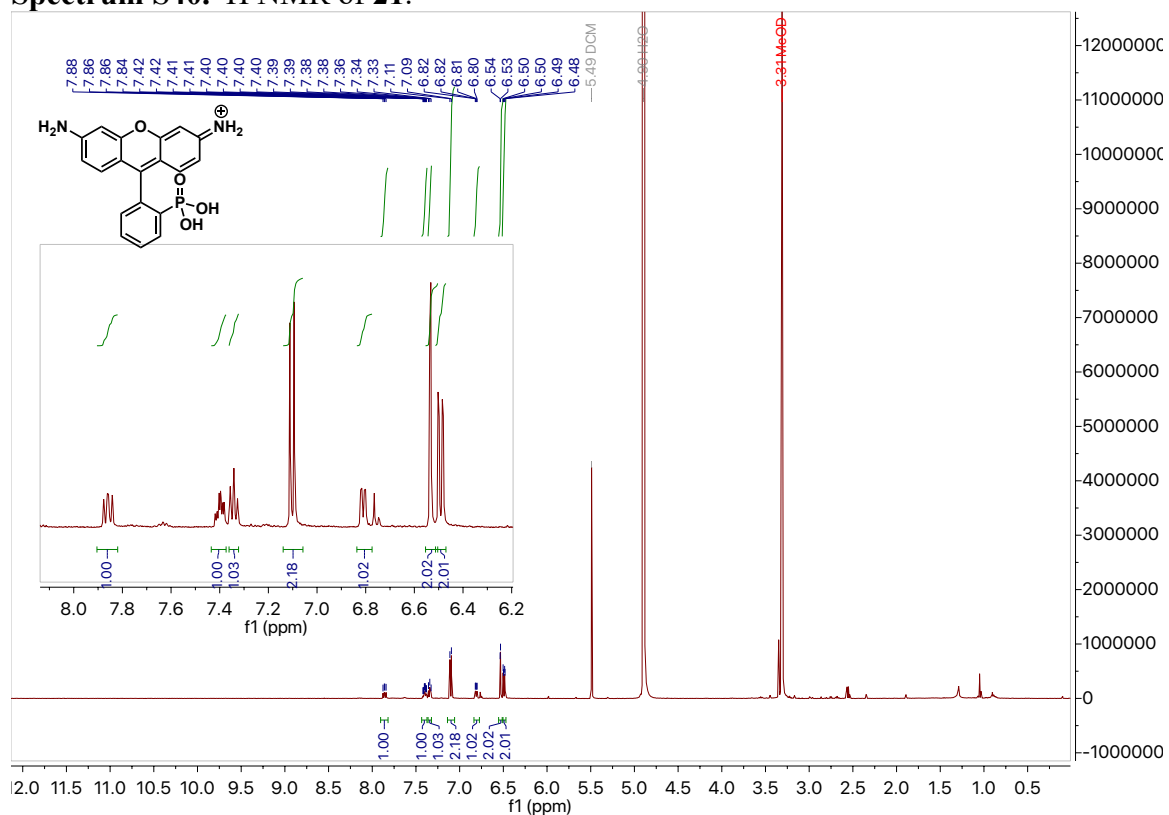
Spectrum S38. ¹H NMR of 20.



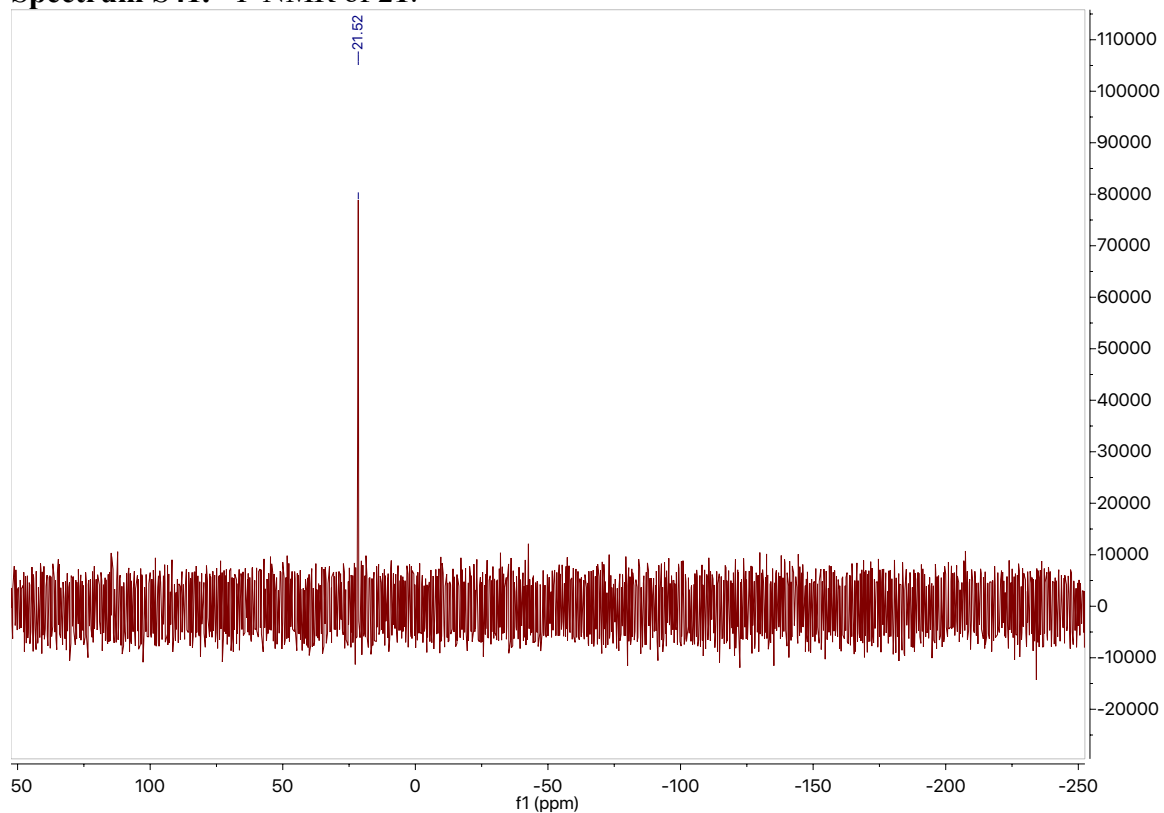
Spectrum S39. ³¹P NMR of 20.



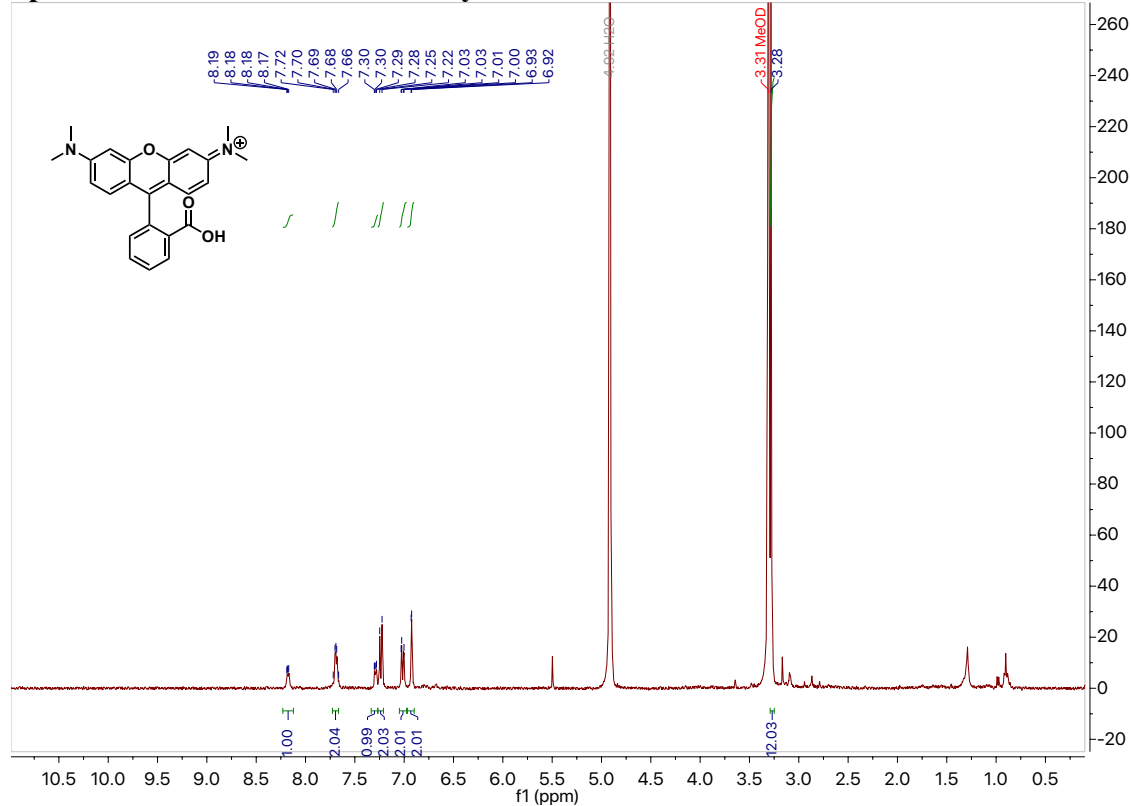
Spectrum S40. ¹H NMR of 21.



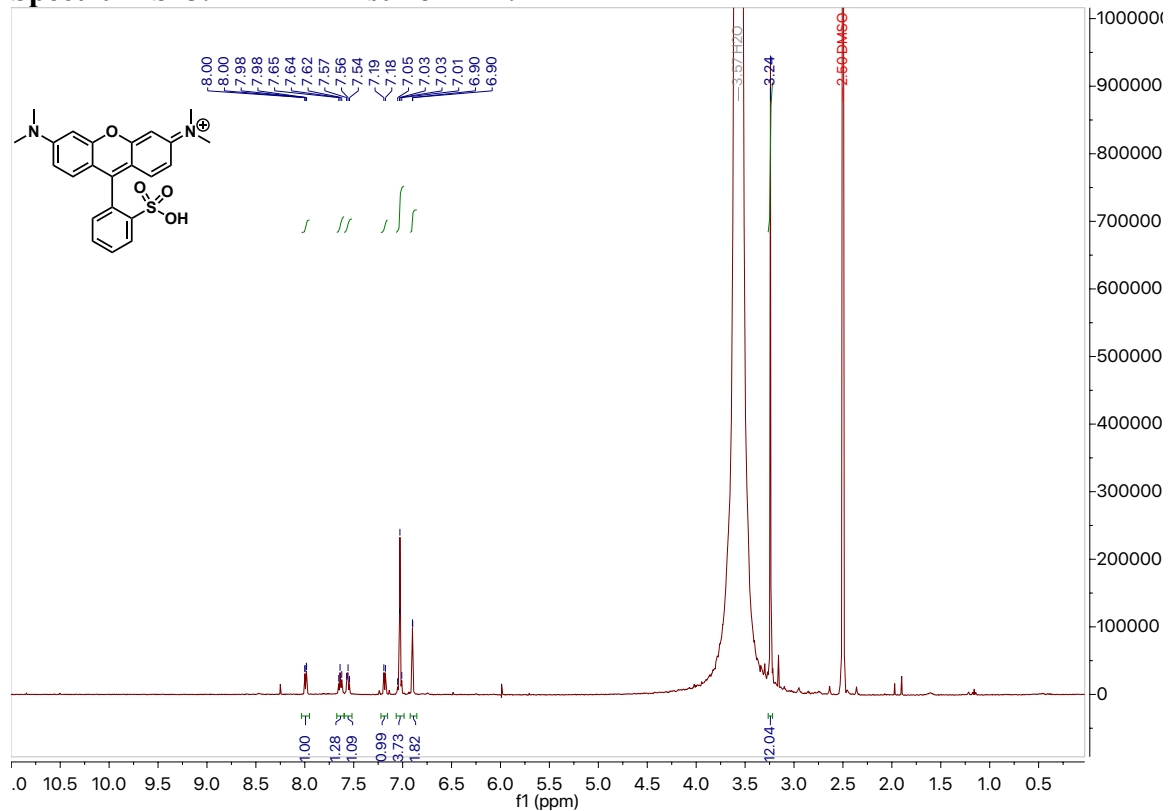
Spectrum S41. ³¹P NMR of 21.



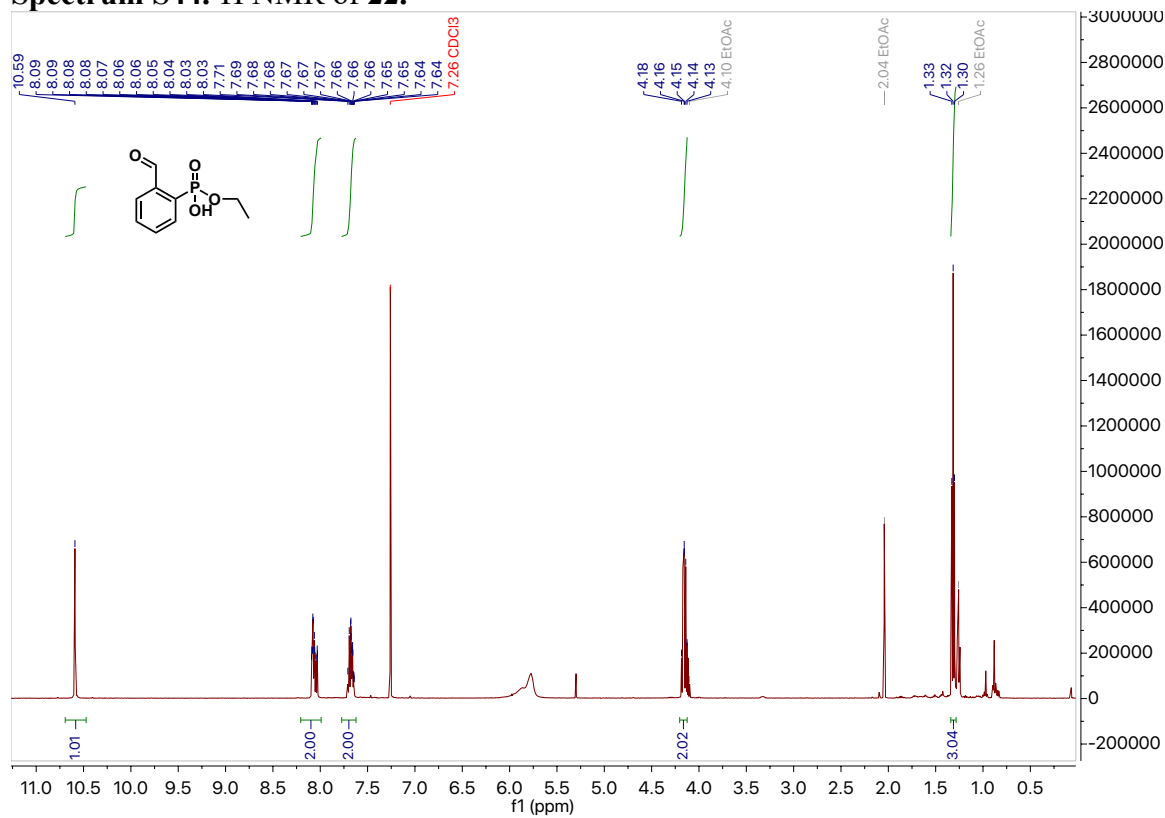
Spectrum S42. ¹H NMR of carboxyTMR.



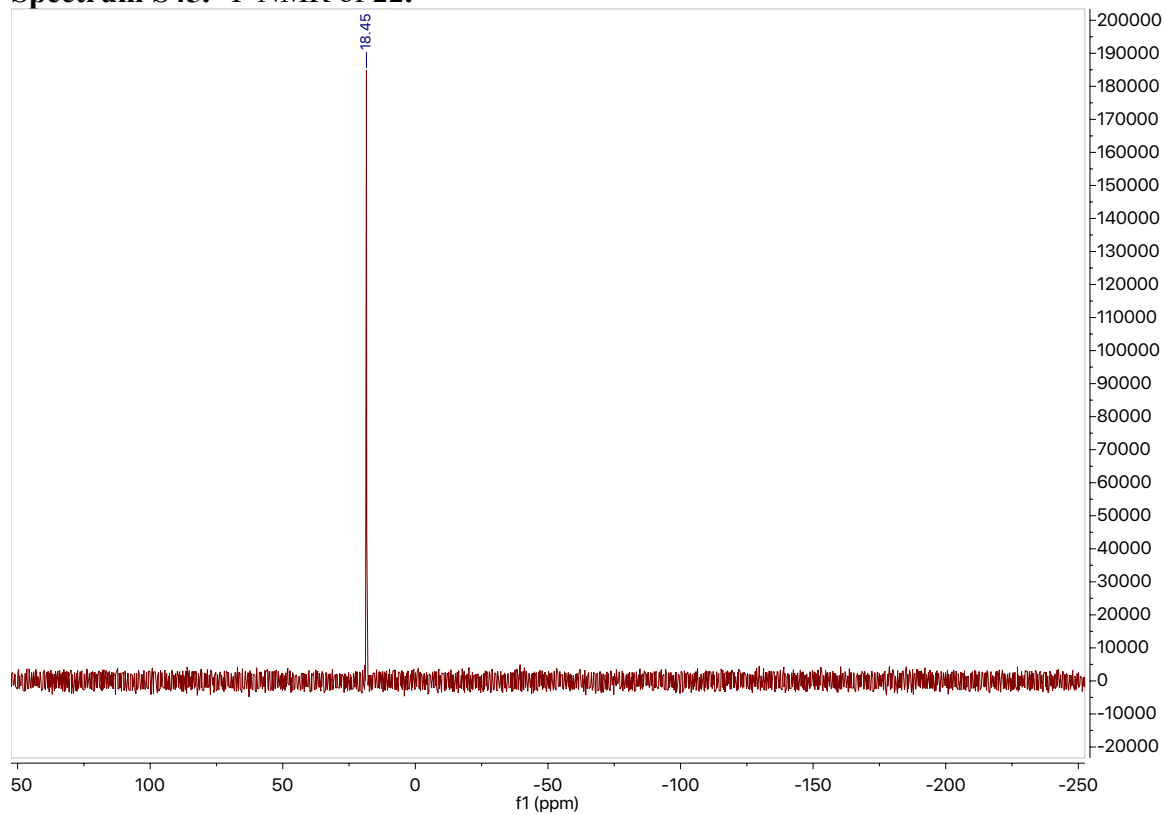
Spectrum S43. ¹H NMR of sulfoTMR.



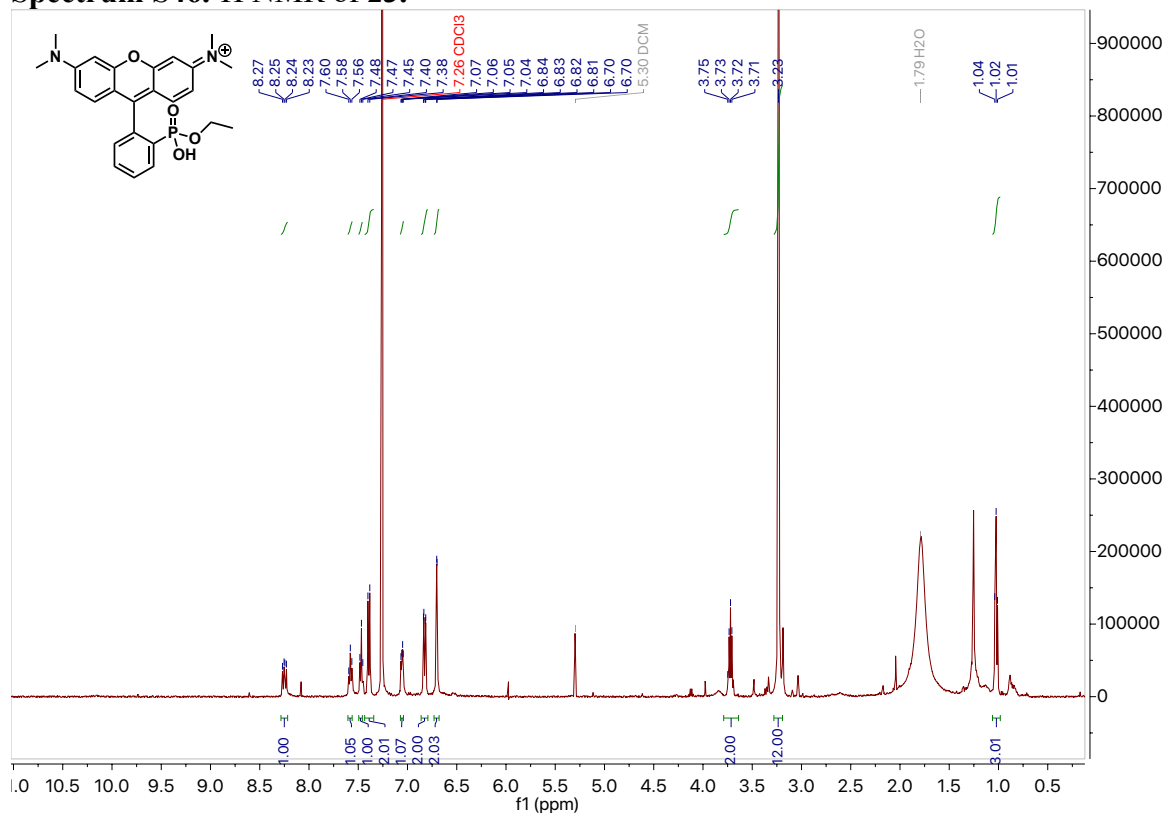
Spectrum S44. ¹H NMR of 22.



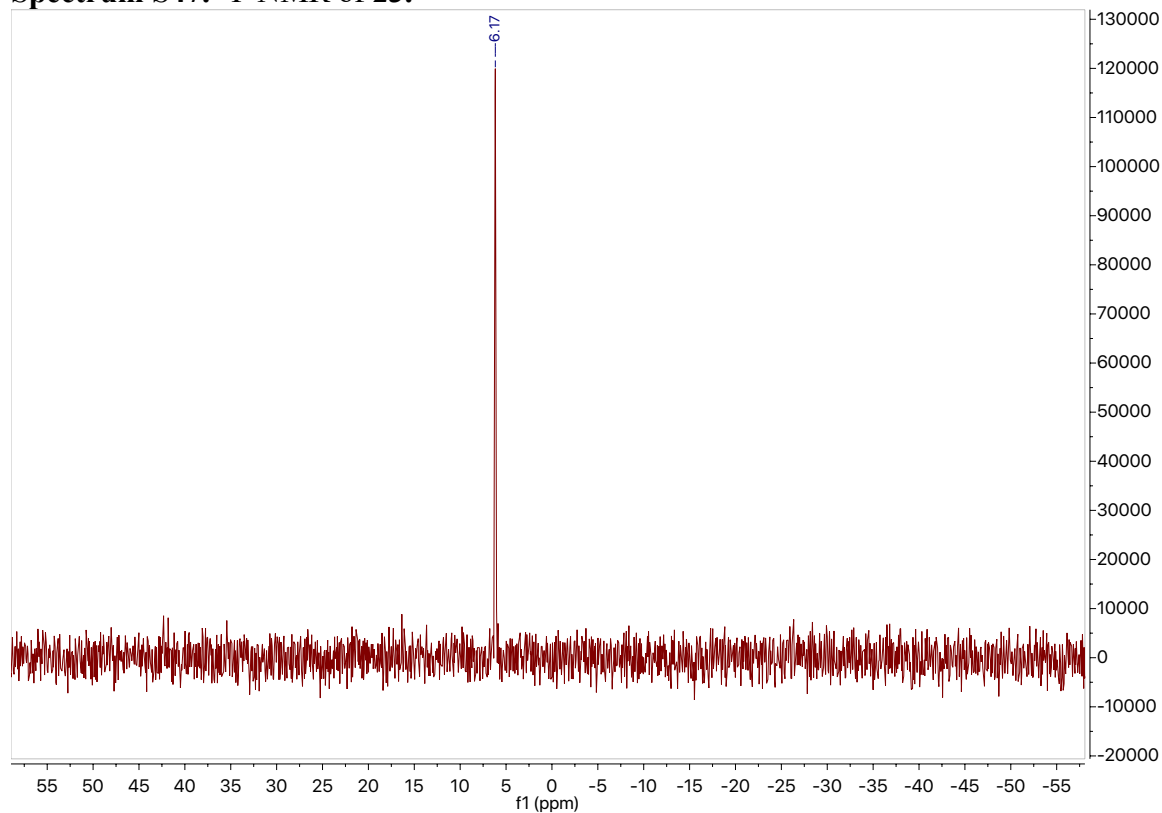
Spectrum S45. ³¹P NMR of 22.



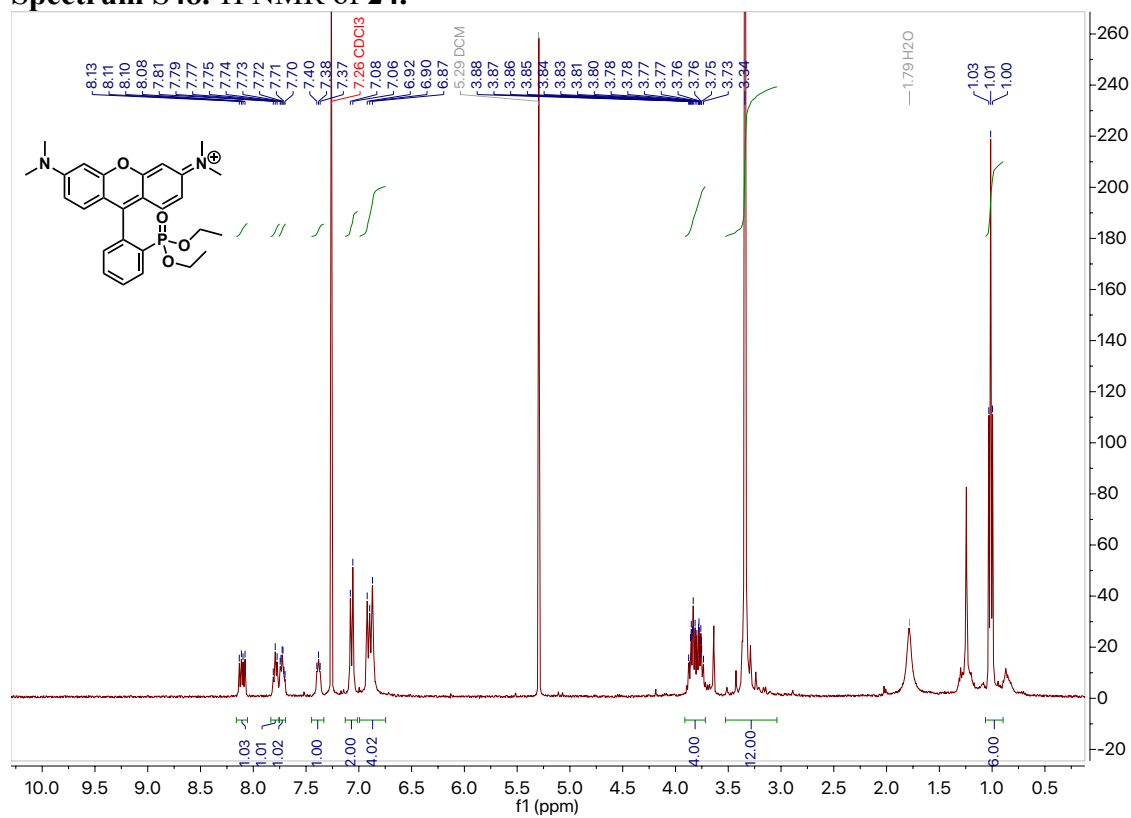
Spectrum S46. ¹H NMR of 23.



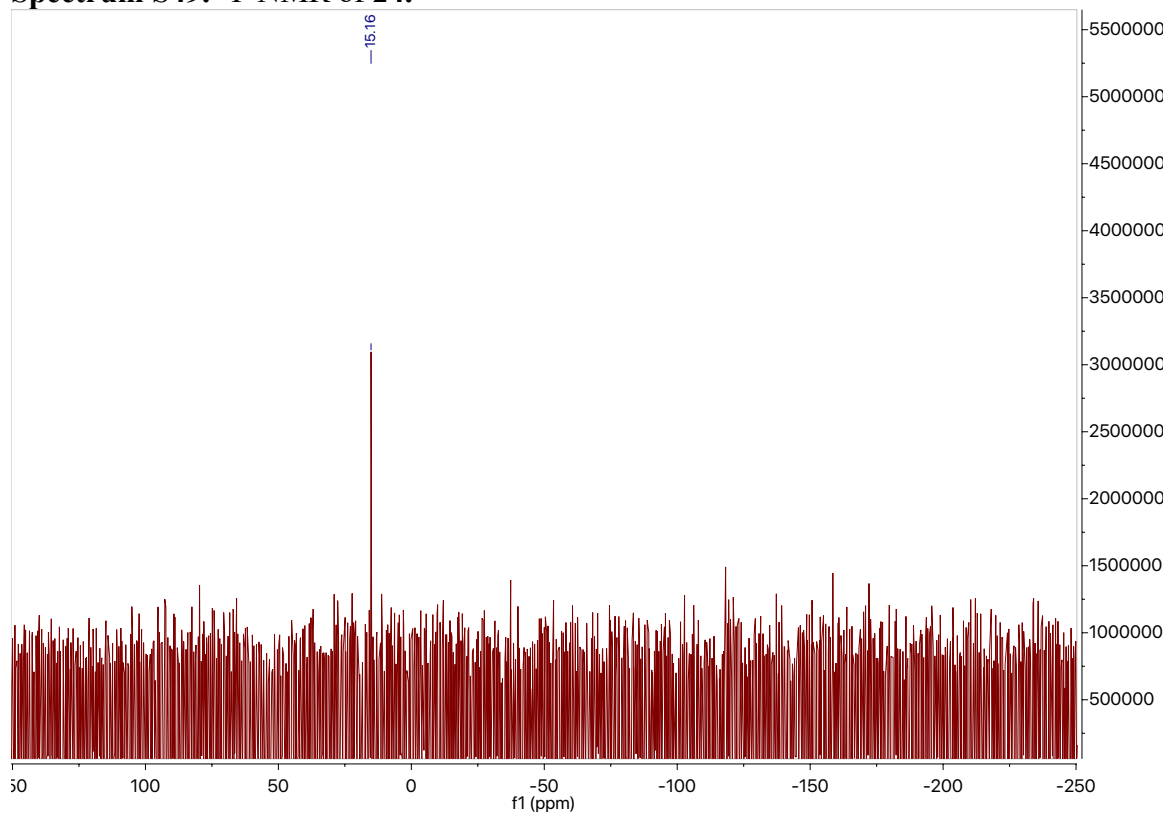
Spectrum S47. ³¹P NMR of 23.



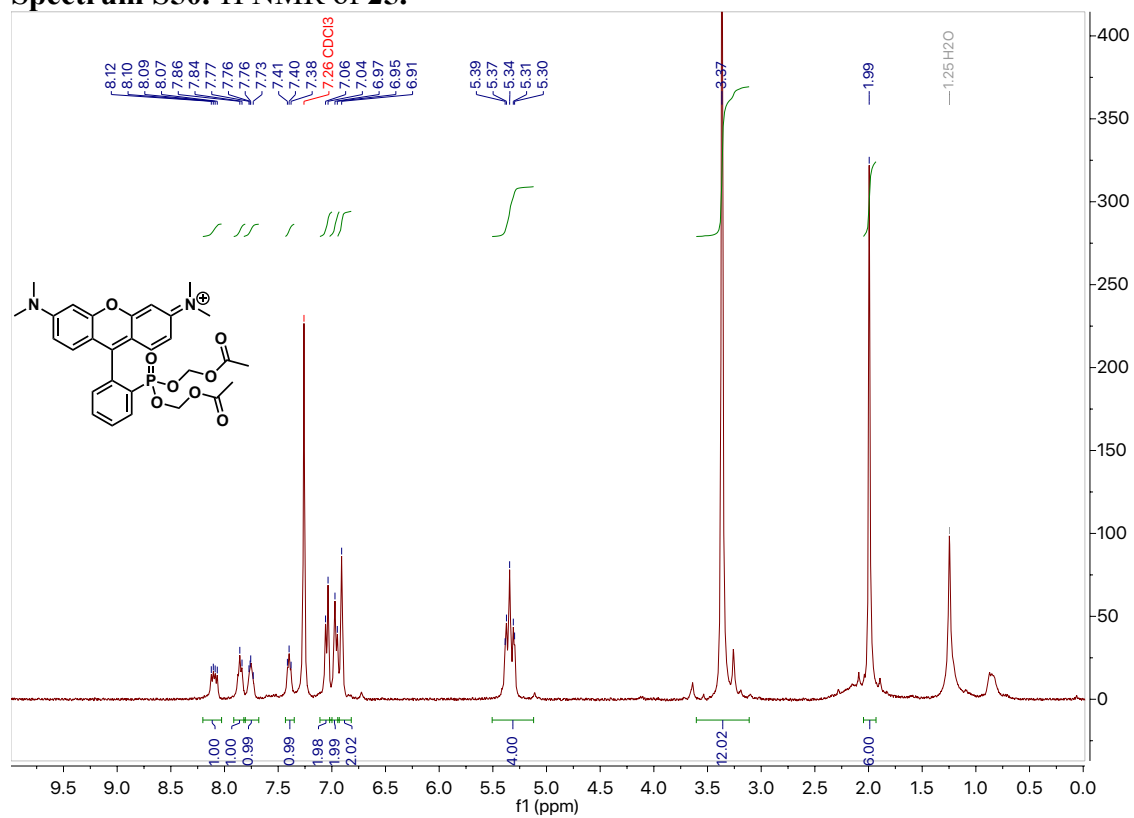
Spectrum S48. ¹H NMR of 24.



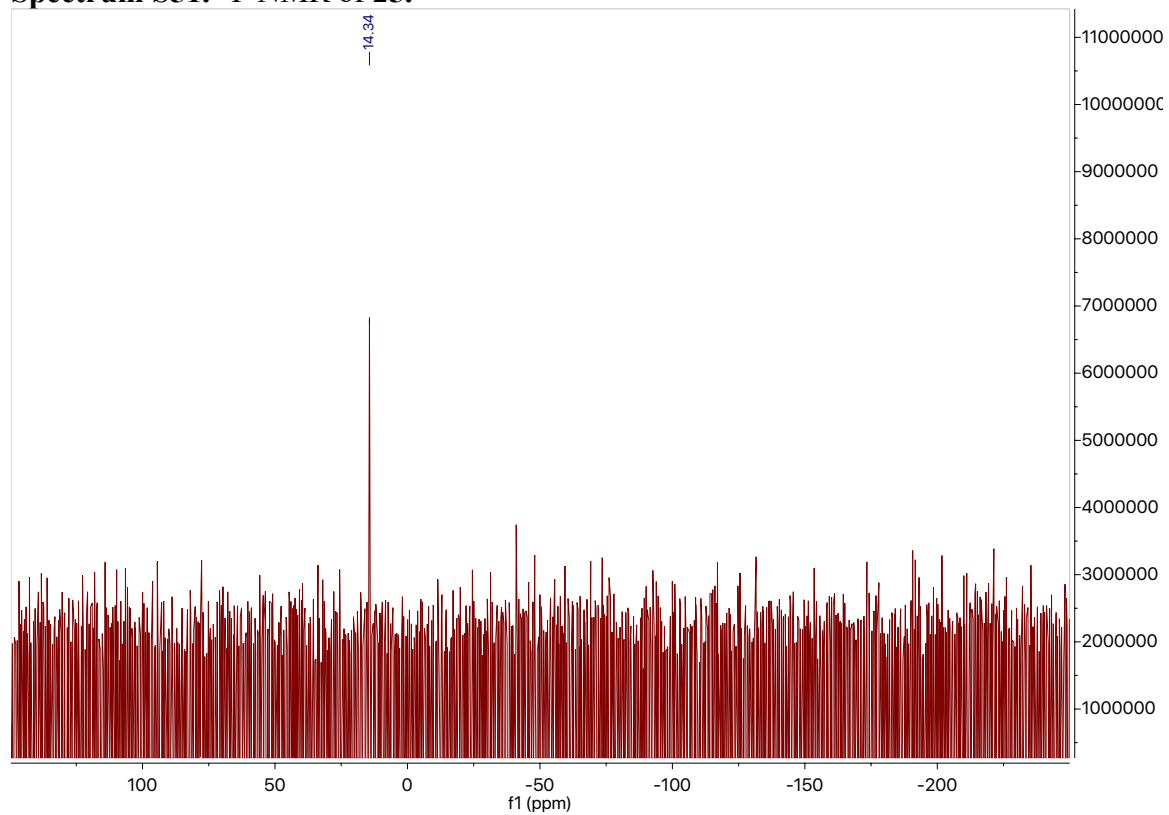
Spectrum S49. ³¹P NMR of 24.



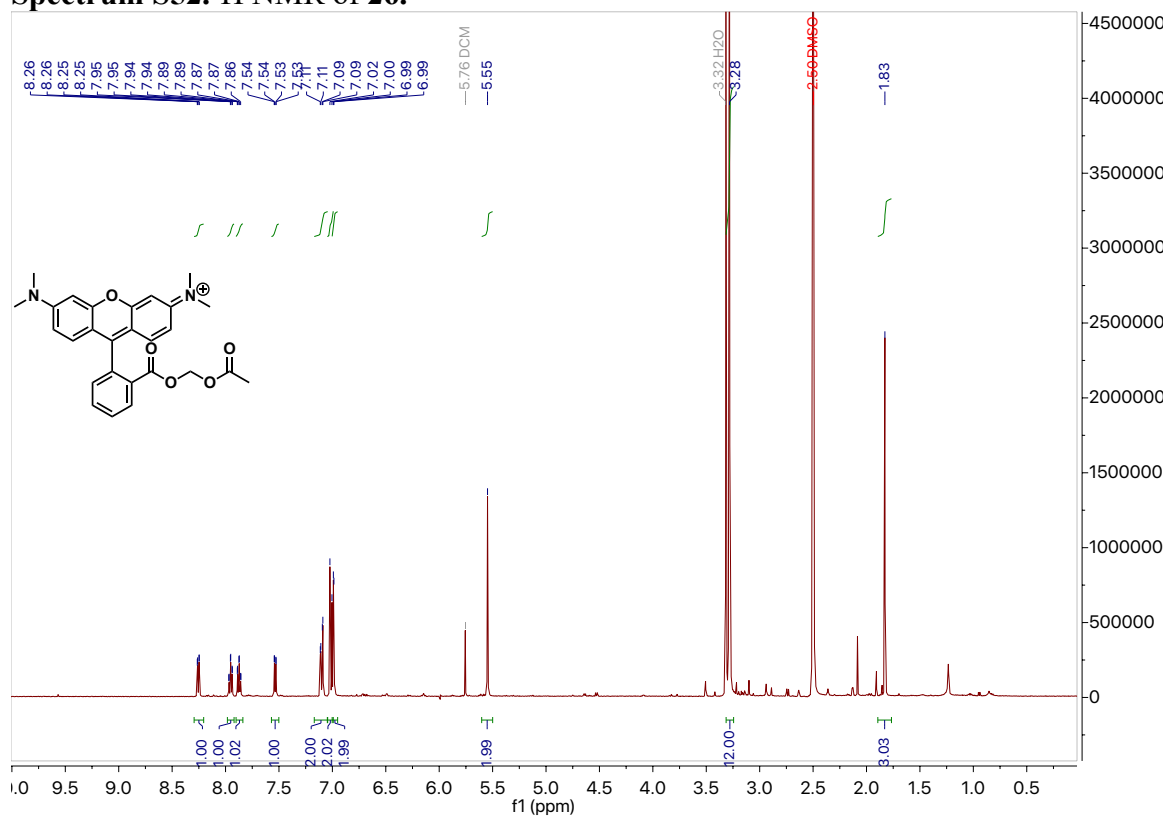
Spectrum S50. ¹H NMR of 25.



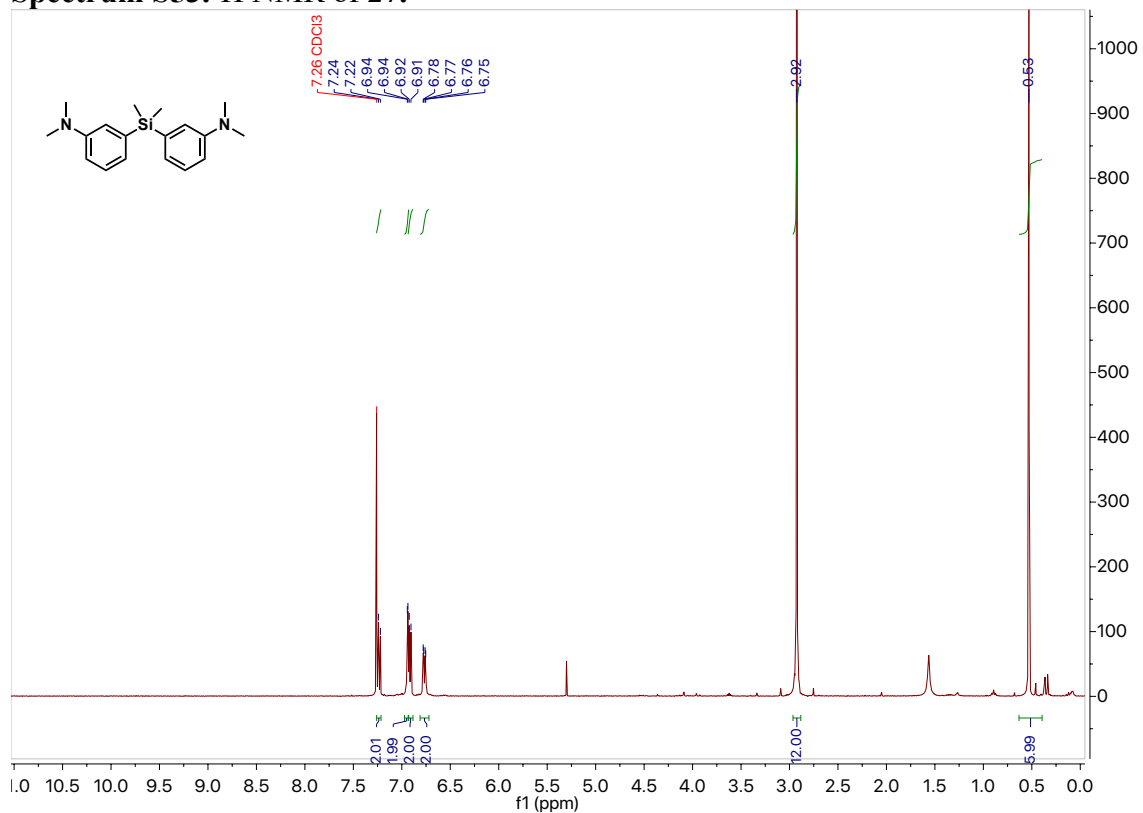
Spectrum S51. ³¹P NMR of 25.



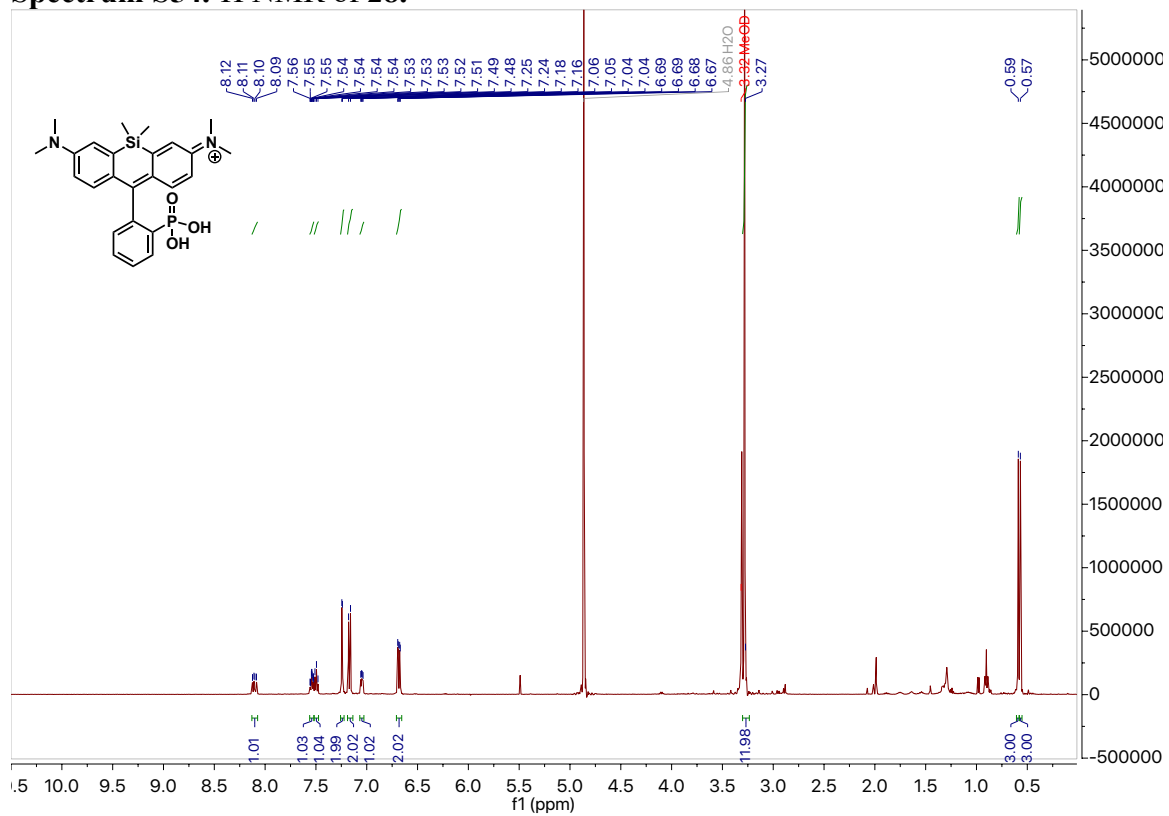
Spectrum S52. ¹H NMR of 26.



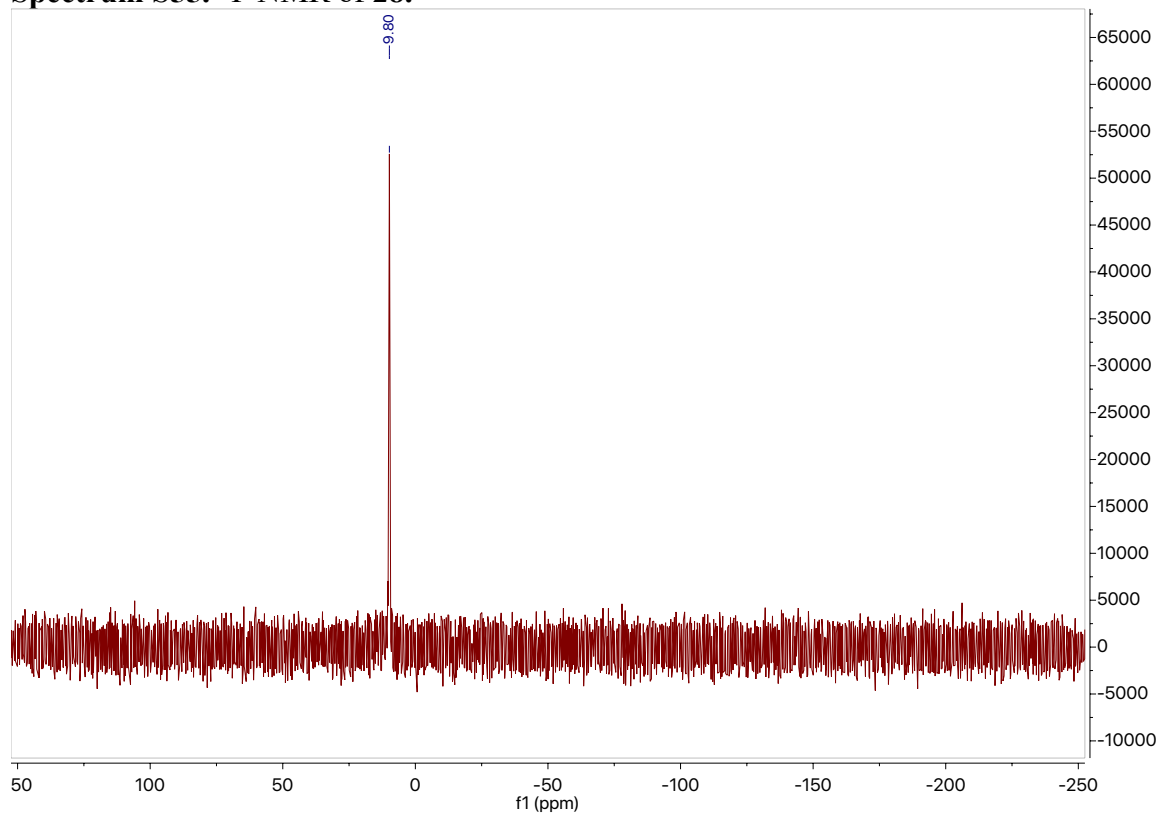
Spectrum S53. ¹H NMR of 27.



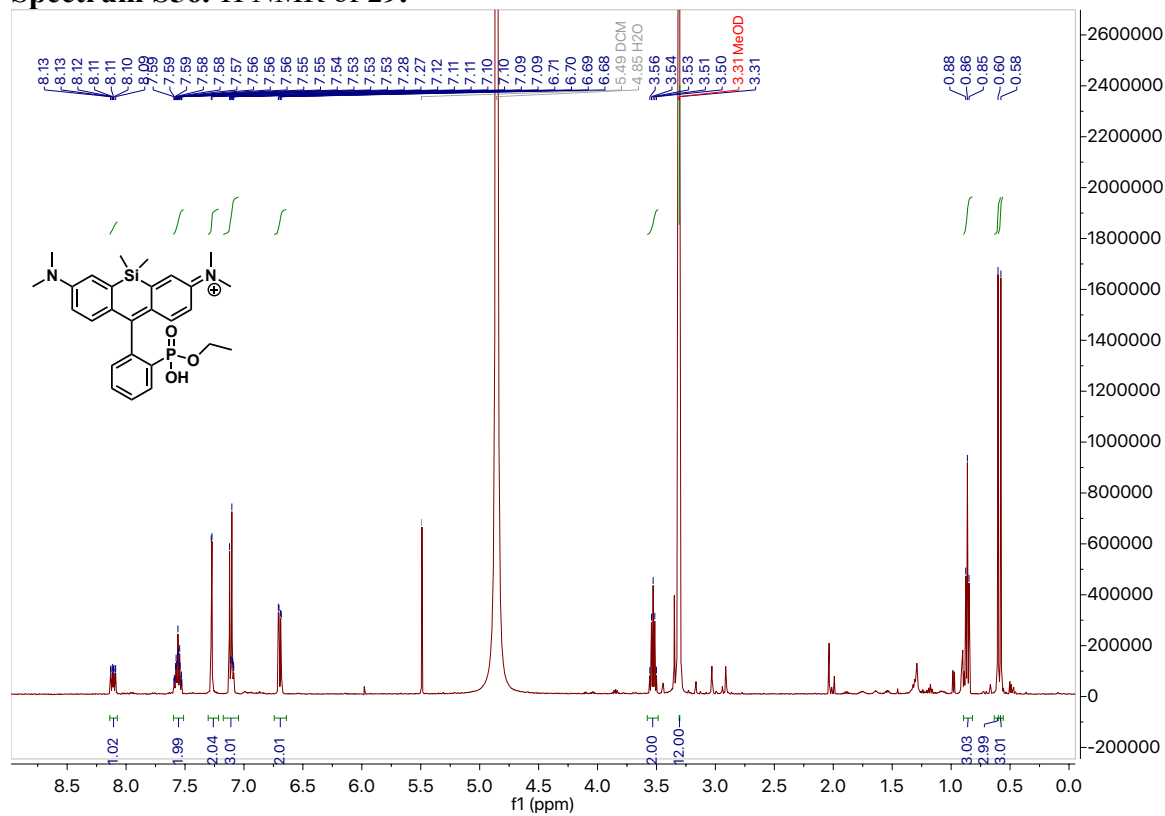
Spectrum S54. ¹H NMR of 28.



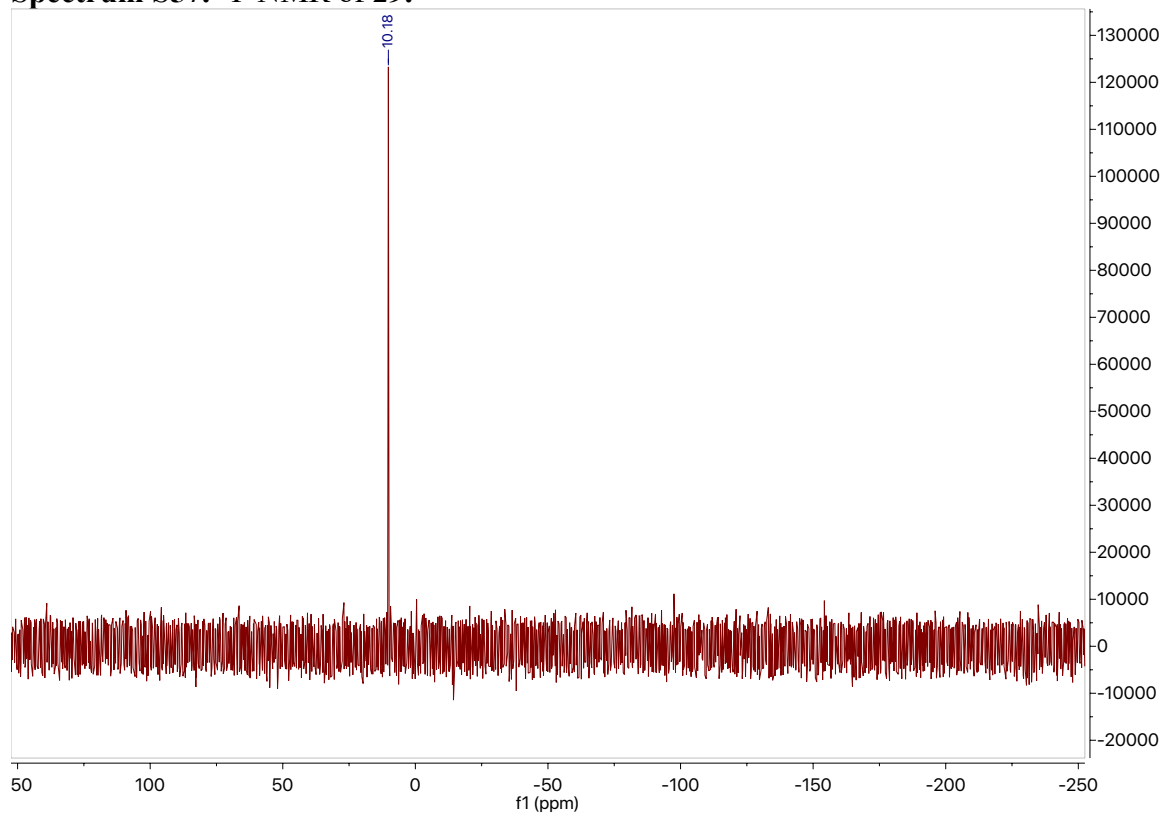
Spectrum S55. ³¹P NMR of 28.



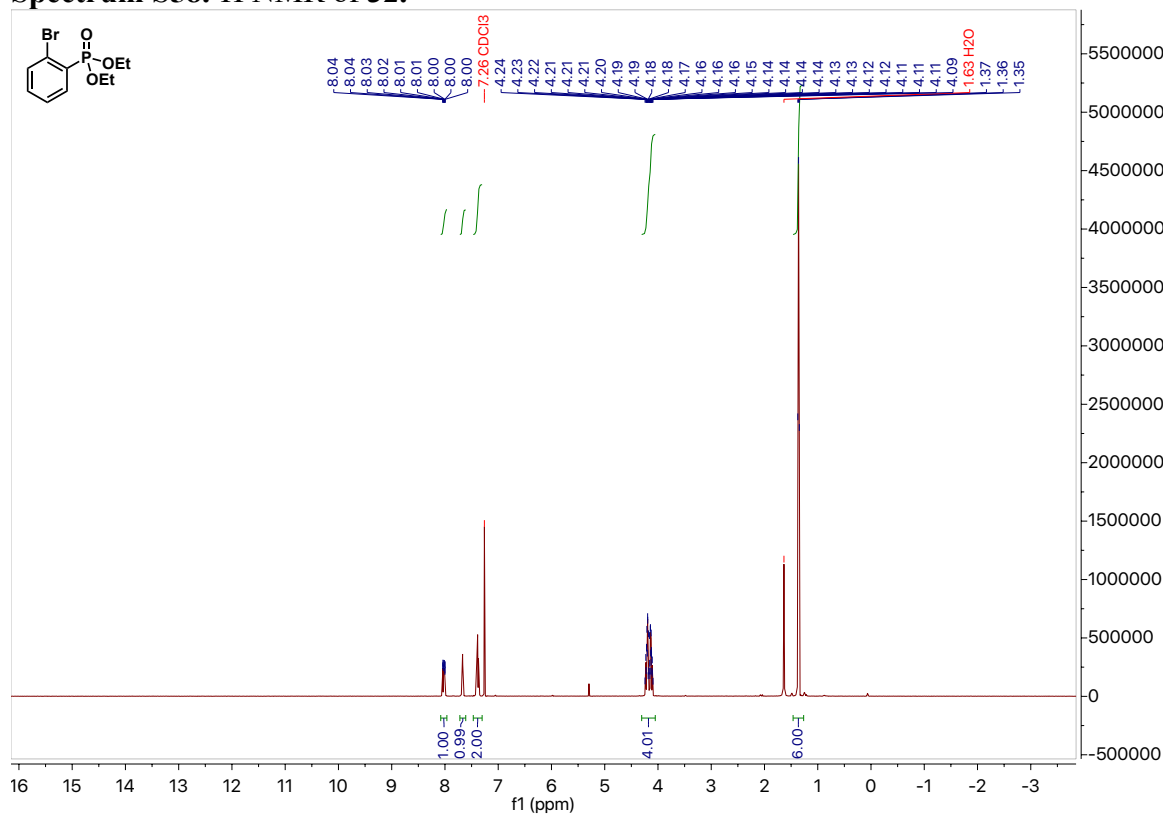
Spectrum S56. ¹H NMR of 29.



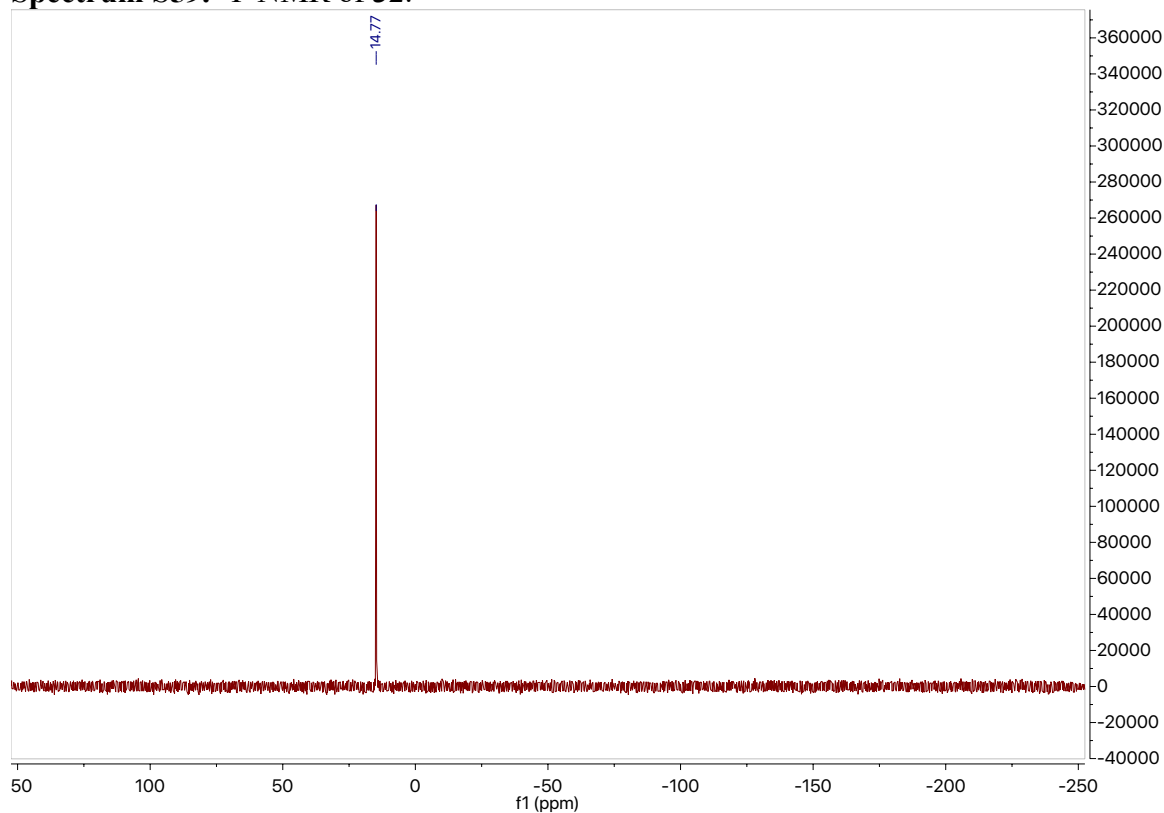
Spectrum S57. ³¹P NMR of 29.



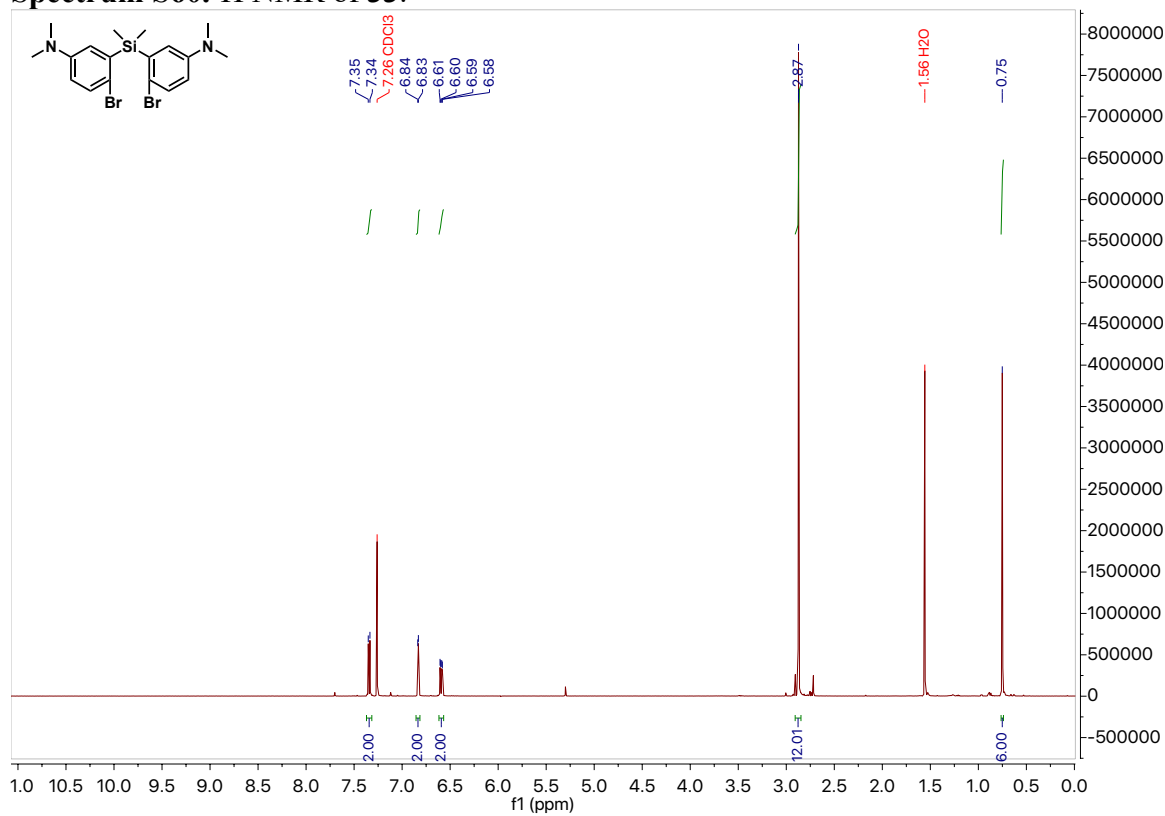
Spectrum S58. ¹H NMR of 32.



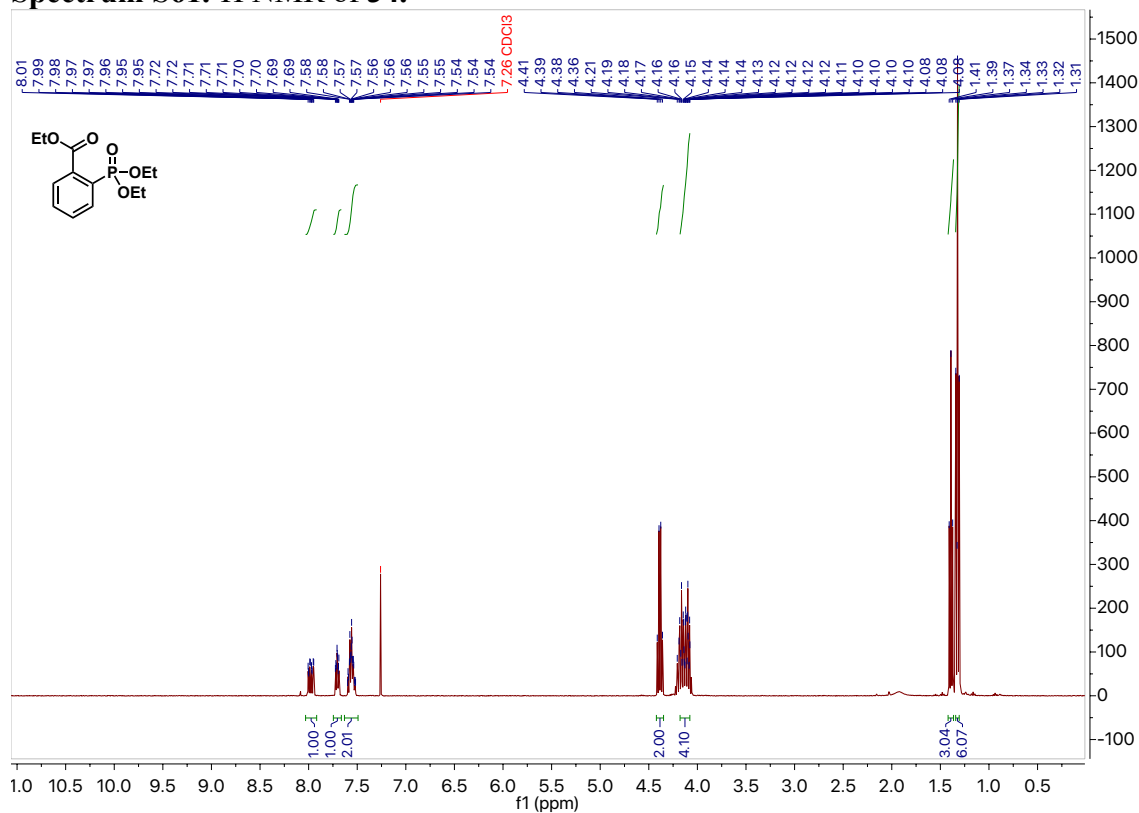
Spectrum S59. ³¹P NMR of 32.



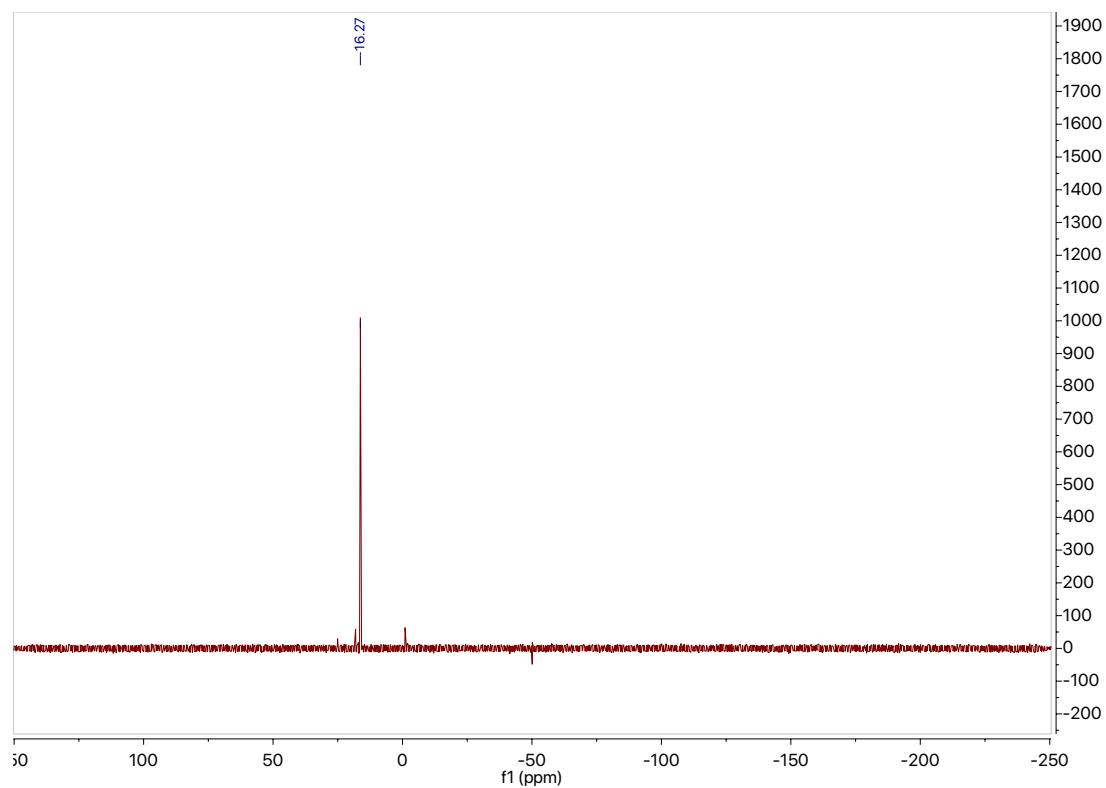
Spectrum S60. ¹H NMR of 33.



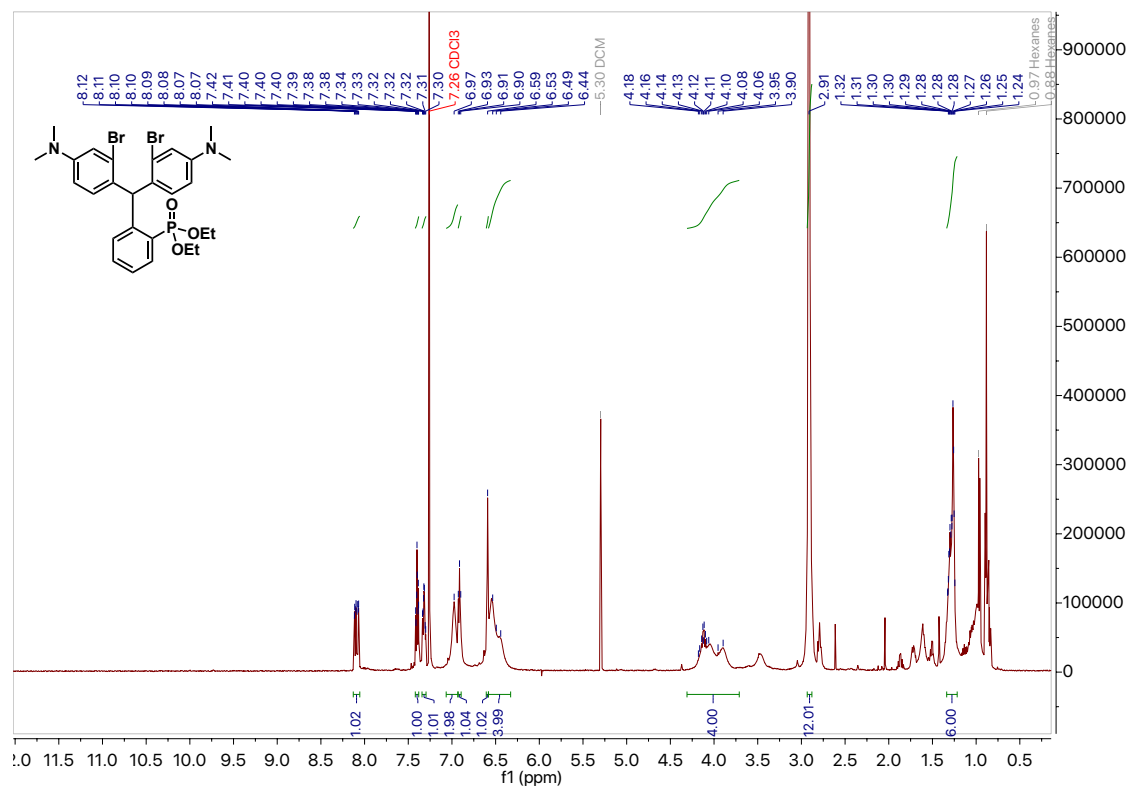
Spectrum S61. ¹H NMR of 34.



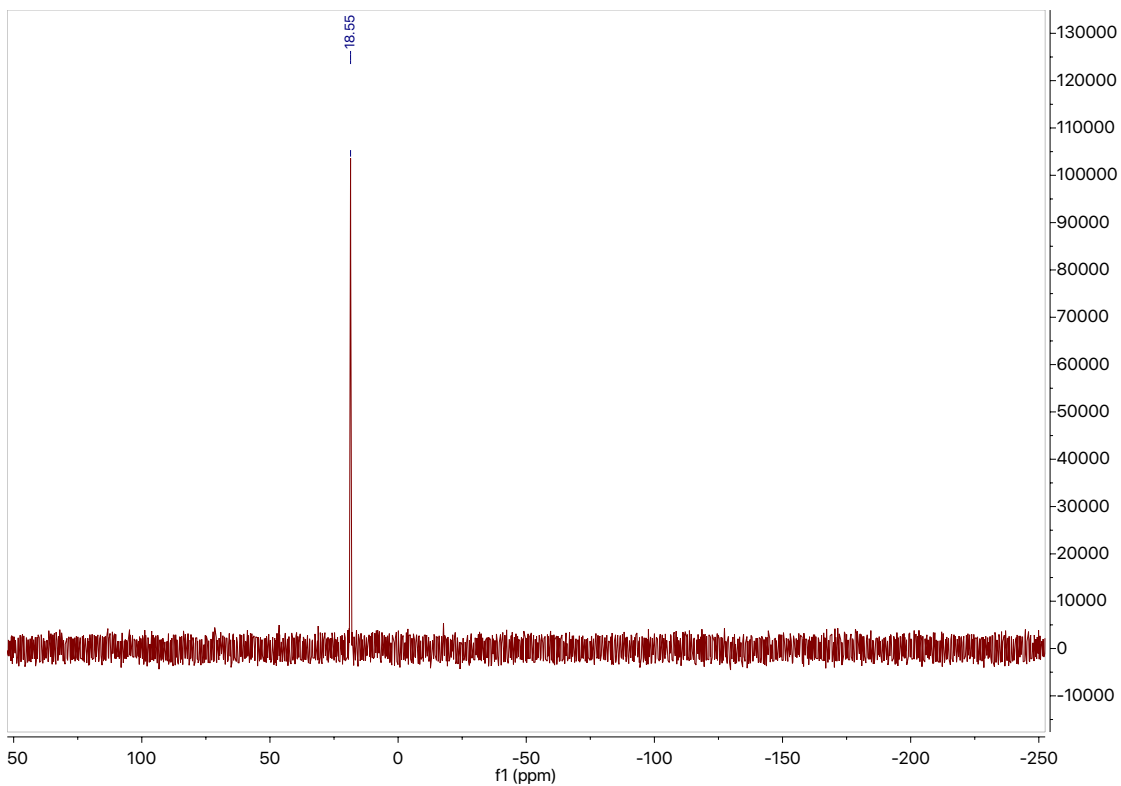
Spectrum S62. ^{31}P NMR of 34.



Spectrum S63. ^1H NMR of 35.



Spectrum S64. ^{31}P NMR of **35**.



Chapter 3

Phosphonated Xanthene Fluorophores for Voltage Sensing Applications

Portions of this work were published as:

[Turnbull, J. L.; Benlian, B. R.; Golden, R. P.; Miller, E. W. Phosphonofluoresceins: Synthesis, Spectroscopy, and Applications. *J. Am. Chem. Soc.* 2021, 143 \(16\), 6194-6201.](#)

Part of this work was performed in collaboration with Brittany Benlian who performed the electrophysiology experiments and Ryan Golden who assisted with chemical synthesis.

Introduction

The universal ability of cells to maintain an uneven distribution of ions across a membrane is fundamental to life itself. Membrane potential dynamics govern the ability for our brain to think, our heart to beat and our body's ability to feel sensation. On a cellular level, membrane potential is critical to a plethora of biological phenomena such as bioelectrical signaling, the cell cycle, and oxidative phosphorylation.^{1,2} In order to further understand the role of membrane potential dynamics in living systems, we need to develop the most effective tools to accurately measure these changes in real time. Traditional methods such as patch clamp electrophysiology are highly sensitive and thereby enable accurate and quantitative measurements of cellular membrane potential. On the other hand, patch clamp electrophysiology is inherently low throughput, provides low spatial resolution and is highly invasive in nature.³ More modern approaches have involved genetically encoded voltage indicators (GEVIs) or small organic fluorophores to alleviate some of these limitations, but competing trade-offs of kinetics, brightness and voltage sensitivities leave much room for improvement in our ability to accurately sense voltage changes in biological systems of increasing complexity.³⁻⁶

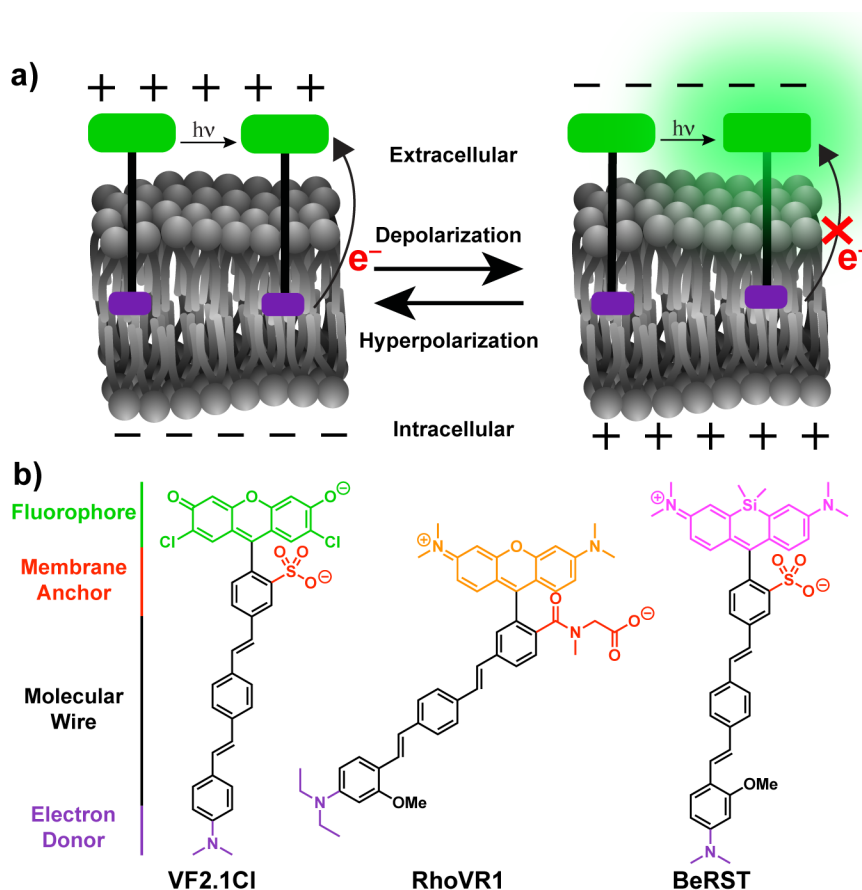


Figure 1. PeT-based voltage sensitive indicators. (a) proposed mechanism of voltage-sensitive indicators and (b) general molecular scaffold of voltage indicators and chemical structures of VF2.1Cl, RhoVR 1 and BeRST.

The Miller lab's research program has largely focused on the development of small molecule voltage-sensitive indicators to alleviate some of the limitations faced with other voltage-sensing approaches (such as resolution, sensitivity, and throughput).⁵ Our voltage-sensing platform makes

use of a common molecular scaffold in which a fluorophore reporter is appended to a lipophilic, aniline-containing phenylene vinylene molecular wire. These electron rich molecular wires donate an electron into the excited state of the fluorophore reporter through photoinduced electron transfer (PeT), quenching fluorescence.⁷ The rate of PeT is sensitive to external electric fields; at a resting membrane potential, PeT is accelerated and fluorescence is quenched but upon depolarization or reversal of membrane potential, PeT is inhibited and an increase in fluorescence can be observed (**Figure 1a**). The fast kinetics of PeT (ns time scale) is instrumental in providing the temporal resolution required to observe rapid membrane potential dynamics (ms time scale). Furthermore, the orthogonal relationship of the fluorophore and molecular wire has enabled access to a variety of colors across the visible spectrum through exchange of the fluorophore.⁷⁻¹³ We have reported a variety of indicators including fluorescein-based Voltage-sensitive Fluorophores (VFs),^{7,8} Rhodamine Voltage Reporters (RhoVRs),⁹ and silicon-rhodamine derived Berkeley Red Sensors of Transmembrane potential (BeRSTs) (**Figure 1b**).¹⁰

While the lipophilic nature of the molecular wire drives voltage sensitive indicators into the hydrophobic plasma membrane of living cells, the properties of the 3-substituent of the fluorophore also play a crucial role in membrane localization. Acidic 3-substituents act as a membrane anchor, dictating orientation, and prevents prohibitive dye internalization.⁷ To inhibit permeability, the 3-substituent must be anionic at physiological pH, impart water solubility and prevent spirocyclization to the neutral non-fluorescent state of the fluorophore and as such we have previously relied on the use of a sulfonate or tertiary amide such as N-methyl glycine.^{8,9} Additionally, this anchoring group has been found to play a major role on the orientation within the membrane, influencing the efficiency of the PeT process and thus voltage sensitivity.⁸ Inspired by the excellent exclusion from cells, high water solubility, and tendency to disfavor spirocyclization, we hypothesized that 3-phosphonate substitution could be readily incorporated into our voltage sensing scaffold.

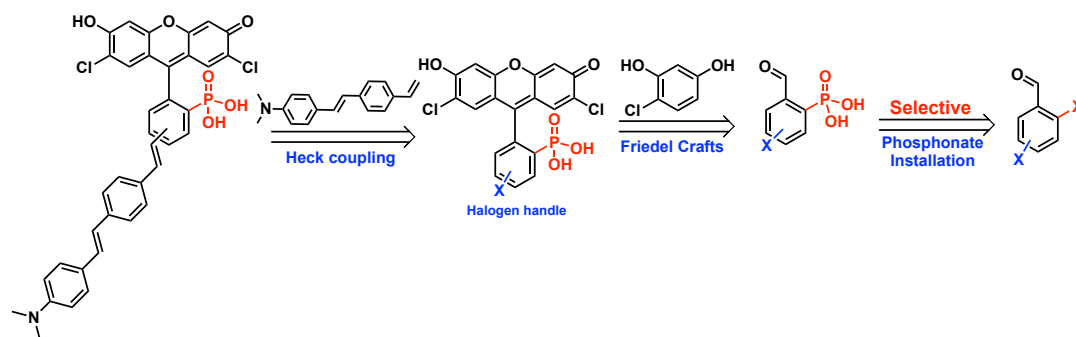
In addition to bearing the key properties for membrane anchoring, 3-phosphonates are readily functionalizable and we have demonstrated by our ability to influence cellular permeability and subcellular localization through esterification of 3-phosphono-fluoresceins and rhodamines (**Chapters 1 and 2**). In fact, functionalization of the 3-substituent has facilitated numerous applications of our voltage sensing indicators. While sulfonate esters are typically unstable and preclude functionalization, coupling of 3-carboxylates to ligands such as a chloroalkane or spy tag peptide enabled chemi-genetic approaches to target voltage indicators specifically to cells expressing the associated targeting enzyme (HaloTag or SpyCatcher).¹⁴⁻¹⁶ This provided improved cellular resolution, where indiscriminate membrane staining is disadvantageous, to study more complex systems such as neuronal circuits, brain slice or intact brains.¹⁷ Conjugation to molecular prosthetics such as triplet state quenchers has been shown to reduce the photobleaching and phototoxicity that is observed under constant illumination and led to the ability to perform prolonged functional imaging of cardiomyocytes.¹⁸ Additionally, protection of sarcosine with biologically labile acetoxymethyl esters facilitated intracellular delivery of RhoVR 1 and enabled imaging of mitochondrial membrane potential dynamics.¹⁹ Conjugation of the 3-carboxylate inherently results in a masking of the associated negative charge, and while this is advantageous for intracellular delivery applications, most useful applications of functionalized voltage sensors still require localization to the extracellular membrane. This meant that incorporation of a negatively charged linker such as cysteic acid was required, thereby adding complexity to the syntheses of these probes.^{15,16} On the other hand, phosphonates contain two functional handles and we envisioned that it would be possible to make use of phosphonate monoesters bearing some

functionality while retaining the negative charge required for membrane anchoring. We hoped this would provide a more generalizable approach to voltage-indicator functionalization and lead to new applications.

In this chapter we describe our synthetic approaches towards phosphonated voltage sensing indicators (phosVFs, phosRhoVRs and phosBeRST), compare how they perform with respect to their analogous sulfo- and carboxy- analogs and explore the utility of these new scaffolds in voltage sensing applications.

Results and discussion

Synthesis of phosphonated voltage sensitive fluorophores (VFs)



Scheme 1. Retrosynthetic analysis of phosphonated voltage sensitive fluorophores (VFs).

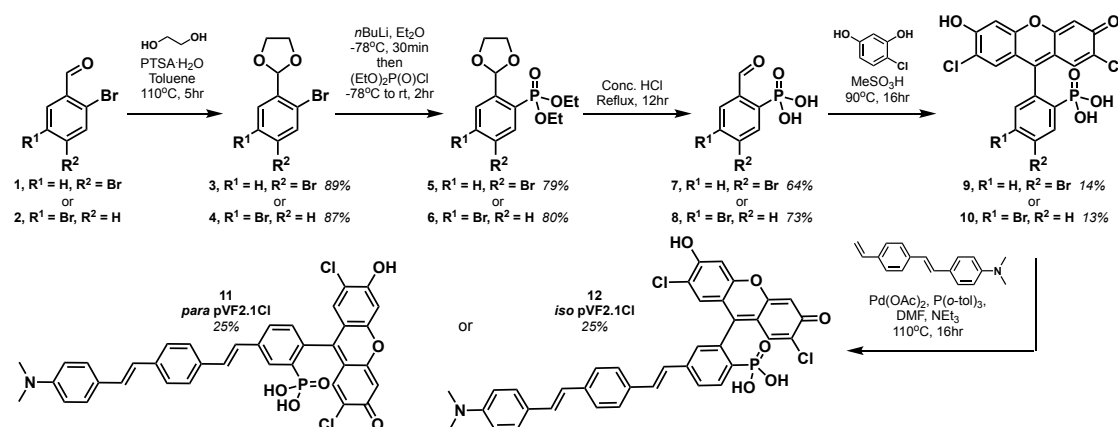
The voltage-sensing molecular wire domains of VFs have typically been installed via Heck coupling to fluoresceins, making use of a 4' or 5' halogen. We recognized that this halogen handle would need to be present on the phosphonobenzaldehyde precursor (**Scheme 1**), however since we had previously made use of a halogen handle to install the phosphonate (**Chapter 1**) our synthetic strategy therefore focused on determining a method for selectively installing a phosphonate in the presence of two aryl halides. Unfortunately, we observe no regioselectivity when exposing 2,5-dibromobenzaldehyde to the same Ni-mediated Arbuzov conditions that had been used previously (**Scheme S1**). We hypothesize that since the oxidative addition step is relatively fast with respect to formation of the phosphonium intermediate, and at such elevated temperatures any directing effects from the aldehyde are negligible.²⁰ To test whether any selectivity for aryl iodides vs. bromides could be achieved, we attempted analogous Arbuzov chemistry with 2-iodo-5-bromotoluene. Interestingly, when using palladium as the catalyst and a lower temperature of 90 °C are able to selectively access 2-phosphono-5-bromotoluene in a 78% yield (**Scheme S1**). Since oxidative addition of aryl iodides is more facile than aryl bromides, careful control of the reaction temperature is sufficient to provide selective phosphonate installation. We do note that since oxidative addition is not the slow step in the reaction,²⁰ the temperature required to see conversion to the aryl phosphonate is substrate dependent and therefore requires some optimization and the scope may be limited. Despite affording regioselectivity, **S3-2** would require some oxidation to the corresponding aldehyde to be used in subsequent fluorescein condensations and 2-iodo-(4- or 5)-bromobenzaldehydes are significantly more expensive than their dibrominated analogs.

We postulated that a pseudohalide approach may be more fruitful as it had previously been reported that aryl triflates can be converted to aryl bromides through use of palladium catalysis.²¹ This would enable us to install the second halogen handle after phosphonate installation, thereby bypassing any regioselectivity challenges. 2-bromo-5-hydroxybenzaldehyde is unreactive when

exposed to nickel chloride and triethyl phosphite, likely due to the acidic phenol poisoning the catalyst. Protection of the 5-hydroxyl with tert-butyl dimethyl silyl chloride enables us to then install the diethyl phosphonate in a moderate yield (**Scheme S2**). Subsequent deprotection of the silyl ether followed by formation of the corresponding triflate provides the pseudohalide intermediate **S7**. In only moderate yield, we can then convert the aryl triflate to the corresponding bromide using $\text{Pd}_2(\text{dba})_3$ and a bulky ligand, ^tBuBrettPhos. Subsequent hydrolysis of the diethyl phosphonate provides us with the desired 5-bromo-2-phosphonobenzaldehyde, **8**, in an overall 9% yield over 6 steps.

Since the fluorescein Friedel Crafts condensations are known to be low yielding, accessing aldehyde precursor **8** in such limited yields is undesirable. We therefore decided to explore alternatives to transition metal catalyzed phosphonate installation. Instead, we first protect 2,4- and 2,5-dibromo benzaldehydes (**1** and **2**) with ethylene glycol and use the corresponding acetals (**3** and **4**) to direct lithium-halogen exchange with *n*-butyllithium exclusively to the *ortho* position (**Scheme 2**). Slow addition of diethyl chlorophosphate provides us with the desired aryl phosphonates (**5** and **6**) in good yields. Simultaneous phosphonate hydrolysis and acetal deprotection in concentrated acid yields 4- and 5-bromo-2-phosphono-benzaldehydes (**7** and **8**) in an overall 45% yield over 3 steps, providing a drastic improvement in both efficiency and cost compared to the transition metal catalyzed alternatives.

Functionalized benzaldehydes **7** and **8** are condensed with 4-chlororesocinol to the corresponding 2',7'-dichloro-3-phosphonofluoresceins (**9** and **10**). As desired, the bromine functional group enables Pd-catalyzed Heck coupling to a styrene molecular wire to produce *para* and *iso* phosVFs (**11** and **12**); however only limited conversion occurs, and significant amounts of dehalogenated and unreacted dye are observed. We initially suspected this could be a result of the presence of the phosphonic acid functional group, but Pd-catalyzed cross coupling of phosphonate-containing precursor **7** and the same styrene results in an almost 3-fold greater 73% yield (**SI compound S3-9**). The desired phosVFs are, however, readily purified by reverse phase silica chromatography to give the desired products in 25% yield for both isomers.



Scheme 2. Synthesis of phosphono voltage fluors.

Characterization of phosphono VFs

Both *para* and *iso* phosVFs possess absorbance and emission spectra nearly identical to 2',7'-dichloro-3-phosphonofluorescein, with the addition of an absorbance band at around 370 nm, corresponding to the aniline-containing molecular wire (**Figure 2a**, **Figure S1**). Both phosVF dyes

localize to cellular membranes of HEK293T cells (**Figure 2b, Figure S2**) and are voltage sensitive (**Figure 1c and d, Figure S3**). Patch clamp electrophysiology coupled with fluorescence microscopy reveal that *para* phosVF2.1Cl has a voltage sensitivity of 26% $\Delta F/F$ per 100 mV (**Figure 2c and d**), roughly the same sensitivity as the sulfonated analog, VF2.1Cl (24%). The same trend was seen for *iso* phosVF2.1Cl and *iso* VF2.1Cl with $\Delta F/F$ per 100 mV values of 11 and 9% respectively (**Figure S3**). No significant differences are observed in the relative brightness or signal-to-noise ratio when both *para* probes are loaded at 250 nM (**Figure S2 and 3**). This suggests substitution of the 3-sulfonate for a phosphonate has negligible effect on the ability of VFs to load into the extracellular membrane of HEK cells. There is likely a negligible effect on the orientation within the membrane since the degree to which both VFs sense the electric field appears relatively unaltered in both the *iso* and *para* cases.

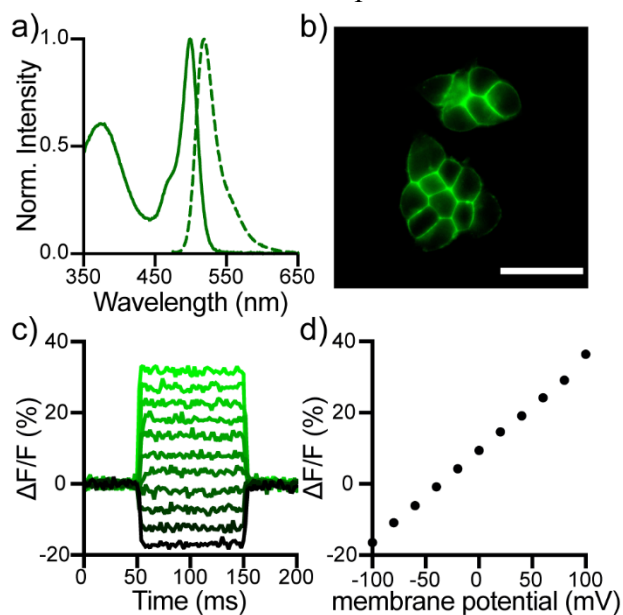


Figure 2. Cellular and *in vitro* characterization of phosphonated VoltageFluors. (a) Normalized absorbance (solid line) and fluorescence emission (dashed line) spectra of *para* phosVF2.1Cl (**17**) in 0.1 M NaOH_(aq). (b) HEK cells stained with 250 nM *para* phosVF2.1Cl (**17**). Scale bar is 40 μ m. (c) Plot of the fractional change in fluorescence of *para* phosVF2.1Cl (**17**) vs time for 100 ms hyper- and depolarizing steps (± 100 mV in 20 mV increments) for single HEK cells under whole-cell voltage-clamp mode. (d) plot of $\Delta F/F$ vs final membrane potential, revealing a voltage sensitivity of approximately 26% per 100 mV. Error bars are \pm SEM for $n=17$ cells. If not visible, error bars are smaller than the marker.

Functionalization of phosphono VFs with acetoxymethyl AM esters.

To date, VFs have served as excellent tools for visualizing voltage changes across plasma membranes, and the most logical application of these tools has been measuring action potential dynamics of excitable cells such as neurons and cardiomyocytes.^{4,5,22} Beyond action potentials, however, bioelectrical chemical gradients can be found across almost any biological membrane, including the intracellular compartmentalization of organelles. In fact, mitochondria, lysosomes, and endoplasmic reticulum are all good examples of how organelle membrane potential dynamics are essential for function.²³⁻²⁶ We recently reported how intracellular delivery of rhodamine voltage indicators can be used to probe mitochondrial membrane potential dynamics, through caging of the negatively charged anchoring 3-substituent with biologically labile acetoxymethyl

(AM) esters.¹⁹ In chapter 2, we described how AM esters could be used to mask the charge of 3-phosphonofluoresceins, enabling permeability across the cellular membrane, and subsequent intracellular release of the anionic fluorophore in a fluorogenic manner. We envisioned this could be extended to phosVFs for intracellular delivery.

Iso phosVF2.1.Cl AM (**S3-10**) can be synthesized in 44% yield from *iso* phosVF2.1.Cl (**12**) and bromomethyl acetate in the presence of silver oxide (**Figure S4a**). Spectroscopic characterization reveals that **S3-10** behaves similarly to the parent fluorophore (pF.Cl AM) in that minimal fluorescence is observed in HBSS but upon AM ester hydrolysis in aqueous base, fluorogenic release of *iso* phosVF2.1.Cl occurs (**Figure S4b**). Notably, this hydrolysis is much slower than with pFCl.AM and it takes 2 hours to see full conversion to *iso* phosVF2.1.Cl. This could be due to several factors such as lower aqueous solubility of **S10**, in solution aggregation or increased stability of the AM esters. While *iso* phosVF2.1.Cl exhibits extracellular membrane localization (**Figure S4c**), HEK cells incubated with *iso* phosVF2.1.Cl AM instead show intracellular cytosolic fluorescence (**Figure S4d**). The apparent cytosolic fluorescence may arise from intracellular membrane saturation, or since excess VF is trapped inside the cell and can no longer be washed away, we are unable to observe much contrast between membrane localized and cytosolic VF. Interestingly at 250 nM, HEK cells stained with **S3-10** are almost 10-fold dimmer than cells stained with membrane localized *iso* VF2.1.Cl (**Figure S4e**). While intracellular brightness can be increased in a concentration dependent manner (**Figure S4e**), the significant decrease in relative brightness could be attributed to the slow kinetics of AM ester hydrolysis observed *in vitro* and may not be representative of the amount of **S3-10** that entered the cell. Alternatively, without any anionic anchor, the hydrophobic nature of **S3-10** may result in membrane embedding and preclude access to cytosolic esterases responsible for uncaging. Future work could involve caging phosVFs with less promiscuous esters (such as methylcyclopropyl acetoxymethyl esters) for fluorogenic targeting to organelles in an analogous manner to what we have previously accomplished on the cell surface.²⁷

Synthesis and characterization of phosRhoVR 1

Rhodamine Voltage Reporters (RhoVRs) are another class of voltage sensing indicators that exhibit absorption and emission profiles in the green to orange regions of the visible spectrum. Making use of a tetramethylrhodamine fluorescent reporter and diethylaniline molecular wire, RhoVRs with remarkable voltage sensitivities (47% $\Delta F/F$ for RhoVR 1) have been developed.⁹ While we have typically relied on 3-sarcosine (RhoVR 1)⁹ or 3-sulfonate (sRhoVR 1)²⁸ functionalities for membrane anchoring, we envisioned expansion to a 3-phosphonate (phosRhoVRs) would allow us to take advantage of the acid-free condensation chemistry discussed in chapter 2 and also provide new opportunities for functionalization. We imagined regioselective alkylation of the 3-phosphonate would now be possible. This contrasts with fluorescein-based indicators where the nucleophilic nature of the phenolic oxygens meant alkylation of the fluorophore and diminishing of fluorescence also occurred with no apparent selectivity.

Reaction of 5-bromo-2-phosphonobenzaldehyde **8** with 3-dimethylaminophenol in 2,2,2-trifluoroethanol, results in clean precipitation of triarylmethane **13** in quantitative yield (**Figure 3a**). Oxidation with chloranil results in clean conversion to the corresponding 6-bromo-3-phosphonotetramethyl rhodamine in an analogous manner to the synthesis of the 3-phosphonorhodamines discussed in chapter 2. We note the remarkable improvement in yield in the condensation to **14** (>99%) relative to the 3-carboxy (57%) and 3-sulfono (44%) analogs.^{9,28}

Additionally the need for silica gel chromatography at this stage is eliminated, reducing the time and cost associated with laborious fluorophore purification. Heck coupling of **14** to a phenylenevinylene molecular wire produces phosRhoVR 1, **15**, as a crude triethylamine salt which can be purified by reverse phase silica chromatography in 76% yield (**Figure 3a**). In the comparable synthesis of RhoVR 1, Heck coupling to the analogous 3-carboxytetramethylrhodamine is followed by a HATU coupling with N-Boc-sarcosine and TFA deprotection, resulting in a substantially lower 9% yield over 3 steps.⁹ The streamlined and greater yielding synthesis of phosRhoVRs not only alleviates the time-consuming bottleneck in voltage reporter synthesis but also enables us to access RhoVRs in much greater quantities (hundreds vs. tens of milligrams at a time). We envision this will be instrumental in easing our ability to further derivatize voltage indicators.

As anticipated, phosRhoVR 1 displays characteristic absorption and emission profiles of 3-phosphono-tetramethylrhodamine, centered at 545 and 562 nm respectively with the addition of an absorption band at 402 nm resulting from the molecular wire (**Figure 3b**). We observe excellent membrane localization in HEK cells as the negatively charged phosphonate is sufficient at preventing internalization despite the positive charge of the rhodamine (**Figure 3c**). Interestingly we note an almost 2-fold improvement in HEK cells stained with 500 nM phosRhoVR 1 in comparison to RhoVR 1 (**Figure S5**). Patch clamp electrophysiology coupled with fluorescence microscopy reveals a voltage sensitivity of 37% $\Delta F/F$ per 100 mV for phosRhoVR 1 (**Figure 3d and e**), which is comparable but lower than the reported 47% for RhoVR 1 and 44% for sRhoVR 1^{9,28}. We envision that at these higher voltage sensitivities, subtle differences in membrane orientation resulting from 3-substitution account for the greater variation in voltage sensitivities than was observed with fluorescein-based VFs.

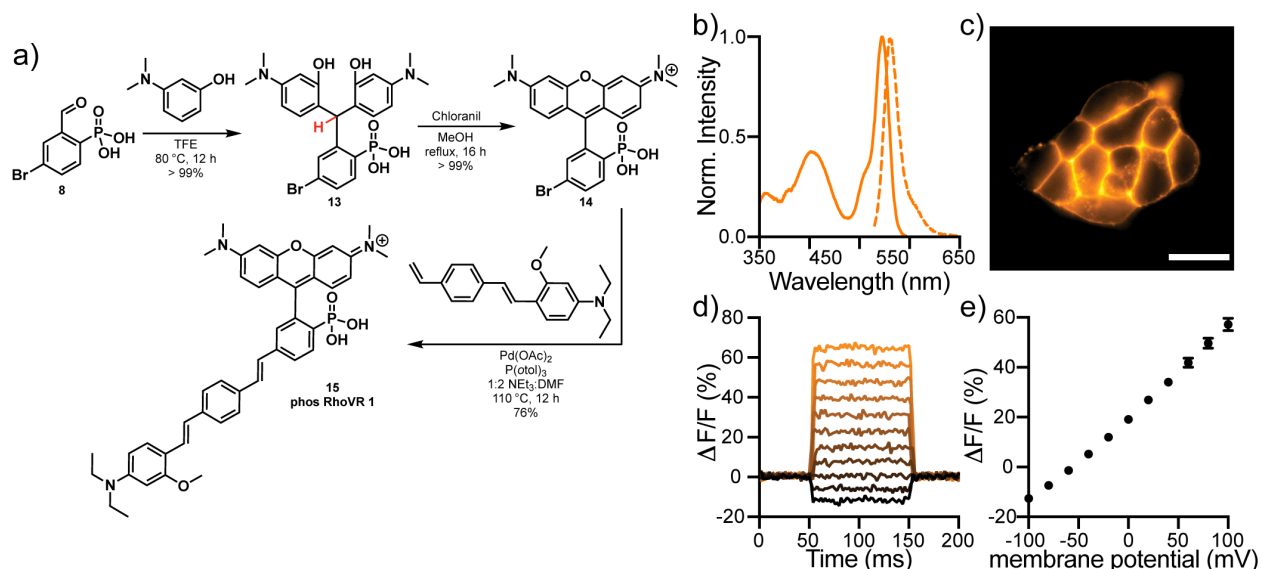
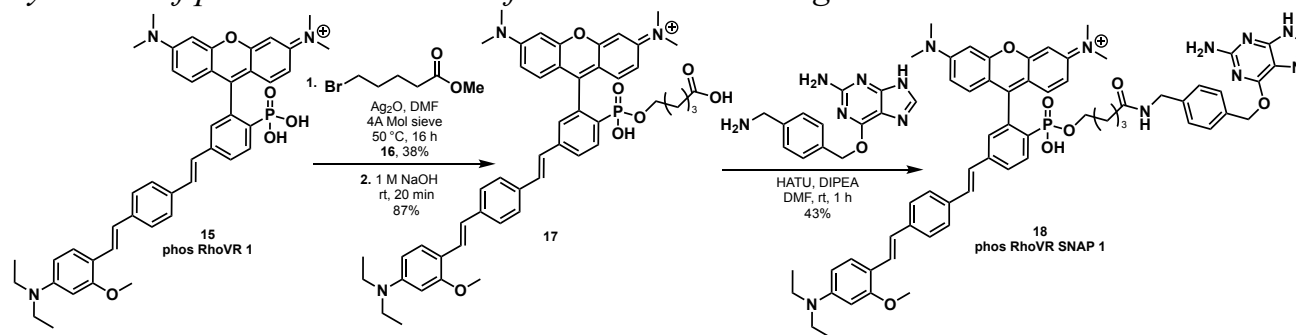


Figure 3. Synthesis and characterization of phosRhoVR 1. (a) Synthesis of phosRhoVR 1, **15** from aldehyde **8** (a) Normalized absorbance (solid line) and fluorescence emission (dashed line) spectra of phosRhoVR 1 in ethanol. (b) HEK cells stained with 500 nM phosRhoVR 1. Scale bar is 20 μ m. (c) Plot of the fractional change in fluorescence of phosRhoVR 1 vs time for 100 ms hyper- and depolarizing steps (\pm 100 mV in 20 mV increments) for single HEK cells under whole-cell voltage-clamp mode. (d) plot of $\Delta F/F$ vs final membrane potential, revealing a voltage sensitivity of approximately 37% per 100 mV. Error bars are \pm SEM for n=6 cells. If not visible, error bars are smaller than the marker.

Synthesis of phosRhoVR SNAP 1 for covalent tethering



Scheme 3 Synthesis of phosRhoVR SNAP 1

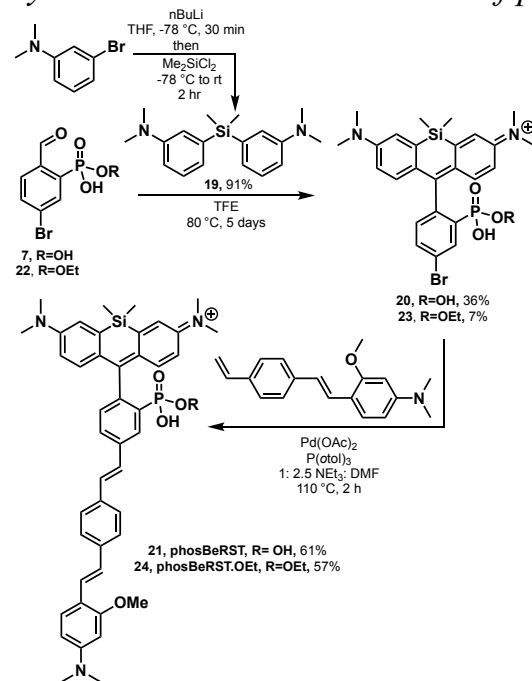
Covalent tethering of voltage indicators, such as RhoVRs, is an attractive chemo-genetic hybrid approach to selective labelling of a specific sub-class of cells. We have previously harnessed HaloTag and SpyCatcher strategies to accomplish covalent tethering of voltage indicators to neurons and demonstrated the implications that discriminate membrane staining can have on improving resolution in more complex systems such as brain slice.^{14,15} SNAP-tag was derived from human O⁶-alkylguanine-DNA alkyl transferase and has emerged as an orthogonal covalent labelling strategy.²⁹ Reaction of O⁶-benzylguanine derivatives with SNAP protein facilitates transfer of the benzyl group and its cargo (i.e. RhoVR) to a reactive cysteine on the protein, coupled with the elimination of guanine.²⁹ When expressed on the cell surface, we anticipated SNAP-tag would yield a complementary approach to covalent tethering of RhoVRs. Specifically, we envisioned functionalization of phosRhoVR 1 to a phosphonate monoester with the SNAP O⁶-benzylguanine ligand could be a suitable substrate for SNAP while retaining the negative charge (on the unfunctionalized phosphonate oxygen) essential for membrane anchoring.

Alkylation of phosRhoVR 1 with methyl 5-bromovalerate followed by saponification of the methyl ester yields phosphonate monoester **17** in 31% yield (2 steps). The low yield of intermediate phosphonate monoester **16** comes from competing formation of the corresponding phosphonate diester, despite careful stoichiometric control. While formation of the diester can be favored (at an improved yield) by use of excess 5-bromovalerate, saponification to the resulting phosphonate monoester requires more forceful hydrolysis conditions. Namely, the elevated temperature required for phosphonate ester hydrolysis causes rhodamine degradation and complicates purification, thus direct alkylation to the phosphonate monoester was deemed a more fruitful approach. HATU coupling of **17** and O⁶-benzylguanine amine provides phosRhoVR SNAP 1 in 43% yield after reverse phase silica chromatography.

Fortunately, functionalization to a phosphonate monoester does not compromise membrane localization and a single negative charge seems sufficient to prevent internalization of phosRhoVR 1 SNAP (**Figure S6**). Incubation of phosRhoVR SNAP 1 with purified SNAP protein *in vitro* yields only slight conversion to the expected SNAP-phosRhoVR adduct, as determined by QTOF-mass spectrometry (**Figure S7**). We hypothesize the large and bulky nature of phosRhoVR could preclude the ability of the benzylguanine substrate portion to reach into the protein active site and thus impedes the desirable rapid labelling kinetics. The valerate linker between the RhoVR and guanine is relatively short (just 5 carbons) and thus future efforts should focus on incorporation of longer linkers to improve reaction kinetics. The incorporation of polyethylene glycol (PEG) linkers in RhoVR HaloTag was found to be important; the flexibility and length of PEG linkers provided sufficient separation of the RhoVR and Halo ligand to facilitate both protein tethering and insertion

of RhoVR 1 into the plasma membrane.¹⁵ This should be considered when developing next generation phosRhoVR SNAP substrates.

Synthesis and characterization of phosBeRST



Scheme 4. Synthesis of phosBeRSTs

Berkeley Red Sensor of Transmembrane potential (BeRST) is a near infrared (NIR) voltage sensing probe that makes use of a 3-sulfonyl tetramethyl silicon rhodamine as the fluorescent reporter.¹⁰ BeRST not only shows comparable voltage sensitivity, but also improved photostability relative to fluorescein based VF2.1Cl. BeRST can be synthesized from 3-bromo-N,N-dimethylaniline, **19** in 3% overall yield over 6 steps.¹⁰ On the other hand, making use of the acid-free condensation of 3-phosphonate substituted silicon rhodamines highlighted in chapter 2, we synthesized phosBeRST, **21** in 20% overall yield, over just 3 steps from the same aniline starting material (**Scheme 4**).

Unlike 3-sulfonyl analog Berkeley Red, phosTMSiR exhibits a propensity to spirocyclize to the colorless lactone at physiological pH (**Chapter 2**) and we were concerned at the implications this would have in the voltage sensing performance and brightness of phosBeRST. We previously demonstrated how monoesterification of the phosphonate was sufficient to favor the open fluorescent form at physiological pH, so we also synthesized phosBeRST.OEt, **24** in which one of the phosphonate handles has been esterified with an ethyl ester (**Scheme 4**). The significantly lower isolated yield of **23** can be accounted for by the lack of purity of aldehyde precursor **22** when this condensation was initially performed and we envision the true yield would be comparable to that of the analogous condensation of **20** (**Supporting Info**).

When loaded on HEK cells at 1 μ M (15 minutes, 37 °C), phosBeRST localizes well to the extracellular membrane (**Figure 4b**) but displays only 24% of the relative brightness of cells loaded with the sulfonated analog, BeRST (**Figure 4a, b g, Table 1**). We hypothesize this substantial decrease in brightness can be attributed to the ability of phosBeRST to spirocyclize at physiological pH. We also note that in the lactonized form we expect the negatively charged

phosphonate to maintain cell impermeability and thus we expect even the closed form to be membrane localized. While it is difficult to visualize the closed form by fluorescence microscopy, we do not observe significant internalization of phosBeRST at this concentration. Surprisingly, loading under identical conditions, phosBeRST.OEt exhibits an almost 7-fold increase in brightness (**Figure 4c, g, Table 1**) compared to the 3-sulfono analog BeRST and an almost 30-fold increase relative to phosBeRST. Given that Berkeley Red, the fluorophore reporter of BeRST, does not show any tendency to lactonize (**Chapter 2**) this stark increase in brightness suggests there is a difference in membrane loading ability brought about by 3-substitution. We were concerned about internalization of phosBeRST.OEt, particularly if the lipophilic nature of the membrane was able to promote spirocyclization to the neutral lactone. While it may appear that there is some propensity for phosBeRST.OEt to internalize, co-loading with Mitotracker Green highlighted there is certainly significant membrane localization (**Figure S8**). Merging of phosBeRST.OEt and Mitotracker Green channels show distinct regions where phosBeRST.OEt is localized and mitotracker green is not, namely the extracellular membrane (**Figure S8c**). While there is perhaps some overlap in the intracellular signals across the two channels, the extent is minimal and Mitotracker gGeen (cyan) signal is much more intense in the mitochondria than phosBerST.OEt (magenta).

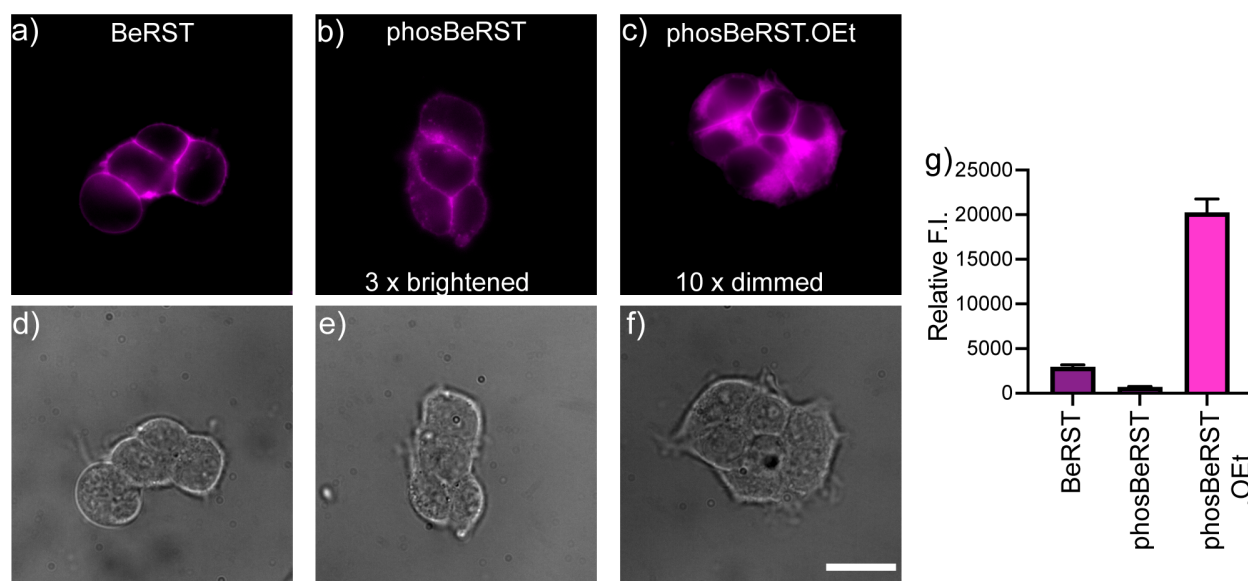


Figure 4. Comparison of BeRSTs membrane and localization and brightness. Widefield fluorescence (a-c) and DIC (d-f) images of HEK293T cells stained with 1 μ M BeRST (a, d), phosBeRST (b, e) and phosBeRST.OEt (c, f). Fluorescence images are normalized to BeRST (a). Image (b) has been brightened by 3-fold and image (c) has been dimmed by 10-fold. Quantification of relative fluorescence intensity (g). Scale bar is 20 μ m. Error bars are \pm SEM for n = 18 images (total) across 3 coverslips.

To further investigate the brightness differences observed in cells we compared absorbance spectra in acidic ethanol and HBSS, the buffer used for cell loading. Surprisingly, we found BeRST to be highly insoluble in HBSS at 1 μ M, accounted for by an almost 90% decrease in absorbance compared to in ethanol (**Figure S9a**). We are confident this decrease is attributed to solubility and not lactonization because we also observe a similar decrease in absorbance of the molecular wire. In the case of phosBeRST, we observe a slight decrease in wire absorbance but dramatic decrease in fluorophore absorbance in HBSS, suggesting both solubility and lactonization are factors at play (**Figure S9b**). It is less clear whether phosBeRST spirocyclizes in HBSS despite a decreased

fluorophore absorption (**Figure Sc**). It is also possible that aggregation due to the amphiphilic nature of BeRSTs could be convoluting our ability to differentiate between these factors. In all cases, absorption is dramatically increased in Tris-Buffered Saline (TBS) containing a detergent (0.1% SDS). It is possible performing cellular loading experiments in alternative buffer solutions or with detergent such as SDS may aid investigation into the large brightness differences. Based on our understanding of silicon rhodamine behavior *in vitro*, we hypothesize phosBeRSTs display improved water solubility and hence loading in aqueous buffer, but the spirocyclization of phosBeRST accounts for its significant reduction in brightness. The ~30-fold difference in brightness observed from simple esterification of the phosphonate may provide future opportunities in controlling the spirocyclization equilibrium for fluorogenic silicon rhodamine voltage sensing platforms.

Table 1. Summary of Voltage Sensitive Indicator Characterization

Voltage Indicator	3-substituent	λ_{\max} (nm) ^a	λ_{em} (nm) ^a	$\Delta F/F$ (%) ^b	Rel. Brightness ^c
<i>Para</i> VF2.1.Cl	-SO ₃ H	512	525	24.4 ± 0.5	1.00
<i>Para</i> phosVF2.1.Cl	-PO ₃ H	499	520	25.7 ± 0.2	1.02
<i>Iso</i> VF2.1.Cl	-SO ₃ H	513	524	9.4 ± 0.4	1.70
<i>Iso</i> phosVF2.1.Cl	-PO ₃ H	500	520	10.8 ± 0.3	1.78
RhoVR 1	-Sarcosine	556	575	47 ± 3	1.00
sulfoRhoVR 1	-SO ₃ H	547	570	44 ± 0.2	-
phosRhoVR 1	-PO ₃ H	545	562	37.3 ± 0.7	1.99
BeRST	-SO ₃ H	658	683	24 ± 5	1.00
PhosBeRST	-PO ₃ H	652	669	-	0.24
PhosBeRST.OEt	-PO ₃ H	653	670	-	6.86

^a in 0.1 M NaOH_(aq) for VFs, 100% EtOH for RhoVRs or 50 mM TBS +0.1% SDS for BeRSTs. ^b per 100 mV in voltage-clamped HEK cells ± SEM. ^c In HEK cells stained with 250 nM (VFs), 500 nM (RhoVRs) or 1 μM (BeRSTs) dye, relative to *para* VF2.1.Cl for VFs, RhoVR 1 for RhoVRs and BeRST for BeRSTs.

Conclusions and outlook

In summary we have expanded 3-phosphonate substitution to the synthesis and characterization of 5 new voltage sensing fluorophores, inspired by previously reported scaffolds. Fundamental to this expansion was our ability to develop a route for selective installation of phosphonates to dihalo-benzaldehydes. This provided 3-phosphonofluoresceins, rhodamines and silicon rhodamines with 5- or 6- halogen handles for molecular wire installation. Fluorescein based phosVFs displayed excellent membrane staining with almost identical voltage sensitivities and relative brightness to their 3-sulfono analogs. Additionally our ability to functionalize phosphonates with AM esters facilitated intracellular delivery of *iso* phosVF2.1.Cl.

Our high-yielding synthesis of 3-phosphonorhodamines enabled us to synthesize phosRhoVR 1 in yields much greater to those reported for RhoVR 1 and sulfoRhoVR 1. While phosRhoVR 1 displays a ~10 percentage point reduction in $\Delta F/F$ (per 100 mV), it remains the most voltage sensitive 3-phosphono probe we described and exhibits a 2-fold increase in brightness relative to RhoVR 1. Additionally, we highlight use of phosRhoVR 1's phosphonate as a functional handle by installing a ligand for chemi-genetic targeting, while maintaining membrane localization. Although our first derivative, phosRhoVR SNAP 1 was a poor substrate for the target protein, we envision future derivatives with increasing linker length could improve labelling efficiency. Synthetic improvements could also be made by construction of the phosphonate monoester before rhodamine synthesis due to fluorophore instability, or incorporation of other pentavalent phosphorus modalities such as phosphinates.

Lastly, we expand 3-phosphonate substitution to a near infrared voltage sensing probe, phosBeRST. Phosphonate substitution increased the propensity to spirocyclize to a non-fluorescent form and as such we observed a significant decrease in cellular membrane brightness relative to the 3-sulfono analog BeRST. In contrast, monoesterification provided phosBeRST.OEt that overcame this flaw, providing a novel probe with greatly improved loading into cellular membranes.

References

- (1) Levin, M. Molecular Bioelectricity: How Endogenous Voltage Potentials Control Cell Behavior and Instruct Pattern Regulation in Vivo. *Mol. Biol. Cell* **2014**, *25* (24), 3835–3850.
- (2) Kadir, L. A.; Stacey, M.; Barrett-Jolley, R. Emerging Roles of the Membrane Potential: Action beyond the Action Potential. *Front. Physiol.* **2018**, *9*, 1661.
- (3) Peterka, D. S.; Takahashi, H.; Yuste, R. Imaging Voltage in Neurons. *Neuron* **2011**, *69* (1), 9–21.
- (4) Kulkarni, R. U.; Miller, E. W. Voltage Imaging: Pitfalls and Potential. *Biochemistry* **2017**, *56*, 7.
- (5) Liu, P.; Miller, E. W. Electrophysiology, Unplugged: Imaging Membrane Potential with Fluorescent Indicators. *Acc. Chem. Res.* **2020**, *53* (1), 11–19.
- (6) Bando, Y.; Sakamoto, M.; Kim, S.; Ayzenshtat, I.; Yuste, R. Comparative Evaluation of Genetically Encoded Voltage Indicators. *Cell Rep.* **2019**, *26* (3), 802–813.e4.
- (7) Miller, E. W.; Lin, J. Y.; Frady, E. P.; Steinbach, P. A.; Kristan, W. B.; Tsien, R. Y. Optically Monitoring Voltage in Neurons by Photo-Induced Electron Transfer through Molecular Wires. *Proc. Natl. Acad. Sci. U. S. A.* **2012**, *109* (6), 2114–2119.
- (8) Kulkarni, R. U.; Yin, H.; Pourmandi, N.; James, F.; Adil, M. M.; Schaffer, D. V.; Wang, Y.; Miller, E. W. A Rationally Designed, General Strategy for Membrane Orientation of Photoinduced Electron Transfer-Based Voltage-Sensitive Dyes. **2016**.
- (9) Deal, P. E.; Kulkarni, R. U.; Al-Abdullatif, S. H.; Miller, E. W. Isomerically Pure Tetramethylrhodamine Voltage Reporters. *J. Am. Chem. Soc.* **2016**, *138*, 29.
- (10) Huang, Y.-L.; Walker, A. S.; Miller, E. W. A Photostable Silicon Rhodamine Platform for Optical Voltage Sensing. *J. Am. Chem. Soc.* **2015**, *137*, 10.
- (11) Franke, J. M.; Raliski, B. K.; Boggess, S. C.; Natesan, D. V.; Koretsky, E. T.; Zhang, P.; Kulkarni, R. U.; Deal, P. E.; Miller, E. W. BODIPY Fluorophores for Membrane Potential Imaging. *J. Am. Chem. Soc.* **2019**, *141* (32), 12824–12831.
- (12) Ortiz, G.; Liu, P.; Htet, S.; Naing, H.; Muller, V. R.; Miller, E. W. Synthesis of Sulfonated Carbofluoresceins for Voltage Imaging. **2019**, *141* (16), 6631–6638.
- (13) Kulkarni, R. U.; Kramer, D. J.; Pourmandi, N.; Karbasi, K.; Bateup, H. S.; Miller, E. W.; Fraser, S. E. Voltage-Sensitive Rhodol with Enhanced Two-Photon Brightness. *PNAS.* **2017**, *114* (11), 2813–2818.
- (14) Grenier, V.; Daws, B. R.; Liu, P.; Miller, E. W. Spying on Neuronal Membrane Potential with Genetically Targetable Voltage Indicators. *J. Am. Chem. Soc.* **2019**, *141* (3), 1349–1358.
- (15) Deal, P. E.; Liu, P.; Al-Abdullatif, S. H.; Muller, V. R.; Shamardani, K.; Adesnik, H.; Miller, E. W. Covalently Tethered Rhodamine Voltage Reporters for High Speed Functional Imaging in Brain Tissue. *J. Am. Chem. Soc.* **2020**, *142* (1), 614–622.
- (16) Ortiz, G.; Liu, P.; Deal, P. E.; Nensel, A. K.; Martinez, K. N.; Shamardani, K.; Adesnik, H.; Miller, E. W. A Silicon-Rhodamine Chemical-Genetic Hybrid for Far Red Voltage Imaging from Defined Neurons in Brain Slice. *RSC Chem. Biol.* **2021**, *2* (6), 1594–1599.
- (17) Kirk, M. J.; Benlian, B. R.; Han, Y.; Gold, A.; Ravi, A.; Deal, P. E.; Molina, R. S.; Drobizhev, M.; Dickman, D.; Scott, K.; et al. Voltage Imaging in Drosophila Using a Hybrid Chemical-Genetic Rhodamine Voltage Reporter. *Front. Neurosci.* **2021**, *15*, 1494.
- (18) Grenier, V.; Martinez, K. N.; Benlian, B. R.; García-Almedina, D. M.; Raliski, B. K.; Boggess, S. C.; Maza, J. C.; Yang, S. J.; Gest, A. M. M.; Miller, E. W. Molecular Prosthetics for Long-Term Functional Imaging with Fluorescent Reporters. *ACS Cent. Sci.* **2022**, *8* (1), 118–121.

- (19) Klier, P. E. Z.; Martin, J. G.; Miller, E. W. Imaging Reversible Mitochondrial Membrane Potential Dynamics with a Masked Rhodamine Voltage Reporter. *J. Am. Chem. Soc.* **2021**, *143* (11), 4095–4099.
- (20) Balthazor, T. M.; Grabiak, R. C. Nickel-Catalyzed Arbuzov Reaction: Mechanistic Observations. *J. Org. Chem.* **1980**, *45* (26), 5425–5426.
- (21) Pan, J.; Wang, X.; Zhang, Y.; Buchwald, S. L. An Improved Palladium-Catalyzed Conversion of Aryl and Vinyl Triflates to Bromides and Chlorides. *Org. Lett.* **2011**, *13* (18), 4974–4976.
- (22) Boggess, S. C.; Gandhi, S. S.; Siemons, B. A.; Huebsch, N.; Healy, K. E.; Miller, E. W. New Molecular Scaffolds for Fluorescent Voltage Indicators. *ACS Chem. Biol.* **2019**, *14* (3), 390–396.
- (23) Jonas, E. A.; Knox, R. J. Giga-Ohm Seals on Intracellular Neurotechnique Membranes: A Technique for Studying Intracellular Ion Channels in Intact Cells. *Neuron* **1997**, *19*, 7–13.
- (24) Matamala, E.; Castillo, C.; Vivar, J. P.; Rojas, P. A.; Brauchi, S. E. Imaging the Electrical Activity of Organelles in Living Cells. *Commun. Biol.* **2021**, *4* (1), 1–12.
- (25) Kuum, M.; Veksler, V.; Kaasik, A. Potassium Fluxes across the Endoplasmic Reticulum and Their Role in Endoplasmic Reticulum Calcium Homeostasis. *Cell Calcium* **2015**, *58* (1), 79–85.
- (26) Xiong, J.; Zhu, M. X. Regulation of Lysosomal Ion Homeostasis by Channels and Transporters. *Sci. China Life Sci.* **2016**, *59* (8), 777–791.
- (27) Liu, P.; Grenier, V.; Hong, W.; Muller, V. R.; Miller, E. W. Fluorogenic Targeting of Voltage-Sensitive Dyes to Neurons. *J. Am. Chem. Soc.* **2017**, *139* (48), 17334–17340.
- (28) Kulkarni, R. U.; Vandenberghe, M.; Thunemann, M.; James, F.; Andreassen, O. A.; Djurovic, S.; Devor, A.; Miller, E. W. In Vivo Two-Photon Voltage Imaging with Sulfonated Rhodamine Dyes. **2018**, *4* (10), 1371–1378.
- (29) Juillerat, A.; Gronemeyer, T.; Keppler, A.; Gendreizig, S.; Pick, H.; Vogel, H.; Johnsson, K. Directed Evolution of O6-Alkylguanine-DNA Alkyltransferase for Efficient Labeling of Fusion Proteins with Small Molecules in Vivo. *Chem. Biol.* **2003**, *10* (4), 313–317.

Chapter 3 Supplementary Information

General procedures

Chemical reagents and anhydrous solvents were purchased from commercial suppliers and used without further purification, besides 4-chlororesorcinol which were recrystallized from toluene prior to use and dimethyl aminophenol which was purified by flash chromatography (100% DCM) prior to use. Previously published molecular wires, VF2.1.Cl, isoVF2.1.Cl, RhoVR and BerST were all synthesized according to literature procedures. Thin layer chromatography (TLC) (silica gel, F254, 250 μm) and preparative thin layer chromatography (PTLC) (Silicycle, F254, 1000 μm) were performed on precoated TLC glass plates and were visualized by fluorescence quenching under UV light. Flash column chromatography was performed on Silicycle Silica Flash F60 (230–400 Mesh) for normal phase or 60 RP-18 (200-400 mesh) for reverse phase, using a forced flow of air at 0.5–1.0 bar. NMR spectra were recorded on Bruker AV-300 MHz, Bruker AVB-400 MHz, Bruker AVQ-400 MHz, Bruker NEO-500 MHz and Bruker AV-600 NMR spectrometers. NMR spectra measured on Bruker AVII-900 MHz, 225 MHz, equipped with a TCI cryoprobe accessory, were performed by Dr. Jeffrey Pelton (QB3). Chemical shifts (δ) are expressed in parts per million (ppm) and are referenced to CDCl_3 (7.26 ppm), DMSO (2.50 ppm), MeOD (3.31 ppm) or D_2O (4.79 ppm). Coupling constants are reported as Hertz (Hz). Splitting patterns are indicated as follows: s, singlet; d, doublet; t, triplet; q, quartet; dd, doublet of doublet; td, triplet of doublets; dt, doublet of triplets; tt, triplet of triplets; ddd, doublet of doublet of doublets; tdd, triplet of doublet of doublets; q, quartet; m, multiplet. High resolution mass spectra (ESI EI) were measured by the QB3/Chemistry mass spectrometry service at University of California, Berkeley. High performance liquid chromatography (HPLC) and low resolution ESI Mass Spectrometry were performed on an Agilent Infinity 1200 analytical instrument coupled to an Advion CMS-L ESI mass spectrometer. The column used was Phenomenex Luna 5 μm C18(2) (4.6 mm I.D. \times 150 mm) with a flow rate of 1.0 mL/min. The mobile phase was MQ-H₂O with 0.05% trifluoroacetic acid (eluent A) and HPLC grade MeCN with 0.05% trifluoroacetic acid (eluent B). Signals were monitored at 210, 254, 350, 460 and 520 nm over 10 min, with a gradient of 10 to 100% eluent B for 8 min, then held at 100% B for 2 min.

Spectroscopy

UV-Vis absorbance and fluorescence spectra were recorded using a 2501 Spectrophotometer (Shimadzu) and a Quantmaster Master 4 L-format scanning spectrofluorometer (Photon Technologies International). The fluorometer is equipped with an LPS-220B 75-W xenon lamp and power supply, A-1010B lamp housing with integrated igniter, switchable 814 photon-counting/analog photomultiplier detection unit, and MD5020 motor driver. Samples were measured in 1-cm path length quartz cuvettes (Starna Cells).

The maximum absorption wavelength (λ_{max}), maximum emission wavelength (λ_{em}) were taken in 0.1M $\text{NaOH}_{(\text{aq})}$ for VFs, 100% ethanol for RhoVRs and 50 mM TBS +0.1% SDS for BerSTs using 1000x dilutions from stock solutions of dyes in DMSO (2 mM).

Cell culture

Human embryonic kidney 293T (HEK) cells were maintained in Dulbecco's modified eagle medium (DMEM) supplemented with 4.5 g/L D-glucose, 10% fetal bovine serum (FBS; Thermo

Scientific) and 1% GlutaMax (Invitrogen) at 37 °C in a humidified incubator with 5% CO₂. Cells were passaged and plated in DMEM (as above) onto 12 mm glass coverslips pre-coated with Poly-D-Lysine (PDL; 1 mg/mL; Sigma-Aldrich) at a density of 50,000 cells per coverslip. Imaging was performed 36–48 hours after plating.

For loading experiments, dye stock solutions in DMSO were diluted 1000- fold in HBSS (1 mL) and incubated with HEK cells at 37 °C for 20 min (VFs and RhoVRs) or 15 min (BeRSTs), prior to transfer to 3 mL fresh HBSS (no dye) for imaging. For electrophysiology experiments, HEK cells were passaged and plated in DMEM (as above) onto 25 mm glass coverslips pre-coated with PDL at a density of 200,000 cells per coverslip. Imaging was performed 12-18 hours after plating. All voltage dyes were loaded as solutions in HBSS at 37 °C for 20 min (VFs and RhoVRs) or 15 min (BeRSTs).

Epifluorescence microscopy

Imaging was performed on an AxioExaminer Z-1 (Zeiss) equipped with a Spectra-X Light engine LED light (Lumencor), controlled with Slidebook (v6, Intelligent Imaging Innovations). Images were acquired with a W-Plan-Apo 63x/1.0 objective (63x; Zeiss) and images were focused onto an OrcaFlash4.0 sCMOS camera (sCMOS; Hamamatsu). The excitation light was delivered from an LED at 475/34 nm (VFs), 542/33 nm (RhoVRs) or 631/28 nm (BeRSTs) and emission was collected with a quadruple emission filter (430/32, 508/14, 586/30, 708/98 nm) after passing through a quadruple dichroic mirror (432/38, 509/22, 586/40, 654 nm LP).

Electrophysiology parameters

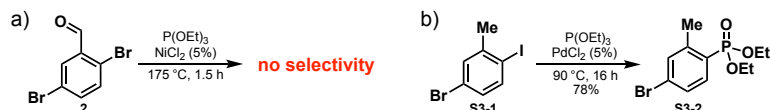
For electrophysiological experiments, pipettes were pulled from borosilicate glass (Sutter Instruments, BF150-86-10), with a resistance of 5–7 M Ω , and were filled with an internal solution; 125 mM potassium gluconate, 1 mM EGTA tetrasodium salt, 10 mM HEPES, 5 mM NaCl, 10 mM KCl, 2 mM ATP disodium salt, 0.3 mM GTP trisodium salt (pH 7.25, 275 mOsm). Electrophysiology recordings were made with an Axopatch 200B amplifier and digitized with a Digidata 1550B (Molecular Devices), sampled at 50 kHz and recorded with pCLAMP 10 software (Molecular Devices) on a PC. Fast capacitance was compensated in the on-cell configuration. Recordings of single cells were only included if they maintained a 10:1 ratio of membrane resistance (R_m) to access resistance (R_a) and an R_a value below 30 M Ω . Once in whole-cell, cells were held at -60 mV resting potential. Depolarizing steps were then applied from -100 to +100 mV in 20 mV increments. Optical traces were captured on an OrcaFlash4.0 sCMOS camera, with 4x4 binning at a framerate of 500 Hz using μ Manager. Excitation light was applied using an LED at 475/34 nm and 542/33 nm and emission collected with using a 540/50 BP emission filter and a 510 LP dichroic.

Image analysis

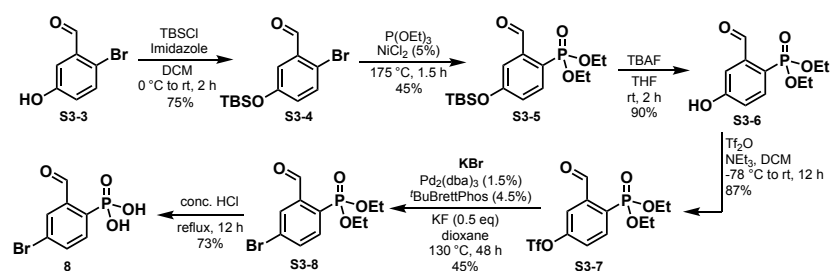
Image analyses were performed in ImageJ (FIJI, NIH). For image intensity measurements, regions of interest were created by thresholding images to create binary masks (cells and background). Background subtracted mean fluorescence intensities were calculated and averaged across five images (each containing at least 15 cells) per coverslip and 4 coverslips were examined for each condition.

For analysis of voltage sensitivity briefly, a region of interest (ROI) was manually drawn around the cell periphery. Fluorescence intensity values were then background subtracted by an area without cells. Changes in fluorescence values (ΔF) with each voltage step were calculated by subtracting baseline fluorescence value (F) at -60 mV. The voltage response is reported as a ratio of change relative to baseline ($\Delta F/F$). All voltage traces are single trial recordings with no averaging.

Supplementary figures



Scheme S1. Halogen selectivity in Pd-catalyzed Arbuzov reactions.



Scheme S2. Alternative synthesis of compound **8** via an aryl triflate.

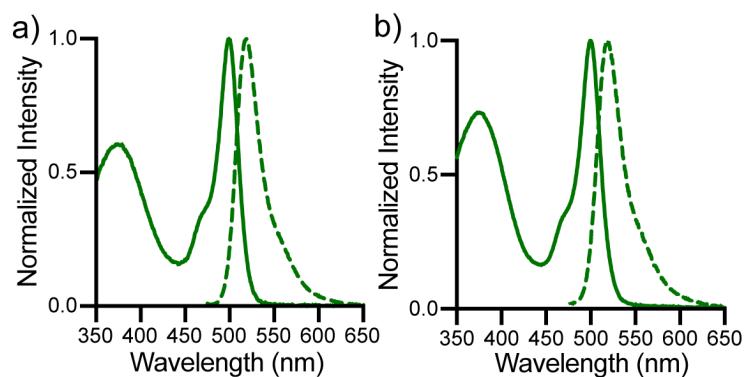


Figure S1. Spectra of phosphonated VoltageFluors.

Normalized absorption (solid) and fluorescence (dashed) spectra of *para* pVF2.1Cl (a) and *iso* pVF2.1Cl (b). Spectra were recorded in 0.1 M NaOH. For fluorescence spectra, excitation was at 465 nm.

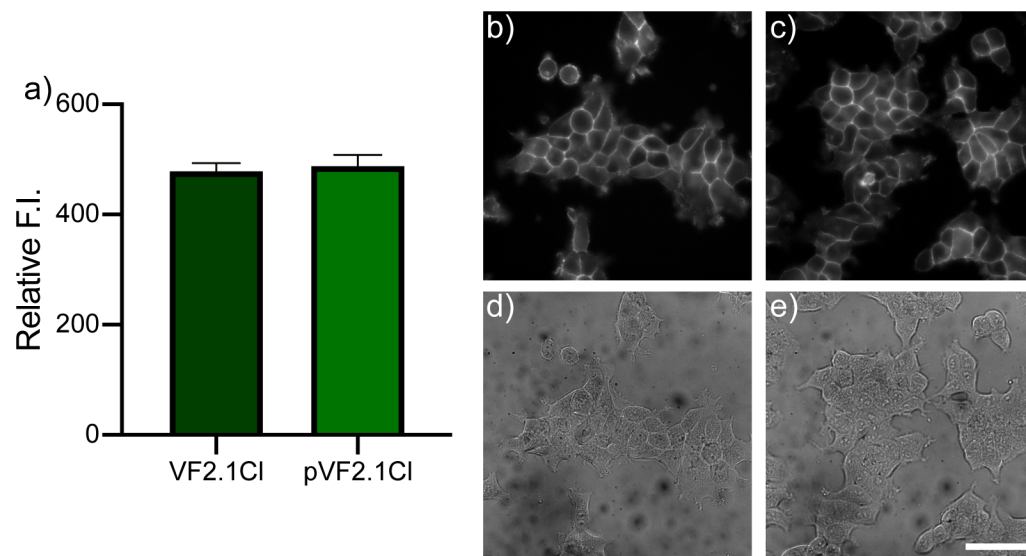


Figure S2. Relative cell brightness of pVF2.1Cl and msVF2.1Cl. Quantification (a), widefield fluorescence (top panel) and DIC (bottom panel) images of HEK cells stained with 250 nM *para* VF2.1Cl (b, d) and *para* pVF2.1Cl. Fluorescence images are normalized to *para* VF2.1Cl (b). Scale bar is 50 μm . Error bars are \pm SEM for $n = 3$ coverslips.

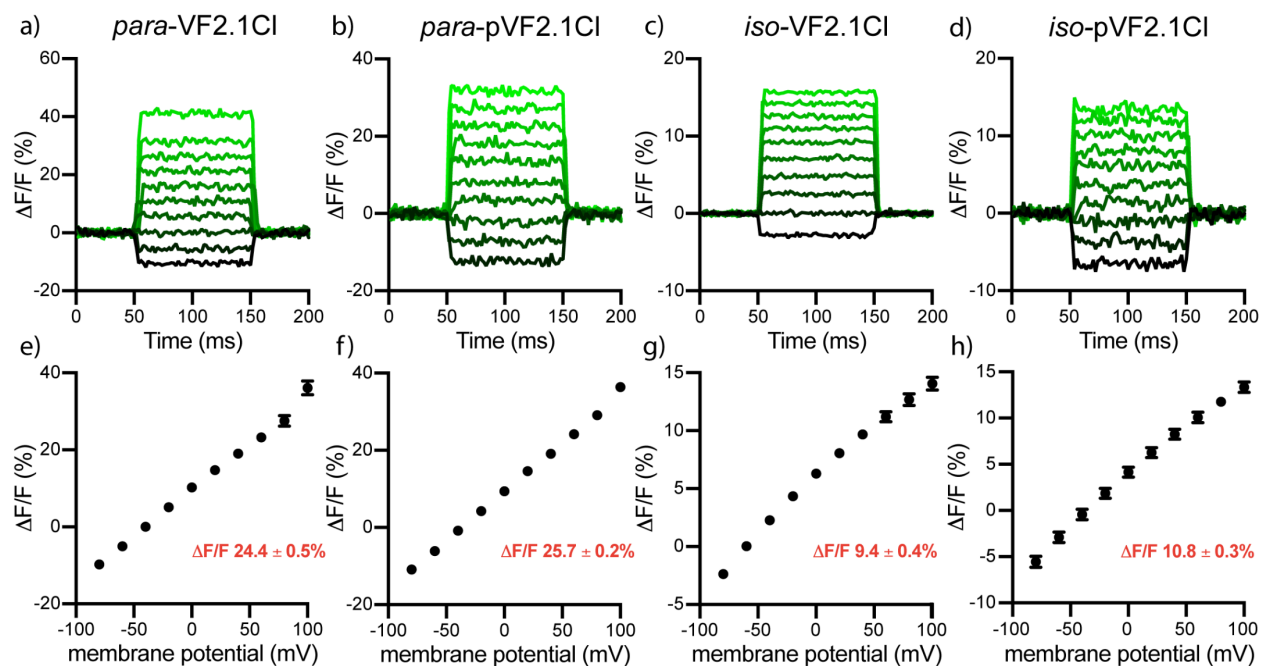


Figure S3. Voltage sensitivity of sulfono- and phsophono- VF dyes. *para* VF2.1Cl (a,e), *para* pVF2.1Cl (b,f), *iso* VF2.1Cl (c,g) and *iso* pVF2.1Cl (d,h). Upper row: The fractional change in fluorescence is plotted vs. time for HEK cells held at -40 mV (-60 mV for *iso* VF2.1Cl) and stepped to 100 ms hyper- and depolarizing steps (-80 to $+100$ mV, 20 mV increments) under whole-cell voltage-clamp conditions. Lower row: Plots of $\% \Delta F/F$ vs. final membrane potential (mV) for $n = 5-6$ HEK cells for each VF dye. Error bars are \pm SEM.

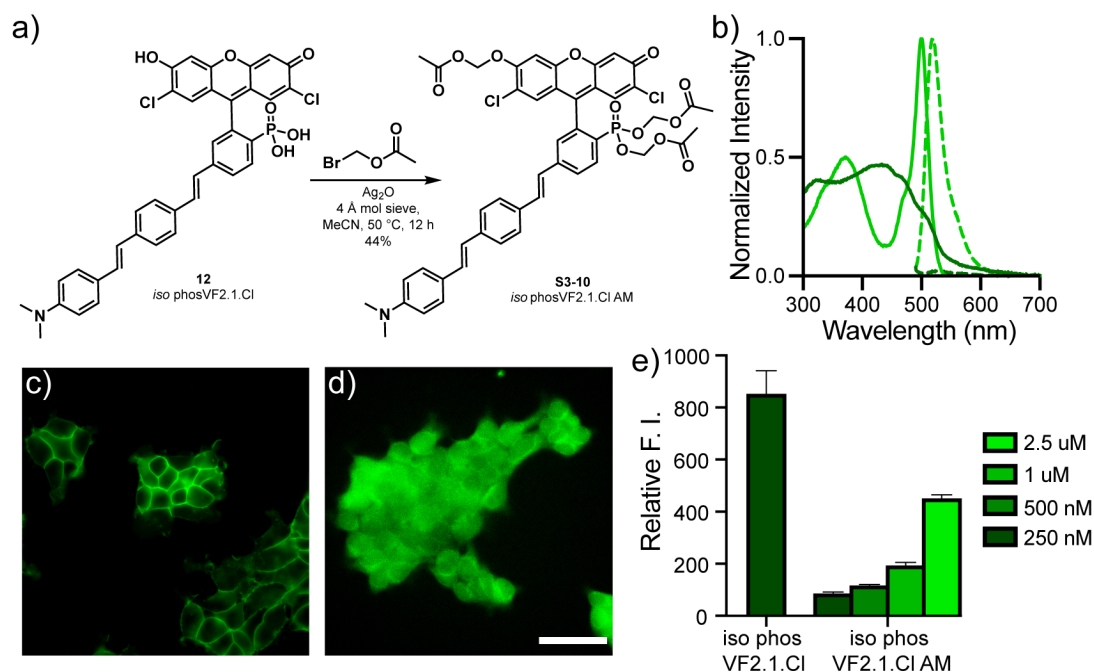


Figure S4. Intracellular delivery of *iso* VF2.1.Cl with acetoxymethyl (AM) esters.

(a) synthesis of *iso* VF2.1.Cl acetoxymethyl (AM) ester, **S3-10**. (b) Absorption (solid) and emission (dashed) spectra of 1 μ M solutions of *iso* phosVF2.1.Cl AM, **S3-10** in HBSS (**dark green**) or after 2 hours in 0.1 M NaOH_(aq) (**light green**). Spectra are normalized to a of 1 μ M *iso* phosVF2.1.Cl standard in 0.1 M NaOH. Widefield fluorescence images of HEK cells loaded with 250 nM solutions of *iso* phosVF2.1.Cl, **12** (c) and *iso* phosVF2.1.Cl, **S3-10** (d). Image d has been brightened 6-fold, scale bar is 50 μ m. (e) quantification of fluorescence images of HEK cells stained with 250 nM *iso* phosVF2.1.Cl, **12** and increasing concentrations of *iso* phosVF2.1.Cl AM, **S3-10**. Error bars are \pm SEM for 7 images.

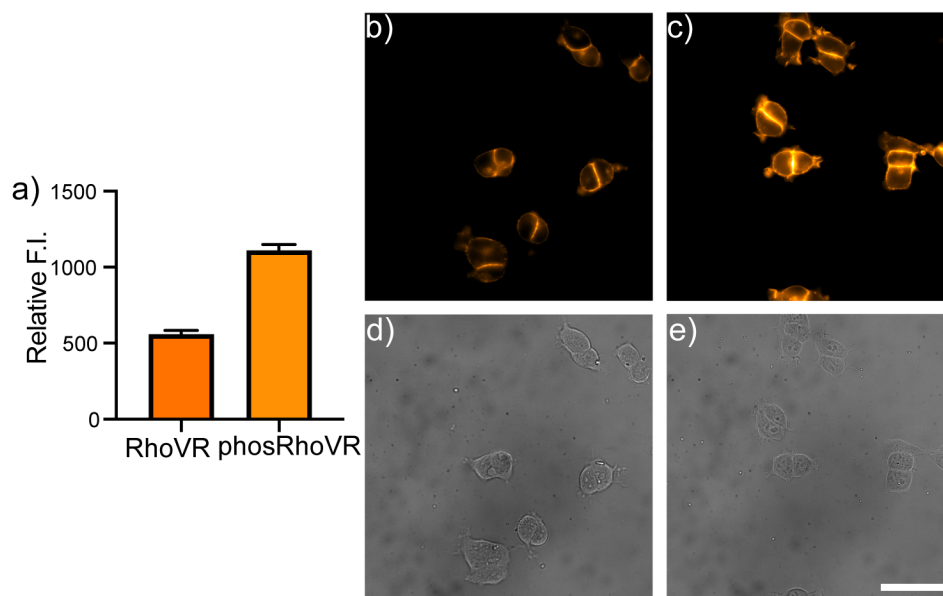


Figure S5. Relative cell brightness of RhoVR 1 and phosRhoVR 1.

Quantification (a), widefield fluorescence (b, c) and DIC (d, e) images of HEK cells stained with 5000 nM RhoVR 1 (b, d) and phosRhoVR 1. Fluorescence images are normalized to phosRhoVR1 (c). Scale bar is 50 μ m. Error bars are \pm SEM for $n = 3$ coverslips.

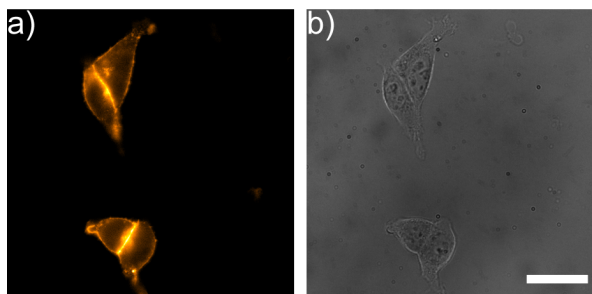


Figure S6. Membrane localization of phosRhoVR SNAP 1. Widefield fluorescence (a) and DIC (b) images of HEK293T cells stained with 500 nM phosRhoVR SNAP 1 in HBSS for 20 minutes at 37 °C. The coverslip was transferred into fresh HBSS prior to imaging. Scale bar is 30 μ m

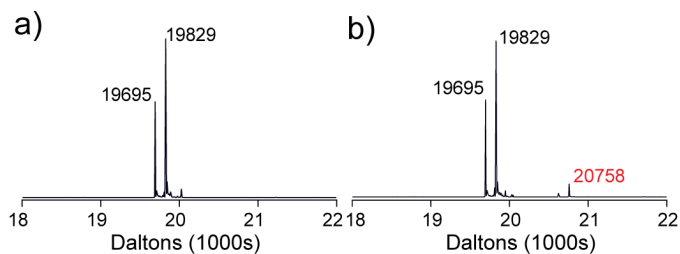


Figure S7. In vitro labelling of SNAP protein with RhoVR SNAP 1. Q-TOF spectra for (a) purified SNAP protein and (b) purified SNAP protein incubated with RhoVR SNAP 1. Masses of 19695 Da and 19829 Da can be observed for SNAP protein and a C terminal DTT adduct respectively (a, b). A mass of 20758 Da for labelling with RhoVR1 SNAP 1 (with loss of guanine) can be observed (b), however very minimal labelling occurred.

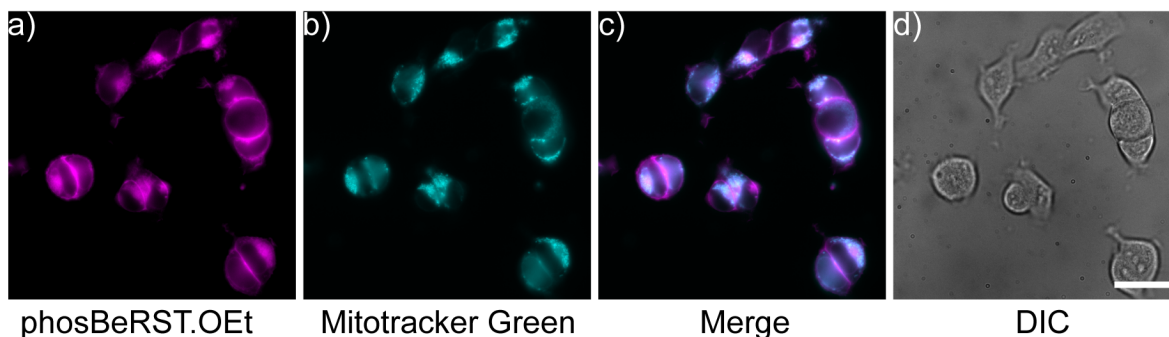


Figure S8. Cell localization of phosBeRST.OEt, 23. Widefield fluorescence images in the red (a) and green (b) channels, a merge of images a and b (c) and corresponding DIC image (d) of HEK293T cells stained with 100 nM 24 and 100 nM Mitotracker Green™ in HBSS for 15 minutes at 37 °C. The coverslip was transferred into fresh HBSS prior to imaging. Scale bar is 30 μ m.

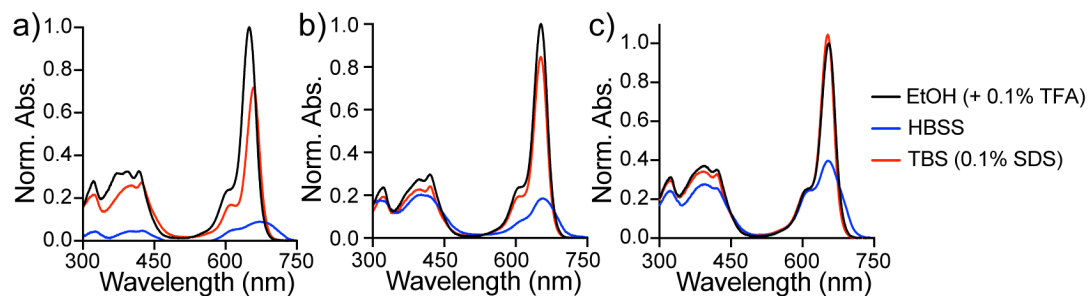


Figure S9. Solvent dependent absorbance profiles of BeRSTs.

Normalized absorbance spectra of BeRST (a), phosBeRST (b) and phosBeRST.OEt (c) in EtOH (+0.1% (v/v) TFA), HBSS or 50 mM TBS (pH 7.5, 0.1% (v/v) SDS) as indicated. Spectra were taken at a dye concentration of 1 μ M and are normalized to the spectra taken in acidic EtOH.

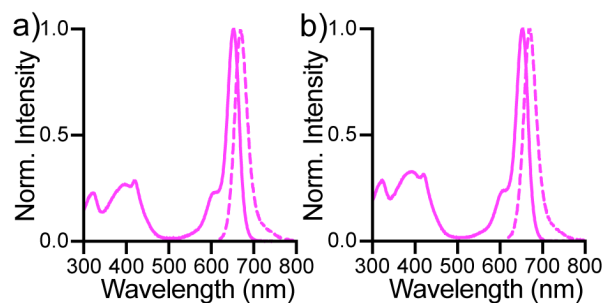
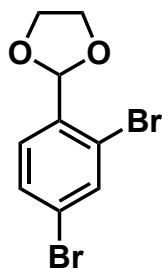


Figure S10. A Spectra of phosBeRSTs.

Normalized absorption (solid) and fluorescence (dashed) spectra of phosBeRST (a) and phosBeRST.OEt (b). Spectra were recorded in 50 mM TBS (pH 7.2 +0.1% SDS). For fluorescence spectra, excitation was at 610 nm.

Synthetic procedures



Synthesis of **3**:

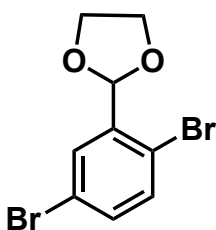
2-(2,4-dibromophenyl)-1,3-dioxolane

2,4-dibromobenzaldehyde (**1**) (1.00 g, 3.8 mmol) and p-toluenesulfonic acid monohydrate (14 mg, 0.08 mmol) were charged into a round bottom equipped with a Dean-Stark trap and dissolved in toluene (4 mL). Ethylene glycol (0.26 mL, 4.74 mmol) was added, and the solution stirred vigorously at 110 °C for 12 hours. Upon cooling to room temperature, the solution was diluted with EtOAc, washed with 2.5 M NaOH (3x), brine (3x) and dried over Na₂SO₄. Solvent was removed in vacuo to obtain **3** (1.04 g, 3.4 mmol, 89%) as a slightly brown oil.

¹H NMR (400 MHz, Chloroform-*d*) δ 7.77 – 7.71 (m, 1H), 7.47 (m, 2H), 6.03 (s, 1H), 4.17 – 4.03 (m, 4H).

¹³C NMR (126 MHz, Chloroform-*d*) δ 135.88, 135.31, 130.65, 129.08, 123.63, 123.52, 102.16, 65.53.

HR-EI-MS m/z for C₉H₈O₂Br₂^{•+} [M]^{•+} calcd: 305.8891 found: 305.8885.



Synthesis of **4**:

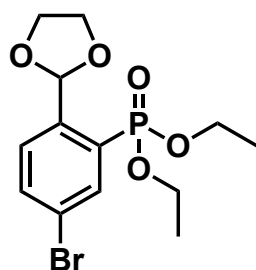
2-(2,5-dibromophenyl)-1,3-dioxolane

2,5-dibromobenzaldehyde (**2**) (2.00 g, 7.58 mmol) and p-toluenesulfonic acid monohydrate (29 mg, 0.15 mmol) were charged into a round bottom equipped with a Dean-Stark trap and dissolved in toluene (8 mL). Addition of ethylene glycol (0.53 mL, 9.47 mmol) was followed by vigorous stirring at 110°C for 5 hours. Upon cooling to room temperature, the solution was diluted with EtOAc, washed with 2.5 M NaOH (3x), brine (3x) and dried over Na₂SO₄. Solvent was removed in vacuo to obtain **4** (2.02 g, 6.56 mmol, 87%) as a waxy tan solid.

^1H NMR (300 MHz, Chloroform-*d*) δ 7.72 (d, $J = 2.4$ Hz, 1H), 7.42 (d, $J = 8.5$ Hz, 1H), 7.34 (dd, $J = 8.5, 2.4$ Hz, 1H), 6.03 (s, 1H), 4.21 – 4.11 (m, 2H), 4.11 – 4.02 (m, 2H).

^{13}C NMR (126 MHz, Chloroform-*d*) δ 138.69, 134.38, 133.56, 130.97, 121.52, 101.98, 65.58.

HR-EI-MS m/z for $\text{C}_9\text{H}_8\text{O}_2\text{Br}_2^{\bullet+}$ $[\text{M}]^{\bullet+}$ calcd: 305.8891 found: 305.8884.



Synthesis of **5**:

diethyl (5-bromo-2-(1,3-dioxolan-2-yl)phenyl)phosphonate

A solution of **3** (1.0 g, 3.25 mmol) in dry diethyl ether (10 mL) was cooled to -78°C under nitrogen. Whilst stirring, *n*-butyllithium (2M in cyclohexane, 1.9 mL, 3.74 mmol, 1.15 eq) was added dropwise via syringe and the solution stirred at -78°C for 30 mins. Diethyl chlorophosphate (0.94 mL, 6.5 mmol, 2 eq) was added dropwise and the solution stirred at -78°C for 1 hour, before warming to room temperature. After another hour of stirring, the reaction was quenched with water (10 mL), extracted with DCM (3x) and dried over Na_2SO_4 . After concentrating in vacuo, the resulting oil was purified by flash column chromatography (50% EtOAc/Hexanes + 1% NEt_3)* to yield **5** (932 mg, 2.55 mmol, 79%) as a waxy white solid.**

^1H NMR (500 MHz, Chloroform-*d*) δ 8.07 (dd, $J = 14.3, 2.1$ Hz, 1H), 7.71 (dt, $J = 9.1, 1.2$ Hz, 1H), 7.64 (dd, $J = 8.4, 5.8$ Hz, 1H), 6.34 (s, 1H), 4.20 – 4.00 (m, 8H), 1.32 (t, $J = 7.1$ Hz, 6H).

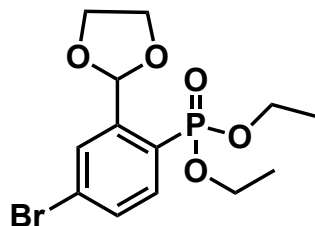
^{31}P NMR (162 MHz, Chloroform-*d*) δ 15.38.

^{13}C NMR (126 MHz, Chloroform-*d*) δ 140.15 (d, $J = 9.6$ Hz), 136.38 (d, $J = 9.7$ Hz), 135.66 (d, $J = 2.8$ Hz), 129.61 (d, $J = 179.9$ Hz), 129.25 (d, $J = 14.5$ Hz), 123.32 (d, $J = 18.5$ Hz), 100.17, 65.58, 62.65 (d, $J = 5.3$ Hz), 16.25 (d, $J = 6.6$ Hz).

HR-ESI-MS m/z for $\text{C}_{13}\text{H}_{19}\text{O}_5\text{BrP}^+$ $[\text{M}+\text{H}]^+$ calcd: 365.0148 found: 365.0157.

*Silica was incubated with the mobile phase for 1 hour prior to use.

**Where necessary residual impurities could be distilled off by heating under vacuum.



Synthesis of **6**:

diethyl (4-bromo-2-(1,3-dioxolan-2-yl)phenyl)phosphonate

A solution of **4** (2.01 g, 6.52 mmol) in dry diethyl ether (20 mL) was cooled to -78°C under nitrogen. Whilst stirring, *n*-butyllithium (2M in cyclohexane, 3.6 mL, 7.2 mmol, 1.1 eq) was added dropwise via syringe and the solution stirred at -78°C for 30 mins. Diethyl chlorophosphate (1.88 mL, 13.04 mmol, 2 eq) was added dropwise and the solution stirred at -78°C for 1 hour, before warming to room temperature. After another hour of stirring, the reaction was quenched with water (20 mL), extracted with DCM (3x) and dried over Na_2SO_4 . After concentrating in vacuo, the resulting oil was purified by flash column chromatography (50% EtOAc/Hexanes + 1% NEt_3)* to yield **6** (1.90 g, 5.21 mmol, 80%) as a yellow oil.

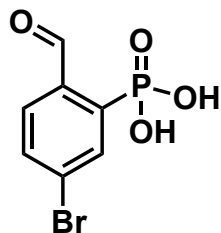
^1H NMR (500 MHz, Chloroform-*d*) δ 7.91 (dd, $J = 4.5, 2.0$ Hz, 1H), 7.80 (dd, $J = 13.6, 8.2$ Hz, 1H), 7.59 (ddd, $J = 8.2, 2.7, 2.1$ Hz, 1H), 6.36 (s, 1H), 4.18 – 4.03 (m, 8H), 1.32 (t, $J = 7.0$ Hz, 6H).

^{31}P NMR (202 MHz, Chloroform-*d*) δ 16.76.

^{13}C NMR (126 MHz, Chloroform-*d*) δ 143.17 (d, $J = 11.0$ Hz), 135.38 (d, $J = 9.7$ Hz), 132.11 (d, $J = 14.6$ Hz), 130.73 (d, $J = 14.1$ Hz), 127.90 (d, $J = 4.0$ Hz), 126.15 (d, $J = 183.5$ Hz), 100.00, 65.63, 62.52 (d, $J = 5.3$ Hz), 16.25 (d, $J = 6.7$ Hz).

HR-ESI-MS m/z for $\text{C}_{13}\text{H}_{18}\text{O}_5\text{BrNaP}^+$ $[\text{M}+\text{Na}]^+$ calcd: 386.9967 found: 386.9967.

*Silica was incubated with the mobile phase for 1 hour prior to use.



Synthesis of **7**:

(5-bromo-2-formylphenyl)phosphonic acid

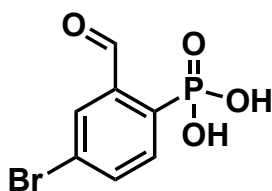
5 (500 mg, 1.37 mmol) was refluxed in conc. HCl (3 mL) for 12 hours. The resulting solution was cooled to room temperature, diluted with water, extracted into 60:40 DCM/PrOH (3x) and dried over Na₂SO₄. The solution was concentrated in vacuo and triturated with DCM and hexanes to yield **7** (232 mg, 0.88 mmol, 64%) as a beige powder.

¹H NMR (500 MHz, DMSO-*d*₆) δ 10.66 (s, 1H), 7.99 (dd, *J* = 13.5, 2.0 Hz, 1H), 7.92 (d, *J* = 7.5 Hz, 1H), 7.82 (dd, *J* = 8.3, 4.9 Hz, 1H).

³¹P NMR (202 MHz, DMSO-*d*₆) δ 6.64.

¹³C NMR (126 MHz, DMSO-*d*₆) δ 192.45 (d, *J* = 4.3 Hz), 139.34 (d, *J* = 170.2 Hz), 136.38 (d, *J* = 9.1 Hz), 135.25 (d, *J* = 8.8 Hz), 134.92 (d, *J* = 2.3 Hz), 129.58 (d, *J* = 12.3 Hz), 128.09 (d, *J* = 16.8 Hz).

HR-ESI-MS *m/z* for C₇H₅O₄BrP⁻ [M-H]⁻ calcd: 262.9114 found: 262.9118.



Synthesis of **8**:

(4-bromo-2-formylphenyl)phosphonic acid

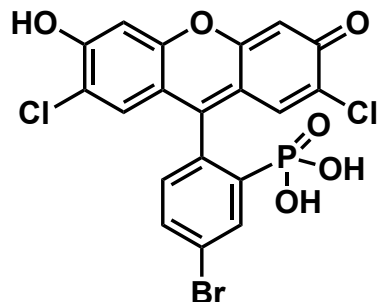
6 (600 mg, 1.64 mmol) was refluxed in conc. HCl (6 mL) for 12 hours. The resulting solution was cooled to room temperature, diluted with water (30mL) extracted into 70:30 DCM/PrOH (3x) and dried over Na₂SO₄. The solution was concentrated in vacuo and triturated with DCM and hexanes to yield **8** (315 mg, 1.19 mmol, 73%) as a pale tan solid.

¹H NMR (500 MHz, DMSO-*d*₆) δ 10.65 (s, 1H), 7.97 (m, 2H), 7.82 (m, 1H).

³¹P NMR (202 MHz, DMSO-*d*₆) δ 8.18.

^{13}C NMR (126 MHz, $\text{DMSO-}d_6$) δ 192.12 (d, $J = 4.2$ Hz), 139.15 (d, $J = 10.6$ Hz), 136.43 (d, $J = 13.2$ Hz), 136.04 (d, $J = 173.7$ Hz), 135.06 (d, $J = 8.8$ Hz), 129.80 (d, $J = 12.3$ Hz), 125.75 (d, $J = 3.7$ Hz).

HR-ESI-MS m/z for $\text{C}_7\text{H}_5\text{O}_4\text{BrP}^-$ $[\text{M-H}]^-$ calcd: 262.9114 found: 262.9118.



Synthesis of **9**:

5-bromo-2',7'-dichloro-3-phosphonofluorescein

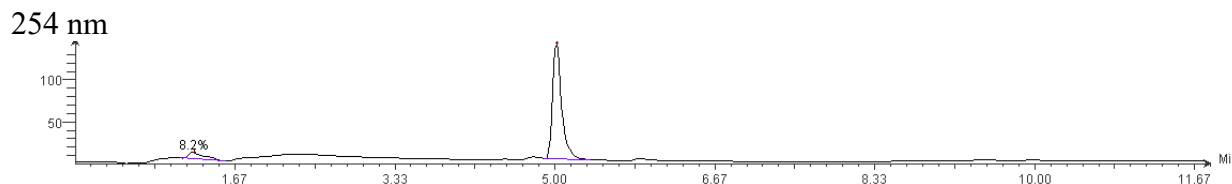
7 (200 mg, 0.75 mmol) and 4-chlororesorcinol (217 mg, 1.5 mmol) were charged into a round bottom that was subsequently evacuated and backfilled with nitrogen (3x). Methanesulfonic acid (2 mL) was added and the solution stirred at 90 °C for 16 hours. Upon cooling to room temperature, 10 mL water was added and the suspension stirred vigorously in an ice bath for 20 minutes before filtering. The orange/brown solid was suspended in 2 mL MeOH and 50 mL ice cold $i\text{PrOH}$ was added before filtering to obtain **9** as a bright orange solid (55 mg, 0.10 mmol, 14%).

^1H NMR (500 MHz, Deuterium Oxide + <1% NaOD) δ 8.20 (dd, $J = 11.8, 2.1$ Hz, 1H), 7.70 (dd, $J = 8.1, 1.5$ Hz, 1H), 7.35 (s, 2H), 6.95 (dd, $J = 8.2, 4.0$ Hz, 1H), 6.73 (s, 2H).

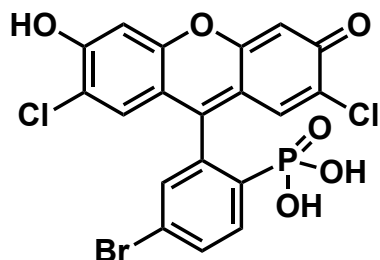
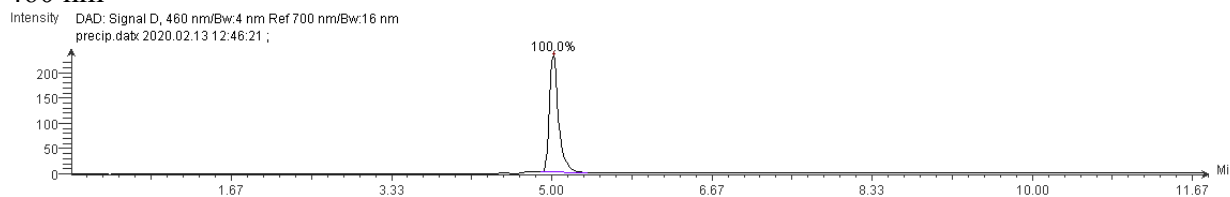
^{31}P NMR (202 MHz, Deuterium Oxide + <1% NaOD) δ 5.34.

^{13}C NMR (151 MHz, Deuterium Oxide + <1% NaOD) δ 174.28, 158.72 (d, $J = 2.3$ Hz), 157.02, 143.74 (d, $J = 158.3$ Hz), 135.27 (d, $J = 8.1$ Hz), 132.18 (d, $J = 6.9$ Hz), 130.93, 130.63 (d, $J = 11.2$ Hz), 129.66, 127.25, 122.61 (d, $J = 14.8$ Hz), 112.83, 103.85.

HR-ESI-MS m/z for $\text{C}_{19}\text{H}_9\text{O}_6\text{Br}_1\text{Cl}_2\text{P}^-$ $[\text{M-H}]^-$ calcd: 512.8703 found: 512.8704.



460 nm



Synthesis of **10**:

6-bromo-2',7'-dichloro-3-phosphonofluorescein

8 (240 mg, 0.91 mmol) and 4-chlororesorcinol (261 mg, 1.82 mmol) were charged into a round bottom that was subsequently evacuated and backfilled with nitrogen (3x). Methanesulfonic acid (2.4 mL) was added and the solution stirred at 90 °C for 16 hours. Upon cooling to room temperature, 10 mL water was added and the suspension stirred vigorously in an ice bath for 20 minutes before filtering. The orange solid was suspended in 2 mL MeOH and 30 mL ice cold MeCN was added before filtering to obtain **10** as a bright orange solid (61 mg, 0.12 mmol, 13%).

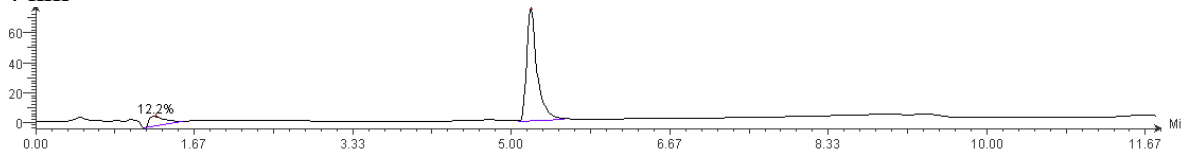
^1H NMR (500 MHz, Deuterium Oxide + <1% NaOD) δ 7.82 (dd, $J = 11.3, 8.4$ Hz, 1H), 7.66 (d, $J = 8.4$ Hz, 1H), 7.17 (s, 2H), 7.02 (d, $J = 2.3$ Hz, 1H), 6.59 (s, 2H).

^{31}P NMR (202 MHz, Deuterium Oxide + <1% NaOD) δ 6.40.

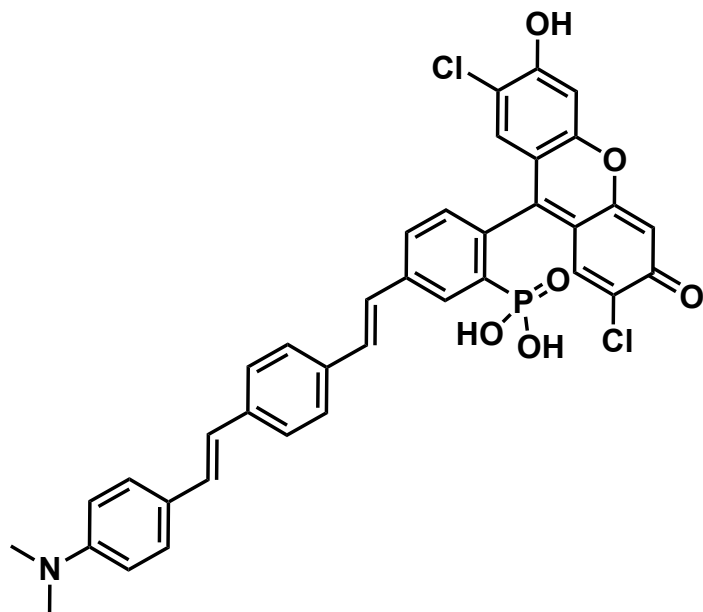
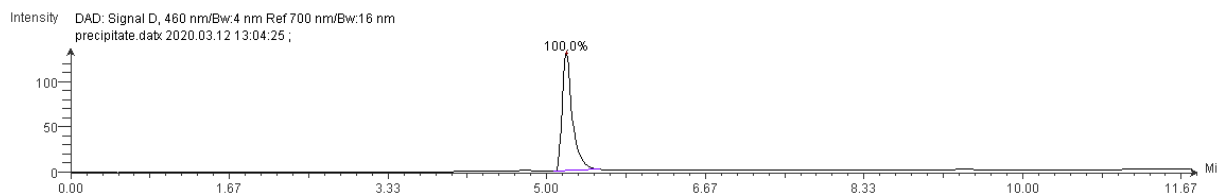
^{13}C NMR (226 MHz, Deuterium Oxide + <1% NaOD) δ 174.52, 158.21, 157.41, 140.63 (d, $J = 158.1$ Hz), 135.51, 134.64, 131.62 (d, $J = 11.2$ Hz), 131.05 (d, $J = 11.1$ Hz), 129.87, 127.39, 121.86, 113.01, 103.90.

HR-ESI-MS m/z for $\text{C}_{19}\text{H}_9\text{O}_6\text{Br}_1\text{Cl}_2\text{P}^-$ [M-H] $^-$ calcd: 512.8703 found: 512.8697.

254 nm



460m



Synthesis of **11**:

Para phosVF2.1.Cl

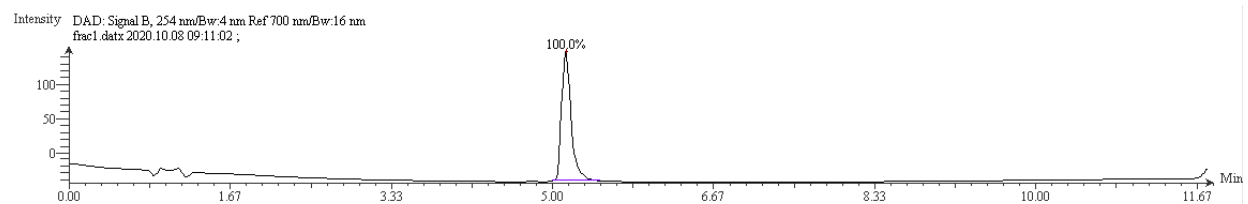
9 (16 mg, 0.031 mmol), molecular wire (10 mg, 0.040 mmol, 1.3 eq), Pd(OAc)₂ (0.75 mg, 0.003 mmol, 0.1 eq), P(*o*-tol)₃ (1.8 mg, 0.006 mmol, 0.2 eq) and 4Å molecular sieves (15 mg) were loaded into a reaction vial, which was subsequently evacuated and backfilled with nitrogen (3x). DMF (0.1 mL) and NEt₃ (0.1 mL) were added and the resulting solution stirred at 110 °C for 12 hrs. The deep red solution was concentrated to dryness, suspended in DCM and filtered over celite. The celite was then washed with MeOH to elute a deep red solution that was purified by reverse phase silica chromatography (75% MeOH/H₂O) yielding *para* phosVF2.1Cl (**11**) as a brick red solid (5.7 mg, 0.008 mmol, 26%).

¹H NMR (900 MHz, Methanol-*d*₄ + <1% NaOD) δ 8.43 (d, *J* = 13.4 Hz, 1H), 7.64 (d, *J* = 7.9 Hz, 1H), 7.59 (d, *J* = 8.0 Hz, 2H), 7.52 (d, *J* = 8.0 Hz, 2H), 7.43 (d, *J* = 8.6 Hz, 2H), 7.39 (d, *J* = 16.2 Hz, 1H), 7.35 – 7.33 (m, 3H), 7.12 (d, *J* = 16.1 Hz, 1H), 7.01 (dd, *J* = 7.7, 3.5 Hz, 1H), 6.96 (d, *J* = 16.3 Hz, 1H), 6.77 (d, *J* = 8.5 Hz, 2H), 6.59 (s, 2H), 2.97 (s, 6H).

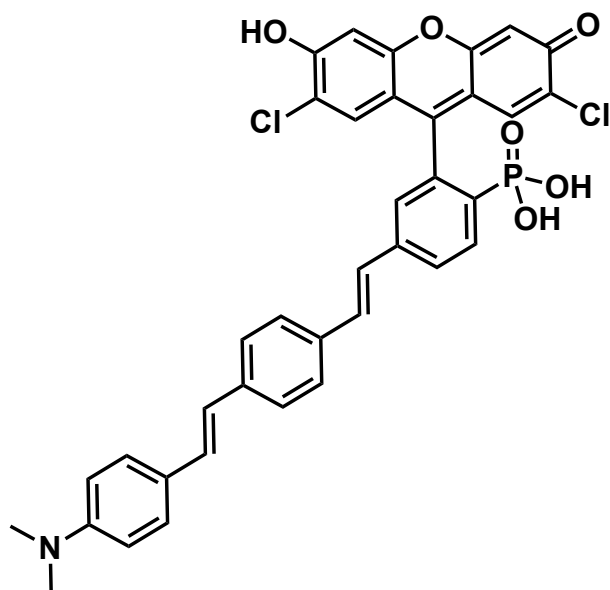
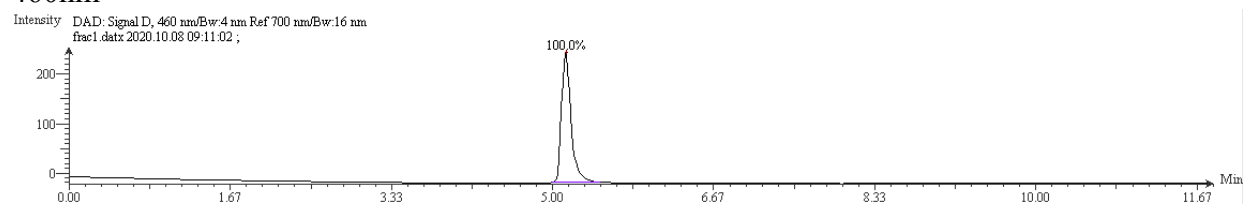
³¹P NMR (202 MHz, Methanol-*d*₄ + <1% NaOD) δ 8.78.

HR-ESI-MS *m/z* for C₃₇H₂₇Cl₂NO₆P⁻ [M-H]⁻ calcd: 682.0959 found: 682.0949.

254 nm



460nm



Synthesis of **12**:

Iso phosVF2.1.Cl

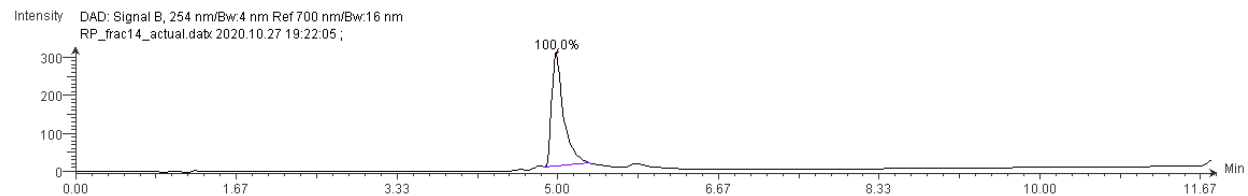
9 (40 mg, 0.078 mmol), molecular wire (23 mg, 0.093 mmol, 1.2 eq), Pd(OAc)₂ (1.8 mg, 0.008 mmol, 0.1 eq), P(*o*-tol)₃ (4.7 mg, 0.016 mmol, 0.2 eq) and 4Å molecular sieves (30 mg) were loaded into a reaction vial, which was subsequently evacuated and backfilled with nitrogen (3x). DMF (0.5 mL) and NEt₃ (0.5 mL) were added and the resulting solution stirred at 110 °C for 12hrs. The deep red solution was concentrated to dryness, suspended in DCM and filtered over celite. The celite was then washed with MeOH to elute a deep red solution that was concentrated and purified by reverse phase silica chromatography (75% MeOH/H₂O) affording *iso* phosVF2.1Cl (**12**) as a bright orange solid (13.2 mg, 0.019 mmol, 24%).

^1H NMR (500 MHz, Methanol- d_4 + <1% NaOD) δ 8.19 (t, J = 9.0 Hz, 1H), 7.75 (d, J = 8.1 Hz, 1H), 7.51 (d, J = 7.8 Hz, 2H), 7.45 (d, J = 7.9 Hz, 2H), 7.39 (d, J = 8.3 Hz, 2H), 7.33 (s, 2H), 7.22 – 7.17 (m, 2H), 7.09 – 7.03 (m, 2H), 6.91 (d, J = 16.0 Hz, 1H), 6.75 (d, J = 8.3 Hz, 2H), 6.61 (s, 2H), 2.95 (s, 6H).

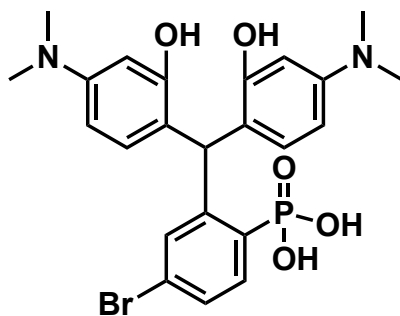
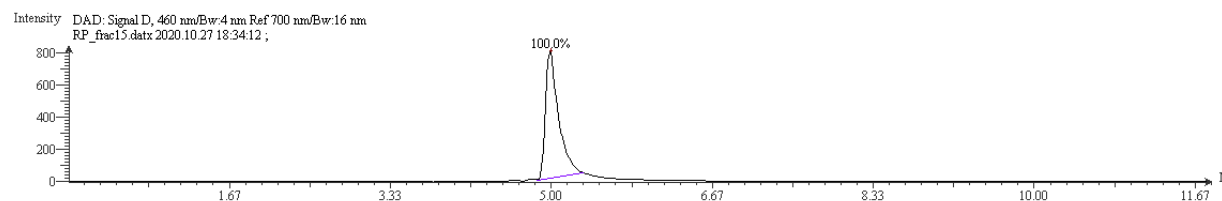
^{31}P NMR (202 MHz, Methanol- d_4 + <1% NaOD) δ 8.82.

HR-ESI-MS m/z for $\text{C}_{37}\text{H}_{27}\text{Cl}_2\text{NO}_6\text{P}^-$ [M-H] $^-$ calcd: 682.0959 found: 682.0961.

254nm



460nm



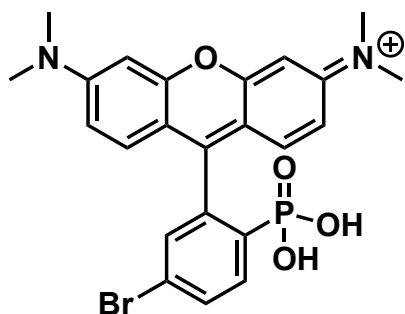
Synthesis of **13**

8 (400 mg, 1.51 mmol, 1 eq) and 3-(dimethylamino)phenol (517 mg, 3.77 mmol, 2.5 eq) were stirred in TFE (30 mL) at 80 °C for 16 hrs. The resulting suspension was concentrated *in vacuo*, and triturated with EtOAc, yielding **13** as a pale purple powder (786 mg, 1.51 mmol, >99%).

^1H NMR (400 MHz, DMSO- d_6) δ 7.61 (dd, J = 13.2, 8.2 Hz, 1H), 7.51 – 7.45 (m, 1H), 7.23 (dd, J = 4.0, 1.7 Hz, 1H), 6.57 – 6.48 (m, 3H), 6.18 – 6.06 (m, 4H), 2.80 (s, 12H).

^{31}P NMR (202 MHz, DMSO- d_6) δ 13.11.

HR-ESI-MS m/z for $C_{23}H_{25}O_5N_2Br_1P_1^-$ $[M-H]^-$ calcd: 519.0690 found: 519.0678



Synthesis of **14**

6-bromo-3-phosphono-tetramethylrhodamine

13 (780 mg, 1.49 mmol, 1 eq) and p-chloranil (445 mg, 1.81 mmol, 1.2 eq) were refluxed in MeOH (50 mL) for 24 hours. Upon cooling to room temperature, the solution was filtered, and the filtrate was concentrated *in vacuo*. Trituration with EtOAc yielded **14** as a dark purple powder (748 mg, 1.49 mmol, >99%).

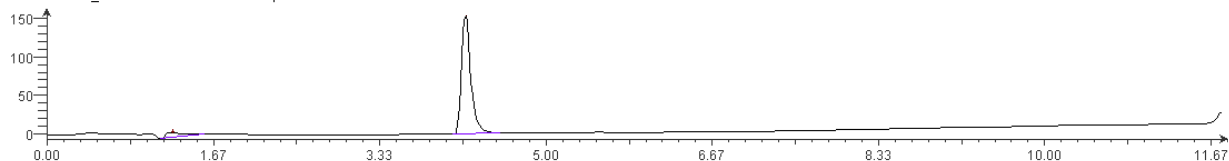
1H NMR (500 MHz, Methanol- d_4) δ 8.06 (dd, $J = 12.9, 8.3$ Hz, 1H), 7.89 (dt, $J = 8.3, 2.0$ Hz, 1H), 7.54 (dd, $J = 3.6, 1.9$ Hz, 1H), 7.17 (d, $J = 9.5$ Hz, 2H), 7.04 (dd, $J = 9.5, 2.4$ Hz, 2H), 6.92 (d, $J = 2.4$ Hz, 2H), 3.30 (s, 12H).

^{31}P NMR (202 MHz, Methanol- d_4) δ 8.70.

HR-ESI-MS m/z for $C_{23}H_{23}O_4N_2Br_1P_1^+$ $[M]^+$ calcd: 501.0573 found: 501.0572

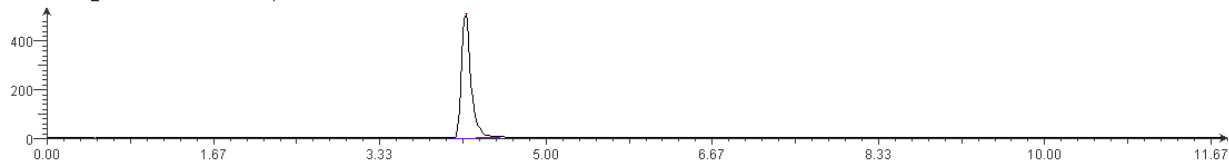
254 nm

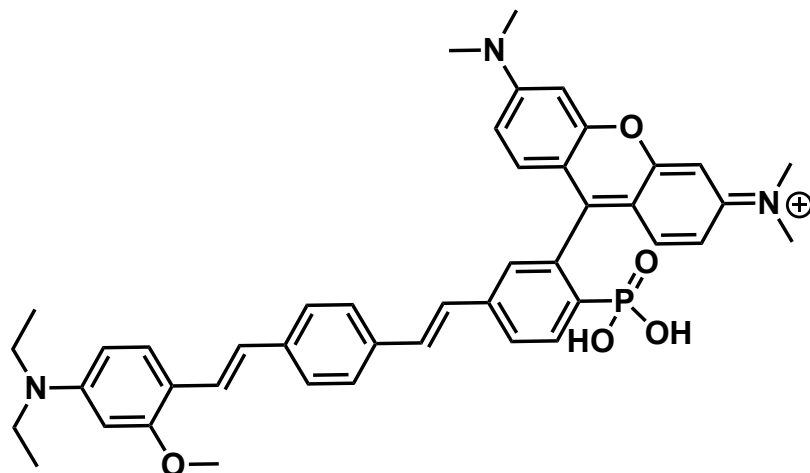
Intensity DAD: Signal B, 254 nm/Bw:4 nm Ref 700 nm/Bw:16 nm
1week_ox.dabx 2020.08.11 20:38:26;



560 nm

Intensity DAD: Signal F, 560 nm/Bw:4 nm Ref 700 nm/Bw:16 nm
1week_ox.dabx 2020.08.11 20:38:26;





Synthesis of **15**

phosRhoVR 1

14 (357 mg, 0.71 mmol, 1 eq), molecular wire (240 mg, 0.78 mmol, 1.1 eq), Pd(OAc)₂ (16 mg, 0.07 mmol, 0.1 eq), P(*o*-tol)₃ (43 mg, 0.14 mmol, 0.2 eq) were charged into a flame dried round bottom flask and was subsequently evacuated and backfilled with N₂ (x3). Upon addition of DMF (10.5 mL) and NEt₃ (5.25 mL), the solution was stirred at 110 °C under static N₂ for 16 hours. After cooling to room temperature, the solution was diluted with DCM and flushed through a celite plug. The filtrate was concentrated *in vacuo* and triturated with EtOAc to yield a crude red solid (658).* **15** could be purified by reverse phase silica chromatography (80% to 100% MeOH/H₂O) (432 mg, 0.59 mmol, 76%).

*Crude solid was a relatively clean NEt₃ salt.

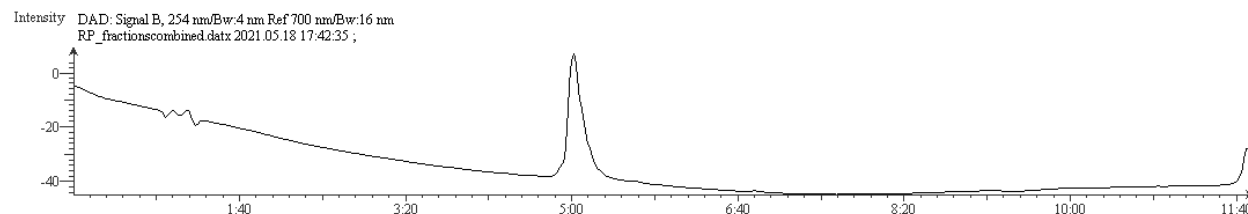
¹H NMR (400 MHz, DMSO-*d*₆) δ 7.53 – 7.43 (m, 3H), 7.45 – 7.32 (m, 4H), 7.31 – 7.22 (m, 3H), 7.07 (d, *J* = 16.6 Hz, 1H), 7.01 (d, *J* = 16.3 Hz, 1H), 6.89 (d, *J* = 16.5 Hz, 1H), 6.62 (s, 1H), 6.44 (dd, *J* = 8.8, 2.4 Hz, 2H), 6.40 (d, *J* = 2.4 Hz, 2H), 6.27 (dd, *J* = 8.7, 2.1 Hz, 1H), 6.19 (d, *J* = 2.0 Hz, 1H), 3.82 (s, 3H), 2.90 (s, 12H), 1.11 (t, *J* = 7.0 Hz, 6H).

Ethyl CH₂'s hidden under H₂O peak

³¹P NMR (202 MHz, DMSO-*d*₆) δ 22.57.

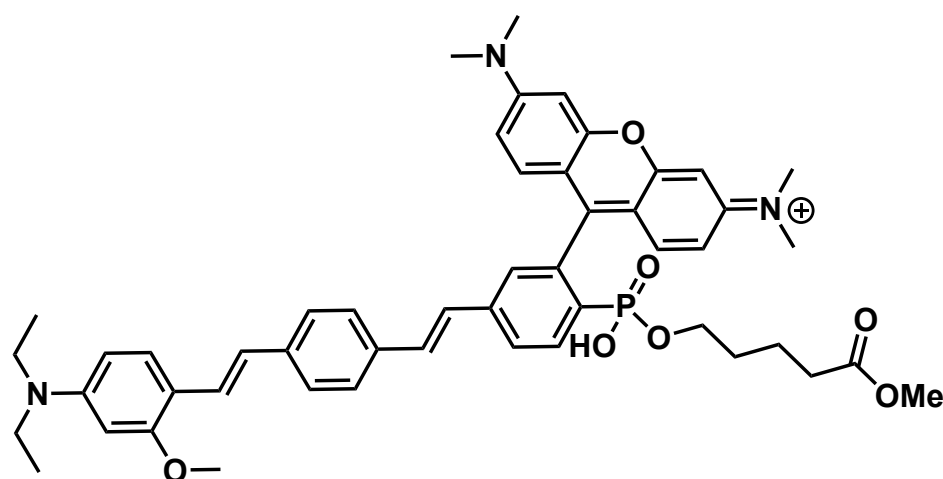
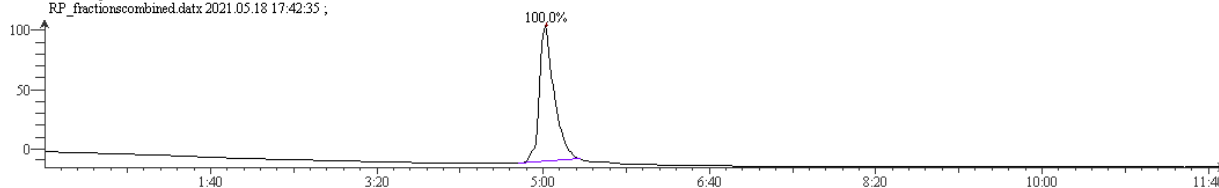
HR-ESI-MS *m/z* for C₄₄H₄₇O₅N₃P⁺ [M]⁺ calcd: 728.3248 found: 728.3236

254 nm



560 nm

Intensity DAD: Signal F, 560 nm/Bw:4 nm Ref 700 nm/Bw:16 nm
RP_fractionscombined.datx 2021.05.18 17:42:35 ;

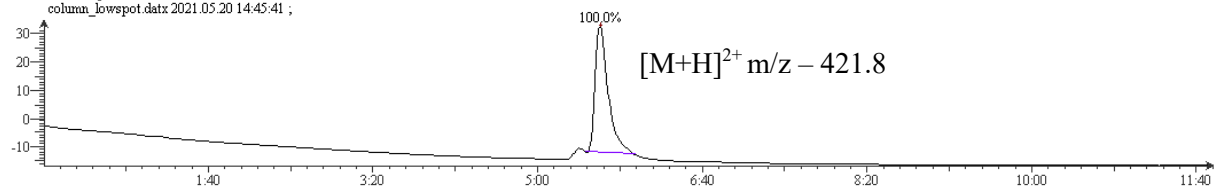


Synthesis of compound 16

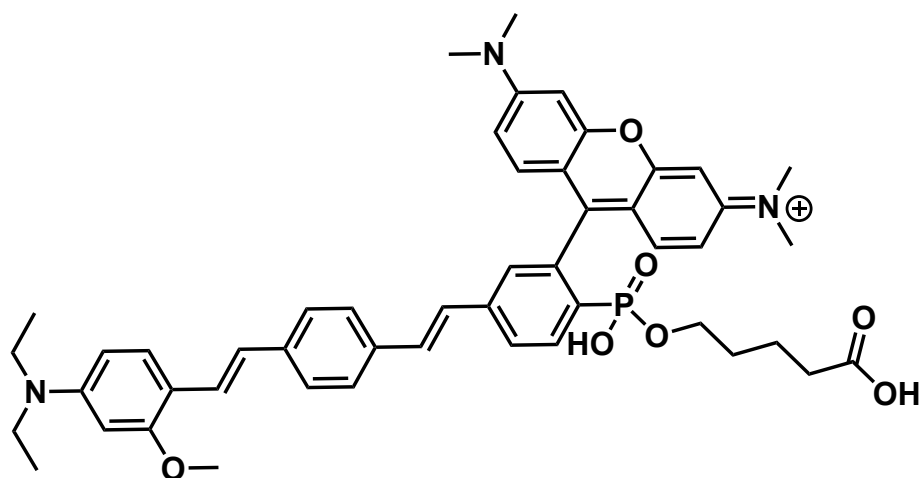
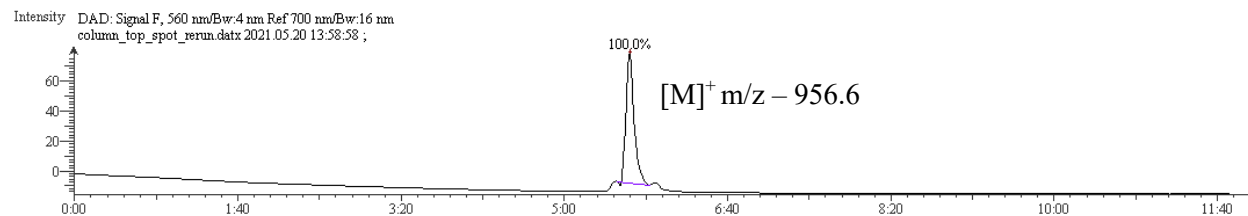
PhosRhoVR 1 (50 mg, 0.07 mmol, 1 eq), Ag₂O (20 mg, 0.09 mmol, 1.25 eq), methyl 5-bromovalerate (17 mg, 0.09 mmol, 1.25 eq) and 4Å molecular sieves (40 mg) were charged into a flame dried round bottom which was then evacuated and backfilled with N₂ (x3). DMF (1.5 mL) was added and the resulting suspension was stirred at 60 °C for 16 hours. Upon cooling to room temperature, the suspension was diluted with DCM and filtered over a short pad of celite. Purification by flash silica chromatography (10 to 25% MeOH/ DCM) yielded **16** as a red powder (22 mg, 0.03 mmol, 38%).

560 nm

Intensity DAD: Signal F, 560 nm/Bw:4 nm Ref 700 nm/Bw:16 nm
column_lowspot.datx 2021.05.20 14:45:41 ;



*note the double phosphonate esterification product was also isolated (12 mg, 0.01 mmol, 18%).

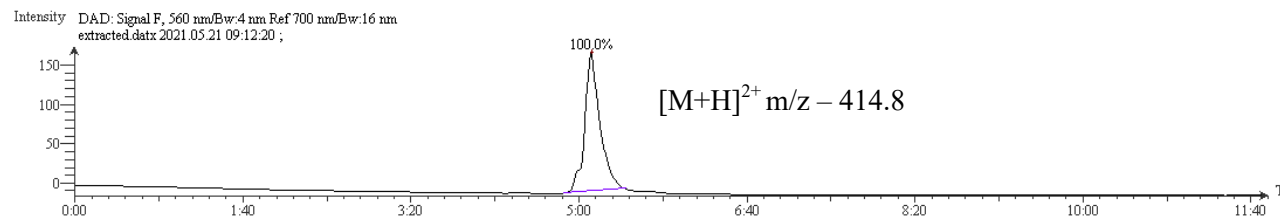


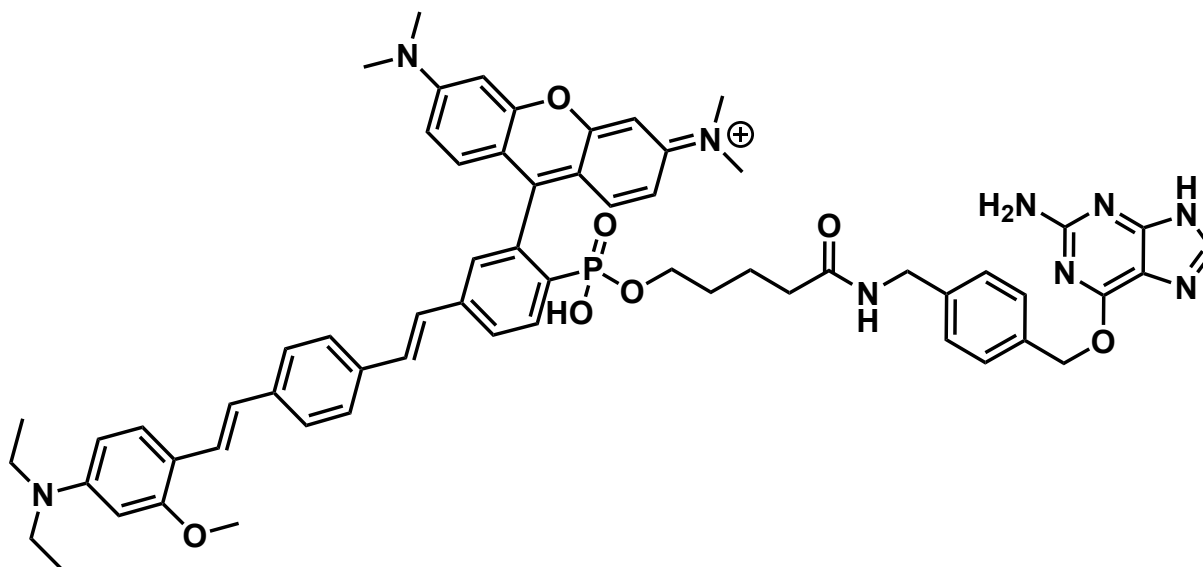
Synthesis of compound **17**

2.5 M NaOH_(aq) (3 mL) was added to a suspension of **16** (17 mg, 0.02 mmol, 1 eq) in water (4 mL), and was stirred at room temperature for 20 minutes. Upon dilution with H₂O (25 mL) the aqueous solution was washed with DCM before acidification with 1M HCl. Extraction with DCM (x6) yielded a red solution that was dried over Na₂SO₄, filtered, and concentrated *in vacuo* to afford **17** as a red solid (14 mg, 0.017 mmol, 87%).

HR-ESI-MS m/z for C₄₉H₅₅N₃O₇P⁺ [M]⁺ calcd:828.3772 found: 828.3773

560 nm





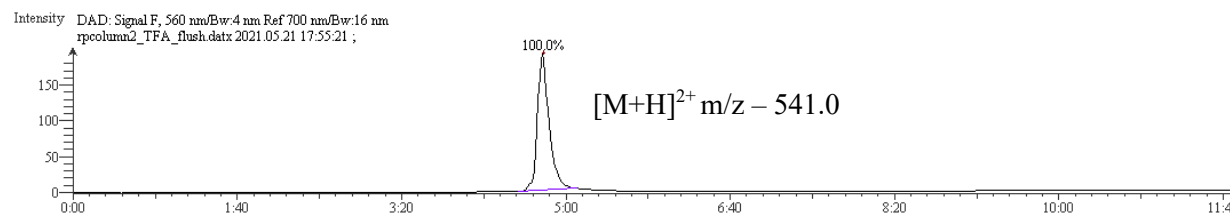
Synthesis of compound **18**

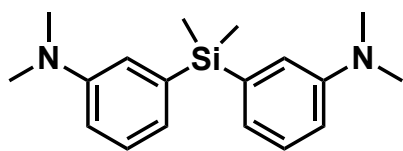
PhosRhoVR SNAP 1

17 (5 mg, 0.006 mmol, 1 eq), benzyl guanine amine (1.6 mg, 0.006 mmol, 1 eq) and HATU (2.3 mg, 0.006 mmol, 1eq) were charged into a small reaction vial and dissolved in DMF (1 mL). Following the addition of DIPEA (2.1 μ L), the vial was flushed with nitrogen and stirred at room temperature for 1 hour. The solution was concentrated *in vacuo* and purified by reverse phase silica chromatography (95 to 100% MeOH/ H₂O) affording phosRhoVR SNAP 1, **18** as a purple solid (2.7 mg, 0.0026 mmol, 43%).

HR-ESI-MS m/z for C₆₂H₆₇N₉O₇P⁺ [M]⁺ calcd:1080.4896 found: 1080.4902

560 nm

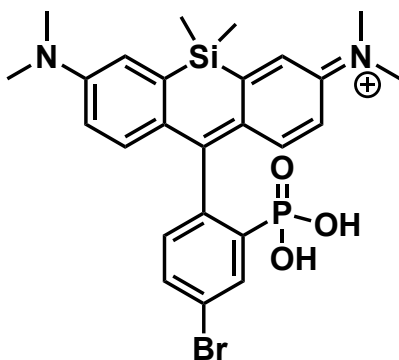




Synthesis of **19**.

3-bromo-N,N-dimethylaniline (1.19 g, 5.9 mmol, 2.4 eq) was charged into a flamed dried Schlenk flask that was subsequently evacuated and backfilled with N₂ (x3). THF (11.8 mL) was added and the solution cooled to -78 °C. nBuLi (2.96 mL, 2M in hexanes, 5.9 mmol, 2.4 eq) was added slowly and the solution stirred at -78 °C for 30 minutes. Dichlorodimethyl silane (0.3 mL, 2.5 mmol 1 eq) was added slowly and the solution was slowly warmed to room temperature over 2 hours. The reaction was quenched with sat. ammonium chloride, followed by extraction into EtOAc (x3). The combined organics were washed with brine (x2), dried over Na₂SO₄ and concentrated *in vacuo*. Purification by flash silica chromatography (5% EtOAc/ Hexanes) yielded **19** as a colorless oil (665 mg, 2.23 mmol, 91%).

¹H NMR (400 MHz, Chloroform-*d*) δ 7.23 (t, *J* = 8.1 Hz, 2H), 6.94 (d, *J* = 2.5 Hz, 2H), 6.91 (d, *J* = 7.1 Hz, 2H), 6.77 (dd, *J* = 8.2, 2.3 Hz, 2H), 2.92 (s, 12H), 0.53 (s, 6H).



Synthesis of **20**

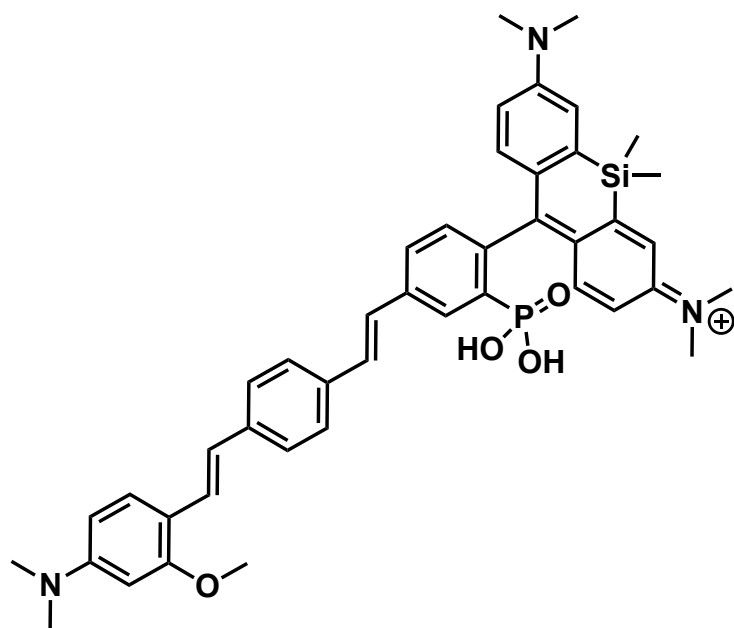
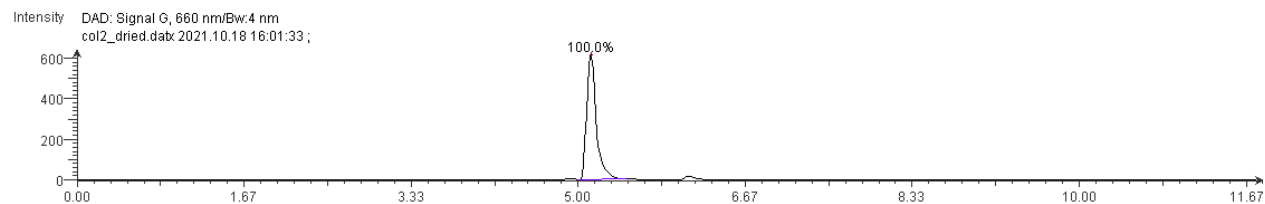
7 (200 mg, 0.75 mmol, 1.15 eq) and **19** (196 mg, 0.66 mmol, 1 eq) were dissolved in TFE (0.5 mL) and the solution was refluxed at 80 °C for 5 days. The deep blue solution was concentrated *in vacuo* and the crude residue was purified by reverse phase silica chromatography (60% to 100% MeOH/H₂O) yielding **20** as a blue solid (129 mg, 0.24 mmol, 36%).

¹H NMR (500 MHz, Methanol-*d*₄) δ 8.26 (dd, *J* = 12.9, 1.9 Hz, 1H), 7.68 (dd, *J* = 8.2, 1.7 Hz, 1H), 7.26 (d, *J* = 2.8 Hz, 2H), 7.12 (d, *J* = 9.6 Hz, 2H), 7.00 (dd, *J* = 8.2, 4.6 Hz, 1H), 6.71 (dd, *J* = 9.6, 2.8 Hz, 2H), 3.30 (s, 12H), 0.58 (s, 3H), 0.56 (s, 3H).

³¹P NMR (202 MHz, Methanol-*d*₄) δ 6.79.

HR-ESI-MS *m/z* for C₂₅H₂₉O₃N₂BrP₁Si₁ [M]⁺ calcd: 543.0863 found: 543.0957

660 nm



Synthesis of compound **21**

3-phosphono-BeRST, phosBeRST 1

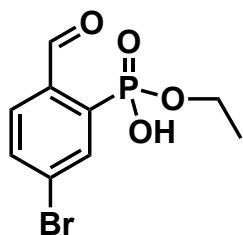
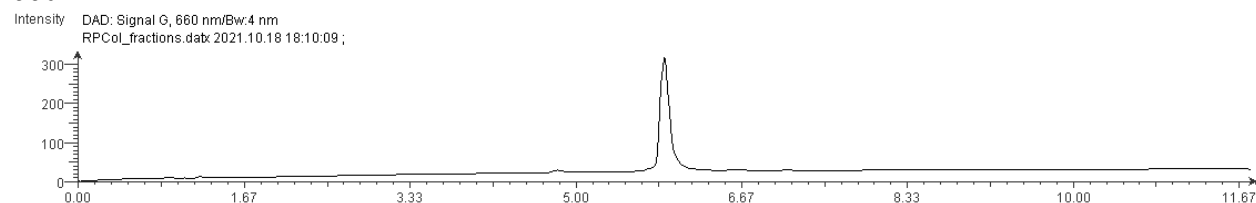
20 (44 mg, 0.08 mmol, 1 eq), molecular wire (25 mg, 0.09 mmol, 1.1 eq), Pd(OAc)₂ (9 mg, 0.04 mmol, 0.5 eq), P(*o*-tol)₃ (25 mg, 0.08 mmol, 1 eq) were charged into a flame dried round bottom flask and was subsequently evacuated and backfilled with N₂ (x3). Upon addition of DMF (1 mL) and NEt₃ (0.4 mL), the solution was stirred at 90 °C under static N₂ for 2 hours. Upon cooling to room temperature, the mixture was diluted with DCM and flushed through a short pad of celite, and the celite was subsequently washed with methanol. Upon concentration *in vacuo* the resulting residue was purified by reverse phase silica chromatography (80% to 100% MeOH/H₂O) to yield **21** as a green solid (37 mg, 0.05 mmol, 61%).

¹H NMR (500 MHz, Methanol-*d*₄) δ 8.29 (d, *J* = 13.6 Hz, 1H), 7.78 (d, *J* = 8.0 Hz, 1H), 7.57 (d, *J* = 8.2 Hz, 2H), 7.49 (m, 3H), 7.43 (d, *J* = 16.4 Hz, 1H), 7.33 (d, *J* = 14.6 Hz, 1H), 7.28 (m, 3H), 7.17 (d, *J* = 9.7 Hz, 2H), 7.14 (dd, *J* = 8.0, 4.9 Hz, 1H), 6.97 (d, *J* = 16.4 Hz, 1H), 6.71 (dd, *J* = 9.7, 2.7 Hz, 2H), 6.43 (dd, *J* = 8.6, 2.0 Hz, 1H), 6.38 (d, *J* = 2.0 Hz, 1H), 3.91 (s, 3H), 3.31 (s, 13H), 3.01 (s, 6H), 0.60 (s, 3H), 0.59 (s, 3H).

³¹P NMR (202 MHz, Methanol-*d*₄) δ 11.35.

HR-ESI-MS m/z for $C_{44}H_{49}O_4N_3P_1Si_1$ $[M]^+$ calcd: 742.3225 found: 742.3213

660 nm

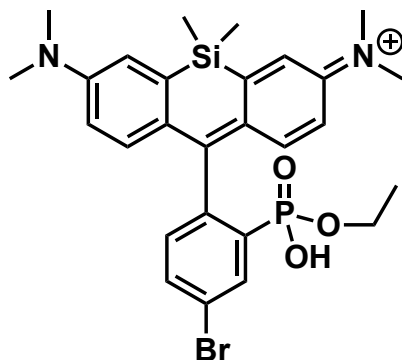


Synthesis of compound **22**.

S3-11 (160 mg, 0.50 mmol, 1 eq) and tetrabutylammonium hydrogensulfate (50 mg, 0.15 mmol, 0.3 eq) were partitioned between DCM (1.5 mL) and 1M NaOH_(aq) (1.5 mL) and the resulting emulsion was stirred vigorously at 40 °C for 16 hours. Upon cooling to room temperature, the mixture was diluted with water and the aqueous phase was washed with DCM (x3). The aqueous phase was then acidified with 1M HCl and extracted into EtOAc (x3), dried over Na₂SO₄ and concentrated *in vacuo* to afford **22** as a hygroscopic white solid (82 mg, 0.28 mmol, 58%).

¹H NMR (500 MHz, Chloroform-*d*) δ 10.50 (s, 1H), 8.16 (dd, J = 14.8, 1.5 Hz, 1H), 7.93 (dd, J = 8.2, 5.7 Hz, 1H), 7.83 (d, J = 8.3 Hz, 1H), 4.19 (p, J = 7.2 Hz, 2H), 1.34 (t, J = 7.1 Hz, 3H).

³¹P NMR (202 MHz, Chloroform-*d*) δ 15.75.



Synthesis of compound **23**.

22 (115 mg, 0.39 mmol, 1 eq) and 3,3'-(dimethylsilanediyl)bis(*N,N*-dimethylaniline) (135 mg, 0.45 mmol, 1.15 eq) were dissolved in TFE and stirred at 80 °C for 5 days. It was determined **21** was only 43% pure with the other 57% being free phosphonic acid **7** leading to a mix of the desired

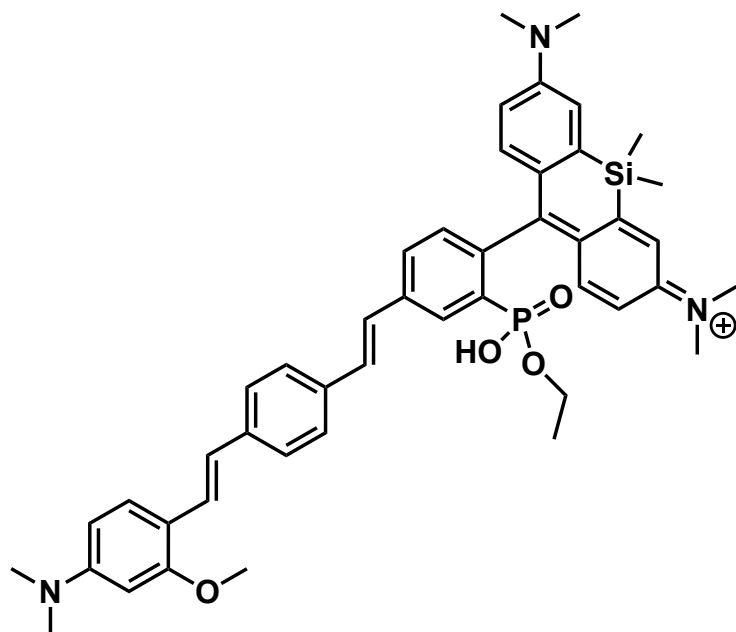
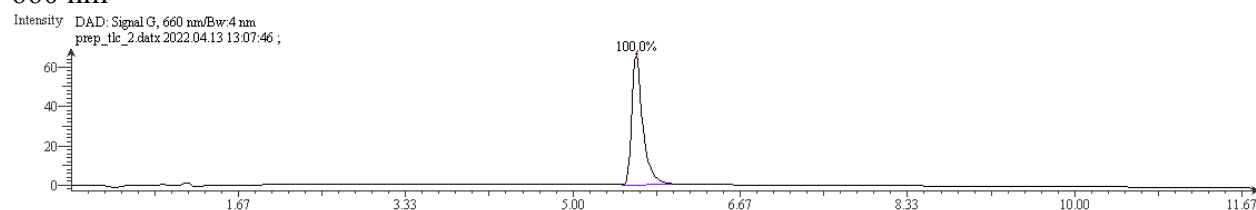
product and **19**. Purification by reverse phase silica chromatography (85% MeOH/ H₂O) followed by preparative TLC separated the two fluorophores and **32** was isolated as a blue solid (17 mg, 0.03 mmol, 7%).

This synthesis should be repeated with a pure sample of **21**.

¹H NMR (400 MHz, Methanol-*d*₄) δ 8.25 (dd, *J* = 12.7, 2.1 Hz, 1H), 7.70 (dd, *J* = 8.2, 2.1 Hz, 1H), 7.28 (d, *J* = 2.9 Hz, 2H), 7.10 (d, *J* = 9.6 Hz, 2H), 7.03 (dd, *J* = 8.1, 4.6 Hz, 1H), 6.73 (dd, *J* = 9.6, 2.9 Hz, 2H), 3.51 (p, *J* = 6.9 Hz, 2H), 0.86 (t, *J* = 7.0 Hz, 3H), 0.60 (s, 3H), 0.57 (s, 3H).

HR-ESI-MS *m/z* for C₂₇H₃₃O₃N₂Br₁P₁Si₁ [M]⁺ calcd: 571.1176 found: 571.1178

660 nm



Synthesis of compound **24**.

3-phosphonoBeRST ethyl ester, phosBeRST.OEt

23 (11 mg, 0.019 mmol, 1 eq), molecular wire (6 mg, 0.021 mmol, 1.1 eq), Pd(OAc)₂ (2.3 mg, 0.01 mmol, 0.5 eq) and P(*o*-tol)₃ (5.8 mg, 0.019 mmol, 1 eq) were charged into a flame dried reaction vial that was subsequently evacuated and backfilled with N₂ (x3). Upon addition of DMF (0.25 mL) and NEt₃ (0.1 mL) the solution was stirred at 90 °C for 2 hours. Upon cooling to room temperature, the solution was diluted with DCM and flushed through a thin pad of celite. The celit

was washed with MeOH to ensure full elution of any fluorophore. Purification by reverse phase silica chromatography (80 to 100% MeOH/H₂O) afforded **24** as a green solid (8.5 mg, 0.011 mmol, 57%).

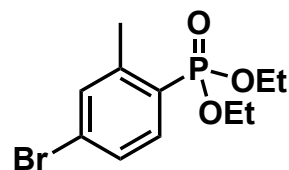
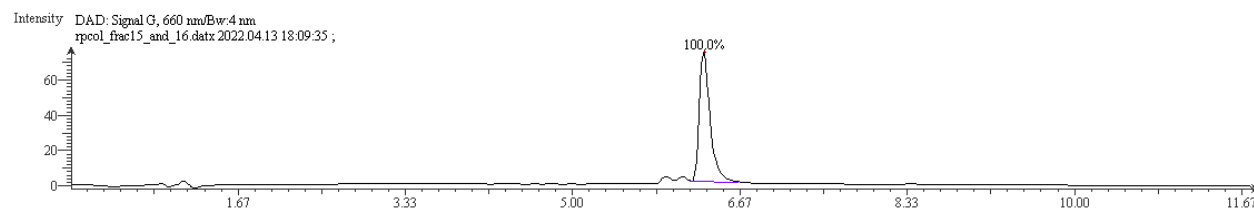
¹H NMR (500 MHz, Methanol-*d*₄) δ 8.31 (dd, *J* = 13.6, 0.7 Hz, 1H), 7.72 (d, *J* = 8.2 Hz, 1H), 7.58 (d, *J* = 8.2 Hz, 2H), 7.49 (d, *J* = 7.8 Hz, 2H), 7.46 (d, *J* = 10.5 Hz, 1H), 7.43 – 7.41 (m, 1H), 7.40 – 7.36 (m, 1H), 7.34 (d, *J* = 14.0 Hz, 1H), 7.28 (d, *J* = 2.7 Hz, 2H), 7.22 (d, *J* = 9.6 Hz, 2H), 7.08 (dd, *J* = 7.6, 4.6 Hz, 1H), 6.97 (d, *J* = 16.3 Hz, 1H), 6.72 (dd, *J* = 9.6, 2.7 Hz, 2H), 6.42 – 6.38 (m, 1H), 6.34 – 6.32 (m, 1H), 3.91 (s, 3H), 3.53 (d, *J* = 7.2 Hz, 3H), 3.00 (s, 6H), 0.87 (t, *J* = 7.0 Hz, 3H), 0.61 (s, 3H), 0.58 (s, 3H).

Note: aniline methyl protons hidden under MeOD peak.

³¹P NMR (202 MHz, Methanol-*d*₄) δ 9.89.

HR-ESI-MS *m/z* for C₄₆H₅₃O₃N₃P₁Si₁ [M]⁺ calcd: 770.3538 found: 770.3538

660 nm



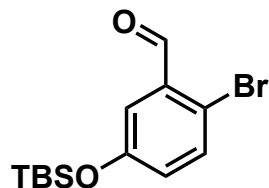
Synthesis of compound **S3-2**.

5-bromo-2-(diethyl)phosphono-toluene

A flame dried reaction vial was charged with Pd(OAc)₂ (40 mg, 0.175 mmol, 0.1 eq) and evacuated and backfilled with N₂ (x3). Upon addition of 2-iodo-5-bromo-toluene (0.25 mL, 1.75 mmol, 1 eq) and triethyl phosphite (0.32 mL, 1.84 mmol, 1.05 eq) the mixture was stirred at 90 °C overnight. The resulting deep red solution was cooled to room temperature and purified by flash column chromatography (15% to 50% EtOAc/ Hexanes) yielding **S3-2** as a colorless oil (420 mg, 1.37 mmol, 78%).

¹H NMR (400 MHz, Chloroform-*d*) δ 7.77 (dd, *J* = 13.9, 8.1 Hz, 1H), 7.41 (m, 2H), 4.10 (m, 4H), 2.54 (s, 3H), 1.32 (t, *J* = 7.0 Hz, 6H).

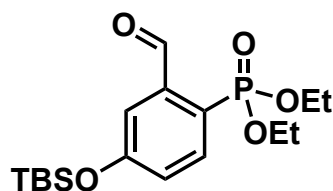
³¹P NMR (162 MHz, Chloroform-*d*) δ 18.67.



Synthesis of compound **S3-4**.

2-bromo-5-hydroxybenzaldehyde (1.00g, 4.98 mmol, 1 eq), imidazole (620 mg, 9.12 mmol, 1.83 eq), tert-butyldimethylsilyl chloride (816 mg, 5.48 mmol, 1.1 eq) were charged into an oven dried round bottom flask which was subsequently evacuated and backfilled with N₂ (x3). Upon cooling to 0 °C in an ice bath, DCM (20 mL) was added and the solution was slowly warmed to room temperature and left stirring for 2 hours. The organic solution was washed with water (x3), brine (x1) and dried over Na₂SO₄ before concentration *in vacuo*. The resulting residue was purified by flash silica chromatography (5% EtOAc/ Hexanes), yielding **S3-4** as a dark brown oil (1.18g, 3.74 mmol, 75%).

¹H NMR (300 MHz, Chloroform-*d*) δ 10.29 (s, 1H), 7.49 (d, *J* = 8.6 Hz, 1H), 7.36 (d, *J* = 2.9 Hz, 1H), 6.95 (dd, *J* = 8.6, 2.9 Hz, 1H), 0.98 (s, 9H), 0.21 (s, 6H).

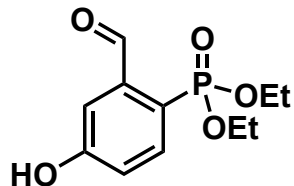


Synthesis of compound **S3-5**.

S3-4 (1.10g, 3.49 mmol, 1 eq) and NiCl₂ (23 mg, 0.18 mmol, 0.05 eq) were charged into an oven dried Schlenk flask which was then evacuated and backfilled with N₂. Upon fitting of a reflux condenser, the system was purged with N₂ for 5 minutes. The flask was then heated to 170 °C and triethyl phosphite (0.72 mL, 4.19 mmol, 1.2 eq) was added slowly over 30 minutes. The solution was stirred at 170 °C for a further hour before cooling to room temperature. The crude residue was purified by flash silica chromatography (50% EtOAc/ Hexanes), yielding **S3-5** as an orange oil (585 mg, 1.57 mmol, 45%).

¹H NMR (400 MHz, Chloroform-*d*) δ 10.59 (s, 1H), 7.95 (dd, *J* = 13.7, 8.3 Hz, 1H), 7.49 (dd, *J* = 4.3, 2.5 Hz, 1H), 7.09 (dt, *J* = 8.4, 2.7 Hz, 1H), 4.27 – 4.07 (m, 4H), 1.32 (t, *J* = 7.1 Hz, 6H), 0.99 (s, 9H), 0.25 (s, 6H).

³¹P NMR (162 MHz, Chloroform-*d*) δ 17.22.

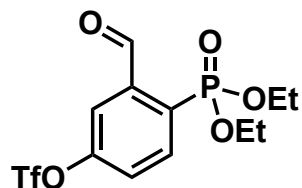


Synthesis of compound **S3-6**.

To a stirring solution of **S3-5** (580 mg, 1.56 mmol, 1 eq) in THF (10 mL) was added a 1 M (in THF) solution of tetrabutylammonium fluoride (7.8 mL, 7.8 mmol, 5 eq) dropwise and the solution was stirred at room temperature for 2 hours. Upon concentration *in vacuo* the residue was dissolved in H₂O and extracted into EtOAc (x3). The combined organics were dried over Na₂SO₄, concentrated, and purified by flash silica chromatography (100% EtOAc), yielding **S3-6** as a golden waxy solid (362 mg, 1.40 mmol, 90%).

¹H NMR (400 MHz, Chloroform-*d*) δ 10.53 (s, 1H), 8.86 (s, 1H), 7.93 (dd, *J* = 13.8, 8.4 Hz, 1H), 7.59 (dd, *J* = 4.5, 2.6 Hz, 1H), 7.18 (dt, *J* = 8.4, 2.7 Hz, 1H), 4.28 – 4.10 (m, 4H), 1.33 (t, *J* = 7.1 Hz, 6H).

³¹P NMR (162 MHz, Chloroform-*d*) δ 17.91.



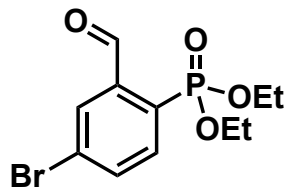
Synthesis of compound **S3-7**.

S3-6 (200 mg, 0.78 mmol, 1 eq) was charged into an oven dried Schlenk flask which was then evacuated and backfilled with N₂ (x3). DCM (1.5 mL) and NEt₃ (0.43 mL, 3.12 mmol, 4 eq) were added and the solution was cooled to -78 °C. Whilst stirring trifluoromethanesulfonic anhydride (0.2 mL, 1.16 mmol, 1.5 eq) was added slowly, the solution was stirred at -78 °C for 2 hours and then warmed to room temperature overnight. The solution was then poured into ice water, extracted into diethyl ether (x3) and upon concentration *in vacuo*, the residue was purified by flash silica chromatography (40% EtOAc/ Hexanes), rendering **S3-7** as a red oil (265 mg, 0.68 mmol, 87%).

¹H NMR (400 MHz, Chloroform-*d*) δ 10.63 (s, 1H), 8.19 (dd, *J* = 13.5, 8.4 Hz, 1H), 7.95 (s, 1H), 7.58 (dt, *J* = 8.4, 2.5 Hz, 1H), 4.33 – 4.14 (m, 4H), 1.36 (t, *J* = 7.1 Hz, 6H).

¹⁹F NMR (376 MHz, Chloroform-*d*) δ -71.87.

³¹P NMR (162 MHz, Chloroform-*d*) δ 13.80.

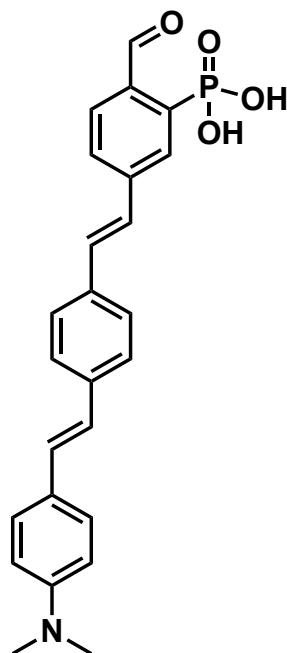


Synthesis of compound S3-8.

$\text{Pd}_2(\text{dba})_3$ (14 mg, 0.015 mmol, 0.015 eq), $^t\text{BuBrettPhos}$ (22 mg, 0.045 mmol, 0.045 eq) were charged into a small flame dried reaction vial that was then evacuated and backfilled with N_2 (x3). Dioxane (1 mL) was added and the solution was heated at 120 °C for 5 minutes. In a separate flame dried reaction vial, was added **S3-7** (390 mg, 1 mmol, 1 eq), potassium bromide (238 mg, 2 mmol, 2 eq), and potassium fluoride (29 mg, 0.5 mmol, 0.5 eq), then evacuated and backfilled with N_2 (x3). Upon addition of dioxane (3 mL), the palladium catalyst solution was added via canula and the solution was stirred at 130 °C for 48 hours. Upon cooling to room temperature the solution was filtered through a small pad of celite, washing with EtOAc and concentrated *in vacuo*. Purification by flash silica chromatography (45% EtOAc/ Hexanes) yielded **S3-8** as a golden oil (144 mg, 0.45 mmol, 45%).

^1H NMR (400 MHz, Chloroform-*d*) δ 10.49 (s, 1H), 8.22 (dd, $J = 4.5, 2.0$ Hz, 1H), 7.94 (dd, $J = 14.1, 8.1$ Hz, 1H), 7.88 – 7.83 (m, 1H), 4.32 – 4.15 (m, 4H), 1.35 (t, $J = 7.1$ Hz, 6H).

^{31}P NMR (162 MHz, Chloroform-*d*) δ 15.66.



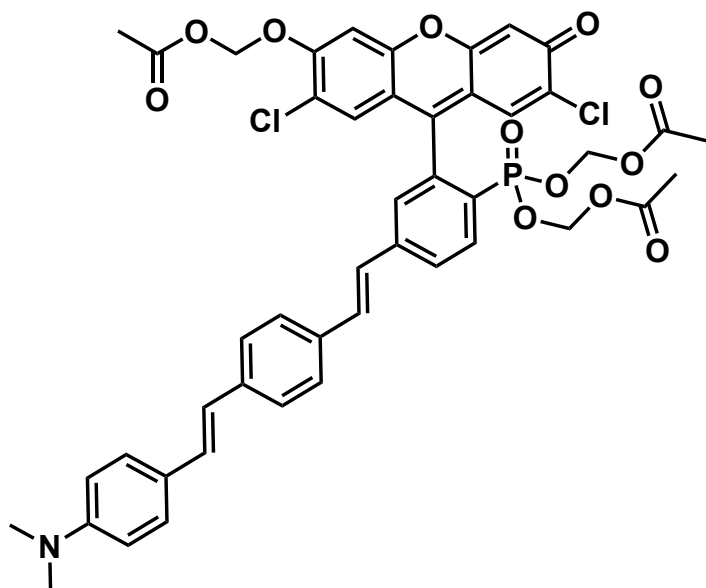
Synthesis of S3-9

7 (80 mg, 0.30 mmol, 1 eq), molecular wire (90 mg, 0.36 mmol, 1.2 eq), $\text{Pd}(\text{OAc})_2$ (3.4 mg, 0.015 mmol, 0.05 eq) and $\text{P}(o\text{-tol})_3$ (9.1 mg, 0.03 mmol, 0.1 eq) were charged into an over dried Schlenk

flask which was subsequently evacuated and backfilled with nitrogen (3x). DMF (0.5 mL) and NEt_3 (0.5 mL) were added and the reaction stirred at 110°C for 2.5 hrs. Upon cooling to room temperature, the suspension was concentrated in vacuo to an orange solid that was triturated with DCM. Vacuum filtration yielded the triethylammonium salt of **S3-9** as a bright orange solid (116 mg, 0.22 mmol, 73%).

^1H NMR (500 MHz, Methanol- d_4 + <1% NaOD) δ 11.06 (s, 1H), 8.35 (d, J = 12.3 Hz, 1H), 7.90 (dd, J = 8.0, 3.5 Hz, 1H), 7.57 (d, J = 8.4 Hz, 3H), 7.51 (d, J = 8.4 Hz, 2H), 7.43 (d, J = 8.8 Hz, 2H), 7.39 (d, J = 16.3 Hz, 1H), 7.25 (d, J = 16.3 Hz, 1H), 7.12 (d, J = 16.3 Hz, 1H), 6.95 (d, J = 16.2 Hz, 1H), 6.77 (d, J = 8.8 Hz, 2H), 2.98 (s, 6H).

^{31}P NMR (202 MHz, Methanol- d_4 + <1% NaOD) δ 7.04.



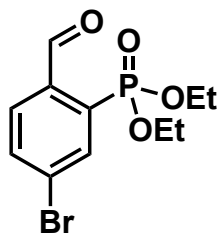
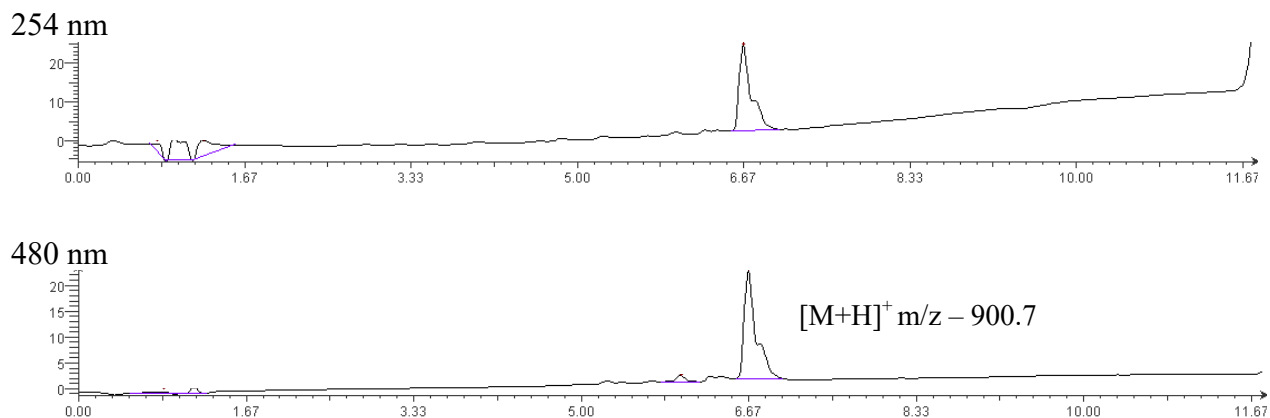
Synthesis of compound **S3-10**.

Iso phosVF2.1.Cl AM

Iso phosVF2.1.Cl, **12**, (10 mg, 0.015 mmol, 1 eq), Ag_2O (14 mg, 0.06 mmol, 4 eq) and 4 Å molecular sieves (15 mg) were charged into flame dried reaction vial, which was subsequently evacuated and backfilled with N_2 (x3). MeCN (1.2 mL) was added, and the suspension was stirred at room temperature for 1 hour. Upon heating to 50°C , bromomethyl acetate (10 μL , 0.09 mmol, 6 eq) was added and stirring was continued overnight. Upon cooling to room temperature, the suspension was diluted with DCM and filtered through a pad of celite. Concentration of the filtrate *in vacuo* followed by purification by flash silica chromatography (75% to 100% EtOAc/ Hexanes) yielded **S3-10** as an orange solid (6 mg, 0.007 mmol, 44%).

^1H NMR (400 MHz, Chloroform-*d*) δ 8.08 (dd, $J = 13.8, 7.7$ Hz, 1H), 7.88 – 7.77 (m, 1H), 7.49 (s, 3H), 7.44 – 7.40 (m, 2H), 7.27 (m, 5H), 7.18 – 7.05 (m, 3H), 7.04 – 6.99 (m, 1H), 6.90 (d, $J = 16.0$ Hz, 1H), 6.71 (d, $J = 8.6$ Hz, 1H), 6.62 (s, 1H), 5.93 (s, 2H), 5.53 – 5.42 (m, 2H), 5.40 – 5.24 (m, 2H), 3.17 (s, 6H), 2.19 (m, 3H), 2.11 – 1.98 (m, 6H).

HR-ESI-MS m/z for $\text{C}_{46}\text{H}_{40}\text{O}_{12}\text{N}_1\text{Cl}_2\text{Na}_1\text{P}_1$ $[\text{M}+\text{Na}]^+$ calcd:922.1557 found: 922.1555



Synthesis of compound **S3-11**

Note this is an adapted synthesis of **5**, but with acetal deprotection in the work up.

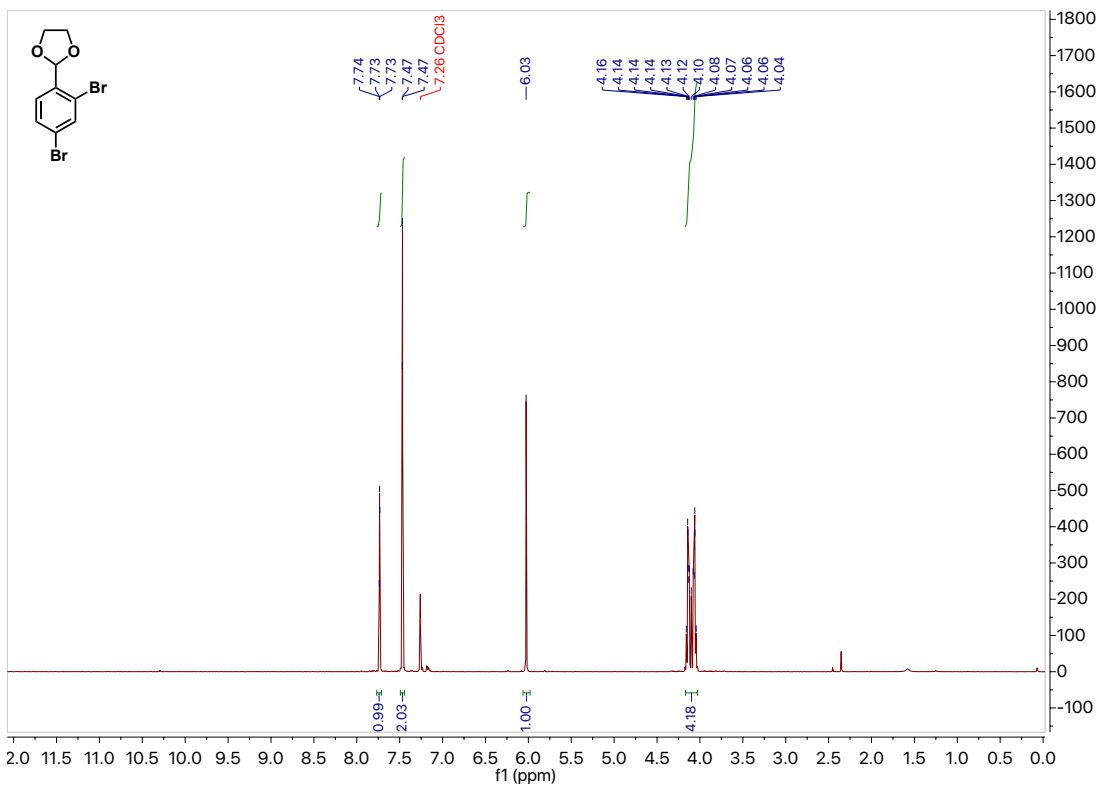
A solution of **3** (1.0 g, 3.25 mmol) in dry THF (10 mL) was cooled to -78°C under nitrogen. Whilst stirring, *n*-butyllithium (2M in cyclohexane, 1.9 mL, 3.74 mmol, 1.15 eq) was added dropwise via syringe and the solution stirred at -78°C for 30 mins. Diethyl chlorophosphate (0.94 mL, 6.5 mmol, 2 eq) was added dropwise and the solution stirred at -78°C for 1 hour, before warming to room temperature. After another hour of stirring, the reaction was quenched with 1M HCl (10 mL), and stirred at room temperature for 3 hours. The solution was then extracted with DCM (3x) and dried over Na_2SO_4 . After concentrating in vacuo, the resulting oil was purified by flash column chromatography (30% EtOAc/Hexanes) to yield **S3-11** (604 mg, 1.88 mmol, 58%) as colorless oil.

^1H NMR (400 MHz, Chloroform-*d*) δ 10.59 (s, 1H), 8.21 (dd, $J = 14.4, 2.0$ Hz, 1H), 7.94 (dd, $J = 8.3, 5.5$ Hz, 1H), 7.88 – 7.78 (m, 1H), 4.26 – 4.09 (m, 4H), 1.34 (t, $J = 7.1$ Hz, 6H).

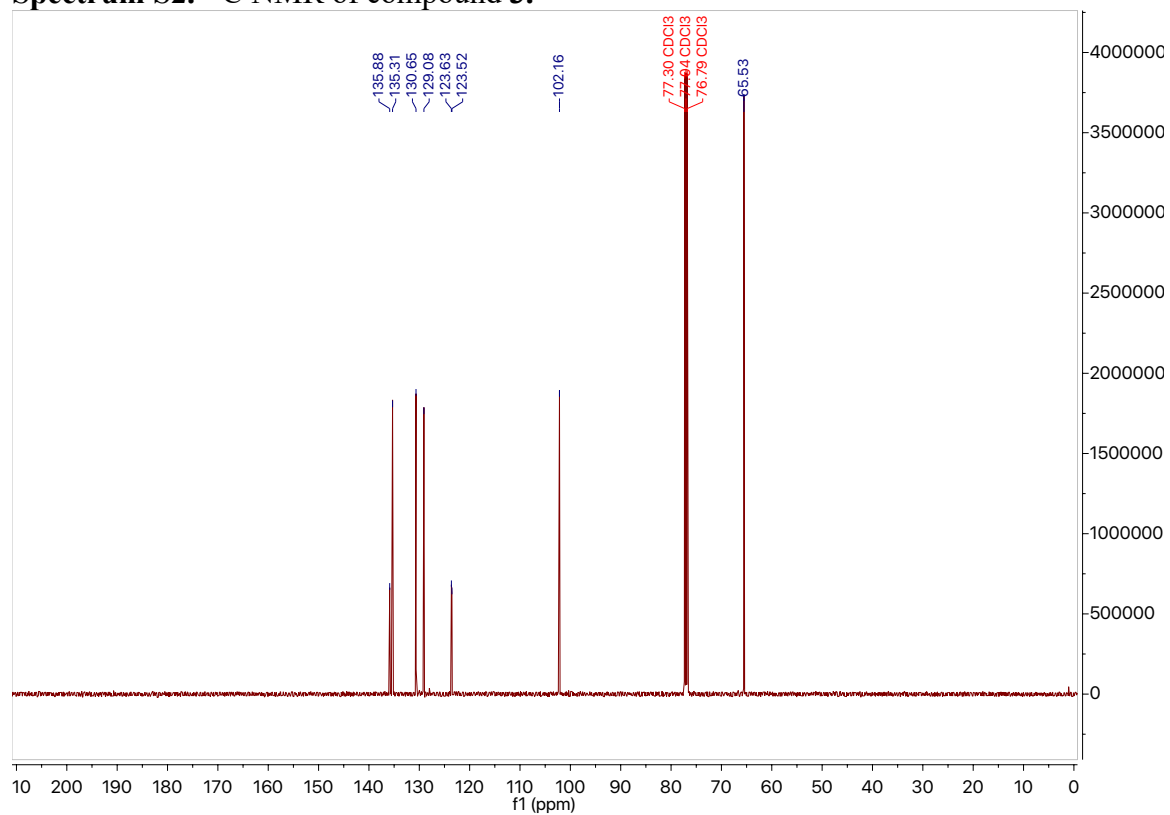
^{31}P NMR (162 MHz, Chloroform-*d*) δ 14.19.

Spectra of compounds

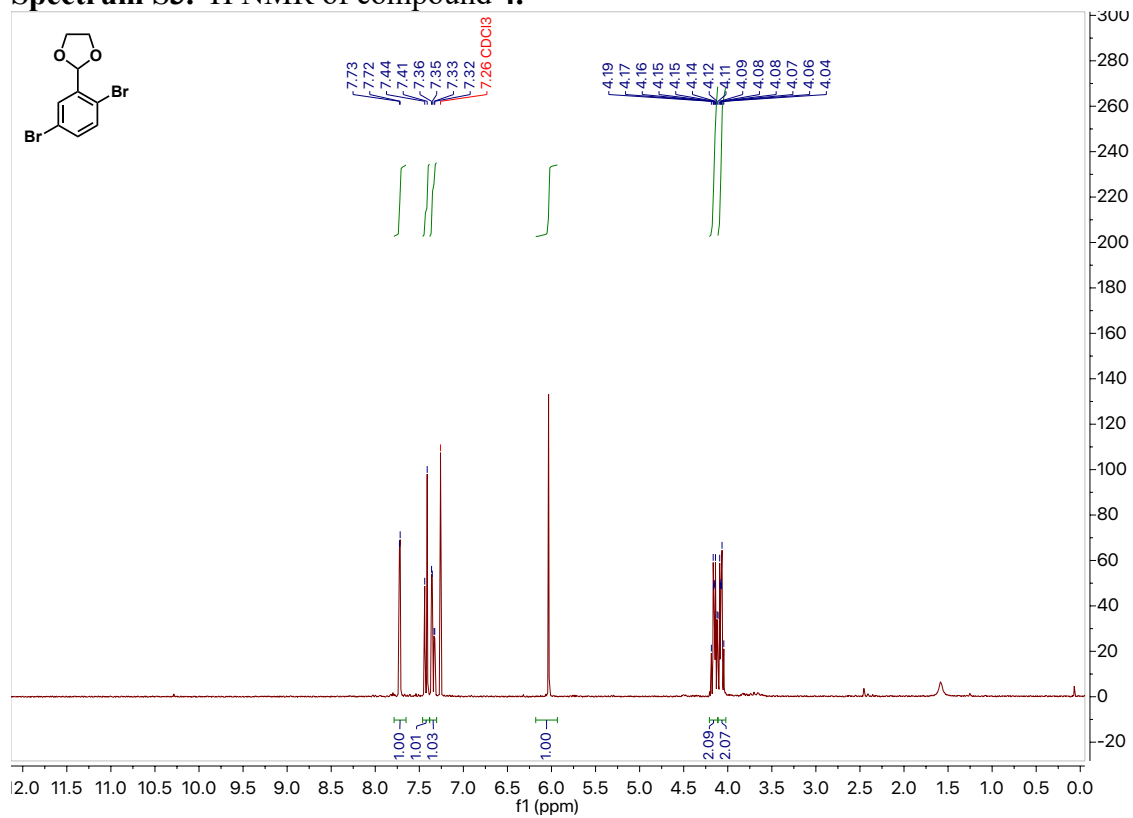
Spectrum S1. ^1H NMR of compound **3**.



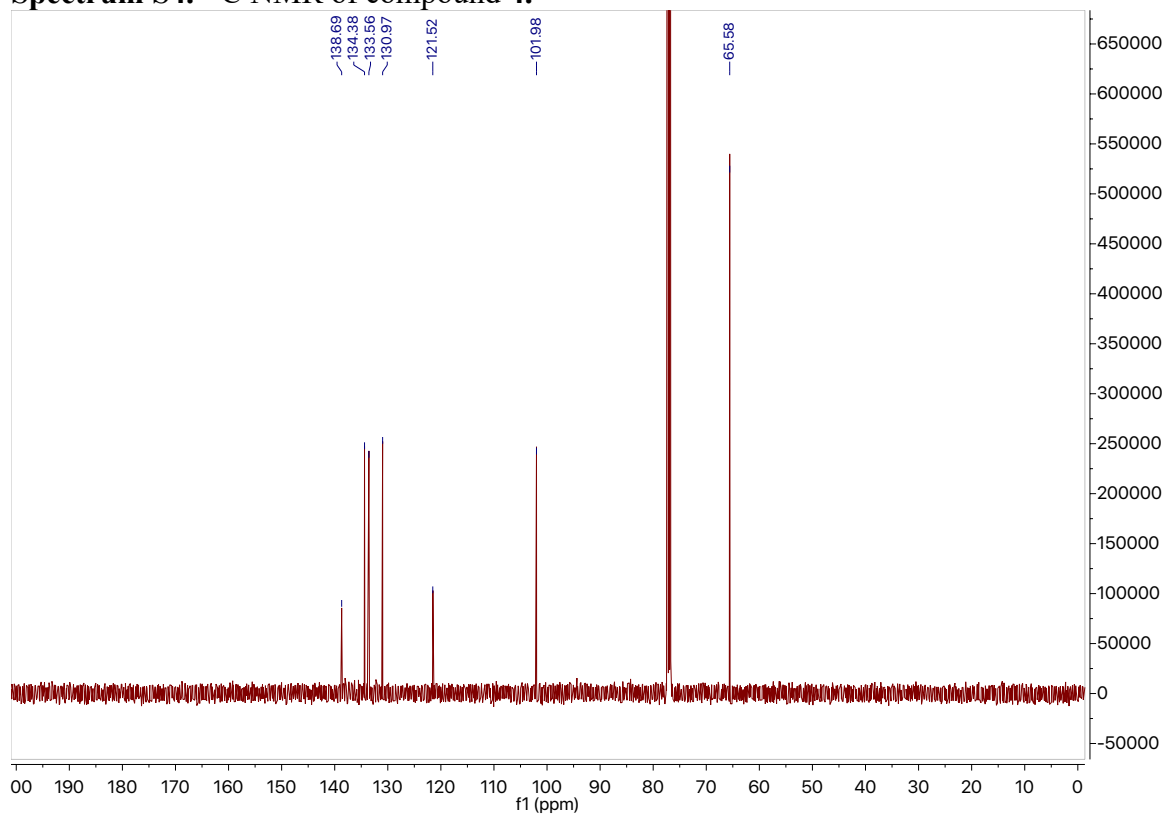
Spectrum S2. ^{13}C NMR of compound **3**.



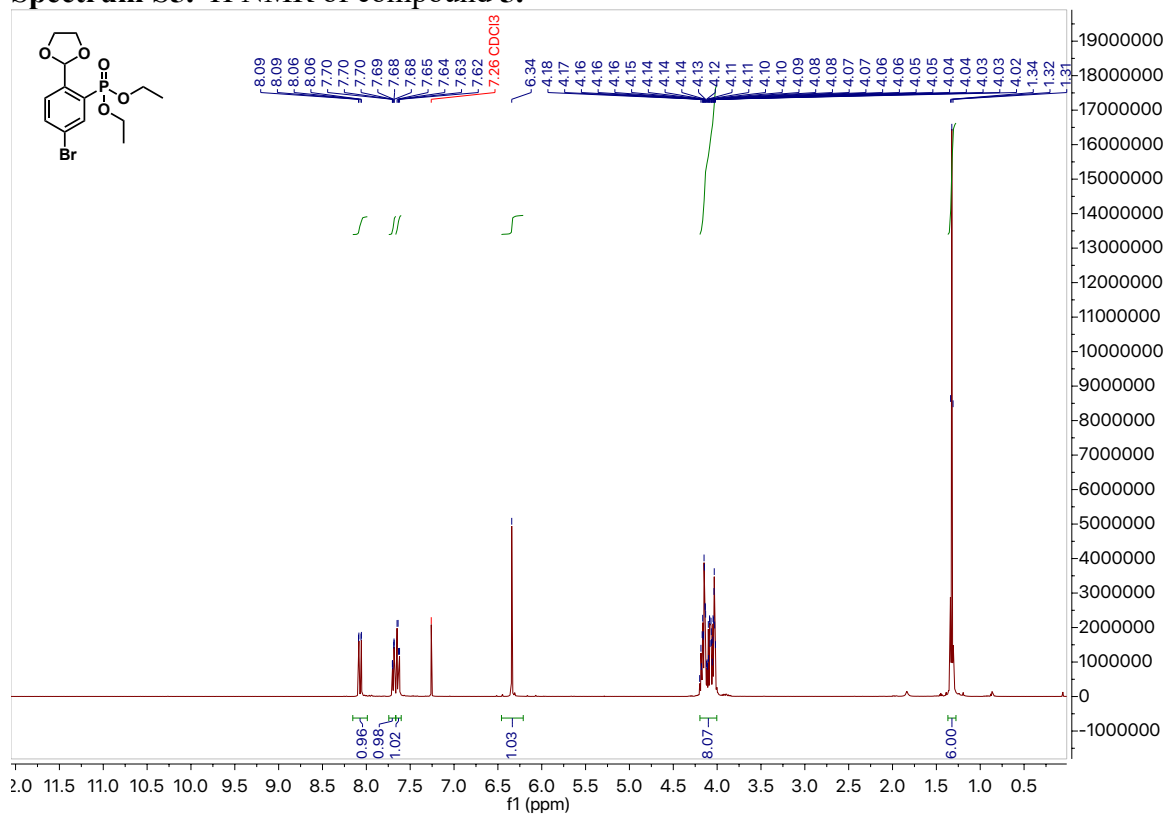
Spectrum S3. ¹H NMR of compound 4.



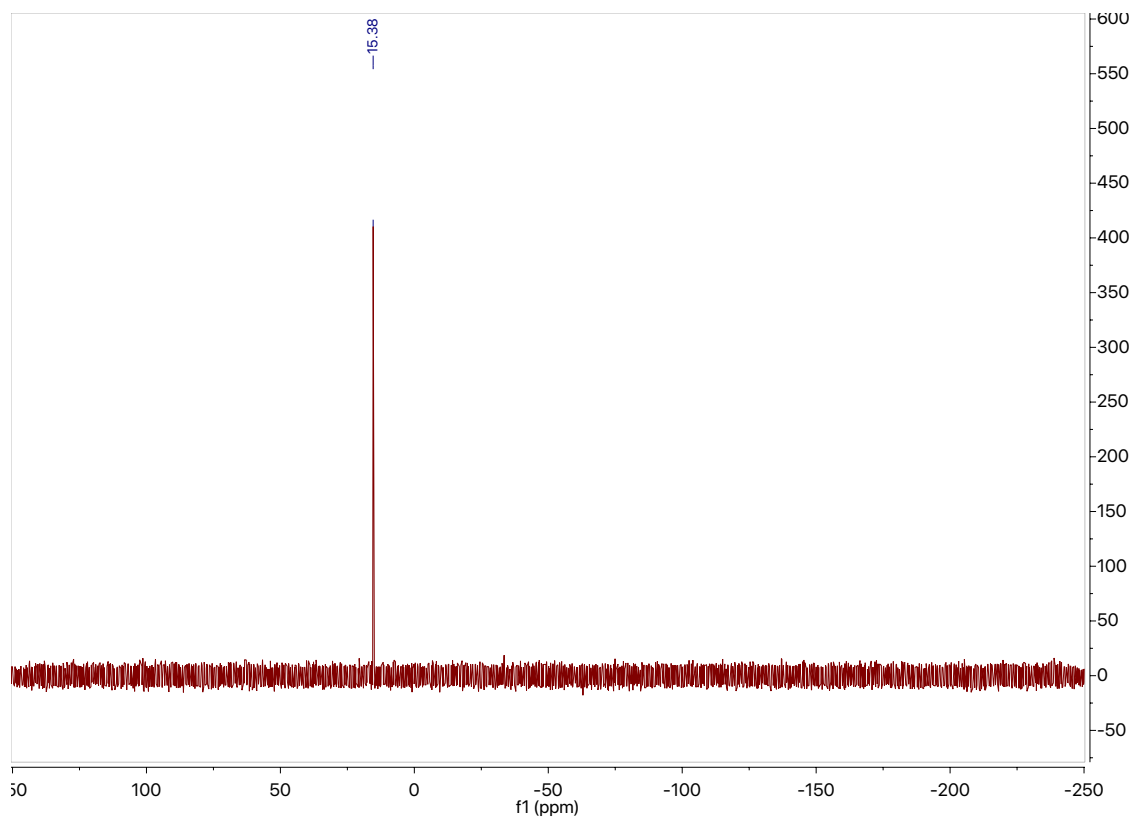
Spectrum S4. ¹³C NMR of compound 4.



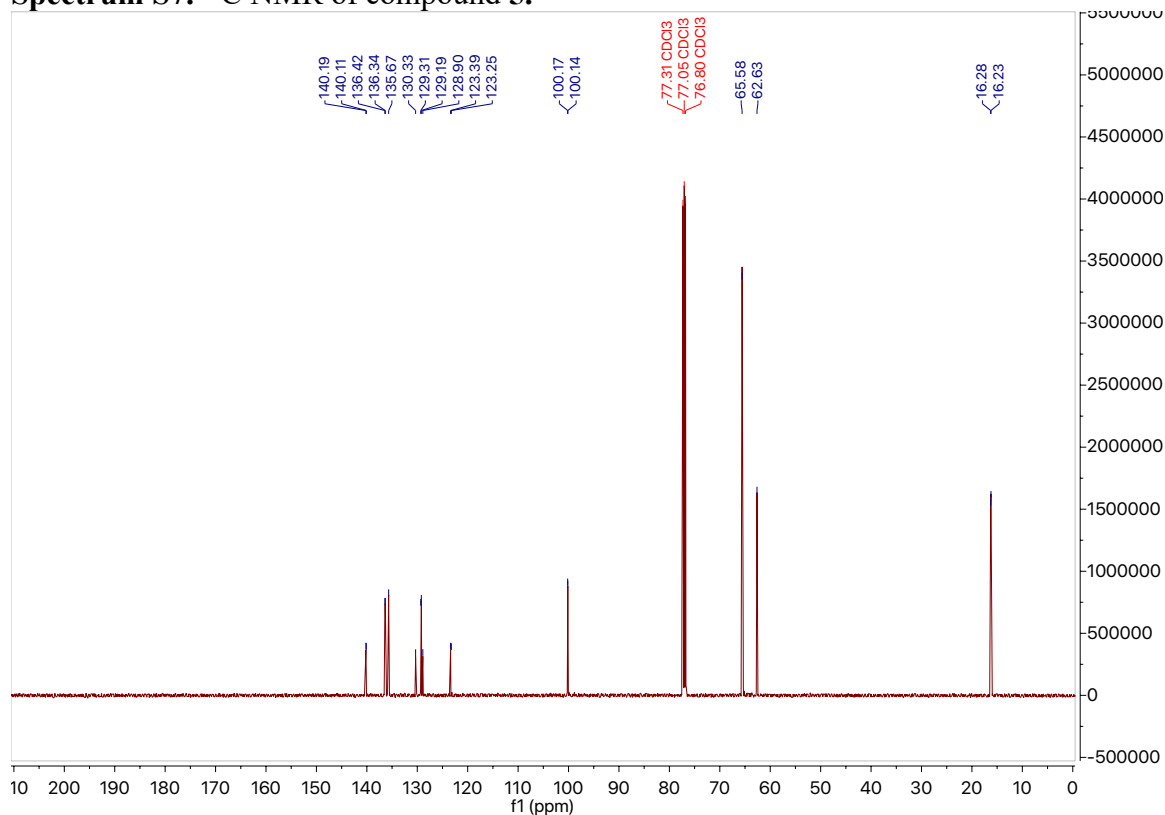
Spectrum S5. ^1H NMR of compound **5**.



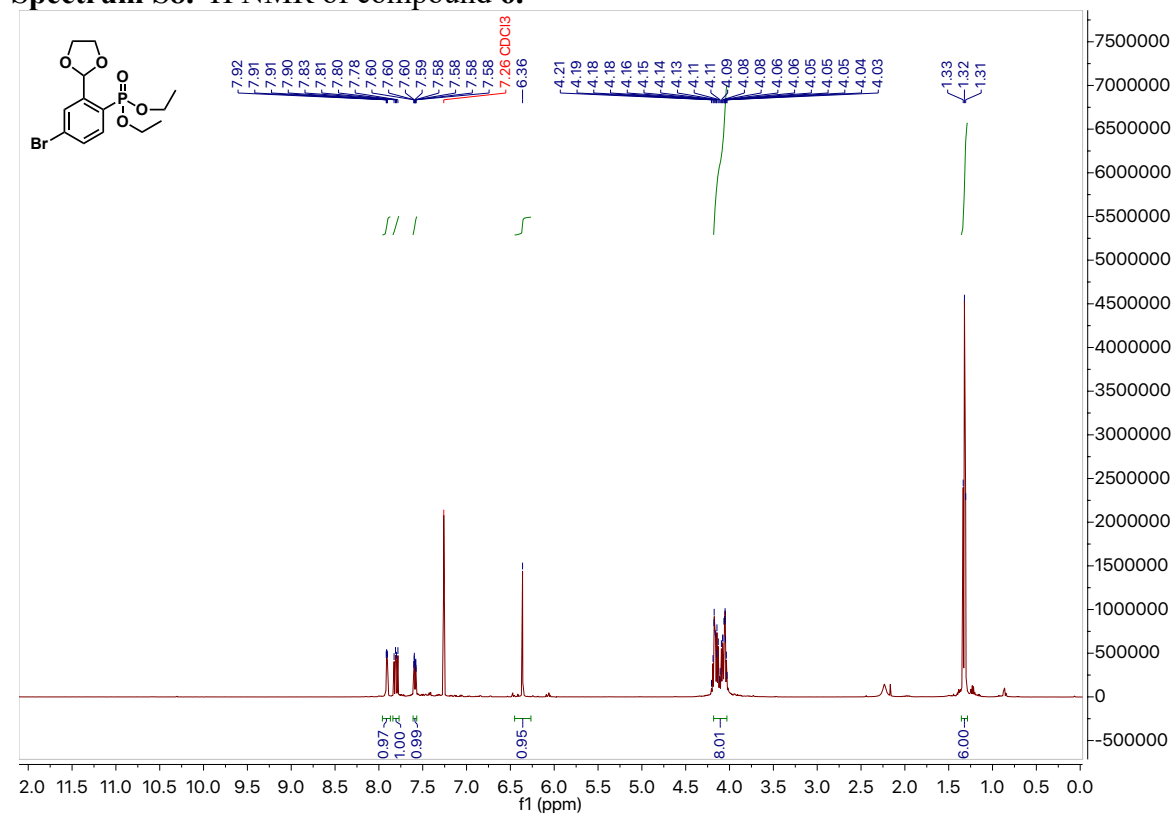
Spectrum S6. ^{31}P NMR of compound **5**.



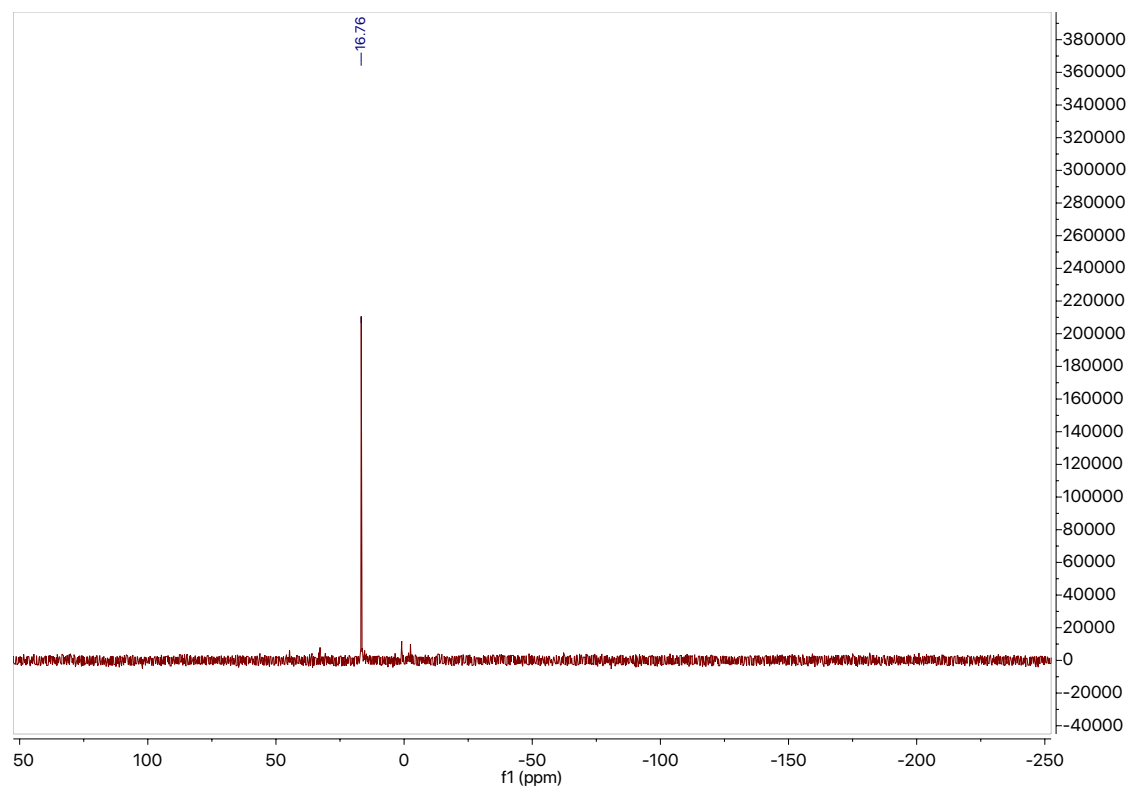
Spectrum S7. ¹³C NMR of compound 5.



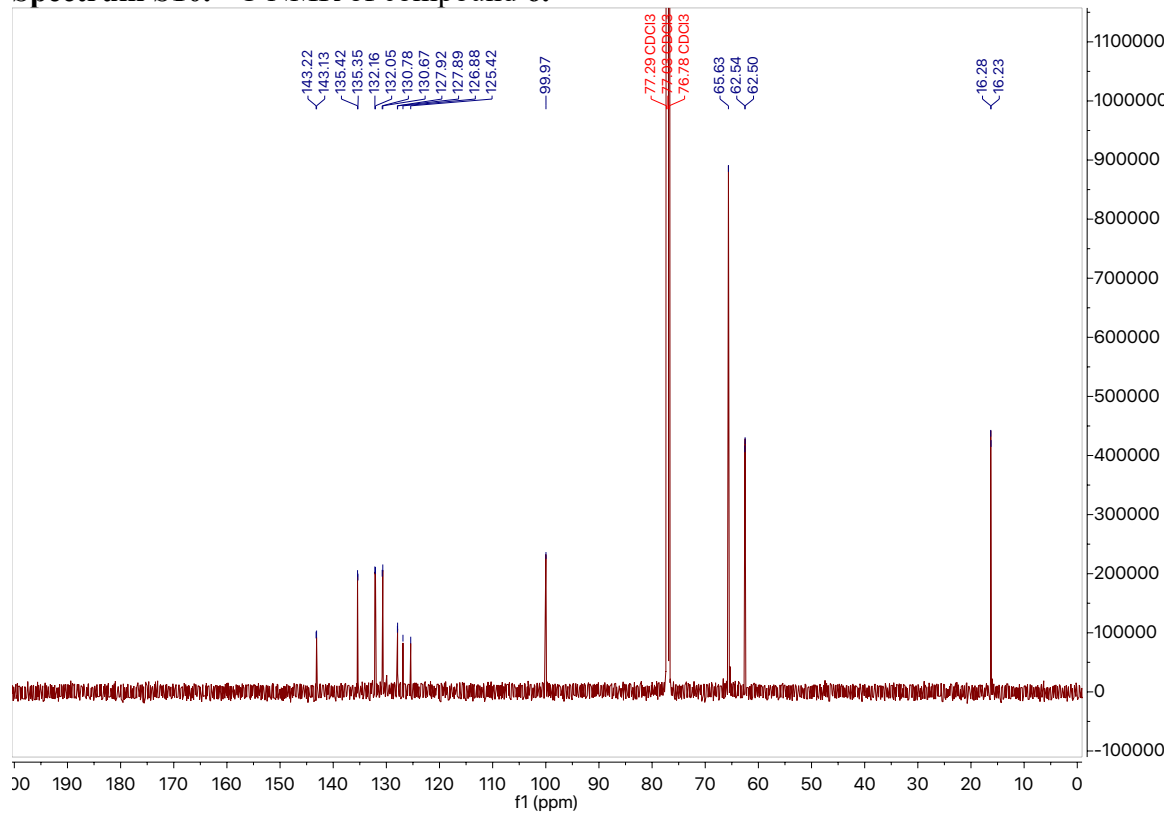
Spectrum S8. ¹H NMR of compound 6.



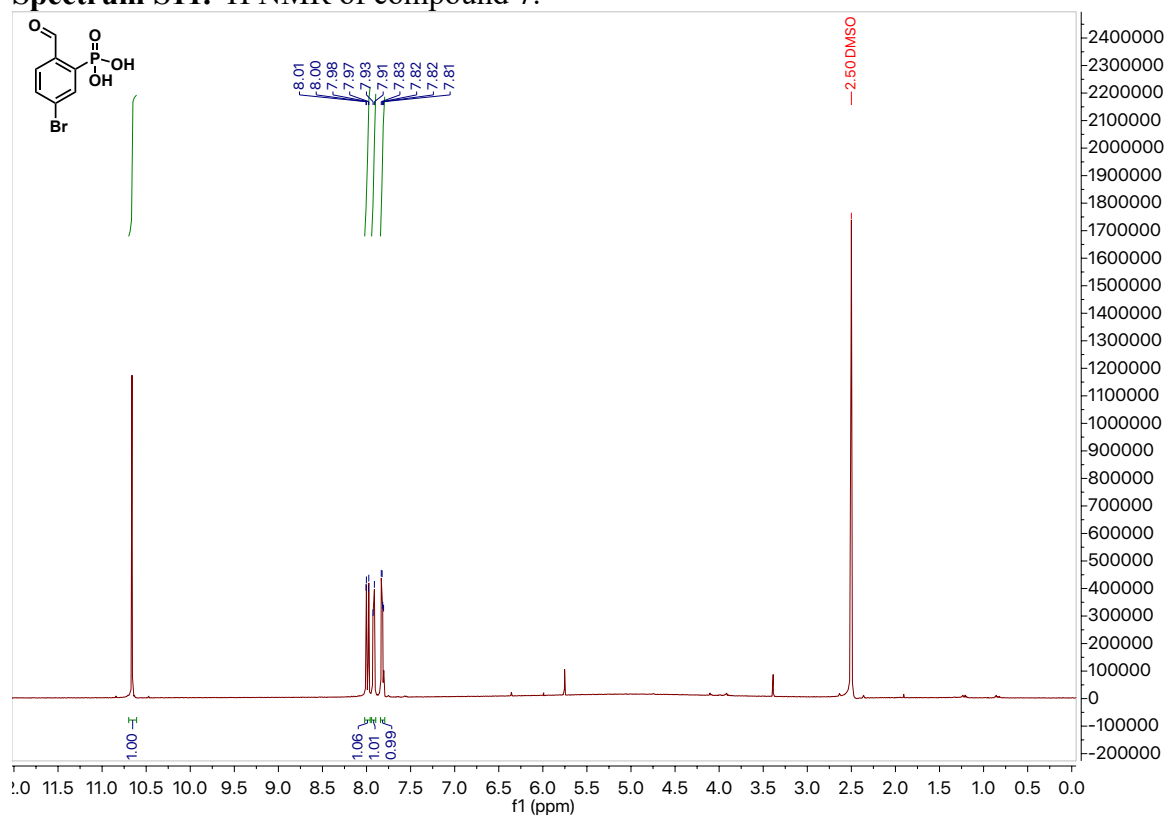
Spectrum S9. ^{31}P NMR of compound 6.



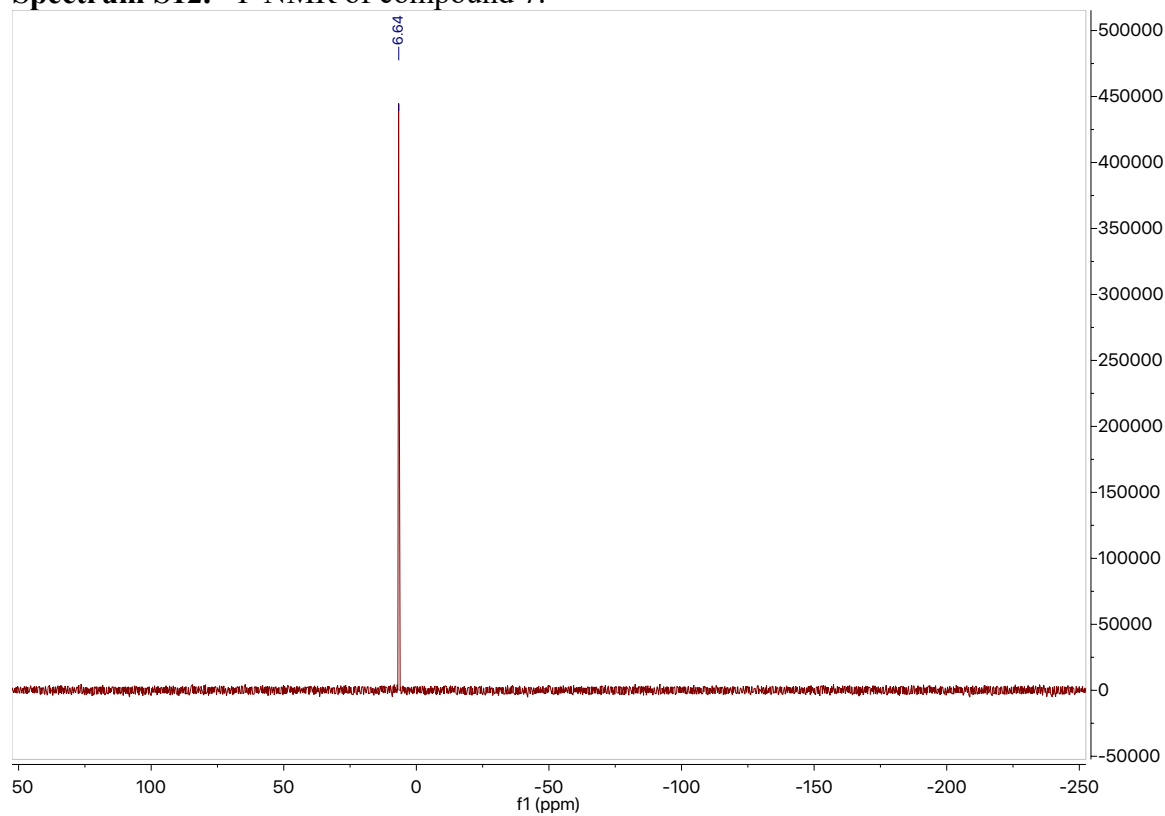
Spectrum S10. ^{13}C NMR of compound 6.



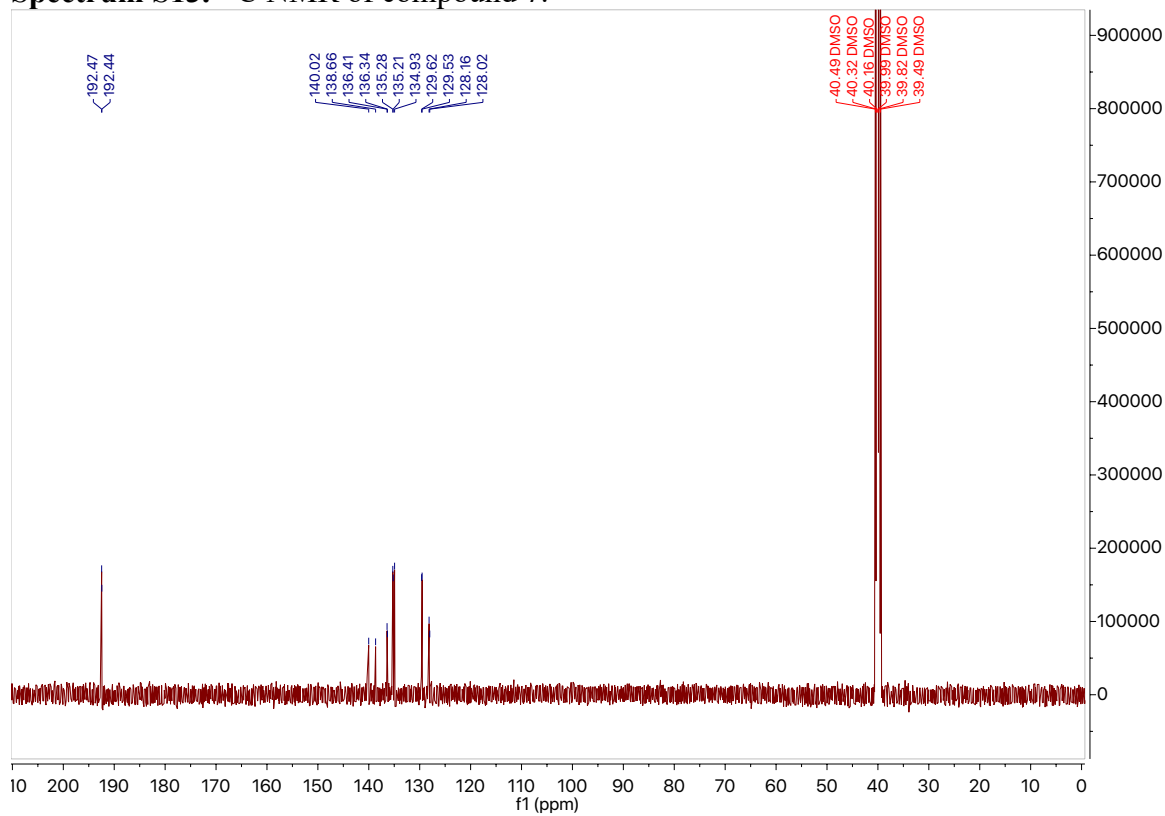
Spectrum S11. ^1H NMR of compound 7.



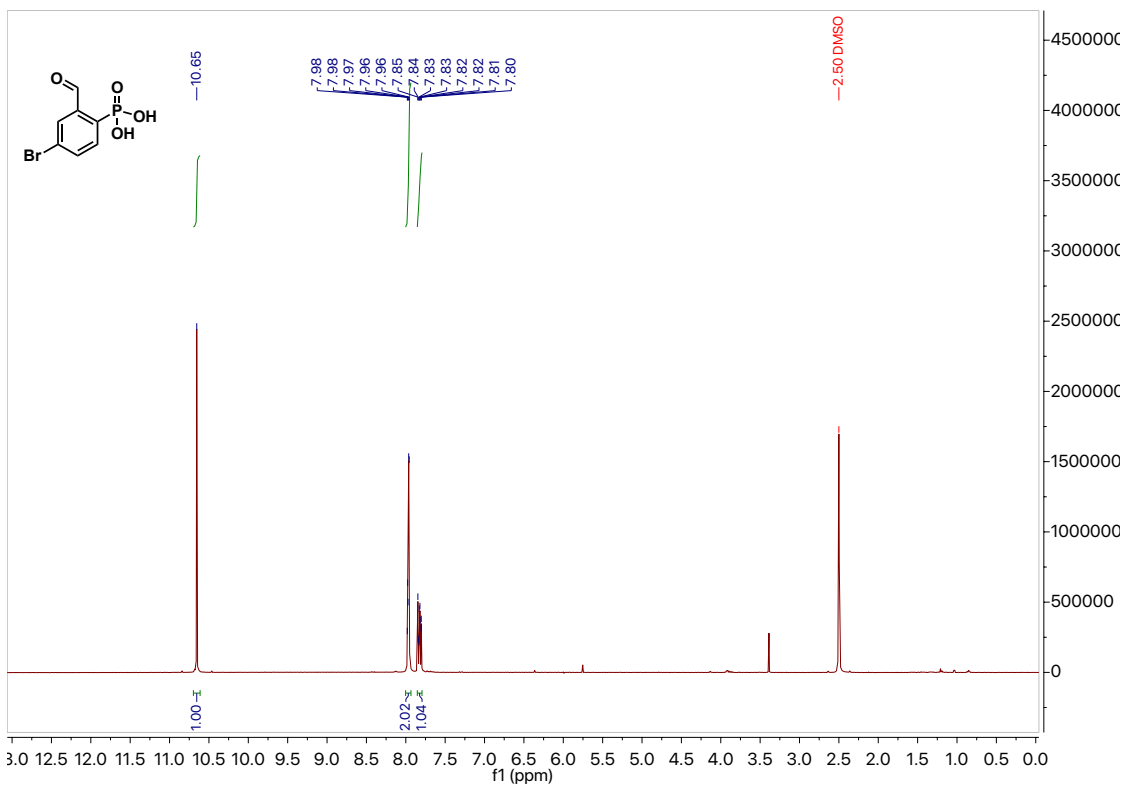
Spectrum S12. ^{31}P NMR of compound 7.



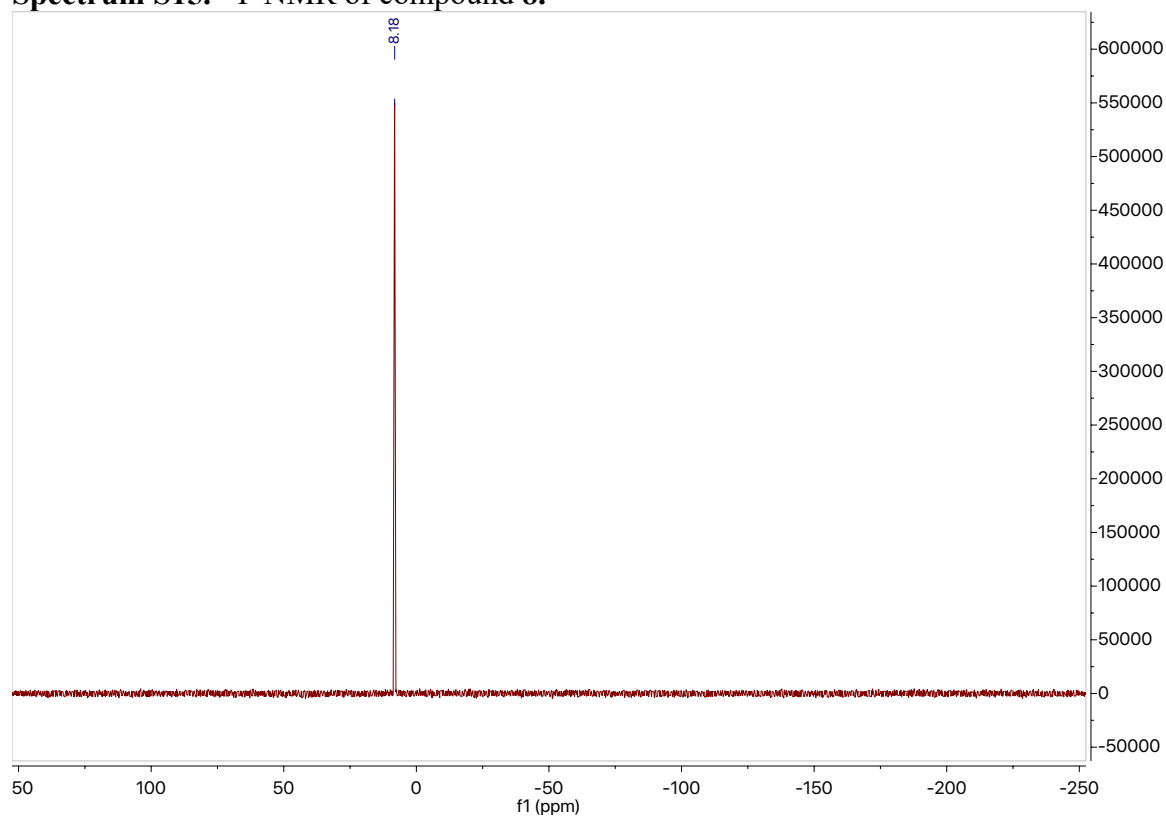
Spectrum S13. ^{13}C NMR of compound 7.



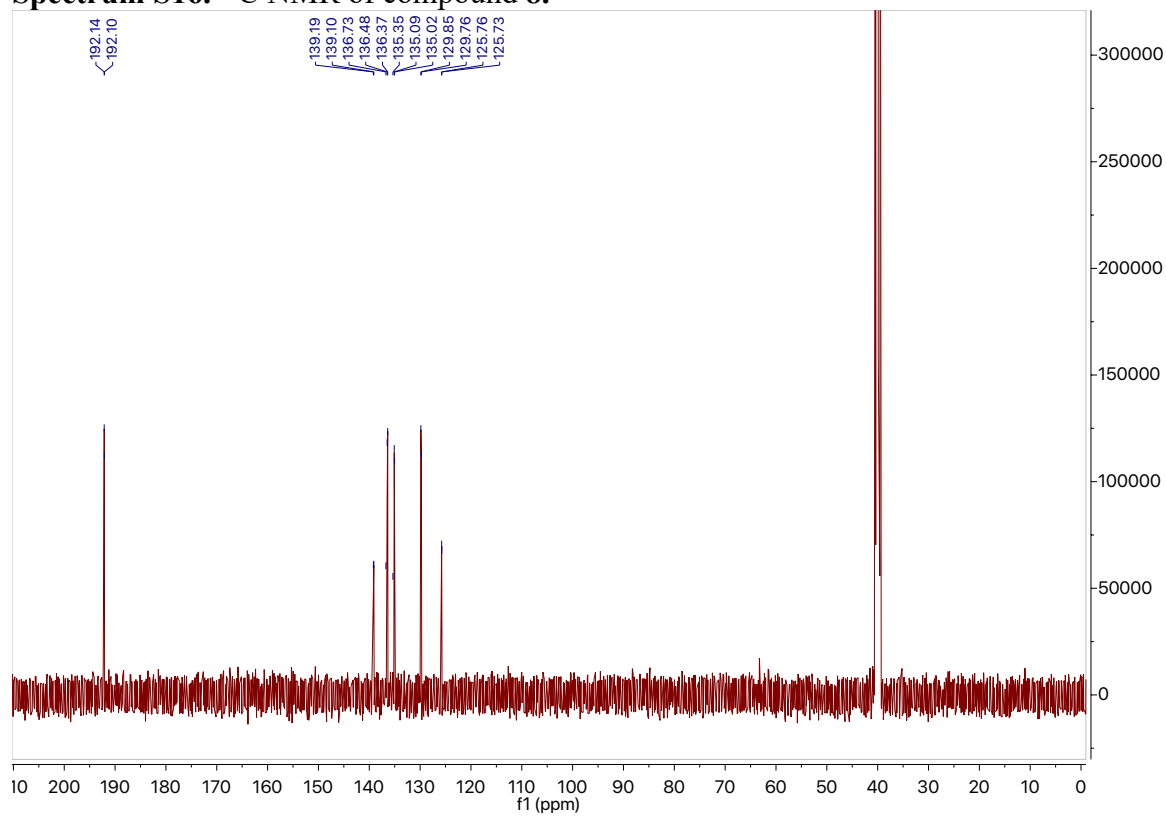
Spectrum S14. ^1H NMR of compound 8.



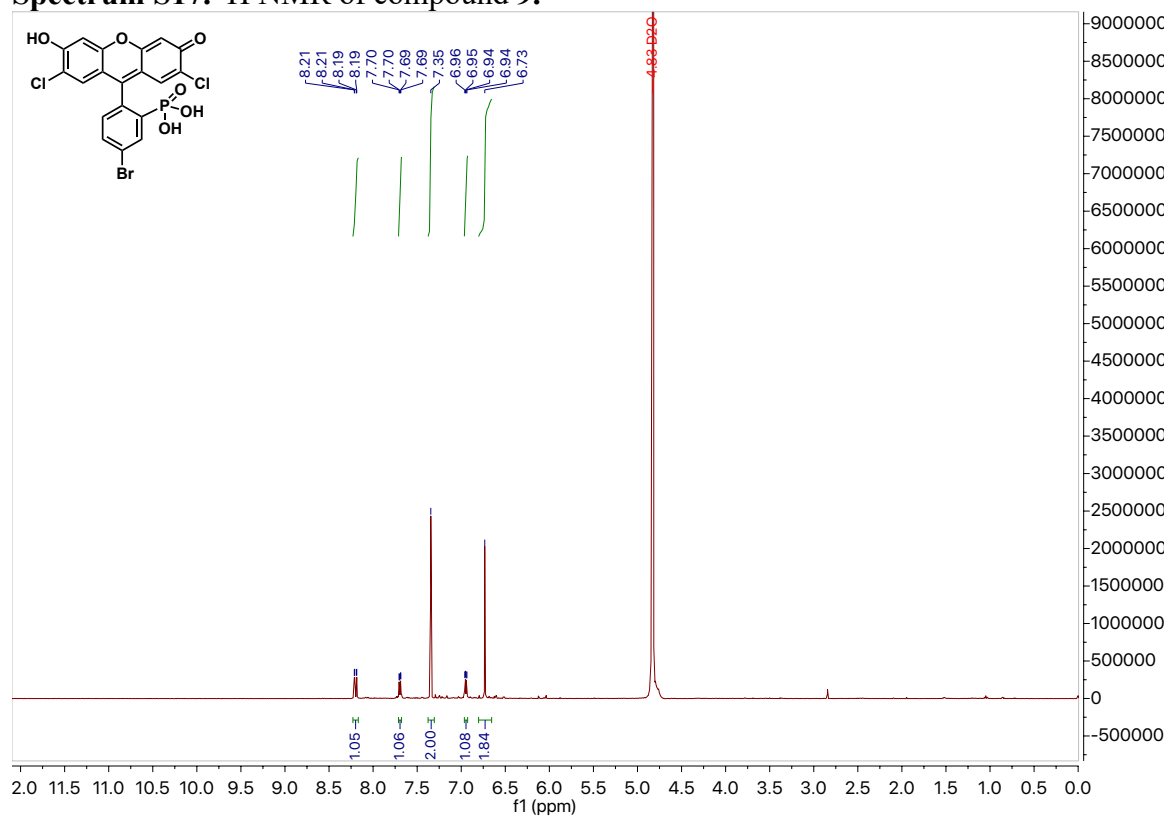
Spectrum S15. ^{31}P NMR of compound **8**.



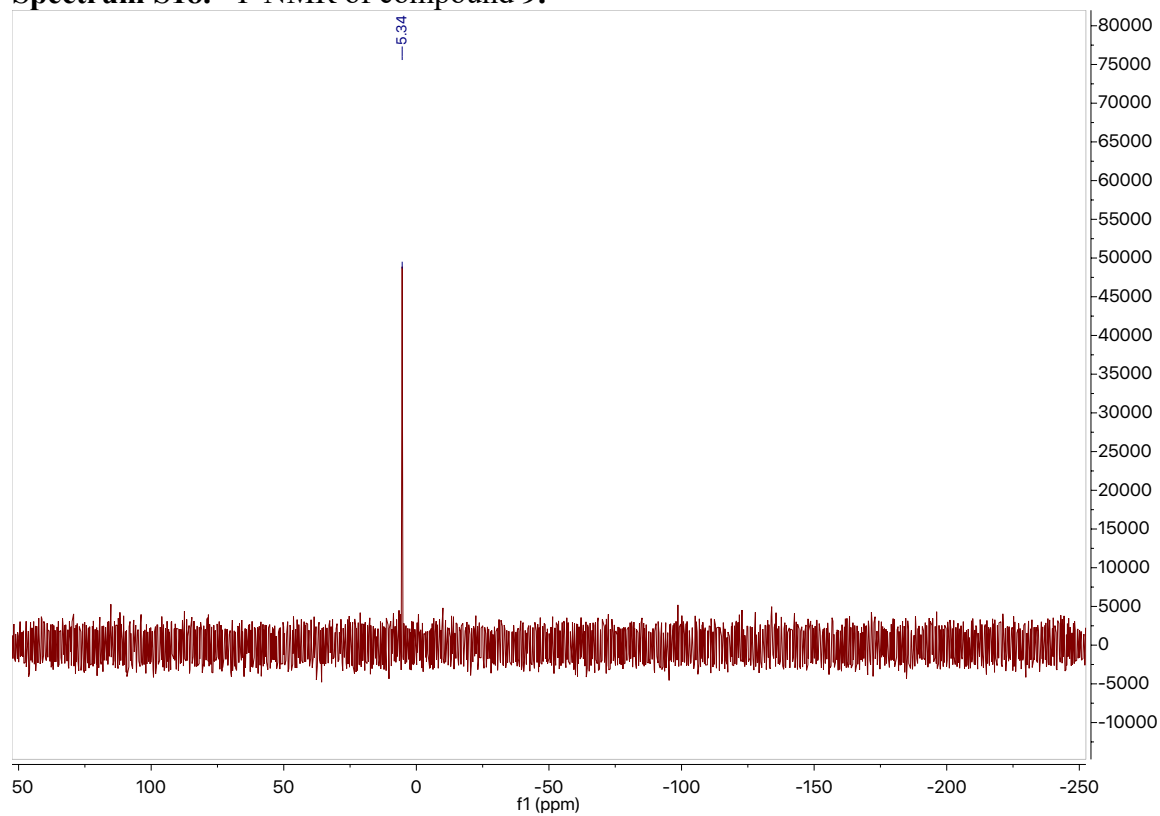
Spectrum S16. ^{13}C NMR of compound **8**.



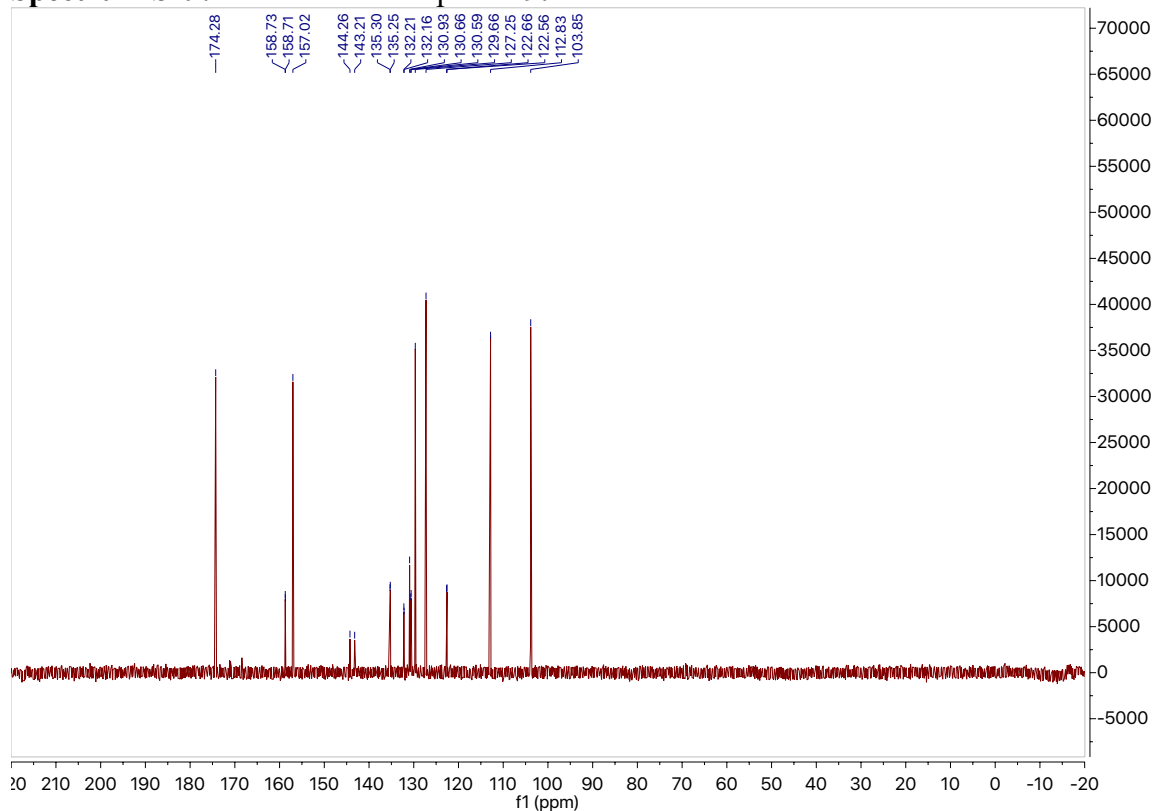
Spectrum S17. ^1H NMR of compound **9**.



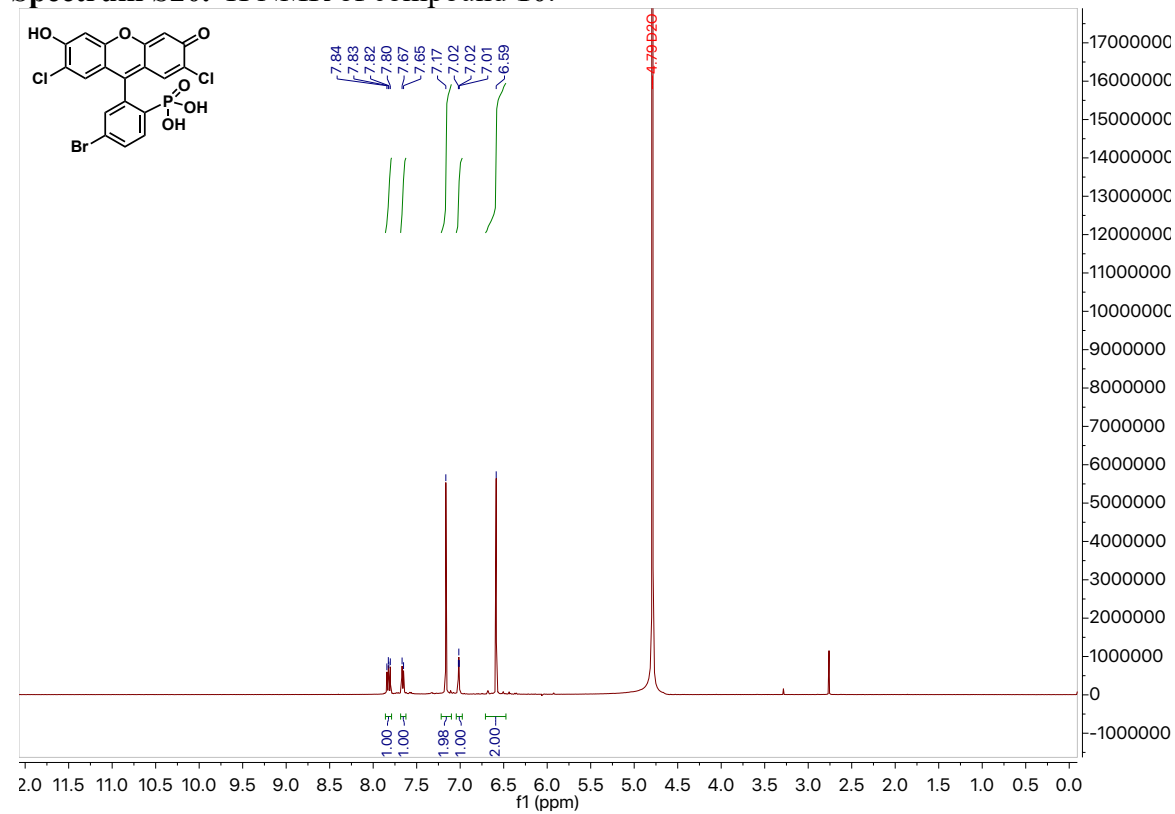
Spectrum S18. ^{31}P NMR of compound **9**.



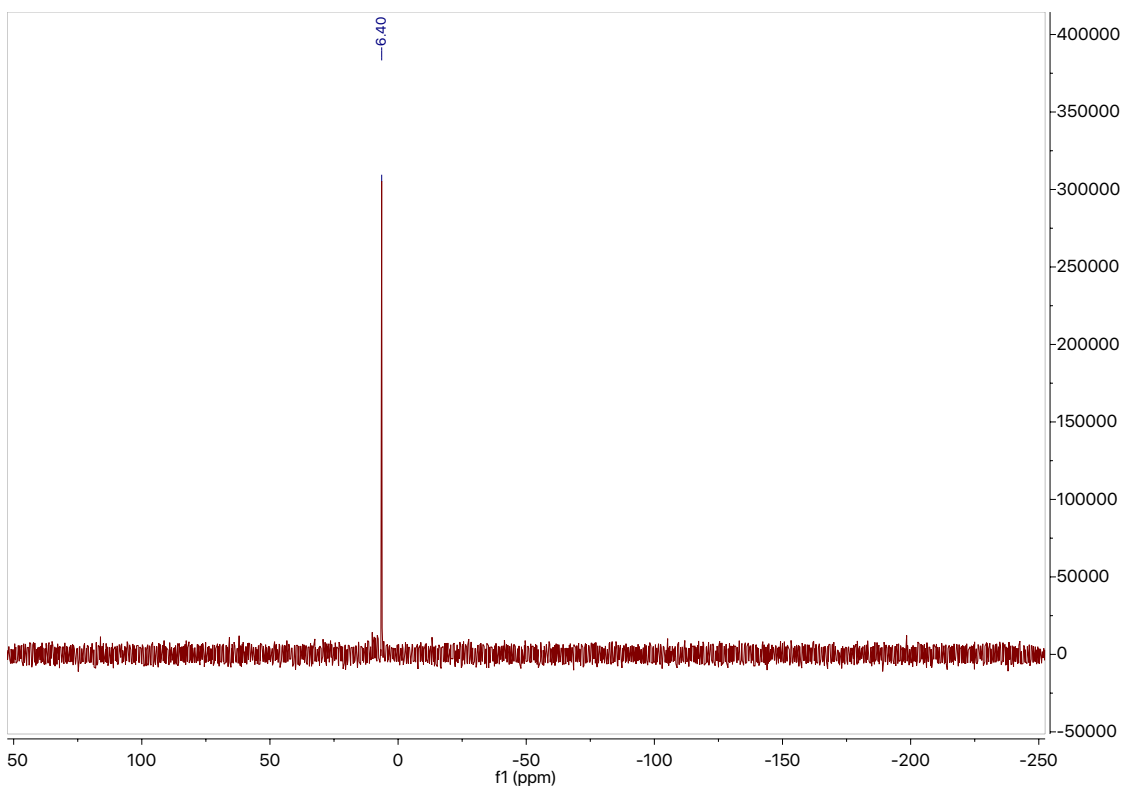
Spectrum S19. ^{13}C NMR of compound **9**.



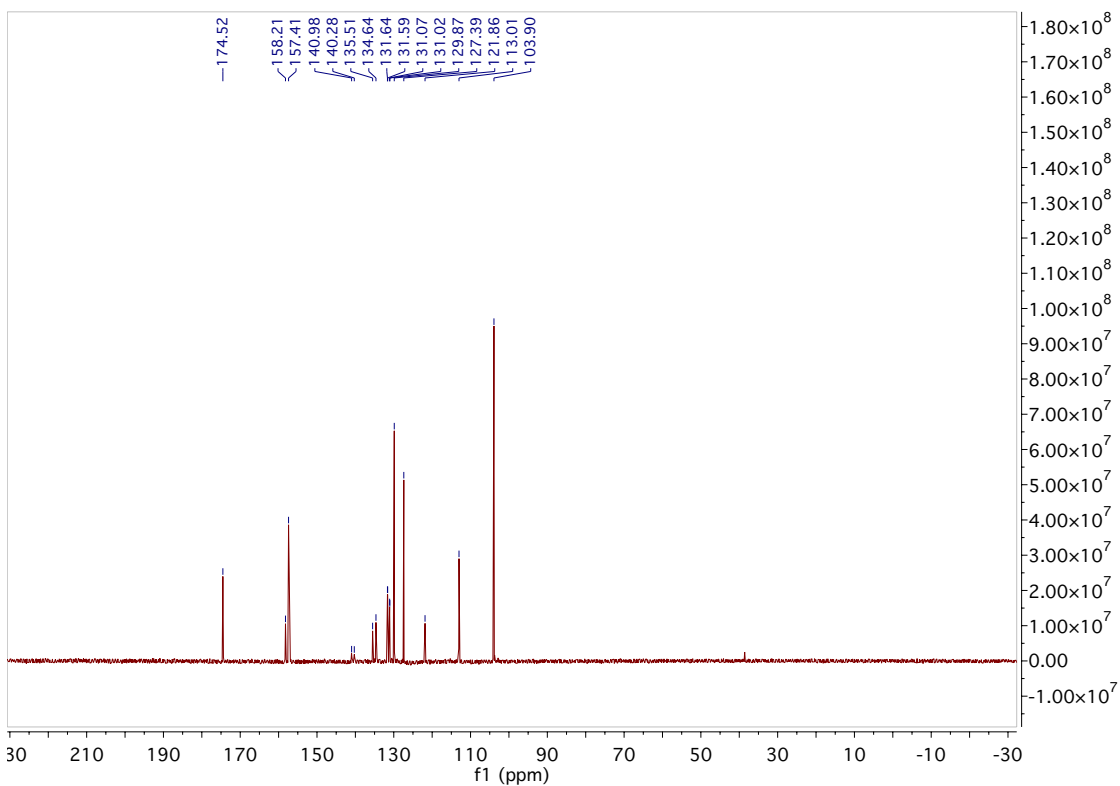
Spectrum S20. ^1H NMR of compound **10**.



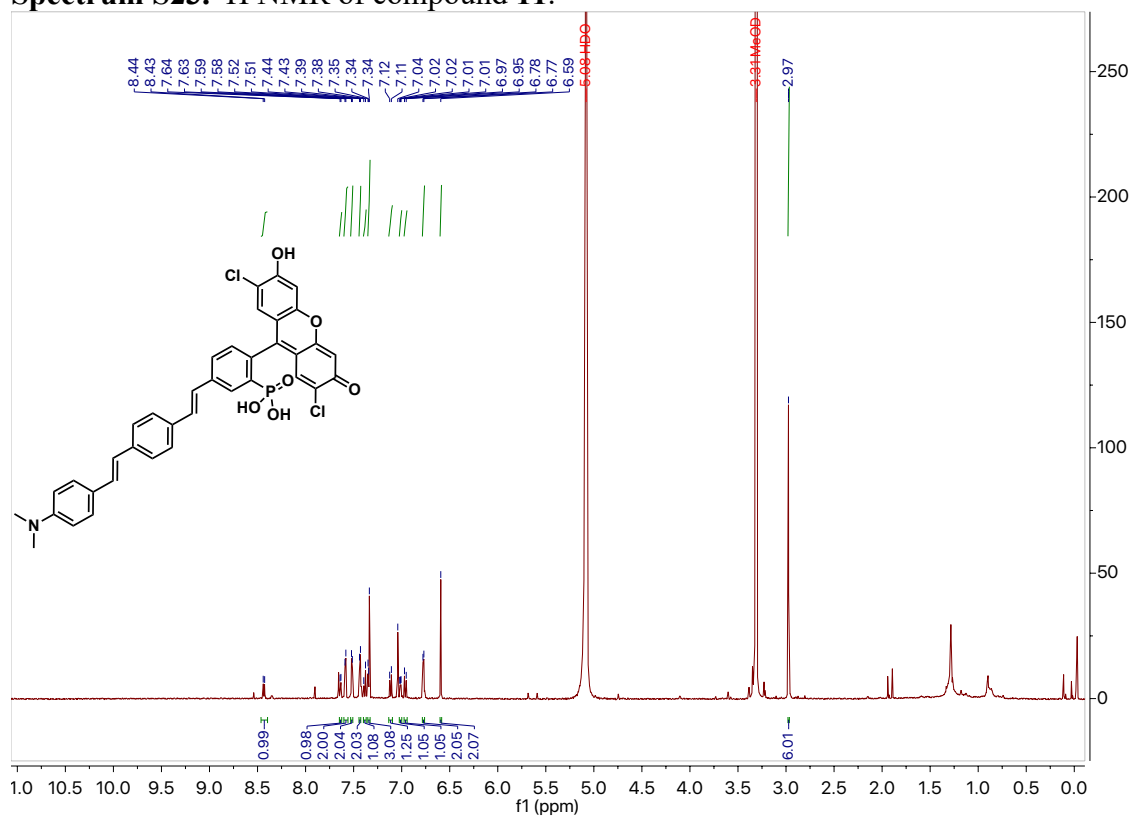
Spectrum S21. ^{31}P NMR of compound **10**.



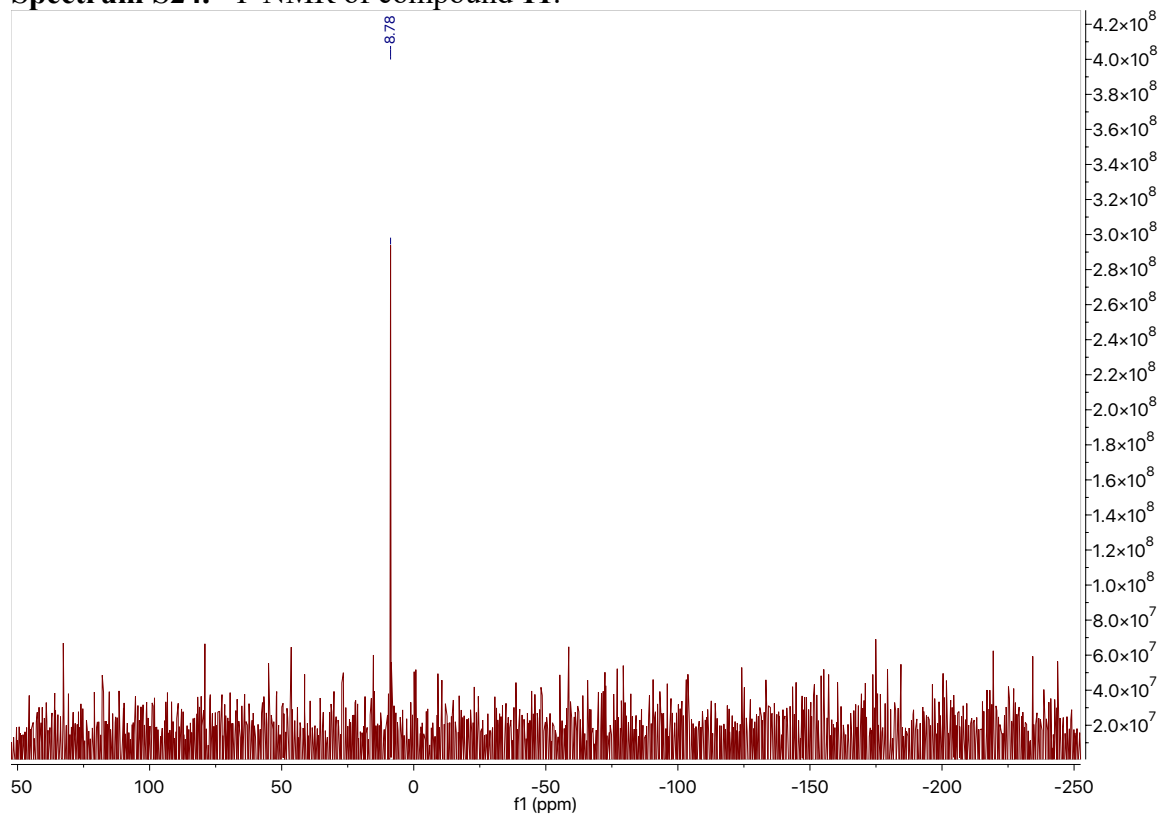
Spectrum S22. ^{13}C NMR of compound **10**.



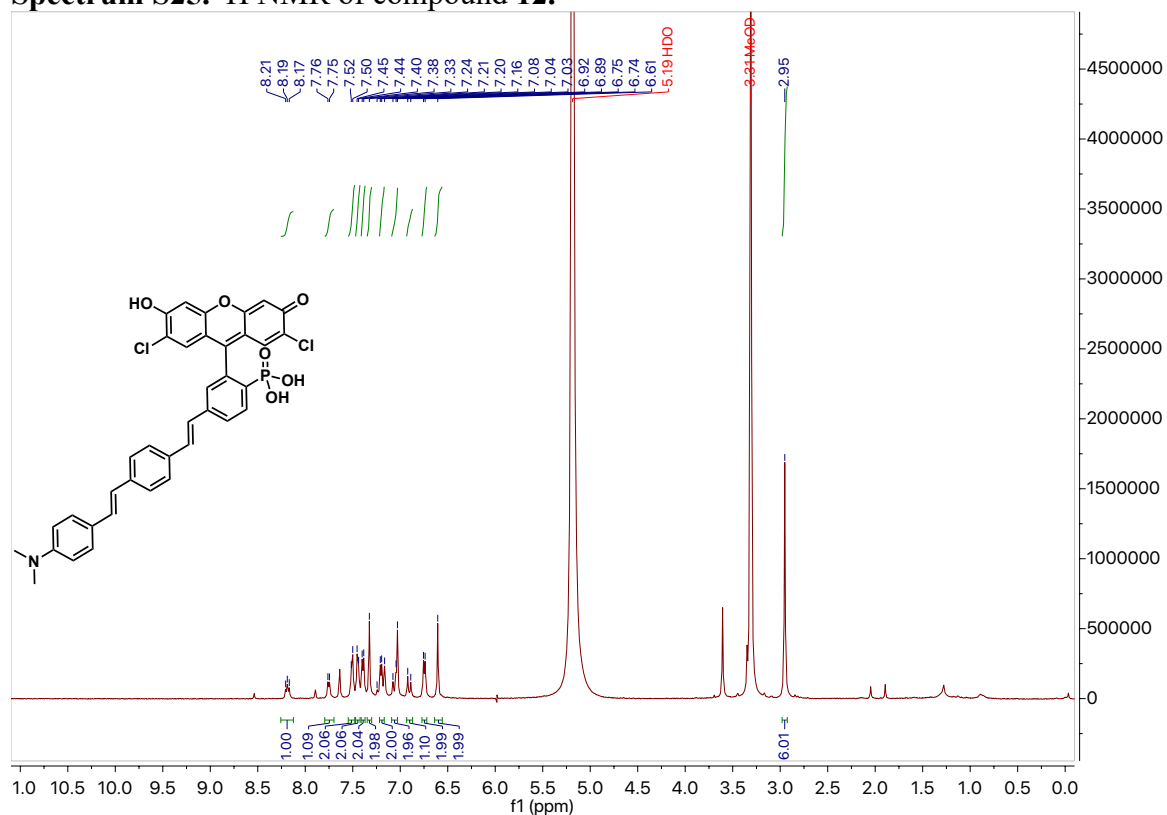
Spectrum S23. ¹H NMR of compound 11.



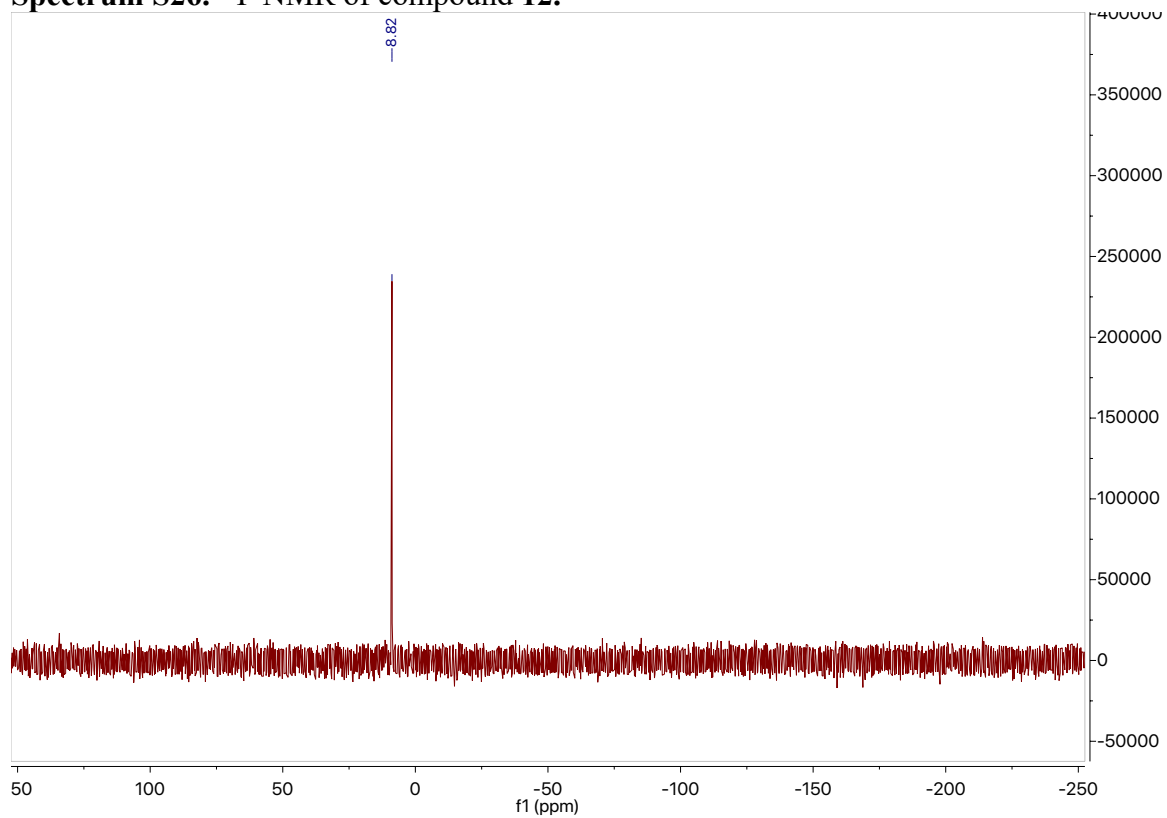
Spectrum S24. ³¹P NMR of compound 11.



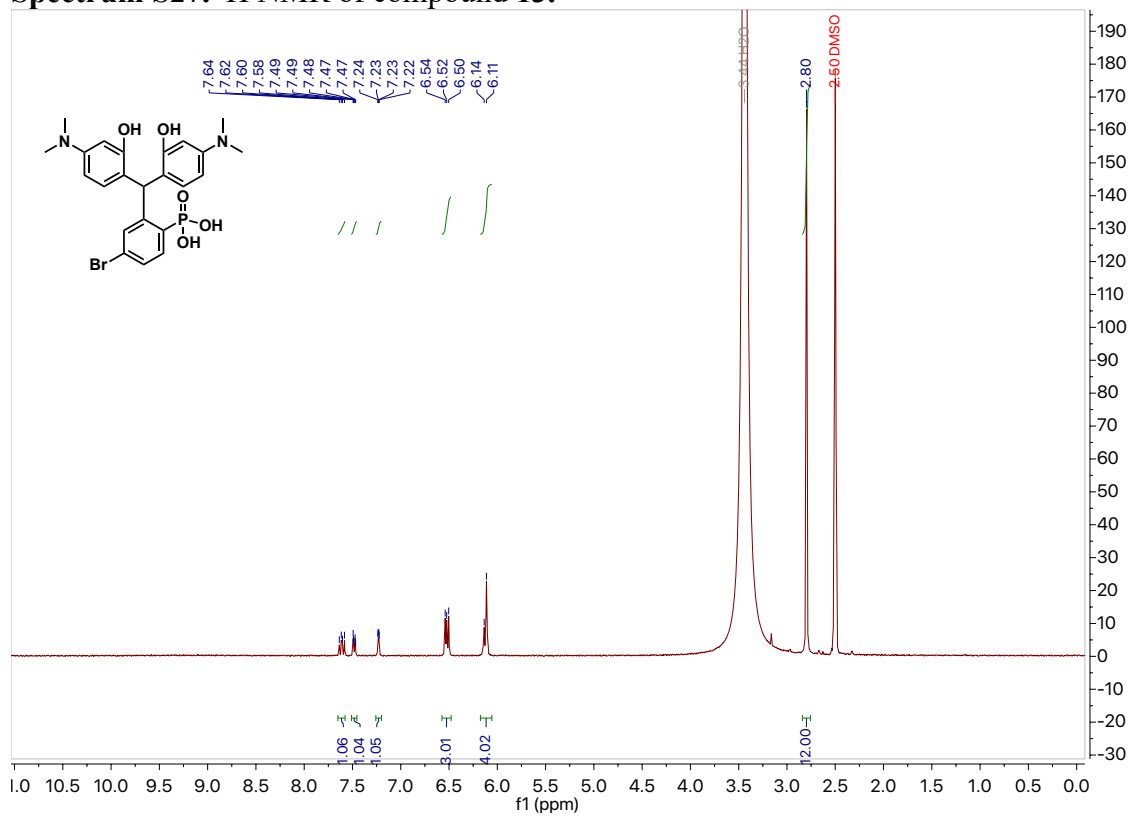
Spectrum S25. ¹H NMR of compound 12.



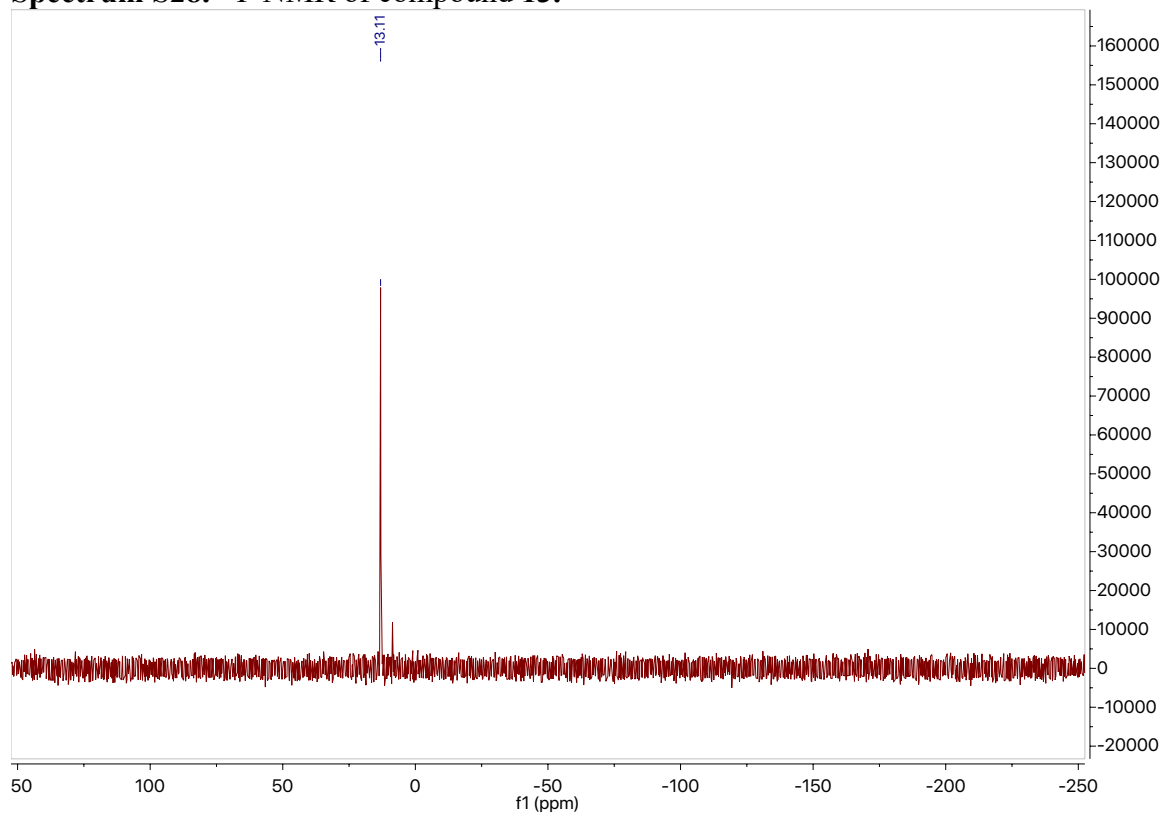
Spectrum S26. ³¹P NMR of compound 12.



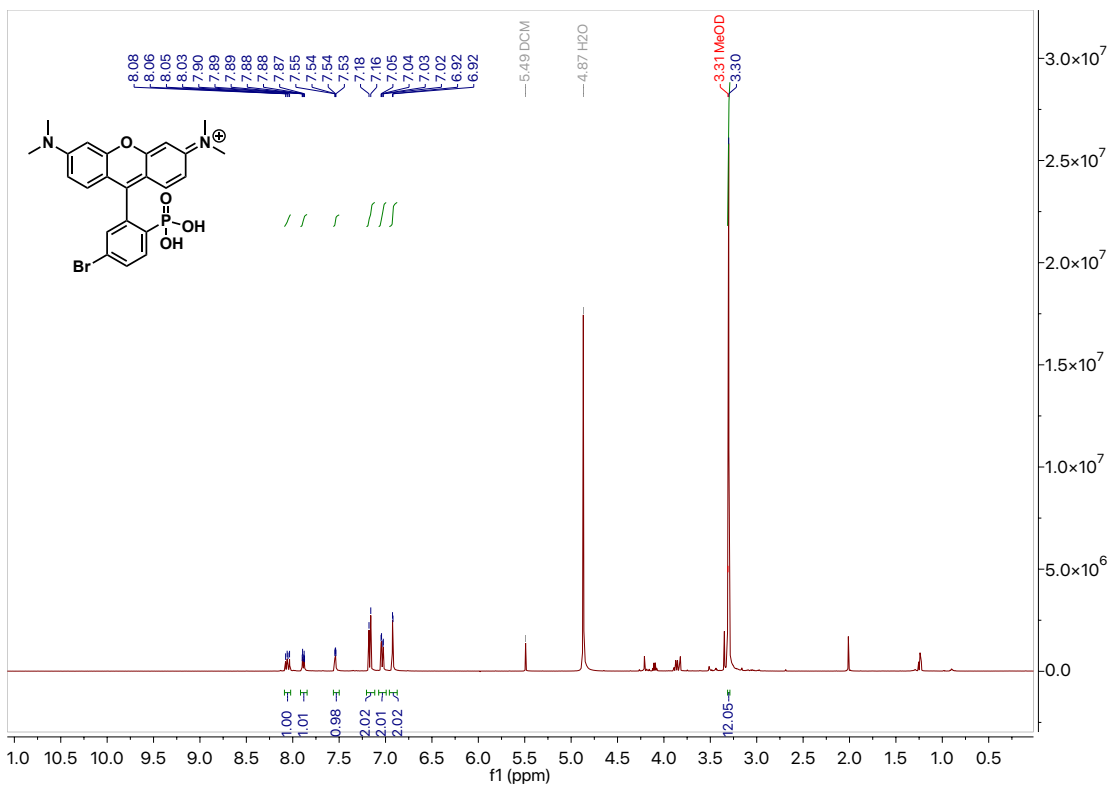
Spectrum S27. ¹H NMR of compound 13.



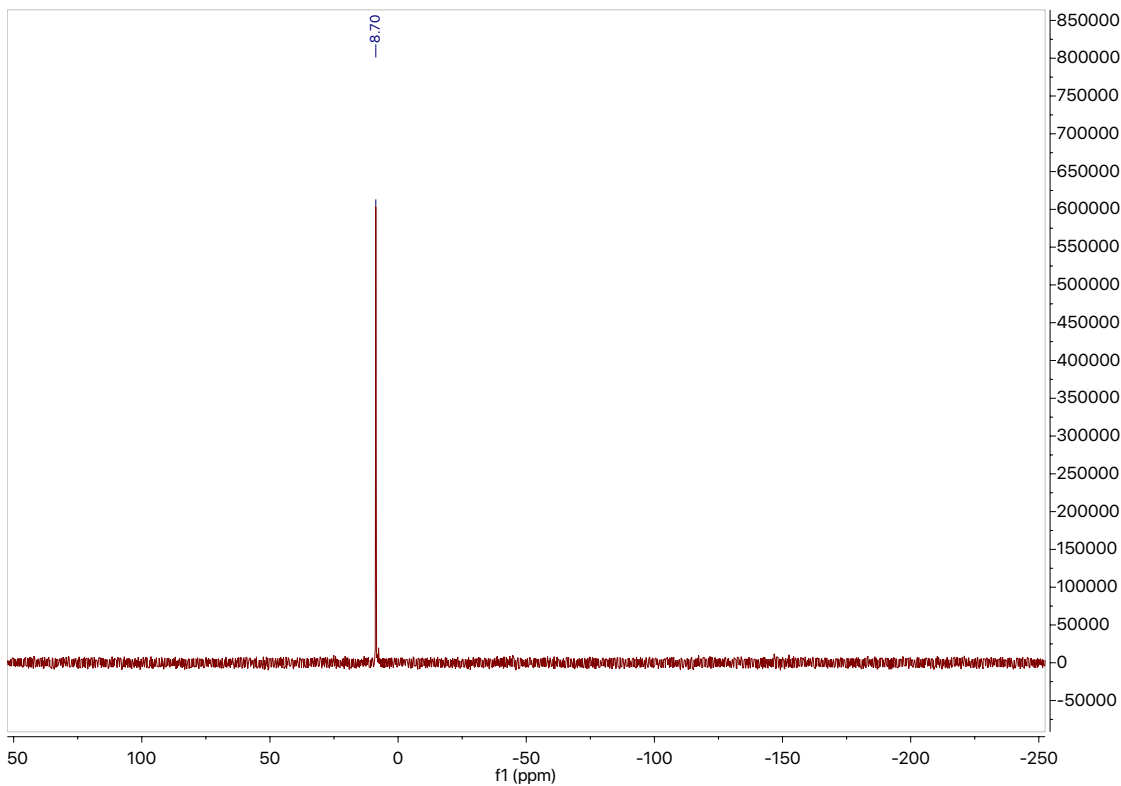
Spectrum S28. ³¹P NMR of compound 13.



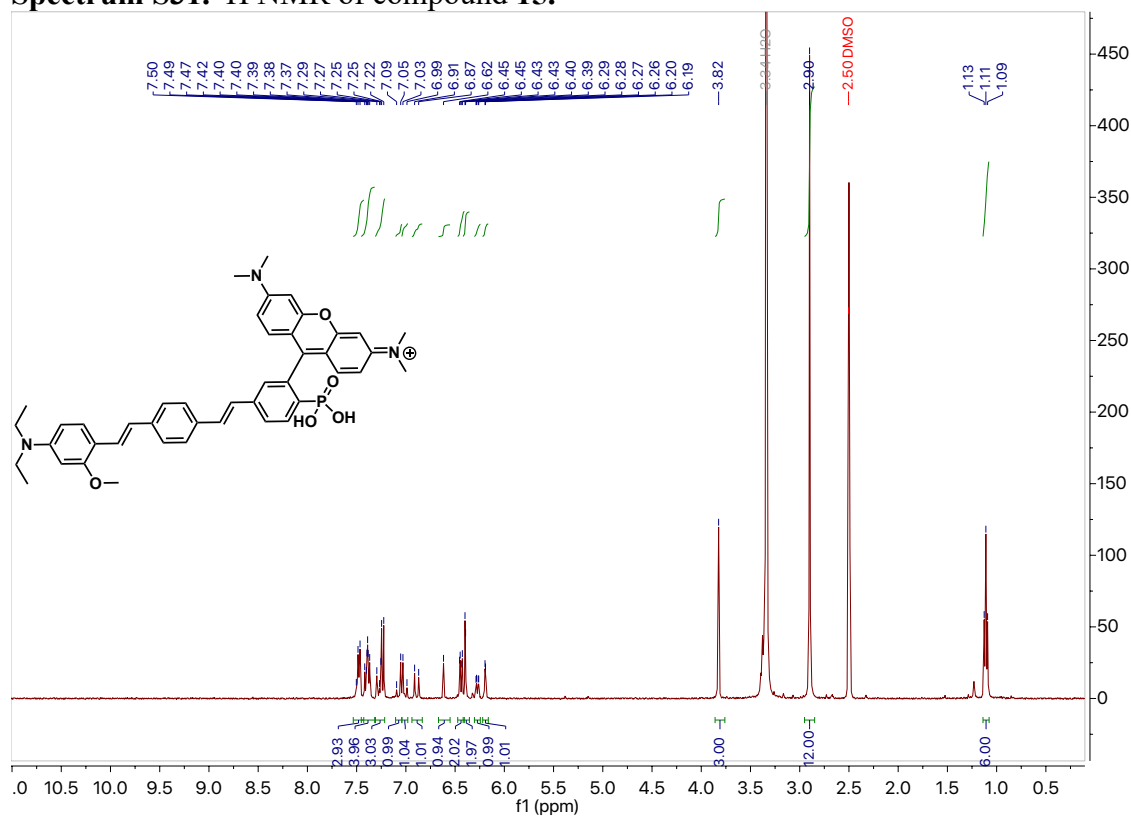
Spectrum S29. ¹H NMR of compound 14.



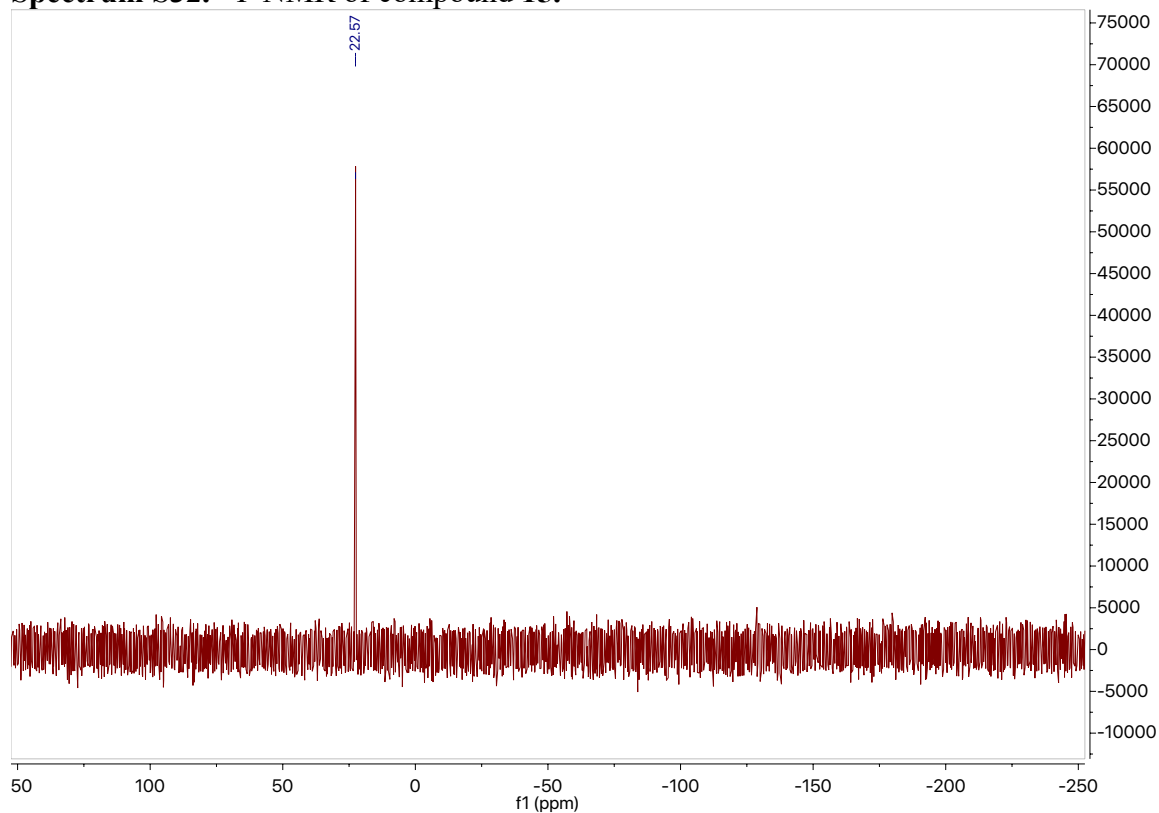
Spectrum S30. ³¹P NMR of compound 14.



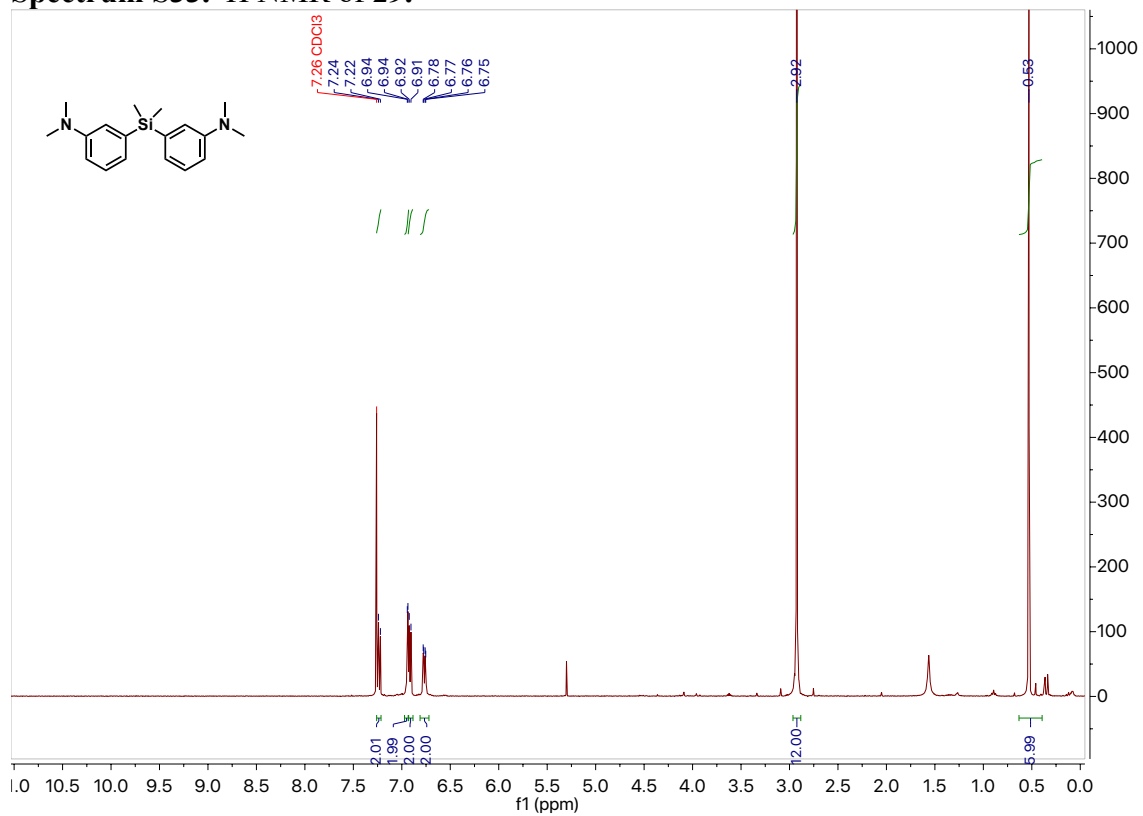
Spectrum S31. ^1H NMR of compound 15.



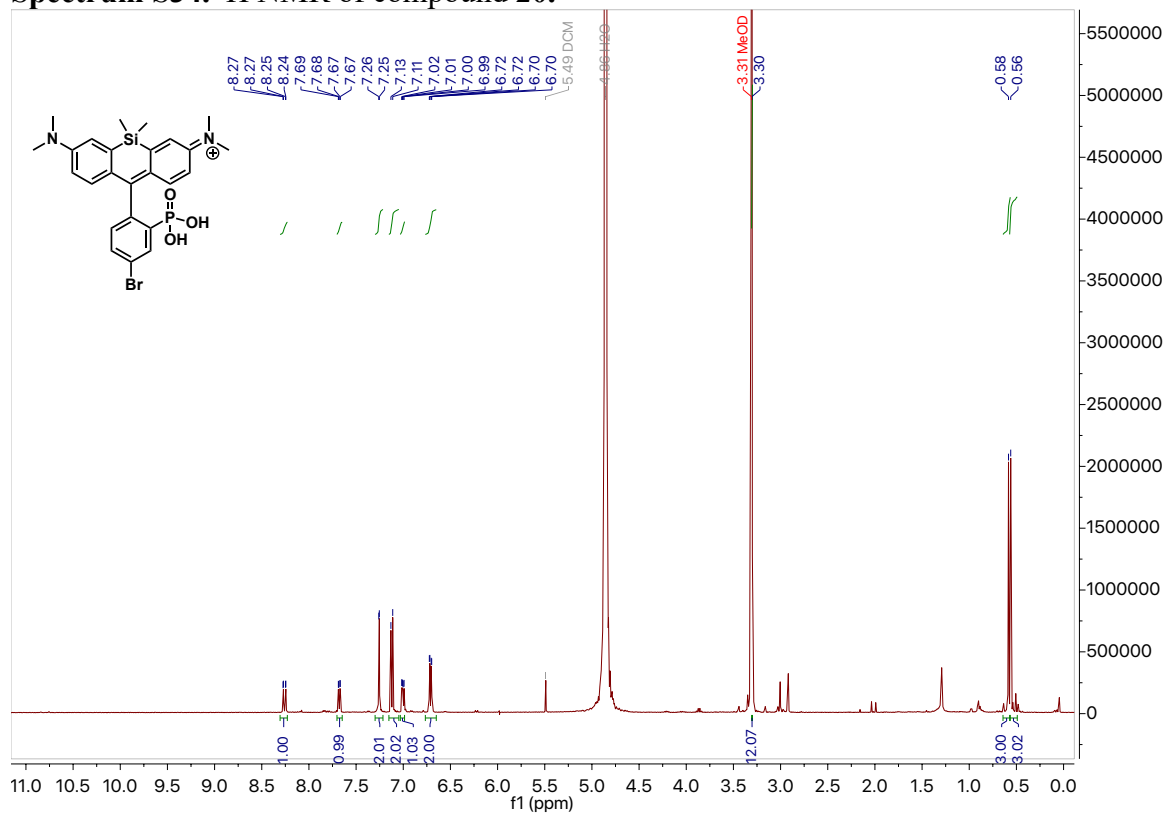
Spectrum S32. ^{31}P NMR of compound 15.



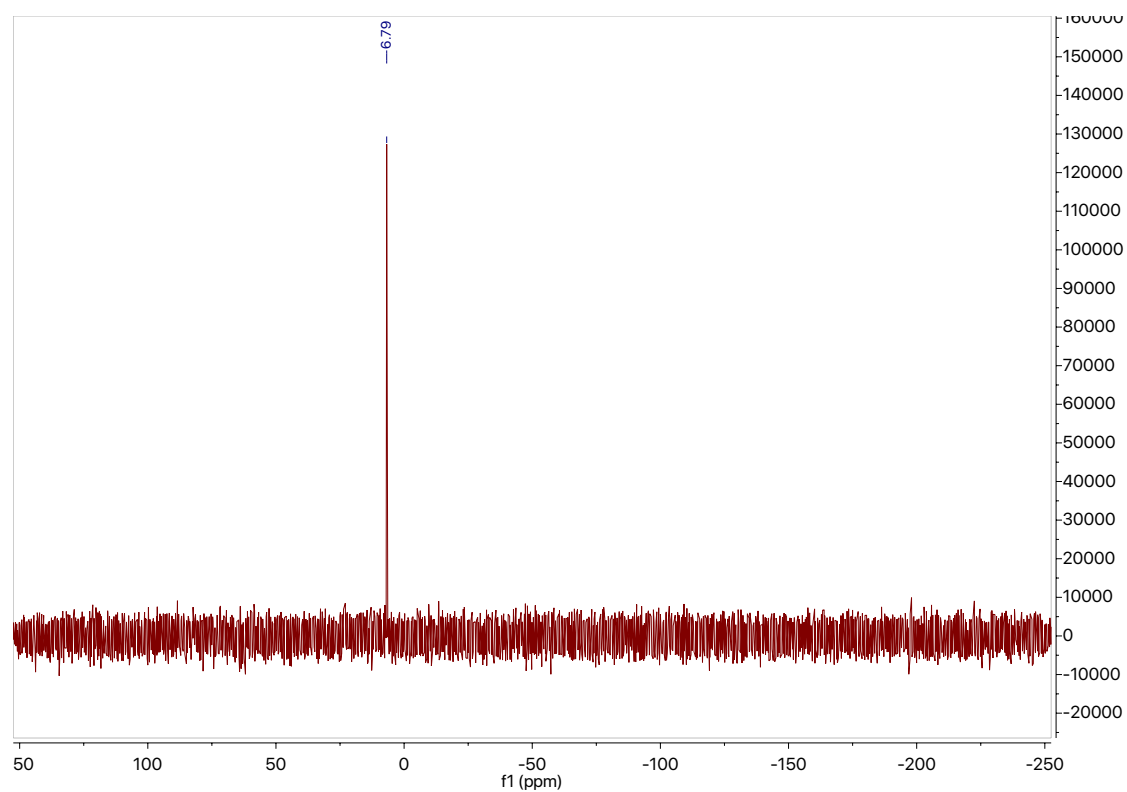
Spectrum S33. ¹H NMR of 29.



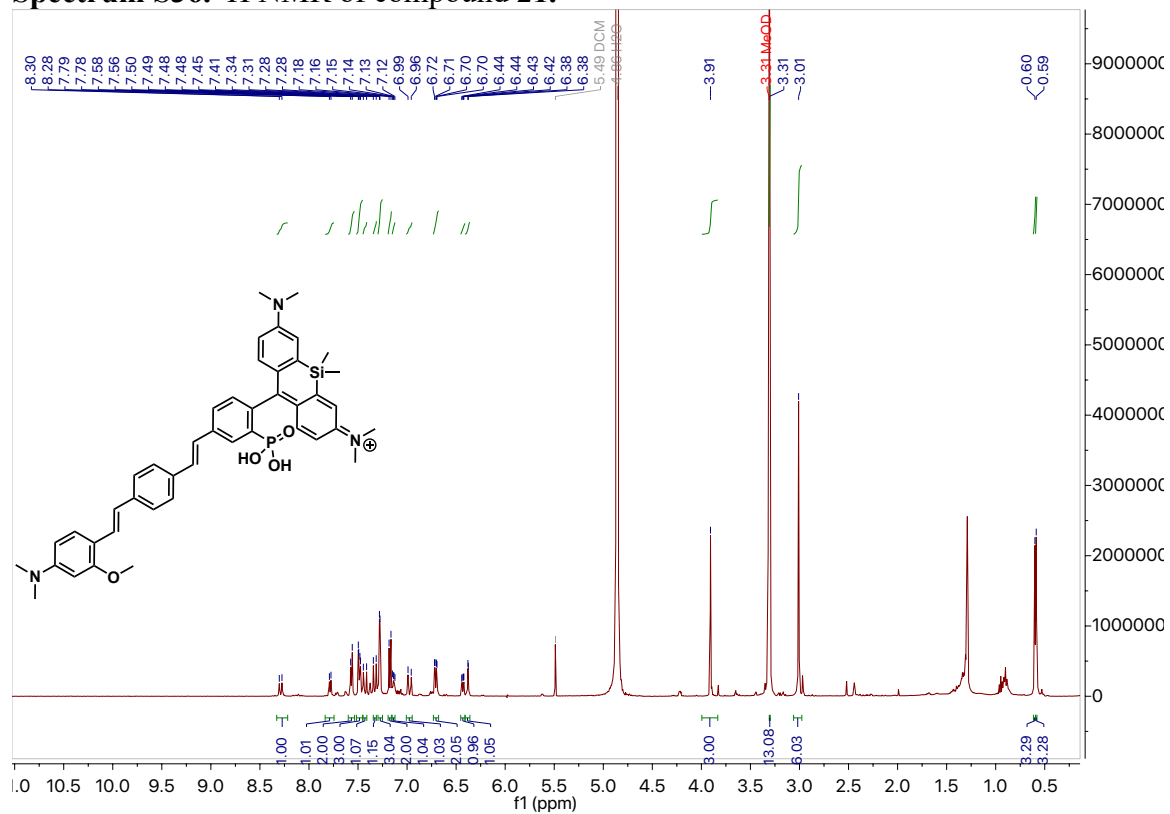
Spectrum S34. ¹H NMR of compound 20.



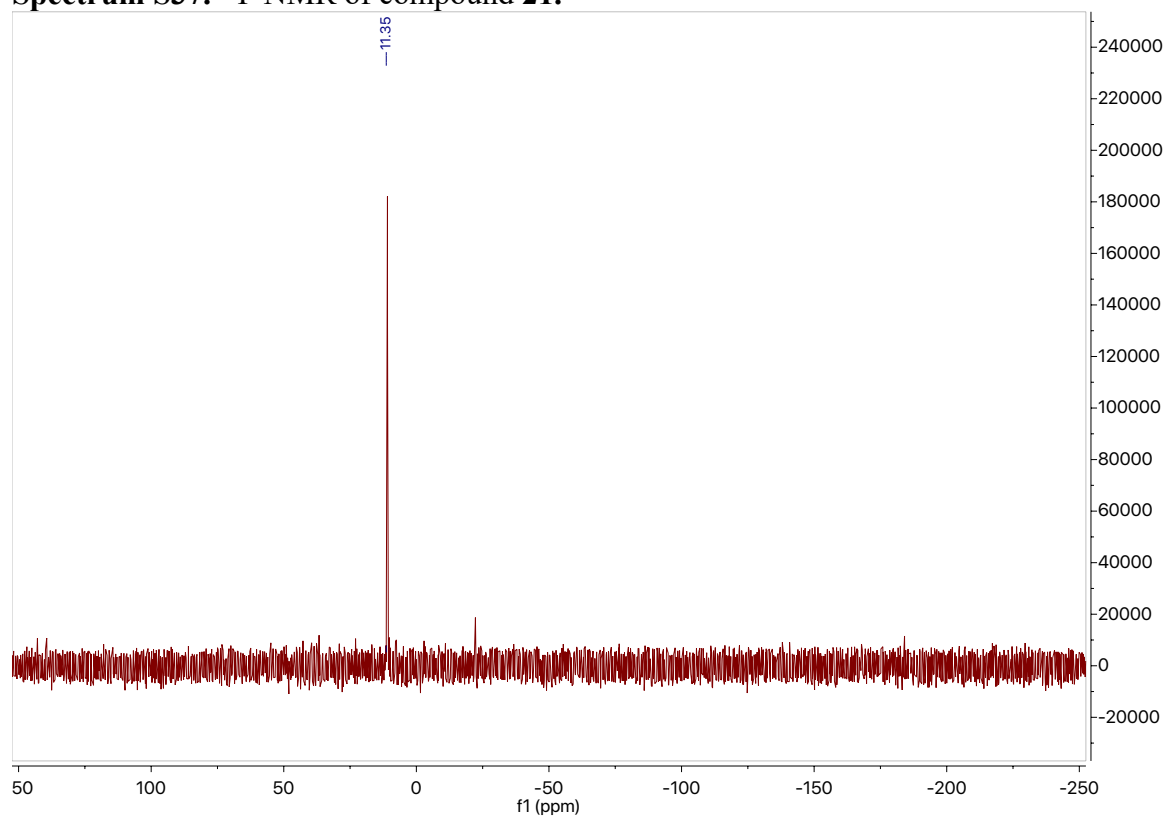
Spectrum S35. ^{31}P NMR of compound 20.



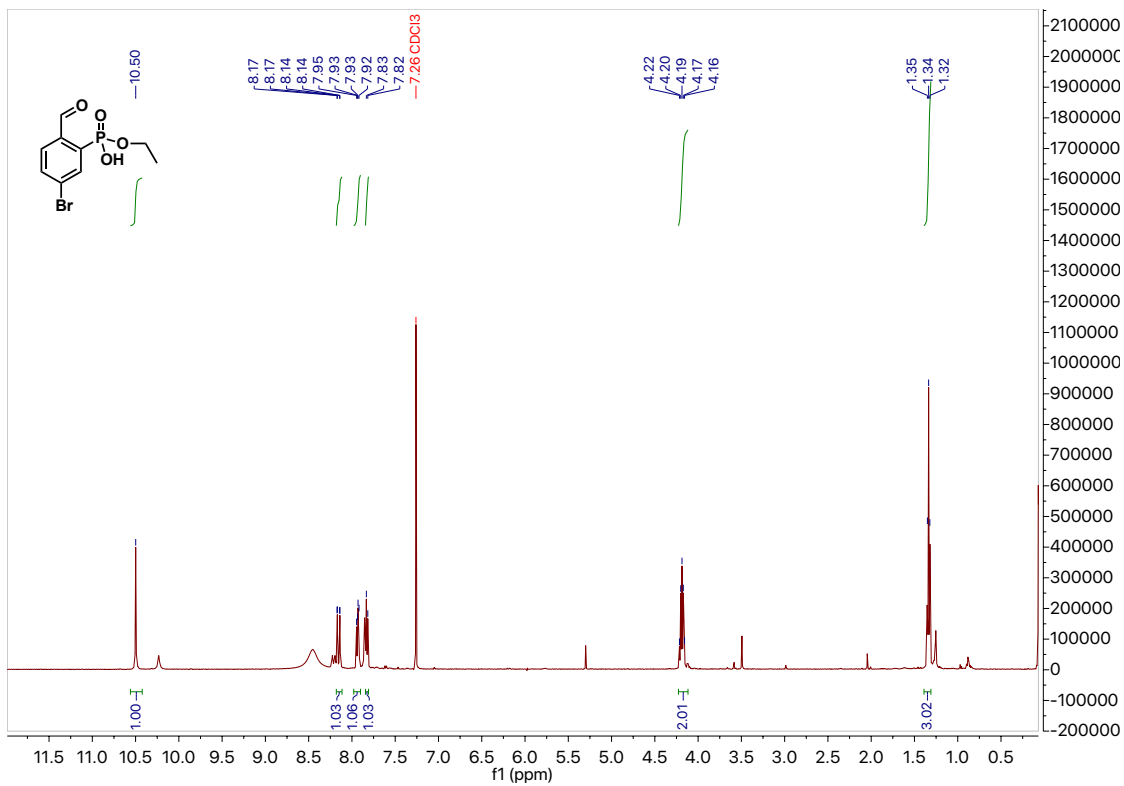
Spectrum S36. ^1H NMR of compound 21.



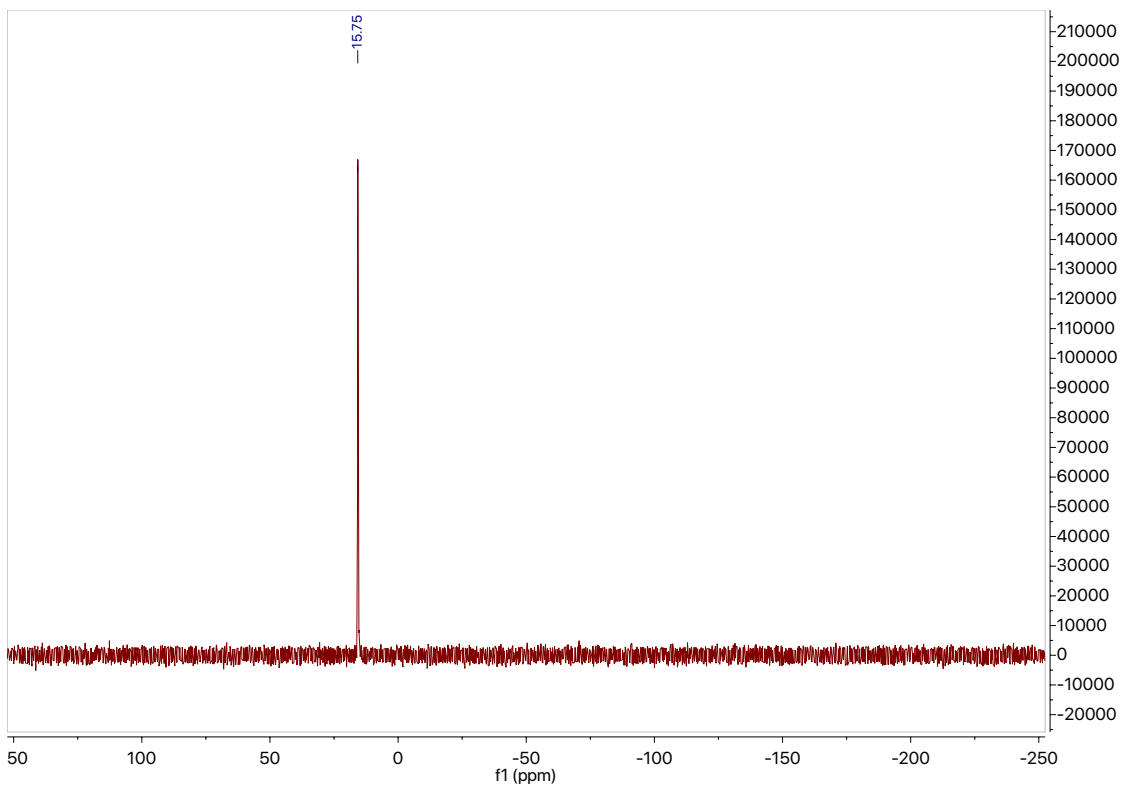
Spectrum S37. ^{31}P NMR of compound **21**.



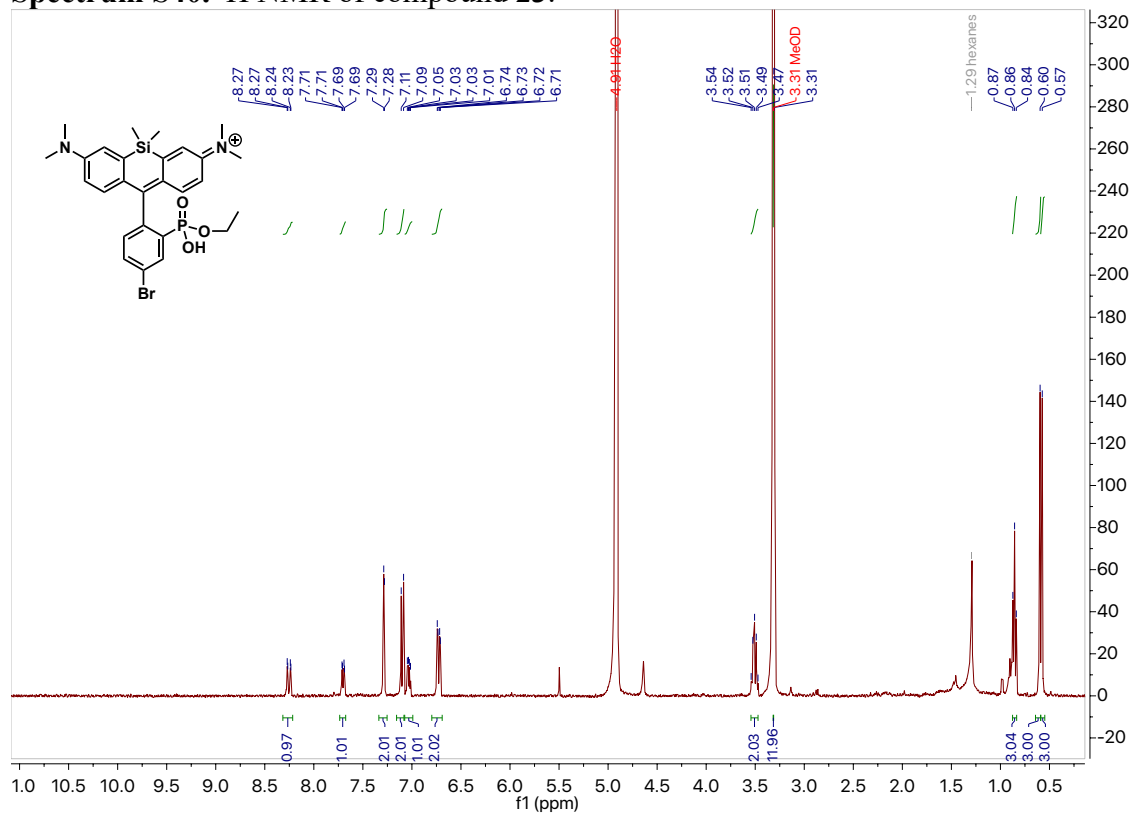
Spectrum S38. ^1H NMR of compound **22**.



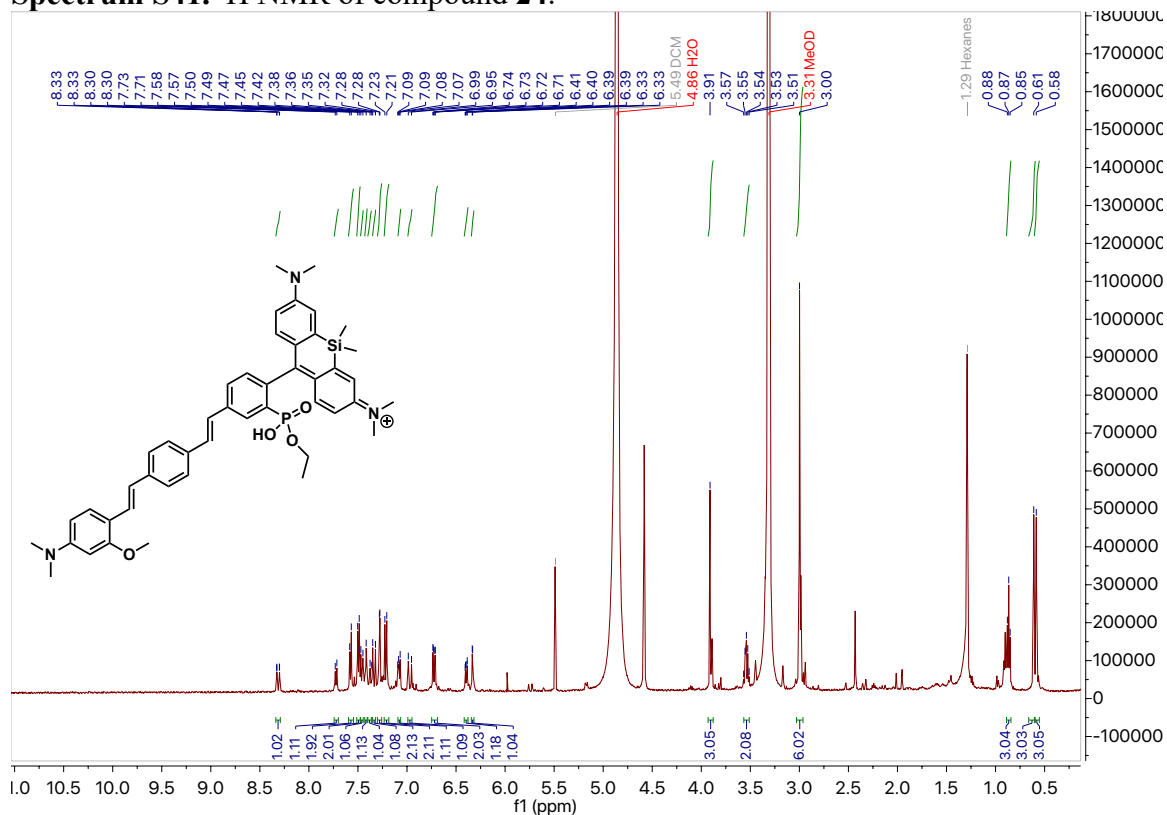
Spectrum S39. ^{31}P NMR of compound **22**.



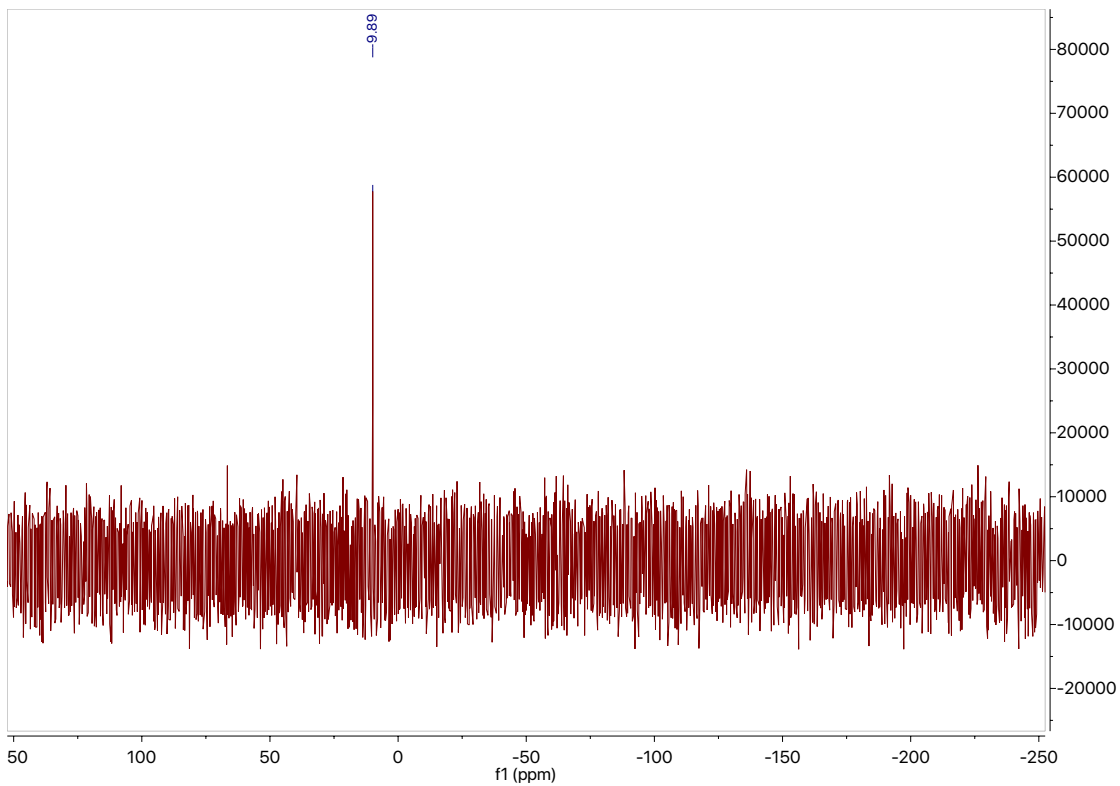
Spectrum S40. ^1H NMR of compound **23**.



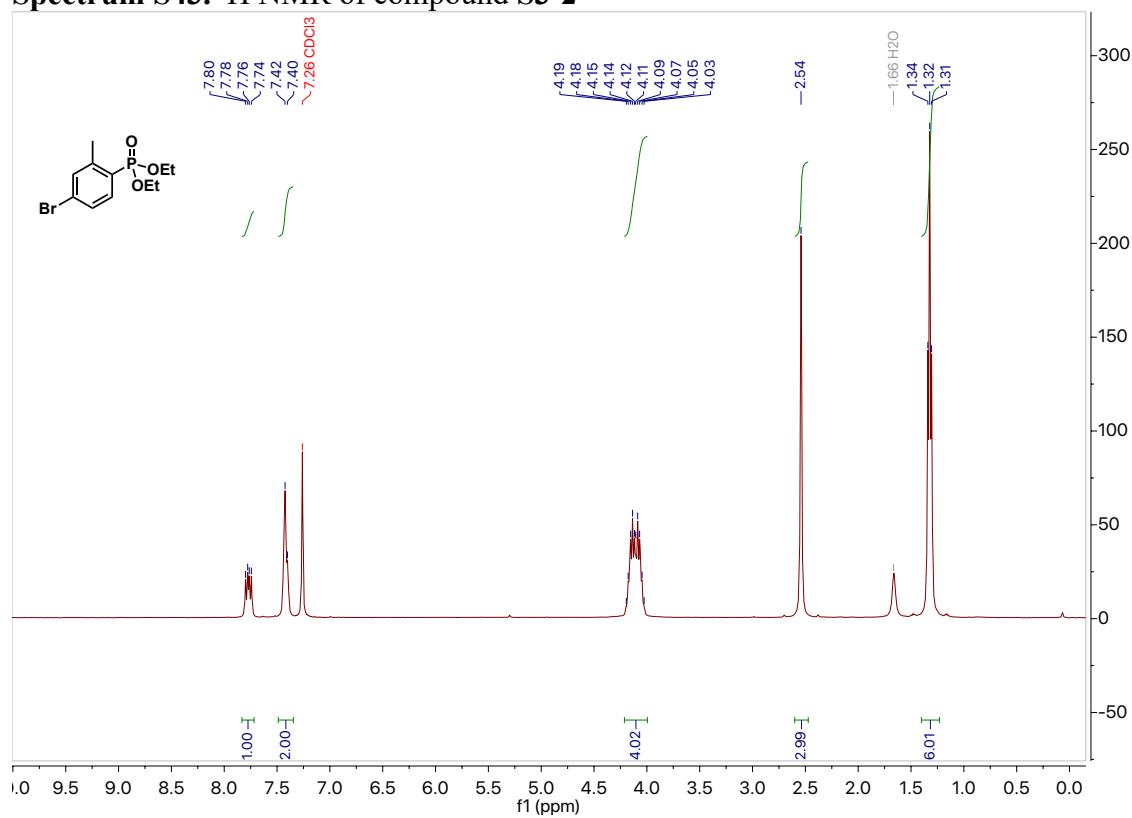
Spectrum S41. ¹H NMR of compound 24.



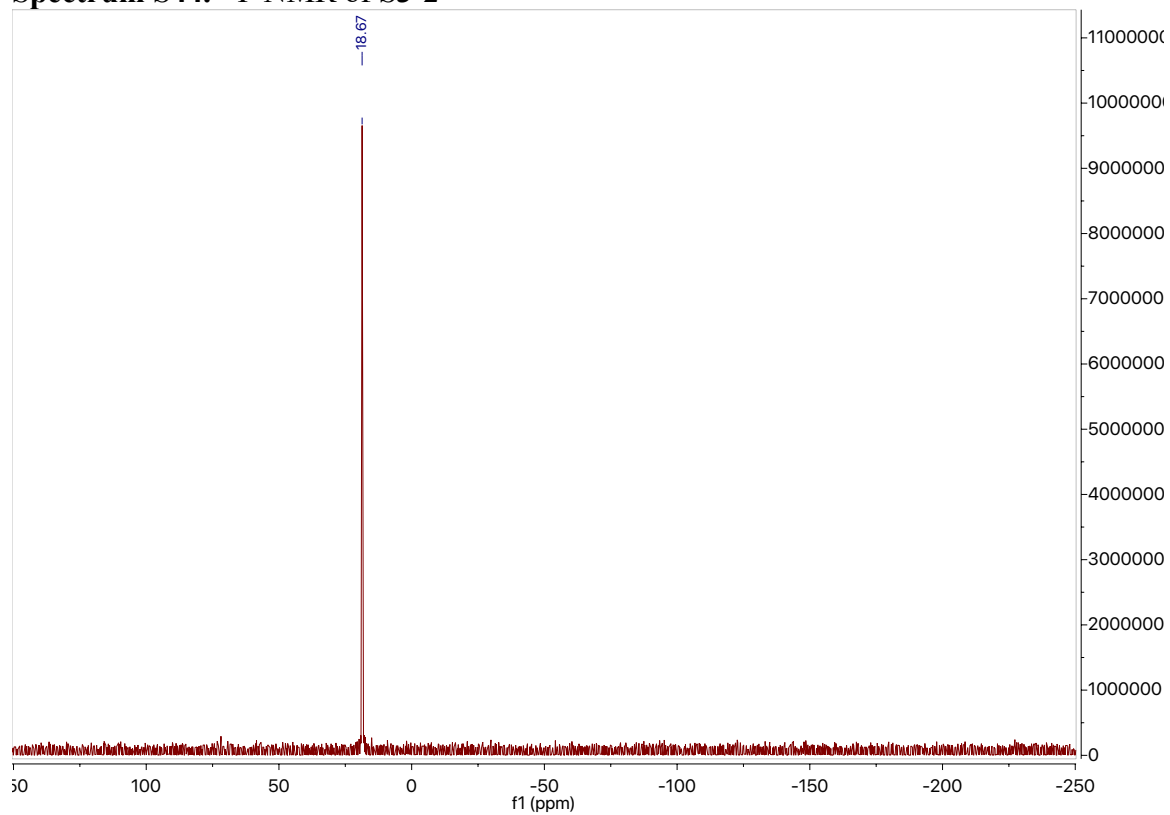
Spectrum 42. ³¹P NMR of 24.



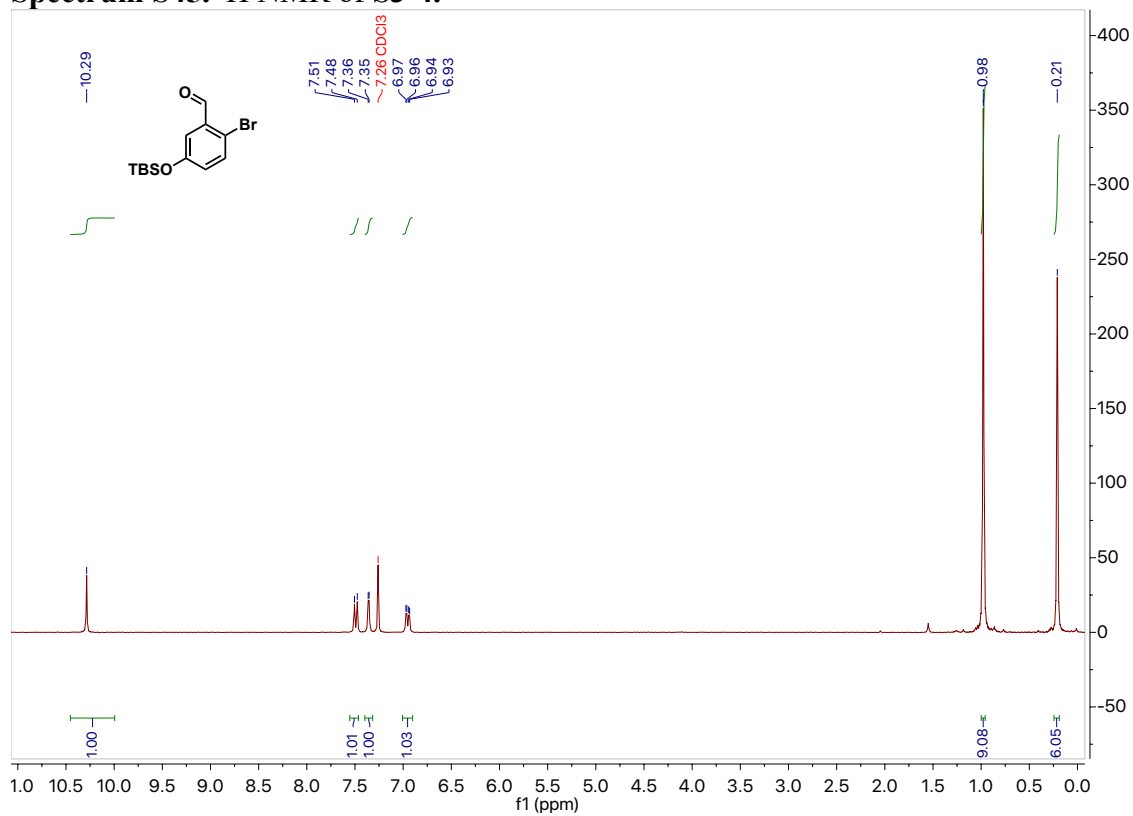
Spectrum S43. ^1H NMR of compound S3-2



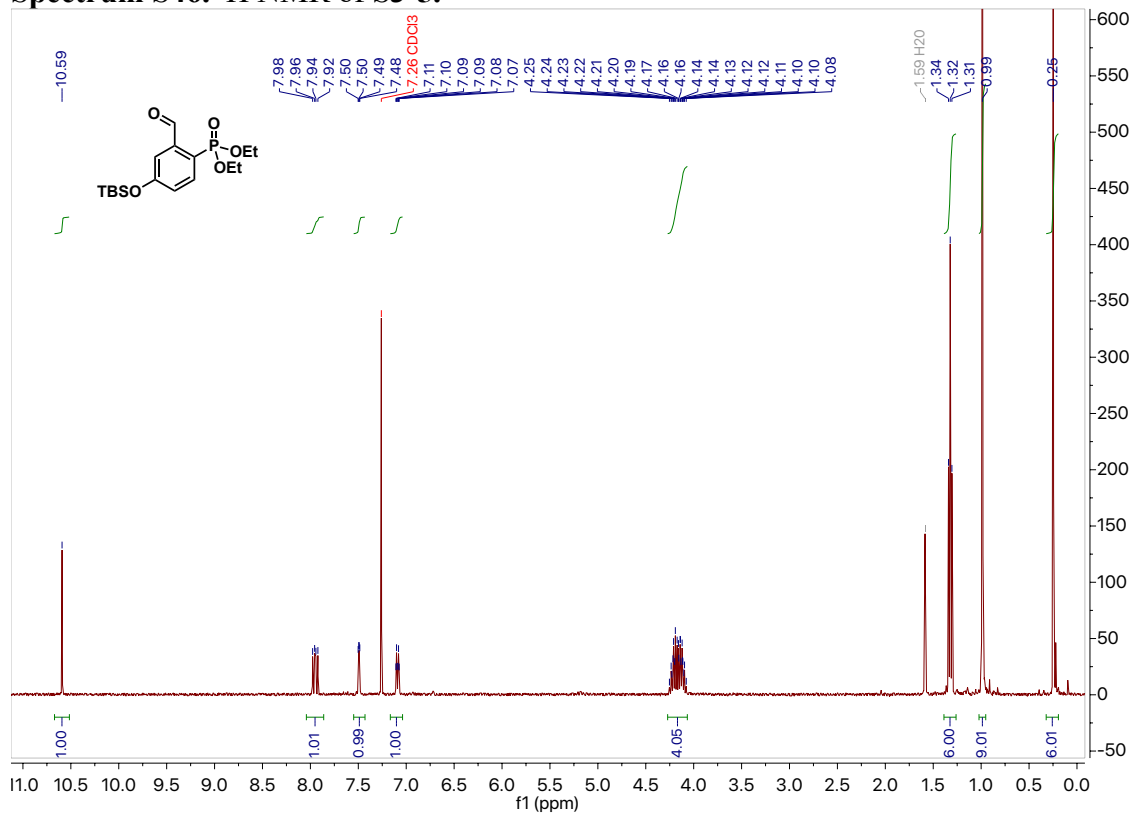
Spectrum S44. ^{31}P NMR of S3-2



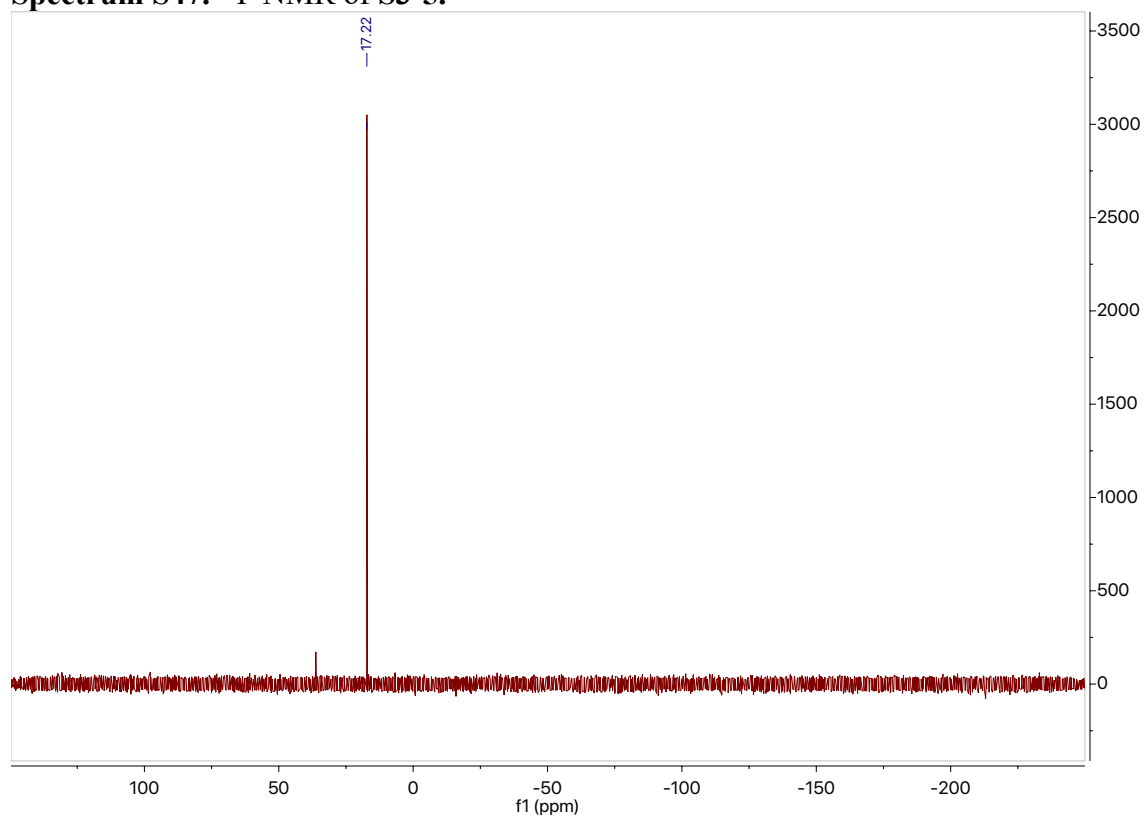
Spectrum S45. ¹H NMR of S3-4.



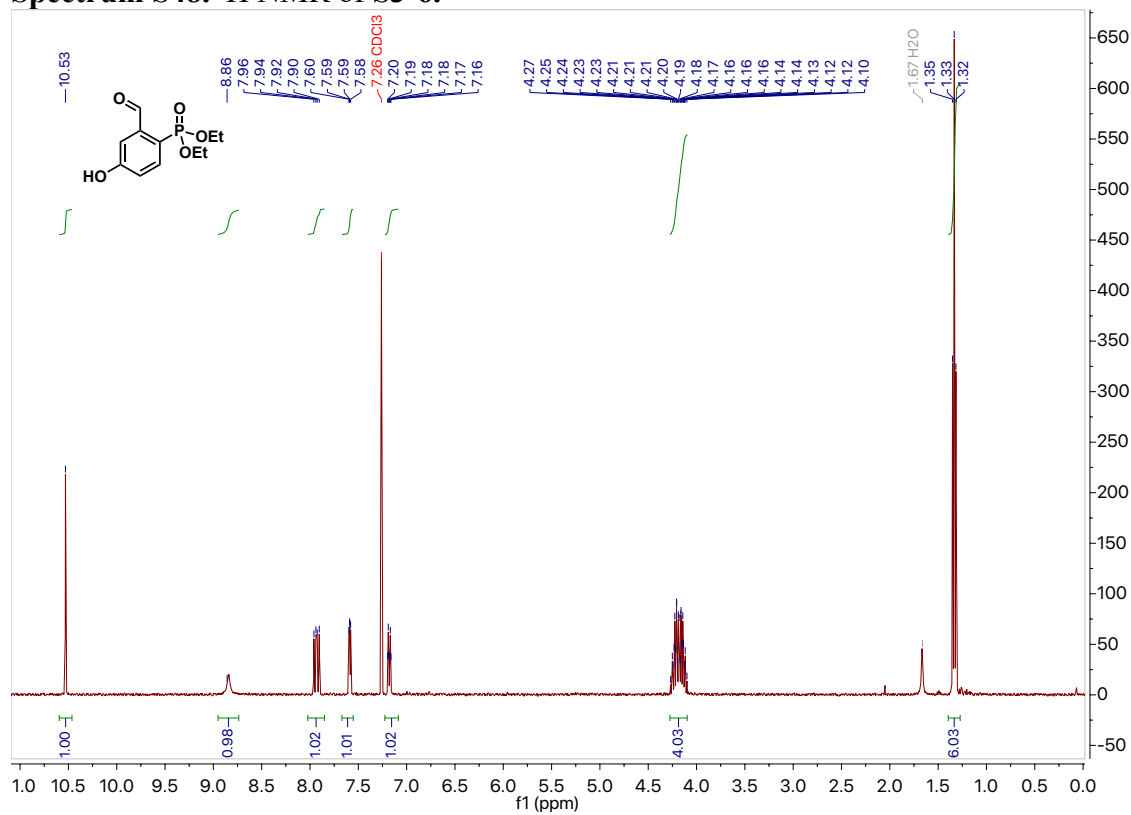
Spectrum S46. ¹H NMR of S3-5.



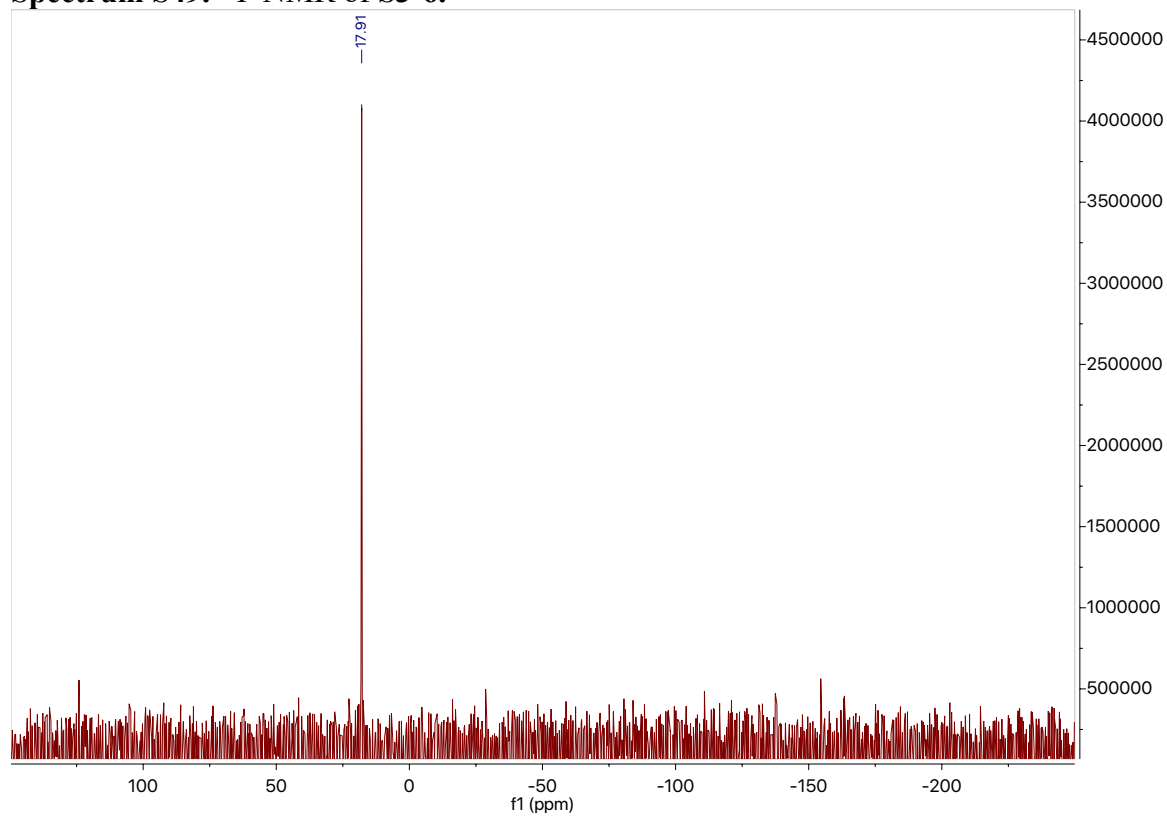
Spectrum S47. ^{31}P NMR of S3-5.



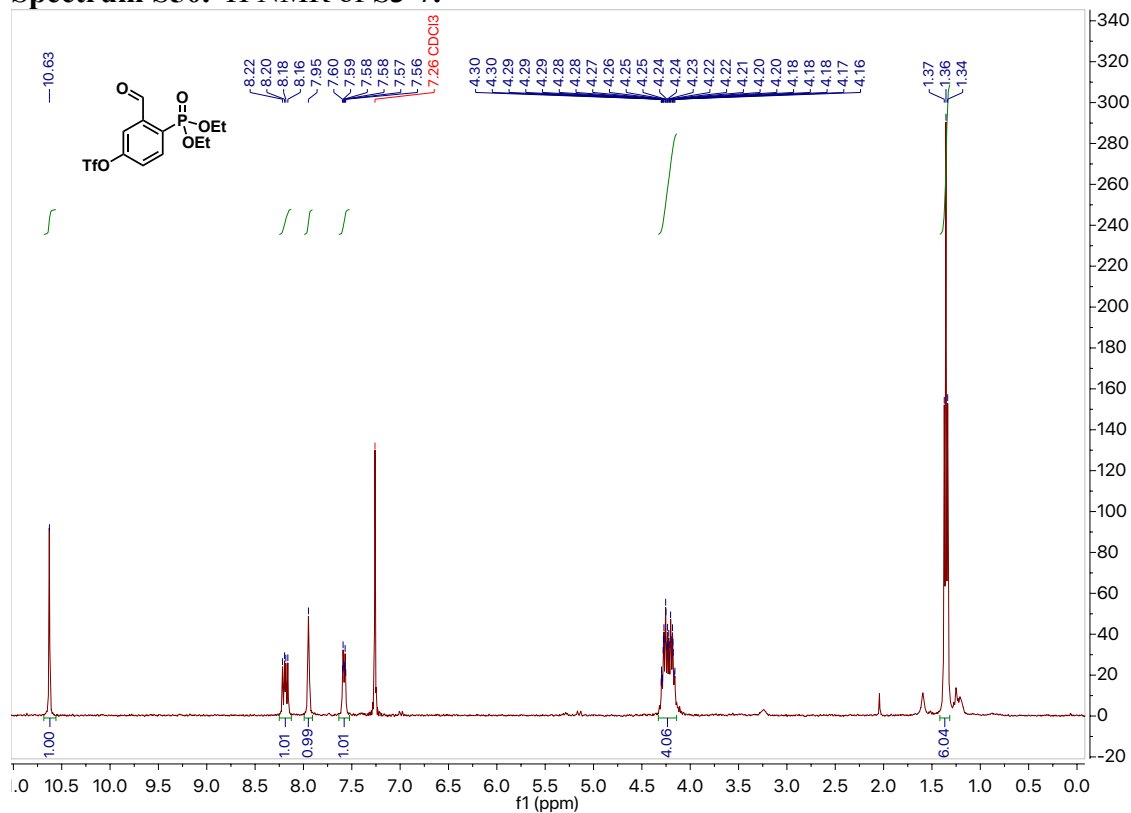
Spectrum S48. ^1H NMR of S3-6.



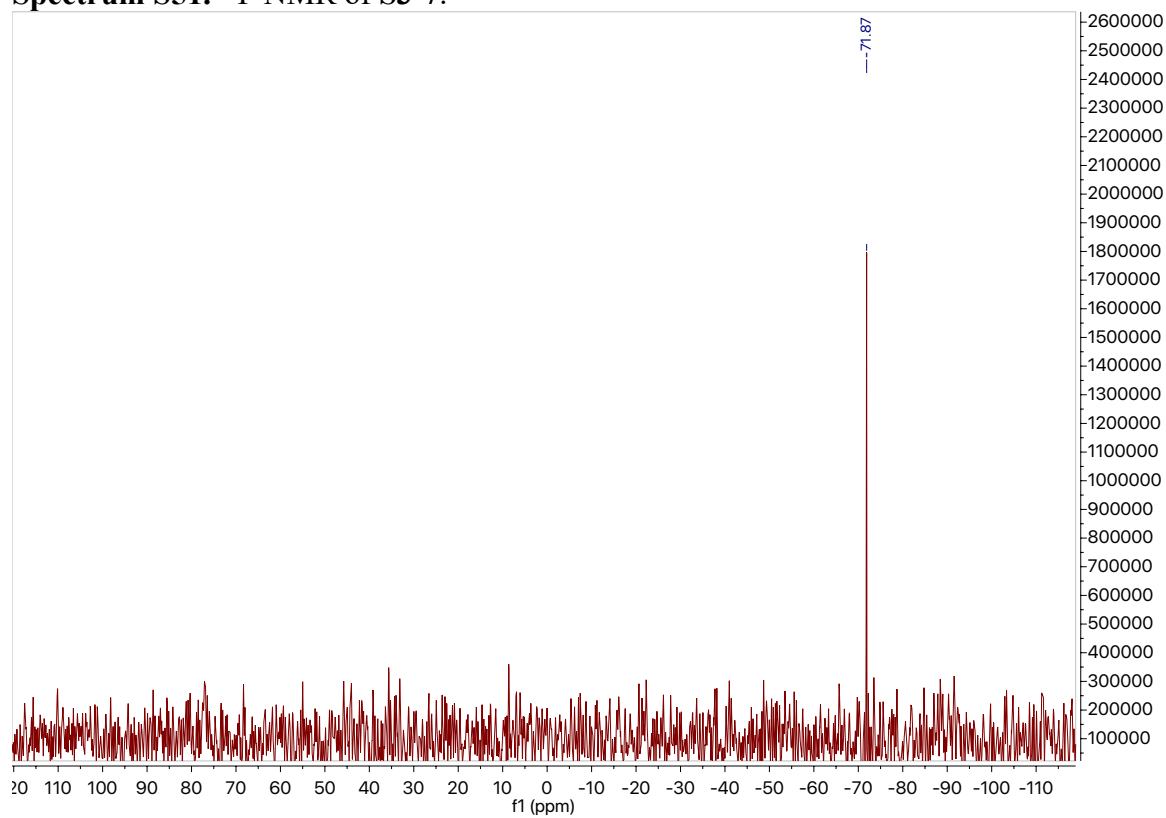
Spectrum S49. ^{31}P NMR of S3-6.



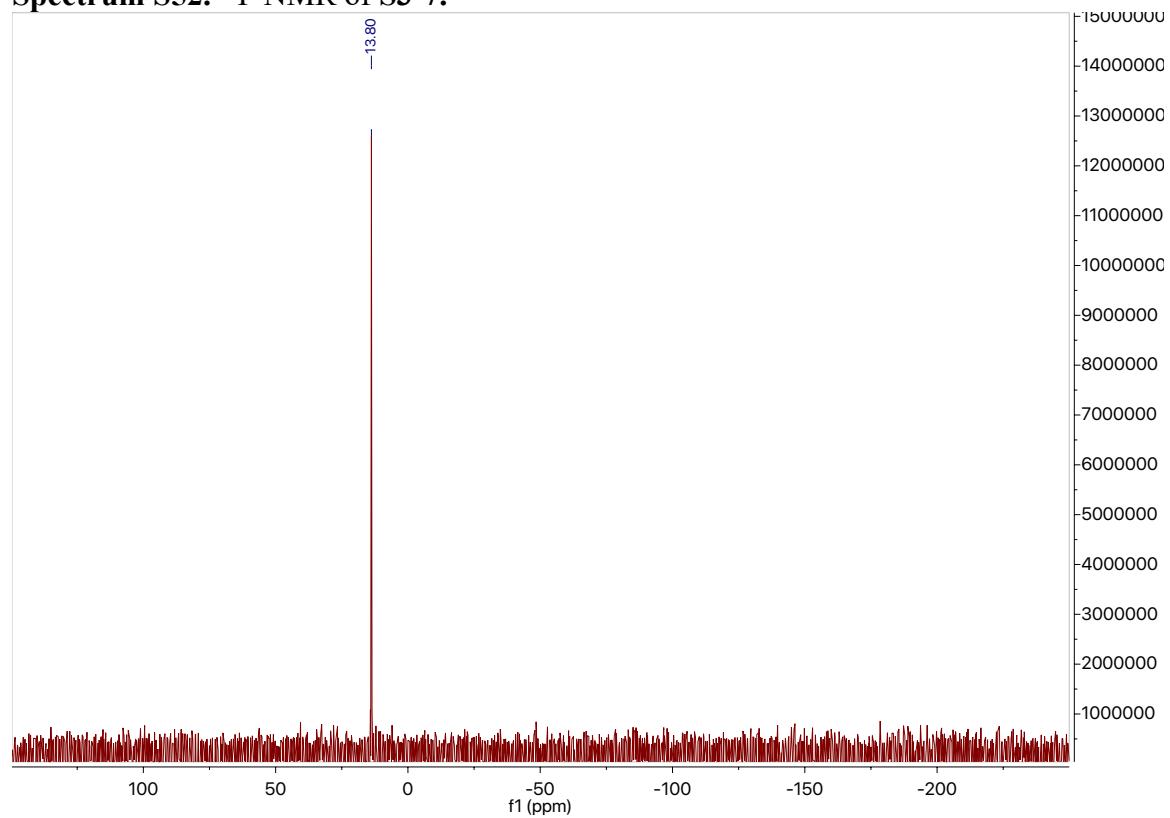
Spectrum S50. ^1H NMR of S3-7.



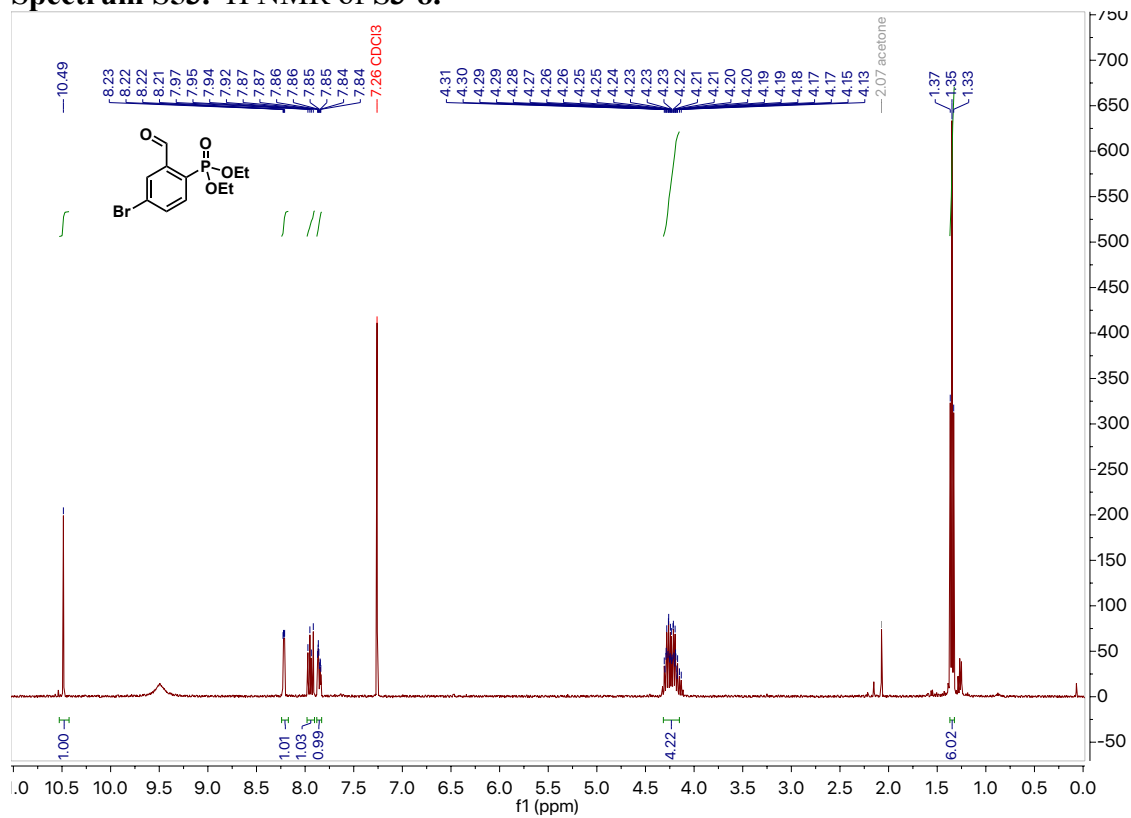
Spectrum S51. ^{19}F NMR of S3-7.



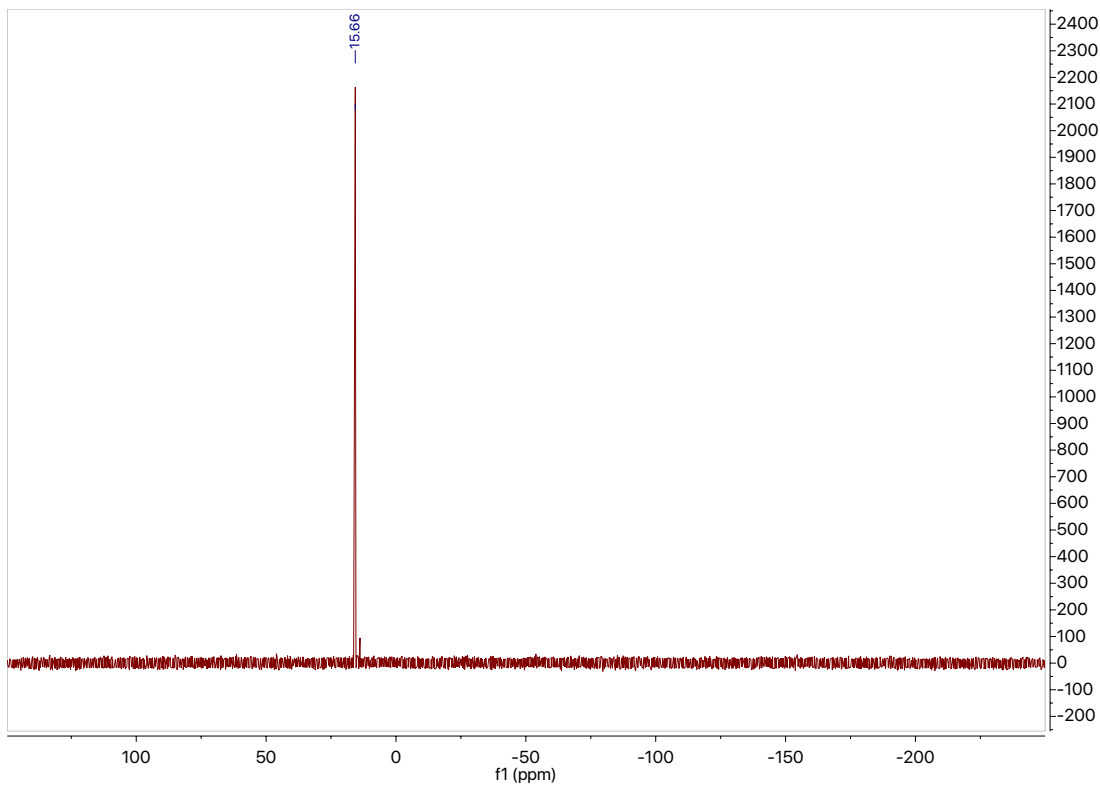
Spectrum S52. ^{31}P NMR of S3-7.



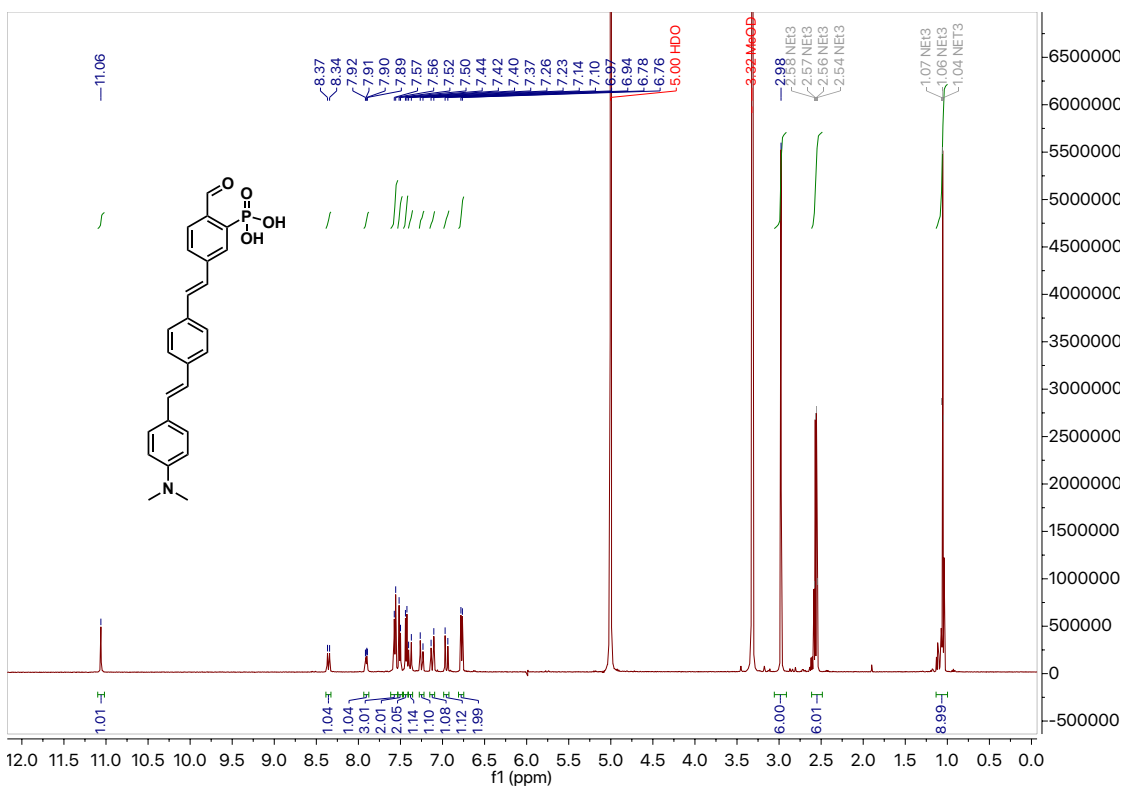
Spectrum S53. ^1H NMR of S3-8.



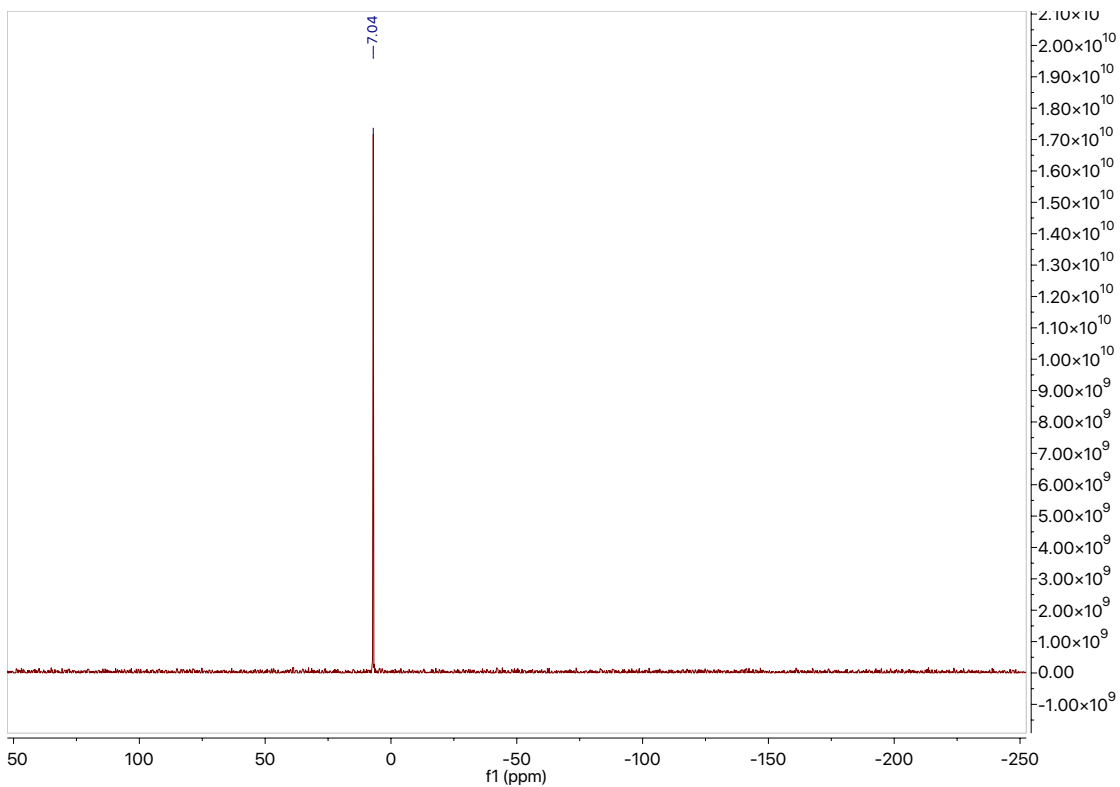
Spectrum S54. ^{31}P NMR of S3-8.



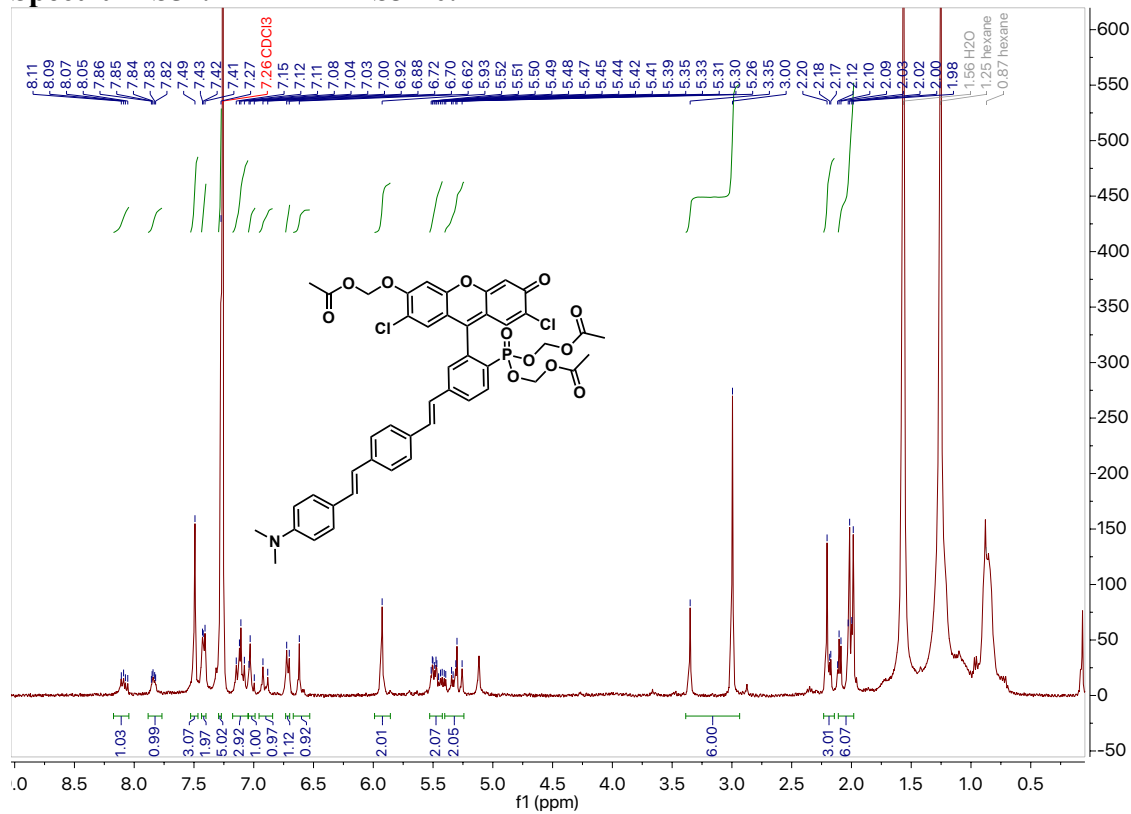
Spectrum S55. ^1H NMR of compound S3-9.



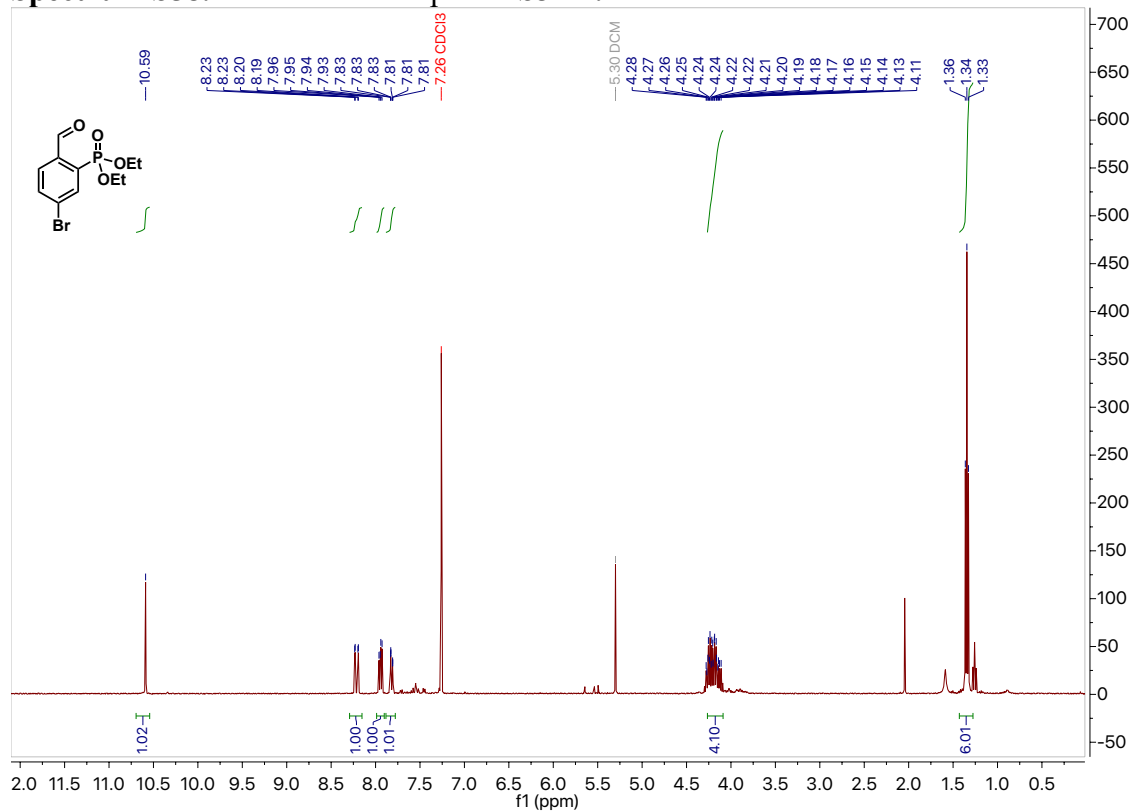
Spectrum S56. ^{31}P NMR of compound S3-9.



Spectrum S57. ^1H NMR of S3-10.



Spectrum S58. ^1H NMR of compound S3-11.



Spectrum S59. ^{31}P NMR of S3-11.

